



**HAL**  
open science

# Lipid excipients and hot-melt coating technology : operational and functional impact

van Trung Tin Huynh

► **To cite this version:**

van Trung Tin Huynh. Lipid excipients and hot-melt coating technology : operational and functional impact. Chemical and Process Engineering. Ecole des Mines d'Albi-Carmaux, 2024. English. NNT : 2024EMAC0002 . tel-04924816

**HAL Id: tel-04924816**

**<https://theses.hal.science/tel-04924816v1>**

Submitted on 1 Feb 2025

**HAL** is a multi-disciplinary open access archive for the deposit and dissemination of scientific research documents, whether they are published or not. The documents may come from teaching and research institutions in France or abroad, or from public or private research centers.

L'archive ouverte pluridisciplinaire **HAL**, est destinée au dépôt et à la diffusion de documents scientifiques de niveau recherche, publiés ou non, émanant des établissements d'enseignement et de recherche français ou étrangers, des laboratoires publics ou privés.

Université Fédérale



Toulouse Midi-Pyrénées

# THÈSE



IMT Mines Albi-Carmaux  
École Mines-Télécom

En vue de l'obtention du

## DOCTORAT DE L'UNIVERSITÉ DE TOULOUSE

délivré par

IMT – École Nationale Supérieure des Mines d'Albi-Carmaux

présentée et soutenue par

**Van Trung Tin HUYNH**

le 26 janvier 2024

### **Lipid excipients and hot-melt coating technology: operational and functional impact**

**École doctorale et discipline ou spécialité :**

MEGEP : Génie des Procédés et de l'Environnement

**Unité de recherche :**

Centre RAPSODEE, UMR CNRS 5302, IMT Mines Albi

**Directrice et Directeur de thèse :**

Maria Inês RÉ, Professeur, IMT Mines Albi

Éric BEYSSAC, Professeur, Université de Clermont-Auvergne

**Autres membres du jury :**

Heiko BRIESEN, Professeur, Technical University of Munich, Rapporteur

Vincent JANNIN, HDR, Directeur R&D, Lonza Capsules & Health Ingredients, Rapporteur

Suênia DE PAIVA LACERDA, Maître de conférences, IMT Mines Albi, Examinatrice

Maëla BERNARD, Chargée de projets, SEPPIC Recherche et Innovation, Examinatrice

Jean-François WILLART, Professeur, Université de Lille, Président du jury

Jean-Flaubert NGUEFACK, Head of Biopharmacy Section, Sanofi R&D, Examineur





## Table of contents

Acknowledgements .....	4
Long version of French summary .....	7
General Presentation .....	20
1. Thesis Context .....	20
2. Thesis Objectives .....	21
3. Thesis Outline .....	21
<b>Chapter 1. Context and Background.....</b>	<b>23</b>
1. Hot-Melt Coating: General Guidelines.....	24
2. Lipid-Based Excipients Used as Coating Materials .....	47
3. Solid Lipid-Based Formulated Products.....	79
4. Some Proposals for a Methodological Approach to Investigating Hot-Melt Coating as the First Deliverable of this Doctoral Thesis after Literature Analysis .....	93
5. Conclusions .....	103
<b>Chapter 2. Methodology .....</b>	<b>105</b>
1. Materials .....	106
2. Methods .....	107
3. Conclusions .....	118
<b>Chapter 3. Hot-Melt Coating with Formulations of Beeswax and Surfactants.....</b>	<b>121</b>
Part 1. Solidification, Melt Viscosity and Adhesiveness of Lipids and Coating Process Performance .....	123
1. Materials and Methods .....	123
2. Results and Discussion .....	130
3. Conclusions .....	159
Part 2 Coating Lipid Composition: Physical Coating Stability.....	161
1. Materials and Methods .....	161
2. Results and Discussion .....	165
3. Conclusions .....	179
<b>Chapter 4. Melt Crystallisation and Hot-Melt Coating of Tristearin-Based Formulations: from Lipid Fundamentals to Applications .....</b>	<b>180</b>
Part 1 A New Fast Lipid-Additive Formulation Screening Approach used in Formulating Solid Lipids for Melt-Processing.....	183
1. Materials and Methods .....	183
2. Results and Discussion .....	189

3. Conclusions .....	208
Part 2. Development of Multifunctional Tristearin-based Formulations for Hot-Melt Coating in Fluidised Bed .....	210
1. Materials and Methods .....	210
2. Results and Discussion .....	215
3. Conclusions .....	238
<b>Chapter 5. Effect of Talc and Vitamin E TPGS on Manufacturability, Stability and Release Properties of Trilaurin-Based Formulations for Hot-Melt Coating .....</b>	<b>240</b>
1. Materials and Methods .....	242
2. Results and Discussion .....	247
3. Conclusions .....	266
<b>Chapter 6. Hot-Melt Coated Substrates: Salt And Amorphous Solid Dispersions Of Praziquantel, Two Different Cases .....</b>	<b>268</b>
Part 1. Hot-Melt Coated Sodium Chloride Crystals: Comparison with a Slow Release Reference Product .....	269
1. Materials and Methods .....	269
2. Results and Discussion .....	269
3. Conclusions .....	271
Part 2. Stability and <i>in vitro</i> Performance of Amorphous Solid Dispersions Hot-Melt Coated with Lipid-based Formulations of Diverse Digestibility.....	272
1. Materials and Methods .....	274
2. Results and Discussion .....	284
3. Conclusions and Perspectives.....	307
General Conclusions and Suggestions for Future Work .....	308
Bibliography.....	313
List of Figures .....	335
List of Tables .....	345
Poster, Presentations and Publications.....	347
Appendix 01 .....	348
Appendix 02.....	357
Appendix 03.....	371
Appendix 04.....	379
Abstract.....	381

## Acknowledgements



At first, I would like to thank sincerely the jury for accepting to evaluate the work of this doctoral thesis, constituted from the collaborative and interdisciplinary work between several parties – IMT Mines Albi (Laboratory RAPSODEE and technological platform GALA), University of Clermont-Ferrand (Laboratory MEDiS) and SEPPIC, in the framework of a thesis financed by Occitania region, Castres-Mazamet. Firstly, Sincere thanks to Prof. H. Briesen for being the reporter whom I have admired for his expertise in process engineering and his quality work with hot-melt coating. Secondly, sincere thanks to Dr. HDR V. Jannin for also being the reporter whom I have admired for his expertise in lipids and lipid-based formulation. Thirdly, sincere thanks to Prof. J.-F. Willart whose expertise I have come across in solid-state pharmaceuticals. Fourthly, sincere thanks to Dr. J.-F. Nguefack who was my training internship supervisor in the department of Biopharmacy at Sanofi. To the jury panel, I am happy to present the multidisciplinary outcome of this doctoral thesis on formulation of solid lipids for pharmaceutical applications.

Further, I would like to thank sincerely the members of the technological platform GALA for their grand contribution to the accomplishment of this doctoral thesis. Firstly, sincere thanks to Mrs. L. Haurie and Mrs. A. Lafon for their expertise of RAMAN spectroscopy and atomic force microscopy. Special thanks again to Mrs. L. Haurie for her project administration and budget management. Thirdly, sincere thanks to Mrs. M. Chambard for her technical interventions on experiments with Crystal16 Crystallization Systems. Finally, I would like to thank greatly Mr. A. Perron for his accompanying in coating operations and technical support, for his willingly listening to exchanges on the thesis subject and the spiritual practice, and for his teaching how to drive a long trajectory so that I became confident enough to accomplish mobility missions. I also did not forget Ms. K. Gelie for her occasional support in coating operations during the early stage of thesis. Their motivation and team work quality are greatly appreciated.

Further, I would like to thank sincerely the technical support at RAPSODEE for their grand contribution to the accomplishment of this doctoral thesis. Firstly, sincere thanks to Mrs. S. d. Confetto for her expertise of thermal analyses and chromatography. Secondly, sincere thanks to Mrs. S. Patry for her expertise of contact angle measurements and dynamic vapour sorption. Thirdly, sincere thanks to Mrs. V. Nallet for her expertise of X-ray powder diffraction acquisition and treatment, work safety and stock management of chemical substances and for training sessions on rheometry with Mr. M. Sauceau. Fourthly, sincere thanks to Mr. P. Acart for his expertise of particle size distribution, pH, and conductivity measurement. Fifthly, sincere thanks to Mr. L. Devriendt for his expertise of powder flow measurements and management of laboratory consumables and devices. Their motivation and team work quality are also greatly appreciated.

Further, I would like to thank sincerely the other technical support at RAPSODEE and at ICA for their participation to the accomplishment of this doctoral thesis. Firstly, sincere thanks to Mrs. C. Rolland – specialist of scanning electron microscopy and optical microscopy. Secondly, special thanks to Mrs. K. Vieilleigne for her accompanying in my experiments with polarised light microscopy. Thirdly, sincere thanks to Mr. D. Marty for equipping an automatic recorder of conductivity which helped us go further in the experimentation. Lastly, sincere thanks to Prof. J.-J. Letourneau, Mr. T. Deleau, Mr. D. Ade, Mr. M. Ribeiro and those whom we might forget for their unspoken contribution to this doctoral thesis.

Further, I would like to also thank MEDiS research group at the University of Clermont-Ferrand for their participation to this doctoral thesis and for their reception during my mission at their workplace. Sincere thanks to Mr. S. Denis, Mrs. S. Chalancon, Mrs. C. Mazal, Mr. C. Durif, Mrs. C. Dhainaut, Mrs. I. Dhifallah, Mrs. E. Lainé for their participation in conduct of experiments using the artificial gastrointestinal digestion model TNO TIM-1. Their contribution is also greatly appreciated.

Further, I would like to thank the support of the doctoral school MEGeP, notably that of Mrs. R. Calvet, Mrs. N. Lyczko, Mrs. L. Barthe. Also sincere thanks to Mrs. H. Belix, Mrs. D. Liret, Mr. P. Diaz and the DOC team for their library service, book rent support, training sessions on literature research, thesis submission and open science... Also, sincere thanks to garage management team, information technology team. Also, sincere thanks to the administration panel, Mrs. S. Perfaure, Mrs. M.-C. Plantié and other administrative personnel. Also, sincere thanks to laboratory secretaries, Mrs. A.-M. Fontes, Mrs. V. Veres and Mrs. C. Auryol for their administrative support. I had such a good opportunity to experience a professional, encouraging and collaborative environment.

Further, I would like to thank A. Verrecchia and L. Azerradj, who contributed to this doctoral thesis as intern or student. Sincere thanks to C.-M. Barcelo, M. Aina, J. V. Jimenez, M.-T. Alves de Lima, L. H. Regua Mangia, L. T. d. Carvalho, L. Maignier, M. Dandignac, T. Massias, G. A. Aruffo, H. Boussoffara for their providing any support in laboratory work and having included me in extra-scholar activities. Also, special thanks to J. Bionatti for her grand support and as a coincidence this doctoral thesis was a continuity of hers i.e. development of amorphous solid dispersions and development of hot-melt coating formulations leading to new pharmaceutical applications.

More importantly, I would like to thank Prof. F. Espitalier for her impartiality, for her creating many favourable conditions for all as well as her willingness to help. Within the framework of this doctoral thesis, I especially thank her for her advice with crystallisation studies and modelling techniques.

Most importantly, I would like to thank the supervision team of this doctoral thesis. Firstly, sincere thanks to Mrs. Maëla Bernard, Mrs. S. Faget, Mrs. S. Lefebvre for their accompanying the long way to the accomplishment, providing industrial insights and financial support. Note that we also received material donations from some providers (e.g., IOI Oleo, Lipoid). I would like to thank Prof. E. Beyssac for his advice on the conduct of *in vitro* performance testing, result analysis and his reception during my sojourn for experiences with TNO TIM-1 and flowthrough cells. I would like to thank Mrs. S. d. Paiva Lacerda for her accompanying the conduct of this doctoral thesis, her technical advice and her being intermediate in exchanges with the technical teams. Their supervision is greatly appreciated.

Most importantly, I would like to thank Prof. M.-I. Ré for my mostly learning how to become a scientist under her direction, for all her support, her advice, and her confidence throughout the progress of this

doctoral thesis. She is willing to listen despite many barriers of language and culture background. She has created for the conduct of this doctoral thesis many favourable conditions such as establishment and purchase of new techniques and materials. She is willing to support when her student has difficulties of communication. My apologies to cause much trouble when being a member of her research group.

Along the farthest journey from my family of my life, I would like to thank Master friends, Y.-Y. Chen, T. V. John, Y.-N. Ngo, D.-N. Ngo and the others, with whom both glad and sad experiences took place during my first two years in France. I also thank the support of the Vietnamese community in Albi, especially Mrs. T.-N. Bui and her husband and those who as students A.-T. Le, just come and go when the time flies. Also, special thanks to Prof. J. Fages and Mr. R. Sescousse for their organising a good Master's training programme which equipped me with enough scientific knowledge and skill for doing this doctoral thesis. Also, special thanks to Prof. D. Pham Minh for his willingness to help and his admission to a Master's internship where I could accumulate my first research experiences.

I also thank my Vietnamese friends in Vietnam D.-T.-T. Phan, N.-L. Nguyen, T.-T.-V. Lieu, H.-Y. Nguyen, T.-H.-H. Lai and my Vietnamese friends in Europe K.-T. Duong, D.-T. Thieu, T. Le and especially both T.-C. Mai and H. Le, for their caring for me from far away as well as their financial aid when I was in need. Also, sincere thanks to the landlords Mr. A. and Mrs C. Jobey in Albi, Mr. C. Depraetere in Montpellier for their kindness. All my journey makes me believe more the words of my teacher of French "Be kind and you will meet kind people". I also thank her, Mrs. P.-L. Pham-Thai and the other teacher Mr. T.-N. Lu for their strict lessons so that I could be confident in managing a new life in France. Also, thanks to my French (Dhagpo Albi KTT), Taiwanese and Vietnamese Buddhist study and meditation communities.

Equally most importantly, beside having good professors, I have been fortunate to receive grand support from my family. I would like to thank my cousin aunt Mrs. T.-L. Nguyen in Paris for her constant care and her first support since my settlement in France and my cousin uncle Mr. V.-H. Phan in Marseille for his support. I also owe a lot to the financial support of my beloved aunts, as foster-mothers, Mrs. T.-T.-A. Nguyen, Mrs. Thi-T.-H. Nguyen, and Mrs. T.-T.-H. Nguyen without which I could not afford to manage such a long journey till now. Finally, to my parents Mrs. T.-T.-H. Nguyen and Mr. V.-T. Huynh, my elder sister T.-P.-O. Huynh, I would like dedicate the outcome of this doctoral thesis in response to their unconditional emotional support, without which I could not have made it this far.

Finally, I apologise for having caused much boredom whilst being a team member. For the sake of the collaboration between IMT Mines Albi, University of Clermont-Auvergne and SEPPIC and the confidence of the supervisors, I tried to have the most work possibly conducted by many parties. This represented a challenge for someone introvert and discreet. I hope any good outcome from this doctoral thesis could be a gift for all, as without a multilateral contribution, it would not be accomplished. I owe to all the parties more than this work. Sincere thanks to all for their patience and perseverance. Thanks to this long journey I realise the purpose in life. I prefer taking time to meditate whilst working and calming the mind in the turbulence of everyday life. Inspired from the teaching words of Venerable Master Chin Kung "for the sake of all beings", I hold no copyright for this doctoral thesis and dedicate all the merits of this doctoral thesis if anyone benefits from it for the good causes to all beings.

Namo Amitabha!

## Long version of French summary

Cette thèse est intitulée « **Excipients Lipidiques et Technologie d'Enrobage à Chaud – Impact Opérationnel et Fonctionnel** ». Sous l'optique de l'ingénierie, l'enrobage à chaud représente une méthode de fabrication sans solvants. Cela permet d'éliminer plusieurs opérations unitaires telles que le séchage et le contrôle de l'humidité dans les produits finis. Sous l'optique des matériaux, les lipides sont, dans sa majorité, généralement sûrs, naturellement abondants et stables dans des conditions thermiques (normalement en-dessous de 200°C) lors de la mise en forme. De ce fait, l'enrobage à chaud et les excipients lipidiques peuvent être considérés comme une combinaison parfaite pour la fabrication durable. D'un point de vue des produits, la formulation avec les lipides solides offre potentiellement des solutions pour lever les défis du développement pharmaceutique tels que (1) émergence des nouvelles modalités thérapeutiques, (2) administration des molécules peu solubles, (3) repositionnement des médicaments, (4) reformulation, (5) développement des génériques, (6) conception des thérapies personnalisées, etc.

Cette thèse traite des trois défis associés au développement des procédés d'enrobage à chaud avec des formulations lipidiques comme agents d'enrobage :

- Premièrement, les avantages et les désavantages de l'enrobage à chaud en lit fluidisé (Voir **Figure 1-2**) n'ont pas été complètement dévoilés face aux procédés existants qui utilisent d'autres types d'enrobant (polymères par exemple) et en ce qui concerne son adéquation avec les propriétés des formulations lipidiques ;

- Deuxièmement, des aspects plus fondamentaux liés à la physique des transformations d'état fondu à solide (cristallisation, polymorphisme) et à la composition de la formulation lipidique (effet de l'ajout d'additifs) ne sont pas entièrement abordés dans la plupart des études menées autour de cette technologie ;

- Troisièmement, les champs d'applications des produits à base de lipides solides n'ont pas été complètement explorés.

Pour cette thèse, la technologie brevetée Innojet Ventilus® – lit fluidisé au système de couches à glissement d'air – a été mise en œuvre. En principe, l'enrobage en lit fluidisé consiste à déposer la formulation fondue sur la surface des particules de substrat en mouvement et à l'y laisser solidifier à l'aide du refroidissement par air (Voir **Figure 1-6**). Cela implique que cette méthode d'enrobage à chaud est une réaction exotherme avec l'échange thermique entre des particules enrobées et de l'air d'entrée au cours de la cristallisation isotherme du lipide.

Concernant les lipides, selon la structure chimique, il y a huit catégories (Voir **Figure 1-11**). La plupart de lipides utilisés pour une mise en forme de formulations lipidiques sont acyles graisses et glycérolipides. Trois représentants de ces deux catégories ont été sélectionnés pour constituer la base des compositions lipidiques étudiées pour un enrobage à chaud : cire d'abeilles (i), trilaurine (ii) et tristéarine (iii).



Dans le procédé d'enrobage à chaud, la cristallisation des lipides, étape cruciale à maîtriser, commence à l'échelle moléculaire lorsqu'un polymorphe déterminé est conditionné par un traitement thermique adéquat. Le réseau cristallin des lipides est de nature fractale et formée par l'agrégation d'une unité structurale à l'autre à travers de multiples échelles de longueur et de temps (Voir **Figure 1-12**). Cette structure devrait être idéalement stable avec le temps et elle détermine les propriétés fonctionnelles du « bulk lipid », telles que la dissolution et/ou la digestion dans des conditions biologiques.

Pour les bonnes pratiques de fabrication et de stockage, la compréhension du processus de cristallisation et post-cristallisation (e.g., transformation polymorphique, murissement Ostwald) est indispensable lorsque la compréhension des propriétés biopharmaceutiques des lipides (e.g., solubilité, mouillabilité, digestibilité) est la clé pour réussir à la conception galénique. En général, la compréhension sur la cristallisation en milieu fondu est essentielle pour développer des formulations à base de lipides solides de bonnes manufacturabilité et stabilité et dotées de bonnes fonctionnalités ainsi que pour sélectionner les techniques de caractérisation pertinentes.

En résumé, cette thèse a pour objectif principal de lever les défis associés aux procédé d'enrobage à chaud, choix de lipides comme agents d'enrobage et champs d'applications des produits à base de lipides solides.

**Le travail expérimental comporte deux parties principales « développement de formulations » et « applications pharmaceutiques ».** Dans la partie « **développement de formulations** », les solutions à chaque défi identifié ont été abordées pour chaque groupe de formulations pour lesquelles le composant majeur est la cire d'abeilles, la tristéarine ou la trilaurine. Les résultats de cette première partie sont fondamentaux pour le développement de la deuxième partie de cette thèse – « applications pharmaceutiques ».

Un plan de caractérisation commun pour la première partie a été conçu pour les trois groupes de formulations (Voir **Figure 2-6**). Il consiste en une étude de pré-formulation (ou caractérisation des matières), une étude de caractérisation de l'équipement utilisé pour l'enrobage à chaud et des produits enrobés, et une étude de stabilité. Chaque groupe fait l'objet de la caractérisation plus ou moins similaire selon les propriétés de formulations.

D'une façon représentative, chaque aspect du développement pharmaceutique est abordé en présentant seulement les résultats typiques d'un groupe dans ce résumé. On commence avec les **formulations contenant de la tristéarine** et leur défi associé à la stabilité. Quant à la tristéarine, il est intéressant de présenter le développement d'une méthode destinée au criblage rapide des combinaisons de lipides et additif(s) en utilisant la technique de turbidimétrie.

Pour développer cette méthode, un appareil commercial Crystal16® Crystallization Systems a été utilisé (Voir **Figure 2-2**). Son principe de fonctionnement consiste à détecter la cristallisation / la fusion via les mesures de turbidité (détection d'apparition / de disparition de cristaux). Avec le Crystal16®, il est possible (1) de simuler les conditions opératoires thermiques et (2) de permettre une analyse avec un débit des échantillons plus élevé que les techniques classiques.

Cette méthode de criblage comporte une étude de cristallisation non-isotherme et une étude de cristallisation isotherme qui complètent l'une l'autre. Deux grandeurs physiques – largeur de la zone métastable et temps d'induction – sont à quantifier dans ces deux études, respectivement.

Dans cette étude de criblage il y a 44 formulations contenant de la tristéarine au total (Voir **Table 4-1**). Selon la lipophilicité de tensioactifs ou combinaison de tensioactifs, ces formulations lipidiques correspondent à différents états physiques : milieux fondus purs, solutions fondues, dispersions fondues et émulsions fondues avec/sans talc. Quatre niveaux de quantité de talc et deux niveaux de concentration de tensioactif ont été utilisés dans cette étude de criblage.

Les résultats typiques d'une étude de cristallisation non-isotherme sont un graphe montrant des points de cristallisation et de fusion mesurés à des vitesses de refroidissement / de chauffe différentes en comparaison avec les températures de fusion de référence des polymorphes  $\alpha$ ,  $\beta'$  et  $\beta$  (Voir **Figure 4-4**). Metastable zone widths (MSZW) map constituted by measurements of melting and crystallisation points of tristearin. Melting points at 0.05°C/min (red open circles), crystallisation points at 0.05°C/min (blue open squares), 5°C/min (blue open triangles) and 10°C/min (blue circles), reference melting points of polymorphs  $\alpha$ ,  $\beta'$  and  $\beta$  (black open squares). Standard deviation (See **Appendix 02**). Le point de cristallisation de  $\beta$  mesuré croît avec l'augmentation de la quantité de talc, ce qui implique raisonnablement une nucléation accélérée. De ce fait, le point de fusion de  $\beta$  mesuré décroît.

Le graphe pourrait être divisé en 5 régions contenant les deux zones métastables où les polymorphes de tristéarine  $\alpha$  et  $\beta$  sont à l'état de surfusion. Selon la recherche bibliographique, les conditions opératoires thermiques se trouvent souvent dans ces deux régions. De ce fait, connaître la largeur de zone métastable peut aider à définir les conditions opératoires thermiques pour les technologies de transformation en milieu fondu.

Cette étude de criblage est associée à une perspective de stabilité dans le développement pharmaceutique. C'est parce que son objectif sous-jacent est de sélectionner les formulations contenant de la tristéarine qui peuvent cristalliser en  $\beta$ , le polymorphe le plus stable. Cela justifie 60°C comme la température choisie dans l'étude de cristallisation isotherme. Seulement après avoir la preuve de faisabilité thermique dans l'étude de cristallisation non-isotherme il est temps de lancer l'étude de cristallisation isotherme. Non pas l'inverse. En effet, dans la deuxième étude, un grand nombre d'essais (environ 40) a été réalisé. L'objectif est de construire une fonction de probabilité de temps d'induction pour chaque formulation. La grandeur physique de nucléation – temps d'induction moyen – peut être estimée grâce à un modèle établi. D'ailleurs, la courbe de fonction de probabilité peut indiquer si les comportements de nucléation sont de nature stochastique ou déterministe.

Les résultats des milieux fondus purs avec/sans talc sont utilisés comme contrôle pour évaluer l'effet de l'ajout de tensioactifs. Quant aux dispersions fondues, leurs comportements de nucléation sont similaires au contrôle. Quant aux solutions fondues, la nucléation de la tristéarine est la plupart décélérée. Le tensioactif lipophile semble modifier l'effet du talc lors de la cristallisation en milieu fondu de la tristéarine et cette interaction est en fonction de la concentration du tensioactif présent dans la formulation (Voir **Figure 4-10**).

Dans une perspective de stabilité encore, il a été rapporté ailleurs dans la bibliographie que les solutions solides, cristallisées des solutions fondues, sont stables tandis qu'il y a des problèmes d'instabilité de la cinétique de relargage pour les dispersions solides. Ces observations peuvent être dues au murissement Ostwald (en anglais « Ostwald ripening »). Par définition, faisant l'objet de ce processus physique, « **le système doit évoluer spontanément vers l'état d'équilibre thermodynamique, à travers la réduction progressive de l'aire interfaciale totale entre les cristaux / gouttelettes liquides dans le réseau cristallin** » (Voir **Figure 1-19**).

En anticipant ces phénomènes comme causes potentielles d'instabilité, la formulation d'émulsions solides ainsi que la cristallisation en  $\beta$  peuvent être une solution double. Ainsi, les émulsions fondues aux ratios de combinaison de tensioactifs différents ont été testées. En présence du tensioactif hydrophile, l'effet indésirable du tensioactif lipophile sur l'effet d'ensemencement du talc est neutralisé. En effet, il a été rapporté ailleurs dans la bibliographie que le mécanisme d'action du talc est associé avec des surfaces de clivage des particules de talc. L'ajout de talc réduit généralement la nature stochastique de la nucléation. Dans le cas de la combinaison de tensioactifs au ratio égal et en présence du talc, la nucléation de la tristéarine semble plus déterministe et indépendante de la concentration de tensioactifs. Il s'agit de l'effet attendu pour la répétabilité d'opérations (Voir encore **Figure 4-10**).

L'étude de criblage avec le Crystal16® nécessite la caractérisation complémentaire. Le polymorphe  $\beta$  a été confirmé via la calorimétrie et la spectroscopie RAMAN. Il est à noter qu'avec les analyses thermiques on risque de surestimer la cinétique de solidification des formulations contenant de la tristéarine. Le microscope à lumière polarisée s'est révélé important pour investiguer les mécanismes de cristallisation et la croissance cristalline (le temps de solidification).

Pour conclure ces résultats, le Crystal16® s'avère être un lien potentiel entre les fondements – cristallisation en milieu – et les applications – définition des conditions opératoires thermiques pour les technologies de transformation telles que l'enrobage à chaud en lit fluidisé. Il est à noter que si une formulation contenant la tristéarine peut cristalliser en  $\beta$  elle peut également cristalliser en  $\alpha$ . La conclusion inverse n'est pas certaine. Il s'agit du principe de développer des formules d'enrobage multifonctionnelles dans cette thèse. Le message clé est de montrer comment définir les conditions opératoires thermiques pour cibler la cristallisation d'un polymorphe déterminé avec une bonne compréhension de la cristallisation en milieu fondu.

Les **formulations contenant de la cire d'abeilles** constituent un bon exemple pour montrer les défis associés à la manufacturabilité. Selon la composition chimique, ce groupe de formulations à l'étude implique deux milieux fondus purs, une solution fondue et une émulsion fondue. Il est intéressant de montrer les scénarios de performance du procédé d'enrobage avec la cire d'abeilles et le monostéarate de sorbitane dont les propriétés de processabilité sont difficiles et puis l'amélioration par formulation.

Le chlorure de sodium a été choisi comme un substrat pour la phase « développement de formulations ». Parmi les raisons, ce substrat est facile de doser avec la conductimétrie et facile d'en trouver le stock avec une taille de particules contrôlable. Il est également facile d'investiguer les mécanismes de relargage des formulations d'enrobage lipidiques et éventuellement les problèmes d'instabilité dus à l'évolution physique.

Une des particularités de cette thèse est l'établissement d'une approche expérimentale dite l'approche à prélèvements multiples (Voir **Figure 1-9**). En effet, cela relève d'un des avantages de l'enrobage en lit fluidisé de générer des produits dont les taux de revêtement varient dans le même lot. Puis tous les échantillons sont à analyser pour évaluer l'efficacité, le régime du procédé et la qualité d'enrobage.

En mesurant l'angle de contact à l'état fondu, les images des gouttelettes en cire d'abeilles et en monostéarate de sorbitane déposées sur la surface de la pastille en chlorure de sodium, indiquant que les deux matières ont une adhésion élevée et une viscosité du milieu fondu élevé aux conditions opératoires thermiques simulées, respectivement (Voir **Figure 3-9**). Quant à la cire d'abeilles, cette propriété a conduit à la formation d'une membrane d'enrobage poreuse avec des particules de sel fines y attachées. Quant au monostéarate de sorbitane, cette propriété a conduit à la formation d'une membrane plane de filaments (Voir **Figure 3-18**). D'ailleurs, la cire d'abeilles et le monostéarate de sorbitane ont une cohésion élevée et une vitesse de solidification élevée, respectivement. Quant à la cire d'abeilles, cette propriété a rendu de plus en plus moins fluides des particules enrobées qui collent aux parois de la chambre de l'appareil lors de l'enrobage. Quant au monostéarate de sorbitane, cette propriété a causé une génération abondante de particules fines. Le graphique de l'efficacité du procédé a des tendances distinctes pour le collage et la génération abondante de particules fines, respectivement (Voir **Figure 3-13**).

En considérant les derniers résultats, il s'avère que la combinaison des deux composants résout les problèmes. En effet, l'adhésion est devenue modérée (Voir **Figure 3-8**). De ce fait, il importe qu'une bonne adhésion ne soit ni élevée ni faible pour un bon enrobage. La viscosité des solution et émulsion fondues s'est approchée de celle de la cire d'abeilles (Voir **Figure 3-6**). De ce fait, une viscosité de la formulation fondue proche de l'huile est à recommander pour son bon étalement sur la surface de substrat. La cohésion est également devenue modérée (Voir **Figure 3-14**). En plus de la coulabilité, il y a un lien entre la faible cohésion et la friabilité élevée, et ainsi la propension à générer de la poudre fine. Ces résultats montrent que pour l'enrobage à chaud, le défi associé à la manufacturabilité d'une formulation relève non seulement de son profil de solidification (Voir **Figure 3-5**). Notamment, le fait d'ajouter une petite fraction de tensioactif liquide ne change pas beaucoup ces propriétés. Cette étude de cas montre un exemple de deux formules d'enrobage dont les propriétés sont contrastées.

Etant confronté à de multiples défis possibles associés à la manufacturabilité, une technique prédictive – goniométrie à chaud – a été établie. Ses principes de fonctionnement sont fondés sur la capture constante de l'évolution de la forme de la gouttelette fondue sur le substrat. La température superficielle et la vitesse d'impact de la gouttelette sur la surface peuvent être ajustées pour représenter les variables de procédé d'enrobage (Voir **Figure 3-11**). Cette technique peut servir à plusieurs finalités telles que prédiction qualitative de la processabilité et évaluation de la relation entre propriétés de formulation, nature de substrat et variables du procédé d'enrobage.

Le fait de combiner la cire d'abeilles avec les deux tensioactifs donne lieu à l'amélioration de la performance du procédé et la qualité d'enrobage. En effet, une particularité du graphique sur l'évolution de l'efficacité d'enrobage est que cette dernière tend vers 100% (Voir **Figure 3-12**). Concernant l'uniformité de dosage, le coefficient de variation doit être égal ou inférieur à 5%. Il arrive alors une

question concernant le taux de revêtement minimal assurant un enrobage complet. L'utilisation de la microscopie électronique à balayage est possible mais il y aurait eu beaucoup d'échantillons à caractériser.

De ce fait, une autre approche a été élaborée. Dans ce cas, tous les produits enrobés d'un lot dont les taux de revêtement varient ont été analysés. Premièrement, la mesure de la cinétique de relargage a été effectuée et puis les données obtenues ont été utilisées pour la modélisation dans le but d'évaluer la qualité d'enrobage (Voir **Figure 3-21**). Deuxièmement, les données de distribution de tailles de particules ont été acquises pour identifier le régime du procédé et estimer l'épaisseur moyenne d'enrobage d'un échantillon. Troisièmement, une corrélation entre une constante cinétique de relargage et l'épaisseur d'enrobage a été construite dans le but d'évaluer la qualité de données (Voir **Figure 3-22**). En plus, les propriétés de formulation doivent être optimisées au préalable pour ne pas impacter négativement la qualité d'enrobage (tels que haute porosité ou revêtement imparfait). En s'appuyant sur les résultats d'uniformité de dosage et de relargage, il est alors possible d'identifier le taux de revêtement minimal requis pour un enrobage complet. Le message clé ici est de montrer comment caractériser le processus d'enrobage à chaud avec des formulations en développement.

La partie expérimentale concernant les **formulations contenant de la trilaurine** est associée aux opportunités de concevoir les produits selon leur digestibilité. Selon la composition chimique, ce groupe de formulations à l'étude implique la trilaurine sans/avec talc, la combinaison de la trilaurine et la vitamine E TPGS avec/sans talc, ce qui représentent des formulations mono-constituant, binaire, ternaire, respectivement et la formulation contrôle (trilaurine et vitamine E TPGS sans talc). Il est intéressant de présenter la preuve du profil de relargage immédiat induit par la digestion des lipides.

Le réseau cristallin de la trilaurine a changé en fonction de l'additif ajouté, ce qui a pu être observé par microscopie à lumière polarisée. Les principes de fonctionnement de cette technique correspondent à la nature chimique des lipides en tant que molécules à longue chaîne. Pour les matériaux anisotropes comme les lipides, la morphologie des cristaux peut être observée avec des motifs biréfringents sous le mode de transmission.

En l'absence de talc, la cristallisation de la trilaurine  $\beta'$ , dont les sphérulites sont de grande taille, a pu être observée. La vitamine E TPGS, qui n'a pas cristallisé à 30°C pendant 2h de cristallisation isotherme, présente des agrégats polycristallins beaucoup plus gros (Voir **Figure 5-11**). Lors de l'ajout de talc, un réseau cristallin de sphérulites plus petites et plus homogènes de trilaurine  $\beta$  s'est formé, que la vitamine E TPGS soit absente ou présente (Voir **Figure 5-10** et **Figure 5-12**). Evidemment, la trilaurine  $\beta'$  se cristallise lentement, tandis qu'en présence du talc, il induit la cristallisation de la trilaurine  $\beta$  beaucoup plus rapidement. Le dernier effet du talc est attendu pour une amélioration de la processabilité et son impact opérationnel a été testé.

Dans l'étude de stabilité, le profil de dissolution comparatif au début ( $t_0$ ) et à 3 mois ne montre aucun changement significatif constaté pour la formulation ternaire alors que la cinétique de libération du sel enrobé de trilaurine pure et de la formulation binaire a été décélérée avec le temps (Voir **Figure 5-14**). Cela est dû à ce qu'on appelle la maturation d'Ostwald. Comme attendu, les conséquences sont une augmentation de la taille moyenne des cristaux et une séparation des phases. Sans talc, la vitamine E

TPGS a eu tendance à s'échapper du réseau cristallin de trilaurine à partir de 6 semaines (Voir encore **Figure 5-12**). La formulation ternaire a présenté peu de séparation de phases solide-solide jusqu'à 12 semaines.

Outre un sujet de recherche pharmaceutique, les lipides sont présents dans notre nourriture quotidienne. Lors de l'ingestion de lipides, ces substances vont être digérées dans l'estomac puis dans l'intestin grêle en présence de lipases. Lors de la digestion, les produits de digestion forment avec les sels biliaires et les phospholipides, en tant que tensioactifs naturels, des structures spécifiques telles que micelles et micelles mixtes qui peuvent solubiliser un médicament peu soluble. Prenons le cas de la digestion des triglycérides. Les triglycérides (trilaurine ou tristéarine) contiennent trois liaisons d'ester hydrolysables. Au cours de la digestion, des réactions hydrolytiques libèrent des acides gras libres. Sur la base de la connaissance de ces réactions, des essais expérimentaux de digestion des lipides peuvent être établis avec un modèle pH STAT dont le principe de fonctionnement consiste à maintenir un point de consigne de pH stable (souvent physiologiquement pertinent) en ajoutant une solution alcaline (par exemple, de l'hydroxyde de sodium) (Voir **Figure 2-4**).

Lors de la mesure de la cinétique de libération du sel dans l'eau, les profils comparatifs de dissolution des trois formulations à  $t_0$  montrent que la trilaurine pure et la formulation binaire donnent une libération prolongée de sel par rapport au médicament de référence (Voir encore **Figure 5-14**). Cependant, quand un milieu biorelevant et des enzymes lipolytiques ont été utilisés pour les tests de libération, toutes les formulations à base de trilaurine (3) donnent une libération immédiate de sel en 1 heure (Voir **Figure 5-16**). C'est le concept de libération déclenchée par la digestion. En plus, si l'on considère l'effet de l'ajout d'additifs, la vitamine E TPGS ne modifie pas vraiment ni la cinétique de libération du sel dans différentes conditions de dissolution ni le degré de digestion finale de la trilaurine par rapport aux autres formulations (2). Le message clé est de montrer à quel point les tests de libération dans les conditions lipolytiques sont importants pour déterminer le vrai profil de libération des formulations à base de lipides solides digestibles.

La première partie « développement de formulations » reflète les approches méthodologiques de caractérisation du procédé, de sélection de matériaux et de conception de produits, ce qui conditionne une bonne compréhension de la deuxième partie « **applications pharmaceutiques** ». Le plan de caractérisation de cette phase comprend deux études : (i) étude de biopharmacie et (ii) étude de stabilité (Voir **Figure 2-7**).

Dans cette partie, le substrat choisi pour l'enrobage est une dispersion solide amorphe d'intérêt pharmaceutique. Son enrobage envisage d'améliorer la stabilité physique de la forme amorphe. Dans ce but, trois formulations d'enrobage ont été sélectionnées parmi les études précédentes avec la cire d'abeille, la tristéarine et la trilaurine. De plus, pour déterminer le profil de libération et les propriétés pharmacocinétiques conférées par ces formulations dont la digestibilité varie, différents modèles de performances *in vitro* ont été appliqués dans l'étude de biopharmacie.

Des dispersions solides amorphes de praziquantel ont été fabriquées via plusieurs opérations unitaires dont l'extrusion à chaud (*hot-melt extrusion*). La formule de ce produit de haute technologie à forte charge en praziquantel a été développée dans une précédente thèse (thèse de Janine Bonniatti, 2021). Le



procédé utilisé englobe l'étape d'extrusion à chaud suivie du découpage des filaments extrudés en pellets et leur broyage. Une fraction granulométrique comprise entre 200 et 640  $\mu\text{m}$  a été utilisée pour l'enrobage. Les paramètres du procédé d'enrobage à chaud sont très proches de ceux utilisés dans les études de la première phase.

Concernant la performance de procédé et la qualité d'enrobage, les courbes de distribution granulométrique des dispersions solides amorphes non enrobées et enrobées ont indiqué la présence d'une fraction fine (Voir **Figure 6-7**). Les images, obtenues via microscopie électronique à balayage, le confirment (Voir **Figure 6-9**). En plus, en considérant la forme des courbes de distribution de tailles des particules et l'évolution des paramètres de distribution (i.e. SPAN,  $D_{v,90}/D_{v,10}$ ), le régime de processus était strictement l'enrobage (Voir encore **Figure 6-7**).

En regardant des micrographies, un revêtement imparfait a été observé pour des produits enrobés des formulations contenant de la tristéarine et de la cire d'abeille (Voir encore **Figure 6-9**). Il s'agit de la conséquence attendue car il y a une fraction fine inférieure à 100  $\mu\text{m}$ , ce qui devrait nécessiter une teneur en revêtement plus élevée pour un enrobage complet. Au contraire, le revêtement obtenu avec la formulation à base de trilaurine apparaît parfait (Voir encore **Figure 6-9**). Il est à noter l'avantage de la cristallisation  $\beta$  avec laquelle une teneur en revêtement plus faible est requis pour un revêtement complet. En effet, dans ce cas, les lipides fondus devraient avoir plus de temps pour s'étaler sur la surface de substrat avant que la nucléation n'ait lieu pour déclencher le processus de solidification. Cette évaluation de la performance de procédé et de la qualité d'enrobage est importante pour interpréter les résultats des études de biopharmacie et de stabilité.

Concernant les résultats des performances *in vitro*, la cinétique de libération du praziquantel à partir des dispersions solides amorphes non enrobées et enrobées (4 au total) a été testée dans des milieux biorelevants contenant des lipases à l'aide du modèle pH STAT comme décrit précédemment. Ainsi, les données de solubilité cinétique peuvent être obtenues pour les quatre produits et comparées avec les valeurs de référence trouvées dans la littérature.

Premièrement, il est à noter que la solubilité cinétique du praziquantel amorphe ou cristallin dans le milieu biologiquement simulé était environ 1,5 fois plus celle dans l'eau. Deuxièmement, il n'y a pas d'effet de solubilisation complémentaire résultant des produits de digestion, ou cet effet est négligeable. Troisièmement, la solubilité cinétique élevée observée pour les deux produits enrobés des formulations contenant de la cire d'abeille et de la trilaurine pourrait être attribuée à l'effet de particules fines.

D'ailleurs, le profil de digestion des quatre produits peut également être obtenu (Voir **Figure 6-17**). Le résultat du produit non enrobé a été utilisé comme blanc. La vitesse de dosage de l'hydroxyde indique la cinétique de digestion de chaque formulation. Les formulations contenant de la trilaurine et de la tristéarine ont été digérées respectivement rapidement et lentement. Quant à la formulation contenant de la cire d'abeille, la consommation d'hydroxyde est probablement due à la dissolution d'acides gras libres ainsi qu'à la digestion de composants digestibles. Ces résultats visent à mettre en évidence l'avantage d'effectuer la digestion et la dissolution dans des conditions *non-sink* pour l'acquisition de ces données. Ces résultats compléteront l'étude en biopharmacie.



L'étude de biopharmacie a été réalisée avec l'utilisation d'un modèle complexe comme TIM-1 (Voir **Figure 6-6**). Ce modèle est composé de quatre compartiments en série simulant l'estomac et les trois segments de l'intestin grêle d'un humain – duodénum, jéjunum et iléon. Il permet de tester la libération du principe actif dans des conditions physiologiques simulées en contrôlant les paramètres mécaniques, physiques et biochimiques tels que la vidange gastrique, le mélange, le pH, la température, les volumes, le transit péristaltique du contenu ingéré et l'ajout continu de sécrétions digestives. Notamment, la caractéristique la plus intéressante de ce modèle est la possibilité d'étudier l'absorption passive de petites molécules dans le milieu biologiquement simulé qui purge continuellement les fibres de filtration installées au niveau des segments jéjunal et iléal. Il fonctionne selon le principe de la séparation membranaire. Le milieu de dissolution concentré se dilue en cédant des petites molécules dissoutes dans le milieu de dialyse pompé en continu depuis la source. Le dialysat enrichi en ces molécules est à collecter à des points de prélèvement prédéfinis et à analyser pour construire un profil d'absorption ou de bioaccessibilité.

Les résultats du modèle pH STAT statique (dissolution dans des conditions non-sink) ont été comparés avec le modèle dynamique TIM-1 (dissolution dans des conditions sink).

Concernant le profil de dissolution du modèle TIM-1, la dissolution dans le compartiment gastrique n'était significative que dans les 30 premières minutes, ce qui simule la vidange gastrique biologique du contenu ingéré à jeun. Une forte variabilité est attendue en raison du caractère aléatoire de la désintégration de capsules et de la vidange gastrique. La concentration du principe actif dans le compartiment intestinal a été mesurée aux moments définis jusqu'à 4 heures, ce qui simule le temps de séjour moyen dans l'intestin grêle (Voir **Figure 6-22**).

Concernant le modèle pH STAT, seul un profil de dissolution dans du liquide intestinal simulé à jeun a été obtenu pour tous les produits jusqu'à 3h (Voir **Figure 6-16**). Pour les dispersions solides amorphes, des effets attendus (effet ressort et effet parachute) ont été observés au cours de la période de test.

Pour tous les deux modèles, une grande variabilité a été particulièrement observée pour les dispersions solides amorphes non enrobées et son profil de libération est apparemment moins performant que celles enrobées avec les formulations contenant de la cire d'abeille et de la trilaurine. Bien qu'inattendu, en pratique, les dispersions solides amorphes non enrobées de praziquantel font l'objet de l'agrégation dans les milieux aqueux, ce qui annule son avantage d'améliorer la cinétique de dissolution. Cela met en évidence un autre avantage de l'enrobage, à savoir l'amélioration de la mouillabilité des dispersions solides amorphes lors de la dissolution. En plus, l'effet des particules fines était également observé pour les produits enrobés avec les formulations contenant de la cire d'abeille et de la trilaurine ainsi que le praziquantel cristallin. Leur cinétique de dissolution était donc rapide. Quelles que soient les conditions sink et non-sink, l'ordre de classement des performances *in vitro* est comparable.

S'agissant d'une information complémentaire, le profil d'absorption montre la bioaccessibilité du praziquantel libéré à partir de tous les produits (Voir **Figure 6-23**). Premièrement, une grande variabilité a également été observée pour les dispersions solides amorphes non enrobées, ce qui doit être évité en cas d'administration orale car cela pourrait affecter l'efficacité du médicament. Plus important encore, l'inclusion des tests de perméation permet de distinguer les propriétés pharmacocinétiques du

praziquantel enrobé des formulations différentes. Un ordre de classement différent peut être observé avec la bioaccessibilité la plus élevée du praziquantel libéré à partir de la formulation contenant de la trilaurine. En plus, son écart de bioaccessibilité avec d'autres produits (par exemple la cire d'abeille) est devenu de plus en plus important. Cela devrait être dû non seulement à la libération continue de praziquantel à partir des produits enrobés, mais également à la digestion continue et à la digestibilité de chaque formulation. Pour expliquer simplement, il devrait y avoir un effet dans lequel le praziquantel a une certaine affinité avec les structures de solubilisation différentes formées par les sels biliaires et les produits de digestion.

Enfin, selon les résultats de l'étude de biopharmacie, on peut conclure que l'enrobage avec les lipides peut fournir une libération soit immédiate soit prolongée et améliorer la bioaccessibilité des dispersions solides amorphes.

Quant à l'étude de stabilité, premièrement, les profils de sorption dynamique de vapeur des quatre produits indiquent que les dispersions solides amorphes non enrobées adsorbent plus de vapeur d'eau que les produits enrobés à tous les niveaux d'humidité relative étudiés (Voir **Figure 6-11**). Le degré maximal d'adsorption était similaire pour tous les produits enrobés et inférieur à celui du produit non enrobé. Du point de vue cinétique, le profil de sorption dynamique de vapeur n'indique aucun signe de recristallisation immédiate lorsque la forme amorphe a été exposée à l'humidité pendant près de 42 heures.

Pour étudier l'état physique du praziquantel, la diffraction aux rayons X de la poudre et la calorimétrie différentielle à balayage ont été utilisées. D'après les diffractogrammes de tous les produits, le praziquantel s'est révélé initialement amorphe et reste stable malgré le fait qu'il a fait l'objet des contraintes mécaniques et thermiques lors du broyage et de l'enrobage à chaud (Voir **Figure 6-12**). Après 3 mois de stockage, la recristallisation a été constatée et s'est produite selon la règle des étapes d'Ostwald. En effet, seuls les polymorphes C et B ont été détectés. A titre d'information, la forme physique initiale du praziquantel avant l'amorphisation est le polymorphe A. En plus, après l'exposition à longue durée à l'humidité, les produits non-enrobés se sont consolidés et leur couleur a aussi changé (Voir **Figure 6-15**). Les produits enrobés présentaient également un changement de couleur mais leur coulabilité restait bonne. Ces résultats complètent les analyses thermiques.

Les thermogrammes des produits non enrobés et enrobés des formulations de la tristéarine et de la trilaurine présentent les pics de fusion distincts des lipides et, si c'est le cas, ceux des polymorphes recristallisés du praziquantel à partir de trois mois (Voir **Figure 6-13**). Pour le produit non enrobé, la température de transition vitreuse a pu être détectée aux trois temps d'analyses et l'enthalpie de relaxation du polymère couvrait une large région de température.

Quantitativement, la recristallisation de la forme amorphe peut être indiquée par l'évolution de la cristallinité de chaque produit en fonction de la durée de stockage (Voir **Figure 6-14**). Concernant la cause de la recristallisation, premièrement, la recristallisation peut être due à une exposition prolongée à l'humidité. Cela affectait les particules fines non enrobées et les surfaces imparfaitement enrobées. Deuxièmement, la recristallisation peut être due au contact entre des dispersions solides amorphes et des lipides. Ce phénomène est latent, comme observé pour les produits enrobés des formulations de la

tristéarine et de la trilaurine. Troisièmement, la recristallisation peut être induite par la fusion des lipides lors des analyses thermiques dans le cas de produits enrobés de la formulation contenant de la cire d'abeille. La cristallinité initiale observée pour ce produit était donc un artefact, ce qui est confirmé par son diffractogramme initial.

D'après les résultats des analyses thermiques, l'humidité s'est révélée être la cause principale de la recristallisation. En outre, les lipides pourraient induire une recristallisation du praziquantel à l'interface à des degrés et à des rythmes différents et le mécanisme n'est probablement autre qu'une nucléation hétérogène. En particulier, de bonnes interactions interfaciales ou une stabilisation du praziquantel amorphe pourraient être dues au contenu amorphe de la cire d'abeille.

Selon l'étude de stabilité, on peut conclure que l'enrobage avec les lipides peut améliorer la stabilité physique de la forme amorphe en réduisant l'exposition à l'humidité, mais la recristallisation induite par les interactions interfaciales est imprévisible.

Ce résumé se termine avec **conclusions** and **perspectives** sur les approches méthodologiques mises en œuvre dans cette thèse.

**Comme la première synthèse**, une des approches de cette thèse de doctorat pour la conception de produits enrobés par des formulations lipidiques solides dont la fonctionnalité repose sur la digestibilité des formulations lipidiques solides (Voir **Figure 1-32**). En fait, trois catégories – bonne digestibilité, faible digestibilité et non-digestibilité – correspondent aux trois lipides étudiés dans cette thèse. Les lipides de chaque catégorie peuvent conférer un profil de relargage soit immédiat soit modifié ainsi qu'un large éventail de fonctionnalités selon leur digestibilité, leur teneur et leur combinaison avec des additifs.

Dans l'étude de cas des dispersions solides amorphes, la formulation contenant de la trilaurine s'est avérée capable d'améliorer la bioaccessibilité du praziquantel amorphe. La libération immédiate et le recouvrement complet de surface observés mettent en évidence sa haute digestibilité et sa digestion rapide. La formulation contenant de la tristéarine, malgré le revêtement partiel, a donné une libération prolongée comme prévu. Quant à la formulation contenant de la cire d'abeille, le revêtement partiel permet une libération immédiate du praziquantel mais s'est révélé efficace pour protéger sa forme amorphe contre l'humidité.

Outre la fonction technologique principale qu'est la stabilisation de la forme amorphe, l'enrobage s'est avéré capable d'empêcher l'agglomération de la poudre due à la recristallisation et d'améliorer sa mouillabilité lors de la dissolution. La qualité de l'enrobage peut être mise en question avec ces conclusions sur les applications des lipides. Il est à noter qu'il est possible de comparer le revêtement partiel au cas de l'ajout de lubrifiants dans un comprimé où seule une petite quantité de ces excipients est normalement recommandée pour éviter un effet négatif sur la cinétique de dissolution.

En plus, l'utilisation d'additifs dans cette thèse a enrichi la base de données des recherches sur l'enrobage à chaud avec les lipides. Un effet de l'ajout d'additifs à constater en premier lieu est d'améliorer la cinétique de libération du principe actif à partir des produits enrobés.

Comme perspective, outre une stratégie de conception des produits basée sur la digestibilité des lipides, des considérations pour choisir des essais de relargage économes en matière ont également été données. L'étude de biopharmacie a montré la pertinence du TIM-1 (avec prise en compte la perméation) pour classer les formulations contenant des lipides solides. Il serait plus utile encore dans le futur d'adopter des modèles miniaturisés pour ce type d'étude.

**Comme la deuxième synthèse**, la deuxième approche de cette thèse de doctorat était l'ajout d'additifs qui permet de concevoir des formulations stables (Voir **Figure 1-31**). Cela s'applique à deux types de lipides : (i) les lipides de haute pureté et (ii) ceux à composition complexe. La sélection d'additifs est normalement envisagée au préalable pour convenir à des applications pharmaceutiques voulues. Ensuite, les additifs sélectionnés sont vérifiés en termes de leur impact sur la manufacturabilité et la stabilité.

Trois mécanismes de stabilisation associés à l'utilisation d'additifs ont été identifiés. Premièrement, la stabilité des formulations contenant de la cire d'abeille repose sur la combinaison de tensioactifs lipophile et hydrophile. Deuxièmement, quant aux formulations contenant de la tristéarine, la  $\beta$ -cristallisation et la formulation d'émulsions solides ont été proposées comme démontré dans l'étude de criblage avec Crystal16®. Pour les lipides de haute pureté, on peut lever le défi du polymorphisme plus tôt (juste après la fabrication), mais il faut se méfier du mûrissement d'Ostwald plus tard. Troisièmement, quant aux formulations contenant de la trilaurine, le mécanisme de stabilisation est associé à l'effet de l'ajout du talc sur la cristallisation des formulations contenant de la trilaurine.

Le défi de la stabilité est toujours là. L'enrobage s'est révélé efficace pour empêcher la recristallisation en réduisant l'exposition à l'humidité du praziquantel amorphe. Cependant, le contact à l'interface entre le noyau des dispersions solides amorphes et la couche de revêtement des lipides peut aussi induire la recristallisation de la forme amorphe, ce qui représente le facteur limitant potentiel pour les applications pharmaceutiques car la stabilité détermine la durée de conservation du produit. L'étude de stabilité a montré que la formulation contenant de la cire d'abeille produisait de bonnes interactions interfaciales tandis que les deux autres induisaient une recristallisation de la forme amorphe. Toutefois, c'est un résultat à ne pas généraliser pour les dispersions solides amorphes contenant des molécules autres que le praziquantel, mais cela doit être traité au cas par cas.

Le message clé de cette deuxième approche est qu'il est recommandé d'utiliser au moins deux additifs pour la formulation avec les lipides solides.

**Il est important considérer l'impact des additifs sur la manufacturabilité, la stabilité et les fonctionnalités dès le début du développement pharmaceutique.** Par conséquent, dans cette thèse, une classification d'additifs basée sur la structure chimique a été proposée pour aider à y voir opportunités et défis associés à l'effet de l'ajout d'additifs dans la formule (Voir **Figure 1-30**).

Pour la formulation avec les lipides solides, les propriétés associées à la manufacturabilité et l'effet de l'ajout d'additifs ont souvent été négligés. Dans cette thèse, un effet peut être constaté. Lors de l'ajout d'un tensioactif liquide, le débit d'alimentation de la formulation fondue doit être réduit. Lors de l'ajout d'un additif solide, ce débit d'alimentation peut être augmenté. Cet effet doit être lié aux comportements de cristallisation des lipides.

**Comme la troisième synthèse**, la dernière approche de cette thèse concerne la mise en place d'une étude intégrant la caractérisation de l'équipement et des considérations sur les propriétés de formulation. Une approche expérimentale fondée sur la physique a alors été établie et validée pour lier les propriétés de formulation, la performance de procédé et la qualité d'enrobage.

L'enrobage à chaud en lit fluidisé est un procédé complexe comportant près de 20 variables. Grâce à l'évaluation des risques, ces variables peuvent être divisées en deux groupes. Le premier groupe concerne les conditions thermiques qui peuvent être définies en fonction des propriétés de formulation. Le second groupe concerne les paramètres mécaniques qui peuvent être ajustés pour cibler un régime d'enrobage ou pour des études exploratoires.

Une cartographie du procédé d'enrobage à chaud a été utilisée pour relier théoriquement les paramètres mécaniques : (1) le débit d'alimentation et (2) le débit d'air de fluidisation, qui peuvent être ajustés en fonction de la taille du lot et de la pression de l'air de pulvérisation (Voir **Figure 1-27**). L'objectif principal est toujours d'obtenir un régime d'enrobage. De nouveau, l'approche expérimentale dans cette thèse a intégré une étude de stabilité et s'est avérée transférable d'un substrat à l'autre.

**En conclusion**, cette thèse a eu pour objectif principal de lever les défis du développement pharmaceutique associés aux matériaux, à la technologie de transformation, aux produits dont leur manufacturabilité, stabilité et fonctionnalités sont à explorer. Trois études de cas représentent une multiplicité de lipides. La cristallisation en milieu fondu est le savoir clé. L'approche expérimentale fondée sur la physique est compatible avec la phase précoce d'un projet de développement pharmaceutique. Une telle approche expérimentale favorise le développement de méthodes analytiques reliant fondements et applications. Parmi ces défis, celui associé à la stabilité des formulations contenant des lipides solides est le plus important. Pour enrober des modèles délicats tels que dispersions solides amorphes, les interactions interfaciales ne doivent pas être négligées. Cette thèse pourrait être utilisée comme exemple d'étude de compatibilité physique pour cribler de bonnes interactions interfaciales. Cependant, il est recommandé de recourir à des méthodes analytiques plus avancées afin d'étudier plus précisément les mécanismes de déstabilisation.

**Comme perspective**, pour surmonter la demande du développement pharmaceutique, il est envisageable de compter sur la polyvalence des excipients lipidiques, les potentiels de l'enrobage à chaud en lit fluidisé en particulier (et technologies de transformation à l'état fondu en général) et l'ajout d'additifs.

# General Presentation

---

## 1. Thesis Context

Melting-based manufacturing processes encompass among others hot-melt extrusion, hot-melt granulation, spray congealing and hot-melt coating (Becker, 2016; Becker et al., 2015). These technologies are gaining more and more attention from drug developers for a number of reasons. The common and most important advantage of these processing techniques is bypassing the need for organic solvents or aqueous vehicles. It is therefore possible streamlining several unit operations such as removal, recovery of solvents (Becker et al., 2015) and control of their residuals in finished products (ICH Q3C, 2022).

As a matter of fact, melting-based processing represents a cost-, time-efficient et eco-friendly manufacturing method (Appelgren & Eskilson, 1993; D. K. Tan et al., 2020) and at the same time relieves compliance burden with environmental and safety regulations (ICH Q3C, 2022). However, each melt technology displays its characteristic potentials and limits not fully unravelled (Becker, 2016) and remains not yet widely embraced in pharma industry (Leane et al., 2015), notably hot-melt coating (D. G. Lopes, Salar-Behzadi, et al., 2017).

In the second instance, lipid-based excipients possess their favourable thermoplastic properties suitable for melt-based processing. For example, the excipients normally ought to be molten and pulverised into droplets in order to coat a substrate (A. S. Achanta et al., 1997) or to form microparticulate solids (Wong, 2015). Amenable to these technical requirements, lipids are endowed with high thermal chemical stability (Nawar, 1969) and low melt viscosity as a function of temperature (Wong et al., 2016). On the other hand, from the biochemistry perspective, lipids, being naturally occurring or (semi-)synthetic, are normally biocompatible and therefore safe (Witika et al., 2020). Nonetheless, polymorphism, crystallisation behaviours from the melt state (Bayés-García et al., 2015; Hondoh et al., 2018; Sato, 2018b), and in addition to these, their subjection to lack of reproducibility from batch to batch of natural “grease ball” substances (Girod Fullana & Aubert-Poussel, 2019) constitute challenges for designing stable solid lipid-based formulations (D. G. Lopes, Salar-Behzadi, et al., 2017).

In synergy with advances in processing technology and materials science, pharmaceutical scientists are always seeking to diversify their formulation methods in response to various challenges in practice such as advent of new modalities (Vargason et al., 2021; W. Yang et al., 2020), reformulation (Bradley, 2007), drug repurposing (Pushpakom et al., 2019) and personalised therapy for vulnerable population (e.g., paediatric and geriatric patients) (Elder et al., 2017; Stegemann et al., 2010). The emergence of new manufacturing technologies also drives innovations in the development of new classes of excipients, combinations or hybrid derivatives (Corzo et al., 2020). Besides polymers, for all time lipids have also represented a versatile class of excipients (Siepmann et al., 2019), which could play multiple roles in product development such as lubricant, control release agent, drug nanocarrier (Aburahma & Badr-Eldin, 2014), solubiliser, emulsifier, matrix agent (Chambin & Jannin, 2005; da Fonseca Antunes

et al., 2013). Despite accumulated understanding of solid lipid-based drug delivery systems in terms of manufacturing methods and stability profile, lacunae in elucidating formulation behaviours and release mechanisms warrant more profound *in vitro* characterisation, for example, using biorelevant media and lipolytic enzymes (Feeney et al., 2016).

## 2. Thesis Objectives

In the context presented, this thesis aims to study hot-melt coating technology with fluidised bed and search for new lipid-based formulations starting from **three basic lipid models** - two triglycerides, and a natural substance (beeswax) whose physicochemical and biological properties are different – and **two substrates in the form of multiparticulate systems** – sodium chloride and amorphous solid dispersions of praziquantel whose solubility is different.

The four principal objectives of this doctoral thesis are:

- Mastering hot-melt coating technology in fluidised bed via tuning process parameters as a function of material properties and predefined product attributes for end-users – *Subject covered in Chapters 3, 4 and 5.*

- Proposing a methodological approach to screening, combining and characterising lipid-based excipients and additives based on a mechanistic understanding of their structure-property-function relationship in order to formulate quality oral solid dosage forms – *Subject covered in Chapters 3, 4 and 5.*

- Providing insights into release mechanisms of orally administered poorly soluble drugs from lipid-based solid lipid-based delivery systems in biologically simulated media – *Subject covered in Chapters 3, 4 and 5.*

- Contributing new functionalities by hot-melt coating in development of amorphous drug solid dispersions such as enhancement of physical stability and bioavailability, and controlled release – *Subject covered in Chapter 6.*

## 3. Thesis Outline

**Figure 1-1** shows the thesis outline giving an overview on the scientific and methodological approach of this thesis work to reach these objectives.



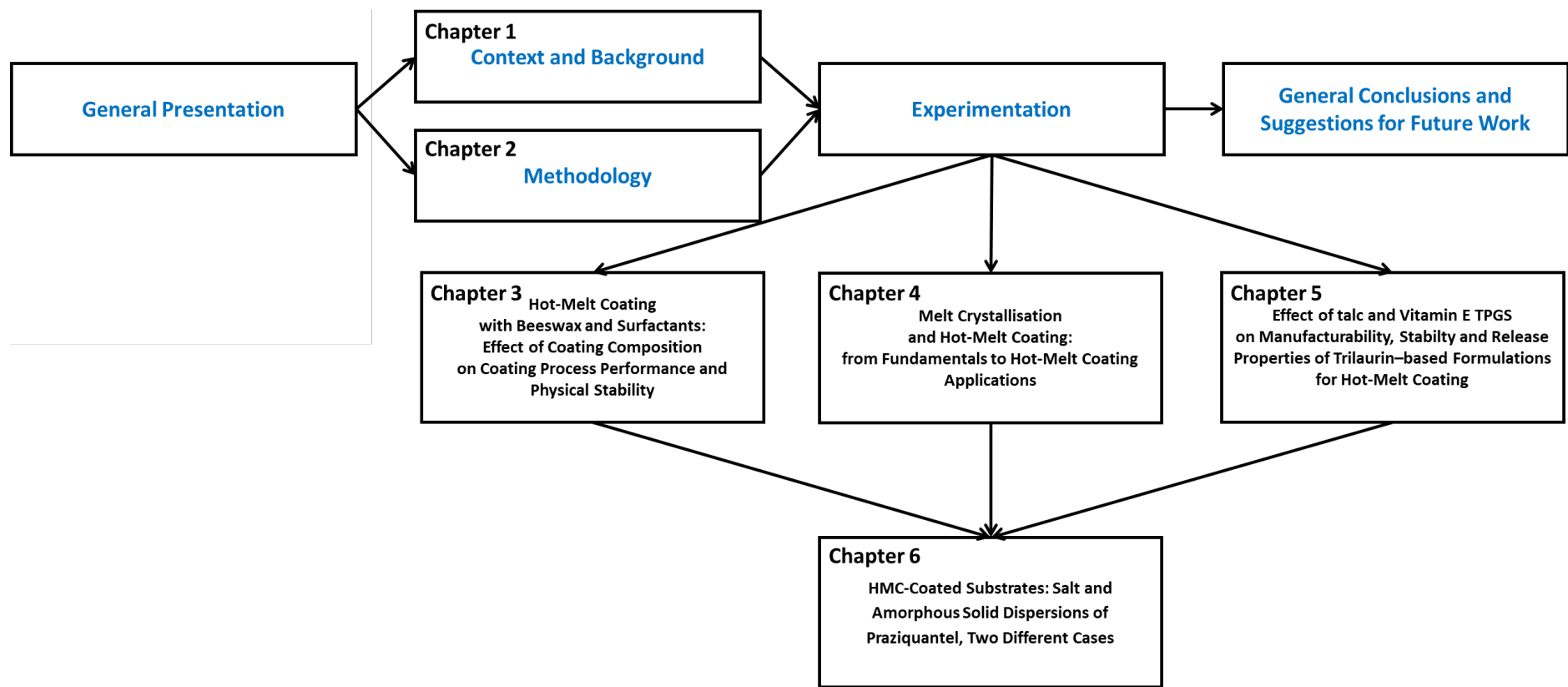


Figure 1-1. Thesis outline

# Chapter 1.

## CONTEXT AND BACKGROUND

---

### **General Introduction**

This first chapter will tackle in some details *process-, material- and product-specific aspects of hot-melt coating technology, lipid-based excipients, and solid lipid-based formulated products*, which form the basic scientific foundation for understanding the scientific approach and working method of this doctoral thesis.

## 1. Hot-Melt Coating: General Guidelines

Nowadays, coating technologies have developed in such a way that they can belong to multiple categories (Benoît et al., 2013; Hautala et al., 2017; Saikh, 2022):

- *Classification based on the use of solvent:* solvent-based, aqueous (e.g. evaporation), or solventless (dry) coating (e.g. coacervation, supercritical fluid processes);
- *Classification based on the nature of dispersing media:* liquid (e.g., interfacial polycondensation, coacervation), gas (e.g., spray-drying, spray-chilling, coating by fluidised bed), plasma, or in supercritical state (e.g., rapid expansion supercritical solution (RESS), supercritical antisolvent (SAS), particles from gas saturated solutions (PGSS));
- *Classification based on the exploited materials:* sugars, (preformed) polymers (e.g., coacervation), monomers (e.g., interfacial polycondensation, polymerisation in a dispersing medium), lipids (e.g., spray coating), minerals (e.g., atomic layer coating) ...
- *Classification based on the end-use properties:* delayed-release coating, extended-release coating ...
- *Classification based on the categories of industrial processes,* grouped according to their working principles: they can belong to (i) physicochemical (e.g., simple coacervation, complex coacervation, thermal gelation of emulsions), (ii) mechanical (e.g., spray coating, spray drying/chilling, prilling, extrusion, 3D-printing) and/or (iii) chemical (e.g., polycondensation, polyaddition) processes.

A specific coating process can belong to more than one classification systems. Coating of pharmaceuticals conventionally concerns mechanical processes (Toschkoff & Khinast, 2013). The coating processes can also be divided into systems integrated with mechanical mixing (e.g. pan coater, high-shear granulator) and systems equipped with mixing by air suspension (e.g., fluidised bed) (Kleinbach & Riede, 1995). A wide definition of coating is based on two successive steps (Appelgren & Eskilson, 1993):

- Distribution of the coating material (in molten/dispersed/dissolved state) on solid particles;
- Formation of a coating membrane via evaporation/solidification.

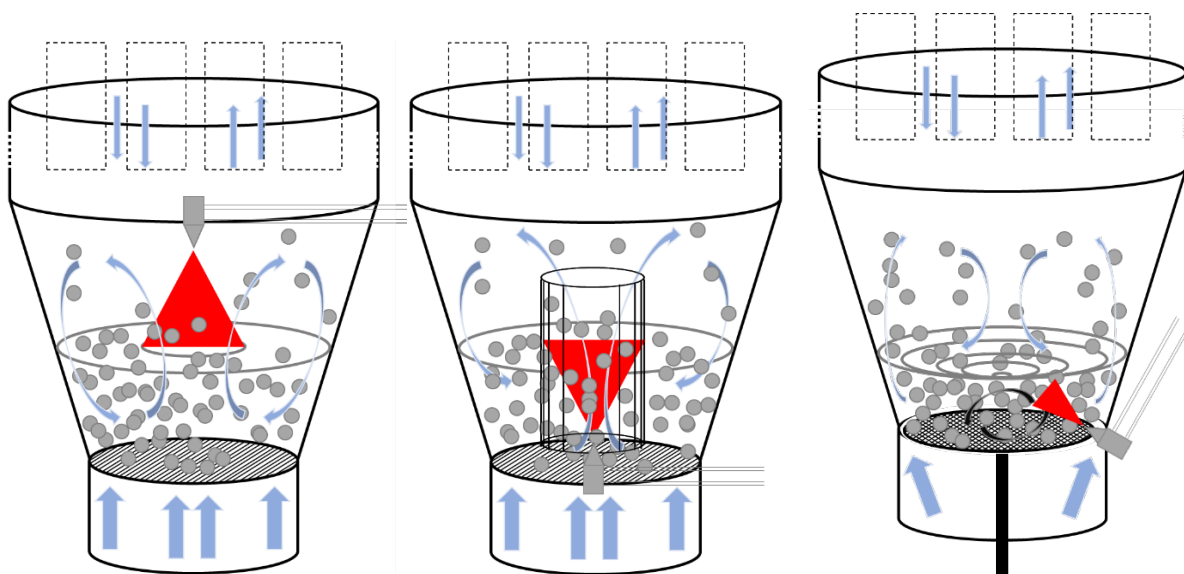
Distribution of coating material can be executed via one of two major routes (Appelgren & Eskilson, 1993): (i) application of the coating material on the surface of solid particles; (ii) suspension of solid particles in the fluid continuous phase containing the coating material. By this definition, coating can be conducted with a rotating pan (drum coater), a high-shear granulator (impeller mixer), an atomiser, an extruder, a prilling tower, a 3D-printer or a fluidised bed (Appelgren & Eskilson, 1993). Hot-melt coating has occasionally been performed via pan coater (Khobragade et al., 2014; Padsalgi et al., 2008), high-shear granulator (Milanovic et al., 2018). Spray-congealing, extrusion, and 3D-printing have also been studied as lipid-processing technologies (Becker et al., 2015; Bertoni, Dolci, et al., 2018; Bertoni et al., 2019; G. Chauhan et al., 2020; Vithani et al., 2019b).

## 1.1. Air Suspension Coating Equipment

### 1.1.1. Conventional air suspension coaters

By a narrow definition, film coating by air suspension consists of delivering dispersed/dissolved polymer in a solvent/aqueous vehicle (or molten lipids, hence the specific term “hot-melt coating”) onto surface of substrate particles in fluidisation and let them solidify with air-drying (or air-cooling) **in isothermal conditions** (Appelgren & Eskilson, 1993; Ronsse et al., 2008).

**Figure 1-1** demonstrates the schematic of three typical types of fluidised bed coaters classified based on the positions of the spraying nozzle: top spray, bottom spray, and tangential spray fluidised bed coaters (Arwidsson & Rudén, 1993; Dewettinck & Huyghebaert, 1999; El Mafadi & Poncelet, 2007; Foroughi-Dahr et al., 2017; Jannin & Cuppok, 2013; Jones, 1988; Kleinbach & Riede, 1995). Based on the similarity in coating principles, the following presentation is almost based on reviews on solvent-based/aqueous coating and adapted to hot-melt coating applications.



*Figure 1-1. Schematic of top spray (left), bottom spray (middle) and tangential spray (right) fluidised beds (adapted from Arwidsson & Rudén, 1993)*

Top spray fluidised bed coaters (**Figure 1-1** (left)) evolved from the fluidised bed dryers (Dewettinck & Huyghebaert, 1999). The spray nozzle is mounted on the top of the fluidised bed. Substrate particles circulate in a random way, there exists a range of gas velocities resulting in a rolling vertical moment of solid particles with a velocity gradient decreasing from the coned section upwards (Arwidsson & Rudén, 1993; Kleinbach & Riede, 1995). In the top-spray configuration, coating material is delivered countercurrently against the fluidised particles (Dewettinck & Huyghebaert, 1999). The position of spraying zone is not controllable. Therefore, abundant spray-chilling might be severe and coating imperfections can occur (Dewettinck & Huyghebaert, 1999). By considering these elements, top spray coaters are adapted for but low coating content (e.g., for taste masking) (Jannin et al., 2005). For high coating content, larger batch size might be required and higher product temperature was reported to yield smoother coating (Jones & Percel, 1994). Coating with the objectives of changing organoleptic

properties of powder (e.g., texture, colour) (El Mafadi & Poncelet, 2007) is viable. It is advisable to perform hot-melt coating substrates with a size between 100 and 750  $\mu\text{m}$  and a bulk density of 0.5 g/mL (Jannin & Cuppok, 2013). Top-spray configuration might probably suit formulations whose solidification rate is limiting. Last but not least, control of the bed height should be considered when targeting a high weight gain of coatings (Knezevic et al., 2009).

Bottom spray fluidised bed coaters (known as Wurster systems) (**Figure 1-1** (middle)) are characterised by the partition (or the Wurster insert) and the distribution plate which is designed to allow for a higher air flowrate passing through in the centre than in the periphery (El Mafadi & Poncelet, 2007; Jannin & Cuppok, 2013; Jones, 1988). This makes substrate particles pursue a fast circulation pattern through the partition to the expansion zone, then fall back into the annular space, finally reach the horizontal transport region above the distribution plate before starting another cycle (Foroughi-Dahr et al., 2017). The spray nozzle is mounted on the distribution plate and just below the partition. Therefore, a spray zone is created inside the partition (therefore also called “coating chamber”) and the coating material is delivered concurrently towards substrate particles. This facilitates wetting and forming of a dense film (Dewettinck & Huyghebaert, 1999). It was reported that coating with Wurster process led to a particular evolution of coating thickness, i.e. coating layer of larger beads thicker than smaller beads (Dewettinck & Huyghebaert, 1999). Furthermore, in the course of coating, it is possible to adjust the gap (height) between the partition and the distribution plate with the increase in particle size and density (Jannin & Cuppok, 2013). This affects the horizontal transportation of substrate particles toward the coating chamber (Jones, 1988). By considering these elements, hot-melt coating with bottom spray coaters could suit fine particles (100  $\mu\text{m}$  or larger) (Dewettinck & Huyghebaert, 1999) dense particles (Jannin & Cuppok, 2013) and is tuneable with the adjustment of the partition height when working with high coating contents. In comparison with coating with top spray configuration, hot-melt coated products generated with the Wurster system were reported to be more porous (Jones & Percel, 1994).

Tangential spray (or rotary) fluidised bed coaters (**Figure 1-1** (right)) are relatively new systems which feature a spray nozzle mounted laterally and a rotating, non-perforated disk. The height of the disk is adjusted to yield a slit between the edge of the disk and the process wall for fluidisation air stream to pass through (Foroughi-Dahr et al., 2017). Substrate particles follow a helicoidal trajectory due to the combined effect of the centrifugal force provided by the rotating disk, the drag force given by the fluidisation air and the gravity (El Mafadi & Poncelet, 2007). The coating material is delivered tangentially to and concurrently towards substrate particles in movement (Dewettinck & Huyghebaert, 1999). By considering these elements, tangential spray coaters are suitable for pelletisation and coating, especially multilayer coating (Foroughi-Dahr et al., 2017) and able to generate similar coating quality as bottom spray coaters. However, due to higher mechanical stress imposed by the systems, tangential-spray coaters might not be suitable to generate coating membrane constituted by lipids which are brittle by its crystalline nature (Salar-Behzadi, Corzo, et al., 2020). In fact, in the comparative study on coating with three spray configurations, hot-melt coated products generated with the rotary fluidised bed whose surface should have undergone much higher shear were also porous but smoother than those produced with the bottom spray coater (Jones & Percel, 1994).

### 1.1.2. Ventilus® V-2.5/1 Romaco Innojet

Ventilus® V-2.5/1 Romaco Innojet (as illustrated in **Figure 1-2** (right)) represents a novel air flow bed technology for drying, coating and granulation at a laboratory scale (Hüttlin, 2011), which is the technique used in the hot melt coating study in this doctoral thesis.

Its name implies the design of a cylindrical product container with 2 types of volume: IPC1 (1 L) and IPC2.5 (2.5 L) (T. T.-L. Nguyen, 2017). This device handles a large range of particles from 10  $\mu\text{m}$  to 30 mm in diameter, such as powders, granulates, pellets, tablets, capsules and numerous other free-flowing bulk materials (Hüttlin, 2011; T. T.-L. Nguyen, 2017). The emergence of Innojet® technology was probably firstly introduced to the pharmaceutical industry in the exhibition TechnoPharm in Nuremberg in 2013 and in the textbook of pharmaceutical technology for students (Bauer, 2015; Schubert, 2022).

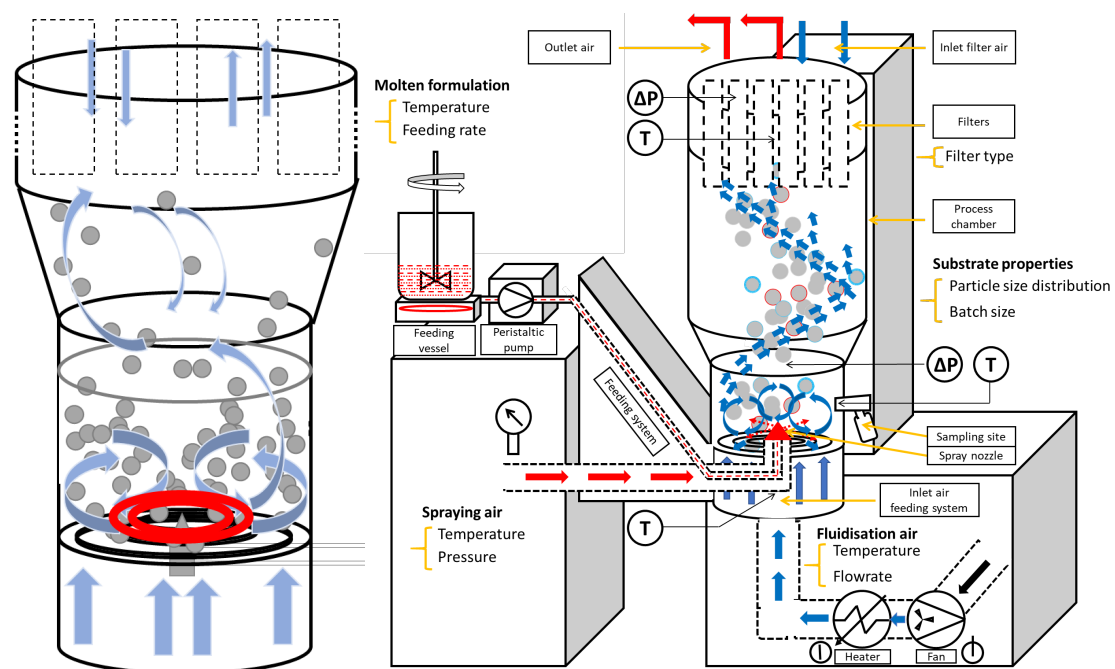


Figure 1-2. Ventilus® Romaco Innojet technology: air flow bed (left) and drawing of the coating technology (right) (Huynh et al., 2024)

This technology comprises of three principal parts that determine its functions. Firstly, the air distributor system Orbiter® Booster consists of overlapping circular plates with a defined number of open air gaps. These bottom plates with concentric air guiding increments in the inferior surface orient the inlet process air radially and tangentially in the direction of the container wall (T. T.-L. Nguyen, 2017). The particle bed is entrained by the inlet air stream to rise upwards along the container wall and then fall back into the centre of the product container where the coating zone is formed around the spray nozzle (**Figure 1-2** (left)). This movement of the particle bed can be redirected in the upward movement and accelerated again and again (Bauer, 2015; T. T.-L. Nguyen, 2017). It is possible to initiate the fluidisation with a smaller air volume and energy savings can be considerable (Schubert, 2022).

Secondly, Rotojet® represents a three-fluid spray nozzle fixed in the bottom centre of the product container (Schubert, 2022). The feeding of the molten formulation is pulverised by means of the two flows of pulverisation air in a circumferential (covering an angle of 360°) and horizontal manner into the particle bed in movement and the spraying also adds more motion kinetics to the particles (Bauer, 2015; T. T.-L. Nguyen, 2017). Furthermore, its configuration also comprises a top of the spray air gap which is rotating to avoid coating deposition and a part underneath which is stationary (T. T.-L. Nguyen, 2017).

Thirdly, Sepajet® represents the upper filter system which provides a separate inlet air stream from above to blow the twelve Sepajet® filters rotationally and in this way to return the powder back into the system or to filter the outlet air stream (Bauer, 2015; Becker, 2016). The blockage raises the power consumption of the inlet air fan to maintain the adjusted fluidisation air flow rate (Becker, 2016). When the maximal differential pressure supported by Sepajet® is surpassed, the fluidisation air flow rate is decreased by a feedback control in a unwanted manner to protect the process in operation.

**Figure 1-2** also demonstrates simply an ongoing coating operation with the position of the sensors (e.g. differential pressure, temperature) of the whole device. The aforementioned descriptions represent a simple demonstration of available fluidised bed technologies. For the reader's curiosity, it is advisable to refer to dissertations (Becker, 2016; T. T.-L. Nguyen, 2017) for more technical details about Ventilus® Romaco Innojet technology. Besides the impact of processing technologies, quality of coatings depends on chemical composition, and resultant physical properties (Kleinbach & Riede, 1995).

## 1.2. Versatility of Air-Suspension Coating for Pharmaceutical Applications

Depending on technical characteristics, different coating technologies can generate coated / encapsulated products in different sizes, forms, morphologies, etc. Based on the morphology, there are basically two types of coated products: (i) reservoir (core/shell) and (ii) matrix (Benoît et al., 2013). If the product is a system of microparticles, those two types represent microcapsules and microspheres, respectively. **Figure 1-3-A** and **-B** show a schematic of microcapsules and microspheres.

Most of developed hot-melt coated products had a morphology of reservoir (**Figure 1-3-A**). Intuitively, reservoir systems should be more efficient than matrix systems when the target functionalities are moisture protection, taste masking or extended release. On the other hand, matrix systems (**Figure 1-3-B**) should be more adapted to fast delivery of poorly water-soluble drugs. The unique article of hot-melt coating in this subject was about the development of diclofenac-loaded amphiphilic lipid bases (Khobragade et al., 2014).



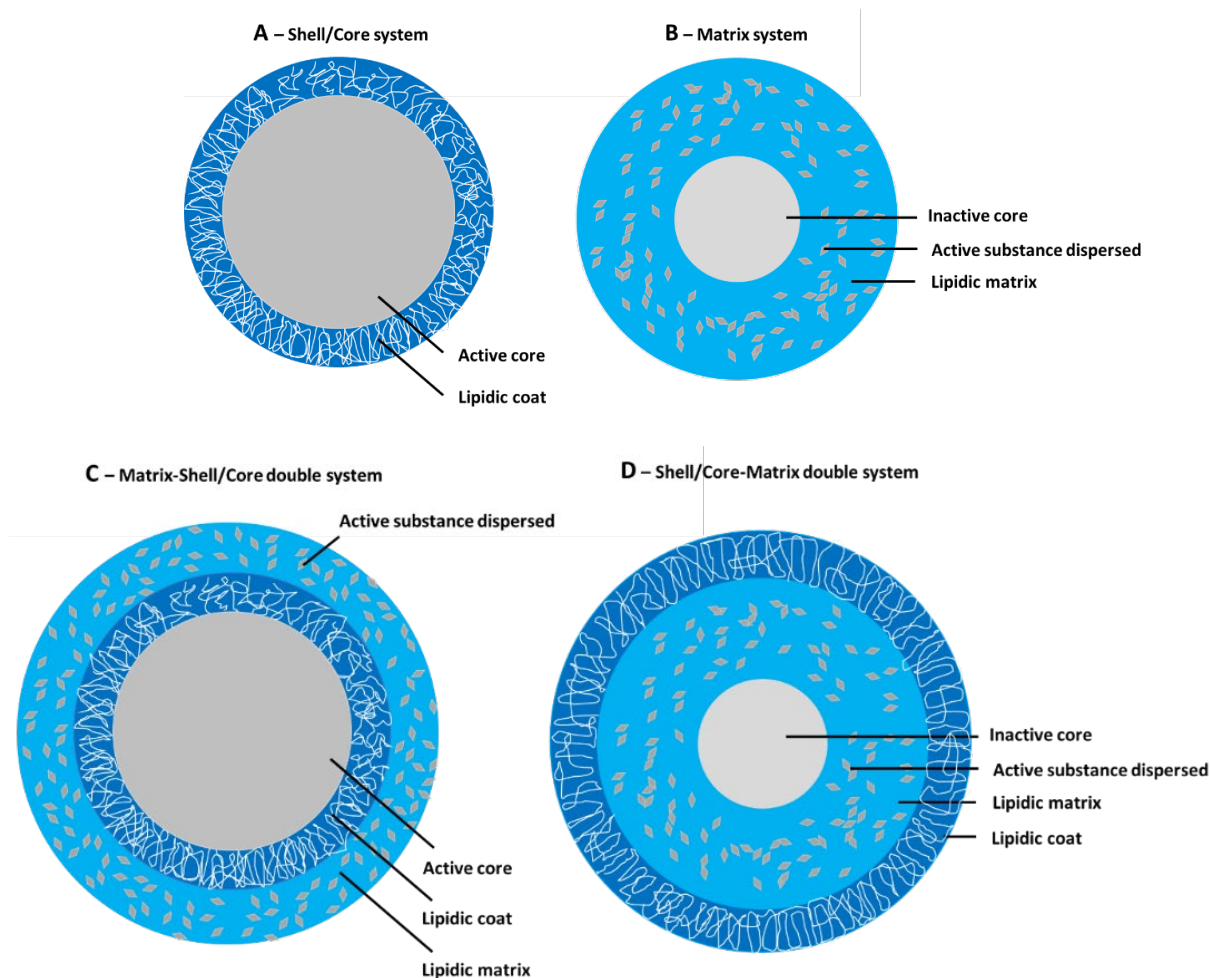


Figure 1-3. Microcapsules and microspheres obtainable with hot-melt coating by fluidised bed

**Figure 1-3-C** shows a matrix-core/shell double system (or **A-in-B**) which comprises the innermost core of highly soluble drug coated by a control-release lipophilic lipid-based membrane and the outermost layer of drug-embedded amphiphilic lipid-based membrane. This is for a design of a pulsatile release system inspired from the case of polymer-based coating (Roy & Shahiwala, 2009).

**Figure 1-3-D** shows a core/shell-matrix structure (or **B-in-A**) for which the inert core might be replaced by the product itself. This product concept is for hot melt coating delicate substrates (e.g., amorphous solid dispersions) to add a value of moisture protection, taste masking, extended release or even bioavailability enhancement. A unique proof of concept was about hot-melt coating of an amorphous drug (Bannow et al., 2020). These examples justify another advantage of hot-melt coating by air suspension. This relies on the possibility to build multiple different structures layer-by-layer from a starting core. Also inspired from polymer-based coating, it is possible to coat the coated products with another formulation without destroying their structures (Frankiewicz & Sznitowska, 2022). **Table 1-1** shows a comparison in product characteristics generated via several popular melt technologies (Benoît et al., 2013; Kyobula et al., 2017; Marie Le Page & Hervé, 2019; Vithani et al., 2019a).

According to **Table 1-1**, each melt technology has its own advantages and drawbacks. For melt spray coating, one can notice at least three advantages, i.e. (i) generation of coated products whose particle

size distribution is narrow, (ii) flexibility to generate reservoir or matrix systems and (iii) possibility of high drug loading.

Table 1-1. Physicochemical characteristics of particles generated via some melt-technologies

Manufacturing process	Technology	Typical product size ( $\mu\text{m}$ )	Product size distribution	Morphology	Drug loading percentage (%)
Spray chilling / cooling / congealing	Spray atomiser	1 – 50	Large	Matrix	< 40
Extrusion/spheronisation	Extruder / spheronisator	> 200	Narrow	Matrix	$\leq$ 50
Co-extrusion	Co-extruder	> 300	Narrow	Reservoir	-
Spray coating / layering	Fluidised bed technology	$\geq$ 100	Narrow	Reservoir / Matrix	40 – 97
	Pan coater	> 1000	Narrow	Reservoir / Matrix	-
Non-spray coating	High shear mixer	> 1000	-	Matrix	-
	High shear mixer	> 1000	-	Matrix	-
Granulation	Extruder	> 200	Narrow	Matrix	$\leq$ 50
	Fluidised bed technology	$\geq$ 10	Large	Matrix	60 – 90
Pastillation	Pastillator / Conveyor crystalliser	> 1000	Narrow	Matrix	-
Prilling	Prilling tower	> 30	Narrow	Reservoir	< 30
Three-dimensional printing	3D-printer	> 1000	Narrow	Matrix	5 – 7
-, No information					

### 1.3. Coating Fundamentals

A good understanding of coating fundamentals at the micro-level time-scale will provide a foundation for anticipating the effects and interactions between process variables and formulation properties. This understanding could be accomplished by identifying and developing the constitutive variables and governing equations underlying the complexity of interdependent and successive microprocesses of the spray coating process (Appelgren & Eskilson, 1993; Ronsse et al., 2008; Werner et al., 2007) as follows:

- movement of substrate particles, spraying of droplets (momentum transfer),
- cooling for hot-melt coating (heat transfer),
- deposition of the molten formulation onto substrate surface (mass transfer).

#### 1.3.1. Fluidisation

Based on the air fluidisation velocity and the quality and quantity of substrate in the particle bed, different fluidisation patterns can be observed according to **Figure 1-4** and described as follows (Leturia & Saleh, 2014; Mörl, 2011):

- Fixed particle bed (**Figure 1-4-A**): at an inlet air velocity inferior to the minimum fluidisation velocity ( $U_{mf}$ ), the particle bed is still immobile and keep its compact state;
- Minimum fluidisation (**Figure 1-4-B** and right): when the minimum fluidisation velocity ( $U_{mf}$ ) is reached, the weight of the entire particle bed is compensated by the buoyancy force of the air. At the moment the substrate particles begin to move and the particle bed behaves like a fluid;

- Bubbling fluidisation (**Figure 1-4-C**): when the inlet air velocity is slightly superior to  $U_{mf}$ , gas bubbles can form in the fluidised bed, move upwards from below and burst on the surface of the fluidised bed. The rising gas bubbles entrain a trail of solid particles from bottom to top, which leads to thorough mixing of the solid particles;
- Turbulent fluidisation (**Figure 1-4-D**): when the inlet air velocity continues to rise, the size and the number of gas bubbles increase progressively and mixing of substrate particles becomes more and more intense. At the moment, the heat, mass and momentum transport processes in fluidised beds are intense, and high mass and heat transfer coefficients can be achieved;
- Entrainment (**Figure 1-4-E**): when the terminal air velocity is overcome, substrate particles are entrained by the fluidisation air stream out of the fluidised bed. This particularly happens to fine particles occurring in the particle bed.

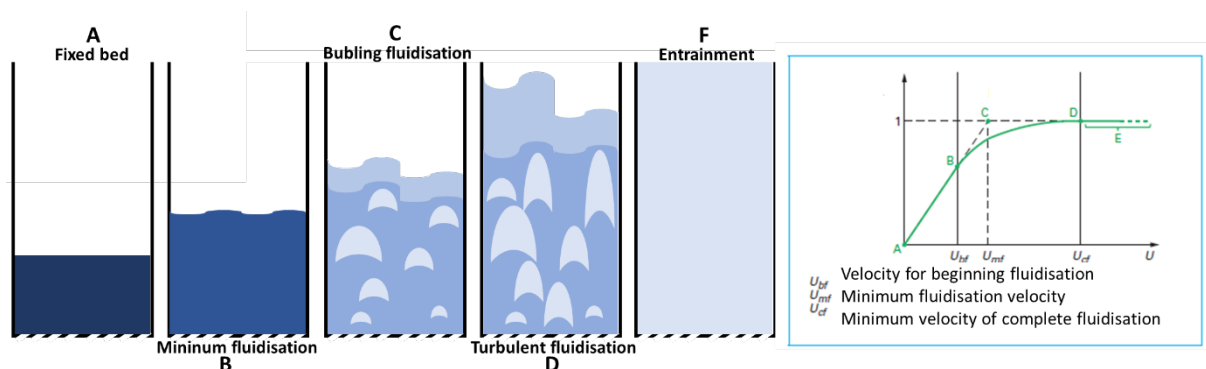


Figure 1-4. Fluidisation patterns (A to F, left) and pressure drop (right) as a function of superficial gas velocity (adapted from Leturia & Saleh, 2014)

Based on the characteristics of the substrate particles (different powders for pharmaceutical use) – relative density and surface-volume diameter, four types of fluidisation (as shown in **Figure 1-5-A**) are predictable according to Geldart classification in order as follows (Dechsiri, 2004; Geldart, 1973; Hüttlin, 2011; Leturia & Saleh, 2014) :

- Group A materials (e.g., granules 20-200  $\mu\text{m}$ ) are **aeratable** particles. Before the occurrence of bubbles, substrate particles of this group expand easily and fluidise with homogeneous patterns with a pronounced expansion of the particle bed. At a higher process air quantity, bubbles start to form from bottom to top and their size hardly surpasses 10 cm. Note that bubbles ascend to the surface of the particle bed more rapidly than interstitial gas.
- Group B materials (e.g. granules 20-200  $\mu\text{m}$ , small pellets 100-400  $\mu\text{m}$ , large pellets 400-1200  $\mu\text{m}$ ) are sand-like particles. Substrate particles of this group are easy to fluidise with the **formation of bubbles large in size and number readily at the start of fluidisation**. Mixing of substrate particles is brought about by the ascending and growing bubbles across the particle bed before reaching the surface (**Figure 1-5-B**).
- Group C materials (e.g., fine powder, crystals 2-20  $\mu\text{m}$ ) are very fine and **cohesive** powders. Substrate particles of this group are extremely difficult to fluidise because interparticle forces are relatively higher than drag and buoyancy forces from the action of gas. The cross-sectional pressure drop is inferior to the apparent weight of the particle bed when channelling occurs.
- Group D materials (e.g. large pellets 400-1200  $\mu\text{m}$ , microtablets 1500-2500  $\mu\text{m}$ , small tablets 3-7 mm) are either very coarse and very dense. Substrate particles of this group are **difficult to fluidise**

at the bottom of the particle bed where large bubbles occur and ascend such slower than interstitial gas. These materials are spoutable with the increase in fluidisation air velocity.

The two substrates used in this doctoral thesis belongs to **group B** as its controlled size will be between 400  $\mu\text{m}$  and 640  $\mu\text{m}$  (or 200  $\mu\text{m}$  and 640  $\mu\text{m}$ ).

Incidentally, almost industrial fluidised beds operate in the regime of bubbling fluidisation as shown in **Figure 1-5-B** (right) (Leturia & Saleh, 2014). For a good design of coating process, control of fluidisation is important (i) to expose all the substrate particles evenly to spraying zone, (ii) to assure an intense movement for decrease of agglomeration (Arwidsson & Rudén, 1993) and (iii) to supply sufficient cooling/drying for hot-melt coating and solvent-based coating, respectively (Appelgren & Eskilson, 1993; Arwidsson & Rudén, 1993).

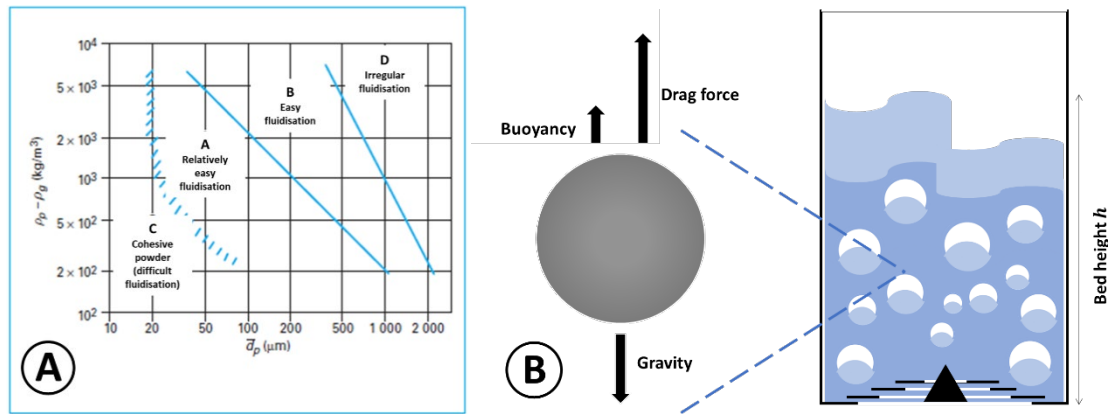


Figure 1-5. Geldart classification (A) and bubbling fluidisation (B)  
(adapted from Leturia & Saleh, 2014; Watano et al., 2004)

For a better understanding of physics, minimum fluidisation velocity and pressure drop are expressed mathematically. The pressure drop when a gas stream flows through a packed particle collective is given by the Ergun equation (S. Fang et al., 2020) as follows:

Equation 1 :

$$\frac{dP}{dh} = C_1 \frac{(1 - \varepsilon_{mf})^2}{\varepsilon_{mf}^3} \frac{\mu U_h}{(\varphi d_p)^2} + C_2 \frac{(1 - \varepsilon_{mf})}{\varepsilon_{mf}^3} \frac{\rho_g U_h^2}{\varphi d_p}$$

$$\begin{matrix} \text{[Pressure} \\ \text{drop]} \end{matrix} = \begin{matrix} \text{[Laminar flow} \\ \text{component]} \end{matrix} + \begin{matrix} \text{[Turbulent flow} \\ \text{component]} \end{matrix}$$

where  $C_1$  is the coefficient of the viscosity term, and  $C_2$  is the coefficient of the inertial term.  $\varepsilon_{mf}$  is the porosity of the particle collective at the incipient fluidised state (-),  $\mu$  the viscosity of the gas stream (Pa.s),  $U_h$  the superficial gas velocity at the h height section of the fluidised bed ( $\text{m}\cdot\text{s}^{-1}$ ),  $\varphi$  the particle sphericity (-),  $d_p$  the particle size (m), and  $\rho_g$  the gas density ( $\text{kg}\cdot\text{m}^{-3}$ ). At  $t_0$ ,  $U_0 = U_{mf,0}$ ,  $H_0$  is the bed height attained at this initial velocity of minimum fluidisation (m).

On the other hand, the minimum force of the gas to maintain fluidisation of the particle bed is:

Equation 2 :

$$dF_{mf} = dP \times A_h$$

Given Newton's second law of motion, the momentum balance between drag, buoyancy and gravity (as shown in **Figure 1-5-B** (left)) can be written as follows:

Equation 3 :

$$dF_{mf} = C_3 \times m_{bed} \times g$$

[Drag]        +        [Buoyancy]        =        [Gravity]

where  $C_3$  is a correction coefficient, for instance, which could reflect the equipment geometry (Knezevic et al., 1998),  $m_{bed}$  the quantity of the bed collective (kg) and  $g$  the gravity ( $m.s^{-2}$ ).

This shows the application of a general momentum balance model in processing by fluidised bed (S. Fang et al., 2020). Having applied an analytical solution to **Equations 1** and **3**, it was found that to achieve the same bed height higher fluidisation velocity is required for larger substrate particles.

On the other hand, pressure drop augments with the increase in weight of the powder bed (S. Fang et al., 2020). These findings are important for considerations of fluidisation control in **hot-melt coating**.

Actually, the most pronounced difference between solvent-based coating and hot-melt coating is that in melt processing 100% coating material is retained after cooling on the surface of substrate particles in comparison with solvent-based methods where only a small fraction of solids in coating liquid remains after drying (Appelgren & Eskilson, 1993). Substrate particles will become significantly denser in the course of hot-melt coating. This might warrant for eventual in-process adjustments of fluidisation air velocity to assure processing performance and coating quality. To the author's knowledge, only one study (Knezevic et al., 2009) has been carried out on this subject till now.

### 1.3.2. Formation of droplets

The spray device plays the most important role in spray coating. There are three typical groups used in spraying with mechanical mixing and with air-suspension mixing: (i) pneumatic spray devices, (ii) hydraulic spray devices and (iii) other spray devices (Arwidsson & Rudén, 1993). The pneumatic spray devices which are dominant in the pharmaceutical industry are the focus of presentation.

Like no other coaters presented in **Section 1**, the coating zone (wet spray zone as illustrated in **Figure 1-6**) for Ventilus® covers an annular space (360°). This represents a strength of Rotojet® technology to provide a larger coating zone tangential to the particle bed entrained by the air flow.

The spray form (cross-section) can be divided into three zones. The spray near the nozzle has a conical form, which then declines and becomes more cylindrical (Arwidsson & Rudén, 1993). The longer the distance between the nozzle and the spray, the more the droplets lose their velocity. For lipids which have an intrinsic fast solidification rate, a sufficient batch size is required to assure the density of substrate particles in the coating zone and therefore to reduce fine overproduction. The most important indicators of a good spray are: (i) mean droplet size, (ii) droplet size distribution, (iii) spray angle and

(iv) physical properties of droplets (viscosity, surface tension, heat of crystallisation) (Arwidsson & Rudén, 1993).

Droplet size is mainly determined by the setup of pulverisation air volume, which is measured indirectly by the pulverisation air pressure. Coating of small particles require correspondingly fine droplet size, hence higher pulverisation air pressure to avoid agglomeration. However, finer droplets can exchange heat more rapidly with the cooling air and hence this possibly results in fine overproduction.

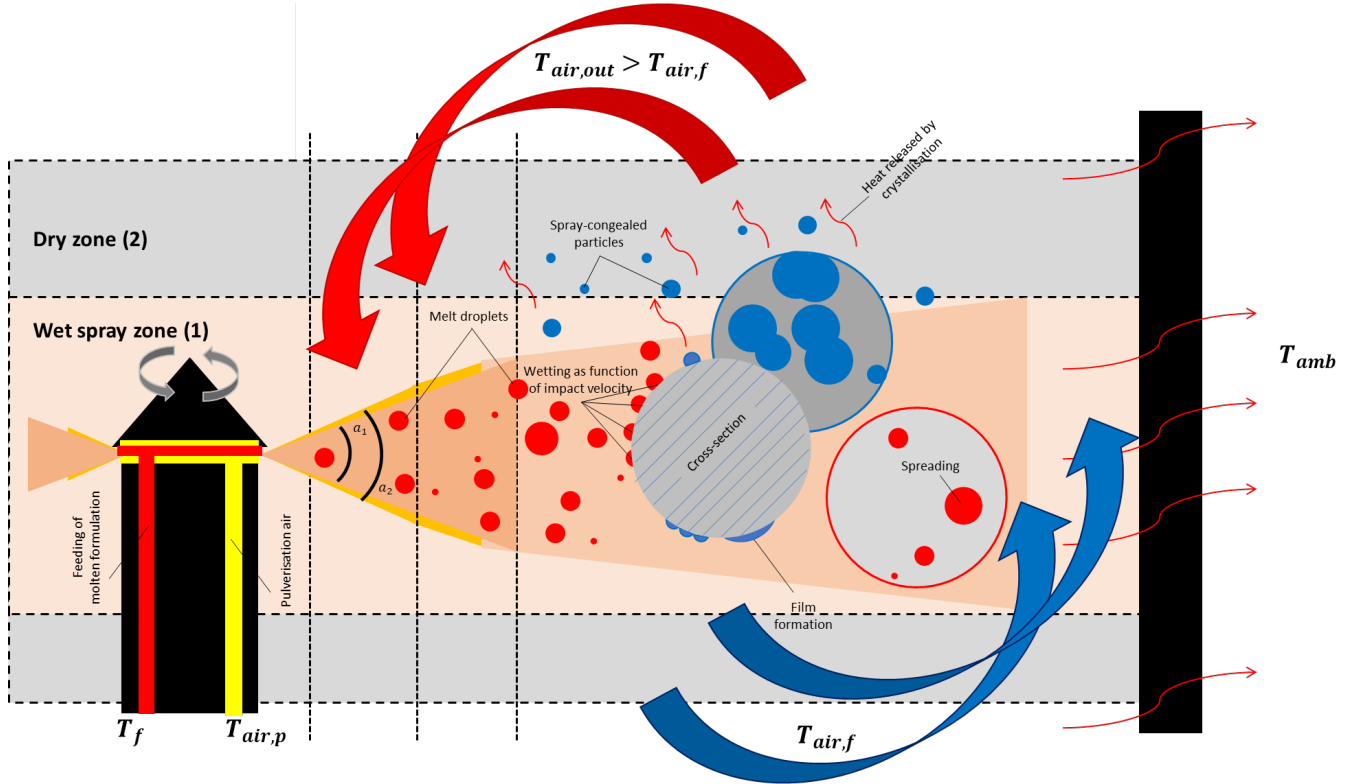


Figure 1-6. Illustrative schematic of spraying by the device Rotojet®, impacting, wetting, film forming and solidifying in coating process (adapted from Arwidsson & Rudén, 1993)

The droplet size of the molten formulation when sprayed is related to the following spray parameters: atomizing air pressure, properties of the molten medium and feeding rate. To predict mean droplet size when the molten formulation is sprayed, it is possible to use mathematical equations such as those proposed in the literature (Arwidsson & Rudén, 1993; Werner et al., 2007):

Equation 4 :

$$D_{3,2} = \frac{A \sigma_{lv}^{1/3}}{U \rho_f^{1/2}} + B \left( \frac{\mu_f / 1000}{\sigma_{lv} \rho_f} \right)^{9/20} \left( 1000 \frac{\dot{m}_f}{\dot{m}_{air,p}} \times \frac{\rho_{air,p}}{\rho_f} \right)^{3/2}$$

which express the mean drop size as the Sauter mean diameter which reflects the same ratio of surface to mass as the total droplet population ( $D_{3,2} = \sum n D^3 / \sum n D^2$ ) and where  $A$  and  $B$  are constants.  $\sigma_{lv}$  is the surface tension of the molten formulation (liquid vapour) ( $N \cdot m^{-1}$ ),  $U$  is the relative outlet air velocity ( $m \cdot s^{-1}$ ),  $\rho_f$  is the density of the molten formulation ( $kg \cdot m^{-3}$ ),  $\mu_f$  is the viscosity of the molten



formulation (Pa.s),  $\dot{m}_f$  is the feeding rate of the molten formulation ( $\text{kg}\cdot\text{s}^{-1}$ ),  $\dot{m}_{air,p}$  is the pulverisation air mass flow rate ( $\text{kg}\cdot\text{s}^{-1}$ ), and  $\rho_{air,p}$  is the density of the pulverisation air ( $\text{kg}\cdot\text{m}^{-3}$ ).

In addition to shear provided by the pulverisation air, the design of Rotojet® technology with a rotary part on the top of the nozzle should effectively contribute to both shearing the melt and preventing sticking of re-melt coated products. Low melt viscosity of lipids (often less than 300 mPa.s) might not be a technical constraint for the spray nozzle in general (D. G. Lopes, Salar-Behzadi, et al., 2017). In the case that melt viscosity is important when solid particles are added (Wong et al., 2016), considerations of nozzle port size are necessary (Jones & Percel, 1994).

As indicated by **Equation 4**, feeding rate of the molten formulation is also a factor determining coating quality and degree of agglomeration via control of droplet size. Generally, low feeding rate leads to less agglomeration (Woerthmann et al., 2023) and better coating uniformity (Jones & Percel, 1994; Jozwiakowski et al., 1990). When coating is complete, the vigour of fluidisation is reduced, and the product should be then cooled to the fluidisation air temperature. Too rapid cooling may cause cracks or fissures in the lipidic coat as lipids might be brittle by crystalline nature (Salar-Behzadi, Corzo, et al., 2020). Therefore, it is advisable to let coated products cool depending on the coating material and the thermal operational condition (Jannin & Cuppok, 2013; Jones & Percel, 1994).

### 1.3.3. Film formation

For solvent-based coating, film forms by the mechanism of entanglement, i.e. intertwining of polymer molecules under evaporation, as the polymer chains are intimately mixed (Felton, 2013; Werner et al., 2007). The quality of the film (surface properties) depends on the evaporation rate. In effect, slow drying allows for better coalescence and facilitate creation of a smooth film but the process is prone to agglomeration in this condition. On the contrary, fast drying leads to formation of a rough and porous film (Arwidsson & Rudén, 1993). **Figure 1-7** illustrates the films prepared by solvent-based coating under slow (**A**) and fast (**B**) evaporation rate.

**Figure 1-7** also illustrates the films resulting from lipid crystallisation. A hypothesis for film formation in hot-melt coating is suggested in the following:

- For spontaneous nucleation (**Figure 1-7-C**), the formed film is smooth and constituted by the layers of deformed droplets. In fact, deformation of droplets depends on the impact velocity (as shown in **Figure 1-6**) as well as the viscosity of the molten formulation at the time of contact. Then, droplets wet the surface in the order of few milliseconds and solidify immediately. There are two of possible failure cases: (i) fine overproduction and (ii) delamination. In the former case, the droplet travel distance is so long that the droplets solidify prior to the contact with the particle surface. In the latter case, the temperature of the particle surface (close to the fluidisation air temperature) is so low that upon impacting the particle surface, the droplets wet poorly, solidify quickly. As a consequence, the film may be deformed with the appearance of filaments (Shepard et al., 2020) or the adhesion may not be sufficient to retain the coating formulation on the particle surface. Spontaneous nucleation is usually the case of metastable polymorphic ( $\alpha$ ) crystallisation;



- For sporadic nucleation (**Figure 1-7-D**), the formed film is rough and porous due to the contraction of lipid in the course of solidification (Kim, 2003; Marie Le Page & Hervé, 2019). In fact, for this case, film formation takes place in isothermal conditions and crystallisation only commences after a certain period called induction time. In this case, solidification rate is limiting for the molten formulation. The droplets always have sufficient time to reach the particle surface, wet it and only after the induction time does it solidify (as shown in **Figure 1-6**). During the solidification time lag, the molten state of the formulation might undergo splashing to create smaller droplets and results in fine overproduction. Simultaneously, the wetted particles might collide to form agglomerates when a solidified bridge is formed. Therefore, three regimes likely occur. As the process of film formation depends on nucleation and crystal growth of the lipid formulation, adjustments of process variables (e.g., for reduction of droplet size) might be not so effective as the modification of formulation properties. Sporadic nucleation is usually the case of stable polymorphic ( $\beta$ ) crystallisation. A unique study on hot-melt coating where there were the two cases of spontaneous and sporadic nucleation shows indeed that  $\beta$  coated products displayed a remarkably higher porosity than  $\alpha$  coated products (D. G. Lopes et al., 2015).

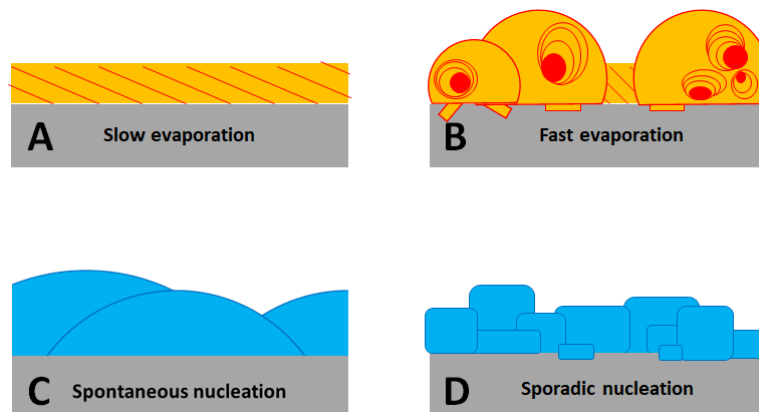


Figure 1-7. Typical films formed in solvent-based coating (A & B) (adapted from Arwidsson & Rudén, 1993) and hot-melt coating (C & D)

#### 1.3.4. Control of thermal operational conditions for hot-melt coating

To understand how to define thermal operational conditions, it is indispensable to understand heat transfer and balance in hot-melt coating. A general heat balance for the case of hot-melt coating has been established in a scale-up study (Kulah & Kaya, 2011). The dynamic heat transfer of the hot-melt coating process by fluidised bed is described by conservation equations of energy. According to the study, the basic assumptions of this model are as follows:

- The powder bed (particle collective) is well-mixed due to the intense mixing in the fluidised bed. At this point, the fluidised bed behaves as a perfectly stirred reactor;
- No material escapes from the powder bed as an adapted filter was put in place;
- The flowrates of the inlet and outlet gas streams are not disturbed during the process;
- The content of solvent/water is zero in the spray liquid;

- Water content of the air streams could be neglected as the film formation of the deposited molten droplets on substrate surface results from its solidification from the molten state;
- Solidification of the formulation takes place immediately after it enters to the particle collective operating at the temperature of the fluidisation air.

From these assumptions, a global energy balance can be given in the following:

Equation 5 :

$$\frac{d(m_{bed} \times H_{bed})}{dt} = \dot{m}_{air,tot\ in} \times H_{air,tot\ in} + \dot{m}_f \times H_f - \dot{m}_{air,out} \times H_{air,out} + Q_{loss}$$

[Rate of change  
in the heat of the particle collective]
=
[Heat exchange between inlet and outlet  
airstreams of the fluidised bed]
+
[Heat loss to the  
surrounding]

where  $\dot{m}_{air,tot\ in}$  is the total flowrate of air streams going into the system ( $\text{kg.s}^{-1}$ ). They encompass the fluidisation air, the inlet air from the filter, and the pulverisation air flowrates.  $H_{bed}$ ,  $H_{air,tot\ in}$ ,  $H_{melt}$ , and  $H_{air,out}$  represent the heat of formation of the powder bed, all the inlet air streams, the melt formulation, and the outlet air stream ( $\text{J.kg}^{-1}$ ).  $\dot{m}_f$  is the feeding rate of the molten formulation (or the melt) ( $\text{kg.s}^{-1}$ ),  $\dot{m}_{air,out}$  is the outlet air mass flowrate ( $\text{kg.s}^{-1}$ ),  $m_{bed}$  the total mass of the bed (kg) at time  $t$  and  $Q_{loss}$  the energy loss to the surrounding (W).

A relationship between absorption of melting heat and release of crystallisation heat is given as follows:

Equation 6 :

$$C_{p,solid} \times T_m + \Delta H_m(at\ T_m) + C_{p,melt} \times (T_{melt} - T_m) = C_{p,solid} \times T_c - \Delta H_c(at\ T_c) + C_{p,melt} \times (T_{melt} - T_c)$$

assumed that  $C_{p,solid}$ , the specific heat capacity of the solid formulation equals to  $C_{p,solid}$ , the specific heat capacity of the solid formulation  $C_{p,melt}$ .  $T_m$  is the melting temperature of the formulation ( $^{\circ}\text{C}$ ), and  $\Delta H_m(at\ T_m)$  is the melting enthalpy of the formulation ( $\text{J.kg}^{-1}$ ) at  $T_m$ .  $T_c$  is the temperature set for crystallisation of the formulation ( $^{\circ}\text{C}$ ) and  $\Delta H_c(at\ T_c)$  is the crystallisation enthalpy of the formulation ( $\text{J.kg}^{-1}$ ) at  $T_c$  (under isothermal conditions).

Taking into account the change of the mass of the bed ( $m_{bed}$ ) with time and substituting the aforementioned equations is rearranged to solve for the outlet air temperature,  $T_{air,out}$  ( $^{\circ}\text{C}$ ), which is equal to the recorded operating temperature of the fluidised bed,  $T_{bed}$  ( $^{\circ}\text{C}$ ), with the condition of a assumed well-mixed bed, as follows:

Equation 7 :

$$\frac{dT_{bed}}{dt} = \frac{Q - Q_{loss}}{(\dot{m}_f \times t + m_{bed,0}) \times C_{p,solid}}$$

where  $m_{bed,0}$  is the batch size (kg) and  $Q$  is the total heat exchange between inlet and outlet air streams as well as the feeding of the melt. Having developed and simplified **Equation 6**,  $Q$  is expressed as follows:

Equation 8 :

$$Q = C_{p,air} \times (\dot{m}_{air,f} \times T_{air,f} - \dot{m}_{air,out} \times T_{bed}) + \dot{m}_f \times [C_{p,solid} \times (T_{air,f} - T_{bed}) - \Delta H_c] + Q_{air,s} + Q_{cooling\ from\ T_f}$$

considering that the temperature of fluidisation air is set with a value of  $T_{air,f} = T_c$  for crystallisation of the formulation.  $C_{p,air}$  is the specific heat capacity of the corresponding process air ( $J.kg^{-1}.^{\circ}C^{-1}$ ),  $\dot{m}_{air,f}$  the mass flowrate of fluidisation air stream,  $Q_{air,s}$  the heat provided by the spray air stream (W) and  $Q_{cooling\ from\ T_f}$  the heat released when cooling the melt till the target crystallisation temperature (W).  $C_{p,solid}$  is assumed to be universal for both solid coating material, substrate, and coated particles while  $C_{p,air}$  is assumed to be universal for inlet and outlet air as the humidity should not change in the case of hot-melt coating.

A analytical solution is possible for **Equation 7** (Kulah & Kaya, 2011) by replacing  $Q$  with Equation 8 and by assuming that a steady-state is established. It then becomes:

Equation 9 :

$$Q_{air,p} + Q_{cooling\ from\ T_f} + \dot{m}_f \times [C_{p,solid} \times (T_{air,f} - T_{bed}) - \Delta H_c] = C_{p,air} \times (\dot{m}_{air,out} \times T_{bed} - \dot{m}_{air,f} \times T_{air,f}) + Q_{loss}$$

As can be seen in **Equation 9** and **Figure 1-6**, it is reasonable to notice that at the equilibrium state the heat provided by process air and hot melt and the heat released from crystallisation of the formulation compensate the heat removed by the fluidisation air and the loss to surrounding (Dewettinck & Huyghebaert, 1999).

Hence, in the contrary to solvent-based coating, one can notice that hot-melt coating is a “macroscopic exothermic process”. The bed temperature (also called “product temperature”) is evidently the **thermodynamic operation point** (Dewettinck & Huyghebaert, 1999) of the heat exchange in the hot melt coating process, while the fluidisation air temperature should be the **target crystallisation temperature** of the formulation. **This knowledge is important to review the two common approaches for controlling thermal operational conditions presented as follows:**

- **When the thermal setpoint is the bed temperature:** the fluidisation air temperature will fluctuate to maintain the bed temperature constant while other thermal parameters are still fixed. This is suitable for coating with lipids, whose crystallisation profile comprises a wide crystallisation temperature range, such as hard fats, beeswax, carnauba wax, candelilla wax and their mixtures (Chansanroj et al., 2007b; Jones & Percel, 1994; Jozwiakowski et al., 1990; Müller et al., 2018; Woerthmann et al., 2021, 2023). This approach might implicitly apply to lipids whose polymorphic profile is complex and less sensitive to short-term exposure to temperature.

- **When the thermal setpoint is the fluidisation air temperature:** the bed temperature will vary but reach a stable value after a period. This is the steady state condition as discussed above. Intuitively, it is like the working principles of differential scanning calorimetry when lipid crystallisation is performed under isothermal conditions. This approach is important for lipids whose polymorphic profile is sensitive to temperature. It is the case of pure substances such as triglycerides whose polymorphs  $\alpha$ ,  $\beta'$  and  $\beta$  can crystallise at different temperatures relatively close to each other. For

instance, this approach has been applied throughout pharmaceutical researches on hot-melt coating with formulations composed of tripalmitin and tristearin (Bannow et al., 2020; Becker et al., 2016; D. G. Lopes et al., 2015, 2016; D. G. Lopes, Koutsamanis, et al., 2017; Schertel, Salar-Behzadi, Karrer, et al., 2021; Schertel, Salar-Behzadi, & Zimmer, 2021; Schertel et al., 2022).

- Among these cited researches, the case of hot-melt coating with tristearin (D. G. Lopes et al., 2015) is particular for discussion. In the cited work, it is noticed that the thermal setpoint was set at two values – 25°C and 60°C – in order to generate the  $\alpha$  and  $\beta$  polymorphs of tristearin, respectively. For the latter case, if the bed temperature of 60°C is the thermal setpoint, a mixture of  $\alpha$ ,  $\beta'$  and  $\beta$  polymorphs will be formed due to temperature fluctuations in the fluidisation air below 60°C. In addition, by this approach, the control feedback can force overheating and require a powerful cooling device to maintain 60°C as constant.

Two independent hot-melt coating research works can be used to validate the applicability of each approach:

- For hot-melt coating hydrogenated soybean oil whose polymorphs  $\alpha$ ,  $\beta'$  and  $\beta$  are the same as tristearin (occurring in high fraction), the product temperature was set at 50-52°C and, after coating, coated products were fluidised until this temperature dropped to 30°C. Besides, simulation of thermal coating conditions was performed with 50°C set for isothermal conditions. Thermal analyses showed that simulative samples show less fraction of  $\alpha$  than that of coated products (Chansanroj et al., 2007b). In fact, when setting the product temperature as 50°C hydrogenated soybean oil should crystallise according to the temperature of fluidisation air and higher  $\alpha$  fraction was obtained. Furthermore, higher  $\alpha$  fraction seemed to transform more in  $\beta$  than  $\beta'$  and higher  $\beta$  fraction induced probably  $\beta'$ - $\beta$  transformation. These should explain the discrepancy between simulative and practical results.

- The other research showed an agreement between simulative and practical results as the isothermal conditions were the same as the fluidisation air temperature (Becker et al., 2016).

Therefore, research studies with different types of lipids performed by different groups of authors converge towards the fact to which case the **thermal setpoint as  $T_{bed}$  or  $T_{air,f}$  is appropriate for hot-melt coating.**

Regarding the first approach,  $T_{bed}$  is recommended to be set at the point where a certain solid fraction content is achieved upon cooling (Jannin & Cuppok, 2013; Müller et al., 2018). In this case, lipids should crystallise almost completely  $T_{air,f} < T_{bed}$ .

Nevertheless, when another property of lipids (e.g. stickiness) is more challenging, this approach could fail. The second approach to defining  $T_{air,f}$  should be based on polymorphism of pure lipids. However, control of thermal operational conditions by  $T_{air,f}$  still lacks considerations of its impact on cohesion, adhesion, and solidification kinetics of droplets on substrate.

By virtue of the heat balance, the effect of the principal mechanical process parameters (i.e., pulverisation pressure, fluidisation air velocity and feeding rate) on  $T_{bed}$  becomes evident. When  $T_{air,f}$  is defined as the thermal setpoint, increase in fluidisation velocity and/or decrease in feeding rate leads to decrease in  $T_{bed}$  as less molten formulation ought to be cooled with more air.

The contribution of pulverisation air stream to heat exchange might be secondary as its specific roles are (i) to form droplets for coating. Definition of high feeding rate can raise  $T_{bed}$  (Woerthmann et al., 2023).

### 1.3.5. Coating efficiency and quality

Coating quality can be evaluated based on the five representative measures (van Kampen, 2018) as follows:

- Mean coating thickness,
- Intraparticle thickness distribution,
- Interparticle thickness distribution,
- Porosity,
- Degree of surface coverage.

In the case of mean coating thickness, the coating efficiency can be evaluated by using a global mass balance modelling the growth of a single particle, as illustrated in **Figure 1-8** (Mörl, 2011).

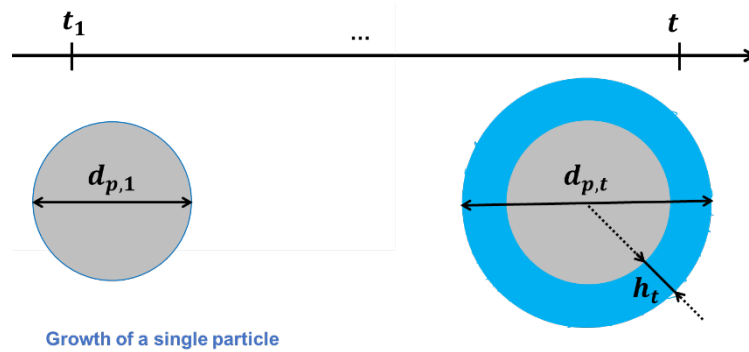


Figure 1-8. Growth regime by layering

For the application of this model, several assumptions are considered:

- Firstly, substrate particles are assumed to be spherical but in practice the sphericity could be used as an adjustment.
- Secondly, the total particulate population is conserved during the coating, implying no birth of new particles due to abrasion, breakage, and agglomeration. Thirdly, particle size distribution is narrow. Fourthly, molten droplets are distributed evenly on all the particles.

The rate of change in the mass of a single particle in the coating process is expressed as follows:

Equation 10 :

$$\frac{dm_p}{dt} = \frac{\dot{m}_f(1-x)}{\sum N_p}$$

[Rate of change in the mass of the particle bed] = [Feeding mass flowrate distributed to the population of the particles]

where  $m_p$  is mass of a particle (kg),  $x$  represents the loss fraction,  $\sum N_p$  the population of the particles.

Converting  $m_p$  into the volume  $V_p$  of the growing particle, it follows that:

Equation 11 :

$$dm_p = \rho_c \times dV_p = \frac{\dot{m}_f(1-x)}{\sum N_p} dt$$

After developing and simplifying **Equation 11**, the coating thickness  $h_t$  (m) of the particle at time  $t$  (s) is given as follows:

Equation 12 :

$$h_t = d_{p,0} \times \left( \sqrt[3]{1 + \frac{\dot{m}_f(1-x)}{m_{bed,0}} t \times \frac{\rho_p}{\rho_c}} - 1 \right)$$

where  $d_{p,0}$  is the mean initial diameter of substrate particles (m),  $\dot{m}_f$  is the feeding rate of the melt ( $\text{kg}\cdot\text{s}^{-1}$ ),  $m_{bed,0}$  the batch size (kg),  $\rho_p$  the apparent density of a particle ( $\text{kg}\cdot\text{m}^{-3}$ ),  $\rho_c$  the apparent density of coating material ( $\text{kg}\cdot\text{m}^{-3}$ ).

This model has been used for estimation of coating thickness in two studies of hot-melt coating where coating quality was evaluated with newly developed analytical techniques – micro-computed tomography and fluorescent spectroscopy (Woerthmann et al., 2021, 2023):

- The first study (Woerthmann et al., 2021) concluded that a coating amount of 10% stearin palm is required for complete and uniform coating microcrystalline cellulose particles ( $d_{50} = 1197\mu\text{m} \pm 113\mu\text{m}$ ). Note that a coating content that assures coating completeness and uniformity should correspond with a certain particle size distribution. In fact, intuitively, coating smaller particles whose surface area is larger will require higher coating amounts for this purpose.

- The second study (Woerthmann et al., 2023) investigated interparticle batch homogeneity using sugar spheres ( $d_{50} = 1140\mu\text{m} \pm 75\mu\text{m}$ ) under the effect of three levels of product temperature and feeding rate. Delamination was found to compromise coating quality by decreasing mean particle layer thickness. As presented in Sections 1.3.2 and 0, decrease in setpoint product temperature should lead to poor wetting on the particle surface and therefore coating was probably prone to delamination.

Another approach based on mass balance is modelling the evolution of coating efficiency monitored by sampling at multiple time points, as illustrated in **Figure 1-9**.

With the dynamic feeding of coating material for its application on substrate particles, they accumulate an increasing coating content with processing time. However, for most of the processing technologies, this approach might be impossible as for each batch or trial a fixed ratio of excipients to substrate has been defined. Spray-coating by fluidised bed allows for sampling at multiple time points where target coating contents are expected. The global mass balance for this approach is expressed as follows:

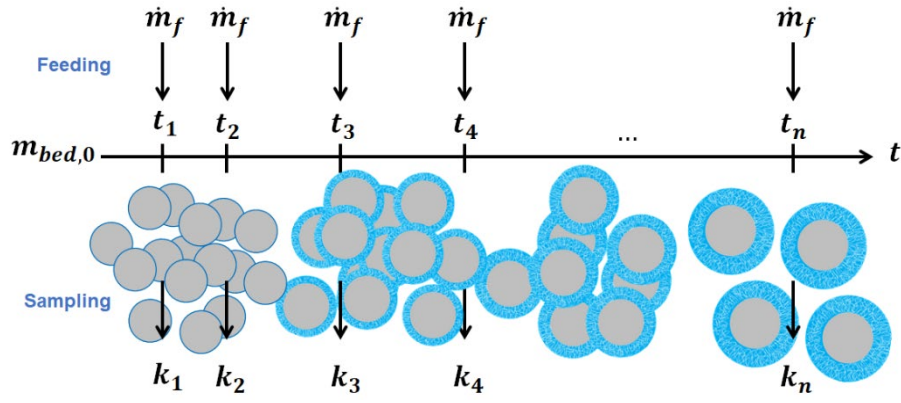


Figure 1-9. Schema of a multiple-sampling experimental approach

**Figure 1-9** highlights the fact that the particulate population diminishes as a function of sampling timepoints. A dynamic model for the accumulative mass of the particle bed during the coating process writes as follows:

Equation 13 :

$$m_{bed}(t) = m_{bed,0} + \dot{m}_f \times t_i - \sum_1^i k_i(t), i = 1, 2, 3 \dots n$$

[Total mass of the particle bed at timepoint t]	=	[Total mass of coating material fed at timepoint t]	-	[Total mass of coated particles sampled at timepoint t]
---	---	---	---	---

where  $m_{bed}$  is the mass of particle bed (kg) at timepoint  $t$ ,  $\dot{m}_f$  is the feeding rate ( $\text{kg}\cdot\text{s}^{-1}$ ),  $k_n(t)$  represents an arbitrary quantity of coated particles (kg) sampled at a timepoint where a coating content  $C_i\%$  w/w is targeted. For the reader's information, coating content of  $C_i\%$  w/w is defined as  $C_i$  g of coating material in 100 g of coated products.

For this purpose, in the course of coating operations, samples are withdrawn from the particle bed when the loss in weight of coating due to feeding approaches the pre-calculated value which allows to achieve the target  $C_i\%$  w/w at the sampling timepoint  $t_i$ . An advantage of coating by fluidised bed is the possibility to generate products with various coating contents in the same batch depending on the sampling time. This allows for design of a multiple-sampling-point experimental approach to evaluate processing performance and coating quality when a formulation is used. Without substrate compensation after each sampling, the number of samples withdrawn at each time should be considered.

Having developed and rearranged the intermediate equations derived from **Equation 13**, at each  $t_i$  to achieve the target  $C_i\%$  w/w, the total mass of fed coating material at this timepoint  $t_i$  is given in the following table by already taking into account the amount of samples withdrawn in the previous sampling  $k_{i-1}$ :



Equation 14 :

$$\dot{m}_f \times t_i = \frac{C_i\% \times m_{bed,0} - k_i(C_i\% - C_{i-1}\%) \dots - k_1(C_2\% - C_1\%)}{100 - C_i\%}$$

and for the first sampling:

Equation 15 :

$$\dot{m}_f \times t_1 = \frac{C_1\% \times m_{bed,0}}{100 - C_1\%}$$

where the condition is that  $m_{bed,0} + \dot{m}_f \times t_i - \sum_{i=1}^i k_i > 0$ .

The strengths of this models rely on the fact that it requires no assumptions, and it has the potential to be associated with the other models (e.g., momentum, heat, mass balance). It reflects the reality of processing performance that calculations of coating efficiency are hardly missing in normal practices.

Final yield and coating efficiency are two key performance indicators that are assessed in the first place regardless of processing methods. However, the construction of a dynamic evolution of coating efficiency alone cannot aid in evaluation of the impact of formulation properties and definition of process variables on coating operations.

In addition, sampled coated products need be analysed by means of a set of characterisation techniques for complementary information to answer the following questions:

- Which is the main process regime of the performed operation: coating, mixed regime of coating and agglomeration, with or without occurrence of overspray?
- Which is the minimum lipid content to assure complete and uniform coating of the substrate with known quality (e.g., chemical nature, particle size distribution) and quantity (e.g., batch size)?

Finally, for evaluation of coating quality, modelling dissolution kinetics is also feasible, and this approach has been performed in studies of solvent-based coating.

In a case study (Van Kampen et al., 2015; van Kampen, 2018), modelling dissolution kinetics of a population of particles coated with a soluble coating material was applied to evaluate coating thickness distribution. This model is given as a convolution:

Equation 16 :

$$c(t) = c_0(t) * x(t)$$

where  $c(t)$  is the dissolution curve of the coated substrate,  $c_0(t)$  the dissolution curve of the uncoated substrate. Given a population of perfectly coated particles, as the particles might be coated differently to some extent, the dissolution curve will have a different value of the time shift  $\tau$  (s) which is represented by a probability density function  $x(t)$ . \* is the convolution operator. Its convolution integral is given as follows:

Equation 17 :

$$c(t) = \int_0^t x(\tau) \cdot c_0(t - \tau) d\tau$$

This model was concluded to serve as a quick method to inform about the distribution of the layer thickness and this make it suitable for daily quality assurance or process optimisation. Concerning the case of lipids, a similar approach can be used to estimate thickness distribution of coating membrane which is amphipathic and readily dispersible like polyethylene glycols, polyoxylglycerides (Khobragade et al., 2014). The most important condition for this approach is that dissolution kinetics of the substrate be measurable (Van Kampen et al., 2015).

On the other hand, modelling dissolution kinetics of particles coated with a non-erodible coating material was also reported (Frenning et al., 2003). The development of this model is complex but one of their correlations could be used to conclude on the complete and uniform coating. It is rewritten as follows:

Equation 18 :

$$\frac{k_{in,i}}{k_{in,i+1}} = \frac{k_{out,i}}{k_{out,i+1}} = \frac{h_{i+1}}{h_i}$$

where  $k_{in,i}/k_{in,i+1}$  is the ratio between the rate constants of liquid inflow obtained for two samples with low and high coating contents,  $k_{out,i}/k_{out,i+1}$  the ratio between the rate constants of drug efflux obtained for two samples with low and high coating contents and  $h_{i+1}/h_i$  the ratio between the mean thickness values obtained for two samples with high and low coating contents. This correlation showing an inverse proportionality function between the coating thickness and the rate constant can be rewritten as follows:

Equation 19 :

$$h_i^n \cdot k_{diss,i} = h_{i+1}^n \cdot k_{diss,i+1} = constant$$

where  $n$  represents the dimension of the dissolution process (-) of coated particles (Sugano & Terada, 2015). With this correlation, it is possible to evaluate the coating quality by measuring release kinetics of several samples with increasing coating amounts and fitting a relationship curve between the coating thickness and the rate constant found by an empirical release kinetics model (e.g., first order, zeroth order). Initial outliers can be indicative of a coating content at which complete and uniform coating should be suspected.

#### 1.4. Experimental approach to characterising coating process

Coating by fluidised bed technology is a complex manufacturing method which involves interdependent and successive microprocesses – fluidisation, pulverisation, collision between droplets and substrate particles, droplet solidification via crystallisation, and film formation.

Regardless of spraying nozzle configuration, design of a coating process encompasses a good definition of nearly twenty process parameters, material properties and product attributes (Jones, 1985; Kulah & Kaya, 2011; Ronsse et al., 2008). As demonstrated in **Figure 1-10**, substrate quality and quantity

(constituting the bed of particle collective), coating material properties, fluidised bed technology dimensions, fluidisation air and spraying air settings represent five groups of coating process variables.

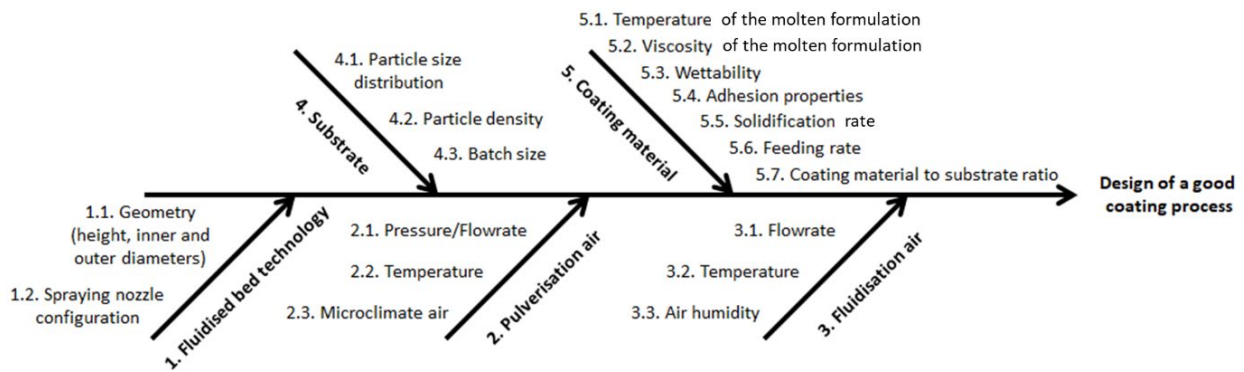


Figure 1-10. Schema of all possible variables for designing a good coating process

When it comes to approaches to characterising the coating equipment, statistics-based approaches (e.g., design of experiments) (A. S. Achanta et al., 1997; Becker et al., 2016; Jozwiakowski et al., 1990; Kennedy & Niebergall, 1996; D. G. Lopes et al., 2016; Milanovic et al., 2018; Rosiaux et al., 2018) are often applied to investigate rapidly the impact of different process variables on the product characteristics.

**Table 1-2** shows the importance associated with each process variable. The common process variables chosen as factors in DoE studies are temperature of the molten formulation and atomisation air, feeding rate, atomisation air pressure, coating amount, additive concentration in coating material, fluidisation air flowrate, and fluidisation air temperature. The choice of process parameters on DoE studies on hot-melt coating and solvent-based coating converges on the implicit importance of feeding rate, atomisation air pressure and fluidisation air flowrate.

DoE studies often bypass the conduct of fundamental researches on coating materials. Therefore, the link between formulation properties, process performance and coating quality (as shown in **Table 1-2**) can be underestimated. In addition, statistics-based approach requires generation of many batches following the statistical design and therefore execution of processing trials and characterisation of products are intensive. This warrants for a development of an experimental approach which could be simple and nimble, which could enable characterisation of the impact of formulation properties and definition of process parameters on processing performance, coating quality and product profile.

A physics-based experimental approach will be proposed (at the end of this chapter) for this thesis.

Table 1-2. Process variables and their importance in **hot-melt coating** by fluidised bed

<i>Process variables</i>	<i>Importance</i>
<b>Pulverisation air</b>	
<b>Pressure</b>	To control melt droplet size distribution
<b>Temperature</b>	Sufficient for preventing clogging/plugging and for keeping the molten formulation sprayable
<b>Microclimate air flowrate / temperature</b>	To form melt droplets of appropriate size distribution Sufficient for preventing clogging/plugging and for keeping the molten formulation sprayable
<b>Fluidisation air</b>	
<b>Flowrate</b>	To expose all the substrate particles evenly to spraying zone To assure an intense movement for decrease of agglomeration To supply sufficient cooling
<b>Temperature</b>	To control lipid crystallisation at this target temperature
<b>Humidity</b>	To facilitate heat transfer (if applicable)
<b>Substrate</b>	
<b>Particle size distribution</b>	For definition of fluidisation patterns
<b>Particle density</b>	For definition of fluidisation patterns
<b>Batch size</b>	For definition of fluidisation patterns To provide a sufficient particle density exposed to spraying zone
<b>Coating material</b>	
<b>Molten formulation temperature</b>	Sufficient for assuring formulation stability, for mixing of components in formulation and for feeding
<b>Molten formulation viscosity</b>	Sufficient for being transported and for being sprayed
<b>Wettability</b>	Sufficient for spreading and not for splashing of droplets on <b>particle surface</b>
<b>Adhesion properties</b>	Sufficient for reducing sticking of <b>coated particles</b> to process wall and for adhering to <b>particle surface</b>
<b>Solidification rate</b>	Sufficient for avoiding agglomeration of particles and for adhering to <b>particle surface</b>
<b>Feeding rate</b>	To control melt droplet size distribution To control cooling rate
<b>Coating material to substrate ratio</b>	To fit functionalities of coated products

## 2. Lipid-Based Excipients Used as Coating Materials

### 2.1. Definition, Classification, and Selection Criteria for Lipid-Based Excipients

Lipids have many applications not only associated with pharmaceuticals, cosmetics, foods but also energy and mechanics (Sato, 2018a). Evidently, they could have a differentiated definition in each field.

The IUPAC's definition that lipids are of biological origin and soluble in non-polar solvents might be restrictive (Couffin & Delmas, 2013). Food scientists' point of view is more relevant to selection of lipid-based excipients for pharmaceutical use and much fundamental research on lipids (both experimentally and theoretically) has been owed to their work. According to their definition, lipids encompass long-chain aliphatic hydrocarbons and their derivatives (Sato, 2018a), excluding cyclic compounds.

From a complementary perspective of biochemists, lipids are subdivided into simple lipids, compound lipids, and steroids (Cole & Eastoe, 1988). Scholars of "lipidomics" adds that lipids are hydrophobic or amphipathic substances whose formation might result entirely or partially from condensations of ketoacyl esters and/or condensations of isoprene units (Fahy et al., 2011). This classification system comprises of eight categories of lipids on the basis of chemical structure.

For the sake of simplicity, three biochemistry-based categories of lipids continue to be considered as almost lipid-based excipients for oral drug delivery fall within these three categories (Gibson, 2007). They are then classified into lipids of natural and synthetic origin.

Naturally occurring lipids are almost complex mixtures, but the most abundant substance (major component) might be deemed as "high-purity" lipids. Beeswax, carnauba wax, hard fats, fatty acids and triglycerides have been largely used in formulation of solid lipid systems (Becker et al., 2015; D. G. Lopes, Salar-Behzadi, et al., 2017).

Synthetic lipids are commercially sourced and often provided with a certificate of analysis on main chemical composition and impurity profile (Jannin et al., 2014). For example, brand mixtures of glyceryl mono-, di- and tristearate (Precirol® ATO 5) or glyceryl mono-, di- and tribehenate (Compritrol® 888 ATO) are prepared with a mass concentration of about 18%, 52% and 28% m/m, respectively (Jannin, 2010; Jannin et al., 2015). An overview of these combined classifications for lipid-based excipients is given in **Figure 1-11**.

**Figure 1-11** can serve as a guide to pick up a major component, i.e. matrix forming agent, for preparation of solid lipid-based formulations suitable for an end-use property. The choice from three categories of lipids – fatty acyls, glycerolipids and glycerophospholipids – is common. The choice of minor components which is determined by their impact on processability, stability and functionalities of the product will be discussed in **Section 4.2**. Classification of the compounded formulations based on biopharmaceutical behaviours (e.g. hydrophilic lipophilic balance-HLB, wettability, digestibility) will be discussed in **Section 3**.

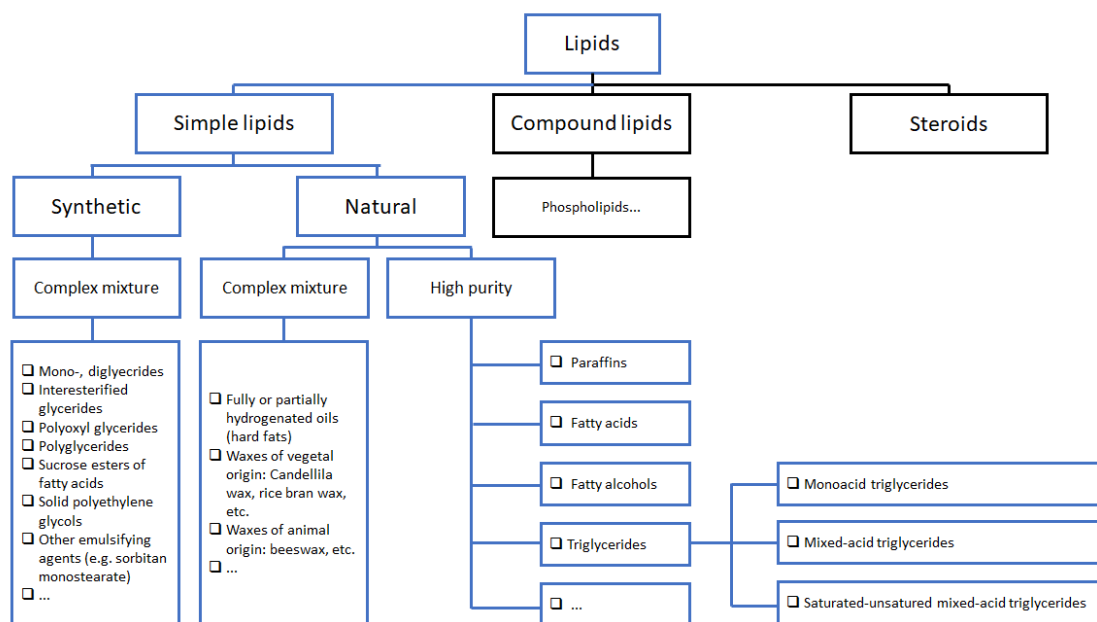
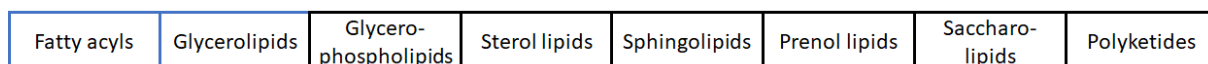


Figure 1-11. Overview of lipids often used for formulating solid dosage forms

Selection of a major component could be empirical with the suggested criteria (A. S. Achanta et al., 1997) in **Table 1-3**:

Table 1-3. Criteria for selection of an ideal lipid used for hot-melt coating

No.	Description of criteria
1	No physical or chemical degradation below 200°C
2	Melting point between 75°C and 80°C
3	Narrow melting temperature range without softening
4	Thermal behaviours independent of preparation and storage conditions (thermal history) between 30°C and 200°C
5	No crystal modifications at 200°C
6	Stability in repeated heating-cooling cycles
7	Availability of excipients having varying HLBS
8	Low melt viscosity for easy flow and spray
9	Conformance to current regulations

Parts of these criteria might be close or open and all of them might not be covered at once. They are still relevant in some way nowadays. Some of them deserve a comment here:

The **second criterion** help eliminate the earlier use of monosaccharides, sugar alcohols, carboxylic acids (Appelgren & Eskilson, 1993) for hot-melt coating as their melting points are close to or above 100°C. This highlights the almost unique utility of lipids for hot-melt coating.

Although solid polyethylene glycols (PEG) are polymers by nature, this group is included in **Figure 1-11** as their melting points respond to this and the **eighth criterion** (Wong, 2015; Wong et al., 2016). Their utilisation (e.g., PEG 6000) was cited as early as in 1953 for a melt-mediated coating application (Appelgren & Eskilson, 1993). PEGs 1500, 4000, 6000 and 20000 had a similar structure to lipid (J. Li

et al., 2011) and were successfully applied for melt coating of tablets or pellets (H. Chen et al., 2010; Kennedy & Niebergall, 1996; Khobragade et al., 2014; K. T. T. Nguyen et al., 2022). They are also adapted to a solventless processing method whose principles are close to hot-melt coating (Capece & Davé, 2014). Besides, lipid-polymer combinations (e.g. lipids with ethyl cellulose, polyvinylpyrrolidone K25) used for melt processing dated back to 1993 (Appelgren & Eskilson, 1993).

The **third criterion** was validated with the emergence of sucrose esters of fatty acids (SEFA) regarded as “extremely functional” in food industry (Ribeiro et al., 2015). The work of a thesis in pharmaceutical research recommended the use of SEFA in crystalline state, not those in amorphous form (Szűts, 2003).

The **fourth criterion** appears ideal as lipid-based products have revealed many stability challenges not limited to polymorphism alone (Delbaere et al., 2016; D. G. Lopes et al., 2015; D. G. Lopes, Koutsamanis, et al., 2017; Salar-Behzadi et al., 2019; Schertel, Salar-Behzadi, Karrer, et al., 2021; Schertel, Salar-Behzadi, & Zimmer, 2021).

The **seventh criterion** holds true at this moment. Representatives of lipophilic and amphipathic lipids are triglycerides and polyoxylglycerides, respectively.

The **last criterion** imposes safety concerns for synthetic lipid-based excipients of new generations as is the case of polyglycerol esters of fatty acids or polyglycerides (Salar-Behzadi, Corzo, et al., 2020). Normally, the safety of conventional lipid-based excipients can be checked in the USA Food and Drug Administration’s generally-regarded-as-safe substances and/or inactive ingredients databases (Becker et al., 2015).

In general, from the very beginning of hot-melt coating adoption, criteria to choose a lipid bulk agent have been based on three aspects of drug development – **manufacturability** (numbers 1, 2, 3, 6 and 8), **stability** (numbers 4 and 5) and **functionality** (numbers 7 and 9) (A. S. Achanta et al., 1997). It was emphasised that for development of melt processing methods the build-up of knowledge on pure substances or combinations is the main driver (Appelgren & Eskilson, 1993; Rosiaux et al., 2022). The following **Sections 2.2, 2.3** and **3** will contribute some updates to this knowledge with the successive syntheses of processing-specific properties, solid-state behaviours and biopharmaceutics characteristics.

## 2.2. Processing-Specific Properties

According to the principles of melt-based processing for preparation of solid dosage forms, control of lipid crystallisation is of utmost importance (Acevedo & Marangoni, 2015).

**Figure 1-12** illustrates at the first sight the nomenclature of the hierarchical structure of lipid crystal networks with the increasing length scale, which is widely recognised in lipid research (Mishra et al., 2023; Tang & Marangoni, 2007):

- At the molecular level, when a determined polymorphic form is conditioned by appropriate thermal treatment, ① triglyceride molecules, for instance, in a conformation of a chair configuration can self-assemble to form ② lamellar structures.
- Stacking of these lamellae then develops into ③ crystallites (also called “nanoplatelets”, “domains” or “primary crystals”) at the nanoscopic scale.



- These crystallites assemble in a fractal manner to build ④ polycrystalline crystal clusters (also called “polycrystalline aggregates”, “spherulite”) at the mesoscopic scale. The length scale of these clusters depends on the crystallisation conditions (target crystallisation temperature and cooling rate).
- At the microscopic scale, loose flocculation of these clusters then results in construction of ⑤ flocs (also called “chains”) and aggregation of these flocs (or polycrystalline) eventually leads to formation of a three-dimensional fat crystal network ⑥, which constitutes bulk fat observed at the macroscopic scale (Acevedo & Marangoni, 2015; R. R. Chauhan et al., 2017; Mishra et al., 2023).

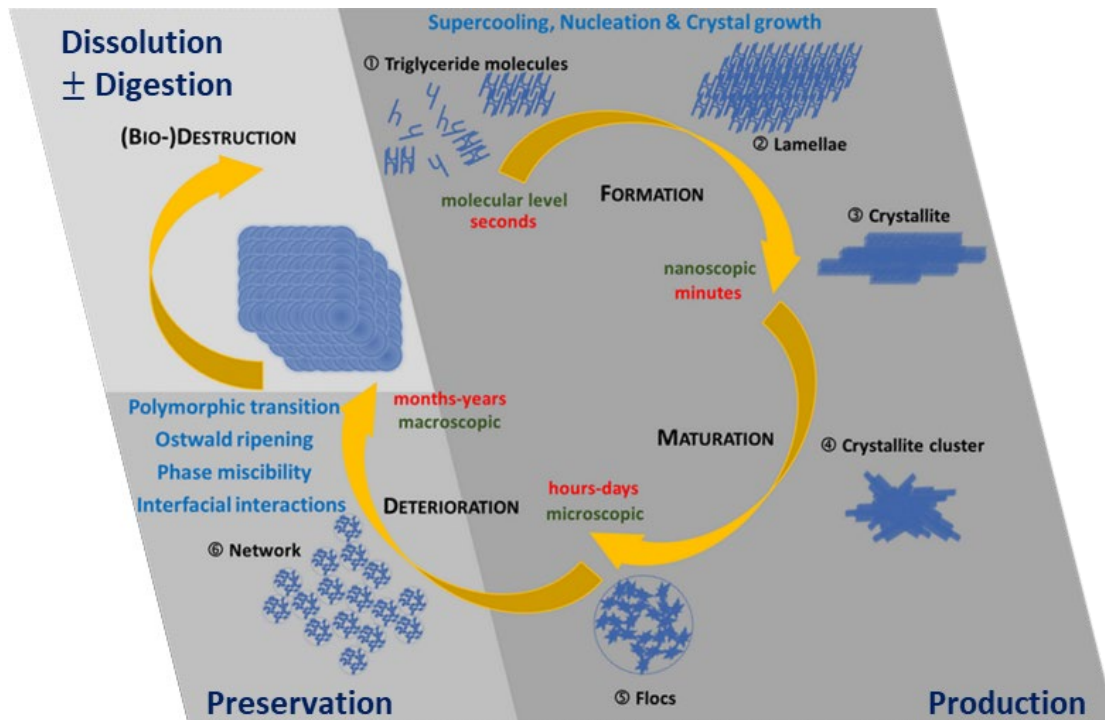


Figure 1-12. Product cycle constituted by formation, maturation, deterioration and (bio-)destruction of lipid crystal network at different times and at different observation scales (adapted from Mishra et al., 2023; Tang & Marangoni, 2007)

From the perspective of formulation science, **Figure 1-12** compares a product cycle of lipids which are produced, then preserved in appropriate conditions before being consumed in drug-loaded products:

- For a good practice of production, knowledge of supercooling, nucleation, crystal growth and network formation is important.
- For a good practice of preservation, understanding post-crystallisation solid-state behaviours such as polymorphic transition, Ostwald ripening, phase miscibility and interfacial interactions is indispensable.
- From the perspective of time scale, crystallisation should be as much momentary as possible whereas post-crystallisation should be less time-dependent for ease of manufacture and product stabilisation, respectively (Sato, 2018a). **Sections 2.2 and 2.3** will treat **crystallisation and post-crystallisation behaviours** which reflect primarily processability and stability of lipids, respectively.

## 2.2.1. Crystallisation

### 2.2.1.1. *Supercooling*

Supercooling ( $\Delta T$ ) is defined as the difference in temperature between the melting point ( $T_m$ ) and the crystallisation temperature ( $T_c$ ) where lipids remain liquid for a period (called induction time  $\tau$ ), that is,  $\Delta T = T_m - T_c$  (Sato, 2018a). This is the case of crystallisation from a neat liquid.

Supercooling is also called undercooling (Piska et al., 2006) or subcooling (Ribeiro et al., 2015). Supercooling has its own impact on the operation, especially in feeding of coating material. Paraffins (hydrocarbons) and fatty acids were known for its low or no supercooling (Beaupere et al., 2018). Certain natural waxes such as beeswax whose composition is quite rich in both of these components (Fratini et al., 2016; Tulloch, 1980) are also probably predisposed to this tendency. Their use should be considered with a risk of clogging if the temperature of the feeding system is not set high enough or if the system itself is not well insulated or in certain cases of applying a low feeding rate or conducting a continuous processing operation. On the other hand, a low supercooling is expected from a triglyceride-based formulation, for instance, with the aims of limiting delamination, facilitating film formation and avoiding agglomeration, to reduce nucleation time of the stable form  $\beta$ . Nucleation will be discussed in the next section.

### 2.2.1.2. *Nucleation*

From a fundamental research point of view, when the melt is being cooled, the occurrence of solids is possible when a spherical crystal of a critical radius  $r^*$  is in equilibrium with its mother phase (melt) assumed that the melting point of this small crystal is below that of a crystal of infinite size (Boistelle, 1988). The condition of this equilibrium is given as follows:

*Equation 20 :*

$$\Delta\mu = \frac{2\gamma v}{r^*} = \Delta H_m \frac{T_m - T}{T_m}$$

where  $T_m$  and  $\Delta H_m$  are the temperature (K) and enthalpy of fusion per molecule ( $J \cdot 1^{-1}$ ), respectively.  $\gamma$  is the interfacial free energy ( $J \cdot m^{-2}$ ) between the nucleus and the melt, and  $v$  the volume of a molecule in the nucleus ( $m^3$ ).

The Gibbs-Thomson equation (**Equation 20**) expresses the chemical potential or driving force for melt crystallisation (**Figure 1-13-A**) and relates crystal size and supercooling.

According to the classical theory of homogeneous nucleation, nucleation is a stepwise addition of molecules to form embryos whose size is less than the critical nucleus. This happens in the mother phase (melt) where the mean energy imposed by the supercooling is constant (Boistelle, 1988). To create a nucleus, a pre-requisite is to overcome an energetic barrier with an activation free energy  $\Delta G_{hom}$  as expressed below:

Equation 21 :

$$\Delta G_{hom}^* = -\frac{4\pi(r^*)^3}{3v} \times \Delta\mu + 4\pi(r^*)^2\gamma$$

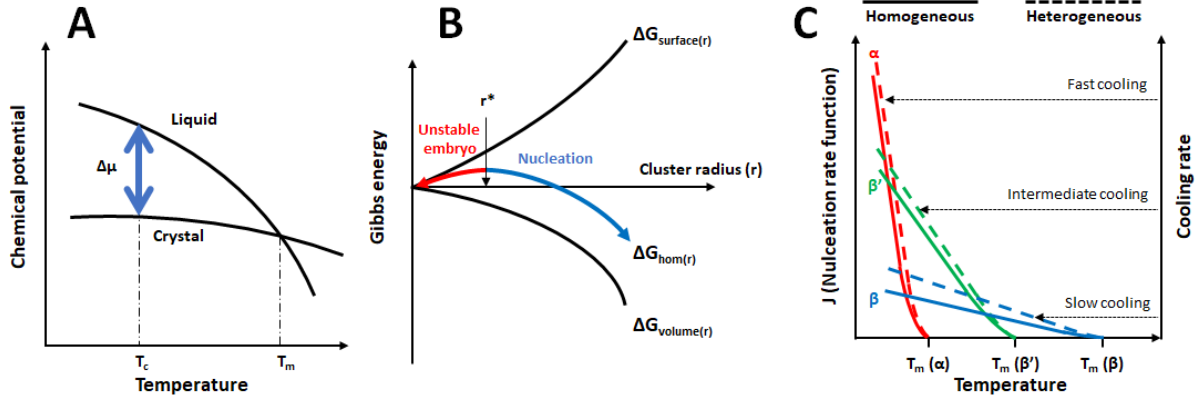


Figure 1-13. Driving force and Gibbs energy in isothermal crystallisation (A, B) and selective crystallisation as a function of cooling rate (C) (adapted from Yoshikawa, 2016)

**Figure 1-13-B** demonstrates this activation free energy in which the first term is the energy to form the nucleus volume of a critical size and the second term the excess energy to create its surface (Boistelle, 1988). For heterogeneous nucleation, the nucleus forms onto surface of foreign particles (Yoshikawa, 2016). The activation free energy for heterogeneous nucleation is written as:

Equation 22 :

$$\Delta G_{het}^* = \Delta G_{hom}^* \times \left( \frac{1}{2} - \frac{3}{4} \cos \theta + \frac{1}{4} \cos^3 \theta \right)$$

where  $\theta$  is the contact angle between the mother phase and the surface of foreign particles (rad). Having the activation free energy, the nucleation rate  $J$  ( $\#.m^{-3}.s^{-1}$ ) as a function of crystallisation temperature (Hondoh et al., 2018) is given as follows:

Equation 23 :

$$J = J_0 \times \exp\left(-\frac{\Delta g}{k_B T_c}\right) \times \exp\left(-\frac{\Delta G^*}{k_B T_c}\right)$$

where  $J_0 = zN_0v$  is the nucleation rate pre-exponential factor.  $z$  is the so-called Zeldovich factor,  $N_0$  the number density of molecules in the mother phase ( $\#.m^{-3}$ ), and  $v$  the frequency of attaching a molecule to the critical nucleus ( $s^{-1}$ ).  $\Delta g$  is the activation free energy of viscosity (J) and  $k_B$  the Boltzmann constant.

Combining **Equations 20, 21, 22** and **23**, a general nucleation rate for both the aforementioned cases (Adachi et al., 2014; Hondoh et al., 2018) is given as follows:

Equation 24 :

$$J = zN_0v \times \exp\left(-\frac{\Delta g}{k_B T_c}\right) \times \exp\left[-4/3 \frac{f\gamma^3 v T_m^2}{k_B T_c \Delta H_m^2 (T_m - T_c)^2} \left(\frac{1}{2} - \frac{3}{4} \cos \theta + \frac{1}{4} \cos^3 \theta\right)\right]$$

where  $J = J_{hom}$  when  $\theta = 180^\circ$ . Otherwise,  $J = J_{het}$ .  $f$  is the shape factor of the crystal.

**Figure 1-13-C** shows the formation of a determined polymorph of a triglyceride as a function of cooling rate for both homogeneous and heterogeneous nucleation (Yoshikawa, 2016). According to the Ostwald step rule, when a lipid can occur in a number of polymorphs from a less stable state to more and more stable states, usually the closest more stable polymorph is formed and not the most stable one whose activation free energy is the least (Aquilano & Sgualdino, 2001; Boistelle, 1988). This rule can be explained with **Figure 1-13-C**. When a melt of a triglyceride is cooled quickly to attain the condition  $T_c < T_{m,\alpha}$ , the  $\alpha$  form can occur spontaneously or sporadically whereas if the condition is  $T_{m,\beta'} < T_c < T_{m,\beta}$ , the  $\beta$  form can also occur spontaneously or sporadically. Cooling rate determines *stricto sensu* how fast the melt reaches the isothermal conditions, and the occurrence of these polymorphs depends on the nucleation rate conditioned by the level of supercooling and the introduction of impurities (accidentally) or additives (intentionally).

Nucleation behaviours of a lipid can be explained using the graph illustrated in **Figure 1-14**.

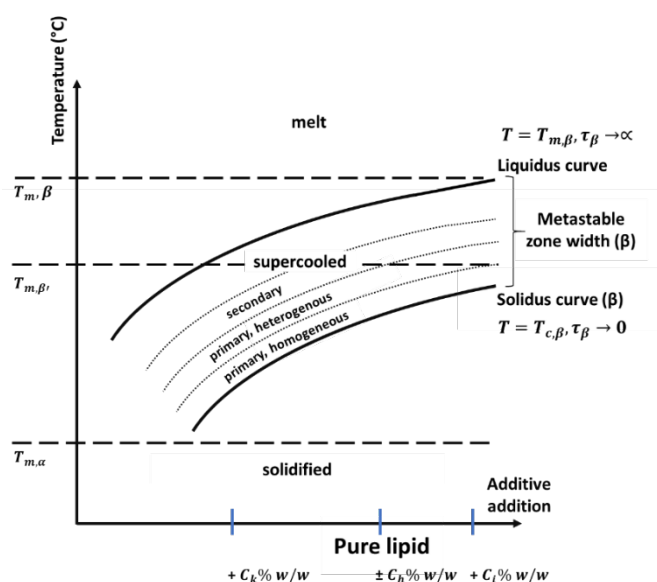


Figure 1-14. Melt crystallisation: Nucleation of a pure lipid model as a function of additive addition associated with two coating approaches (adapted from Dasgupta, 2017; Marie Le Page & Hervé, 2019)

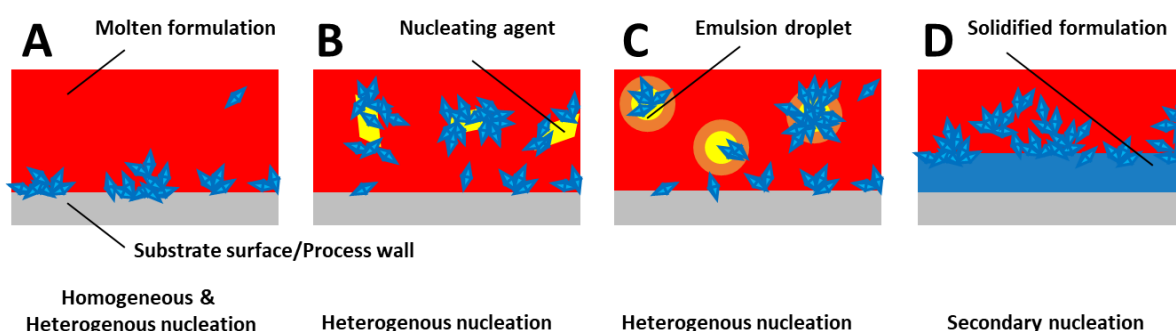
**Figure 1-14** demonstrates the melt crystallisation of the lipid being cooled at different rates. These curves are indicated by  $T_m$  and  $T_c$ , respectively. Above the liquidus curve, triglyceride molecules remain in the molten state. When the temperature of the system reaches  $T_m$ , there is a potential to crystallise the lipid but its induction time tends to infinity. Below the solidus curve, the system changes immediately to solidified state. When the temperature of the system reaches  $T_c$  upon cooling at a specific rate, it crystallises spontaneously induction time of the lipid tends to 0.

The region delineated by the two curves is called the metastable zone width (MSZW) (Dasgupta, 2017; Marie Le Page & Hervé, 2019). The lipid remains supercooled in the metastable zone and has the potential to crystallise after a period of induction. MSZW can be divided further depending on the

mechanisms of nucleation: (i) (primary) homogeneous nucleation, (ii) (primary) heterogeneous nucleation, and (iii) secondary nucleation.

In the case of heterogeneous nucleation, presence of impurities and additives is likely the cause. Even a little amount sometimes can have an impact on the nucleation rate by several orders of magnitude (Boistelle, 1988). For instance, the effect of talc (of a median size 0.6  $\mu\text{m}$ ) on  $\beta$  trilaurin was demonstrated down to a mass concentration of 0.1% (Yoshikawa, 2016; Yoshikawa et al., 2015). On the other hand, sorbitan monostearate of various commercial sources whose impurity profile should be different had a different effectiveness as a  $\alpha$  form crystal preservative for tristearin (Garti et al., 1982). Impurities and additives affect the nucleation kinetics through the thermodynamic factor (e.g., interfacial energy, melting point, supercooling) and the kinetic factor (e.g., frequency of attaching a molecule to the critical nucleus) (Boistelle, 1988; K. W. Smith & Sato, 2018). The effectiveness of the additive(s) can be evaluated in terms of some related quantities (e.g., induction time, stochastic nature of nucleation, supercooling, cloud point (drop point), metastable zone width) (Boistelle, 1988; Kulkarni et al., 2013). This effectiveness can be evaluated by constructing a MSZW graph (as given in **Figure 1-14**) as a function of additive category and concentration.

The effect of additive addition will be discussed in **Section 2.4** but here mechanisms of primary and secondary nucleation are presented graphically. **Figure 1-15** illustrated four nucleation mechanisms possibly encountered in processing lipid-based formulations.



*Figure 1-15.  $\beta$  nucleation mechanisms possibly encountered in lipids processing (adapted from Stewart et al., 2017; Yoshikawa et al., 2015)*

In the actual context of lipids processing, it is hardly possible for homogeneous nucleation (**Figure 1-15-A**) to occur because of the presence of impurities or foreign surface (e.g. that of substrate, process wall) that may catalyse the nucleation process (Hondoh et al., 2018). In addition, secondary nucleation (**Figure 1-15-D**) can be the case where pre-existing crystals of lipids are present or the process wall acts as nucleation catalyst (Boistelle, 1988; Hondoh et al., 2018). Actually, take the example of hot-melt coating with tristearin at 60°C (D. G. Lopes et al., 2015). For the successful production, a two-step feeding was applied when delivering tristearin on substrate particles. The first feeding rate was set at 0.5 g/min during the first 5 min, which implies that it was a step to facilitate nucleation of  $\beta$  form. This step was short in comparison with much longer induction time of homogeneous nucleation of  $\beta$  tristearin (Bertoni et al., 2021; Da Silva et al., 2009; Oh et al., 2002). Then, the second feeding rate was raised up

to 10 g/min after that, which implies that secondary nucleation is faster than primary nucleation of  $\beta$  tristearin.

In the case of adding an additive(s), heterogeneous nucleation represents the main mechanism of crystallisation. For example, talc serves as a nucleating template (**Figure 1-15-B**) for fast crystallisation of trilaurin and tripalmitin (Yoshikawa, 2016; Yoshikawa et al., 2015). Another example is about crystallisation of tripalmitin at the interface of dispersed phase (oily droplet) and dispersing phase (melt) (**Figure 1-15-C**) (Stewart et al., 2017). By considering these application evidence, nucleation of a polymorphic form at a specific temperature can be regarded as its proof of thermal feasibility.

Knowledge of nucleation mechanisms is practically a key to (i) formulating combinations of lipid and additive(s) and (ii) mastering melt processing by adjustment of process variables. However, control of nucleation only contributes partially to crystallisation of lipids. Solidification kinetics is also determined by crystal growth, which will be presented in the next section.

### 2.2.1.3. Crystal growth

Once the formation of nuclei of an excessive critical size, they develop into crystallites (or nanoplatelets) (See again **Figure 1-12**) whose growth hinges on both external factors (e.g., temperature, presence of impurities and/or additives) and internal factors (e.g., structure, bonds, defects) (Boistelle, 1988). Concerning the structure, according to the periodic bond chain theory, there are three types of faces of a crystal on which a lipid molecule could assemble in the course of grow: F (flat), S (step) and K (kink) (Boistelle, 1988). These types of growth sites are given in **Figure 1-16-A**. K faces display only kinks (i.e., growth sites) so that lipid molecules incorporate directly thereon. F faces, being flat and exhibiting not many kinks, grow either by a two-dimensional nucleation mechanism or by a spiral growth mechanism. S faces which are corrugated faces grow by a one-dimensional nucleation mechanism (Boistelle, 1988).

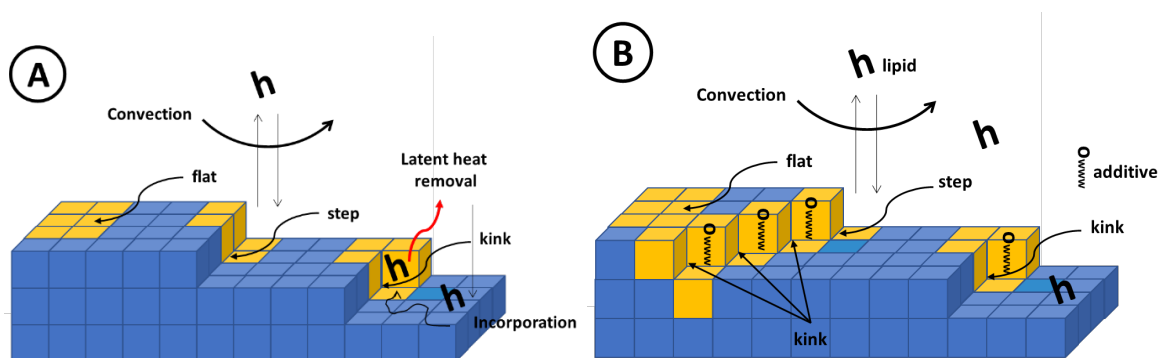


Figure 1-16. Crystal growth processes (A) and mechanisms of action of additive impact on these processes (B) (adapted from Thakore et al., 2020)

**Figure 1-16-A** also shows three kinetic processes involved in crystal growth: (i) transportation, (ii) incorporation and (iii) latent heat removal. Firstly, growth units (triglycerides in a chair configuration) are transported as a flux onto the surface by convection or diffusion under the effect of supercooling. Once these molecules arrive at the surface (F faces), it diffuses thereon until it finds a kink site (K faces) to be incorporated. Latent heat (or crystallisation enthalpy) is released after this process. Growth units



can also detach from the surface. In melt crystallisation the crystals in the mother phase sometimes display a rough surface on which the density of kink sites is high thanks to small chemical potentials between solids and melt. Then, incorporation of growth units can be accelerated and the local temperature near the growing surface increases rapidly. As a consequence, supercooling decreases drastically and this reduces the crystal growth rate and therefore the solidification kinetics (Hondoh et al., 2018).

Knowledge of the **crystal growth mechanism** is also useful for design of a melt-based process. For instance, it was reported with the case of tripalmitin extrudate (Witzleb et al., 2012). Extrusion with 1.0- and 0.3-mm dies made such a difference that tripalmitin was cooled slowly or rapidly at ambient conditions under the effect of extrudate surface and friction imposed by pression. In this case, slow cooling maintained the thermal condition favourable for  $\beta$  crystallisation ( $T_{m,\alpha} < T_c < T_{m,\beta}$ ) whereas rapid cooling (fast heat removal) led to  $\alpha$  crystallisation ( $T_c < T_{m,\alpha}$ ). On the contrary, fast removal is an advantage for hot-melt coating thanks to control of fluidisation air flow rate and feeding rate of molten lipids. The cooling rate in fluidised bed was said to be de facto between 2 and 10°C/min (Becker et al., 2016; Chansanroj et al., 2007b). Furthermore, the fluidised bed can maintain a constant target crystallisation temperature by defining the setpoint as  $T_{air,f}$ .

**Figure 1-16-B** shows the negative mechanism of action when adding an emulsifier as an additive. The retardation of the crystal growth may not be associated with convection or diffusion of lipid molecules as illustrated with **Figure 1-16-A**. Emulsifier molecules inhibit the incorporation of lipid molecules into kink sites instead. However, for a high effectiveness, this interaction requires two conditions: (i) adsorption of the emulsifiers which should display a similarity in fatty-acid moieties at the kink sites and (ii) repulsion of the lipid molecules to be incorporated which should bear a dissimilarity in polar head groups with the emulsifier molecules (Hondoh et al., 2018). In this case, the emulsifier molecules poison the growth sites on the crystal surface (Boistelle, 1988). For a better understanding of the physics, an expression of the crystal growth rate (Adachi et al., 2014) is given as follows:

Equation 25 :

$$G = \frac{fk_B T_c}{3\pi a_0^2 \eta} \left[ 1 - \exp\left(\frac{-\Delta G_c}{RT_c}\right) \right]$$

where  $f$  is the fraction of sites on the crystal surface available for attachment,  $a_0$  is the thickness per molecular layer (m),  $\eta$  the viscosity (Pa.s) and  $R$  the gas constant. As can be seen in **Equation 25** and **Figure 1-16-B**, the number of growth sites, the viscosity of the mother phase and the supercooling are probably the determining factors of crystal growth as discussed above.

Note that additive addition can have four effects on crystallisation behaviours: (i) both nucleation and crystal growth promoted, (ii) nucleation promoted and crystal growth retarded, (iii) nucleation retarded and crystal growth promoted and (iv) both nucleation and crystal growth retarded. The four effects might be useful for design of a specific lipid-based formulated product but in the case of pharma manufacturing the first effect is evidently expected. In effect, while nucleation of a lipidic formulation at a specific thermal condition determines its feasibility, crystal growth determines its ease of manufacture. For



instance, MSZW of  $\beta'$  tristearin informs of its crystallisation temperature and when working with this polymorph definition of a sufficiently slow feeding rate is necessary to avoid agglomeration. The underlying cause is its slow crystallisation kinetics compared to that of  $\alpha$  and  $\beta$ .

Furthermore, nucleation and crystal growth kinetics of a lipid can be different from each other in terms of rate and extent. In other words, nucleation kinetics might be maximal at the one temperature (range) while crystal growth reaches its maximum rate at another temperature (range) (Descamps & Dudognon, 2014; Kim, 2003). This knowledge highlights selection and if necessary, combination of appropriate additives with different effects.

Though separately discussed, the two processes – *nucleation and crystal growth* – constitute the whole solidification process of high-purity lipids whose melt crystallisation is more controllable in comparison with complex-mixture lipids. Melt crystallisation determines the processability via melt-based processing in general and hot-melt coating in particular. **Good understanding of melt crystallisation** is indispensable for control of process regime, long-term stability, and functionalities of end products (Ribeiro et al., 2015).

#### 2.2.1.4. *Particular case of complex-mixture lipids*

Crystallisation profile of complex-mixture lipids (including those of natural origin like beeswax, one of lipids investigated in this doctoral thesis) is usually characterised by a wide melting/crystallisation temperature range (Brubach et al., 2007; Bucio et al., 2021; Müller et al., 2018; Otun et al., 2015) or by several net melting/crystallisation peaks (Chansanroj et al., 2007b).

On the one hand, low melting fraction can work as solvent in crystallisation of high melting fraction (Hondoh et al., 2018). Unlike high-purity lipids whose crystallisation of a polymorph is almost independent of cooling rate but target crystallisation temperature, slow cooling rate could lead to phase separation or fractionation in complex-mixture lipids.

Fast cooling could result in formation of one lamellar phase (at the nanoscopic scale) (Brubach et al., 2007) or one homogeneous system (at the microscopic scale) (Otun et al., 2015). A hypothetical explanation for this observation is that at a higher cooling rate high melting fraction crystallises and traps low melting fraction in its crystal network at the same time. These systems could be “kinetically stable” (Jannin, 2010; Jannin et al., 2015; Salar-Behzadi et al., 2019) and additive addition or further thermal treatment might disturb this kinetics. Slow crystallisation of the most stable polymorphic state could also continue in these systems (Garti & Yano, 2001).

On the other hand, the supercooling of high melting fraction can be regarded as the supercooling of the whole system. In this case, low supercooling could be a problem of certain waxes (e.g. beeswax, candelilla wax, paraffin) as it can cause discontinuity of production operations. This behaviour is ascribed to the natural occurrence of alkanes in their chemical composition (Bucio et al., 2021). For instance, this justifies the difference in the crystallisation temperature measured via calorimetry and oscillation rheometry. The fact that the rheological  $T_c$  obtained at slow cooling rate was close to the onset of the crystallisation of high-melting fraction detected via calorimetry indicates low supercooling of beeswax and candelilla wax. On the other hand, the thermal  $T_c$  identified at the end of the

crystallisation of low-melting fraction detected via calorimetry served as a guide to defining thermal conditions for hot-melt coating (Müller et al., 2018).

Due to the complexity of the crystallisation process, nucleation and crystal growth mechanisms can be investigated by applying the Avrami model which is familiar to food researchers (Foubert et al., 2003; Metin & Hartel, 1998; Narine et al., 2006; Otun et al., 2015) which is given as follows:

*Equation 26 :*

$$SFC = \frac{F(t)}{F_{\infty}} = 1 - \exp(-kt^n)$$

where *SFC* is the solid fraction contents (-) at time *t*, *k* the crystallisation rate constant ( $s^{-n}$ ) and *n* the Avrami exponent (-). The values of *n* correspond to spherulitic growth, continuous nucleation, growth in less than three dimensions, and heterogeneous nucleation on planar or linear defects (Narine et al., 2006). Estimation of *k* and *n* necessitates the values of *F(t)*, the crystallinity at time *t* (J/g), and *F<sub>∞</sub>*, the total crystallinity after complete crystallisation (J/g), obtained via differential scanning calorimetry or solid state nuclear magnetic resonance. The construction of SFC as a function of time or temperature (also called crystallisation/solidification profile) can also be used for definition of thermal conditions in hot-melt coating (Jannin et al., 2005; Jannin & Cuppok, 2013; Müller et al., 2018).

To change crystallisation behaviours of these lipids, mixing them with another crystalline lipid could make a difference (Müller et al., 2018). For instance, mixing palm fat with beeswax or candelilla wax created eutectic mixtures while mixing beeswax and candelilla wax formed a solid solution. This is ascribed to dissimilarity and similarity in chemical composition of the three lipids, respectively. Note that this case risks forming a complex polymorphism.

### 2.2.2. Adhesion

#### 2.2.2.1. *Considerations for processing fluidity*

Lipids with good adhesion properties are expected to well adhere to substrates **during solidification** when performing the coating trials. However, coating materials which are too adhesive can disturb processing fluidity and cause loss in productivity (Adhikari et al., 2001). This is therefore called a stickiness issue which is not solely the problem for hot-melt coating, but also aqueous film coating and tableting (Ammar et al., 2016; J. Lee, 2004).

An additional requisite for selection of lipids in hot-melt coating seems to be a moderate adhesiveness that should assure both good “fluidisability” of coated particles and good coating quality, which will be one of the subjects of study in this thesis.

For complex-mixture lipids, notably those of natural origin, certain classes of chemical substances can impart a high adhesiveness such as paraffins (W. Li et al., 2012). Beeswax which is rich in these components (Bucio et al., 2021) was reported not to be a suitable “monocomponent” formulation for hot-melt coating (Müller et al., 2018). Combinations of candelilla wax and beeswax from the ratio 7:3 were observed to work for hot-melt coating. In effect, candelilla wax as vegetally sources is known to

contain mainly esters of very long fatty acids and fatty alcohols (Sato, 2018a). From these two cases, stickiness issues originate in chemical composition of the formulations. Solutions for these issues could be adding anti-adhesive agents such as magnesium stearate, sodium stearyl fumarate, talc or glyceryl monostearate (Ammar et al., 2016; J. Lee, 2004). The common point is that they are all crystalline by nature. As a precaution, additive addition needs careful consideration on the polymorphism of new systems as well as the impact on release properties (Ammar et al., 2016).

#### 2.2.2.2. Considerations for coating quality

As mentioned in the previous section, lipids with good adhesion properties should wet-out the particle surface in the molten state and then well adhere to it after solidification. One can compare the application of a droplet of the molten formulation onto a particle surface to the application of a hot-melt adhesive on an arbitrary plan as illustrated in **Figure 1-17**:

- **Figure 1-17-A:** the open time is the period between the moment where after the application the hot-melt formulation can flow and wet-out the substrate particle and the moment where it begins to solidify and lose its tackiness in the course of cooling (Moyano et al., 2019). The set time is counted from the application till the onset of the hot-melt formulation re-crystallisation which marks the change in storage modulus  $G'$  and the duration of its sharp increase with the decrease of temperature (Moyano et al., 2019). Adhesion can be explained as the ability of the hot-melt formulation to bond with the substrate surface in a short time with a minimal contact force (O'Brien et al., 2007).

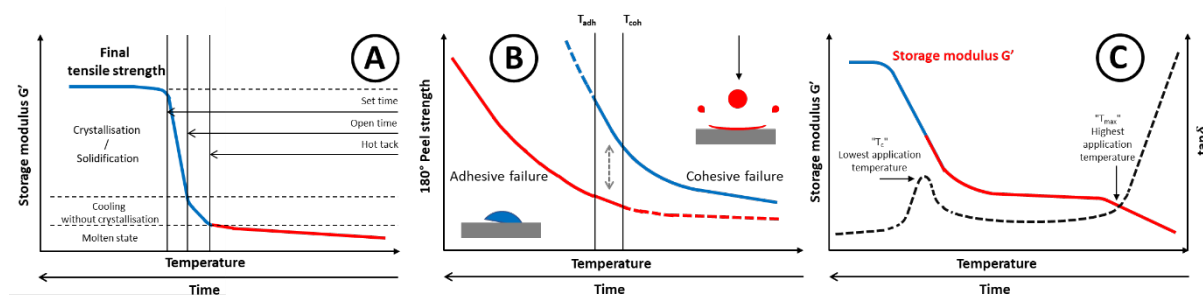


Figure 1-17. Relevance between crystallisation kinetics, adhesion, cohesion and viscoelasticity to defining  $T_c$  (adapted from Kondo & Toda, 2009; Moyano et al., 2019; O'Brien et al., 2007).

- **Figure 1-17-B:** the peel strength decreases in adhesive failure mode when the temperature continuously increases. Till a certain value, the peeling mode is subject to a transition from the adhesive failure mode to the cohesive failure mode, followed by a recovery of peel strength. This transition is ascribed to the change in the viscoelastic properties of the hot-melt formulation with temperature (Kondo & Toda, 2009).  $T_{adh}$  and  $T_{coh}$  are the lower temperature limit of the adhesive failure and the upper temperature limit of the cohesive failure, respectively.

- **Figure 1-17-C:** the storage modulus  $G'$  can be related to the re-crystallisation of the hot-melt formulation as shown in **Figure 1-17-A**. It is stated that the steeper the slope of change in storage modulus  $G'$  the faster the solidification of the system (Costard, 2017). The first moment at which  $\tan \delta$  reaches a peak indicates the re-crystallisation of the hot-melt formulation together with a change in the viscoelastic behaviours. At the second moment where  $\tan \delta = 1$ , the temperature at this point is defined as the highest temperature at which the hot-melt formulation significantly loses its cohesive strength. Consequently, droplets of the molten formulation become more subject to splashing.

These graphs originating from the researches of hot-melt adhesives show the potential link between crystallisation, adhesion and viscoelastic behaviours of lipid-based formulations in the liquid-solid transition. In effect, the information of those researches is relevant as addition of lipids (e.g., paraffins) in formulating hot-melt adhesives was reported to help them crystallise rapidly at the time of their application onto a contact surface (Kalish et al., 2015). This link might help define an optimal value for the crystallisation temperature in hot-melt coating or predict the performance of one lipid-based formulation to adhere to the substrate surface in the case of isothermal conditions.

The temperature scale applies to the case of spontaneous nucleation while the time scale applies to the case of sporadic nucleation (as shown in **Figure 1-17**). Concerning the relevance of the adhesion to the coating quality, **Figure 1-17-B** can be used for a hypothetical explanation. In the case of spontaneous nucleation, when  $T_c$  is defined too low, droplets of the molten formulation undergo the adhesive failure as they cannot wet-out and well adhere to the substrate particles. This probably leads to delamination. In the case of sporadic nucleation, when the solidification rate of the molten formulation is limiting, both adhesive and cohesive failure modes can occur. This likely causes both delamination and agglomeration. Solutions for the case of sporadic nucleation are strongly linked to improvement in formulation properties (e.g. addition of additives which act as an inductor of both nucleation and crystal growth, e.g., talc, polymeric derivatives).

### 2.2.3. Viscosity and viscoelastic behaviours

#### 2.2.3.1. *Considerations for formation of melt droplets*

For the spray nozzle to pulverise the molten formulation into a sufficient droplet size distribution, its melt viscosity should be sufficiently low. The melt viscosity of 300 mPa.S is taken in literature as a reasonable upper limit (D. G. Lopes, Salar-Behzadi, et al., 2017). By considering **Figure 1-17-C**,  $T_{max}$  can serve as the upper temperature limit for the melt (the molten formulation) and/or the pulverisation air temperature. This might help avoid the splashing of droplets and therefore the fine overproduction.

#### 2.2.3.2. *Considerations for film formation*

For a good film to form, good viscoelastic behaviours are also requisite. The thermal operational conditions, which involve temperature of the molten formulation for feeding, pulverisation air temperature and crystallisation temperature  $T_c$  (fluidisation air temperature), should be considered together so that the droplets arrive at the particle surface with a sufficient melt viscosity to facilitate spreading and film forming. Viscoelastic behaviours could also reflect the crystallisation kinetics of the lipidic formulations (Toro-Vazquez et al., 2002). In the case of spontaneous nucleation,  $T_c$  should not be too low because delamination might be its effect. In the case of sporadic nucleation, an induction time is required for the molten formulation to solidify. In the meantime, in liquid state it might undergo splashing to result in fine overproduction or cause agglomeration when the wetted particles collide with each other. Slow crystallisation might also lead to its weak adhesion on the particle surface (see **Figure 1-17-B**). As a matter of fact, addition of viscosity thickeners, adhesives, crystallisation inductor might be necessary.

The two topics just discussed (**adhesion, viscosity and viscoelasticity**) highlight the potential link between crystallisation, adhesion and viscoelastic behaviours of lipid-based formulations to define ideally an optimal crystallisation temperature that assures feasibility of the formulation and its facility for the production, coated product quality and process productivity. It is also advisable to avoid extreme cases where crystallisation, adhesion, and viscoelastic behaviours of the lipidic formulation could cause processing issues, as suggested in **Table 1-4**.

*Table 1-4. Possible consequences when processing-specific properties are in an extreme case*

Processing-specific properties	Possible scenarios	Possible consequences
<b>Crystallisation rate (nucleation, crystal growth)</b>	Both too fast	Fine overproduction
	Too slow nucleation Too fast crystal growth	Agglomeration
	Too fast nucleation Too slow crystal growth	Fine overproduction Agglomeration
	Both too slow	Fine overproduction Agglomeration Long processing time
<b>Adhesion</b>	Too high	Accumulation of coated particles sticking to process wall
	Too weak	Delamination
<b>Viscoelastic behaviours</b>	Too high	Delamination
	Too weak	Fine overproduction

#### 2.2.4. Thermal stability

##### 2.2.4.1. *Considerations for the coating*

As melt-based processing conditions are relatively high in comparison with those imposed by solvent-based production, a definition of thermal conditions based on thermal stability profile is necessary.

Concerning lipids commonly exploited for coating, for example, trilaurin, trimyristin, tripalmitin and tristearin were found to be decomposed starting from 150°C, 150-181°C, 170-184°C and 180-187°C, respectively (Ravotti et al., 2020).

In the case of fatty acids, capric acid and myristic acid were reported to be degraded starting from about 95°C and 111°C, respectively (Majó et al., 2021). Stearic acid was found to be decomposed at the temperature range of 360-380°C whereas paraffin wax started to be degraded at 450°C (Jaw et al., 2001).

As a representative of complex-mixture lipids, beeswax was found to undergo thermal decomposition over a wide temperature range of 125-370°C (Al-Shehri et al., 2022). Another study revealed that the decomposition of beeswax, candelilla wax and paraffin wax started from 209°C, 220°C and 216°C,

respectively (Bucio et al., 2021). These data were quite abundant in the research subjects of phase change materials and food.

Concerning additives which are organic compounds, documented thermal stability data appear to be rarer. However, these data could be requested from the manufacturers as their chemical profile and thermal stability could diverge. For example, vitamin E D- $\alpha$ -tocopherol polyethylene glycol (1000) succinate is informed to be subject to oxidative degradation at 219°C and above. According to published data on the manufacturer's website, decomposition temperature of sugar esters is in general above 220°C. In case that these data are missing, in-house thermal stability could be conducted. One can refer to an example study was performed on palmitic acid, citric acid ester of monoglyceride and their mixture 50:50 (Schertel et al., 2022).

#### 2.2.4.2. Considerations for the core

The thermal stability of substrate is important for decision making to work with hot-melt coating. Stereotypically, it has been said that high temperature setup in melt-based processing do not generally suit thermolabile active substances and even delicate intermediates (e.g., amorphous solid dispersions).

In practice, as was explained the heat exchange of hot-melt coating in **Section 1.3.4**, although high-temperature is set for the sake of operational fluidity (i.e. transporting and spraying of melt), substrate particles are subject to fast cooling by virtue of fluidisation air flowrate. The higher the flowrate of fluidisation air, the higher its cooling capacity and the shorter the residence time of substrate particles in the spraying zone and therefore the less the exposure time of sensitive substrate to heat.

In addition, one can consider defining a low setpoint of fluidisation air temperature so as not to compromise the substrate. For example, hot-melt coating with tripalmitin-based formulations has been successfully applied on a thermosensitive active substance – N-acetyl cysteine – and a delicate substrate – amorphous carvedilol (Bannow et al., 2020; Becker et al., 2016). In these cases, the ambient temperature around 25°C was chosen as the fluidisation air temperature.

Knowing the thermal stability profile of lipid-based formulations and substrate is useful for design of coating process. As discussed above, setup of all the thermal process parameters ( $T_f$ ,  $T_{air,f}$  and  $T_{air,s}$ ) as well as an appropriate fluidisation air flowrate is important. Batch size is a factor also noteworthy. In fact, as discussed in **Section 1.3.1**, it could affect pressure drop of the product bed and, therefore, particulate population density in the spraying zone. Besides, processing time dictated by the feeding rate of the molten formulation and a target coating content should be considered since long exposure to heat possibly denatures the formulation in molten state and/or the substrate.

### 2.3. Solid-State Behaviours

After solidification (production stage), aging of lipid crystal network is naturally occurring in accordance with thermodynamic laws (Sato, 2018a) as one or several post-crystallisation events (as shown in **Figure 1-12**) could arise. Control of these events, also called solid-state behaviours, is indispensable to stabilise the final products till the use of the end customers (Sato, 2018a). These solid-

state behaviours could be discussed in four principal categories as follows: **polymorphism, Ostwald ripening, phase miscibility and interface interactions.**

### 2.3.1. Polymorphism

#### 2.3.1.1. High-purity lipids

Polymorphism can be defined in terms of the ability to manifest different unit cell structures in crystal, resulting from a variety of molecular conformations and molecular packings (Ribeiro et al., 2015; Sato & Garti, 1988). Long-chain compounds such as fatty acids and their derivatives can occur in more than one polymorphs by virtue of different molecular interactions via, for example, methyl end stackings, polar head groups, or bulky aliphatic chains (Ribeiro et al., 2015; Sato & Garti, 1988). In other words, dealing with polymorphism is often unavoidable when formulating lipids (Girod Fullana & Aubert-Poussel, 2019). For instance, despite the level of simplicity according to the classification (see **Figure 1-11**) fatty acids whose number of hydrocarbon atoms ranges from 12 to 18 (i.e. lauric acid, myristic acid, palmitic acid, stearic acid) have between three and four polymorphs (Sato, 2018b).

Saturated monoacid triglycerides are the main pure lipids of interests for discussion here thanks to their abundant availability of hot-melt coating applications (Bannow et al., 2020; Becker et al., 2016; D. G. Lopes et al., 2015, 2016; D. G. Lopes, Koutsamanis, et al., 2017; Schertel, Salar-Behzadi, Karrer, et al., 2021; Schertel, Salar-Behzadi, & Zimmer, 2021; Stocker et al., 2017). A triglyceride (e.g. tripalmitin, tristearin) has three polymorphs  $\alpha$ ,  $\beta'$  and  $\beta$  whose stability increases with the melting point ( $T_{m,\alpha}$ ,  $T_{m,\beta'}$  and  $T_{m,\beta}$ ), as shown in **Figure 1-18**. Its polymorphism is monotropic and their molecular packings are hexagonal (H), orthorhombic ( $O_{\perp}$ ) and triclinic ( $T_{//}$ ) (Sato, 2018b).

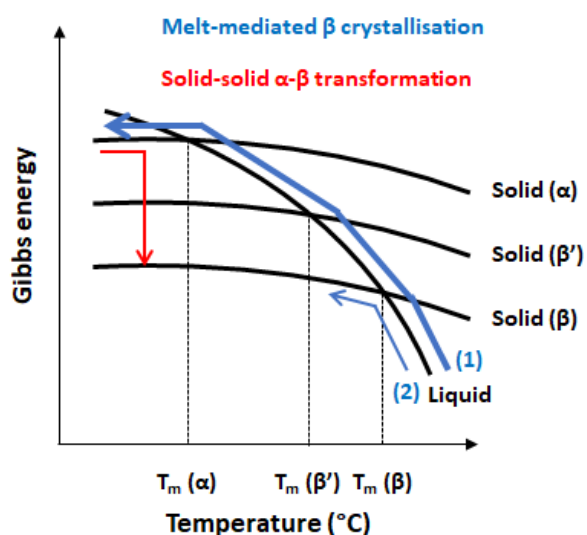


Figure 1-18. Monotropic polymorphism and two processing approaches for generation of the stable form  $\beta$  (adapted from Yoshikawa, 2016)

The polymorphic stability of metastable forms  $\alpha$  and  $\beta'$  increases with the increase in chain length of fatty acids constituting the triglycerides (Yoshikawa, 2016). For example, pure trilaurin crystallised in  $\beta'$  and  $\beta$  forms and self-converted into completely  $\beta$  form with a day at ambient temperature while  $\alpha$



tripalmitin and tristearin took one day and more than 48 days to transform into their  $\beta$  form at 40°C, respectively (Windbergs et al., 2009c).

Solid-solid (e.g., thermal treatment by tempering, maturing or curing), melt-mediated (i.e. recrystallisation from metastable modifications, direct crystallisation from melt) and solvent-based (i.e. direct crystallisation from solution) pathways are three modes of polymorphic transformation (Aquilano & Sgualdino, 2001).

Other than the process engineer's point of view in **Figure 1-14**, **Figure 1-18** illustrates two of the pathways to obtain the most stable polymorph relevant to hot-melt coating in particular (Becker et al., 2015):

- On the one hand,  $\alpha$  polymorph can crystallise with ease at thermal processing conditions set less than  $T_{m,\alpha}$  and the production operations are often necessarily followed by a tempering process to convert  $\alpha$  into  $\beta$  (Becker et al., 2016).

- On the other hand, it is more challenging to have  $\beta$  polymorph crystallise at thermal processing conditions set greater than  $T_{m,\alpha}$  (D. G. Lopes et al., 2015) as the three processes of melt crystallisation – supercooling, nucleation and crystal growth (as shown earlier in Figure 1-14) should be treated with particular caution. This non-traditional approach to generating directly  $\beta$  polymorph has been unique for hot-melt coating till now but it has been largely exploited for hot-melt extrusion (Windbergs, 2009; Windbergs et al., 2009e, 2009d, 2009a). The advantage of the non-traditional hot-melt coating approach is that it can make this process greener and leaner by bypassing the need for tempering, i.e. polymorphic transformation. Actually,  $\alpha$  tristearin had to undergo 12h at 50°C to be converted into  $\beta$  (D. G. Lopes et al., 2015). However, this approach is not suitable to thermolabile substrate.

From a stability point of view, lipids can be classified according to their polymorphic transformation behaviours:

- **Lipids whose polymorphic transformation is sensitive to short-term exposure to temperature:** this is the case of natural lipids of high purity (e.g., triglycerides). This process can be accelerated by setting an appropriate tempering temperature (Windbergs et al., 2009c) and adding additives alone or in combination (J. Aronhime et al., 1990; J. S. Aronhime et al., 1987, 1988; Becker et al., 2016; Bertoni et al., 2021). Normally, the tempering thermal conditions should be less than the melting point of unstable form (Chansanroj et al., 2007b; D. G. Lopes et al., 2015).

- **Lipids whose polymorphic transformation requires long-term exposure to temperature:** this is the case of natural or synthetic complex-composition lipids such as beeswax, hard fats, glyceryl behenate, behenoyl polyoxyl-8 glyceride, glyceryl palmitostearate (A. S. Achanta et al., 1997; Chansanroj et al., 2007b; Jones & Percel, 1994; Jozwiakowski et al., 1990; Kushwah et al., 2020, 2022; Milanovic et al., 2018; Padsalgi et al., 2008; Reitz & Kleinebudde, 2007; Rosiaux et al., 2018; Salar-Behzadi et al., 2019; Xu et al., 2017). The tempering/annealing process often lasts for days to months and require a combination of several factors (e.g., temperature, additive addition, humidity) (Kushwah et al., 2020).

▪ **Lipids which occur in solely one polymorph  $\alpha$ :** this is the case of a new class of lipid-based excipients – polyglycerides (Corzo et al., 2020; Corzo Dardón, s. d.; Salar-Behzadi, Corzo, et al., 2020; Salar-Behzadi, Karrer, et al., 2020).

The impact of additive addition on polymorphic transformation will be treated in **Section 2.4**.

#### 2.3.1.2. *Complex-mixture lipids*

Polymorphic profile of complex-mixture lipids (natural and synthetic) is generally difficult to control and subject to **composition lot-to-lot variations** (Gibson, 2007; Girod Fullana & Aubert-Poussel, 2019). For example, the naturally occurring polymorphs are  $\beta'$  for soybean oil, corn oil, coconut oil, palm kernel oil, cocoa butter and  $\beta$  for cottonseed oil and palm oil (Ribeiro et al., 2015). Another study reported controversially that preferential polymorphisms of soybean, cottonseed, palm and crambe hard fats were  $\beta$ ,  $\beta'$ ,  $\beta'$  and  $(\beta' + \beta)$ , respectively (J. D. Lopes et al., 2015).

Hydrogenated soybean oil, castor oil, partially hydrogenated cotton seed oil, carnauba wax, have been occasionally used for hot-melt coating researches where a **post-production thermal treatment for tempering is rare** (A. Achanta, 1999; Chansanroj et al., 2007b; Jones & Percel, 1994; Jozwiakowski et al., 1990; Padsalgi et al., 2008; Xu et al., 2017). Polymorphic transformation is not necessary when such complex-mixture lipids (e.g. hydrogenated palm oil, carnauba wax, rice bran wax, **beeswax**, stearin) are used for hot-melt coating researches whose objectives consist of method development, characterisation of hot-melt coating performance as a function of formulation properties (Müller et al., 2018; Woerthmann et al., 2021, 2022, 2023).

**Treatment of polymorphic transitions which can be finished in the early stage for high-purity lipids** was excellently discussed by Becker et al. (Becker et al., 2015) by proposing some approaches that could suit hot-melt coating as follows:

- Tempering during processing;
- Tempering after processing;
- Addition of seeds (templating agents);
- Addition of polymorphic controllers;
- Selection of lipid-based excipients with stable polymorphism;
- Definition of appropriate storage conditions.

On the contrary, polymorphic evolution of complex-mixture lipids requires a long and careful treatment. By a rare study on this subject, it was demonstrated the effect of tempering at different temperatures on release kinetics of a drug coated with hydrogenated soybean oil (Chansanroj et al., 2007b). However, this effect should be monitored in a longer period.

Like natural lipids, synthetic mixtures of lipids also exhibit complex polymorphism. Examples are commercial products Compritol® 888 ATO (glyceryl behenate) and Precirol® ATO 5 (glyceryl palmitostearate). They have a fixed ratios between mono-, di- and triglycerides (Jannin, 2010). Note that each component is a crystalline matter itself. The most precious information is that formation of “stable

phase” metastable forms sub- $\alpha$  and  $\beta'$  was obtained at a cooling rate of 10°C/min when cooling down to 10°C (Brubach et al., 2007). Note the (final) crystallisation temperature and the cooling rate, whose importance was discussed in **Section 0**. This cooling rate is feasible with hot-melt coating as stated by a study (Becker et al., 2016). For the reader’s information, the form sub- $\alpha$  is a less ordered phase equivalent to the orthorhombic perpendicular subcell  $\beta'$  of triglycerides (Jannin, 2010). The occurrence of a “stable phase” metastable form is possible for a complex mixture of crystalline matters or with the addition of a crystal modifier (e.g. sorbitan monostearate) and in this case the form sub- $\alpha$  is probably stabilised for a long period and the transformation into  $\beta$  is delayed but not inhibited (J. S. Aronhime et al., 1988).

Glyceryl behenate has been used for hot-melt coating a hydrophilic and thermosensitive substrate (Salar-Bezadi et al., 2019). The trial was performed with an inlet air temperature of around 25°C at a coating ratio of 70% w/w. The study showed that release kinetics was relatively stable for 3 months of storage at 20°C ( $f_2 = 68$ ) but unstable at 40°C ( $f_2 = 42$ ). It was found that a new peak of  $\beta$  form was observed for samples stored at 40°C (not at 20°C) and this phase modification probably altered release profile. In another study where glyceryl behenate was used as matrix for spray congealing, addition of a pore former at low concentration and annealing at 40°C and/or 50°C during 7-21 days helped convert partially into  $\beta$  form (Kushwah et al., 2020, 2022). In another study where this lipid was used an excipient for controlled release tablets, it was found that release kinetics was stabilised from 3 to 6 months for tablets stored at 40°C. In addition, curing at 50°C for 24h did not change release kinetics of the hydrophilic drug (Jannin et al., 2015). **These example studies showed that understanding the formation conditions (cooling rate and crystallisation temperature) of a “stable phase” metastable form  $\beta'$  for a synthetic complex-mixture lipid is important, polymorphic transformation needs a sufficient exposure to temperature for its significant effect on release kinetics and in certain cases it would be rather keep this phase than force a polymorphic transformation into the most stable form.**

It is stated that the  $\beta'$  form is stabilised (but not “the most stable form”) when mixed-acid triglycerides are present (Sato, 2018b). Stabilisation of the  $\beta'$  form is conditioned by (i) fatty-acid-chain-length diversity, (ii) triglyceride carbon-number and diversity, (iii) triglyceride structure, (iv) concentration of liquid oil and (v) temperature fluctuation (Sato, 2018b). These statements are true for the fact that many hard fats tend to occur in  $\beta'$  form (Ribeiro et al., 2015). The case of glyceryl behenate can be deemed “similar”.

In general, polymorphic transitions of complex-mixture lipids are more or less chronological with other post-crystallisation events (Ribeiro et al., 2015), which add to difficulties dealing with stabilisation of lipid systems. In the next sections, solid-state behaviours induced by Ostwald ripening (e.g., evolution of crystal size distribution and liquid-solid phase separation) will be discussed.

### 2.3.2. Ostwald ripening

#### 2.3.2.1. *Crystal size redistribution*

Nucleation and crystal growth lead to the formation of a lipid crystal network constituted by multiple building units one on another throughout multiple length-scales, as shown in **Figure 1-12**. Once these

processes have finished, crystals of different sizes and shapes are present in the lipid crystal network. Even if only the most stable form occurs, the system is still not stable because the conditions of thermodynamic equilibrium are not fulfilled (Boistelle, 1988).

An adapted definition of Ostwald ripening states that “*the system must evolve spontaneously toward the thermodynamic equilibrium, through the progressive reduction of the total interfacial area between the crystals in the crystal network*”. In fact, only crystals that obey the Gibbs-Thomson equation (**Equation 20**) are stable (Aquilano & Sgualdino, 2001; Boistelle, 1988). Probably, at the time scale of the shelf-life of a pharmaceutical product, Ostwald ripening is hardly finished. If it is finished, only the crystal of the largest initial size would exist in the system and all the other crystal would have disappeared (Boistelle, 1988).

The expected effect of Ostwald ripening is the evolution of the crystal size distribution and the modification of the crystal morphology as a function of time. After crystallisation, coarse crystals continue to grow at the expense of smaller crystals with time (as illustrated in **Figure 1-19-A**). As a consequence, the total surface energy of the system decreases spontaneously (Aquilano & Sgualdino, 2001). This is called recrystallisation, one of post-crystallisation behaviours. It is necessary to differentiate between isothermal recrystallisation (or Ostwald ripening itself) and non-isothermal recrystallisation (also called kinetic ripening). The former occurs in saturated systems at a constant temperature whereas the latter occurs merely in the presence of supercooling conditions, created by thermal fluctuations, by contamination of impurities or addition of additives (Aquilano & Sgualdino, 2001).

According to the definition of Ostwald ripening, it is reasonable to state that **lipid blooming** – *observations of petal-like structures on the lipid surface after a certain period* – and post-crystallisation crystal growth are ascribable to Ostwald ripening. There have been several reports of these observations in the studies on hot-melt coating (D. G. Lopes et al., 2015; D. G. Lopes, Koutsamanis, et al., 2017; Schertel et al., 2022; Schertel, Salar-Behzadi, Karrer, et al., 2021; Schertel, Salar-Behzadi, & Zimmer, 2021).

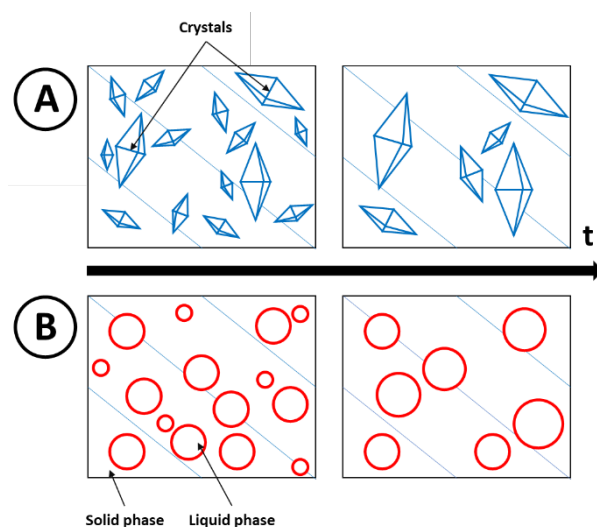


Figure 1-19. Demonstration of Ostwald ripening: growth of crystals (A) and oil droplets (B)

In the first place, lipid blooming is crystal growth on the surface of lipids (Delbaere et al., 2016). In fact, take the case of triglycerides as examples, when the melt of triglycerides was cooled quickly in the operation of hot-melt coating with tristearin, the  $\alpha$  form occurred with the formation of a dense network of small crystals. After the  $\alpha$ - $\beta$  conversion, the converted  $\beta$  form displayed larger crystallite size and developed bloom on the surface of coated particles (D. G. Lopes et al., 2015). Additionally, the difference between the crystallite size of the converted  $\beta$  form and that of the directly crystallised  $\beta$  form implies that the crystal size distribution of the converted  $\beta$  form would continue to evolve. Probably for lipids which occur in several polymorphs (including their combinations with surfactants), their crystal size distribution could evolve and continue to evolve during and after polymorphic transformation, respectively (D. G. Lopes et al., 2015; D. G. Lopes, Koutsamanis, et al., 2017).

Again, lipid blooming is a consequence of crystal size redistribution. Lipid blooming can be detected early after production and after maturation (Bertoni et al., 2021; Chansanroj et al., 2007b; D. G. Lopes et al., 2015; D. G. Lopes, Koutsamanis, et al., 2017) or it can occur slowly in the course of preservation (Witzleb et al., 2012). In these cases, the crystal size redistribution in the crystal network of lipidic formulations and the surface properties appear to be good indicators of stability worth monitoring.

There are several possible solutions to treat Ostwald ripening. In the first place, it is possible to enhance the evolution kinetics of the crystal size redistribution by creating temperature fluctuations with an amplitude and a frequency depending on the lipidic formulation (Boistelle, 1988). One can learn from the case of chocolate to create, for instance, a number of temperature fluctuation cycles (Castro-Alayo et al., 2023; T. L. T. D. Silva et al., 2017; Sonwai & Rousseau, 2006). In these cycles, the rise of temperature is to melt-out all unstable crystals (possibly an application of kinetic ripening) and the fall of temperature is to crystallise a mixture of unstable and stable crystals (possibly an application of secondary nucleation). A series of case studies on hot-melt coating reported that crystal size redistribution was observed for combinations of tripalmitin and polysorbate at different ratios, at different coating contents, at contact of different cores and at different storage conditions (D. G. Lopes, Koutsamanis, et al., 2017; Schertel, Salar-Behzadi, Karrer, et al., 2021; Schertel, Salar-Behzadi, & Zimmer, 2021). This implies that the converted  $\beta$  form of tripalmitin was prone to crystal growth and in this case setup of temperature fluctuations might be a solution, but this strategy has not been adopted in pharmaceutical applications so far.

In the second place, the primary crystal size of the freshly crystallised system represents can limit Ostwald ripening process (Boistelle, 1988). By this effect, Ostwald ripening is fast for crystals having size about 1  $\mu\text{m}$  but neglectable when the crystal size reaches around 100  $\mu\text{m}$  (Aquilano & Sgualdino, 2001). This effect reflects the benefit of  $\beta$  crystallisation in non-traditional hot-melt coating (as presented in **Figure 1-14**) in comparison with  $\alpha$  crystallisation in traditional hot-melt coating. There was already a proof of concept for hot-melt coating with tristearin (D. G. Lopes et al., 2015), which shows the difference between the crystallite size of the converted  $\beta$  form and that of the directly crystallised  $\beta$  form. Furthermore, the directly crystallised  $\beta$  form of tristearin displayed no blooming while this secondary structure was observed on the lipid surface of the converted  $\beta$  form right after production or after  $\alpha$ - $\beta$  conversion (D. G. Lopes et al., 2015; Windbergs et al., 2009e, 2009b). Furthermore, another

proof of concept on extrusion of  $\beta$  trimyristin without melting was reported to yield a stable release profile up to 9 months at 40°C (Reitz & Kleinebudde, 2007).

In the third place, as Ostwald ripening involves both dissolution of unstable crystals and growth of stable crystals, contamination of impurities or addition of additives can have an inhibitor effect (Boistelle, 1988). For this effect, surfactants (e.g. sorbitan esters, lecithins) as anti-blooming agents have been used in food researches since long (Cottrell & Peij, 2014; Garti & Aserin, 2012). As an interesting example of food research, combinations of sorbitan monostearate and polysorbate 60 at ratios of 3:1, 1:1, 1:3 were reported to have the maximal antiblooming effect in comparison with sorbitan monostearate or polysorbate 60 alone (Garti et al., 1986). As another interesting example, it was reported that even at 0.1% w/w level addition of a phospholipid can be effective to reduce lipid blooming (J. Chen et al., 2021). Still, drug formulation scientists have not been familiar with the use of antiblooming agents for solid lipid-based formulations. One of rare findings in pharmaceutical research shows that addition of sorbitan monooleate and lecithin at 10% w/w resulted in a smooth surface of spray-congealed microparticles containing  $\beta$  tristearin (Bertoni et al., 2021). This validated the use of these antiblooming agents in pharmaceutical applications.

In general, the cause of post-crystallisation crystal growth on surface (fat blooming) and in bulk observed in many pharmaceutical researches with solid lipidic formulations is ascribable to Ostwald ripening. Three possible solutions to overcome these stability issues are derived from experiences in food research: (i) tempering with a defined number of temperature fluctuation cycles, (ii) direct crystallisation of the most stable form with a larger crystal size and (iii) additive addition.

#### 2.3.2.2. *Oil migration*

For the definition, like the case of post-crystallisation continuous crystal growth in the crystal network, if liquid phase and solid phase co-exist in the crystal network, this system is also subject to Ostwald ripening. In this case, the initial distribution of dispersed liquid (oil) droplets in the crystal network tends to change in such a similar manner that large droplets grow at the expense of small droplets (as illustrated in **Figure 1-19-B**) in order to minimise the total surface area between the two phases (Green & Rousseau, 2018). A familiar stability problem is a phase-separated system, or oil migration, or liquid leaching, which has been encountered with some pharmaceutical applications (Bertoni et al., 2021; D. G. Lopes, Koutsamanis, et al., 2017).

For the possible solutions to treat Ostwald ripening, unlike the case of post-crystallisation continuous crystal growth in the crystal network, the first precaution is to avoid a high storage temperature that could facilitate Ostwald ripening. In fact, it was reported that the system of tripalmitin/polysorbate 65 90:10 exhibited microphase separation when being stored at 40°C (D. G. Lopes, Koutsamanis, et al., 2017). It was not significantly phase-separated for 6 months at 20°C. The cause of this incidence was said to be that preservation at 40°C melted out polysorbate 65 and in liquid state it leaked out to form larger hydrophilic channels among lipophilic crystalline clusters of tripalmitin. As discussed in the previous section, it is also possible that the parallel crystal growth of converted  $\beta$  tripalmitin was catalysed by the surfactant and then this incidence contributed to this phase separation.



The second solution could be the formation of a dense crystal network with large crystal size ( $\beta$  crystallisation) (Delbaere et al., 2016). For  $\beta$  crystallisation, it is unavoidable to execute the non-traditional hot-melt coating. As a precaution, in the presence of a liquid surfactant,  $\beta$  crystallisation might be retarded (as discussed in **Section 2.2.1.3**) and processing issues (e.g., agglomeration) might occur. Therefore, this approach might warrant for a combination of additives of different types. However, no known study has been performed with non-traditional hot-melt coating and lipid-surfactant systems.

The third solution could be the formation of a dense crystal network with small crystal size ( $\alpha$  crystallisation), which is stabilised by adding additives. The one possibility is to formulate with a liquid lipid which is soluble in the solid lipid. For instance, tristearin was formulated with oleic acid, ethyl oleate, isopropyl myristate, glyceryl monooleate, sorbitan monooleate, lecithin and vitamin E to form microparticles whose release kinetics was stable for one year (Bertoni et al., 2021). The other possibility is to formulate a solidified emulsion which is composed of a lipid and two surfactants with complementary HLBs. In this case, the melt of this system occurs in an “hydrophilic fraction/lipophilic fraction” emulsion which solidify upon cooling. By the effect of a binary surfactant combination, the crystal size distribution of this system is expected to be stabilised after  $\alpha$ - $\beta$  conversion in the long run. In fact, this formulation strategy inspires from the proof of concept that combinations with a mixture of surfactants have successfully aided in the stability of emulsion systems (Pichot, 2012).

### 2.3.3. Phase miscibility

To distinguish with Ostwald ripening of liquid-solid systems, phase miscibility concerns combinations of lipidic crystalline matters (Macridachis-González et al., 2020) rather than incorporation of liquid minor component(s) in solid lipid systems as discussed in the previous section. Understanding of this concept could help create new formulation recipes of great interest in industrial applications (Macridachis-González et al., 2020). Furthermore, as phase miscibility could be mistaken for the specific (liquid-solid) phase separation observed in the previous hot-melt coating researches, it is relevant to discuss.

#### 2.3.3.1. *Solid solution*

When a homogeneous liquid binary mixture of a lipid system is cooled, both of the components solidify simultaneously and incorporate into crystal network of each other to certain extent (Floeter et al., 2018). The crystallised system is a solid solution whose phase diagram is shown in **Figure 1-20-A**. All the binary mixtures display intermediate melting temperatures between the melting points of the pure substances as a function of varying molar ratios. As an example, combination of triglycerides whose physicochemical properties are similar (e.g., trilaurin and trimyristin, tripalmitin and tristearin) was reported to form solid-solution mixtures (Floeter et al., 2018). However, their mixing behaviours depend on polymorphism. In fact, their occurring  $\alpha$  and  $\beta'$  are miscible whereas their stable polymorphs  $\beta$  exist in eutectic mixtures (Macridachis-González et al., 2020). Another example is the case of tristearin and sorbitan monostearate. Addition of the latter inhibit  $\beta$  crystallisation of the former (Aronhime et al., 1987). A solid solution should form between sorbitan monostearate and  $\alpha$  tristearin upon cooling



whereas de-mixing is observed when their mixtures are subject to isothermal crystallisation at 60°C for hours. In pharmaceutical researches, mixtures of triglycerides have been used for preparation of suppositories (Grant et al., 1983; Grant & Liversidge, 1983; Liversidge, 1983; Liversidge et al., 1981; Liversidge & Grant, 1983). These freshly crystallised systems should exist in solid solution.

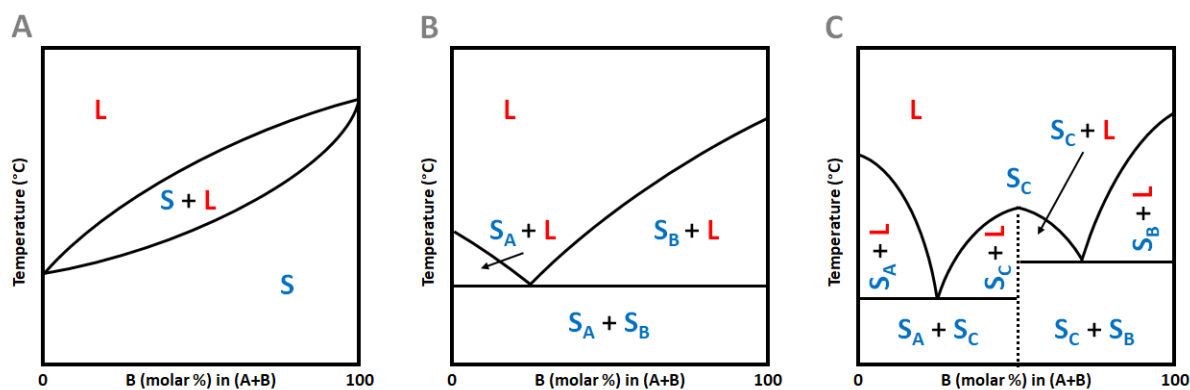


Figure 1-20. Three typical phase mixing behaviours of solid lipid systems (adapted from Bayés-García et al., 2005)

### 2.3.3.2. Eutectic mixture

**Figure 1-20-B** shows an illustrative phase diagram for a eutectic mixture system. The diagram depicts the temperatures at which one component starts to crystallise from the homogeneous neat liquid. The two components exist in molten state above the borders delineating the regions where crystals of the one component occur in molten liquid of the other and vice versa. The eutectic temperature is a characteristic point identified at a specific molecular ratio of the two components. At this point, the melting of the binary solid mixtures begins. Below this point, the total system is solidified (Bayés-García et al., 2005). Formation of an eutectic system is common for binary mixtures of monoacid  $\beta$  triglycerides (Floeter et al., 2018) and those of fatty acids different in chain length (M. C. Costa et al., 2007, 2009; Inoue, Hisatsugu, Ishikawa, et al., 2004; Inoue, Hisatsugu, Suzuki, et al., 2004; Inoue, Hisatsugu, Yamamoto, et al., 2004). Effectively, it was demonstrated in pharmaceutical researches that the binary systems of palmitic acid and stearic acid at 50:50 and 70:30 interacted with alkaline buffer media (pH 8) more pronounced than the systems of a pure component (Qi et al., 2006, 2008). This knowledge could be inspired for potential applications such as preparation of delayed release pharmaceuticals hot-melt coated with fatty acids (e.g., palmitic acid, stearic acid) (Patil et al., 2012; Schertel et al., 2022; Sudke et al., 2013). The release mechanism is based on their pH-dependent solubility by which fatty acids and their derivatives are saponified in alkaline media and therefore the lipid membrane is eroded to release active substance (Dudzińska, 2017).

### 2.3.3.3. Molecular compound

Two components of a binary system can combine to form a molecular compound at a defined ratio. If a molecular compound can coexist in equilibrium with a neat liquid of the same composition, this compound has a congruent melting point shown by the point  $S_C$  (**Figure 1-20-C**). By considering this point, the phase diagram for this system can be split into two sub-diagrams comparable to that of a

eutectic system. In fact, the molecular compound forms with its constituent a eutectic mixture (Bayés-García et al., 2005). The occurrence of molecular compounds is often observed with saturated-unsaturated mixed-acid triglycerides. It is stated that the ability to form molecular compounds is based on the combined interactions between aliphatic chain packing, glycerol conformation and methyl end stacking (Floeter et al., 2018). Some examples are binary mixtures of 1,3-dipalmitoyl-2-oleoyl-glycerol and 1,2-dipalmitoyl-3-oleoyl-glycerol (POP/PPO 1:1), 1,3-dipalmitoyl-2-oleoyl-glycerol and 1,3-dioleoyl-2-palmitoyl-glycerol (POP/OPO 1:1), 1,3-distearoyl-2-oleoyl-glycerol and 1,2-distearoyl-3-oleoyl-glycerol (SOS/SSO 1:1), 1,3-distearoyl-2-oleoyl-glycerol and 1,3-dioleoyl-2-stearoyl-glycerol (SOS/OSO 1:1) (Floeter et al., 2018; Macridachis-González et al., 2020). Note that the formation of these binary mixtures is dependent on cooling rate (Nakanishi & Ueno, 2020) and fortunately, for instance, the equimolar mixture of POP/OPO can be found at cooling rate similar to that provided by hot-melt coating. These compounds are interesting as their chemical composition hints at a digestibility higher than saturated monoacid long-chain triglycerides.

#### 2.3.4. Interfacial Interactions

##### 2.3.4.1. *Impact of the substrate on lipids*

This is the case when **physical stability of lipidic formulations is more limiting than that of substrates**. As a substrate, the active substance should occur in the most stable polymorph in pure forms (e.g., crystals (Becker et al., 2016; D. G. Lopes et al., 2015; Schertel, Salar-Behzadi, & Zimmer, 2021; Stocker et al., 2017; Xu et al., 2017)) or in intermediate products (e.g., granulates (D. G. Lopes et al., 2016), extrudates (H. Chen et al., 2010)). To demonstrate the impact of the substrate on lipids, two case studies are discussed.

In one study, combinations of tripalmitin/polysorbate 65 in different ratios were used to coat a hydrophilic drug and another lipophilic drug (Schertel, Salar-Behzadi, & Zimmer, 2021). It was reported that for the hydrophilic drug its release kinetics was accelerated with time, and it tended to separate from the lipidic coating. For the lipophilic drug its release kinetics was decelerated with time, and it was likely the cause of crystal size redistribution of the crystal network.

In another study, three active substances whose solubility in glyceryl behenate were coated with this coating agent and then subject to direct tableting with lactose (Jannin, 2004). It was reported that sticking to tableting die was not observed for the least soluble drug and this phenomenon worsens with the increase of solubility of the drugs in the coating material. For the most soluble drug, the trial had to be stopped after about 100 tablets were produced.

Both cases showed that the lipophilicity of the drug can influence processability of the lipidic formulations and long-term stability of their release kinetics. Solutions could be based on the choice of the coating methods, for example, coating with hydrophilic polymers in the case of lipophilic substrates.

##### 2.3.4.2. *Impact of lipids on the substrate*

This is the case when **physical stability of lipidic formulation is less limiting than that of substrates**. Substrates of this type are often delicate in terms of their inherent challenging properties (e.g., low glass

transition temperature) and they might comprise amorphous drugs (Bannow et al., 2020), amorphous solid dispersions, etc. The failure of the first attempt to hot-melt coat an amorphous drug with the objective of improving stability of the amorphous state should not negate the possible suitability of hot-melt coating for other substrates.

**How can one apply solid lipid-based formulations to functionalise delicate substrates (e.g., amorphous solid dispersions), whose stability is technologically and scientifically unpredictable? The must condition is that those solid lipid-based formulations should not compromise their physical stability.** One approach is that more profound studies should be performed to identify the mechanisms underlying stabilisation given by one lipidic formulation and destabilisation caused by another with respect to one formulation of amorphous solid dispersions. This would be labour-intensive and resource-consuming, and the problems continue to arise. For information, several destabilisation mechanisms via heterogeneous recrystallisation have been proposed, which should be relevant to coating induced re-crystallisation of amorphous drugs (Thakore et al., 2020). Another approach that could be more straightforward is to perform “physical compatibility” studies between a large number of candidate (stable) lipidic formulations and the delicate substrate following the official guidelines (ICH Q8 (R2), 2009).

In conclusion, the question of interfacial interactions is which structural component – core or coat – is more thermodynamically stable. This supports the use of a stable and simple active substance (e.g., sodium chloride) as a core in the early stage for developing a number of lipidic formulations. Note that this active substance should be ideally a stable crystalline matter and its melting point should be above the thermal operational conditions. The variety of lipidic formulations can then be used for hot-melt coating the delicate substrates in a “physical compatibility” screening study. The application of this approach could be useful to anticipate a certain attrition rate of developed lipidic formulations which can cause destabilisation the delicate substrates, as one of the models that will be used in this thesis (solid amorphous dispersion of praziquantel).

#### **2.4. Effect of Additives on Lipid Crystallisation and Polymorphism**

From the beginning of hot-melt coating adoption (Appelgren & Eskilson, 1993) and the early evidence of solid lipid-based formulations for pharmaceutical use (Liversidge et al., 1981) till 2004, almost solid formulations were composed of a single lipid major component. One possible reason for this trend is that the use of solid lipids has been thought to be used specifically for controlled-release coating (Rosiaux et al., 2015).

On the other hand, the history of bio enabling (liquid) lipid-based formulations began more than 50 years ago and the use of surfactants in these systems was also evidenced in the same period (Alany, 2017; Feeney et al., 2016). The early solid (binary) lipid-surfactant systems were noticed in 2000s (Jannin, 2004; Jannin et al., 2006) with surfactants acting as both polymorphic controller and release modifier. Since then, there is a time gap till mid 2010s that the interests to formulate this type of binary system re-emerged together with the introduction of hot-melt coating by air flow bed technology

(Becker, 2016; Becker et al., 2016). One of the advantages of this combination was to reveal an immediate release for products with thick coating.

**Table 1-5** provides information about hot-melt coating formulations containing at least one surfactant recorded till nowadays. The double role of surfactants as **polymorphic controller and release modifier** retains more and more formulators' attention not only in hot-melt coating (Bertoni et al., 2021; Kushwah et al., 2020, 2022). Actually, polymorphism is the well-known issue when working with lipids for both food and drug formulation scientists (Bayés-García et al., 2005; Becker et al., 2015; Girod Fullana & Aubert-Poussel, 2019; Sato, 2018b).

Take the case of solvent-based or aqueous film coating, the composition of polymer-based formulations has been well established since long (Arwidsson & Rudén, 1993). Other than the main polymer(s), many types of additives include plasticisers, colorants, opacifiers, surfactants or water-soluble materials, anti-adherents and antimicrobials which are of importance in the descending order. In effect, plasticisers are attributed an important role in stabilisation of the polymer (Arwidsson & Rudén, 1993; Kucera et al., 2013; Siepmann & Siepmann, 2013).

*Table 1-5. Hot-melt coating formulations composed of a lipid and at least a surfactant*

Lipid-based excipients	Surfactants (HLB) (if applicable)	Ratios	Roles	References
<b>Glyceryl behenate</b>	PEG-32 stearate (9.5), polysorbate 60 (15), and PEG-8 caprylic/capric glycerides (12)	80:20	Polymorphic controller; Release modifier	Jannin, 2004; Jannin et al., 2005
<b>Tripalmitin</b>	Polysorbate 65 (10.5)	98:2, 90:10, 80:20, 70:30	Polymorphic controller; Release modifier	Bannow et al., 2020; Becker et al., 2016; D. G. Lopes, Koutsamanis, et al., 2017; Schertel, Salar-Behzadi, Karrer, et al., 2021, 2021; Schertel, Salar-Behzadi, & Zimmer, 2021; Stocker et al., 2017
<b>Cetostearyl alcohol + Beeswax</b>	olive oil, polysorbate 60 (15), ethyl cellulose, hydroxypropyl methyl cellulose	97:3, 96:4, 95:5, 94:6, 87:13	Release modifier	Jacobsen et al., 2021
<b>Palmitic acid</b>	Citric acid esters of fatty acids (11)	50:50	Release modifier	Schertel et al., 2022

Surfactants in solid lipid-based formulations used for hot-melt coating can be regarded as the equivalent of plasticisers in polymer-based formulations used for solvent-based or aqueous film coating. However, the current practice of additive selection is mainly focused on its effect on polymorphic transformation and release modification (Becker et al., 2015). Other types of additives might be necessary for optimal design of solid lipid-based formulated products.

It is possible to review food research to select additives according to their effects. As the principal strategy, the use of surfactants has been intensely investigated since the past century for their effects on nucleation, crystal growth and polymorphic transformation of lipids (J. Aronhime et al., 1990; J. S. Aronhime et al., 1988; Garti & Yano, 2001; K. W. Smith & Sato, 2018). These two physical processes condition the formation of lipid crystal network reflected in the number of crystal nuclei, the size distribution of crystal particles, the crystal morphology, polymorphic crystallisation and transformation

(K. W. Smith & Sato, 2018). By considering this overview, potentials of surfactants have not been thoroughly explored in pharmaceutical research in the subject of solid lipid-based formulations. In food research, “emulsifier” is often used as an alternative for “surfactant”. Surfactants are amphiphilic molecules having lipophilic aliphatic chains and hydrophilic head group (Garti & Yano, 2001). For the sake of simplicity, almost the cases which will be presented concern triglycerides only.

#### 2.4.1. Additive effect on the crystallisation of the most stable form $\beta$

In the first place, the effects of additive addition on crystallisation behaviour (i.e. nucleation and crystal growth) of the most stable form  $\beta$  are presented. **Dealing with nucleation of solid lipid-based formulations has not been the subject of extensive research within the pharmaceutical industry** (Otun et al., 2015). However, benefits of nucleation behaviours in melt processing have been exploited unwittingly. The case of successful extrusion of  $\beta$  trilaurin,  $\beta$  tripalmitin and  $\beta$  tristearin at 40°C, 55(or 60)°C and 65°C (all higher than  $T_{m,\alpha}$ ) was a proof of concept (Windbergs et al., 2009e). Furthermore, extrusion at the same conditions was also performed successfully for trilaurin and tripalmitin with the addition of polyethylene glycol 10000 at a ratio 9:1 (Windbergs et al., 2009a). Furthermore, extrusion at the same conditions was also performed successfully for equivalent-ratio combinations of tripalmitin/poly-ethylene glycol whose molecular weight ranged from 10000 to 700000 (Windbergs et al., 2009a). Extrusion at the same conditions was also performed successfully for combinations of tripalmitin/polyethylene glycol 10000 at ratios 9.5:0.5/9:1/8:2/7:3/6:4/5:5 (Windbergs et al., 2009d). Additionally, all the solid lipid-based formulations above were combined with a drug in a ratio 1:1. From this evidence, either drug, polyethylene glycol of varying weights or even process wall could be crystallisation inductor or at least neutral.

For hot-melt coating, the first proof of concept with tristearin was obtained but no additive was used (D. G. Lopes et al., 2015). The knowledge on the nucleation of a lipid and the effect of additives thereon (as presented in **Figure 1-14**) can help adapt thermal processing conditions of compounded lipidic formulations to a particular melt technology and to chemical stability profile of one substrate as well as overcome certain stability issues (e.g. polymorphism, Ostwald ripening).

Applications of additives in food research have various established evidence. Measurements of the melting point of  $\beta$  tristearin in combination of a substance can help identify whether this substance influences nucleation or not. In this case, if the measured value of the combination fluctuates around the melting point of pure  $\beta$  tristearin, the substance has an effect of nucleation inductor. This was observed for sorbitan monolaureate, sorbitan monooleate, polysorbate 60, octadecane, stearic acid, stearyl alcohol, methyl stearate (J. S. Aronhime et al., 1988). Note that there were three surfactants which are liquid or semi-solid and four other substances whose structure has a stearic acid moiety.

Recently, food researchers discovered new substances (other than surfactants) which also have an effect on nucleation of triglycerides (Yoshikawa, 2016; Yoshikawa et al., 2014). Talc, carbon nanotube, graphite, theobromine, ellagic acid dihydrate, terephthalic acid were found based on the principles of the first approach (Kaneko et al., 2020; Yoshikawa, 2016; Yoshikawa et al., 2014, 2015). Templating was revealed to be the mechanism of action of talc and graphite particles. All the results presented above

were obtained via a conventional screening approach for lipidic formulations which is based on measurements of  $T_m$  at a slow cooling rate. Another screening approach for phase change materials for energy storage based on the nucleation behaviours was also reported (Adachi et al., 2013, 2014). A system like the second approach could be used for high throughput screening of surfactants based on their effects on the nucleation behaviours. These examples in food research show that for an effect of nucleation inductor the choice could be grounded on but not limited to the similarity in fatty acid moieties borne by the additives.

Till the moment, the possible question is **which principles** underlies the effect of an additive on the nucleation and crystal growth.

Thermodynamically, these effects can be related to the melting point ( $T_m$ ) of the crystallisable lipidic formulation or the solubility of an additive in the lipid major component.

As indicator of the effect of additive addition, when the additive increases  $T_m$ , it tends to induce the nucleation of the system in the mother phase (the melt) because the supercooling increases at the same thermal condition and vice versa (K. W. Smith & Sato, 2018). Concerning the relevance of the solubility of the surfactant to its effect on nucleation, in a supercooled melt, if the solubility of the surfactant is high or its concentration is lower than the solubility limit, it might not crystallise before the lipid and retard the nucleation of the system by preventing the formation of nuclei via attractive molecular interactions.

On the other hand, if the solubility of the surfactant is low or its quantity is higher than the solubility limit, it might induce the nucleation of the system (K. W. Smith & Sato, 2018). The solubility of a surfactant in the lipid major component depends on the similarity in molecular shape between the two, especially in the fatty-acid moieties or the acyl groups (K. W. Smith et al., 2011; K. W. Smith & Sato, 2018).

From a point of view of kinetics, the effects of additive addition can be understood on the basis of the fundamentals on nucleation and crystal growth (K. W. Smith & Sato, 2018), as presented in **Sections 2.2.1.2** and **2.2.1.3**. There are four possible effects of additive addition:

- **clustering agent** when the additive acts against the formation of crystal nuclei (e.g., tristearin with sorbitan monostearate/sorbitan tristearate/glyceryl-1-stearate/citric acid ester of glyceryl-1-stearate/triglycerol-1-stearate (J. S. Aronhime et al., 1988)),
- **templating agent** when the additive serves as seeds for nucleation (e.g., tristearin with octadecane, stearyl alcohol, stearic acid, stearyl alcohol, methyl stearate (J. S. Aronhime et al., 1988)),
- **poisoning agent** when the additive adsorbs on available growth sites of the growing crystals (e.g., trilaurin with glyceryl-1,2-dilaurate, glyceryl-1,3-dilaurate (P. R. Smith et al., 1994)),
- **kink-forming agent** when the additive creates new growth sites on the growing crystals (e.g., trilaurin with lauric acid, glyceryl monolaurate (P. R. Smith et al., 1994)).

For melt processing, a fast solidification is expected and intuitively an ideal additive should promote both nucleation and crystal growth of the lipid major component. Otherwise, it is recommended to combine at least two additives which have a promotional effect on either nucleation or crystal growth.



#### 2.4.2. Additive effect on polymorphic transformations of the metastable form $\alpha$

In the second place, the effects of additive addition on polymorphic transformations of the metastable form  $\alpha$  are presented. In the more common practice of melt processing, the lipidic formulation in molten state will be cooled quickly below a temperature at which it should solidify spontaneously, as shown earlier (see **Figure 1-14**). In this case, the metastable forms ( $\alpha$  ( $\beta'$ ) for triglycerides) usually occur in the freshly crystallised lipidic formulation. Then, an extra unit operation – tempering, curing, maturing – is required to convert these metastable forms into the most stable form ( $\beta$  for triglycerides) (Becker et al., 2016; Bertoni et al., 2021).

The question that may arise today is **why** the additives are always needed. On the one hand, unless it is a co-processed mixture, a monocomponent formulation often has limited end-use properties. On the other hand, pure triglycerides (e.g., tripalmitin, tristearin) often transform slowly from  $\alpha$  to  $\beta$  at ambient conditions (Windbergs et al., 2009c) and the longer the aliphatic chains borne by triglycerides the longer the transformation process (Yoshikawa, 2016). Actually, addition of additives (e.g., surfactants) not only accelerates this polymorphic transformation under influence of the additional factors (e.g. temperature, exposure time) but also modifies the release kinetics of the active substance (Becker et al., 2016; Bertoni et al., 2021).

There are two interesting case studies of pharmaceutical applications. For hot-melt coating, systems of tripalmitin/polysorbate 65 are a good example. It was reported that the increase in surfactant concentration (10-20-30%) and temperature (25-30-35°C) accelerates the  $\alpha$ - $\beta$  conversion (Becker et al., 2016). The effect of polysorbate 65 on polymorphic transformation of tripalmitin is so remarkable that  $\alpha$ - $\beta$  conversion is complete within 210 min at maximum, even at 25°C. This is compared to the fact that the  $\alpha$  form of tripalmitin is stable for more than 60 days at room conditions in the absence of additives (Windbergs et al., 2009c). For spray-congealing, combinations of tristearin and various liquid lipids are a good example. It was reported that  $\alpha$ - $\beta$  conversion of tristearin could be complete from 6h to 7 days at room temperature in the presence of 10% w/w additive and oils (isopropyl myristate, oleic acid, ethyl oleate and medium chain triglycerides) accelerated this process more than liquid surfactants (glyceryl monooleate, sorbitan monooleate and lecithin) (Bertoni et al., 2021). Note that the  $\alpha$  form of tristearin is stable for more than 60 days at room conditions (J. S. Aronhime et al., 1988; Bertoni et al., 2021; Windbergs et al., 2009c). Normally, tempering of hot-melt coated products represents in principle a solid-solid transformation process (i.e. under the melting point of the metastable forms) (Chansanroj et al., 2007b). The use of surfactants is still limited to their double roles of polymorphic controller and release modifier while their effects on nucleation, crystal growth as well as other post-crystallisation behaviours (e.g., Ostwald ripening) were overlooked.

Applications of additives in food research also have various established evidence. As presented in two case studies of pharmaceutical applications, measurements of the melting enthalpy of the  $\alpha$  form crystallised in the lipidic formulation in isothermal incubation as a function of time can help identify the effect of an additive on the polymorphic transformation. This approach was adopted since long in food researches (J. Aronhime et al., 1990; J. S. Aronhime et al., 1987, 1988). Based on the effects on

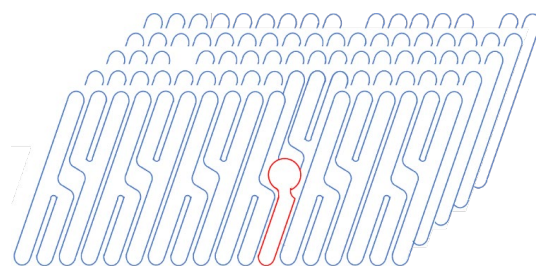


polymorphic transformation of tristearin, surfactants were divided into two groups: (i) dynamic controllers of polymorphic transformation and (ii) crystal modifiers.

The former group can accelerate the  $\alpha$ - $\beta$  conversion process to an extent and a rate both of which depends on other external factors such as temperature, heating rate, and exposure time. Tested surfactants of this group are glyceryl-1-stearate, lactic acid esters of glyceryl-1-stearate, citric acid esters of glyceryl-1-stearate, stearic acid, stearyl alcohol, methyl stearate, octadecane, sorbitan monolaurate and other liquid surfactants (e.g., sorbitan monooleate, polysorbate 60, polysorbate 65, polysorbate 80).

On the other hand, the latter group can decelerate the kinetics of  $\alpha$ - $\beta$  conversion but cannot inhibit this process completely. Tested surfactants of this groups are sorbitan monostearate and triglycerol-1-stearate. Generally, surfactants can modify the kinetics of polymorphic transition of lipids through the preferred adsorption at or inclusion in the lipid crystal network by changing the mobility of the lipid molecules (Garti, 1988; Garti & Yano, 2001). Thermodynamically, surfactants were said not to change crystallographic properties (e.g., occurrence of new polymorphs) which are reflected in the arrangement of the lipid molecules (Garti, 1988). Particularly, surfactants (e.g., sorbitan monostearate, triglycerol-1-stearate) should have a steric compatibility between their polar head group and that of the lipid molecules, which can prevent  $\alpha$ - $\beta$  transformation temporarily (J. Aronhime et al., 1990; J. S. Aronhime et al., 1988; Garti, 1988). This is called “the button syndrome”, as illustrated in **Figure 1-21**. As completed by the results of pharmaceutical researches, any liquid lipids (including oils and liquid surfactants) significantly accelerates the transformation from  $\alpha$  to  $\beta$  (Garti & Yano, 2001).

This section presented certain representative case studies on the effects of additives on the nucleation, the crystal growth and the polymorphic transformation in pharmaceutical applications and food research. The objectives are also dual. On the one hand, these data hint at how to choose additives. In fact, a remarkable fact from these data is that almost the interesting surfactants bear fatty acid moieties or acyl groups in their chemical structures which should predispose these surfactants to adsorb or include in the lipid crystals and exert their effects (as shown in **Figure 1-21**). On the other hand, these data suggest the principles underlying an imminent screening approach which is efficient and fast-track to select adequate surfactants or combinations from many candidates.



*Figure 1-21. Incorporation of a surfactant molecule in triglyceride crystal network (J. S. Aronhime et al., 1988)*

Inspired by this literature review, a classification of additives used in solid lipid-based formulations will be proposed at the end of this chapter, considering the impact of additive addition on manufacturability, stability and functionalities of lipid coated products.

The next section, dedicated to solid lipid based formulated products, will present the link of additive addition and product characteristics to functionalities developed into hot-melt coated products.

### 3. Solid Lipid-Based Formulated Products

#### 3.1. Classification of Lipid-Based Formulations

Lipid-based formulations cover different dosage forms (e.g., tablets, creams, solutions) in different physical states (solid, semi-solid, liquid) prepared in different length scales (e.g., monolithic, microparticulate, nanoparticulate systems) for different administration routes (e.g., oral, topical, parenteral). Concretely, lipid-based formulations range from subcutaneous depots or implants (Kreye et al., 2008; Sharma et al., 2023), intravenous emulsions (Hippalgaonkar et al., 2010), liposomal formulations (Fan & Zhang, 2013), topical preparations (Palefsky, 2022), lipid nanoparticles (Couffin & Delmas, 2013; Scioli Montoto et al., 2020; Severino et al., 2012), (liquid) bioenabling lipid-based formulations (Feeney et al., 2016) to conventional oral solid lipid-based dosage forms (Becker et al., 2015). This section is focused on the last type of formulations – **solid lipid-based formulations**.

The words “conventional” and “solid” are to distinguish this type with solid lipid nanoparticles and (liquid) lipid-based formulations for oral delivery of poorly water-soluble drugs, respectively. The applications of liquid lipid-based formulations are bio-enabling or for bioavailability enhancement.

In an attempt to compare solid and liquid lipid systems, one can review the Professor Pouton's classification system for lipid-based formulations (LFCS) introduced for the first time in 2000 (Holm et al., 2023; Kalepu et al., 2013; Pouton, 2000, 2006; Pouton & Porter, 2008).

Lipid-based formulations were classified into four principal categories – I, II, IIIA, IIIB and IV as illustrated in **Figure 1-22** – based on the chemical composition which includes lipid-based excipients, surfactants, cosolvents, polymers... (Holm et al., 2023; Jannin, 2010; Pouton, 2006).

**Type I** lipid-based formulations are oily solutions, which are composed of triglycerides or mixtures of mono- and diglycerides. **Type II** lipid-based formulations are water-insoluble self-emulsifying drug delivery systems. **Type III** lipid-based formulations are more water-soluble self-micro-emulsifying drug delivery systems which contain a small fraction of amphiphilic surfactants and/or cosolvents (**Type IIIA**) or a greater proportion fraction of water-soluble components (**Type IIIB**). **Type IV** lipid-based formulations contain no oils but mostly amphiphilic surfactants and cosolvents. Concerning the particularities of the four types, the oil-rich Type I lipid-based formulations are susceptible to *in vivo* digestion which leads to generation of amphiphilic products in the gastro-intestinal fluid. Type II to Type IV lipid-based formulations contain a sufficient quantity of amphiphilic surfactants to promote a spontaneous dispersion in the luminal fluid. In general, by changing the chemical composition from Type I to Type IV lipid-based formulations, amphiphilicity, dispersibility and risk of loss in solvency capacity upon dilution increase whereas lipophilicity and digestibility decrease (Holm et al., 2023; Jannin, 2010; Kalepu et al., 2013; Pouton, 2006).

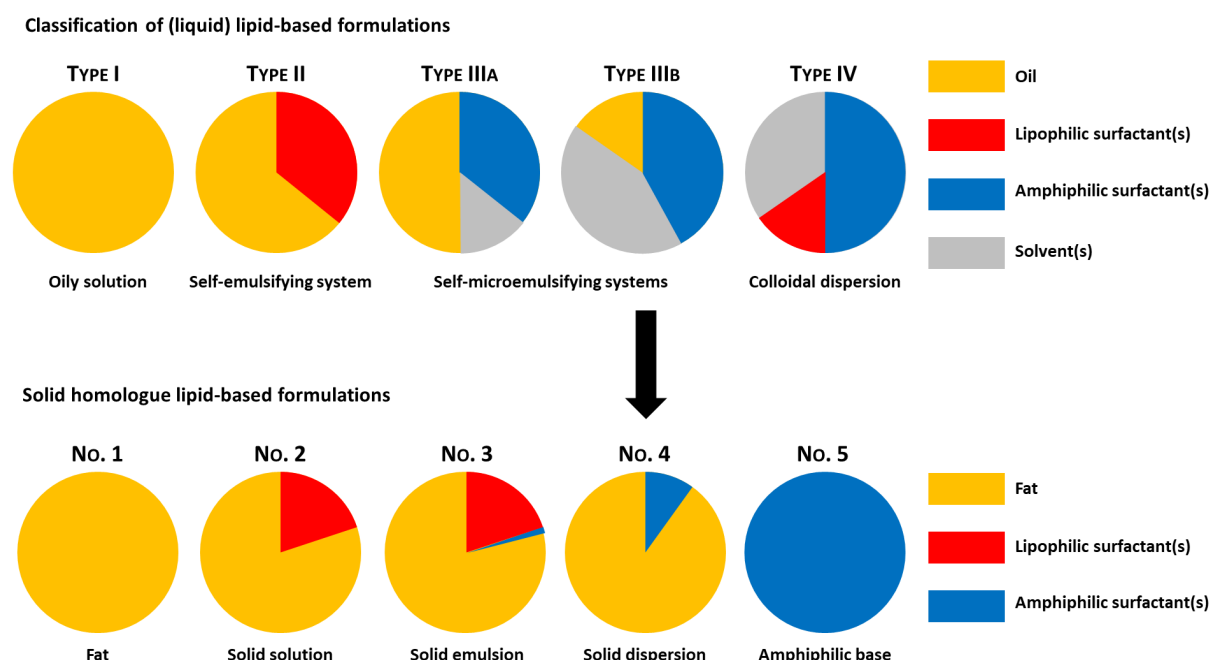


Figure 1-22. Chemical-composition based comparative classification of solid and liquid lipid-based formulations (adapted from LFCs Consortium 2010 - <http://www.lfcs-consortium.org/background.aspx>)

As can be seen, both solid and liquid lipid-based formulations found some similarities in the chemical composition. While the chemical composition of liquid lipid-based formulations implies their occurring physical structures in liquid state, a classification for solid lipid-based formulations could be based on their developed functionalities which are technological or biopharmaceutical (Girod Fullana & Aubert-Poussel, 2019). “Liquid” lipid systems are advantageous due to the fact that the poorly water-soluble drug is presented in liquid state in the dosage form (Pouton, 2006). The purpose to develop liquid lipid-based formulations justifies their common immediate release profile. On the contrary, mostly solid lipid-based formulations have a sustained release profile (D. G. Lopes, Salar-Behzadi, et al., 2017). As a matter of fact, release testing with the use of biorelevant media and lipolytic enzymes are usually indispensable to evaluate *in vitro in vivo* correlations (Berthelsen et al., 2019; Feeney et al., 2016). On the contrary, these practices of release testing are occasionally performed (Albertini et al., 2019; Becker et al., 2015; Feeney et al., 2016).

Screening of lipid-based excipients could be based on the solubility of drugs in liquid lipid-based formulations (Pouton & Porter, 2008). On the contrary, their functionalities often determine the choice of lipid-based excipients (Banerjee et al., 2021; Rosiaux et al., 2015). Last but not least, new trends for development of liquid lipid-based formulations consist of (i) solidifying self-emulsifying drug delivery systems (e.g., removal of solvents) and (ii) combining with other formulation technologies (e.g., amorphous solid dispersions (Nora et al., 2022)). The last feature converges with the development of solid lipid-based formulations. For instance, hot-melt coating of amorphous drugs is an encouraging example (Bannow et al., 2020). The comparison between liquid and solid lipid-based formulations is summarised in **Figure 1-6**.

Also illustrated in **Figure 1-22**, another categorisation based on physical structures for solid lipid-based formulations as a function of chemical composition can be homologous to this classic classification of (liquid) lipid-based formulations.

Concretely, in the first place, solid formulations composed of solely one lipid major component (**number 1**) are fats at room temperature which are equivalent to solidified forms of Type I formulations.

In the second place, solid formulations composed of one lipid major component and one solid/liquid lipophilic additive (**number 2**) are solid solutions which are equivalent to solidified forms of Type II formulations.

In the third place, solid formulations composed of one lipid major component and one solid/liquid amphiphilic additive (**number 4**) are solid dispersions which are equivalent to solidified forms of Type IIIB formulations. In the fourth place, solid formulations composed of solely one solid amphiphilic additive (**number 5**) are amphiphilic bases which are equivalent to solidified forms of Type IV formulations.

In the fifth place, solid formulations composed of one lipid major component, one solid/liquid lipophilic additive and one solid/liquid amphiphilic additive (**number 3**) are solid emulsions which are equivalent to solidified forms of Type IIIA formulations.

According to the database of hot-melt coating researches, mostly solid lipid-based formulations pertain to the category **number 1** (e.g., hydrogenated vegetal oils, triglycerides, glyceryl dibehenate), as they have been exploited for development of sustained release dosage forms (Rosiaux et al., 2015).

In a few publications, several lipid-based formulations can be classified into the category **number 5** (e.g., polyethylene glycols, poloxamers, stearyl macrogol-32 glycerides) (H. Chen et al., 2010; Khobragade et al., 2014).

All the hot-melt coating formulations composed of a solid lipid and an amphiphilic surfactant ( $HLB > 9$ ) (as shown in **Table 1-5**) constitute the category **number 4**.

Beside hot-melt coating, solid lipid-based formulations of the category **number 2** were evidenced by the combinations between tristearin with oils/lipophilic surfactants ( $HLB < 9$ ) used for spray congealing (Bertoni et al., 2021).

Solid lipid-based formulations of the category **number 3 – solidified emulsions**, there is no proof of concept found for melt technologies (e.g. spray congealing, hot-melt coating, extrusion) by a narrow definition. In fact, during processing, solid lipid can be molten with an amphiphilic surfactant and a lipophilic surfactant to form a hot-melt emulsion. The solidification of this molten formulation results in a solidified emulsion. By a wide definition, solidified self-emulsifying drug delivery systems can also represent the category **number 3**. This should be a common point in development of solid and liquid lipid-based formulations.

**Type III lipid-based formulations** were reported to be the most marketed developed products (Bennett-Lenane et al., 2020; Kalepu et al., 2013). This might imply at least a superior stability of emulsion systems composed of lipophilic and amphiphilic surfactants in comparison with other liquid lipid-based

formulations. In fact, since long, formulation of stable emulsions has been based on the quest for the required HLB by combining a surfactant and a co-surfactant (Bendjaballah et al., 2010; J. Boyd et al., 1972; Fernandes et al., 2013; Gore et al., 2023; Greth & Wilson, 1961; Nursakinah et al., 2013; Rohan et al., 2014; Schmidts et al., 2010; Wangpradit et al., 2022), this quest has been applied throughout studies in different categories of lipid-based formulations presented at the beginning of this section. Note that the concept “required HLB value” was implicitly revealed to relate to a combination of a surfactant and a co-surfactant which have a stabilisation effect on a specific emulsion system via specific interactions at the molecular level (J. Boyd et al., 1972; Lin et al., 1977; Pouton, 1997). These emulsions occur in liquid and semi-solid state. **The elements are to highlight the relevance of a combination of surfactants to the development of solid lipid-based formulations.**

For liquid/semi-solid systems of emulsions, coalescence – size-independent particle size redistribution – might be predominant whereas Ostwald ripening – size-dependent particle size redistribution – has been shown to be the main driver of destabilisation of solid systems (Urbina-Villalba et al., 2009). Note that both coalescence and Ostwald ripening take place in the direction that the total interfacial energy of the system becomes minimised with time. In the database of solid lipid-based formulations, there are implicitly two example studies.

The one case concerns the lipid-surfactant of tripalmitin/polysorbate 65 at different ratios which were reported with many stability issues related to Ostwald ripening (as presented in **Section 2.3.2**) (D. G. Lopes, Koutsamanis, et al., 2017; Schertel, Salar-Behzadi, Karrer, et al., 2021; Schertel, Salar-Behzadi, & Zimmer, 2021). One possible reason is the solid dispersion system formed by this combination in which the lipophilic tripalmitin and the amphiphilic polysorbate 65 (HLB 10.5) are confirmed again to be not miscible.

The other case also concerns various combinations of tristearin with one oil/liquid surfactant 90:10 which were reported to all yield a relatively stable release kinetics of a model drug within a year (Bertoni et al., 2021). One possible reason is the formation of the solid solution systems in which the lipophilic tristearin and the lipophilic oil/liquid surfactant are soluble in each other. In a relevant and interesting food research where combinations of sorbitans and polysorbates at different ratios were tested for an effect of anti-blooming, most of combinations were reported to yield a better anti-blooming effect in cocoa butter than a surfactant alone (Garti & Aserin, 2012). Note that lipid blooming is also related to Ostwald ripening (Delbaere et al., 2016).

This evidence suggests that the choice of surfactants based on HLB values in formulating solid lipid-based formulations should not only be based on release modification but also physical stabilisation. However, when adding liquid additives, it is advisable to consider their limit concentration in order not to compromise the processability of solid lipid-based formulations (i.e. crystallisation, adhesion, viscoelastic properties). This evidence also agrees with the suggestion to combine two surfactants whose lipophilicity and amphiphilicity are complementary in order to evade stability issues possibly encountered for hot-melt coating formulations.

Table 1-6. Comparison of liquid and solid lipid-based formulations with cited references (not exhaustive)

No.		Classic (liquid) lipid-based formulations	Solid lipid-based formulations
1	Classification	Five categories, I, II, IIIA, IIIB and IV based on composition and formulation properties (Pouton, 2000; Pouton & Porter, 2008)	Possibly two categories (Girod Fullana & Aubert-Poussel, 2019): technological functions (e.g., moisture protection, lubrication); biopharmaceutical functions (e.g., taste masking, extended release)
2	Stability indices	Droplet size distribution, viscosity, zeta potential, centrifugation, conductivity (Gore et al., 2023; Nursakinah et al., 2013; Schmidts et al., 2010)	Solid-state behaviours (e.g. polymorphism, Ostwald ripening, substrate-lipid interactions) (D. G. Lopes, Salar-Behzadi, et al., 2017; Becker, 2016; Windbergs, 2009)
3	Physical state	Liquid state (most of the case); (semi-)solid state (encapsulated in soft or hard capsules) (Bennett-Lenane et al., 2020; Feeney et al., 2016; Porter et al., 2007; Pouton, 2006)	Solid state (A. S. Achanta et al., 1997; Appelgren & Eskilson, 1993; Becker et al., 2015; Jannin & Cuppok, 2013; Jones & Percel, 1994; D. G. Lopes, Salar-Behzadi, et al., 2017; Rosiaux et al., 2015)
4	Release profile	Immediate release (most of the cases) based on the advantage of “pre-dissolved” drug (Feeney et al., 2016); modified release (e.g., coated hard and soft capsules) (Siepmann et al., 2019; Siew, 2017; Soares & Crema, 2020)	Often sustained release (most of the case) (Rosiaux et al., 2015, 2022); immediate release (less common, e.g., using reservoir system with combinations of lipids and surfactants (Bannow et al., 2020; Becker et al., 2016; Jannin, 2004; Jannin et al., 2005; D. G. Lopes et al., 2016; D. G. Lopes, Koutsamanis, et al., 2017; Schertel, Salar-Behzadi, Karrer, et al., 2021; Schertel, Salar-Behzadi, & Zimmer, 2021; Stocker et al., 2017), or formulating with hydrophilic lipid derivatives (Khobragade et al., 2014)
5	Release / Uptake tests	Very often with biorelevant media or <i>in vivo</i> model to provide IVIVC (Feeney et al., 2016)	Largely based on compendial dissolution tests using simple buffered media (Becker et al., 2015; Feeney et al., 2016), rare use of biorelevant media for release testing (Albertini et al., 2019; Witzleb et al., 2012)
6	Need for digestion	Recommended for understanding the impact of digestion (either desirable or undesirable) on drug performance (Berthelsen et al., 2019; Feeney et al., 2016; Mu et al., 2013)	Occasionally performed for special formulations such as amorphous drug (Bannow et al., 2020), delivery of macromolecules (Albertini et al., 2019; Bertoni, Albertini, et al., 2018; Bertoni et al., 2020; Christophersen et al., 2013a; Christophersen, Vaghela, et al., 2014a; Christophersen, Zhang, et al., 2014a; Traub-Hoffmann et al., 2020)
7	Formulation screening	Intensive (e.g., via design of experiments), including formulations of five classes or with a specific class (e.g., IIIA, IIIB) via many combinations; as a bioenabling technology platform, classic lipid-based formulations intended for oral delivery of poorly water-soluble drugs (BCS II/IV drugs) based on drug solubility in lipids or solvent capacity of lipid-based formulations (Kohli et al., 2010; Mu et al., 2013; Pouton & Porter, 2008)	Empirical choice of excipients based on targeted functions for mostly highly soluble drugs (BCS I/III drugs) (Becker, 2016; Jannin, 2004; Rosiaux et al., 2015)
8	New trends	Solidification of self-(micro-)emulsifying drug delivery systems (Feeney et al., 2016; Joyce et al., 2019; A. Tan et al., 2013; Zupančič et al., 2022); Combination of lipid-based formulation and amorphous solid dispersions (Nora et al., 2022)	Coating of amorphous solid dispersions (Bannow et al., 2020); Lipid-based solid dispersions for improvement of bioavailability (Khobragade et al., 2014)

IVIVC, *in vitro in vivo* correlations; BCS, biopharmaceutics classification system;

## 3.2. Versatility of Lipid-Based Excipients for Pharmaceutical Applications

### 3.2.1. Versatility in release patterns

Despite being a grand class of excipients as that of polymers, versatility for formulating solid dosage forms is commonly recognised for polymers but uncommonly for lipids (Gibson, 2007; Siepmann et al., 2019). To address this stereotype, from the database of hot-melt coating researches, the release profile of hot melt-coated products can be classified into the four types which correspond to typical drug delivery scenarios (Selen et al., 2014), as illustrated in **Figure 1-23**.

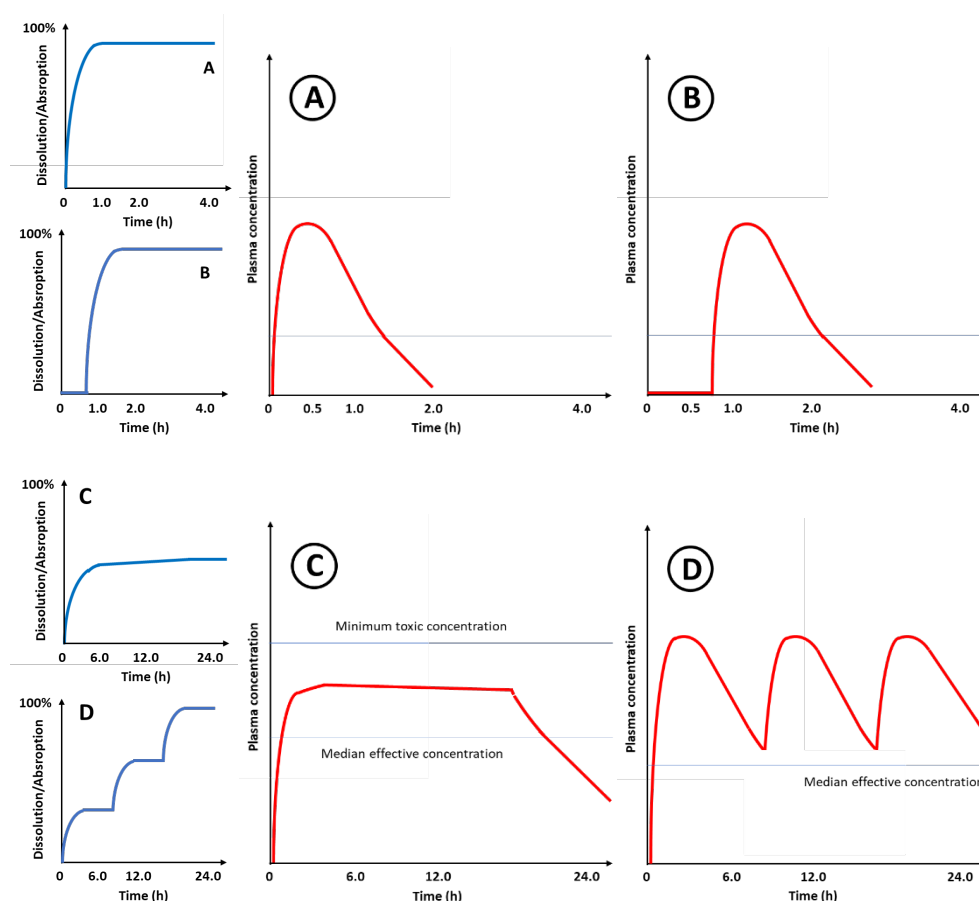


Figure 1-23. Possible release patterns of solid lipid-based formulated products: immediate release (A), delayed release (B), sustained release (C) and pulsatile release (D) (adapted from Selen et al., 2014)

The first scenario (**Figure 1-23-A**) is envisaged for a case where a very rapid onset of action of the drug is wanted. Therefore, the therapeutic goal is rapid achievement of therapeutic concentrations at the site of action. Analgesics and for acute treatments (e.g., asthma, common cold, angina pectoris) often require an **immediate release** oral dosage form (Selen et al., 2014). In pharmaceutical applications, lipids can also be used for taste masking based on their hydrophobic effect. With this mechanism, the lipidic coat constitutes a physical barrier to reduce wetting of the coated core and delay the onset of drug release in the buccal cavity (Banerjee et al., 2021).

Some proofs of concept with hot-melt coating show a successful dual achievement of an immediate release profile and a function of taste-masking (e.g., for N-acetylcysteine, ibuprofen sodium,



paracetamol, potassium chloride) (Becker, 2016; Becker et al., 2016; Jannin, 2004; Jannin et al., 2005; D. G. Lopes et al., 2016; D. G. Lopes, Koutsamanis, et al., 2017; Rosiaux et al., 2018; Schibschid, 2017). With the high coating amount, a mass concentration of 10% polysorbate permitted attainment of 85% drug dissolved within 45 minutes. For the reader's information, a specification of 85% of formulated drug dissolved within 60 minutes is acceptable for an immediate release product from the regulatory point of view (FDA, CDER, 1997). For taste-masking a criterion of less than 10% drug dissolved within the first 5 minutes could help evaluate taste-masking efficiency of the dosage forms *in vitro* and a multiple-point sampling during this period is recommended (Siewert et al., 2003).

The second scenario (**Figure 1-23-B**) is intended for a case where the timed onset of action (**delayed release**) is important for the therapeutic outcome. For oral administration, this scenario corresponds to delivery of gastric irritants (e.g., aspirin) or acid-sensitive agents (e.g., probiotics) as well as **site-specific** delivery (Selen et al., 2014). Some examples of hot-melt coated products include enteric coating with fatty acids (e.g., palmitic acid, stearic acid) (Patil et al., 2012; Schertel et al., 2022; Sudke et al., 2013) or fatty alcohols in combination with plasticisers (e.g., cetyl alcohol, myristyl alcohol, stearyl alcohol, cetostearyl alcohol (Jacobsen et al., 2021)). For colon-specific delivery, selection of very long fatty acids whose pKa should be higher than 7 could be a solution (Zaid, 2020) as the higher the fatty acid chain length the higher the pKa value (Pashkovskaya et al., 2018).

The third scenario (**Figure 1-23-C**) is envisaged for a case where the maintenance of a target exposure over a time period with repeated dosing, a profile of **extended release** is expected, or drugs exhibit short half-life. In these cases, a minimal acceptable residence time (or occupancy) at a receptor or adequate "averaged" exposure is desirable to achieve the intended therapeutic outcome (e.g., delivery of antibiotics, antihypertensives, chronic pain management) (Selen et al., 2014). Some examples of hot-melt coated products corresponding to the cited therapeutic categories include extended release oral dosage forms of ofloxacin (Wankhade et al., 2018), chloroquine (Faham, Prinderre, Piccerelle, et al., 2000), metoprolol tartrate (Chansanroj et al., 2007a, 2007b; Y. Yang et al., 2017), nifedipine (Le, 2004), hydrochlorothiazide (Schertel, Salar-Behzadi, Karrer, et al., 2021), propranolol hydrochloride (Sinchaipanid et al., 2004), paracetamol (Knezevic et al., 2009), oxcarbazepine (N. Patel & Jani, 2021b), levetiracetam (N. Patel & Jani, 2021a), theophylline (Barthelemy et al., 1999; Faham, Prinderre, Farah, et al., 2000; Padsalgi et al., 2008), fenoverine (Suresh & Dinesh, 2013), pregabalin (Jeong et al., 2015) and venlafaxine hydrochloride (Guan et al., 2011).

The fourth scenario (**Figure 1-23-D**) is intended for a case where **pulsatile delivery** of a drug substance or delivery of a **fixed dose combination** product is desirable. The therapeutic goal might not only rely on rapid achievement of therapeutic concentrations at the site of action but also the maintenance of the desirable effect. This drug delivery scenario is beneficial for patient compliance by reducing the dosing frequency and avoiding the confusion with polypharmacy. For the case of fixed dose combination, their pharmacokinetic properties should be adequate as obtained with their corresponding dosage forms. The fourth scenario applies well to combined therapy like antihypertension or treatment for circadian disturbances such as antihistamines, antidiabetics and anti-insomniacs (Selen et al., 2014). No scientific research of hot-melt coating responded to pulsatile drug delivery. However, in the near future, it is

possible to generate layer-by-layer hot-melt coated products based on experiences acquired with polymer-based coating (Roy & Shahiwala, 2009). Furthermore, some research on a homologous melt technology – spray congealing with lipids proved that lipid-based formulated products can also respond to this scenario. For a pulsatile release of melatonin, three types of devices with enhanced-, delayed- and controlled-release were generated separately and mixed together using stearyl macrogol-32 glycerides, stearic acid and carnauba wax, accordingly (Albertini et al., 2014).

Above are presented representative hot-melt coated drugs that could respond practically to the four typical delivery scenarios. This just shows the versatility of solid lipidic formulations for pharmaceutical applications. Nevertheless, note that almost the developed hot-melt coated drugs had a morphology of microcapsules (core-shell) and the attribution of a release profile was based mostly on dissolution testing in simple buffers, not all based on dissolution testing in biologically simulated buffers in the presence of lipolytic enzymes. In effect, when biorelevant dissolution with/without lipolysis is performed on solid lipid-based formulations, release patterns of hot-melt coated drugs could change completely (Albertini et al., 2019; Reitz, 2007; Witzleb et al., 2012).

### 3.2.2. Role of wetting and digestion

Release profile of solid lipid-based formulated products is a function of morphology, size of and coating content in the finished product, biopharmaceutical properties (e.g., penetrability, wettability, digestibility) of the formulation, solubility of the active substance and its affinity with the formulation.

The term “penetrability” is used to reflect interactions between water (i.e., penetrant species) and lipid system (i.e., penetrated front) in dissolution media. In fact, the mainly affected subject is water penetration mechanisms (i.e., how water is transported inwards and outwards the system) and kinetics (i.e., to which rate and extent) (Sanopoulou & Papadokostaki, 2017).

Concerning wettability of lipids, lipids are classified depending on polarity and interactions with water (Kegel et al., 2009). Lipids can be non-polar and water-insoluble species (e.g., paraffin, unsubstituted aromatic compounds) which do not spread to form a monolayer. Lipids can be polar species which are divided into three groups depending on their solubility.

The first group (I) comprises insoluble non-swelling amphiphiles (e.g., cacao butter, di-, triglycerides, non-ionised fatty acids, fatty alcohols, waxes (esters of fatty acids and fatty alcohols), vitamin E, sterols). They have a surface solubility, shown by the ability to form a stable monolayer.

The second group (II) comprises insoluble swelling amphiphiles (e.g., monoglycerides, ionised fatty acids, lecithins, phospholipids). They also have a surface solubility and moreover can swell to form liquid crystalline structures which can incorporate large volume fraction of water molecules.

The third group (III) comprises soluble amphiphiles (e.g., bile salts). They form an unstable monolayer at the air-water interface and form micelles over a critical concentration which can solubilise other insoluble lipids (Small, 1968). Almost the lipids commonly selected as bulk agent represent non-polar species or lipids of the first group (I).

The knowledge of lipid wettability is useful for several purposes. On the one hand, wettability of lipids might determine their selection for fast or slow-release kinetics of a model drug.

On the other hand, wettability of lipids aids to decide the use of biologically simulated media when performing release testing of solid lipid-based formulations.

In the case of non-polar lipids, the use of biorelevant media might not be necessary. For instance, paraffins were found to be technically inert to either fed state simulated intestinal fluid or aqueous solution of high-concentration of polysorbate 20 (Witzleb et al., 2012). In fact, release kinetics of a model drug from paraffin-based matrix did not change when augmenting the concentration of polysorbate 20 as well as at different timepoints in biorelevant media.

In the case of polar lipids, the use of biorelevant media might not be exempted. For instance, release kinetics of a model drug from poorly- or non-digestible solid lipid-based formulations (e.g. cetyl palmitate, glyceryl dibehenate) was shown to be faster in biorelevant media than in simple buffer media (Witzleb et al., 2012). When the total surface area of an erodible lipid system (e.g., fatty acids) becomes important, its erosion kinetics might also become important especially in the presence of bile salts.

Concerning digestibility of lipids, lipids are classified into three groups: highly digestible lipids (e.g., short- and medium-chain triglycerides), poorly digestible lipids (e.g., long-chain (saturated) triglycerides) (Mu, 2004) and non-digestible lipids (e.g., non-polar lipids, esters of fatty acids and fatty alcohols, fatty acids, fatty alcohols) (Witzleb et al., 2012).

Evidently, testing with lipolytic enzymes might also be exempted for non-polar lipids or non-digestible lipids (Witzleb et al., 2012). In the case of digestible lipids, involvement of digestion might change the release kinetics of a model drug from digestible lipid systems completely (Christophersen, Zhang, et al., 2014a; Reitz, 2007). For instance, trilaurin was used as a coating agent for delayed-release (Yoshiteru et al., 1990; Yoshitomi et al., 1992, 1993). In fact, this application was based on the digestion of trilaurin in gastro-intestinal media. Without digestion, trilaurin-coated products would have a prolonged-release pattern.

Following is another example on the comparison between two dissolution tests in simple buffer and biorelevant media, release kinetics of a model drug was increased fourfold in the presence of pancreatin (Reitz, 2007). Following is another example on the comparative digestion profile between long-chain triglycerides, about 100%, 80% and 20% of a macromolecule released from microparticulate systems constituted by trimyristin, tripalmitin and tristearin were reported in *in vitro* lipolysis in comparison with around 30%, 40% and 10% released in the absence of enzymes, respectively (Christophersen, Zhang, et al., 2014a). Hence, the effect of digestion should be not ignored when formulating solid lipid-based formulations which are digestible.

To compare the digestibility of solid lipids, it is important to normalise not only the quantity of substrate but also the total surface area of the solid lipid systems (Arnold et al., 2012; Bertoni, Albertini, et al., 2018).

For large monolithic systems whose specific surface area is limited, digestion kinetics becomes less important and therefore digestibility might become neglectable, except the case of digestible

amphipathic lipids. For instance, with the same lipid composition, it was reported that the higher the specific surface area of the geometry of 3D-printed tablets, the higher the dispersion kinetics and the higher the resultant digestion kinetics (Vithani et al., 2019a).

Digestion of solid lipids was said to take place at the interface between the solid and the liquid (Christophersen et al., 2013a; N’Goma et al., 2012). Digestion kinetics depends on several factors such as liquid or solid state of lipids (Witzleb et al., 2012), polymorphism (Olbrich et al., 2002), as well as level of solubilisation of lipids (Christophersen et al., 2013a; Witzleb et al., 2012), enzyme activity and food effects (Christophersen, Vaghela, et al., 2014a). With the role of an additive, digestible surfactants could be added to impart an immediate release to lipid-based formulations (Bannow et al., 2020; Koehl et al., 2020; Vithani et al., 2017). For instance, high concentration and digestibility of polysorbate 65 permitted an immediate release to tripalmitin-coated drugs (Bannow et al., 2020).

Some surfactants and polymers can exert an effect on digestion kinetics of solid lipid-based formulations. In fact, certain commonly used surfactants or polymers (e.g., polysorbate 80, vitamin E D- $\alpha$ -tocopherol polyethylene glycol (1000) succinate, sucrose laurate, polyethylene glycol) were reported to decelerate digestion kinetics by diverse mechanisms (e.g. competition at lipolysis site with lipid major components) (Arnold et al., 2012; Christiansen et al., 2010; Feeney et al., 2014).

In conclusion, design of solid lipid-based formulations warrants for understanding of lipid biopharmaceutical behaviours (e.g., polarity, digestibility) in *in vivo* processing of the gastro-intestinal tract (N’Goma et al., 2012; Small, 1968). Despite the rarity of its applications (Albertini et al., 2019; Feeney et al., 2016), only conduct of biorelevant and lipolytic testing for solid lipid-based formulations might help in most cases reveal their true release profile and therefore anticipate their pharmacokinetic properties. To summarise the aforementioned elements, the link between the choice of release testing methods for hot melt coated drugs and biopharmaceutical properties of solid lipids is given in **Figure 1-24**.

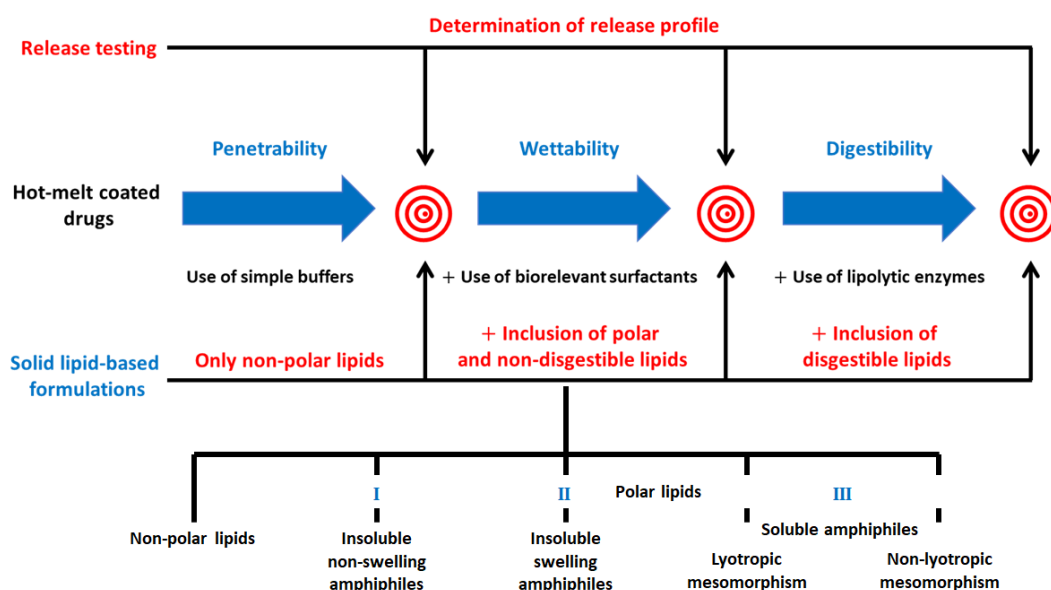


Figure 1-24. Link between the choice of release testing methods and biopharmaceutical properties of solid lipids

### 3.3. Classification of Drugs and Its Relevance to Solid Lipid-based Formulations

To begin with this section, the classic biopharmaceutics classification system is presented to remind that the main objective of the galenic formulation is to deliver a drug to the patients with the most appropriate administration method (i.e., dosage forms, processing technologies, excipients) by considering its physicochemical and biological properties and the pathophysiology of the patients (Langguth et al., 2012).

Solubility and permeability are key determinants of the absorption of a drug (also called “active substance, active pharmaceutical ingredient, chemical entity, small molecule, etc.”) which determines ultimately its availability at the site of action. Based on these two criteria active substances are divided into four classes: (BCS I) high solubility-high permeability, (BCS II) low solubility-high permeability, (BCS III) high solubility-low permeability and (BCS IV) low solubility-low permeability (Amidon et al., 1995) (as shown in **Figure 1-25**).

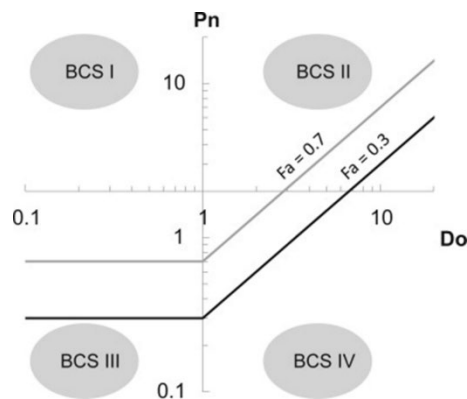


Figure 1-25. BCS plane ( $Pn$ - $Do$  plane) and DCS lines presented via dimensionless numbers;  $Fa$  lines, representing the estimated fraction of dose absorbed, distinguish the case of dissolution-limited and solubility-limited following the concept of maximal dose absorbable in DCS (Sugano & Terada, 2015)

The BCS in **Figure 1-25** is also related to the developability classification system (DCS) (Butler & Dressman, 2010) and the fraction absorbed classification system (FaCS) (Sugano & Terada, 2015). In effect, these three classification systems can be based on the two characteristic dimensionless numbers:  $Do$ , dose number and  $Pn$ , permeation number (Amidon et al., 1995; Sugano & Terada, 2015).

Equation 27 :

$$Do = \frac{Dose}{V_{GI} \times S_{dissolv}} = \frac{Volume\ of\ gastro \cdot\ intestinal\ fluid\ available\ to\ dissolve\ the\ dose}{Drug\ solubility\ in\ gastro \cdot\ intestinal\ fluid}$$

Equation 28 :

$$Pn = \frac{2 \times DF \times P_{eff}}{R_{si}} \times \langle T_{si} \rangle = \frac{Radial\ permeation\ rate}{Axial\ convection\ rate}$$

where  $V_{GI}$  is the volume of gastrointestinal fluid ( $m^3$ ),  $S_{dissolv}$  the solubility of drug in gastrointestinal fluid ( $kg/m^3$ ),  $DF$ , the degree of flatness (physiologically dependent),  $R_{si}$  the mean radius of GI tract (m),  $L_{si}$  the length of GI tract (m),  $P_{eff}$  the effective permeability of drug ( $m \cdot s^{-1}$ ),  $\langle T_{si} \rangle$  the residence

time in GI tract (s).  $k_{perm}$  is the permeation rate coefficient ( $s^{-1}$ ) and  $k_{perm} = \frac{2 \times DF \times P_{eff}}{R_{si}}$ . If  $Do > 1$ , drugs exhibit solubility-limited absorption with the defined dose. If  $Pn < 1$ , drug absorption is permeability-limited. In DCS, the gastric volume 250 mL of BCS is replaced by 500 ml considering the volume of gastro-intestinal fluid. Furthermore, DSC introduced the concept of solubility limited absorbable dose (SLAD) expressed as follows (Butler & Dressman, 2010):

Equation 29 :

$$SLAD = S_{dissolv} \times V_{GI} \times M_p$$

where  $M_p$  is the permeability dependent multiplier. For highly permeable drugs,  $M_p$  is the permeation number (Pn) whereas for poorly permeable drugs, it is kept at unity. Also, by another dimensionless number – dissolution number (Dn), DCS suggests the particle size of drug substance in order to overcome dissolution rate limited bioavailability issues (Butler & Dressman, 2010):

Equation 30 :

$$Dn = \frac{3 \times D \times S_{dissolv}}{\rho_p \times r_p^2} \times \langle T_{si} \rangle = \frac{\text{Small intestine transit time}}{\text{Mean dissolution time}}$$

If  $Dn < 1$ , it is the case of dissolution rate limited drug absorption. Following **Equation 30**, a recommended size for a drug whose dissolution rate is limiting can be calculated. The modified BCS, FaCS, considers the fraction of dose absorbed for classifying drug substances based on the three dimensionless numbers presented above. According to FaCS, drug absorption could be dissolution rate limited, permeability limited, and solubility permeability limited. It also guides bioenabling formulation approach in response to each problem statement (Sugano & Terada, 2015). For the case of solubility-permeability limited, fraction of dose absorbed could be estimated by the expression given below (Sugano & Terada, 2015):

Equation 31 :

$$Fa = \frac{SLAD}{Dose} = \frac{k_{perm} \times S_{dissolv} \times V_{GI} \times \langle T_{si} \rangle}{Dose} = \frac{Pn}{Do}$$

This justifies the boundaries, Fa lines, of DCS based on Pn/Do in **Figure 1-25**. At the moment, a possible question is **how relevant the BCS/DCS/FaCS is to the development of hot-melt coating formulations**.

Firstly, most publications of hot-melt coating research were related to development of extended release/sustained release/prolonged release dosage forms. Incidentally, these applications of hot-melt coating with lipids concern almost **BCS I/III drugs**. These drugs should be highly soluble with a Fa which should be at unity, i.e. fraction of dose absorbed is total within the small intestine transition time  $\langle T_{si} \rangle$ .

Publications on hot-melt coating (not exhaustive) are demonstrated in **Table 1-7** and **Figure 1-26** depending on the purpose of hot-melt coating researches as well as the BCS classes of active substances used in the development work.

Table 1-7. Publications on hot-melt coating per technological or biopharmaceutical function

Function	Publications
<b>Technological functions</b>	
<b>Moisture protection</b>	A. Achanta, 1999; A. S. Achanta et al., 2001; Bannow et al., 2020; H. Chen et al., 2010; D. G. Lopes, Koutsamanis, et al., 2017; Sinchaipanid et al., 2004; Sorgatz, 2011
<b>Lubrication</b>	Jannin, 2004; Jannin et al., 2003; Milanovic et al., 2020
<b>Method development</b>	Hohl et al., 2017; Kennedy & Niebergall, 1996; Woerthmann et al., 2021, 2022, 2023
<b>Biopharmaceutical functions</b>	
<b>Taste masking with immediate release</b>	Becker, 2016; Becker et al., 2016; Hate, 2015; Jannin, 2004; Jannin et al., 2005; D. G. Lopes et al., 2016; Rosiaux et al., 2018; Salar-Behzadi, Corzo, et al., 2020; Schibschid, 2017; Stocker et al., 2017
<b>Extended release / Sustained release</b>	Barthelemy et al., 1999; Chansanroj et al., 2007b, 2007a; Faham, Prinderre, Farah, et al., 2000; Faham, Prinderre, Piccerelle, et al., 2000; Guan et al., 2011; Ignjatović et al., 2021; Jeong et al., 2015; Jozwiakowski et al., 1990; Kennedy & Niebergall, 1998; Knezevic et al., 2009; Le, 2004; D. G. Lopes et al., 2015; Milanovic et al., 2018; Padsalgi et al., 2008; N. Patel & Jani, 2021b, 2021a; Pham & Christensen, 2014; Salar-Behzadi et al., 2019; Schertel, Salar-Behzadi, Karrer, et al., 2021; Schertel, Salar-Behzadi, & Zimmer, 2021; Suresh & Dinesh, 2013; Wankhade et al., 2018; Xu et al., 2017; Y. Yang et al., 2017
<b>Delayed release</b>	Jacobsen et al., 2021; Kulah & Kaya, 2011; Patil et al., 2012; Schertel et al., 2022; Sudke et al., 2013; X. Wang et al., 2017
<b>Bioavailability enhancement</b>	Khobragade et al., 2014

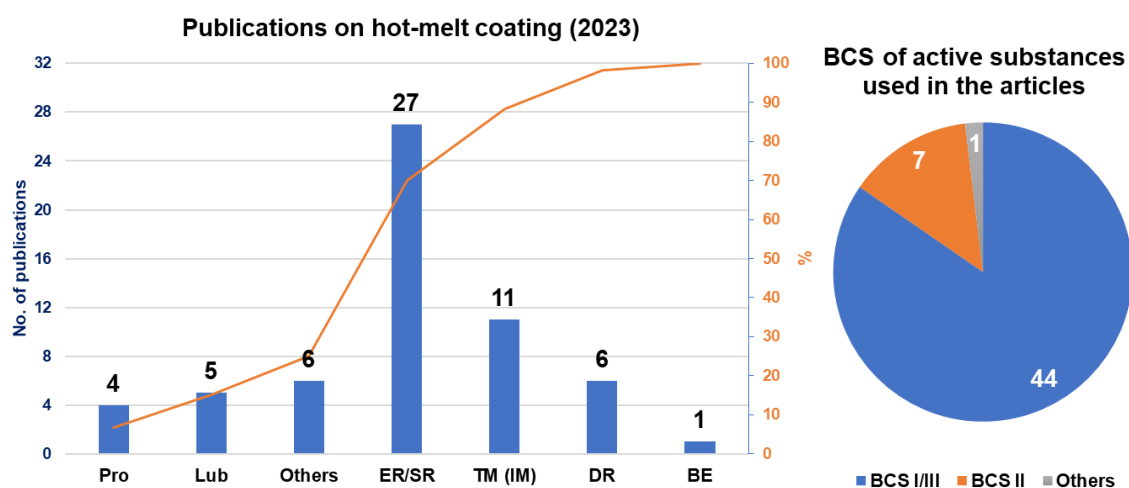


Figure 1-26. Key numbers: number of publications per functionality (left) and per BCS class (right) (not exhaustive). Pro, moisture protection; Lub, lubrication; Others (left), for example, method development; TM, taste masking with immediate release; ER/SR, extended release / sustained release; DR, delayed release; BE, bioavailability enhancement; Others (right), for example, probiotics

**BCS II drugs** are not a popular subject of hot-melt coating research and their applications are limited to development of taste masking. It is probably due to the stereotype that lipid solids were used for formulating sustained release dosage forms (Kegel et al., 2009; Rosiaux et al., 2015, 2022). Almost



these BCS II drugs, often acidic such as ibuprofen sodium, have a pH dependent solubility and their dissolution in alkaline intestinal fluid should not be limiting when being hot-melt coated.

On the other hand, almost solely one publication on development of a bio-enabling formulation concerns diclofenac – a BCS II drug (Khobragade et al., 2014). Note that this application was based on formulating amphipathic lipid-based dispersions which served as a matrix. Layering drug-loaded lipid-based dispersions and the use of amphipathic lipids are not much exploited for development of bioenabling formulations with the potentials of hot-melt coating by air suspension. In fact, if a poorly soluble drug is dispersed molecularly into the amphipathic lipid-based matrix, its solubility will be enhanced manifold so that its absorption should not be limited any more by solubility and dissolution rate according to **Figure 1-25**.

By considering **Equation 30** (effect of particle size reduction), lipid-based excipients could be regarded as “grease ball”. In this case, when hot-melt coating is performed with a system of microparticles rather than a monolithic system, **biopharmaceutical properties of lipids (e.g., solubility, wettability, erodibility, digestibility) can become important**. For instance, it was reported that 3D-printed amphiphilic lipid-based formulations tended to erode/disperse into aqueous media more rapidly with the increase in specific surface area (Vithani et al., 2019a). With an another example, under the form of microparticles, trimyristin was shown to be digested more rapidly in smaller size (75-100  $\mu\text{m}$ ) than in larger size (200-250  $\mu\text{m}$ ) (Bertoni, Albertini, et al., 2018). In effect, the higher the specific surface area of substrate per unit volume the higher the amount of lipases adsorbable thereon and as a result the higher the lipolysis rate of lipids (N’Goma et al., 2012).

Last but not least, by also considering **Equation 30** (effect of particle size reduction), note that for coated products the use of small substrate particles does not mean that in most cases it will be dissolved from the encapsulated system faster than coarse substrate particles coated. For instance, hot-melt coated theophylline monohydrate loaded granules were reported to have an increasing release kinetics in the increasing order of granule size, i.e. < 100  $\mu\text{m}$ , 100-200  $\mu\text{m}$ , 200-400  $\mu\text{m}$  and > 400  $\mu\text{m}$  (Faham, Prinderre, Farah, et al., 2000). In effect, on the one hand, in the same coating batch, smaller substrate particles tended to accumulate more coating material due to larger available surface and hence their coating membrane became thicker than that of coarser substrate particles.

On the other hand, even with a similar thickness, the volume occupied by smaller substrate particles is evidently smaller in comparison with that occupied by coarser substrate particles and therefore the fact that less fluid could diffuse inside to dissolve the substrate probably leads to a decrease in drug gradient.

Nonetheless, if the coating material is digestible or erodible, dissolution kinetics of smaller substrate particles now can be in synergy of digestion or erosion kinetics of the coating material which is in proportion to the total surface area of the coated microparticles. For instance, in a study where stearic acid, glyceryl dibehenate and carnauba wax were spray congealed with a model drug, its release kinetics from microcapsules whose size is between 100-250  $\mu\text{m}$  was reported to be enhanced significantly in comparison with those whose size is between 250-500  $\mu\text{m}$  (Albertini et al., 2019). Glyceryl dibehenate-based matrices whose size are below 250  $\mu\text{m}$  were found to have a non-neglectable digestibility (Albertini et al., 2019; Bertoni, Albertini, et al., 2018).

*For the two substrates – sodium chloride and amorphous solid dispersions of praziquantel, all the aforementioned considerations will be integrated into a systematic proposal for design of lipid-coated products based on the target functionalities and the biopharmaceutical properties of lipids. This proposal will be tested in all the experimental Chapters 3, 4, 5 and 6.*

#### **4. Some Proposals for a Methodological Approach to Investigating Hot-Melt Coating as the First Deliverable of this Doctoral Thesis after Literature Analysis**

After the summary of the literature, it is possible to propose a few approaches for contributing to hot melt coating studies, which will be explained in greater detail in the following, related to:

- Definition of process parameters with Ventilus<sup>®</sup> technology as a function of formulation properties;
- Additive selection with considerations on manufacturability, stability and functionalities of solid lipid-coated products;
- Design of solid lipid-coated products depending on the formulation digestibility.

##### **4.1. Definition of Process Parameters with Ventilus<sup>®</sup> as a Function of Formulation Properties**

To start with a research on spray-coating in fluidised bed in general and hot-melt coating in particular, one can choose one of the aforementioned approaches (e.g., momentum balance (Knezevic et al., 2009), heat balance (Kulah & Kaya, 2011), mass balance (Woerthmann et al., 2021)) depending one's experiences and availability of experimental tools.

The methodological approach involving multiple sampling points and the establishment of a systematic characterisation plan, may prove the most comprehensive and straightforward for beginners in the development of hot melt coating formulations.

As discussed before, the process variables could be divided further into two categories, thermal operational conditions, and mechanical parameters. Thermal operational conditions should have a strong relationship with the properties of coating materials (e.g., melt viscosity, crystallisation profile, polymorphism) as well as the substrate cores (e.g., thermal stability, glass transition temperature). On the other hand, definition of fluidisation air flowrate and feeding rate contributes largely to removal of crystallisation heat and cooling of the melt till the thermodynamic operation point (product temperature at steady state).

By considering lessons learned from solvent-based coating, a process window for successful operations is contingent on formulation properties, process variables and the fluidised bed technology (van Kampen, 2018). Generally, principles of coating by fluidised bed apply to both solvent-based and hot-melt coating (as given in **Section 1**), the difference is that drying of coating material on particles (removal of liquid fraction) is homologue for cooling. Technically, in the past, studies of solvent-based coating proposed the dimensionless flux number ( $FN_m$ ) which is logarithm of fluidisation air mass flowrate ( $\dot{m}_{air,f}$ ) to feeding rate ( $\dot{m}_f$ ) ratio as follows:

Equation 32 :

$$FN_m = \log_{10} \left( \frac{\dot{m}_{air,f}}{\dot{m}_f} \right)$$

According to the application,  $2 < FN_m < 3.5$  indicates occurrence of agglomeration while  $FN_m > 3.5$  informs of a coating regime and high overspray loss occurs if  $FN_m > 4.5$  (Boerefijn & Hounslow, 2005; Hede et al., 2008). Intuitively,  $FN_m$  represents the ratio of drying rate (provided by fluidisation air flowrate) to wetting rate (or feeding rate). Therefore, the limits of  $FN_m$  indicates when drying rate overwhelms wetting rate and vice versa. However, this correlation should be treated carefully with formulation properties.

These examples and a study on modelling overspray of solvent-based coating (Ronsse et al., 2008) served as an inspiration to propose a process window for hot-melt coating diagrammed in **Figure 1-27**.

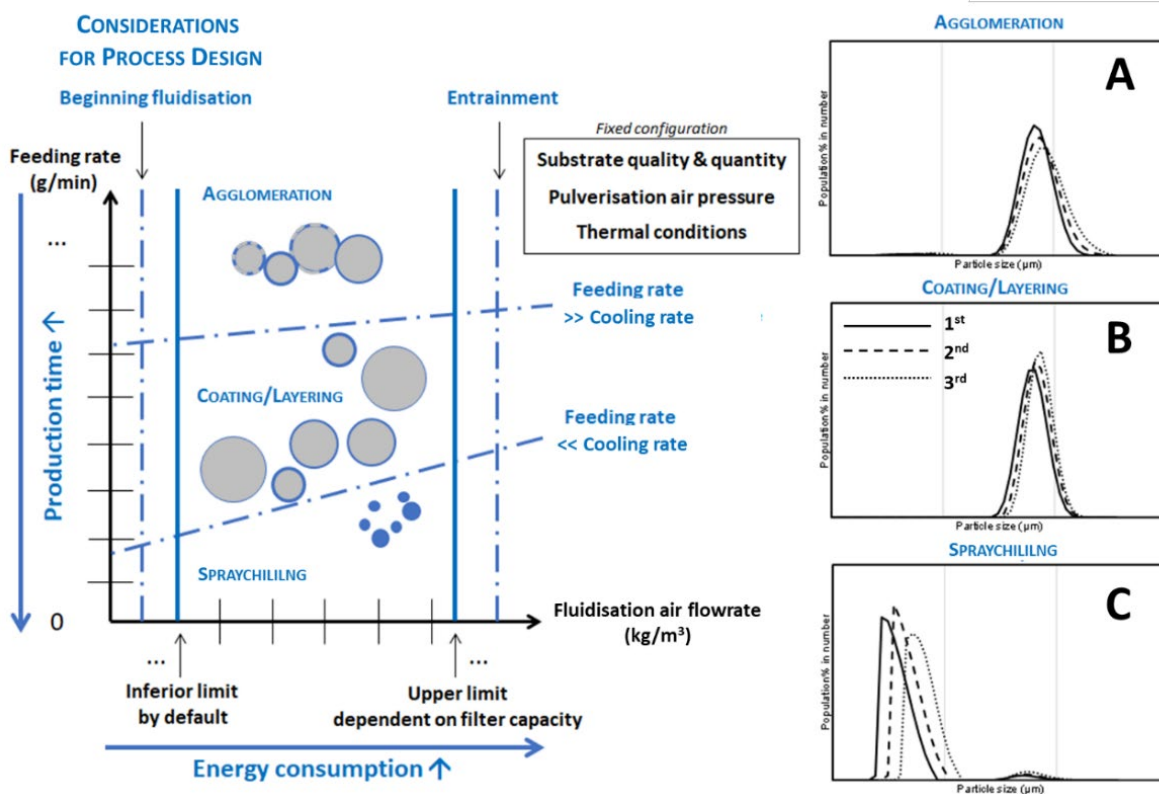


Figure 1-27. A projective process window for hot-melt coating studies with Ventilus® technology (adapted from Ronsse et al., 2008)

For constructing this process window:

- Particle size distribution (quality) and batch size (quantity) of substrate are firstly defined.
- For definition of thermal operational conditions, fluidisation air temperature ( $T_{air,f}$ ) is firstly regarded as target crystallisation temperature. This temperature should also be determined by considering wettability and adhesion of melt droplets onto particle surface (as explained in this review, **Table 1-2**).
- Other thermal conditions are set for a good flowability of molten formulation from transport to spray. Pulverisation air pressure ( $p_{air,p}$ ) should be set at a value which allows for a droplet size

distribution corresponding to substrate quality. At the moment, nearly twenty process variables can be reduced to definition of two parameters: fluidisation air flowrate ( $\dot{Q}_{air,f}$ ) and feeding rate of the molten formulation ( $\dot{m}_f$ ).

At a fixed fluidisation air temperature, a fluidisation air flowrate can be first set to fluidise sufficiently substrate particles. When working with Ventilus® technology, this flowrate is limited by a lower value by default and by an upper value by filter capacity. The latter value risks being surpassed when high overspray chilling is predominant. This technology is for direct applications and not for fundamental research to determine minimum fluidisation and entrainment.

For feeding rate, two limit values can also be determined for each fluidisation air flowrate depending on its relative magnitude in comparison with cooling rate. The four limit lines of fluidisation air flowrate and feed rate divide the graph into three regions:

- coating when there is a relative balance between feeding rate and cooling rate;
- occurrence of agglomeration (and coating) when feeding rate (wetting rate) is far greater than cooling rate;
- coating with abundant spray chilling when feeding rate is to a lesser degree compared to cooling rate.

An *imaginary* process window is therefore established. For this process window, solidification rate is assumed to be so great that the coating performance is determined by defining fluidisation air flowrate and feed rate of the molten formulation. However, in case that control by these two process parameters does not allow for a strict coating regime, this signifies that solidification rate is likely a limiting factor for the coating performance. Therefore, formulation properties need improvement, for instance, by adding or adjusting the concentration of additive(s).

When agglomeration is observed, this might be due to setting a high feeding rate. This fact was suggested in the early development of hot-melt coating (Jones & Percel, 1994) and validated with a recent study of the same subject (Woerthmann et al., 2023). In the latter study, when varying feeding rate from 3 to 20 g/min for coating with hydrogenated palm oil, signs of agglomeration was initially observed at 20 g/min. In fact, agglomeration could be due to larger droplet size (Hampel et al., 2018) formed at high feeding rate when pulverisation air pressure was fixed. Therefore, adjustment of feeding rate should be accompanied by re-definition of pulverisation air pressure, if necessary. A DoE study also found that increase in feeding rate together with higher surfactant amount in coating formulations led to agglomeration (Becker et al., 2016). In this case, agglomeration is associated with higher droplet size and likely with higher intraparticle adhesiveness or slower solidification rate. Another DoE study also found that a high feeding rate and a low pulverisation air pressure led to agglomeration whereas increase in this pressure resulted in coating only (Milanovic et al., 2018).

Statistics-based experimental approach enables quick identification of key process variables influencing product functionalities, especially in development of new products and processes or evaluation of material alternatives (Montgomery, 1999). However, sometimes the choice of responses seems not be relevant to factors and the design space obtained after optimisation of coated products might be applicable solely to one type of drug product. On the other hand, physics-based approaches not only

contribute more insights into this interdependent relationship but also drive development of novel analytical methods specific to characterisation of hot-melt coated products (e.g., oscillation rheometry, X-ray computed tomography, fluorescent spectroscopy) (Müller et al., 2018; Woerthmann et al., 2021, 2023). Their results could be plausibly transferable from substrate to substrate and independent of coating processes.

Furthermore, the **choice of substrate** has been proved equally indispensable for formulation development. It should be easy to measure in release testing so that coating quality could be evaluated at the same time (Kleinbach & Riede, 1995). Otherwise, selection of an active substance whose molecular weight higher often leads to development of a correspondingly selective assay method such as liquid chromatography (Siewert et al., 2003). Research works with active substances should be reserved when it comes to testing possible functionalities with the developed formulations whose processability and stability will have been mostly evaluated. There are some simple substrate such as citric acid (Jones & Percel, 1994; D. G. Lopes et al., 2015; Sorgatz, 2011; Xu et al., 2017), paracetamol (Milanovic et al., 2020), potassium chloride (Jones & Percel, 1994; Rosiaux et al., 2018), sodium chloride (Cai & Lee, 2020; Jones & Percel, 1994; Van Kampen et al., 2015; van Kampen, 2018), and salicylic acid (Frenning et al., 2003), which are measurable via simple conductometry or spectrophotometer, accordingly.

In conclusion, the experimental approach consisting of sampling at multiple timepoints represents a way forward for characterising hot-melt coating with candidate formulations. By applying this approach, expected tendencies of process efficiency evolution are given in **Figure 1-28**.

**Figure 1-28-A** indicates a good process efficiency but does not identify occurrence of agglomeration.

**Figure 1-28-B** informs about accumulated sticking of coated particles to the process wall from the second sampling while **Figure 1-28-C** pinpoints abundant overspray chilling. Samples collected in the course of processing operations can also be analysed for constructing a granulometric growth tendency as illustrated in **Figure 1-27-A, B** and **C**. For instance, **Figure 1-27-C** which shows the presence of fine fraction in all samples corresponds to **Figure 1-28-C**. **Figure 1-27-A, B** can apply to **Figure 1-28-A** or **Figure 1-28-B**. This justifies the need for other complementary characterisation for coating quality.

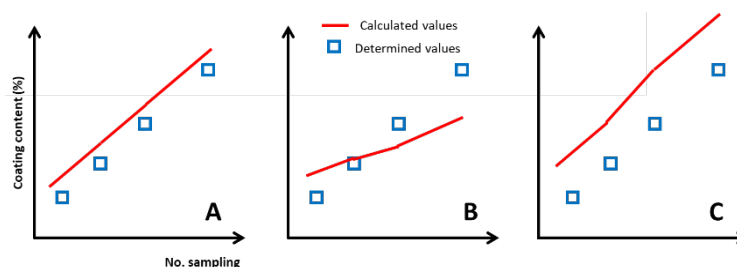


Figure 1-28. Expected process efficiency evolution obtained with multiple-sampling experimental approach

Once an optimal formulation is developed, process optimisation should be executed the next by considering not only key performance indicators (i.e., yield, efficiency, process regime and coating quality) but also time- and energy-efficiency. As illustrated in **Figure 1-27**, low  $\dot{m}_f$  will prolong processing time unnecessarily and simultaneously energy consumption for generation of fluidisation

flow rate becomes important. Considerations for process optimisation should be based on the trade-off between four variables  $T_{air,f}$ ,  $p_{air,p}$ ,  $\dot{Q}_{air,f}$  and  $\dot{m}_f$ .

In practice, this imaginary process window will be used in this doctoral thesis to define the operational conditions for different studies in **Chapters 3, 4 and 5**. First, a multiple-sampling experimental approach will be tested with beeswax-based formulations (Chapter 3). After that, the tested approach will be adapted to two other groups of formulations containing high-purity lipids (i.e. tristearin and trilaurin) in Chapters 4 and 5, respectively.

## **4.2. Additive Selection Basis on Manufacturability, Stability and Functionalities**

### 4.2.1. Considerations for classification of additives used in solid lipid-based formulations

The proposal for a classification aims at supporting development of fast screening methods whether this is based on the impact of additive addition on manufacturability, stability and functionality.

*How can one define these aspects of pharmaceutical development relevant to hot-melt coating?*

For the sake of simplicity, by “**manufacturability**”, it is understandable that the principal objectives are (i) feasibility of the formulation, (ii) facility for manufacture, (iii) coating quality and (iv) productivity.

By “**stability**”, it is understandable that the principal objective is to assure the robustness of product quality (e.g., organoleptic properties, impurities, release kinetics) throughout a defined shelf-life (e.g. for 12, 24 or 36 months) under appropriate storage conditions.

By “**functionality**”, it is understandable that the product should respond to its intended use whether it is technological (e.g., identification, lubrication, moisture protection) or biopharmaceutical (e.g., taste-masking, modified release) (Sato, 2018a).

This classification could be grounded on effects which additives exert on lipid crystallisation (i.e. de-clustering, templating, poisoning, and kink-forming), on effects which additives have on stabilisation of lipid systems (e.g., polymorphic control, anti-bloom) or hydrophilic lipophilic properties which allows additives to customise product functionalities (e.g., immediate release, modified release). By considering functions of additives, this classification diverges but by considering structures of additives it converges. In fact, it is the structure of a surfactant whose lipophilic aliphatic chain and hydrophilic head group determine its effect and mechanism(s) of action (K. W. Smith et al., 2011; K. W. Smith & Sato, 2018). Traditionally, pharmacists often select lipid-based excipients and surfactants on the basis of HLB system (Jannin, 2004; Salar-Behzadi, Corzo, et al., 2020; Salar-Behzadi et al., 2019) so as to design a target release profile for formulated products.

A structure-based classification should not constrain selection of surfactants but should also propose considerations of candidate surfactant whose structure is similar to that of the lipid major component in terms of fatty-acid moieties or aliphatic chains (Pasquali et al., 2008). **Figure 1-29** illustrates for formulating with tristearin a suggestion of surfactants which all bear the same fatty-acid moiety, but have different HLB values.



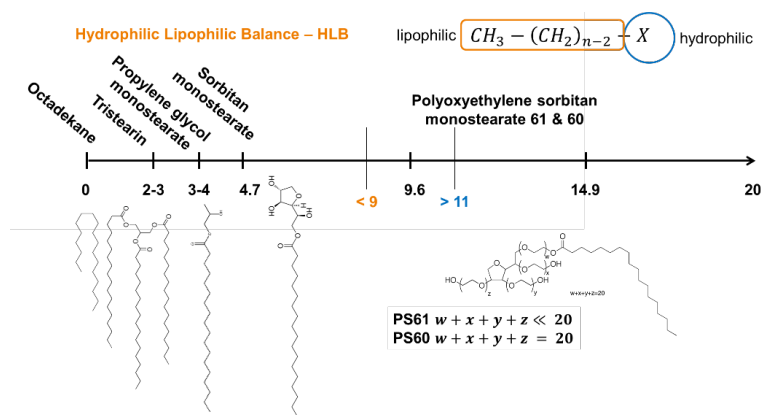


Figure 1-29. Molecules bearing a stearic-acid moiety on the basis of HLB (Source: Wikipedia)

From the reasons above, as illustrated in **Figure 1-30**, additives could be classified into four categories:

- The **first category** contains **polymer- and fatty-acid-based derivatives** (hybrid). Some representatives of this category are polyoxyethylene sorbitan esters of fatty acids (e.g., polysorbate 20 (HLB 16.7), polysorbate 40 (HLB 15.6), polysorbate 60 (HLB 14.9), polysorbate 65 (HLB 10.5) and polysorbate 80 (HLB 15.0)), fatty acid esters of polyethylene glycol (PEG) (e.g., PEG-32 glyceryl laureate (HLB 14), PEG-32 glyceryl palmitostearate (HLB 13)) and fatty acid esters of polyglycerol (e.g., polyglyceryl-3-stearate (HLB 7)) (Cottrell & Peij, 2014; Gibson, 2007). They are hydrophilic if HLB is greater than 11 and lipophilic if HLB is less than 9 (Gibson, 2007).

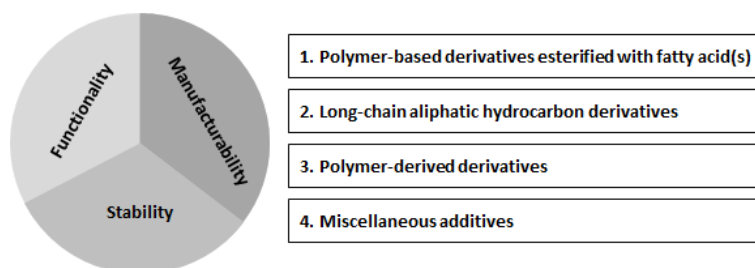


Figure 1-30. Proposed classification of additives used for solid lipid-based formulated products

- The **second category** contain **lipid-based derivatives which bear fatty acid moieties or aliphatic chains in the structure**. Some representatives of this category are esters of non-polymerised alcohol and fatty acids such as fatty acid monoesters of glycerol (e.g., glyceryl monolaurate (HLB 3-4), glyceryl monostearate (HLB 3-4), glyceryl monooleate (HLB 3.4-3.8)), sorbitan esters of fatty acids (e.g., sorbitan monolaurate (HLB 8.6), sorbitan monopalmitate (HLB 6.7), sorbitan monostearate (HLB 4.7), sorbitan tristearate (HLB 2.1), span monooleate (HLB 4.3)), acetic acid esters of mono-/diglycerides (ACETEM), lactic acid esters of mono-/diglycerides (LACTEM), citric acid esters of mono-/diglycerides (CITREM), salts of fatty acids, and sucrose esters of fatty acids (e.g., sucrose mono-/di-/trimer of palmitic acid (HLB 16), sucrose mono-/di-/trimer of stearic acid (HLB 16)) (Cottrell & Peij, 2014; Garti & Yano, 2001; Gibson, 2007; Szűts, 2003). Others could be alkanes (e.g., octadecane), and fatty acids (e.g., stearic acid, oleic acid), fatty alcohols (e.g., stearyl alcohol), esters of fatty acids (e.g., methyl stearate, ethyl oleate, isopropyl myristate), soya lecithin (HLB ~7), oil-soluble vitamin E (J. S. Aronhime et al., 1988; Bertoni et al., 2021).



- The **third category** contains **polymer-based derivatives**. Some representatives of this category which are surfactants include poloxamer 188 (HLB ), polymer 407 (HLB ) (Jannin et al., 2006; Kushwah et al., 2020, 2022). This category also includes polymers that can self-assemble into micellar structures in aqueous media (e.g., polyethylene glycol 10000, polyethylene glycol 20000, polyethylene glycol 100000, polyethylene glycol 1000000, polyethylene glycol 7000000) (Windbergs et al., 2009d, 2009a).

- The **fourth category** contains other substances which have **miscellaneous** chemical structures (e.g., talc, carbon nanotube, graphite, theobromine, ellagic acid dihydrate, terephthalic acid) (Kaneko et al., 2020; Yoshikawa, 2016; Yoshikawa et al., 2014, 2015). This category can be extended to additives used to modify drug release following different mechanisms. For instance, orlistat as lipase inhibitor was reported to be effective to modify drug release kinetics from a digestible lipid-based formulation (Murshed et al., 2022).

#### 4.2.2. Considerations for additive addition

**First consideration:** it is recommended (i) *to select additives or surfactants based on chemical structures* in order to facilitate molecular interactions between themselves and the lipid major component.

As a precaution, combinations of more than one crystalline matters are discouraged as they could give rise to occurrence or stabilisation of metastable solid forms as is the case of crystal structure modifiers (e.g., sorbitan monostearate) (Garti et al., 1982) or mixtures of triglycerides (e.g., tripalmitin/tristearin) (J. Aronhime et al., 1990). Combination of more than one crystalline matters might require an intensive study for their established uses (Aburahma & Badr-Eldin, 2014; Jannin, 2010).

**Second consideration:** concerning the additive addition, it is recommended (ii) to combine at least two emulsifiers whose lipophilicity and hydrophilicity are complementary.

There are several reasons for this practice.

- In the first place, it starts with ① **Functionalities** to be developed into solid lipidic formulations from the early stage of development. The combination of a surfactant and a co-surfactant is not new for pharmaceutical applications (e.g., emulsification). As a hypothesis, this combination should aid in tuning release kinetics of substance actives from solid lipidic formulations by varying the combination ratios between two surfactants. From a point of view of stability, the lipophilic surfactant should also stabilise the incorporation of the hydrophilic surfactant in the solid lipidic formulations for which adding a hydrophilic surfactant alone is suspected to give rise to stability issues (e.g., Ostwald ripening) (D. G. Lopes, Koutsamanis, et al., 2017; Schertel, Salar-Behzadi, Karrer, et al., 2021).

- In the second place, for the combination it is safe to select a liquid lipophilic surfactant rather the one in crystalline state. From the perspective of ② **Stability**, this is to avoid the occurrence of new polymorphs. In addition, liquid lipids (including surfactants) should accelerate  $\alpha$ - $\beta$  polymorphic transformation in the case of spontaneous nucleation (as presented in **Section 2.4.2**) and therefore polymorphism of solid lipidic formulations is controllable. In the case of sporadic nucleation, this

combination is worth testing for an effect on crystallisation behaviours (nucleation and crystal growth) of solid lipidic formulations.

- In the third place, from the perspective of ③ **Manufacturability**, as the sporadic nucleation underlies the non-traditional hot-melt coating approach (i.e., definition of the thermal operational condition above  $T_{m,\alpha}$  (D. G. Lopes et al., 2015)), it is justifiable to state that the lipidic formulations are multifunctional when they can also be produced at this condition (see **Figure 1-14**). Multifunctionality resides in the fact that they can be adapted to the thermal stability profile of substrates. Note that by non-traditional hot-melt coating approach it is possible to eliminate the tempering unit operation which might be time- and energy-consuming. Furthermore, again from the perspective of ② **Stability**, non-traditionally hot-melt coated products might be less susceptible to Ostwald ripening (as presented in **Section 2.3.2**).

- As a back-up strategy, as the addition of liquid surfactants could retard the crystal growth process (as presented in Section 1) by the mechanism of poisoning, it is recommended (iii) to add a third additive which can counter an possible adverse effect of the binary surfactant combination by a stronger effect to promote both nucleation and crystal growth rates. Solving crystallisation issues might help overcome processing issues such as fine overproduction, agglomeration, and delamination (see **Table 1-4**). All these considerations which apply to the case of formulating with high-purity lipids are schematised in **Figure 1-31**.

**CONSIDERATIONS FOR ADDITIVE ADDITION**

Hot-melt coating	Production			Preservation	Applications
<p style="text-align: center;"><b>High-purity lipids</b></p> <p style="text-align: center;">Narrow crystallisation temperature peak</p> <div style="border: 1px solid white; padding: 5px; margin: 5px;">                     Traditional approach  <math>T_{air,f} &lt; T_{m,\alpha}</math> </div> <div style="border: 1px solid white; padding: 5px; margin: 5px;">                     Non-traditional approach  <math>T_{air,f} &gt; T_{m,\alpha}</math> </div>	<p style="text-align: center;">Formulation Feasibility</p> <div style="border: 1px solid white; padding: 5px; margin: 5px;">Solidification</div> <div style="border: 1px solid white; padding: 5px; margin: 5px;">Nucleation</div> <div style="border: 1px solid white; padding: 5px; margin: 5px;">Crystal growth</div>	<p style="text-align: center;">Operation Fluidity</p>	<p style="text-align: center;">Coating Quality</p> <div style="border: 1px solid white; padding: 5px; margin: 5px;">Agglomeration</div> <div style="border: 1px solid white; padding: 5px; margin: 5px;">Fine overproduction</div> <div style="border: 1px solid white; padding: 5px; margin: 5px;">Delamination</div>	<div style="border: 1px solid black; padding: 5px; margin: 5px;">Ostwald ripening</div> <p style="text-align: center;">Crystal size re-distribution? Bloom? Oil migration?</p> <div style="border: 1px solid black; padding: 5px; margin: 5px;">Interfacial interactions</div>	<div style="border: 1px solid black; padding: 5px; margin: 5px;">Technological functions</div> <p style="text-align: center;">Improvement of organoleptic properties ...</p>
<p style="text-align: center;"><b>Complex-mixture lipids</b></p> <p style="text-align: center;">Wide crystallisation temperature range</p> <div style="border: 1px solid black; padding: 5px; margin: 5px;">                     Traditional approach  <math>T_{bed}</math> with SFC <math>\geq 90\%</math> </div> <div style="border: 1px solid black; padding: 5px; margin: 5px;">                     Other approach                      Hot air blow through a (fixed-ratio) mixture of lipid and substrate                 </div>	<div style="border: 1px solid white; padding: 5px; margin: 5px;">Slow crystallisation</div>	<div style="border: 1px solid white; padding: 5px; margin: 5px;">Supercooling</div> <div style="border: 1px solid white; padding: 5px; margin: 5px;">Stickiness</div>	<p style="text-align: center;">Coating Quality</p> <div style="border: 1px solid white; padding: 5px; margin: 5px;">Agglomeration</div> <div style="border: 1px solid white; padding: 5px; margin: 5px;">Fine overproduction</div> <div style="border: 1px solid white; padding: 5px; margin: 5px;">Delamination</div>	<div style="border: 1px solid black; padding: 5px; margin: 5px;">Polymorphic transition</div> <div style="border: 1px solid black; padding: 5px; margin: 5px;">Ostwald ripening</div> <p style="text-align: center;">Crystal size re-distribution Bloom Oil migration</p> <div style="border: 1px solid black; padding: 5px; margin: 5px;">Interfacial interactions</div>	<div style="border: 1px solid black; padding: 5px; margin: 5px;">Biopharmaceutical functions</div> <p style="text-align: center;">Release modifier (e.g. pore former, surfactants with varying HLB) ...</p>
<b>③ Manufacturability</b>					
<b>② Stability</b>					
<b>① Functionalities</b>					
<b>Additive addition</b>					
$\geq 3$			$\geq 2$		$\geq 2$

$T_{air,f}$ , fluidisation air temperature;  $T_{m,\alpha}$ , melting point of metastable form(s);  $T_{bed}$ , bed temperature (product temperature); SFC, solid fraction content (%); CSr/D, crystal size re-distribution

Figure 1-31. Proposal for additive selection by considering manufacturability, stability and functionalities

**Third consideration:** concerning the case of complex-mixture lipids, they can be processed via only one traditional approach. The possible presence of slow crystallisation fraction in their composition

dictates another strategy to define thermal processing conditions (as presented in **Section 1.3.4**). Their polymorphism is difficult to control as were reported in certain case studies. In fact, polymorphic transitions of complex-mixture lipids might be chronological with other post-crystallisation behaviours (e.g., Ostwald ripening, interfacial interactions). However, it is possible to learn from multiple stability issues encountered with high-purity lipids. Actually, while polymorphic transitions might retard release kinetics of an active substance with time, solid-state behaviours related to Ostwald ripening such as lipid blooming, or crystal size re-distribution accelerate or decelerate its release kinetics. In other words, all the possible solid-state behaviours of complex-mixture lipids can compensate each other in terms of release kinetics of the active substance. Depending on the extent of this trade-off, it is also possible to tune with the combination of a surfactant and a co-surfactant and this combination could also comprise a solid surfactant.

Below are the proposed combinations of lipids and additives to be tested in **Chapters 3, 4 and 5**:

- Beeswax plus sorbitan monostearate with/without polysorbate 80;
- Tristearin plus sorbitan monostearate and polysorbate 20 with/without talc;
- Trilaurin with/without talc and D- $\alpha$ -tocopherol polyethylene glycol (1000) succinate.

The choice of one lipophilic surfactant and one hydrophilic surfactant for beeswax relies on the fact that it is a complex-mixture lipid. From a point of view of manufacturability, its chemical composition might cause stickiness or supercooling and additive addition is for processability improvement. From a point of view of stability, addition of two surfactants is also to deal with several solid-state behaviours which are not chronological.

The choice of one lipophilic surfactant and one hydrophilic surfactant for tristearin relies on exploratory studies based on the concept of metastable zone width which has been overlooked in development of solid lipid-based formulations. One objective is to develop multifunctional formulations containing additives. These should be adapted to different thermal operational conditions. Talc is also included to anticipate a possible effect of surfactants on crystallisation rate of the compounded formulations. The other objective is to investigate if the non-traditional approach can help overcome stability issues of Ostwald ripening.

The choice of D- $\alpha$ -tocopherol polyethylene glycol (1000) succinate for trilaurin relies on its favourable biopharmaceutical properties for delivery of poorly water-soluble drugs in combination with a highly digestible triglyceride – trilaurin as well as its melting point is also close to trilaurin. In the case of hot-melt coating with trilaurin, a non-traditional approach is inevitable for targeting  $\beta$  crystallisation because its  $\alpha$  form ought to be liquid at ambient conditions. The effect of the selected surfactant on crystallisation of trilaurin is unknown and therefore talc whose effect was confirmed thereon is included as a back-up strategy.

#### **4.3. Proposal for Design of Solid Lipid-Coated Products as a Function of Formulation Digestibility**

Both immediate release and modified release are obtainable with solid lipid-based formulations whose digestibility is either high, poor or neglectable (as presented in **Section 3.2.2**). Instead of considering

the final functionalities of solid lipid-based formulations (technological or biopharmaceutical), design of hot-melt coated drugs can be based on the digestibility of the formulation itself. In effect, considerations of digestibility of one formulation imply considerations the chemical composition, the target functionalities envisaged for the substrate, the projective release mechanisms, and the need for additive addition. This proposal (**Figure 1-32**) could be time-saving for decision making in pharmaceutical development with some details provided as follows:

- For **highly digestible lipids** (e.g., trilaurin), technological functionalities (e.g., moisture protection, lubrication) and taste masking could be achieved by creating an integral and sufficiently thick to control drug release in the buccal cavity (Banerjee et al., 2021). The thickness of this lipid-based membrane determines immediate release or delayed release of the coated products (Yoshiteru et al., 1990; Yoshitomi et al., 1992, 1993). Furthermore, digestion of this lipid could give rise to amphiphiles which can aid in improvement of bioavailability of poorly water-soluble drugs as was reported for trilaurin (Nishihata et al., 2011; Watanabe et al., 1993; Yoshitomi et al., 2011);

- For **poorly digestible lipids** (e.g., long-chain triglycerides), for development of technological functionalities when an immediate profile is desirable, additive addition is indispensable. For instance, it is the case of the combination of tripalmitin and polysorbate 65 at different ratios which was able to release totally a highly soluble drug within 60 min (Becker et al., 2016; D. G. Lopes, Koutsamanis, et al., 2017; Stocker et al., 2017). On the other hand, digestion of this formulation in which polysorbate 65 constitute 20% w/w was required to enable an immediate release of a poorly water-soluble drug (Bannow et al., 2020). For development of extended-release, many strategies are possible. One can use lipophilic lipids (e.g., hydrogenated vegetal oils, long-chain triglycerides, mixtures of synthetic glycerides) with or without additives and vary coating contents;

- For **non- or almost non-digestible lipids** (e.g., beeswax, carnauba wax, paraffins), to target both taste masking and immediate release, the same formulation approach for poorly-digestible lipids such as tripalmitin applies. As an exception, for this purpose one can use polyethylene glycols of different grades which are not digestible (H. Chen et al., 2010). To target delayed release, the same formulation approach for poorly-digestible lipids such as tripalmitin also applies. For instance, inclusion of digestible surfactants or additives (e.g., oils) in fatty alcohols plus beeswax was reported to successfully deliver probiotics in gastro-resistant dosage forms (Jacobsen et al., 2021). Parallely, one can use fatty acids whose solubility is pH-dependent for enteric release and even for colon-specific delivery. For extended release, the same formulation approach for poorly-digestible lipids also applies.

For all these cases, the coating quality, i.e. complete and uniform coating, should be assured with a minimal coating content (Van Kampen et al., 2015; Woerthmann et al., 2021) which varies as a function of substrate particle size distribution

Each formulation from the three groups of formulations tested will be selected for hot-melt coating amorphous solid dispersions of praziquantel which was developed within a precedent doctoral thesis (Boniatti, 2021). In fact, the digestibility of these three groups should increase in the ranking order: beeswax-, tristearin- and trilaurin-based formulations.

Not only biorelevant and lipolytic release testing methods but a dynamic artificial gastrointestinal model, which integrates peristaltic movement, dissolution, digestion, and absorption, will be deployed for biopharmaceutics evaluation of uncoated and coated products in **Chapter 6**. In this chapter, stability studies will also be performed to investigate the impact of different coatings on the amorphous state of praziquantel.

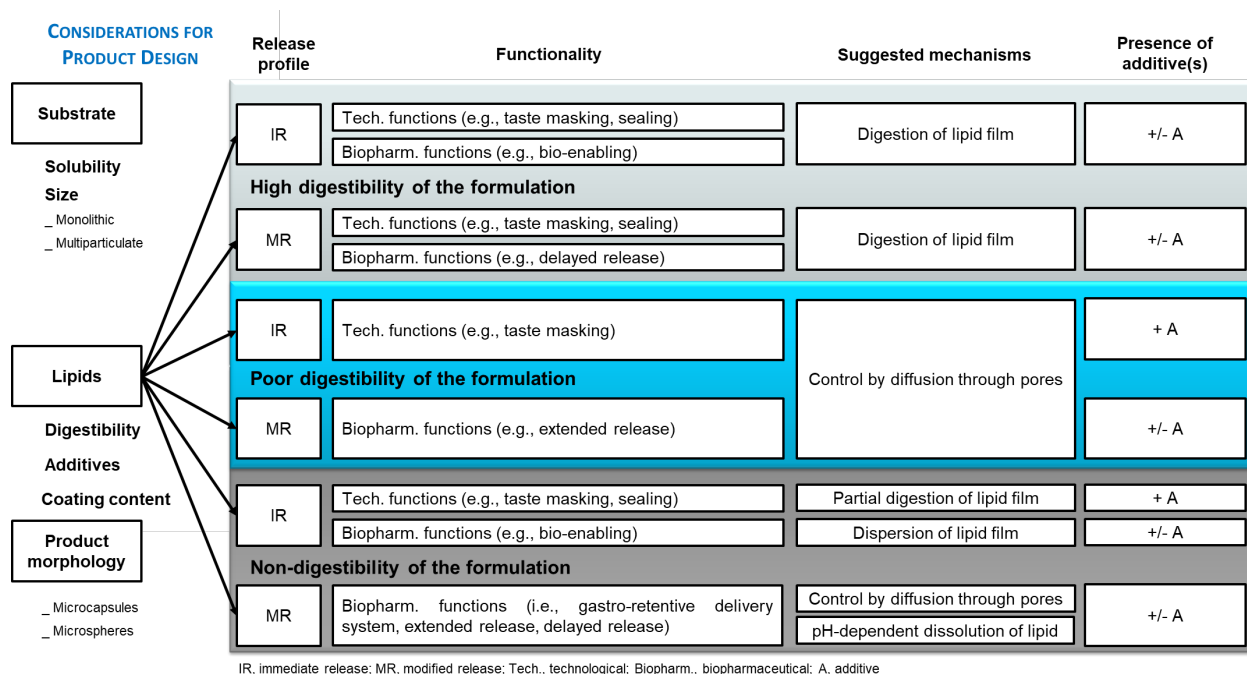


Figure 1-32. Proposal for design of solid lipid-coated products as a function of formulation digestibility

## 5. Conclusions

This chapter addressed, **firstly**, the common lack of thorough considerations of the three interlinked aspects – **manufacturability, functional performance and stability** – in the current development of hot-melt coating formulations (ICH Q8 (R2), 2009).

Most of hot-melt coating research has been focused on development of a pharmaceutical application with limited availability of stability data, while characterisation of coating equipment might also be missing. Few but precious development works which follows Q8 guidelines can serve as role models (Becker et al., 2016; D. G. Lopes et al., 2016; Stocker et al., 2017).

**Secondly**, this chapter brought together considerations of **process design, materials selection, and product design**. Based on this literature review, for process design, a theoretical framework underlying a physics-based experimental approach proposed here will be applied in **Chapters 3, 4 and 5** for simple and nimble development of formulations in the early stage. In this approach, the importance of defining thermal conditions for lipid crystallisation and how to control these conditions by three key process variables was explained. For materials selection, relevant and systematic knowledge of crystallisation and post-crystallisation behaviours was extracted from the base of literature to back up engineering of processable and stable formulations. For product design, considerations on structures of solid lipid-

based formulations as a function of chemical composition, digestibility and morphologies are indispensable.

This chapter aimed, **thirdly**, at resolving three stereotypes. In the first place, hot-melt coating does suit thermosensitive substrates. In fact, for this type of substrates a low fluidisation air temperature can be defined in such a manner that this allows for solidification of lipids or select formulations whose melting point of the most stable form is appropriate. In the second place, stability of lipids appears not so difficult to control but lack of knowledge about crystallisation and post-crystallisation behaviours makes it challenging. In fact, two categories of high-purity (e.g. trilaurin, tristearin) and complex-mixture lipids (e.g., beeswax) were treated in parallel and the proposed strategy for additive selection will be tested in **Chapters 4 and 5**. In the third place, lipids represent a versatile tool for design of solid dosage forms with diverse release patterns. In fact, understanding physicochemical and biopharmaceutical properties of lipids and advantages of melt spray-coating can give rise to new functionalities of solid lipid-based formulations.

This chapter supports, **fourthly**, the fact of having an open mindset when dealing with the subject of hot-melt coating. From a point of view of process, the comparison with solvent-based/aqueous coating was to help elucidate the working principles of hot-melt coating. From a point of view of materials, applications of lipids are abundant. By sticking to the principles of lipid crystallisation and polymorphism for development of hot-melt coating formulations, one can refer to other research fields so that data (e.g. thermal stability) not be duplicated. One can also apply the results of food research on the effect of additives and treatment of lipid polymorphism. One can also inspire from nucleation triggering screening of phase change materials for thermal energy storage. One can also learn from hot-melt adhesives industry to define a crystallisation temperature linked with quality coating. From a point of view of products, polymer and lipid are life-long companions (Siepmann et al., 2019) so that scientific ideas should be interchangeable. In fact, as bead coating by air suspension bed is possible with polymer-based amorphous solid dispersions, it should also be technically viable with lipid-based solidified emulsions/dispersions. This could open a new trend of hot-melt coating studies on poorly water-soluble drugs.

## Chapter 2. METHODOLOGY

### General Introduction

The purpose of this chapter is not to describe in detail the characterisation techniques used in the thesis, but rather to present the rationale behind the choice of materials and techniques used.

The selection of the chosen characterisation techniques will be aligned with the three aspects of pharmaceutical development (as presented in **Chapter 1**) in responding to the following questions:

- Firstly, concerning evaluation of material processability and product feasibility, *will the technique(s) be able to simulate the most possible operational conditions under which lipids are processed?*
- Secondly, concerning characterisation of equipment, *will the technique(s) be reliable to conclude yield, efficiency, process regime and coating quality?*
- Thirdly, concerning evaluation of pharmaceutical applications, *will the technique(s) be specific and sensitive to determine concentration of model drugs? Could in vitro conditions for measurements of release kinetics mimic the most possible in vivo conditions to conclude a relevant release profile for solid lipid-based coated products?*
- Finally, concerning characterisation of product stability, *will the technique(s) be specific and sensitive to identify and quantify solid-state behaviours of either lipids (e.g., polymorphism, Ostwald ripening) or model drug (e.g., glass transition temperature) in coated products?*

In order to answer these questions and, based on the literature review given in **Chapter 1**, certain characterization techniques are inspired by other fields of research and developed within the framework of this doctoral thesis. **Figure 2-1** shows the interlink between theoretical work and experimentation for the conduct of this doctoral thesis.

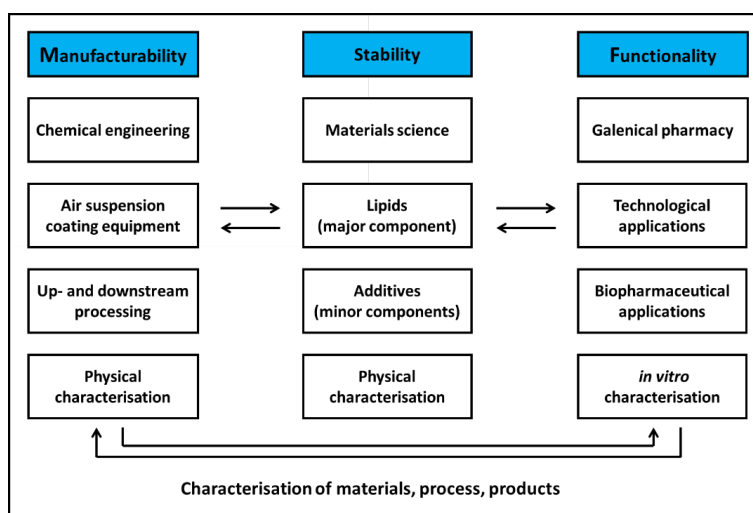


Figure 2-1. Importance of characterisation in formulation development and pharmaceutical applications

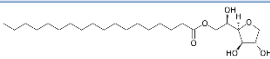
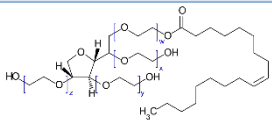


## 1. Materials

### 1.1. Coating materials

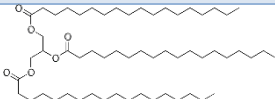
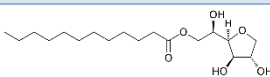
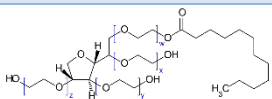
Three groups of formulations that will be tested in the experimentation of this doctoral thesis are presented as follows in the order of decreasing digestibility.

Table 2-1. Beeswax and surfactants

Material	Beeswax	Sorbitan monostearate	Polysorbate 80
Organoleptic properties	Yellowish waxy pastilles	Greenish waxy pastilles	Viscous liquid
Molecular weight (g/mol)	-	430.63	1309.66
Chemical formula	* hydrocarbons, free fatty acids, free fatty alcohols, monoesters, diesters, triesters, hydroxy monoesters, acid monoesters, acid polyesters, hydroxy polyesters	<b>C<sub>24</sub>H<sub>46</sub>O<sub>6</sub></b>	<b>C<sub>64</sub>H<sub>124</sub>O<sub>26</sub></b>
Chemical composition			
* (Dobrosielska et al., 2023)			

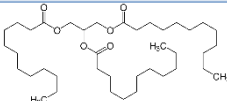
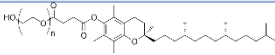
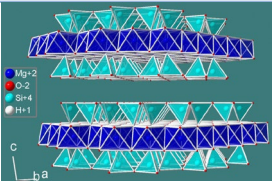
All materials in **Table 2-1** will be used for compounding beeswax-based formulations in **Chapter 3**.

Table 2-2. Tristearin and additives

Material	Tristearin	Sorbitan monolaurate	Polysorbate 20
Organoleptic properties	White powder	Yellowish viscous liquid	Yellowish viscous liquid
Molecular weight (g/mol)	891.48	346.46	approx. 1200
Chemical formula	<b>C<sub>57</sub>H<sub>110</sub>O<sub>6</sub></b>	<b>C<sub>18</sub>H<sub>34</sub>O<sub>6</sub></b>	<b>C<sub>58</sub>H<sub>114</sub>O<sub>26</sub></b>
Chemical composition			

Together with sorbitan monostearate (**Table 2-1**) and talc (**Table 2-3**), all materials in **Table 2-2** will be used for compounding tristearin-based formulations in **Chapter 4**.

Table 2-3. Trilaurin and additives

Material	Trilaurin	Vitamin E D- $\alpha$ -tocopherol polyethylene glycol 1000 succinate	Talc
Organoleptic properties	White powder	Yellowish waxy matter	White powder
Molecular weight (g/mol)	638.55	574.80	379.27
Chemical formula	<b>C<sub>45</sub>H<sub>86</sub>O<sub>6</sub></b>	<b>(C<sub>2</sub>H<sub>4</sub>O)<sub>n</sub>C<sub>33</sub>H<sub>54</sub>O<sub>5</sub></b>	<b>Mg<sub>3</sub>Si<sub>4</sub>O<sub>10</sub>(OH)<sub>2</sub></b>
Chemical composition			

All materials in **Table 2-3** will be used for compounding trilaurin-based formulations in **Chapter 5**.

Almost the presented information about chemical formula and chemical composition was sourced from the online free encyclopaedia **Wikipedia**.

## 1.2. Substrate

### 1.2.1. Sodium chloride

Salt crystals (salt purity >99,9%) were commercially sourced from Baleine SA, Salins, France. It can be regarded as a model drug (Clarkson et al., 1971). In fact, it is the active pharmaceutical ingredient of a medicine which has been marketed since 1998 under the commercial name Slow Sodium Tablets® (PL 44490/0004). However, the first motivation to use salt as a model substrate was the simplicity of checking membrane integrity during release tests on coated products (salt dissolves instantaneously in the dissolution media used in this thesis if it is not coated).

Salt crystals were sieved and the size fraction of solids between 400 and 630 µm were retained for coating trials without prior co-processing with any other excipients.

Sodium chloride will be the substrate for hot-melt coating investigations in **Chapter 3**, **Chapter 4** and **Chapter 5**. In addition, some lipid formulations selected from these chapters will be briefly compared with the coated commercial salt form (Slow Sodium Tablets®) in terms of release profile.

### 1.2.2. Amorphous solid dispersions of praziquantel

Within the framework of this doctoral thesis, solid amorphous dispersions of praziquantel, as a challenging model drug in terms of physical stability and drug release rate, was tested to valorise hot-melt coating applications. This high-tech product was developed in a previous thesis (Boniatti, 2021). Solid amorphous dispersions of praziquantel will be the substrate for hot-melt coating investigations in **Chapter 6**.

## 2. Methods

### 2.1. Characterisation of Materials

#### 2.1.1. Solidification (kinetics in isothermal & non-isothermal conditions)

As presented in **Chapter 1**, solidification or crystallisation is the most important property of lipids as this underlie the principles of hot-melt coating. Crystallisation involves the two physical processes: nucleation and crystal growth. To investigate lipid crystallisation behaviours, three principal characterisation techniques – *differential scanning calorimetry (DSC)*, *turbidimetry* and *polarised light microscopy (PLM)* – were used in the experimentation. While a crystallisation profile (solid fraction content as a function of time) can be obtained with DSC, turbidimetry and PLM tend to target the information of nucleation and/or crystal growth.

##### 2.1.1.1. *Differential scanning calorimetry*

All the thermal analyses (DSC) were performed with DSC Q200 (TA Instrument, USA). Its working principles are based on uptake and loss of heat. In fact, in the course of thermal analyses of this type, samples are subject to heating or cooling at a constant rate. When a phase transition (e.g., polymorphic

transformation, fusion, crystallisation) in samples occurs, heat is transferred to keep the temperature difference constant the energy needed for this event is registered (Nyqvist, 1993).

The applications of DSC in this doctoral thesis are as follows:

*In preformulation:*

- To construct a solidification profile for defining thermal operational conditions (Fernanda, 2018; Müller et al., 2018). This is adapted to beeswax-based formulations whose spontaneous crystallisation is the core principle of the traditional approach of hot-melt coating;
- To construct a solidification profile of triglyceride-based formulations at a target crystallisation temperature (in an isothermal condition) higher than the melting point of metastable form(s) (Bertoni et al., 2021);

*In stability study (other than investigation of crystallisation behaviours):*

- To identify the polymorph(s) or the polymorphic profile occurring in the samples.
- To determine the crystallinity of the model drug in the amorphous solid dispersions.

More details about its procedures and applications will be presented in **Chapter 3, Chapter 4 and Chapter 5.**

#### 2.1.1.2. Turbidimetry with Crystal16<sup>®</sup> crystallization systems

Turbidimetry with Crystal16<sup>®</sup> crystallization systems was deployed as a **fast screening method in development for selection of their lipid-additive systems based on nucleation behaviours.**

Crystal16<sup>®</sup> is a device used to monitor crystallisation at the scale of mL. This device is capable of (1) controlling the temperature of vials of 1.5 mL, (2) probing dissolution/precipitation during crystallisation via turbidity measurements by laser (detection of crystal appearance), and (3) having a small well-stirred system in each vial. This device has four blocks (and 4 vials/block) which are equipped with a temperature controller. When using the same lipid in the four blocks, adding in each block (4 vials) a different amount of the same additive or combination and specifying one identical temperature programme for four blocks, it is possible to test the effect of additive in 16 samples at the same time. **Figure 2-2** shows the simple design of Crystal16<sup>®</sup> and its working principles of turbidimetry, which consist of measuring disappearance or appearance of melting or crystallising trilaurin in molten media, respectively.

Some of the advantages of this device rely on the possibilities (1) to simulate processing thermal conditions with a maximal cooling/heating rate up to 20°C.min<sup>-1</sup> and (2) to provide a higher analysis throughput than conventional techniques such as DSC. Note that a transmissivity of 1% at the time of nucleation does not mean a complete solidification or crystallisation.

More details about its procedures and applications will be presented in **Chapter 3, Chapter 4 and Chapter 5.**

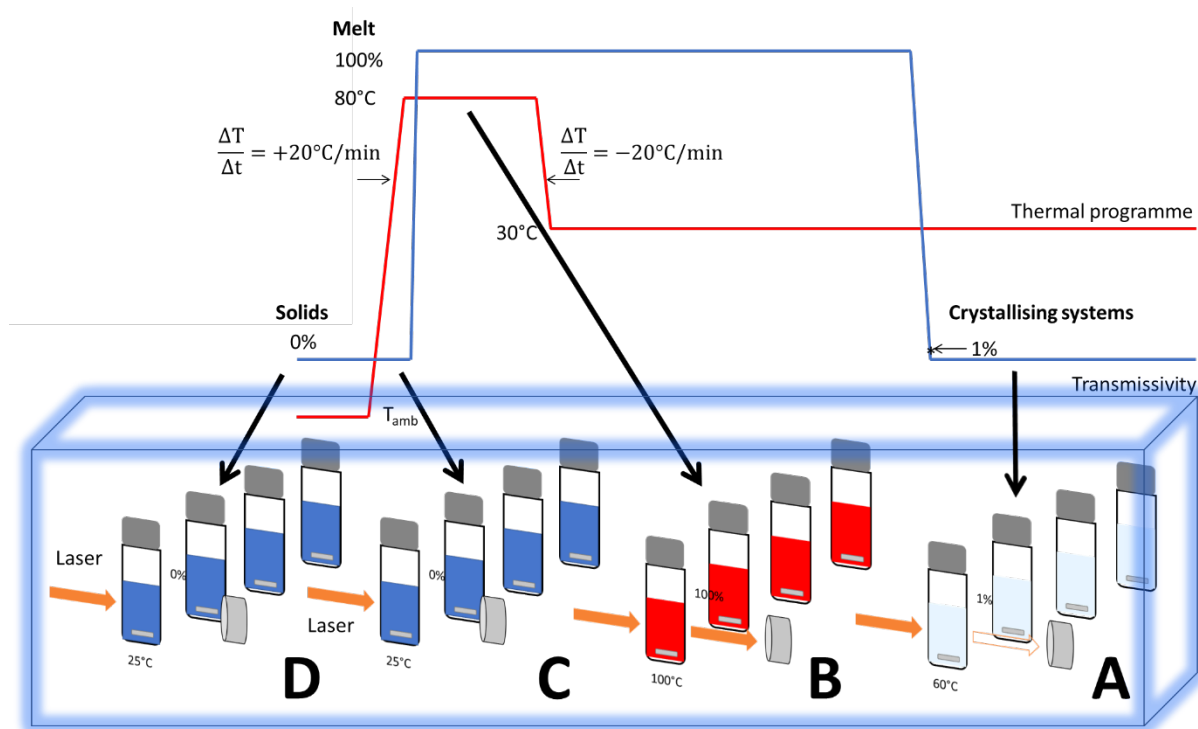


Figure 2-2. Working principles of Crystal16® Crystallization systems (adapted from Yakugaku Zasshi, 2014)

### 2.1.1.3. Polarised light microscopy

Polarised light microscopy (PLM) was performed using the microscope Zeiss IMAGER.M2m equipped with a tube lens 1.25x, integrated with Aixocam 305 Color (additional magnification 10x) and accompanied by a temperature-controlled platinum plate (Linkam). It is possible to observe a length-scale of 50  $\mu\text{m}$  with a good resolution using two external long-distance objectives 20x and 50x. Its working principles are based on the chemical nature of lipids as long-chain molecules. In fact, when the incident polarised light interacts with long-chain molecules which arrange in different planes in lipid crystal network, its intensity will diminish to different extent (possibly down to extinction) depending on the angle between the plane of lipid arrangement and the plane of electromagnetic field. Therefore, for anisotropic materials like lipids, morphology of crystals can be observed with birefringent patterns. PLM does not work for amorphous matter and crystallite matter with cubic geometry (Nyqvist, 1993; Wolman, 1975).

More details about its procedures and applications will be presented in **Chapter 3**, **Chapter 4** and **Chapter 5**.

### 2.1.2. Other processing-specific properties (viscosity, contact angle)

#### 2.1.2.1. Rheometry (rotation)

FT Rheometer (Fischer, Germany) was deployed for rheometry. The rotation mode with plate-plate geometry was applied for measurement of shear viscosity of the lipid-based formulations in molten state as a function of shear rate and as a function of temperature (Wik & Wik, 1993). Shear viscosity is

important for spray coating as it represents a measure of their resistance to flow in thermally relevant unit operations such as pumping, spraying and spreading on the surface of substrate and coated substrate (Carnicer et al., 2021).

More details about its procedures and applications will be presented in **Chapter 3** and **Chapter 4**.

### 2.1.2.2. Hot-melt goniometry

The system Drop Shape Analyzer DSA30 (Krüss) was deployed for contact angle measurement. Based on a research work done on pastillation technology (Kim, 2003), the system was adapted to experimentation with lipid-based formulations in molten state for the preformulation work. It is therefore called “hot-melt goniometry”. **Figure 2-3** shows a simple schematic of this system. Its working principles are based on imaging the shape evolution of a droplet on a substrate. The temperature of the substrate surface and the delivery velocity can be set to be representative of the process variables. Therefore, this technique can serve multiples purpose for evaluating qualitatively the interlink between formulation properties, substrate properties and process variables.

More details about its procedures and applications will be presented in **Chapter 3**, **Chapter 4** and **Chapter 5**.

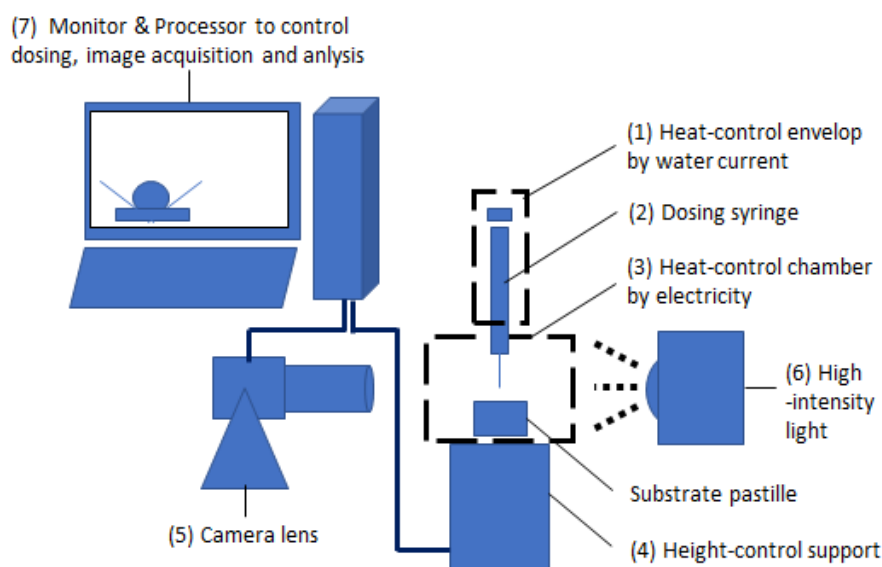


Figure 2-3. Setup of goniometry for contact angle measurements in molten state (Huynh et al., 2024)

## 2.2. Process Characterisation

Characterisation of the coating equipment is performed indirectly on coated products by evaluating the impact of each formulation on processing performance and coating quality. Processing performance is assessed by considering four key indicators: (i) yield, (ii) efficiency, (iii) target process regime and (iv) coating quality. Coating quality is assessed by considering some of five quantitative indicators: (1) mean coating thickness, (2) interparticulate thickness distribution, (3) intraparticulate thickness distribution, (4) porosity and (5) surface completeness (Van Kampen et al., 2015; Woerthmann et al., 2021).

Yield and efficiency can be evaluated by virtue of quantifying coating contents in coated samples collected in different timepoints according to the multiple-sampling experimental approach (proposed in the conduct of this doctoral thesis). Assay of coating contents can be performed directly by DSC and indirectly by assay of model drug in the finished coated products by a method that is specific to the model drug itself. This will be presented in **Assay**. Process regime and certain indicators of coating quality can be qualitatively and quantitatively assessed by measurement of particle size distributions by laser diffraction, microscopical techniques and measurement of release kinetics.

#### 2.2.1. Measurement of particle size distributions by laser diffraction

Mastersizer 3000 (Malvern) was deployed for measuring particle size distributions of raw materials and coated products. Its working principles are based on measuring the angular variation in intensity of light scattered as the incident laser beam (red or blue) traverses a sample of dispersed particles. Coarse particles diffract incident light at small angles compared to its axis while fine particles diffract incident light at wide angles. The intensity-as-a-function-of-scattering-angle data are then converted into particle size distributions. The Mastersizer uses the full Mie theory which completely solves the equations for interaction of light with matter (Ebnesajjad, 2014; *Laser Diffraction Particle Size Analysis | Malvern Panalytical*, s. d.). Mie theory assumes the particle is spherical, as opposed to Fraunhofer, which is a projected area prediction. The penalty for this complete accuracy is that the refractive indices for the material and medium must be known and the absorption part of the refractive index must be known or estimated.

Based on the particle size distribution measured for a sample of coated particles, it is possible to determine which process regime (e.g., growth, breakage) occurred in a unit operation (Stiller, 2016). Besides, in the normal practice, mean coating thickness can be obtained by calculating the difference between the volume-weighted diameter of coated particles and that of uncoated particles (initial substrate) (D. G. Lopes et al., 2015) *provided that a coating regime is established in the operation*.

More details about its procedures and applications will be presented in **Chapter 3**, **Chapter 4** and **Chapter 5**.

#### 2.2.2. Optical microscopy

Optical microscopy was performed with the optical microscope Leica under transmission mode. Its working principles are based on collection of scattered electromagnetic radiations (corresponding to visible light whose wavelength ranges from 390 nm to 700 nm) after the light beam travelling from the source either passing through the sample (transmission mode) or reflected by the sample (reflection mode) (Fernanda, 2018). This technique is simple, non-destructive and able to perform *in situ* for qualitative evaluation of process regime and coating quality.

More details about its procedures and applications will be presented in **Chapter 3**, **Chapter 5** and **Chapter 6**.

### 2.2.3. Scanning electron microscopy

TM3000 TableTop Scanning Electron Microscope (Hitachi, Japan) was deployed for evaluation of coating quality and surface properties of lipid-coated products subject to effect of additive-addition, processing conditions and aging (stability study). SEM is an imaging technique. Its working principles consist of illuminating the sample with a beam of electrons and detecting these back-scattered electrons to construct the image (Fernanda, 2018). Following are several types of electrons detected associated with types of the acquired information:

- Back-scattered elastic electrons constitute chemical contrast image of the surface. Observable features of an object are based on the molecular weight of chemical components in its composition. The higher the molecular weight of its constituents the brighter the object reflected in its image. This mode is used for evaluation of coating completeness.
- Secondary electrons originating from inelastic interactions between the primary electrons and the sample surface constitute topographical contrast image. This mode offers more resolution for evaluation of surface properties. For low-conductivity materials like lipids, they are often sputtered with metal before analyses.

More details about its procedures and applications will be presented in **Chapter 3**, **Chapter 4**, **Chapter 5** and **Chapter 6**.

## **2.3. Characterisation of Products**

Stability of coated products depends on the control of solid-state behaviours (e.g., polymorphism, re-crystallisation from amorphous state, Ostwald ripening) under long-term storage conditions. The possible consequences are reflected on surface properties of coated products and release kinetics of model drugs. Techniques to characterise the corresponding phenomena will be presented below.

### 2.3.1. Polymorphism or solid forms

#### 2.3.1.1. *X-Ray powder diffraction*

Besides thermal analyses with DSC, solid-state behaviours could be investigated by X-ray diffraction which was performed using Malvern PANalytical Empyrean diffractometer with reflection mode. X-ray diffraction gives resolution of the crystal lattice geometry based on the fact that the characteristic distance between the identity periods of the crystal lattice is close to the wavelength of X-rays. Its working principles consist of “accumulation or amplification” of the elastic scattering electrons in the directions in which the amplitudes of the radiation scattered from different atoms in the crystal lattice are in phase. The diffractogram is a record of coherent scattering intensities (Bragg peaks) as a function of diffracted angle  $\theta$ . Bragg peaks in the wide-angle region ( $10^\circ < 2\theta < 30^\circ$ ) and small-angle region ( $1^\circ < 2\theta < 8^\circ$ ) polymorphism provide information about polymorphism and crystallite size, respectively (Fernanda, 2018; Nyqvist, 1993).

Measurement of X-ray powder diffraction was performed in stability studies with the objectives:



- To identify the lipid polymorph(s) or the polymorphic evolution in the samples;
- To determine approximately the crystallize size of lipids in coating;
- To monitor the solid-state behaviours of amorphous drug.

More details about its procedures and applications will be presented in **Chapter 3**, **Chapter 4**, **Chapter 5** and **Chapter 6**.

#### 2.3.1.2. *Raman spectroscopy*

RAMAN spectroscopy was performed with RAMAN-AFM Alpha 300 AR (WITec, Ulm, Germany). Its working principles were based on polarizability of the molecule in the chemical bonds of a sample after being exposed to an incident laser. Resulting from vibrations in the chemical bonds the interactions with photons lead to specific energy shifts in the back scattered light (inelastic scattering) recorded in RAMAN spectrum (*Raman Spectroscopy*, 2018; *WITec Raman Imaging*, s. d.). This technique is rapid, non-destructive and able to perform *in situ* for qualitative evaluation of lipid polymorphism and polymorphic transformation.

More details about its procedures and applications will be presented in **Chapter 4**.

#### 2.3.2. Surface properties

The use of SEM for evaluating surface properties subject to aging was described above. These properties can also be evaluated by atomic force microscopy and dynamic vapour sorption.

##### 2.3.2.1. *Atomic force microscopy*

AFM was also performed with RAMAN-AFM Alpha 300 AR (WITec, Ulm, Germany). Its working principles consist of recording movement of the probe (a sharp tip mounted on a cantilever) and its interaction forces with the sample surface on a piezo-driven scanning stage which provides spatial adjustment parallel or perpendicular to the sample surface. Thereby, the tip traces topography as well as adhesion, stiffness of the sample surface at the nanometric scale (*Atomic Force Microscopy (AFM) - WITec Raman Imaging*, s. d.). This technique is non-destructive, able to provide high resolution and to perform *in situ* for (1) measurement of adhesion of different coatings and (2) qualitative and quantitative evaluation of the surface of hot-melt coated particles subject to polymorphic transformation.

More details about its procedures and applications will be presented in **Chapter 3** and **Chapter 4**.

##### 2.3.2.2. *Dynamic vapour sorption*

Dynamic vapour sorption profiles were recorded using a DVS Resolution instrument (Surface Measurement Systems, London, UK). Its working principles consist of measuring gravimetrically the content of adsorbed water onto materials exposed to specified levels of relative humidity and temperature for a fixed time. In effect, materials when exposed to a controlled humidity environment at a temperature are susceptible to adsorb water vapour to certain extent and rate. A cycle of exposure to increase and decrease in humidity provides information about the type of water bonding (Nyqvist, 1993).

Based on the literature analysis on hot-melt coating, DSV was applied (i) to investigate an effect of moisture protection of lipids (A. Achanta, 1999; A. S. Achanta et al., 2001; H. Chen et al., 2010; Sorgatz, 2011) and (ii) to evaluate surface properties subject to aging (Schertel, Salar-Behzadi, & Zimmer, 2021).

More details about its procedures and applications will be presented in **Chapter 5** and **Chapter 6**.

### 2.3.3. Miscellaneous

For accompanying the selection of these physical characterisation techniques, other devices include, for example, climatic chamber, hot even, centrifuge, balances, etc. Evaluation of powder flow properties was also performed using Freeman FT4 powder rheometer and its protocol was presented in **Chapter 3 – Part 1**.

## 2.4. *In Vitro* Characterisation

### 2.4.1. Measurement of digestibility/Combination of digestion and dissolution

The pH STAT Titrand 901 equipped with a dosing unit Dosino 800 (Metrohm, Switzerland) was used for measurement of digestibility of solid lipid-based formulations or combination of coating digestion and dissolution of model drug from coated products. Its working principles consist of real-time measurement of pH value susceptible to change in the course of lipolysis and maintenance of a stable pH setpoint (often physiologically relevant) by adding an alkaline solution (e.g., sodium hydroxide) (Arnold et al., 2012; Williams et al., 2012).

The establishment of this method consists of two steps:

- Determination of lipase activity in pancreatin powder (commercial);
- Preparation of pancreatin extract whose lipase activity should be physiologically relevant or adapted to the tested lipid systems.

It is important to use the same lipase activity in all *in vitro* lipolysis tests, for instance, to assure (i) a good comparison in digestibility of different solid lipid-based formulations and (ii) a good link between two study sites RAPSODEE and MEDiS (UCA) (Brodkorb et al., 2019; Grundy et al., 2021).

For *in vitro* lipolytic testing, definition of testing parameters (e.g., concentration and dosing rate of NaOH solution, pH dynamics) based on digestibility of lipids is also important to obtain a good digestion profile. **Figure 2-4** shows the simple schematic of pH Stat, thermostat and conductometer for measurement of release kinetics of coated salt particles.

More details about its procedures and applications will be presented in **Chapter 3**, **Chapter 5** and **Chapter 6**.

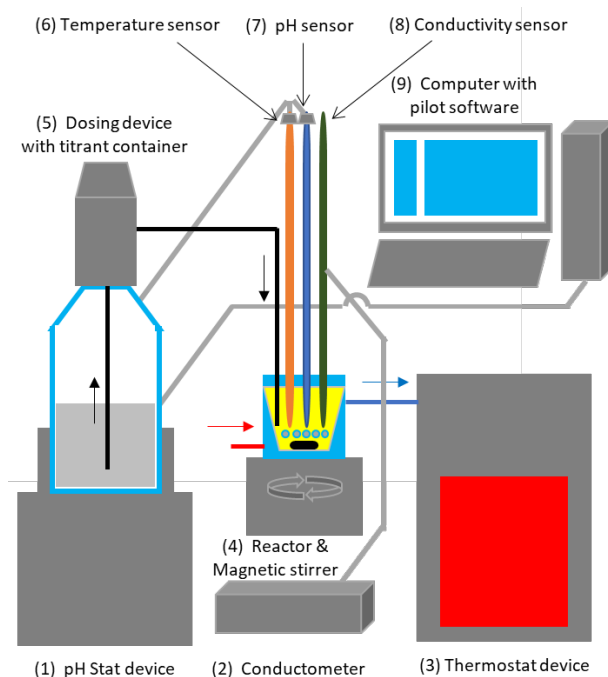


Figure 2-4. Setup of pH STAT for release kinetics measurements in biorelevant media (Huynh et al., 2024)

#### 2.4.2. Assay of model drugs

In this doctoral thesis, sodium chloride and praziquantel which are highly and poorly water-soluble drugs were used for development of solid lipid-based formulations and pharmaceutical applications. Conductometry and liquid chromatography coupled with UV-Vis detector represent two assay methods adapted to each model drug, accordingly.

##### 2.4.2.1. Conductometry

Conductometry was conducted using CDM10 (RadiometerLab, Copenhagen) and pPhenomenal® CO 3100 H (VWR). Conductometry is applied to quantify **sodium chloride** contents in the finished coated products as well as its concentration in real time measurement of release kinetics. There have been applications of this test relevant to coating by fluidised bed and pharmaceutical research (Claviez et al., 1999; Van Kampen et al., 2015; van Kampen, 2018). Its working principles are based on the conductivity of sodium chloride in aqueous. Despite the simplicity of testing, interference of other ionisable components in testing media, limits of quantification and temperature dependence of conductivity should be considered.

More details about its procedures and applications will be presented in **Chapter 3**, **Chapter 4** and **Chapter 5**.

##### 2.4.2.2. Chromatography coupled with UV-Vis

An integrated UPLC system (Agilent 1260 Infinity II) was used for assay of **praziquantel** in amorphous solid dispersions and coated products. This device comprises the liquid chromatography and the detector UV-Vis. Its working principles consist of (i) separating the active substance dissolved from other

components in the complex media (e.g., biorelevant media) in the diluent (mobile phase) through hydrophilic/lipophilic/steric interactions with the column packed with microparticles (stationary phase) and (ii) detecting it by its characteristic absorption UV wavelength. The latter step comprises of identification and quantification by the appearance of the characteristic peak of model drug at a retention time and by the area under peak at that position in the chromatograph, respectively. It is important to consider selection of an appropriate diluent and definition of pumping rate, run time of an analysis for both separation of peaks and good maintenance of the device. Normally, validation is necessary by considering specificity, linearity and range, accuracy, precision and robustness of the method in development (Siewert et al., 2003).

More details about its procedures and applications will be presented in **Chapter 6**.

### 2.4.3. Measurement of release kinetics

At first, the physical process of dissolution is presented for a better understanding of release testing models. Dissolution kinetics of a drug with a single size bin of particles (presumably spherical) is described in a mechanistic meaning by the Nernst-Brunner equation as follows (Sugano & Terada, 2015):

*Equation 33 :*

$$\frac{dM}{dt} = \frac{3D}{\rho_p h r_{p,0}} Dose^{1/3} M_{s,t}^{2/3} (C^{eq} - C^b(t))$$

where  $\mathcal{D}$  is the diffusion coefficient ( $m^2/s$ ),  $\rho_p$  the true density of drug particles ( $m^3.kg^{-1}$ ),  $h$  the thickness of unstirred water layer (m),  $r_{p,0}$  the initial radius of the dissolving particles (m),  $Dose$  the initial amount of drug to be dissolved (kg),  $M_{s,t}$  the remaining amount of drug to be dissolved at time  $t$  (kg),  $C^{eq}$  the equilibrium solubility of drug in the dissolution media ( $kg.m^{-3}$ ),  $C^b(t)$  the bulk concentration of drug in the dissolution media at time  $t$  ( $kg.m^{-3}$ ) and  $V$  the volume of dissolution medium ( $m^3$ ).

Intuitively, dissolution rate of drug particles is directly related to its physicochemical properties (e.g., solubility, molecular weight, dose, particle size) and hydrodynamic conditions (e.g., mixing rate, volume, viscosity of dissolution medium).

The Nernst-Brunner equation could be expressed alternatively by regrouping involved physical parameters (Bransford et al., 2019):

*Equation 34 :*

$$\frac{df}{dt} = \frac{1}{\tau} (1 - f)^{2/3} \left(1 - \frac{f}{f_\infty}\right)$$

where  $\frac{1}{f_\infty} = \frac{Dose}{C^{eq}V}$  is the ratio of the final concentration reached when the dose is completely dissolved in the volume of dissolution medium to the equilibrium solubility of drug. In fact, it is the dose number  $Do$ , equivalent to **Equation 27** presented in **Chapter 1**.  $\frac{1}{\tau} = \frac{3DC^{eq}}{\rho_p h r_{p,0}}$  is the reciprocal of the mean dissolution time (MDT), representing the formulation properties (e.g., drug particle size distribution,

solubility, state of being coated or uncoated). For information, MDT is equivalent to **Equation 30** presented in **Chapter 1**.

When  $f_{\infty}$  is greater than 3, a three-fold sink condition is achieved, the time required to reach 85% dose dissolved becomes relatively constant. Based on the dose number  $Do$ , the sink condition is achieved when the volume of dissolution medium for dissolution of the dose to reach a concentration at least 3 times less than the equilibrium solubility of drug. With this condition, dissolution depends primarily on the formulation properties and its processing history. In fact, when performing numerical solution for the second Nernst-Brunner equation, it was shown that time to 85% dissolved as multiples of  $\tau$  remain almost constant when  $f_{\infty}$  is greater than 3. (Bransford et al., 2019). This justifies the application of a sink condition in quality control (QC) dissolution tests to discriminate the influence of process parameters and formulation variables on product performance without the interference of dissolution testing conditions.

When  $f_{\infty}$  is smaller than 3, the time required to reach 85% dose dissolved is no longer relatively constant. In this instance, dissolution rate becomes more sensitive to perturbations in the experimental conditions (Bransford et al., 2019). Application of non-sink condition is often associated with biorelevant dissolution practice in order to rank-order bioenabling technologies or formulations as well as to study the influence of systems biology parameters (e.g., dynamic changes in pH, volume) on product performance.

Following the explanation of the physical process of dissolution, experimental dissolution conditions could be decided based on the availability of current dissolution models:

- (i) stirred vessel methods: USP 2 paddle apparatus and pH Stat model;
- (ii) continuous flow methods: USP 4 flow-through cells apparatus;
- (iii) artificial gastro-intestinal models: TNO-TIM 1 (for absorption measurements).

In the case of measuring release kinetics of **sodium chloride** from coated products, the use of stirred vessel methods is sufficient. A dissolution volume of 250 mL (minimum) in comparison with the normal practice (900 or 1000 mL) responds to the sink-condition (Siewert et al., 2003). As conductometry is not specific, pure water could be selected as dissolution medium. In the case of testing with lipolysis, the baseline of conductivity should be taken into account as well as the salt content in biorelevant composition is removed.

In the case of measuring release kinetics of **praziquantel** from uncoated and coated amorphous solid dispersions, all the current dissolution models are chosen. As praziquantel is a poorly water-soluble drug, the specificity of the assay method is dispensable and this justifies the use of liquid chromatography coupled with UV detector. Two testing approaches based on the sink and non-sink conditions should be considered in order to establish (i) a quality-oriented method (using simple buffers) and (ii) a biorelevant method (with pH Stat model or flowthrough cells, among others).

On the one hand, the quality-oriented method should be sensitive and discriminative to detect any changes in formulation design, manufacturing operation and stability monitoring (Nicklasson, 1993). On the other hand, the biorelevant method could help evaluate the physiological impact (e.g., presence

of bio-surfactants, digestion) on the release kinetics and the apparent solubility of praziquantel amorphous solid dispersions uncoated and hot-melt coated with formulations whose digestibility is different. Biorelevant data could be useful to complement the results of other complex models (Eason et al., 2022).

Furthermore, flow-through cells are deployed for testing release kinetics of solid lipid-based formulated products. It's also a method that allows to work under standardized solid-liquid interface conditions. One of the most important parameters in comparative dissolution is to ensure that the results obtained (e.g. differences) are not due to the method. The use of a cell provides a laminar flow and more rigorous control of the solid-liquid interface between the formulation and the dissolution medium. These experiments are performed with both fasted state and fed state simulated intestinal fluids to reflect different levels of wetting (Nicklasson, 1993). Finally, the application of TNO TIM-1 system, as the most complex *in vitro* model (e.g. a digestion model in which dissolution and, above all, absorption are measured), could simulate multiple aspects during the *in vivo* processing. In fact, TNO TIM-1 is a multicompartamental and dynamic system that integrates *in vivo* features such as biorelevant media, change in volumes, pH, secretions, transit and other conditions found in the upper GI tract of studied subjects (Blanquet et al., 2004, 2005; Déat et al., 2009). The system also possesses an absorptive sink by means of hollow fibre ultrafiltration.

Within the framework of this doctoral thesis, the most important objective is to determine the most suitable release profile of each type of the developed solid lipid-based formulations where other three models might be not able to provide a suitable sink condition by considering a high dose of praziquantel amorphous solid dispersions, potential effects of digestion, solubilisation, supersaturation and precipitation (Nora et al., 2022; Z. Wang et al., 2023). However, the more complex the models, the lower the throughput of *in vitro* testing. This justifies the application of TNO TIM-1 only for testing pharmaceutical applications. All of the elements presented for selection of release testing conditions are summarised in **Figure 2-5**.

### **3. Conclusions**

This short chapter not only gives an overview of the analytical devices used in the experiments of this doctoral thesis, but also provides their working principles. Understanding these principles is important for both appropriate selection of conventional techniques and successful adoption of new characterisation in hot-melt coating researches.

All the aforementioned characterisation techniques will be eventually deployed in the experimentation and can be integrated into two characterisation plans corresponding to the two phases of this doctoral thesis development – “formulations development” for **Chapter 3, Chapter 4 and Chapter 5 (Figure 2-6)** and “pharmaceutical applications” for **Chapter 6 (Figure 2-7)**, respectively.

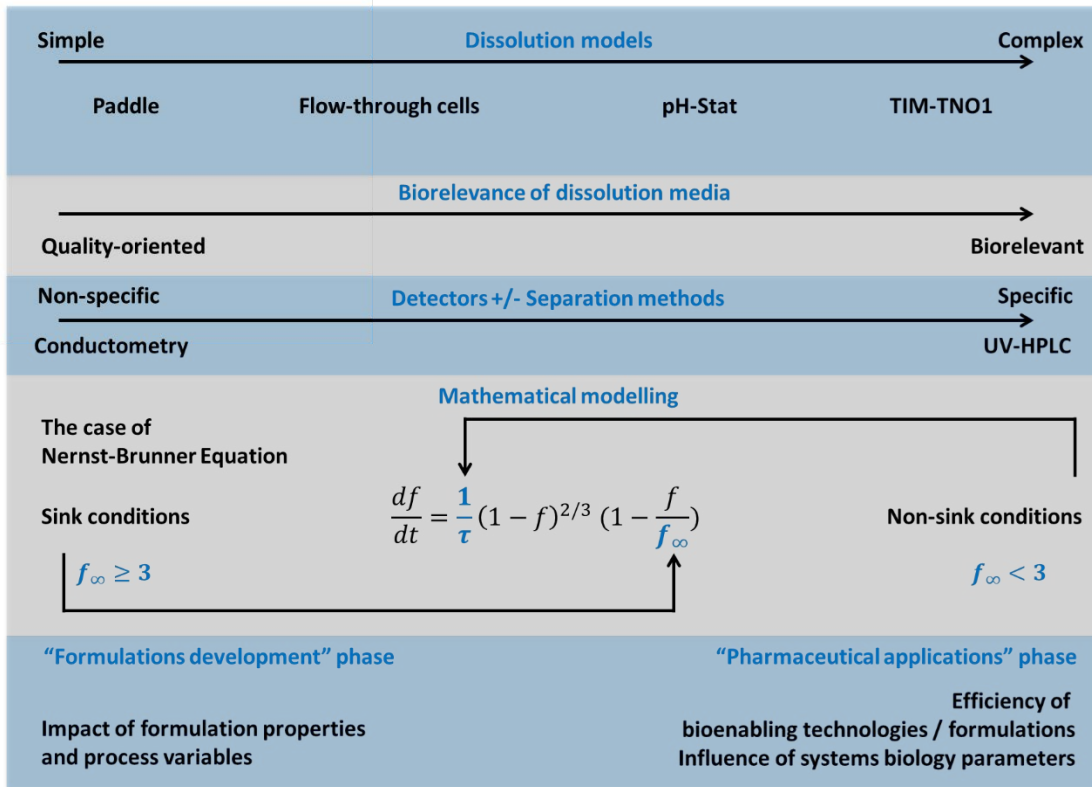


Figure 2-5. Considerations for selection of release testing conditions

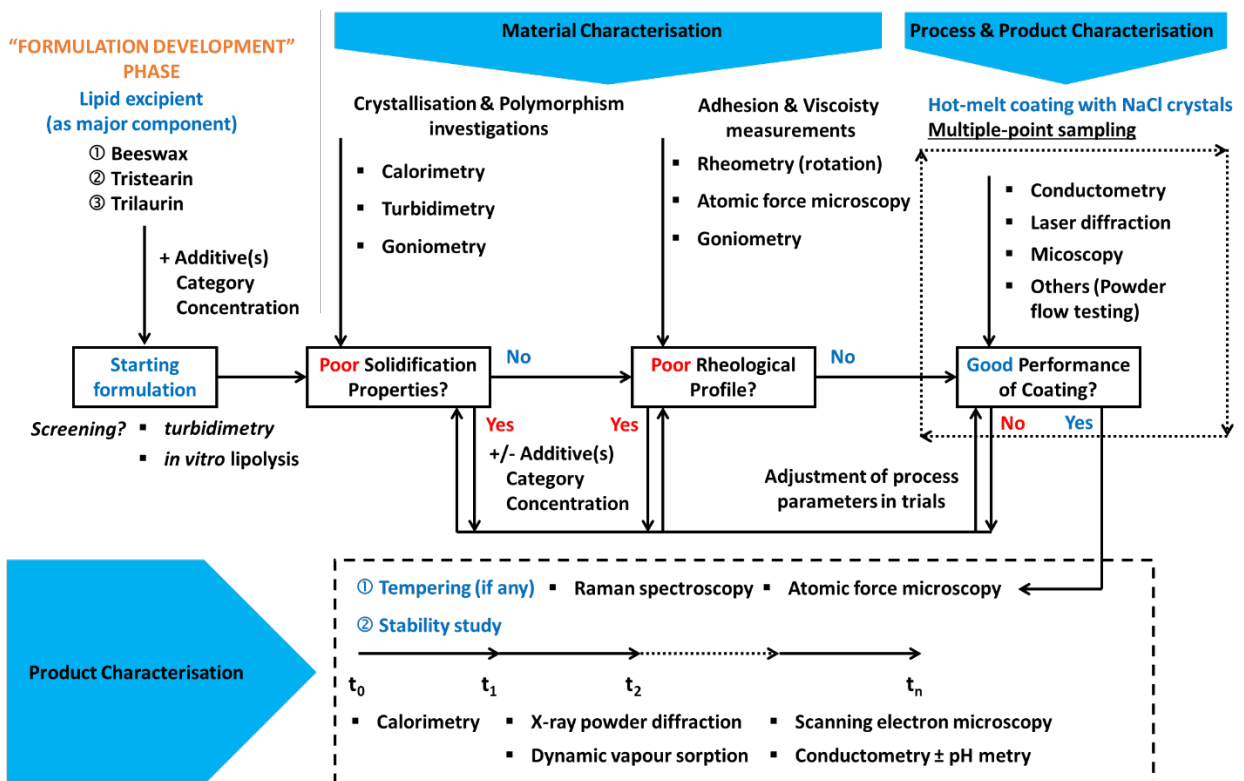


Figure 2-6. Characterisation plan in the “formulation development” phase



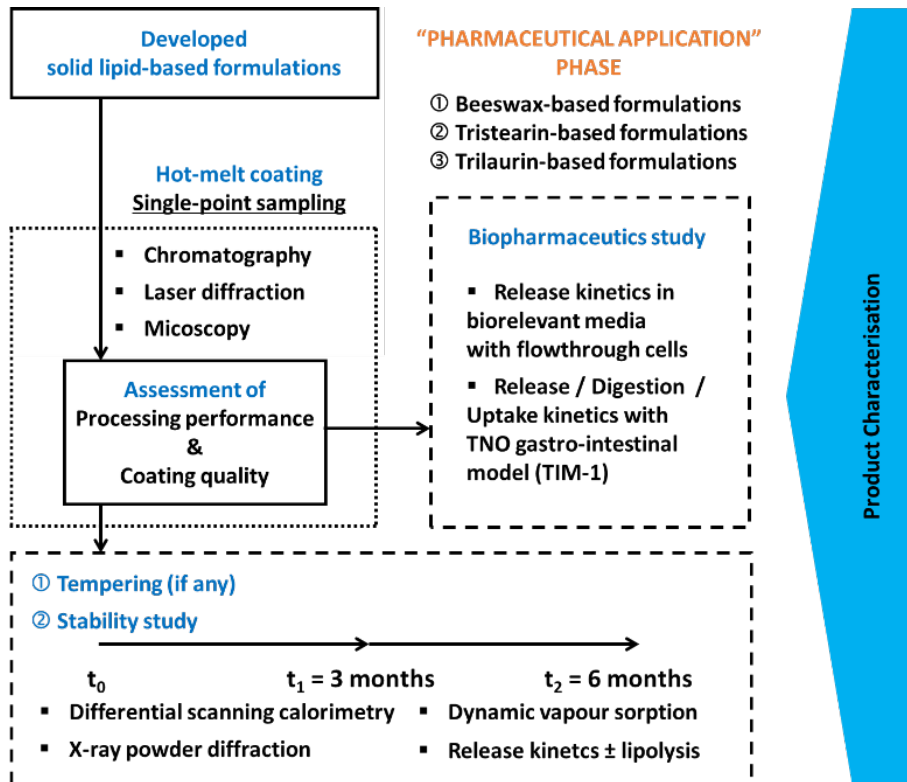


Figure 2-7. Characterisation plan in the “*pharmaceutical application*” phase

## Chapter 3.

# HOT-MELT COATING WITH FORMULATIONS OF BEESWAX AND SURFACTANTS

---

### General Introduction

Hot-melt coating with lipid-based excipients can respond to a wide range of demands in drug development, from moisture protection (A. S. Achanta et al., 2001; H. Chen et al., 2010), lubrication (Jannin et al., 2003) to taste masking (Becker et al., 2016; Rosiaux et al., 2018) as well as control of drug release in the gastrointestinal tract (Jacobsen et al., 2021; Knezevic et al., 2009; Patil et al., 2012; Schertel et al., 2022; Sinchaipanid et al., 2004).

However, successful development of hot-melt coating formulations for an intended use should be based on a good understanding on physicochemical and functional properties of coating materials together with appropriate definition of process parameters. Throughout drug research database, lipids have often been combined with additives in order to target a specific release. However, this results in a certain effect of additive-addition on formulation properties that might change product manufacturability and stability. **The studies on these two impacts constitute the two parts of this chapter.**

Beeswax (BW), as a complex-mixture lipid, was an interesting coating model for these studies. It is combined with additives (one lipophilic surfactant – sorbitan monostearate (SMS) – and one hydrophilic surfactant – polysorbate 80) to make up two studied formulations. We worked thus on 4 different systems:

- two monocomponent systems (BW and SMS, corresponding respectively to high and low adhesive coating lipids). These systems were expected to serve as positive and negative control with respect to adhesiveness and solid-state behaviours.
- two binary and ternary combinations of BW with surfactants.

NaCl crystals are used as a model substrate.

In the **Part 1** of this chapter, the focus is put on the impact of coating composition on formulation processability. The experimental work was divided in two parts: (1) lipid characterisation comprising thermal analyses (solidification), measurements of viscosity, contact angle, adhesiveness and (2) characterisation of process and coated product (assay uniformity, granulometry, images from microscopy, powder flow, and release testing on coated pellets).

**Part 1** not only investigated the impact of formulation properties like melt viscosity, adhesiveness and improvement on the processability of BW, but also proposed experimental approaches to evaluating process performance and coating quality:

- multiple-point sampling with assay, optical microscopy (or PSD), release testing for early development of hot-melt coating formulations

- single-point sampling (conventional) with assay, SEM, PSD, release testing for quality control.

**Part 2** of the chapter is dedicated to the investigation of coating composition and in particular, the effect of binary/ternary BW-based compositions, on product stability under the conditions 25°C/60% relative humidity for three months. Solid-state behaviours such as crystallisation, polymorphic transformation, modification of surface and crystal network, were monitored using conventional techniques DSC, XRPD, SEM and PLM. Release testing was performed in both simple and biologically simulated media to evaluate the impact of both factors -*solid-state evolution and lipid digestion* - on release kinetics.

The chapter ends with a general summary of the main conclusions drawn from this study with beeswax and surfactants.

# Part 1.

## Solidification, Melt Viscosity and Adhesiveness of Lipids and Coating Process Performance

### 1. Materials and Methods

#### 1.1. Materials

##### 1.1.1. Strategy for choice of single, binary and ternary lipids for this study

The use of beeswax as a hot-melt coating material is challenging. From a point of view of processability, beeswax was reported to be sticky (Müller et al., 2018) and high fraction of alkanes in its chemical composition is likely the cause. To overcome this challenge, mixing with another crystalline matter (for example, carnauba wax) has been proved as a possible solution. However, combining two complex-mixture lipids, like the case of two natural lipids, could lead to a complicated polymorphism. Therefore, a criterion for selection of the other lipid component is that its polymorphism should be simple.

Formulating with a crystalline surfactant was proved as a good choice for melt processing (Szűts, 2003). Monosorbitan stearate was then selected as it occurs only in  $\alpha$  polymorph (Nilsson et al., 2020).

Besides, addition of hydrophilic surfactants (like polysorbate 80) could be useful to modulate release kinetics of coated product, as already shown for a drug formulated with its very small fraction (Dong et al., 2019). It will be also investigated in this work. This leads to 4 formulations for this work, which will be presented next.

##### 1.1.2. Description of used materials

Beeswax (BW) and additives dedicated to pharmaceutical applications, Montane™ 60 PHA PREMIUM (sorbitan stearate) (SMS) and Montanox™ 80 PHA PREMIUM (polysorbate 80) (PS80), were provided by SEPPIC (Castres, France).

NaCl salt crystals (salt purity >99,9%) used as model substrates were commercially sourced from Baleine SA, Salins, France. They were sieved and the size fraction of solids between 400 and 630  $\mu\text{m}$  were retained for coating trials without prior co-processing with any other excipients.

Compositions of the studied formulations are provided in **Table 3-1**. **F0**, **F1** and **F2** stand for formulations containing beeswax alone, with one and two additive(s), respectively. In addition, the solid additive SMS was also used as a coating formulation itself (F3).

Table 3-1. Lipid-based coating formulations composition

Formulation	Excipients (% w/w)		
	BW	SMS	PS80
F0	100	-	-
F1	qsp 100	1 to 20	-
F2	qs 100	1 to 20	1 to 10
F3	-	100	-

## 1.2. Methods

### 1.2.1. Molten coating characterisation

Four characterisation techniques were deployed: measurement of thermal properties, measurement of viscosity, measurement of adhesion forces and measurement of contact angle in molten state.

#### 1.2.1.1. *Thermal properties*

Thermal properties of formulations such as melting point ( $T_m$ ), phase transitions were studied using DSC Q200 (TA Instrument, USA). All the analyses were performed in non-hermetic aluminium pans under nitrogen purge at 50 mL min<sup>-1</sup>. The thermal programme, spanning over a temperature range of 0°C and 100°C, included a first heating-cooling cycle followed by a second heating. A heating rate of 5°C min<sup>-1</sup> was chosen as this rate allows for net separation of thermal events. In the cooling step, a rate of 5°C min<sup>-1</sup> was chosen to simulate the cooling rate of lipids in a hot coating operation in a fluidized bed (Becker et al., 2016; Chansanroj et al., 2007b).

Thermal data in the first cooling step was further exploited to construct solidification profile, i.e. solid fraction content (SFC) (%) as a function of temperature and/or time with **Equation 35** (Fernanda, 2018; Müller et al., 2018):

Equation 35 :

$$SFC(t) = \frac{\int_0^t h dt}{\int_0^{t_\infty} h dt} \times 100 = \frac{\int_0^t h dt}{\Delta H_c} \times 100$$

where  $h$  is specific heat flow at the time  $t$  (W/g) and  $\Delta H_c$  is the crystallisation enthalpy of the formulation (J/g).

#### 1.2.1.2. *Measurements of melt viscosity*

Using FT Rheometer (Fischer, Germany) with the geometry plate-plate, the viscosity of molten formulations were evaluated as a function of temperature profile over a range of 70°C and 100°C with a shear rate 100 1/s and an integration time of 10 s in linear patterns. In addition, shear rate sweep was performed from 10 1/s to 500 1/s at 70°C and 90°C, with an acquisition time of 300 s in linear patterns in order to simulate and evaluate the impact of shear variability during peristaltic pumping on feeding of molten media (Carnicer et al., 2021). Both types of viscosity measurements were carried out using a setup of 20 mm diameter smooth disc in rotation mode.

### 1.2.1.3. Measurements of adhesion force and topography

As part of a complementary and exploratory study in adhesion measurements, adhesion force measurements of coating formulations were performed using RAMAN-AFM Alpha 300 AR (WITec, Ulm, Germany) based on a microscope with a magnification of x20 and a laser of 532 nm wavelength. Topography map and adhesion map were obtained using digital pulsed force mode (DPFM) – tapping mode – at ambient temperature and a relative humidity of 40–60%. The pyramidal cantilevers were used, with a spring constant of 0.28 N/m. Briefly, in DPFM measurements the force-distance curves were recorded **Figure 3-1**).

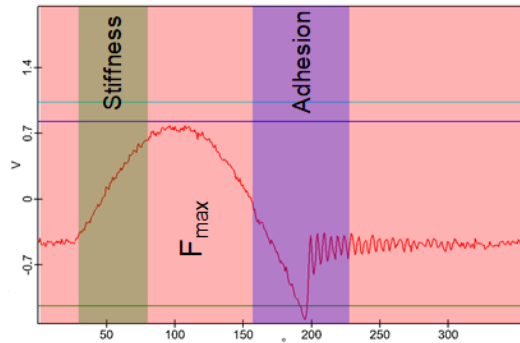


Figure 3-1. Force-distance curve recorded by digital pulsed force mode DPFM

At the beginning, AFM tip is far above the surface of the sample, subsequently moving closer to snap into contact (the attractive forces between the tip and the sample prevail). After reaching the contact, the piezo table pushes the tip into the sample and the repulsive forces reach the maximum ( $F_{\max}$  point). Then the piezo table is pulled back, the repulsive forces decrease and the force signal changes from repulsive to attractive one. Finally, the tip loses contact with the sample surface and the free oscillation of the cantilever is observed. Then the cycle is repeated (Abramczyk et al., 2019). Initially, the adhesion map recorded by DPFM has V (Volt) as unit. To convert the adhesion into N (Newton), the following expression is applied with **Equation 36**:

Equation 36 :

$$Adhesion = k \times S \times V_{adhesion}$$

where  $V_{adhesion}$  is the adhesion value in each image pixel of the map (V),  $k$  the cantilever spring constant (N/m),  $S$  the sensitivity of the detector (nm/V).

Other parameters include a setpoint of 0.8, P-gain and I-gain of 5, driving amplitude of 2 V, times/line for 1-2 s and 1 s, respectively. Measurements were carried out on three separate areas of 7-9  $\mu\text{m}$  x 7-9  $\mu\text{m}$  on the sample surface ( $n = 3$ ). Two types of samples were tested: cast film and coated surface of salt particles.

#### 1.2.1.4. Measurements of contact angle in molten state

To evaluate the wetting behaviours of coating formulations and therefrom induce their affinity to the substrate, measurements of contact angle in molten state could be used (Woerthmann et al., 2022). The experimental setup developed for this purpose is shown in **Figure 3-2**.

It comprises (1) a metallic insulated envelope accommodating (2) the dosing syringe capable of controlling heat by water current and (3) a chamber equipped with a Platin plate whose temperature is controlled by electricity. This chamber is placed on (4) a support (DSA30, Kruess) the height of which can be adjusted manually, and its internal temperature is verified using an external numerical thermometer (Chauvin Arnoux C.A 861). For image acquisition, (5) a camera lens (Namitar 1-6010) fixed at x 0.7 magnification and (6) a tungsten light (dedolight DLH4) of 3400K intensity is placed in opposite positions. (7) Image acquisition and analysis is piloted by the software DSA4. Each formulation is prior melted in an oven at 80°C, agitated and poured into a single-use 1 mL syringe. The latter is then placed in the heat-control box of the goniometer. For each formulation, measurements ( $n = 3$ ) were performed at a temperature close to that of the temperature of the fluidised bed of the model substrate to be coated during HMC processing, and at five distances 1, 3, 5, 7 and 9 cm to reflect the impact of droplet velocity on its wetting behaviours. During a measurement, the evolution of the droplet was captured each in a 1-minute video at a rate of 5 frames per second and contact angles were directly estimated from taken images using the software Image (1.54d) which was calibrated against Krüss templates.

The wetting substrates for these experiments were salt pastilles produced using a hydraulic press Atlas Power T15 Specac 13 mm die. About 1.7 g of fine salt was compressed under a pressure of 2 tons during 15 s as relaxation time and the surface of pastilles generated in this manner were sufficiently smooth.

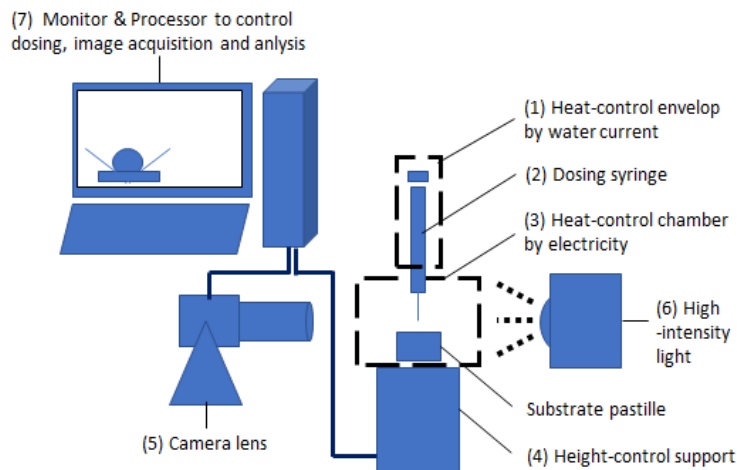


Figure 3-2. Simplified experimental setup for measurements of contact angle in molten state

#### 1.2.2. Hot-Melt Coating (HMC) with F0, F1, F2 and F3 Coating Formulations

HMC trials are performed using 1L lab-scale Ventilus® fluidised bed technology (Romaco© Group, Germany) shown in **Figure 1-2 (B)**. Process parameters were selected based on preliminary trials and are presented in **Table 3-2**. Prior to each coating test, the treatment chamber was cooled/heated with the



inlet of fluidizing and spraying air streams. The substrate particles (batch sizes between 250g to 300g) were then introduced to equilibrate with the temperature briefly and the coating operation was initiated. All the coating formulations were maintained in the molten state for feeding at 100°C, and the temperature of spraying air was fixed at 80°C.

In the course of one trial, regular sampling was carried out at the moment where one desired coating level was reached, i.e. 5%, 10%, 15%, 20%, 30% and 40% w/w. The molten coating feeding rate was calculated based on the mass of the coating agent delivered in the intervals of one or two minutes.

In this study, coating content is defined as the mass percentage of coating material present in the finished product. After each coating operation, the yield (%) is calculated based on **Equation 37**, where,  $m_{tot,sampled}$  is the total mass of samples taken during the coating trial (g),  $m_{tot,recovered}$  the total mass of coated product obtained at the end of trial (g),  $m_{substrate}$  and  $m_{ca,dispensed}$  the total mass of substrate and that of coating agent dispensed for the trial (g), respectively.

Equation 37 :

$$Yield (\%) = \frac{m_{tot,sampled} + m_{tot,recovered}}{m_{substrate} + m_{ca,dispensed}} \times 100\%$$

Table 3-2. Process parameters and their values specified for each formulation

Parameters	Values specified for each formulation		
	F0	F1, F2	F3
Formulation			
Temperature of fluidisation air (°C)	-	20 (setpoint)	20 (setpoint)
Temperature of product bed (°C)	33 (setpoint)	-	-
Volumetric air flowrate (m <sup>3</sup> /h)	45	37	37
Molten coating feeding rate (g/min)	≈2	≈7	≈20

### 1.2.3. Characterisation of coated products

#### 1.2.3.1. *Assay of coating contents*

To evaluate process efficiency, lipid-based coating content was indirectly assayed by quantification of salt amount by conductometry using one of two models CDM10 (RadiometerLab, Copenhagen). In a glass flacon 80 mL, around 40 mg coated products were firstly wetted with about 5 mL of ultrapure water and then heated at 100°C to melt the lipid shell. Next, about 55 mL of ultrapure water was added to dissolve salt contents and conductivity measures were performed. Assay was carried out in triplicate (n = 3) via gravimetric method. Before analysis conductivity sensors were calibrated with a conductivity standard solution 1413 μS/cm at 25°C (Hamilton, USA). The efficiency of coating process was evaluated with the following formula:

Equation 38 :

$$Efficiency = \frac{m_{ca,assayed}}{m_{ca,dispensed}} \times 100$$

where  $m_{ca,assayed}$  is the real amount of coating agent assayed in the final product and  $m_{ca,dispensed}$  the total amount of coating agent dispensed at time of sampling. Both  $m_{ca,assayed}$  and  $m_{ca,dispensed}$  are used to calculate the practical and theoretical coating content, i.e. the mass percentage of coating formulation recovered in the finished product.

### 1.2.3.2. Particle Size Distribution

Measurements of particle size distribution (PSD) were performed using laser diffraction particle size distribution analyser Mastersizer 3000 (Malvern Instruments, Malvern, United Kingdom) under dry dispersion mode.

The mean size of the population of particles is expressed in  $D_{[4,3]}$ . PSD in volume can be interpreted in order to identify the process regime in this study. Three PSD parameters, i.e. PSD width (*SPAN*) and the ratio  $D_{v(90)}/D_{v(10)}$ , are calculated from  $D_{v(10)}$ ,  $D_{v(50)}$  and  $D_{v(90)}$  from the following formula:

Equation 39 :

$$SPAN = \frac{D_{v(90)} - D_{v(10)}}{D_{v(50)}}$$

where  $D_{v(10)}$ ,  $D_{v(50)}$  and  $D_{v(90)}$  represent the maximal particle size of 10%, 50% and 90% volume of the whole particulate population.

### 1.2.3.3. Optical microscopy

By optical microscopy the evolution of particle size, agglomeration and salt surface coverage were investigated. A representative number of coated products were inspected with an optical microscopy Leica. Observations were carried out under transmission mode with a magnification capacity of 0.4x of camera and 10x resolution using a KL 300 LED. Two modes of lighting conditions, (1) dark background and (2) white background, were set for those observations depending on the angle  $\alpha$  (**Figure 3-3**) between the rough surface of the reflecting mirror and the horizontal surface, i.e. around 45-60°C and 120-135°C, respectively.

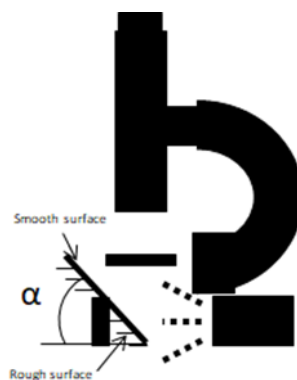


Figure 3-3. Optical microscope setup

#### 1.2.3.4. Scanning electron microscopy (SEM)

SEM provides qualitative information about surface quality such as rugosity and lipid deposition rate. Images of coated products were taken using TM3000 TableTop Scanning Electron Microscope (Hitachi, Japan) with an incident voltage of 15 keV under low vacuum.

Two specific detectors ABS (angular back-scattered) and ETD (Everhart-Thornley detector) were deployed for the chemical contrast mode and the topographical contrast mode, respectively. Each analysis required a small quantity of samples, which was glued to an adhesive strip.

#### 1.2.3.5. Coated powder flow properties

To evaluate the stickiness of all formulations, powder flow properties were measured using a Freeman FT4 powder rheometer. For these measurements, one batch size of 250 g salt was coated with **F0**, **F1**, **F2** and **F3** coating formulations to generate samples.

A split vessel of 85 mL volume and a blade of 48 mm diameter were chosen for this purpose. Yield loci were obtained by applying pre-shear and shear stresses at 4 and 5 levels as shown in **Table 3-3**, respectively. From yield loci obtained, unconfined yield strength and maximal consolidation stress were extracted to construct a flow function for each type of powder. Measurements were performed at ambient temperature and relative humidity in triplicate (n = 3).

Table 3-3. Details about pre-shear and shear stresses used in measurements.

Pre-shear (kPa)	Shear (kPa)
<b>3</b>	1.0, 1.25, 1.5, 1.75, 2.0
<b>6</b>	2.0, 2.5, 3.0, 3.5, 4.0
<b>9</b>	3.0, 4.0, 5.0, 6.0, 7.0
<b>15</b>	5.0, 6.0, 7.0, 8.0, 9.0

#### 1.2.3.6. Release kinetics

Experimental measurements

Release kinetics of coated salt were experimentally obtained with a USP type II apparatus (paddle) (ERWEKA DT light, Heusentamm, Germany). In all experiments, a quantity of samples equivalent to 600 mg NaCl was placed inside a 100-mesh sinker basket with lid (316 SS). A quantity of glass beads (160 – 200 µm) equivalent to one quarter of substrate total mass was introduced to prevent agglomeration inside the sinker (Frenning et al., 2003). As for testing conditions, each test was performed in 250 mL ultrapure water at  $37 \pm 1^\circ\text{C}$ .

The rotation speed was set at 100 rpm. As for sampling, conductivity values are automatically recorded every 5 s using conductivity meters (models CDM10, RadiometerLab). Conductivity sensors were calibrated before analysis with a conductivity standard solution 1413 µS/cm at 25°C (Hamilton, USA). For each sample, release testing was performed in triplicate (n = 3).

## Data analysis

To investigate mechanisms governing salt release, release testing data were fitted to some selected empirical models zero order, first order, Korsmeyer-Peppas, Peppas-Sahlin, Higuchi and Hopfenberg expressed in **Table 3-4**, where  $F_d$  (%) is the percentage of salt released at time  $t$ .  $k_0$  ( $\text{h}^{-1}$ ),  $k_1$  ( $\text{h}^{-1}$ ),  $k_{KP}$  ( $\text{h}^{-n}$ ),  $k_D$  ( $\text{h}^{-m}$ ),  $k_{R-E}$  ( $\text{h}^{-2m}$ ),  $k_H$  ( $\text{h}^{-0.5}$ ) and  $k_\beta$  ( $\text{h}^{-1}$ ) represents constant release specific to each mode,  $m$  and  $n$  are release exponents (P. Costa & Sousa Lobo, 2001).

Table 3-4. Model-dependent equations for release kinetics

Model	Equation	Equation number
Zeroth order	$F_d = 100 \times k_0 \times t$	40
First order	$F_d = 100 \times (1 - e^{-k_1 \times t})$	41
Korsmeyer-Peppas	$F_d = 100 \times k_{KP} \times t^n$	42
Peppas-Sahlin	$F_d = 100 \times (k_D \times t^m + k_{R-E} \times t^{2m})$	43
Higuchi	$F_d = 100 \times k_H \times t^{0.5}$	44
Hopfenberg	$F_d = 100 \times [1 - (1 - k_\beta \times t)^3]$	45

## 2. Results and Discussion

### 2.1. Thermal Analyses

#### 2.1.1. Impact of the lipid-based coating composition

Thermal properties of all studied formulations (**F0**, **F1**, **F2** and **F3**) were analysed by DSC aiming to define good processing parameters for each composition and they are presented in **Figure 3-4**. In each thermogram, continuous red lines, continuous blue lines, and discontinuous red line are displayed representing respectively the first heating step, the first cooling step and the second heating step. The first cooling step informs the crystallisation of formulations in simulated thermal processing conditions, while the second heating step identifies the polymorphic profile of formulations formed after the crystallisation.

##### 2.1.1.1. *Single-lipid formulations – F0 (beeswax) and F3 (SMS)*

In the **first heating** cycle, **F0** is characterised by a broad melting range in the range 20°C-68.2°C (with two shoulders around 46.6-48°C and 52.6-54.3°C as well as a one peak at 63.8°C) and a total melting enthalpy of 184.0 J/g. This thermogram displays similar shoulders and melting peak close to characteristic melting peaks of both white beeswax (42.7°C and 60.0°C) and yellow beeswax (51.4°C and 61.0°C) of the species *Apis mellifera* (Buchwald et al., 2008). It should be noted that beeswax is a natural wax which is composed of several classes of chemical substances (e.g., alkanes, fatty acids, esters of long-chain fatty acids and alcohols (Sato, 2018a). The number and the positions of peaks and/or shoulders in the thermal curves of the present beeswax could be then attributed to the occurrence of several classes of long carbon chain substances. In fact, beeswax being a natural wax, it is likely subject to variability in composition due to harvesting seasons, geography, and cultured bee species (Girod Fullana & Aubert-Pouessel, 2019). In turn, **F3** exhibits a narrower melting range 40.5-61.3°C (with

merely a peak at 54.5°C). **F3** is also a complex-mixture lipids resulting from esterification of sorbitol and fatty acids (Cottrell & Peij, 2014).

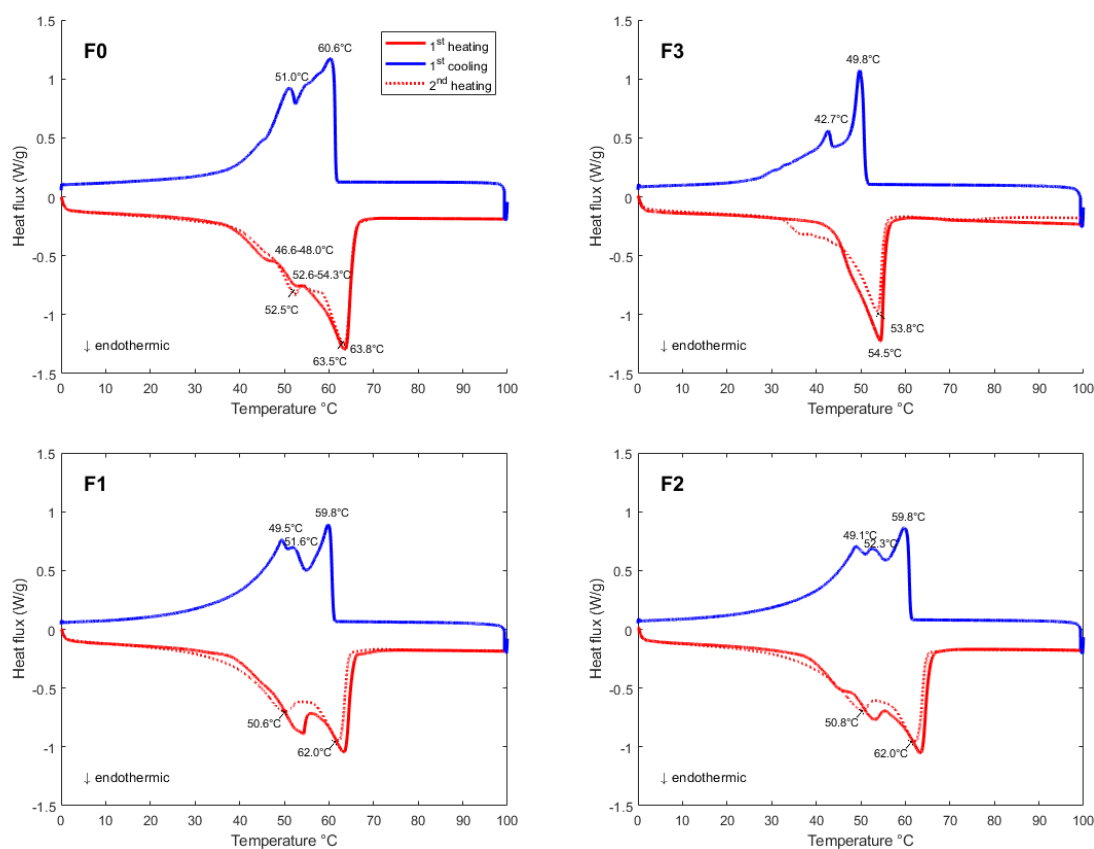


Figure 3-4. Thermograms of formulations **F0**, **F1**, **F2** and **F3**: red continuous line (first heating), blue line (first cooling), red discontinuous line (second heating).

Thermal curves during **crystallisation** (cooling step) are demonstrated via continuous blue lines in **Figure 3-4**. Both crystallisation thermograms of **F0** and **F3** display two separate peaks at 60.6°C and 51.0°C, and at 49.8°C and 42.7°C, respectively. As for **F3**, a long tail following those peaks implies slow crystallisation of shorter-chain derivatives in the principal classes of chemical substances as already discussed that ends at about 26.4°C. Unlike **F3**, thermal curve of **F0** upon crystallisation demonstrates three shoulders around 58.8°C, 55.4°C and 45.6°C accompanying the remarked crystallisation peaks.

**In the second heating** step (discontinuous red line in **Figure 3-4**), **F0** displays two separate peaks, 52.5°C and 63.5°C, followed by a shoulder around 46.2°C and a tail spanning an interval of 53.9°C-58.2°C. Regarding **F3**, before the appearance of a melting peak (53.8°C), there is a wide temperature range probably indicating melting of compounds which are chemically similar and polymorphic.

### 2.1.1.2. Binary (F1) and ternary (F2)-lipid formulations

Concerning **F1** and **F2**, as a combination of **F3** and **F0**, their respective thermograms display similar shoulders (49.7°C-50.6°C and 50°C-50.8°C, respectively) and similar peaks (62.3°C and 62.4°C, accordingly). Compared to the DSC second heating curve of **F0** and **F3**, depression in principal melting peaks (about minus 1.5°C-2.5°C) is observed. This indicates the resultant effect of SMS addition into beeswax, i.e. solid-state interactions.

**F1** and **F2** display similar **crystallisation** thermal curves with three separate peaks, 59.8°C, 51.6°C, 49.5°C and 59.8°C, 52.3°C, 49.1°C, respectively. The total crystallisation enthalpies of these two formulations are close (about 163.6 J/g and 161.5 J/g, respectively) in comparison with about 177.5 J/g of **F0** and 87.39 J/g of **F3**. Addition of SMS leads to a slight depression in the first crystallisation point of formulations **F1** and **F2** compared with the most remarked peak of **F0**, disappearance of shoulders in thermograms of **F0** or **F3**, as well as appearance of a new peak at 51.57°C or 52.27°C. These observations result likely from interactions between SMS and other components occurring in beeswax.

Concerning the second heating diagrams, **F1** and **F2** also display similar **melting** curves with two separate peaks around 50.6°C-50.8°C and 60°C preceded by a long tail. **F3** was noticed to also depress the high melting fraction temperature in **F1** and **F2**.

Both the heating steps of **F0** and **F3** are important because they show the (initial) presumably stable and metastable polymorphism of each substance. For **F1** and **F2** the second heating is more important as it indicates the formation of a new phase mixing system. All this information is indispensable for stability monitoring which will be treated in the second part of this chapter.

### 2.1.1.3. Solidification profiles

The thermal data of the four formulations in the cooling step were exploited to construct their **solidification profile** as shown in **Figure 3-5**:

- **F0**: a complete solidification is apparently achieved within more or less than 8 minutes.
- **F3**: appears to solidify at the greatest rate in comparison with the three other formulations.
- **F1** and **F2**: a slight depression in crystallisation point (compared to **F0**) as well as a comparable solidification process which is prolonged and completed within 10 minutes. In summary, addition of surfactants exerts an impact not only on polymorphic behaviours of beeswax-containing formulations but also on their solidification profile.

It was important to study the solidification properties of **F0**, **F1**, **F2**, and **F3** in order to define the operating conditions for hot melt coating with these lipid formulations. The bed temperature was set based on the solidification profiles shown in **Figure 3-5**. Initially, the bed temperature was set 33°C to achieve over 90% solid fraction content (as can be seen in **Figure 3-5**) and therefore to avoid agglomeration (Müller et al., 2018).

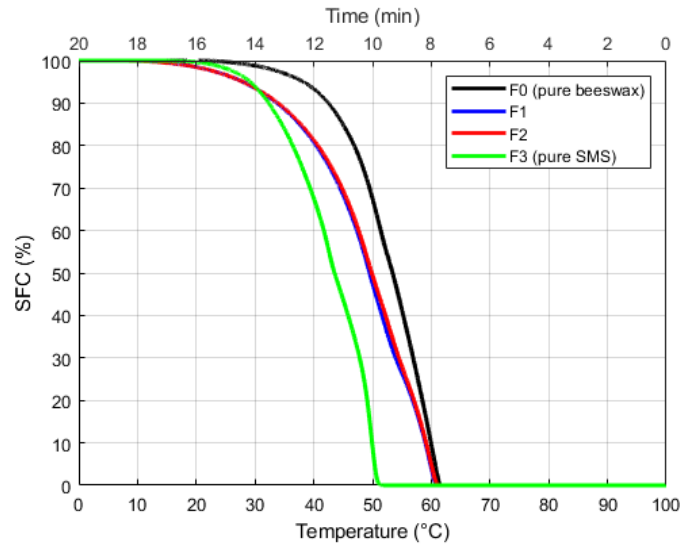


Figure 3-5. Comparative solidification profile of three formulations **F0** (black line), **F1** (blue line), **F2** (red line) in comparison with that of **F3** (green line)

### 2.1.2. Rheological Analyses

**Figure 3-6-A** shows flow curves of **F0** to **F3** molten formulations measured then at two temperatures - 70°C and 90°C - as these represent the lower and upper temperature limits of the melt in the transport system. A shear rate range of 50-500 1/s was chosen as it might reflect the shear rate of pumping in practice (Carnicer et al., 2021). The relationship between dynamic viscosity and shear rate indicates that these molten formulations behave like Newtonian fluids.

In the measuring thermal conditions of respectively 70°C and 90°C, the melt viscosities of **F0** to **F3** varied between 30 and 15 mPa.s for **F0**, 200 and 70 mPa.s for **F3**, 31 and 18 mPa.s for **F1** and between 32 and 14 mPa.s for **F2**. The melt viscosities of **F1** and **F2** are comparable to that of **F0**. In addition, the value of melt viscosity measured for all formulations is below the limit 300 mPa.s given by the pioneer researchers in the field of spraying for coating of surfaces (Kennedy & Niebergall, 1996; D. G. Lopes, Salar-Behzadi, et al., 2017).

**Figure 3-6-B** demonstrates the viscosity-temperature relationship for a shear rate fixed at 50 1/s. A temperature range of 75°C and 105°C was chosen to represent the temperature set for keeping formulations in molten state and the temperature at the end of feeding nozzles in operation which were kept hot with the atomisation air temperature of 80°C.



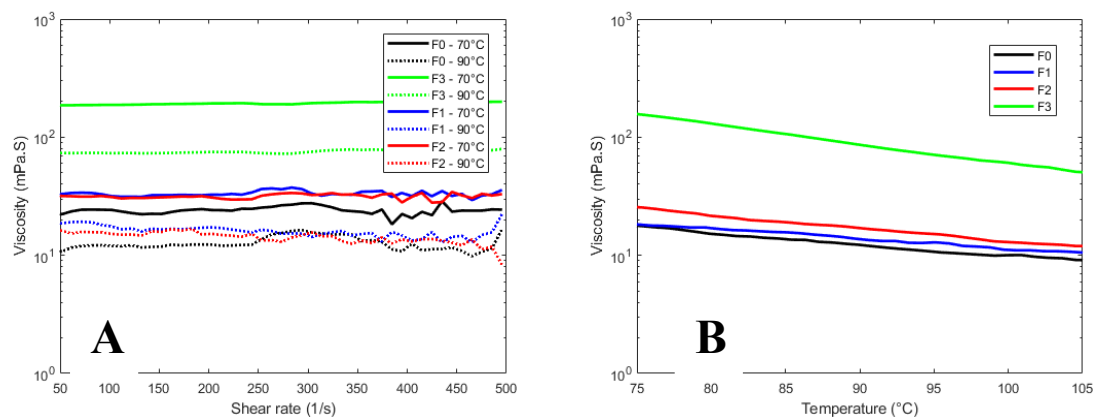


Figure 3-6. Melt dynamic viscosity of **F0** to **F3** formulations as a function of shear rate at 70°C and 90°C (A) and that as a function of temperature when shear rate is fixed at 50 1/s (B)

In general, melt viscosity is inversely proportional to temperature. In fact, from 75°C to 105°C, viscosity of SMS (**F3**) decreases from around 150 to 50 mPa.s while that of beeswax (**F0**) diminishes from about 20 to 10 mPa.s. The addition of SMS to beeswax appears to have an influence on the melt viscosity of lipid formulations (**F1**). Theoretically, for an ideal mixture of SMS (**F3**) and **F0**, an arithmetic mean viscosity value should be obtained but the viscosity of **F1** is almost equal to that of **F0**. This might imply that **F0** dissolves SMS (**F3**) in a mass ratio of 80:20. On the other hand, addition of a small fraction of PS80 (<2% w/w) raises viscosity of this melt mixture at a shear rate of 50 1/s, as observed at logarithmic scale (as shown in **Figure 3-6-B**). Due to their composition, this system behaves as a dispersion constituted by a dispersed phase (PS80) and a dispersing phase (melt solution of SMS and BW). This effect will be linked to their wetting and deformation behaviours.

### 2.1.3. Investigation of Adhesion Forces by AFM Analyses

The objective of the application of this method is to analyse adhesion properties on solid surfaces produced from different lipid compositions.

From an AFM image, adhesion value is the mean adhesion of all the probed points within a selected area (on three separate areas of 7-9 μm x 7-9 μm) and of three analyses (n = 3) on the surface of a cast film made of the solid lipid-based formulations.

As shown in the **Figure 3-7**, an adhesion map (left) and topography (right) of a solid surface of **F0**, **F1**, **F2** and **F3** were the expected results obtained from AFM analyses. For illustration purposes, some results (one measured surface) are shown in **Figure 3-7**. For the selected area, adhesion force values range between 669 and 1500 nN, between 196 and 1027 nN, between 242 and 1040 nN and between 95 and 464 nN for **F0**, **F1**, **F2** and **F3**, respectively.

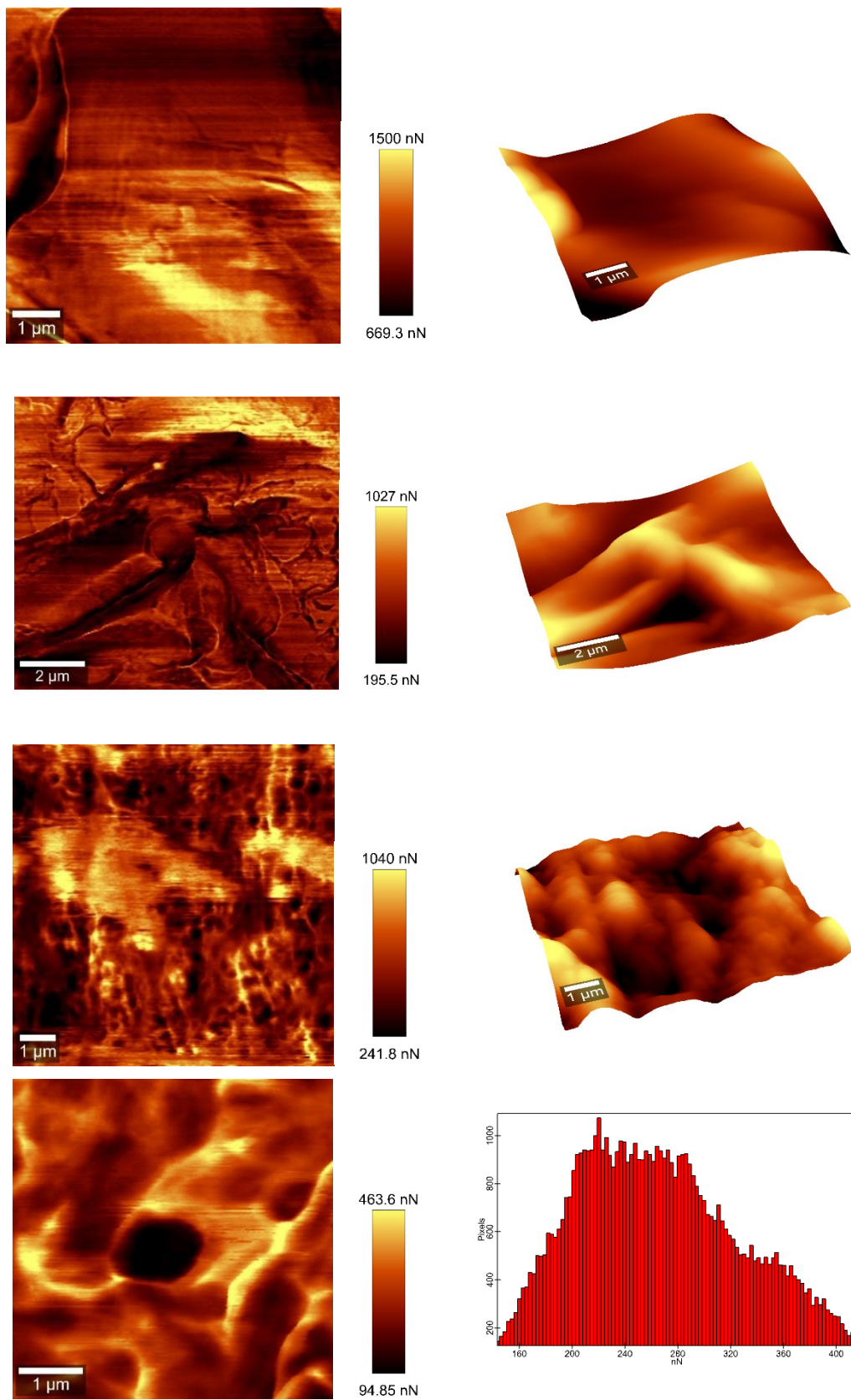
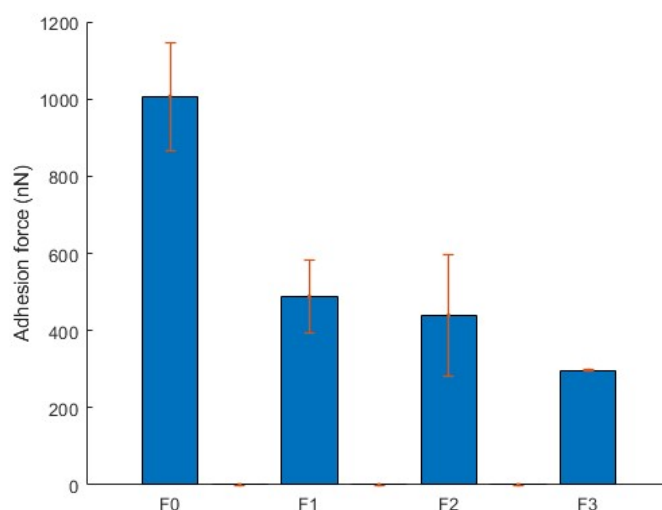


Figure 3-7. Measurements of adhesion of four formulations **F0**, **F1**, **F2** and **F3** (from top to bottom)

Images of AFM taken surface (**cast film**) made of each formulation **F0**, **F1** and **F2**: adhesion map (left) and topography map (right). In the map, colour gradient varies from light to dark, the higher brightness of which indicates the higher extent of adhesion or the higher relief, respectively. Higher relief is associated with higher adhesion. Adhesion force is the mean value of a distribution of probed points on the measured surface (J. Lee, 2004; N. Zheng et al., 2018). In general, a high relief region exhibits high adhesion as this might be due to larger contact between the measured surface and the tip.

Measurements conducted on the cast films yield the following results:  $1007 \pm 140$  nN for **F0**,  $488 \pm 94$  nN for **F1**,  $439 \pm 158$  nN for **F2** and  $297 \pm 52$  nN for **F3**. They are shown graphically in **Figure 3-8**. They demonstrate firstly a lower adhesion force on **F3** film surface compared to **F0** film surface, confirming the initial hypothesis of an adhesiveness tendency of **F3** > **F0**. A remarkable effect of surfactant addition to BW is also observed on adhesion forces (**F2**~**F1**<**F0**, with a reduction of almost 2 times).



*Figure 3-8. Values of adhesion force measured for each formulation cast in film*

The expected trend being identified, note that these results should be treated with caution. To validate the method and the results, it would be necessary to increase the number of measurements, as was done by some experimenters (J. Lee, 2004; N. Zheng et al., 2018) who tested the method before this work (more than 80 measurements equivalent to the number of surface areas measured of the same particle). More extensive mapping would also reduce the variability of measured adhesion forces. However, considering the standard deviations from three measurements, each AFM measurement can be said to be representative of the adhesion of each formulation. The trend that emerges from the graphic is clear, and the capacity of this technique to discriminate formulation properties in the same measuring conditions is what we wish to highlight here.

As a condition of measurements, the samples should be the freshly prepared ones to simulate the situation where substrate particles are being coated with each formulation. The surface properties of the sample should also be smooth and the film casting appeared to be a good choice. In fact, as confirmed by SEM observations at the same scale, the surface of a cast film is smooth while that of a coated particle

is rough due to film formation process via the mechanism of solidification. This process will be discussed in the next.

#### 2.1.4. Measurements of Contact Angle in Molten State

The advantage of the current setup for contact angle measurements in molten state relies on the fact that the transparency of the droplet can be observed. Qualitatively, a change of background from white to black implies the start of solidification.

Images of solidified droplets of each formulation deposited on NaCl surface (the first model substrate to be coated in this research work) and on the surface of the same formulation itself to simulate surface coating and onion coating effect (layer-by-layer coating) were taken by hot-melt goniometry, as described in the methodology. Pictures taken on the moment of melt lipid drop deposition ( $t_0$ ) and up to 60 s can be seen in **Figure 3-9**.

For these measurements, the temperature of the chamber was around 20°C, close to the temperature of inlet air for HMC experiments. The temperature of the syringe that delivers the molten formulation in the form of droplets was controlled by the hot water whose temperature was set around 97.5°C for **F0**, **F1** and **F2**, not more than 80°C for **F3**. This temperature setting was for not disturbing measurements due to low supercooling of **F0**, **F1** and **F2** rather than for simulating processing conditions.

From the experiments shown in **Figure 3-9**, it could be seen that only **F0**, **F1** and **F2** solidify completely upon contact, but **F3** still appeared to remain a little transparent in this same contact time (at 0 s). According to the solidification profile shown previously in **Figure 3-5**, all the four formulations ought to almost solidify and solidification kinetics of **F3** is the fastest. Note that the solidification of these formulations is a spontaneous crystallisation process. In the case of **F3** (SMS), by considering the start of its crystallisation process at 51°C at a cooling rate of 5°C/min, the measuring thermal conditions (between 20°C and 30°C) might create a high temperature gradient and as a consequence lead to a significant increase in melt viscosity (like the case of glass forming) (Descamps & Dudognon, 2014). This slows down nucleation rate but does not inhibit it, as in several seconds, SMS (**F3**) starts to solidify.

Contact angles are considered at this time point. These values of contact angles,  $35.6^\circ \pm 1.4^\circ$  for **F0**,  $38.8^\circ \pm 1.9^\circ$  for **F1**,  $38.7^\circ \pm 1.5^\circ$  for **F2** and  $81.0^\circ \pm 2.2^\circ$  for **F3** at 1.17 m/s, show that beeswax-containing formulations wet the NaCl surface better than SMS (**F3**). The wetting behaviours in this case did not correlate with the lipophilicity of the formulations but with other properties. In fact, it was already evidenced that three lipids (i.e., hydrogenated palm oil, rice bran wax and carnauba wax) at 100°C wetted well the surface of cellulose, sugar spheres, citric acid, glucon- $\delta$ -lactone and sucrose at 23°C (Woerthmann et al., 2022).

The fact that **F3** is resistant to deform upon impacting the substrate surface could be attributed to its crystallisation retarded by a high melt viscosity. In the presence of beeswax, the viscosity of these formulations is lower and there might be an advantage of low- and high-melting fractions occurring in beeswax.

At 10 s, all the formulations appear to solidify completely and therefore measurements of (static)

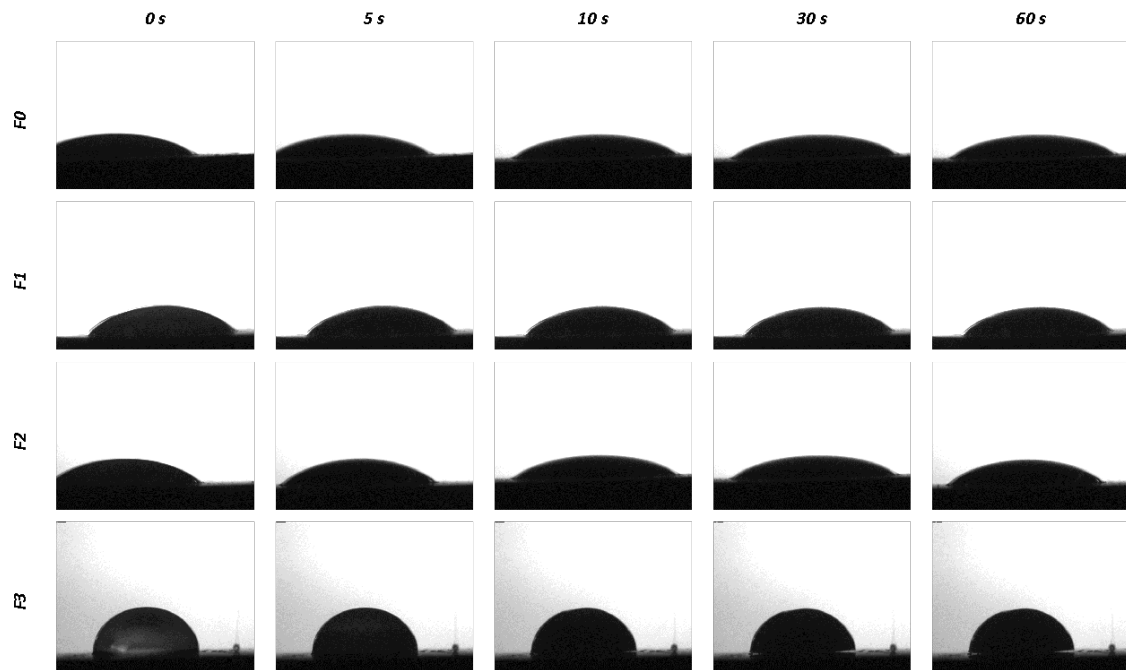


Figure 3-9. Droplets of each formulation (F0 to F3) deposited at a velocity of 1.17 m/s being solidified within 1 minute on NaCl surface

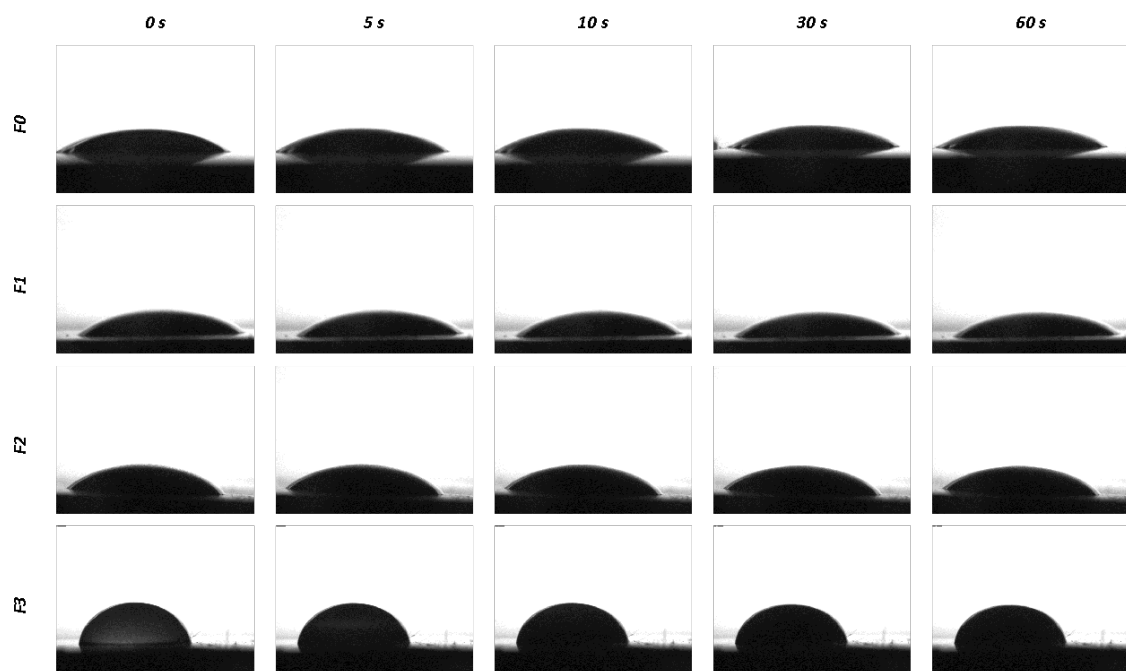


Figure 3-10. Droplets of each formulation (F0 to F3) deposited at a velocity of 1.17 m/s being solidified within 1 minute on that of the same formulation itself

Furthermore, these contact angle measurements also demonstrated delamination of solidified **F3** membrane from NaCl surface (see **Figure 3-9**) while the formulations containing beeswax appeared to adhere well to this surface. Also, this does not happen for the case of **F3** membrane deposited on **F3** cast film (See **Figure 3-10**). It hints at a more stable SMS-SMS bond (cohesion) than that of SMS-NaCl (adhesion). In addition, in comparison with **F0**, solidified deposited **F1** and **F2** droplets on NaCl surface

are easily removable with little trace from NaCl surface after measurements of contact angle in comparison with those of **F0**. This corroborates the decrease in adhesion strength between NaCl surface and the formulation in the order of **F0**, **F1** and **F2**, **F3**. This justifies the combinations of SMS and BW, which is used in performant adhesive formulation (Gaillard et al., 2011). These observations agree with the measurements of adhesiveness.

**Figure 3-11** shows the shape of deposited droplets as a function of impact velocity (**A**) and relationship between contact angles measured and impact velocity (**B**) for all the studied coating formulations. While performing these measurements the height between the dosing syringe and the sample surface was adjusted from 01 to 09 cm and then deduced into impact velocity using the kinematic equation for a free-falling object -  $v_{impact} = \sqrt{2gh}$ , where  $g$  is the gravity ( $m/s^2$ ) and  $h$  the distance between the tip of syringe and the substrate surface (m).

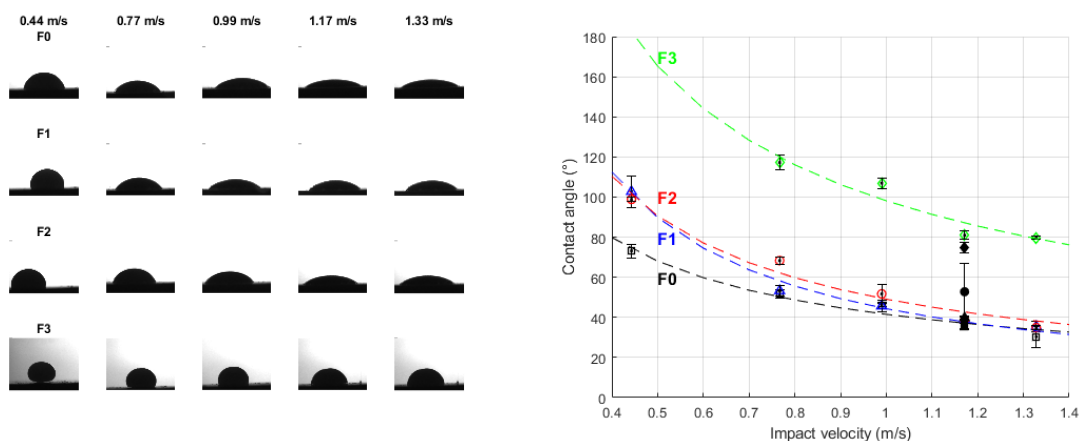


Figure 3-11. Images (A) of solidified droplets of each formulation deposited on NaCl surface and contact angles (B) obtained at different velocities.

The objective of adjusting various heights is to simulate impact of melt droplets from the spray and particles in random movement (product bed). Implicitly, this is to verify whether despite poor solidification, viscosity and adhesion behaviours impact velocity, representative of the influence of the process parameters, can have an effect on feasibility of a good coating.

Qualitatively, shape of droplets deposited on NaCl surface as a function of impact velocity shows that mixing with SMS leads to decrease in wetting but no delamination was observed. However, from 0.99 m/s there seems to be no significant change for F0, F1 and F2 as is noticed in the graph that their values of contact angle are close at each impact velocity. As for F3, there are 03 observations. At the lowest impact velocity, it does not wet and adhere to the NaCl surface. At intermediate impact velocities, contact between the SMS membrane and NaCl surface displays delamination. At the highest impact velocity, no detachment occurs.

The shape of the droplets deposited on the surface of a cast film of NaCl, visible in **Figure 3-11-(A)**, are like those found before, deposited onto the surface of a film of same nature (see **Figure 3-11-(B)**).



Quantitatively, **Figure 3-11-B** shows an inverse power-function relationship between contact angle and impact velocity for **F3** ( $R^2 = 0.896$ ), **F0** ( $R^2 = 0.967$ ), **F1** ( $R^2 = 0.990$ ) and **F2** ( $R^2 = 0.973$ ). This obtained relationship agrees with an inverse power model to prove the link between deformation of a droplet (ratio of final to initial droplet diameter) and Reynolds number (which involves impact velocity by definition) (Kim, 2003; Kim & Ulrich, 2003). In other word, the graph (**Figure 3-11-B**) implies that for adhesive coatings (contact angles between  $60^\circ$  and  $80^\circ$  without delamination) less impact velocity is required to overcome viscous flow of the droplets. This means that the higher the impact velocity, the lower the contact angle, and wetting is therefore facilitated. As a consequence, the higher the wetting, the higher contact surface for the formulation, and its formulation is therefore improved.

**To conclude the part of coating material characterisation**, the observations with contact angle measurements provide many types of information:

- Firstly, it shows that to have the molten formulation solidify on the substrate setting of an appropriate crystallisation temperature is key. In fact, when it is too low in comparison with crystallisation onset of **F3**, slow crystallisation occurring at high melt viscosity leads to adhesive failure between the coating and the substrate;
- Secondly, it shows that good adhesiveness of a formulation is necessary for coating. In fact, no delamination observed for BW (**F0**) and mixtures with SMS (**F1** and **F2**).
- Thirdly, inadequate crystallisation rate, melt viscosity and adhesiveness of the formulation can be improved by adjusting either crystallisation temperature (fluidisation air temperature) or impact velocity (fluidisation air flowrate, feeding rate and atomisation pressure) or both. In the following part, the link of these three formulation properties, i.e. solidification, melt viscosity and adhesiveness, to processing performance and coating quality will be investigated.

## 2.2. Process Performance Assessment

### 2.2.1. Impact of lipid coating composition on process yield and efficiency

Coating with fluidised bed technology has a unique advantage, i.e. the possibility to prepare products with different drug loadings or coating contents in the same operation via sampling. The proposed experimental approach relies on sampling particles for characterisation at different timepoints at which a target coating content should be known.

Process yield is calculated right after each coating operation. As shown in **Figure 3-12**, the coating process efficiency is indicated by the red continuous line, and it could be alternatively expressed by the gap between the theoretically calculated values (black line) and the practical assay results (blue columns).

The efficiency is low at the very first sampling (target 5-10% coating contents) as a stable contact between melt droplets and substrate surface has not been established. The coating efficiency observed with **F1** and **F2** increases from the second sampling onwards, becoming well established above 25% w/w coating content. Note that normally overspray may occur but appear not to be overwhelming. In this case, fine particles are not always detected in PSD measurements. As for **F0**, no or very low coating



content was found for the initial samplings. This could be linked to sticking of coated particles onto the fluid bed wall at the beginning. From the second sampling to final sampling, coating contents increased in a linear pattern with a calculated efficiency over 100% at the end. In fact, in the coating trials with **F0**, sticking of coated particles was observed and it worsened with the processing time. From second sampling, particles stuck onto the process wall and re-fell with coating time, which reduced the population of fluidised particles. As a consequence, those particles tended to receive more coating material during coating and a higher coating content was the result.

Concerning coating with **F3**, despite setting the same target coating contents as with **F1** and **F2**, coating efficiency remained low for all the samplings and attained a maximal value of about 75%. In fact, in the coating trials with **F3**, generation of fine particles was observed with a gradual increase of the filter pressure differential.

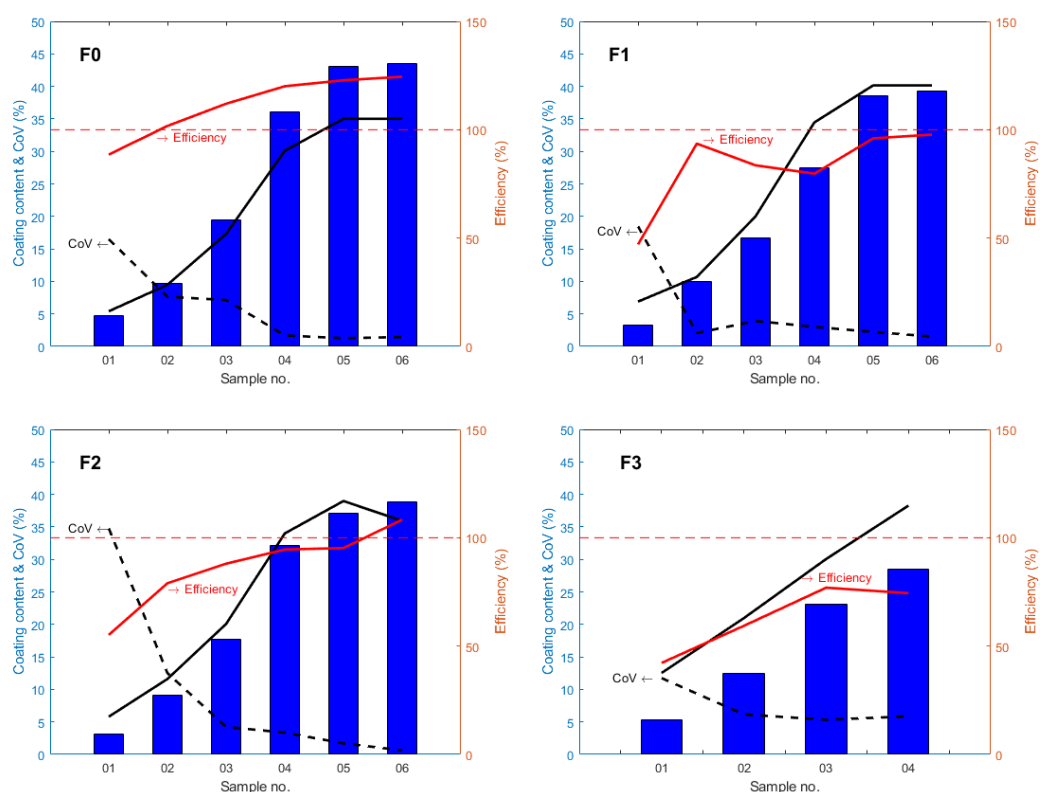


Figure 3-12. Assay of samples taken during coating trials with formulations **F1**, **F2**, **F0** and **F3**.

Calculated coating contents (black line), determined coating contents (blue bars), efficiency (red line), coefficient of variation-CoV (black dashed line). *Efficiency in excess of 100%* observed on some graphs is explained as follows: For process yield calculation, in this study, only particles still in fluidisation were counted, excluding the fraction of product sticking to the process wall and the filter system, or segregating upper in the fluidised bed.

From these observations, by collating with measurements of adhesion and contact angle for **F0**, high adhesiveness of **BW (F0)** is confirmed to be a problem for processing – stickiness of the formulation. On the other hand, by collating with all **F3** characterisation results, fine overproduction was due to combined factors of high cooling rate (by setting a low crystallisation temperature) of the fluidised bed,

its high melt viscosity, and low adhesiveness. Combinations of BW and SMS – formulations **F1** and **F2**, yield good efficiency.

For information, with the current experimental approach, once the experimental efficiency of a specific formulation with a determined set of process parameters is known, a compensated amount of material feeding could be applied to attain the target coating content.

In addition to the efficiency trends, the coefficient of variation (CoV) based on the assay ( $n = 3$ ) could presumably be used as an indicator of coating quality. Coating quality is based on the minimal coating content to yield coating homogeneity and completeness and it could be evaluated by examining both the mean coating thickness of the whole particles and the CoV by X-ray micro-computed tomography (Woerthmann et al., 2021). Emphasis is also put on the fact this coating content target should be considered together with the granulometry of substrate particle size used. As can be seen with assay results, a value of CoV (also called “relative standard deviation”) equal to or less than 5% indicates a good assay uniformity (Bánfai et al., 2007). – As a hypothesis to correlate CoV with uniform and complete coating, for the four formulations, a coating content from above 15% w/w was supposed to yield good coating quality together with a CoV less than 5%. This finding will be evaluated with results obtained with microscopy and release testing.

**To conclude this part**, with this multiple-sampling experimental approach, an evolution of coating efficiency could be constructed. This can help predict poor processing performance. For instance, low efficiency indicates abundant loss of coating material for **F3** while excessive efficiency indicates accumulated sticking of coated particles to the process wall for **F0**. These trends inform to discontinue product characterisation, to adjust process parameters or to improve formulation properties. However, all the coated particles would be analysed with different techniques to determine how formulations properties affect processing performance and coating quality.

### 2.2.2. Identification of process regime

Various process regimes are possible with the fluidised bed: agglomeration, coating/embedding, spray-congealing or mixed regimes (Ronsse et al., 2008). This depends on the specification of process parameters based on the understanding of formulation properties. The process regime could be determined by interpreting PSD and its parameters (Stiller, 2016) but this has still not been clear how to identify a coating regime when working with a fluidised bed.

As a hypothesis, when a coating regime dominates, fine particles tend to gain more coating materials with time in comparison with larger particles, this presumably leads to a reduction of the width of PSD, a sharpening of the median peak  $D_{v(50)}$  and a reduction in the ratio between  $D_{v(90)}$  and  $D_{v(10)}$ . On the other hand, granulation should result in an expansion of particle size range and a rapid shift of PSD to greater class size bins as the particles agglomerate with the three features following an inverse trend. Appearance of a peak in the region of finer particle class size bins might indicate occurrence of abundant overspray of lipids. Following this hypothesis, a certain process regime could be attributed to trials with **F0**, **F1**, **F2** and **F3** formulations by considering PSD evolution of coated particles sampled at a defined target coating content.

**Figure 3-13** shows overlapping PSD curves expressed in volume measured for initial NaCl particles, first, second and third sampled particles during coating trials.

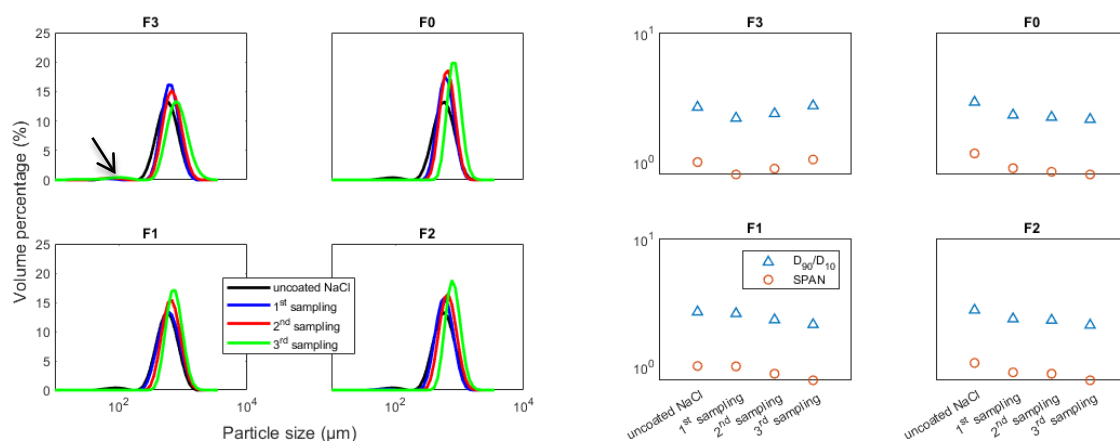


Figure 3-13. PSD curves (left) and parameters (right) obtained for salt particles coated with **F0**, **F1**, **F2** and **F3**. Left graphs: initial uncoated NaCl (black line), first sampling (blue line), second sampling (red line), third sampling (green line). Right graphs:  $D_{v90}/D_{v10}$  ratio (blue triangles), SPAN (red circles)

In all PSD graphs, the black line indicates polydispersed nature of initial salt particles after sieving. The substrate used in this study contains a fraction of fine particles despite a careful sieving operation. The absence of the peak in the region of finer particle size classes after initiating the coating operation might suggest two hypotheses:

- (1) segregation or loss of fine salt particles entrained by inlet air out of the filter;
- (2) agglomeration of those particles onto larger particles subject to coating.

From a qualitative perspective, the PSD curves could be interpreted. According to the hypothesis proposed at the beginning of this section, for three formulations **F0**, **F1** and **F2**, the fact that the median peak augmented and the PSD width reduced with the time points of sampling should indicate a coating regime. For the formulation **F3**, the same features for the first sampling informs a coating regime at the beginning of coating. However, an inverse trend was observed, which should indicate an on-going agglomeration.

These PSD interpretations complement the efficiency results. Firstly, a good efficiency and a coating regime were obtained when processing with **F1** and **F2**. Secondly, processing with **F0** yielded a poor efficiency but a coating regime. This means that high adhesiveness should not always be the cause of agglomeration. Thirdly, abundant loss in coating material (low efficiency) observed for processing with **F3** can be confirmed with abundant fine overproduction. Agglomeration also observed in this case was probably due to setting high feeding rate of **F3** (20 g/min).

From a quantitative perspective, PSD parameters could be interpreted. The parameter *SPAN* and  $D_{v(90)}/D_{v(10)}$  (see **Figure 3-13**) could be used as an indicator to differentiate the two process regimes.

When overspray or spray-congealing of lipids is abundant (as indicated by the black arrow in **Figure 3-13**), a second population of fine particles with a size less than 100  $\mu\text{m}$  might appear in PSD, which was observed for coating with **F3** in all the samplings. The rather constant ratio  $D_{v(90)}/D_{v(10)}$  could be

used as an indicator of coating regime (D. G. Lopes et al., 2015). This study (**Figure 3-13**) adds further that although not significant  $D_{v(90)}/D_{v(10)}$  diminishes as a function of coating time and this suits the hypothesis mentioned above for a coating regime.

PSD parameters of **F0**, **F1** and **F2**-coated particles showed the same decreasing tendency of *SPAN* and  $D_{v(90)}/D_{v(10)}$ . This implies narrowing of particle size distribution width and gradual levelling of particle size in the full batch. Therefore, a coating regime is expected.

On the other hand, as for coating with **F3**, from the start of the trial to first sampling both indicators inform a coating regime but later on agglomeration should take place.

**To conclude this part, concerning the application of PSD measurements in hot-melt coating, both qualitative and quantitative interpretations of PSD data can be applied interchangeably in a multiple-sampling experimental approach.** Solely a quantitative interpretation is possible in a single-sampling experimental approach, which suits quality control practices. As a precaution, the process regime should be evaluated using volume-based PSD data.

### 2.2.3. Contribution of cohesion

**Table 3-5** shows physical properties of salt particles coated with all formulations used for this study. Their particle size and bulk density could be regarded as similar.

Table 3-5. Micromeritic properties of salt particles coated with four formulations

Formulation	PSD parameters			Bulk density (g/mL)
	$D_{v(10)}$ (μm)	$D_{v(50)}$ (μm)	$D_{v(90)}$ (μm)	
<b>F0</b>	506	758	1160	0.79
<b>F1</b>	527	728	1010	0.77
<b>F2</b>	514	728	1050	0.72
<b>F3</b>	476	762	1200	0.70

As stickiness could be due to cohesion of particles (Adhikari et al., 2001), measurements of flow properties were performed on coated particles to complement measurements of adhesiveness presented above. By the definition in the cited publication, cohesion/adhesion is "a measure of force holding two similar/different surfaces/particles".

**Figure 3-14** shows an example result with flow measurements at 9 kPa as consolidation stress (**A**) and flow functions obtained for all formulations (**B**). **Figure 3-14-A** shows that cohesion of each formulation can be deduced from the value of the intercept.

As can be seen in **Figure 3-14-B**, cohesion decreases in the order of **F0**, **F2**, **F1** and **F3**. This shows an effect of surfactant addition. Interestingly, adding PS80 at a small percentage also results in a slight increase in cohesion. For this case, characterisation with FT4 appears to be sensible.

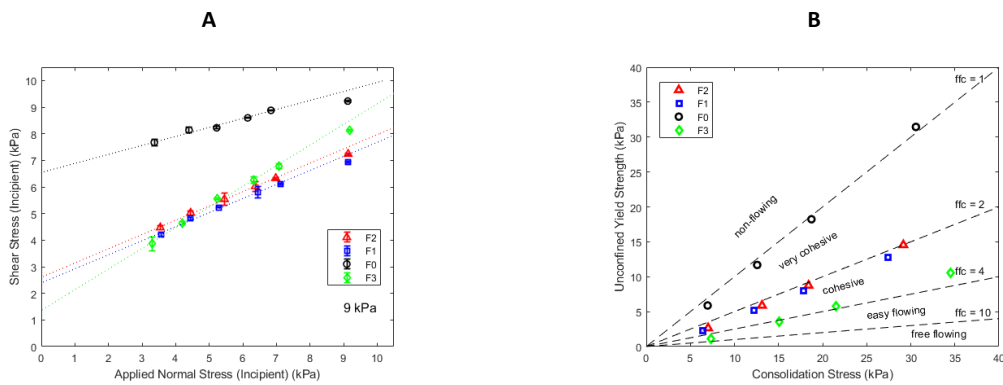


Figure 3-14. Yield locus (A) obtained under a representative consolidation stress 9 kPa and flow function (B) of salt particles coated with: **F0** (black circles), **F1** (blue squares), **F2** (red triangles) and **F3** (green diamonds)

The flow function graph in **Figure 3-14-B** shows regions indicative of different flow behaviours: very cohesive **F0**, cohesive **F1** and **F2**, easy flowing **F3**. These measurements contribute to explain accumulated sticking onto process wall observed whilst coating with beeswax (**F0**).

**To conclude this part**, on the one hand, **it is advisable that adhesion and cohesion should be investigated prior to coating** because a larger quantity of samples are needed for powder flow measurements as well as there are difficulties in processing challenging formulations. AFM and measurements of contact angle in molten state could be good predictive tools in development of hot-melt coating formulations.

On the other hand, **BW was shown to exhibit both high adhesion and cohesion which cause accumulated sticking of coated particles with time in the course of coating**. On the contrary, SMS was found to be less adhesive and cohesive, which cause abundant delamination. This incidence is related to adhesive failure of coating on substrate (especially at low crystallisation temperature) and cohesive failure of coating on coated substrate. Note that a material could have a low adhesion but a high cohesion and vice versa (Von Fraunhofer, 2012). A material could have both a low viscosity and a high cohesion and vice versa, both low viscosity and cohesion and vice versa (Wongprasert et al., 2022). The combination of BW (**F0**) and surfactants gave rise to a coating formulation with moderate adhesion, cohesion and low viscosity.

#### 2.2.4. Considerations on Operational Impact

One of the main objectives of this study was to evaluate the impact of formulation properties on processing performance. Therefore, the operational conditions were kept as close as possible. However, adhesion or solidification properties might dictate a specific set of process parameters (as shown previously in **Table 3-2**) whilst working with each formulation.

Firstly, for **F1** and **F2**, process parameters were optimised in preliminary trials and served as the starting conditions to be modified whilst coating with **F0** and **F3**. A fluidisation rate at 37 m<sup>3</sup>/h was sufficient to suspend particulate population with known quantity and quality, a spray-air pressure differential of 0.5 bar to pulverise molten medium and a feeding rate of about 7 g/min to deliver lipid medium appeared to be suitable to its solidification kinetics.

Initially, coating with **F1** and **F2** was based on a strategy to define product temperature (or bed temperature) as a setpoint. Later, in order to assure the stability of temperature control, this strategy was oriented to the inlet air temperature into the fluidized bed of substrate to be coated. As a precaution, stable control of thermal conditions is important as adhesion of **F1** and **F2** could increase with temperature (Pustan et al., 2022). As a result, this might reduce processing yield.

As for coating with **F0**, a higher fluidisation air flow rate, a very low feeding rate and a higher spray-air pressure differential were set in an attempt to improve processing performance and to generate samples for characterisation to force particle movement by considering their poor flow behaviours. A higher batch size was also required to increase density of fluidised bed. Otherwise, generation of fine fractions occurred (batch data not shown). Till this point, it can be noticed that in spite of better solidification kinetics of beeswax, coating performance was still better using **F1** and **F2** at the similar thermal conditions. In this case, adhesion properties should be moderate by combining BW and a material of low adhesion such as SMS.

As for coating with **F3**, a higher feeding rate was set by considering its rapid solidification kinetics. The same feeding rate as applied to coating with **F1** and **F2** was not viable as it led to almost generation of fine fraction with few coated particles. However, at this feeding rate, a mixed regime – coating and agglomeration – was obtained for **F3**. Fine fraction was always present in all samples. On the one hand, this incidence was due to low adhesiveness of SMS. On the other hand, setting of low fluidisation air temperature was likely to be the cause of adhesive failure or delamination. In conclusion, it was important to define thermal operational conditions based on formulations properties evaluated and then set other mechanical process parameters correspondingly.

**To conclude this part**, among the thermal processing conditions, fluidisation air temperature is the most important. It influences solidification, melt-viscosity for film formation and adhesion of the tested formulations in the course of coating but setting this temperature is also constrained, mainly by adhesion in this case. Other than re-definition of thermal processing conditions, adjustment of mechanical process parameters, i.e. fluidisation air flow rate, atomisation air pressure and feeding rate, was possible but only for feasibility of coating with **F0** and **F3**. It is not so effective as modification of formulation properties. In fact, the combinations of **F0** and **F3** – **F1** and **F2** have a good processing performance. Evaluation of coating quality will be presented in the following parts.

## **2.3. Coating Quality Assessment**

### **2.3.1. Optical Observations**

Observations with optical microscopy provide further information on morphology of particles (white background with light reflected on background) as well as allow for quick assessment of surface coverage and process regime (black background with light reflected on object). For these observations, a large quantity of particles were investigated to assure the representativity. The two modes of observations show no difference for transparent objects such as uncoated salt crystals.

**Figure 3-15** shows uncoated salt crystals and salts coated with **F0** on white and black background. In general, on white background observed particles look polygonal-shaped and the coating increases the roundness of particles with time. Coating quality could be evaluated with respect to evolution in overall particle size and reduction in transparency of salt crystals. These figures show uneven transparency of not completely coated salt crystals and grey scale of coated particles, which indicates lack of coating completeness and homogeneity. Observations of particles on black background help discern particle borders or whether particles are agglomerated or not. Therefore, they permit identification of the process regime. In this case, a coating regime was obtained with F0 processing, and it agrees with interpretation of PSD measurements.

Salt crystals coated with **F1**, **F2** and **F3** were also observed by the same optical technique, on white and black background. Optical images of salt crystals coated with **F2** and **F1** showed a similar trend (and for this reason, images for **F1** are not shown). For salt crystals coated with **F2** (See **Figure 3-16**), as observed with particles coated with **F0**, an evolution of particle size, a coating regime and absence of fine particles were noted. However, good coating completeness and uniformity could be expected according to an even distribution of grey scale throughout all the samplings.

All **F3** coated images display fine particles and occurrence of agglomerates (see **Figure 3-17**). In addition, an even distribution of grey scale may hint at a good surface overage. With **F3** agglomerates appear from second sampling. Therefore, these images also lead to the same interpretation of PSD measurements performed on particles coated with **F3**. From these observations, it could be concluded that CoV of assay observed with particles sampled at the end of coating with **F0** and **F3** (corresponding respectively to **Figure 3-15-D** and **Figure 3-17-D**) cannot be used as an indicator of coating completeness and homogeneity.

**To conclude this part**, utility of PSD measurements and optical observations could be concluded for certain cases in HMC research:

- Optical observations can be useful in a multiple-point-sampling approach tested in the current study. PSD measurements can be alternative. However, one PSD measurement could be deployed in order to get quantitative information, i.e. PSD parameters.
- PSD measurements are normally applied in the conventional single-point-sampling approach and confirmed to suit quality control when coating with lipid formulations prepared for use in hot coating (Becker et al., 2016).



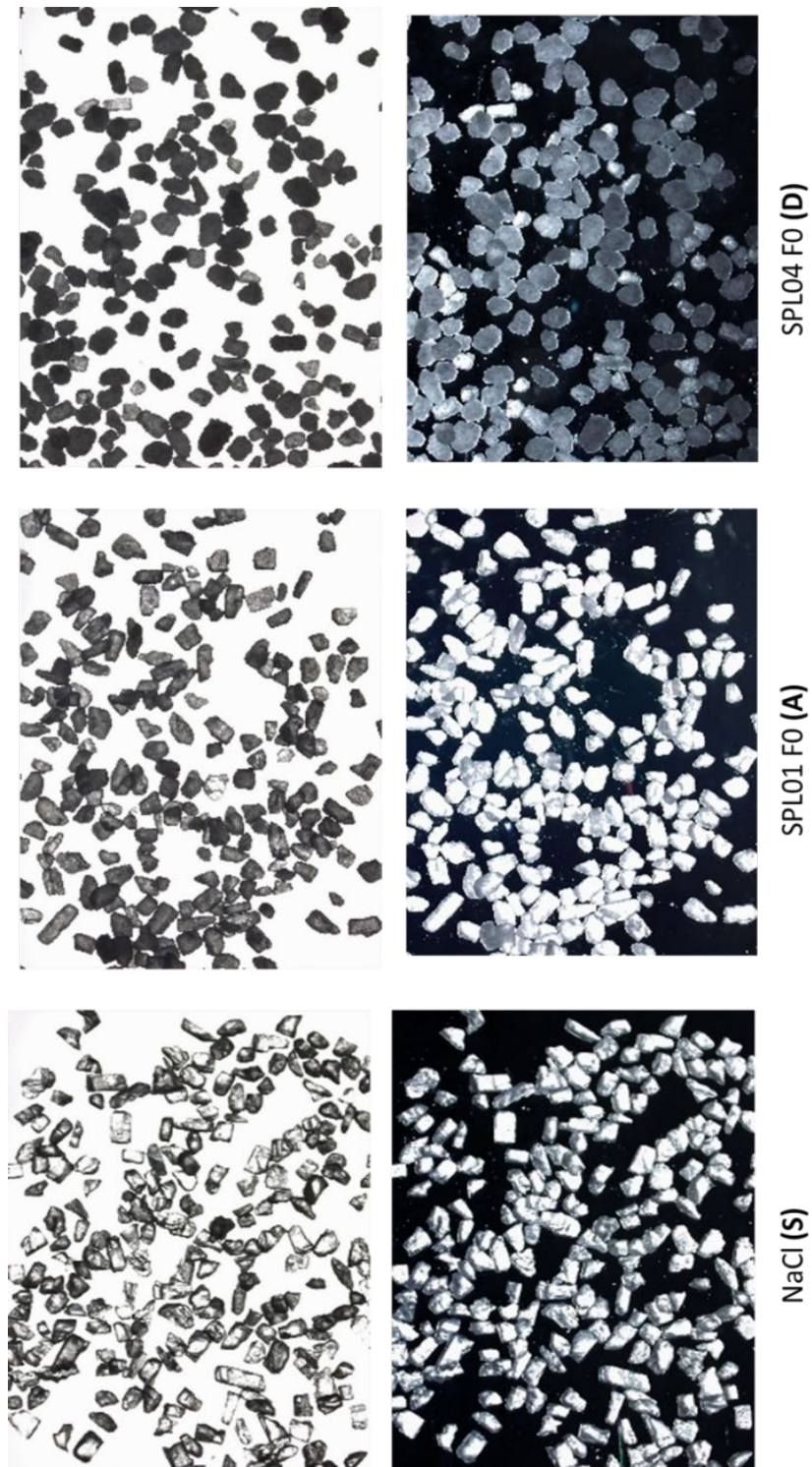


Figure 3-15. Optical microscopic images of samples taken from coating trial with formulation F0. S, uncoated salt, A, first sampling, D final sampling

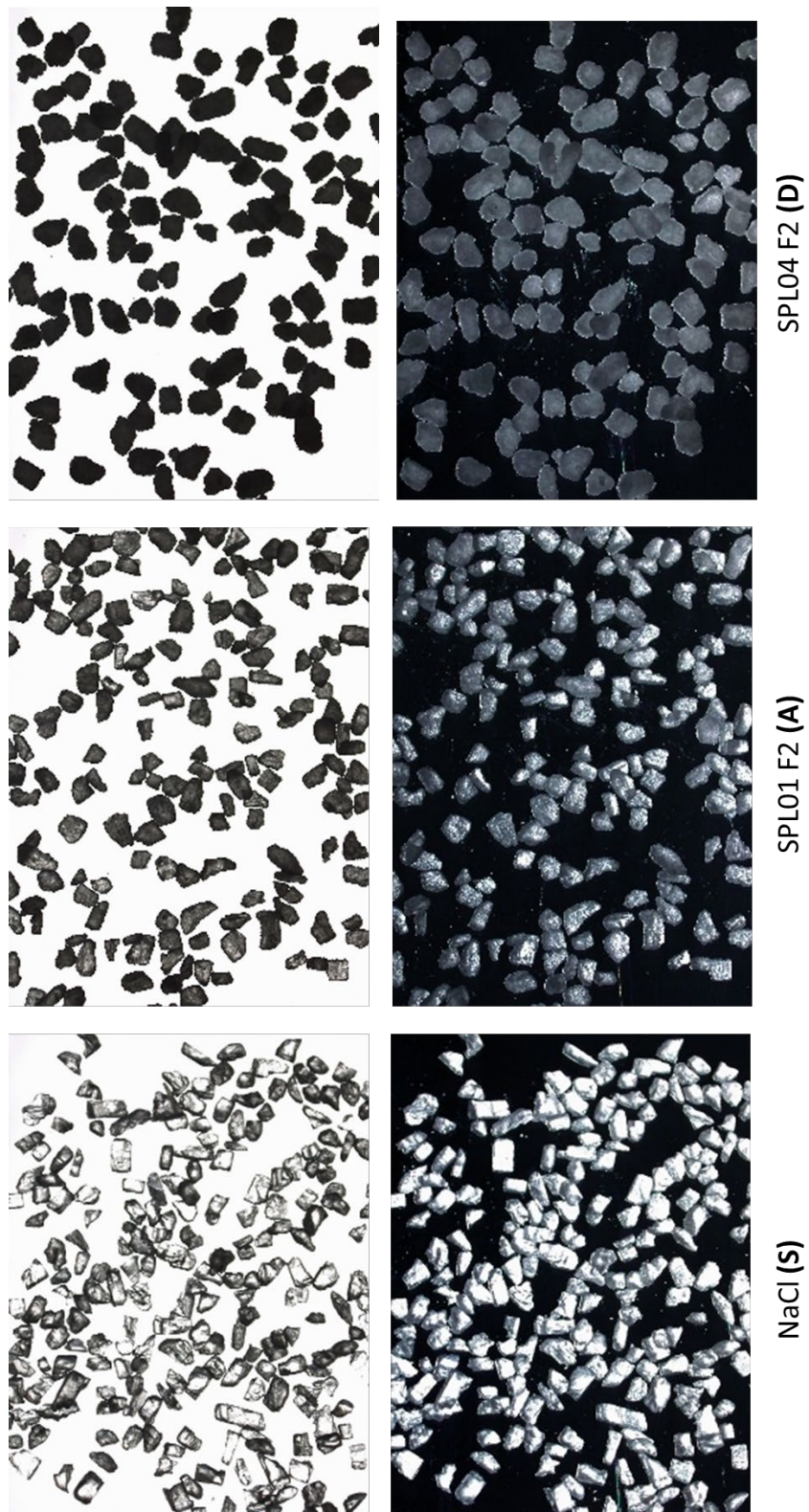


Figure 3-16. Optical microscopic images of samples taken from coating trial with formulation F2. S, uncoated salt, A, first sampling, D final sampling



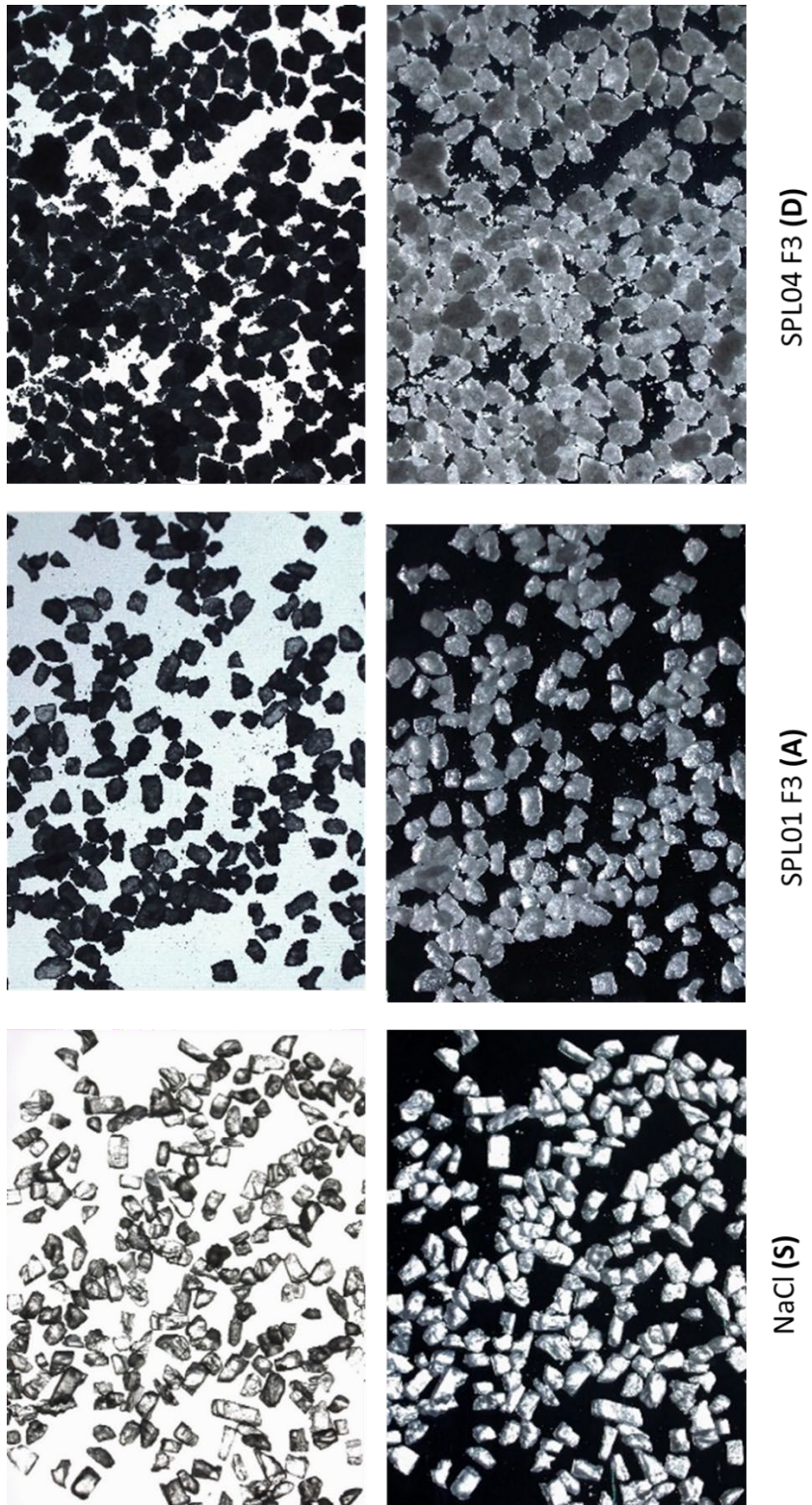


Figure 3-17. Optical microscopic images of samples taken from coating trial with formulation F3. S, uncoated salt, A, first sampling, D final sampling

## 2.3.2. SEM Observations

### 2.3.2.1. Chemical contrast mode

This mode enables evaluation of coating completeness based on the interactions of chemical elements with X-ray. Higher-atomic-weight elements display a brighter aspect compared to lower-atomic-weight elements. Therefore, NaCl crystals brighten, and coated parts of these crystals darken. All the SEM images are displayed in 500  $\mu\text{m}$  scale in **Figure 3-18**.

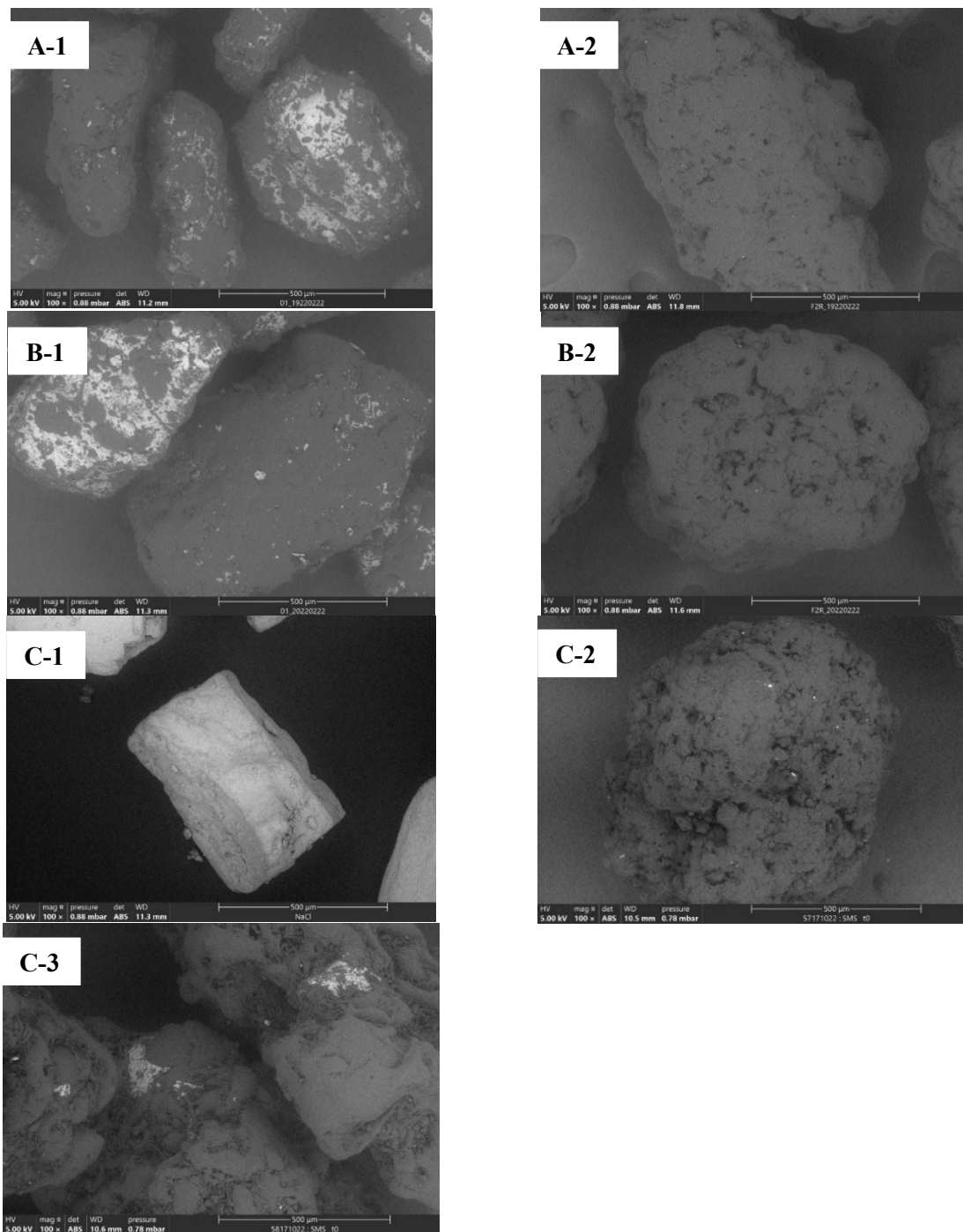


Figure 3-18. Images taken on chemical contrast mode (length-scale of 500  $\mu\text{m}$ ): uncoated salt (C-1) and salt coated with different formulations at different ratios: 3.2% and 39.3% **F1** (A-1 & A-2), 3.2% and 38.9% **F2** (B-1 & B-2), 33.8% **F0** (C-2), and 32.6% (C-3) **F3**

**Figure 3-18-A-1** and **B-1** show particles not completely coated with 3.2% w/w F1 and F2, respectively. Particularity of these images is that small spots could be observed on the bright surface of non-coated salt particles.

**Figure 3-18-A-2, B-2** and **C-2** show particles coated with 39.3% **F1**, 38.9% **F2** and 33.8% **F0**. With such high coating contents, all the observed particles were almost completely coated. As reported in literature, solidification led to formation of a porous surface (Mostefa & Muhr, 2019). Qualitatively, particles coated with **F1** and **F2** exhibit less rough surface (less developed porosity) in comparison with that of **F0**. In fact, this might be due to setting of a higher atomisation air pressure differential for coating with **F0**, which probably lead to generation of smaller droplets of BW.

**Figure 3-18-C-1** shows uncoated salt particles which display bright and angular aspects, whereas coated particles possess rounded edges regardless of their coating contents or nature. As shown in **Figure 3-18-C-3**, particles coated with **F3** display large defects of non-coverage. This might be due to its propensity to delaminate and its poor adhesiveness. Furthermore, on the surface displays filaments, the cause of which will be discussed considering observations on topographical mode.

#### 2.3.2.2. *Topographical contrast mode*

At a smaller scale of observations (50  $\mu\text{m}$ ), surface quality could be observed more clearly (**Figure 3-19**).

The surface of uncoated NaCl appeared to be partly smooth (**Figure 3-19-A-1**) and covered with fine particles (**Figure 3-19-C-1**) whereas the surface area coated with lipids is rather rough. There are also fine salt particles attached to a gross particle.

**Figure 3-19-A-1** and **B-1** show images of particles not completely coated with **F1** and **F2**. Primary structures include discrete hemispheres of different diameters attached to the smooth surface of salt particles and continuous fin-like surface. Observations of lipid deformation during solidification corroborate the formation of these structures.

**Figure 3-19-A-2, B-2** and **C-2** also display primary structures with open pores the size of which are less than 50  $\mu\text{m}$ . In addition, secondary structures appear more clearly with small plaques like flower petals. This is the so-called phenomenon "lipid blooming", often encountered with lipid-based formulated products (Delbaere et al., 2016; D. G. Lopes et al., 2015; Witzleb et al., 2012). These particles were conserved at room temperature until the date of SEM imagery. The sustained presence of a small salt particle (at the observation scale of 10  $\mu\text{m}$  – **Figure 3-19-C-2**) can indicate a high adhesiveness of BW.



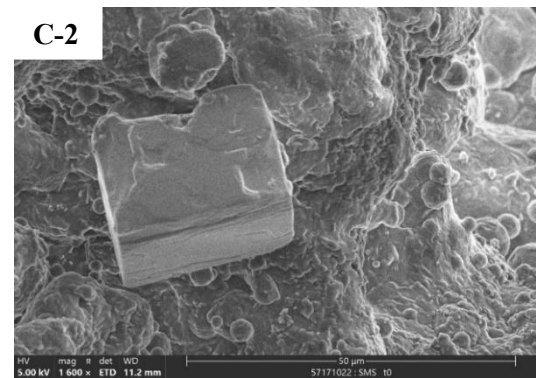
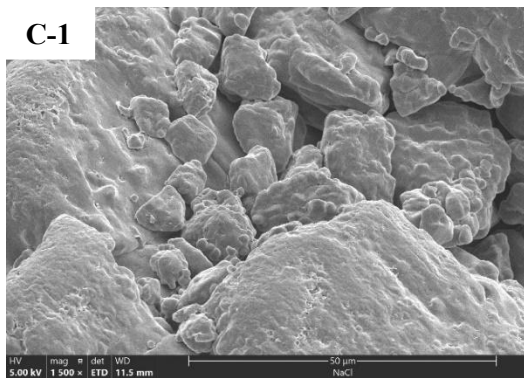
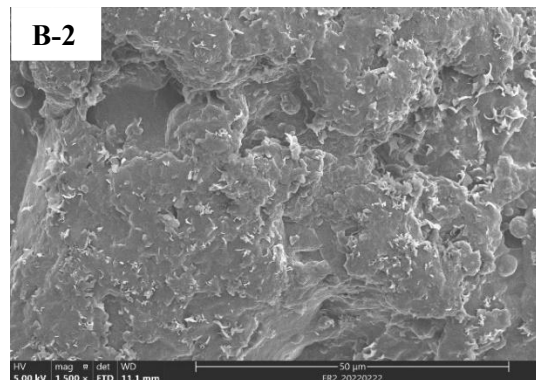
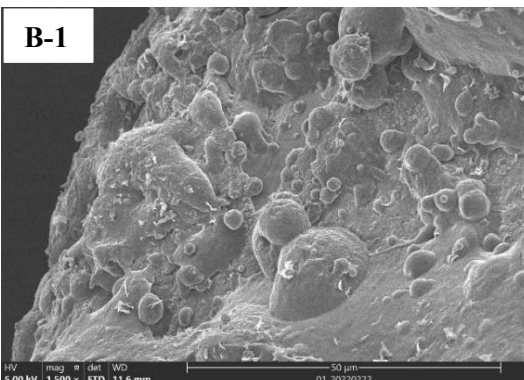
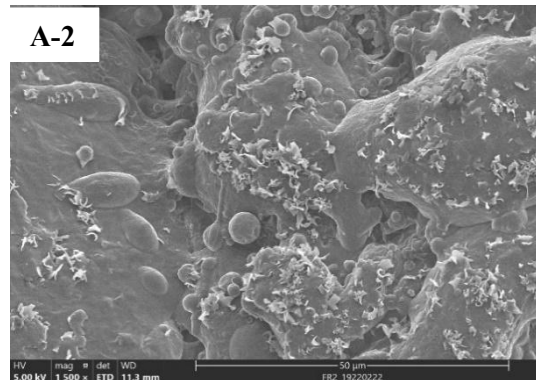
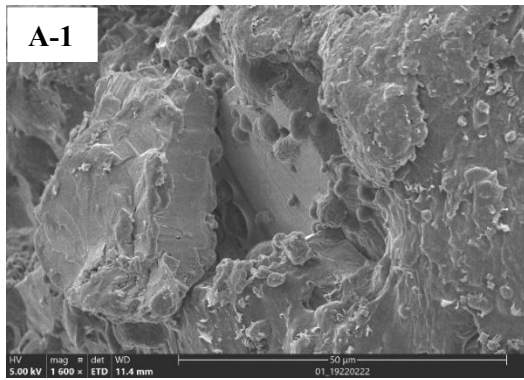


Figure 3-19. Images taken on topographical contrast mode (length-scale of 50  $\mu\text{m}$ ): uncoated salt (C-1) and salt coated with different formulations at different coating contents: 3.2% and 39.3% **F1** (A-1 & A-2), 3.2% and 38.9% **F2** (B-1 & B-2), 33.8% **F0** (C-2) and 32.6% **F3** (C-3)

**Figure 3-19-C-3** shows a particular case of salt coated with SMS (**F3**). Filaments were observed and should originate from solidification of SMS. The cause of their occurrence could be deduced from a recent study on spray drying (Shepard et al., 2020). In fact, low inlet temperature, low spraying pressure as well as its rapid solidification profile and high viscosity should likely be the cause as presented with the measurements of contact angle.

**To conclude this part**, SEM could be counted as a technique applied in single-point sampling approach to evaluate coating coverage (via chemical contrast) and coating topography (via topographical contrast). For instance, salt particles with the least and the most coating contents of **F1** and **F2** were analysed to search for a correlation on film formation observed with hot-melt goniometry and to determine a coating content that assures a complete coating. Even with the highest coating content, salt particles coated with **F3** were found to be not fully covered and its film formation was not normal. Intuitively, at the temperature of processing conditions, **F3** should exhibit high melt viscosity and as a consequence this should prevent it from sufficient spreading for a good coating. SEM observations are qualitative for identification of coating defects and topography. Quantitative evaluation of coating quality will be presented in the next parts.

### 2.3.3. Assessment of release kinetics

#### 2.3.3.1. *Effect of coating composition*

As can be seen with the results on process performance already presented, coating with either beeswax (**F0**) or sorbitan monostearate (**F3**) alone displays challenges related to their solidification, melt viscosity and adhesiveness property.

Despite that, release testing was performed with salt particles coated with all those formulations, the coating contents was approximately the same (with a range between 29% to 35% w/w). All the tests were conducted during one hour to check if an immediate release profile could be obtained with formulations being studied (Siewert et al., 2003).

The results are presented in **Figure 3-20** showing that uncoated salt dissolved in about 5 min and product coated with **F3** released the salt completely within 15 min. The products coated with a relatively close coating content of **F2** and **F1** exhibits a difference in release rate but a close release extent (more or less than 60% salt dissolved) at the end of release testing.

The product coated with **F0** shows a prolonged salt release which attains just above 20% salt dissolved within 1h. In definitive, all the formulations exert a coating effect on salt release kinetics in comparison with uncoated salt. All the standard deviations are below 5% for all measurements of release kinetics, except **F1** (> 5% from 50 min).

By mathematical fitting up-to-40%-salt release data of coated beads with selected empirical models (Vergnaud, 1993), release mechanisms of salt in pure water were evaluated in the following. Release parameters of empirical models are shown in **Table 3-6**.

The model drug, NaCl, is a very water-soluble substance (about 362.6 g/L) (Pavuluri, 2014). As an assumption, coated products were treated as spherical particles. The simple release models (zeroth and



first order) were applied to verify if dissolution is mainly diffusion-controlled and concentration-dependent with the effect of coating already taken into account (Siepmann & Siepmann, 2009)

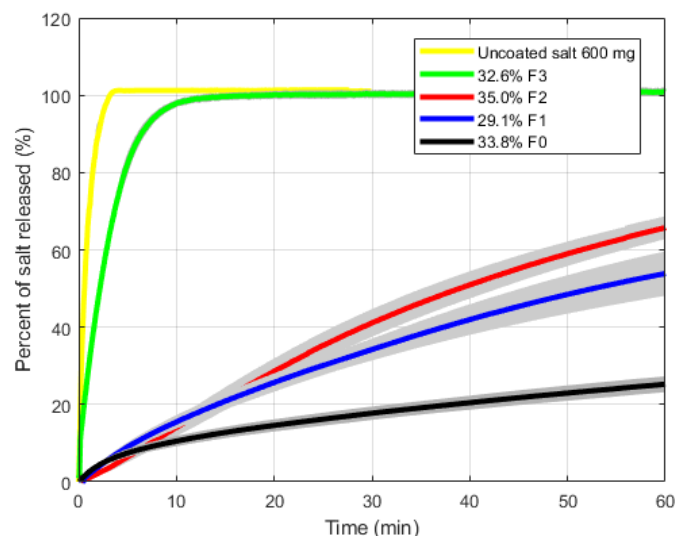


Figure 3-20. Comparative dissolution profile of uncoated salt particles and salt coated with four formulations at a similar coating content (% w/w): uncoated salt (yellow line), salt particles coated with 33.8% **F0** (black line), 29.1% **F1** (blue line), 35.0% **F2** (red line) and 32.6% **F3** (green line). Standard deviation (grey region).

Table 3-6. Release constants and exponents obtained after data fitting to selected models for salt coated with four formulations at a similar coating content (%w/w)

Coating content (%w/w) and Formulation	Zero order		First order		Korsmeyer-Peppas			Peppas-Sahlin			Higuchi		Hopfenberg		
	$k_0$ ( $h^{-1}$ )	$R^2$	$k_1$ ( $h^{-1}$ )	$R^2$	$k_{KP}$ ( $h^{-n}$ )	$n$	$R^2$	$k_D$ ( $h^{-m}$ )	$m$	$k_{R-E}$ ( $h^{-m}$ )	$R^2$	$k_H$ ( $h^{-1}$ )	$R^2$	$k_B$ ( $h^{-1}$ )	$R^2$
33.8% F0	0.30	0.6411	0.35	0.7356	0.25	0.50	0.9977	0.25	0.50	0.00	0.9977	0.25	0.9977	0.11	0.7064
29.1% F1	0.71	0.9461	0.87	0.9851	0.57	0.73	0.9991	0.57	0.73	0.00	0.9991	0.46	0.9385	0.27	0.9754
35.0% F2	0.85	0.9988	1.00	0.9918	0.85	1.00	0.9988	0.85	1.00	0.00	0.9988	0.47	0.8374	0.32	0.9958
32.6% F3	15.44	0.9100	19.11	0.9611	4.33	0.67	0.9929	4.08	0.66	1.04	0.9929	2.20	0.9597	5.94	0.9477

Kormeyers-Peppas model was applied to identify release mechanisms based on the value of release exponent  $n$  estimated. If  $n = 0.5$ , the release mechanism is purely diffusion (Fickian transport). If  $0.5 < n < 1$ , the mechanism is non-Fickian or anomalous transport. If  $n = 1$ , the mechanism is a zeroth order or Case 2 transport. If  $n > 1$ , the mechanism is a super Case 2 transport (P. Costa & Sousa Lobo, 2001). The difference between the four mechanisms relate to water diffusion and lipid membrane relaxation (swelling) in this case. In fact, Fickian diffusion is characterised by high water diffusion rate and low membrane relaxation kinetics while for non-Fickian diffusion, water diffusion rate and membrane relaxation kinetics occur to a similar rate. For Case II transport, water diffusion rate is less important than membrane relaxation kinetics while for Super Case II transport, water diffusion rate is much higher than membrane relaxation kinetics (« Mathematical Models of Drug Release », 2015).

Application of Peppas-Sahlin model was to account for both release mechanisms by diffusion and relaxation/erosion. The applicability of Higuchi model, normally used for release of active substance from matrix systems, was tested as it has been used to model drug release subject to long-term storage in some hot-melt coating researches (D. G. Lopes et al., 2015; Schertel, Salar-Behzadi, & Zimmer,

2021). Finally, Hopfenberg model was also deployed to verify as its use is for surface-erodible systems (applicable to coating) (P. Costa & Sousa Lobo, 2001; Katzhendler et al., 1997).

As discussed above, **F0**-coated salt particles were a sustained release dosage form. All the coated particles appeared to behave like a homogeneous matrix system in which drug is entrapped and slowly released by diffusion. In fact, dissolution data can be well integrated in a Higuchi model ( $R^2 = 1$  – **Table 3-6**). Release kinetics of salt coated with **F3** involves diffusion and probably both membrane relaxation and erosion as indicated by the Peppas-Sahlin imodel.

Note that both **F3**- and **F1**-controlled salt release data well fitted Kormeyers-Peppas but an erosion mechanism should make a difference for **F3**. In fact, by considering aqueous interactions based on their chemical composition, SMS is a polar swelling insoluble amphiphile while BW is composed of non-polar or insoluble polar lipids according to a classification of lipids based on aqueous interactions (Small, 1968).

NaCl release from **F1** follows a first order kinetic process ( $R^2 = 0.99$  – **Table 3-6**). This corresponds with release kinetics from a reservoir with non-constant active source (Siepmann & Siepmann, 2009). For this system, water penetration in and out of the coating is limiting. Partial dissolution of salt trapped in the centre in a limited volume of water creates a concentration gradient that governs salt diffusion out of the coating. Salt concentration decreases gradually and a first order release is therefore observed as such. **As presumptions, characteristics of the membrane and the dimension of the system should be time-independent during salt release, i.e. no dissolution or swelling of the membrane.** Not only the first order was well fitted but also the release exponent ( $n = 0.73$  – **Table 3-6**) indicates a transport mechanism dictated by both water diffusion and membrane relaxation in similar kinetics. Note that **F1** is a combination of **F0** and **F3**. Therefore, **F1** contains non-polar, non-swelling and swelling insoluble polar lipids (Small, 1968).

Finally, **F2**-coated salt release kinetics can be well integrated in a zero or first order model ( $R^2 = 1$  – **Table 3-6**). Its release kinetics agrees with a reservoir system with constant active source applies (Siepmann & Siepmann, 2009). The coating acts as a non-erodible membrane and water penetration in and out of the membrane might not be a limiting process. More salt-concentrated solution is created inside the core by rapid replacement of water and salt dissolved diffuses out of the membrane following a stable gradient. This is the zeroth order release. In the late stage, once salt is completely dissolved, salt concentration inside the core decreases with time. A first order release is then observed. This model holds the same presumptions aforementioned. Not only the zeroth order was well fitted but also the release exponent ( $n = 1.00$  – **Table 3-6**) indicates a transport mechanism dictated by membrane relaxation to a higher rate than water diffusion. In fact, note that **F2** differs from **F1** in the fact that a small fraction of polysorbate 80 is added. Therefore, **F2** contains non-polar, non-swelling and swelling insoluble polar lipids and a small fraction of soluble amphiphile that should enhance water penetrability of the coating (Small, 1968).

Fitting with Hopfenberg model complements these suggested release mechanisms. Addition of polysorbate 80 could be said to render **F2** more erodible ( $R^2 = 1$  – **Table 3-6**) in comparison with **F1**

and **F3**. **F0** is more resistant to erosion in water according to this model and this agrees with its chemical composition.

To finish with this part, the use of empiric release models could help propose a hypothetical explanation on release mechanisms associated **with the chemical nature of different coatings**. In fact, relaxation (swelling behaviours) of lipid coating was revealed to be the main contributing factor. This justifies that some models suit better with a particular system than another:

- Higuchi model for **F0** (BW) which contains non-polar/polar insoluble non-swelling lipid-based coating (as discussed in DSC thermal analyses)
- Peppas-Sahlin model for **F3** (SMS) which is an insoluble swelling amphiphile
- First order release model for **F1** which is the combination of **F0** and **F3**
- Second order release mode for **F2** which is **F1** with a small fraction of PS80 added
- Kormeyers-Peppas model reasonable to correlate release mechanism(s) with interactions of a lipid coating in aqueous media as a function of its chemical composition
- Hopfenberg model as indicator of lipid coatings susceptible to erosion
- Peppas-Sahlin equation – a good model that can inform most of release mechanism(s) of all the lipid coatings tested.

#### 2.3.3.2. *Effect of physical barriers*

**F1** and **F2** were selected to study the influence of coating contents on NaCl release taking into account the above *in vitro* dissolution results.

**Figure 3-21** shows the dissolution profile of salt particles, those uncoated and coated with different coating contents of **F1** (**A**) and **F2** (**B**). For all the batches produced with different amount of coating (from 15.3% to 49.3% for **F1** and 11.5 to 44.2% for **F2**), a coating regimen has been obtained and confirmed by PSD measurements (data not shown). As expected, there is a great influence of coating level on NaCl release. The increase in coating amount decreases the release there is a low influence on the type of release kinetic.

**Tables 7** and **8** gathered main model parameters estimated for all dissolution profiles obtained with salt coated with **F1** and **F2**, respectively. As discussed above, for **F1** coated products, almost all the different coating amount formulations exhibits first order release kinetics while for **F2** coated products almost all the different coating amount formulations exhibits a zeroth order kinetics.

**Figure 3-22-A** and **-B** shows that all **F1** and **F2** release constants from first order, zeroth order, Korsmeyer-Peppas and Hopfenberg models were plotted against the estimated mean coating thickness of **F1** and **F2** coated products respectively. In this case, first order, zeroth order and Hopfenberg are selected because they express the coating effect. Release constants ( $k$ ) are based on the fact that this release constant has an exponent of 1 in these equations.

For coated dosage forms, the release constant was found to be inversely proportional to the coating thickness, i.e.  $k \times h = \text{constant}$  (Frenning et al., 2003). Therefore, a power relationship was chosen for all these data in Excel. The exponents were found relatively close between first order (-1.81), zeroth order (-1.73) and Hopfenberg (-1.78) for **F1** (Figure 3-22-A). The exponents were also found relatively close between first order (-1.76), zeroth order (-1.73) and Hopfenberg (-1.75) for **F2** (Figure 3-22-B).

From these results, firstly, an observed value of  $R^2 > 0.9$  shows that this inverse exponential relationship between coating thickness and release constant exists. This implies that a uniform and complete coating could be achieved for all the particles at one of these coating contents.

Secondly, the exponent of the reference relationship (1) obtained with a mechanistic modelling approach is different from the exponent of the inverse exponential relationship estimated for empirical models (nearly 2). In fact, the dissolution constant often includes diffusion term and total surface area of the tested system (P. Costa & Sousa Lobo, 2001; Katzhendler et al., 1997; Sugano & Terada, 2015).

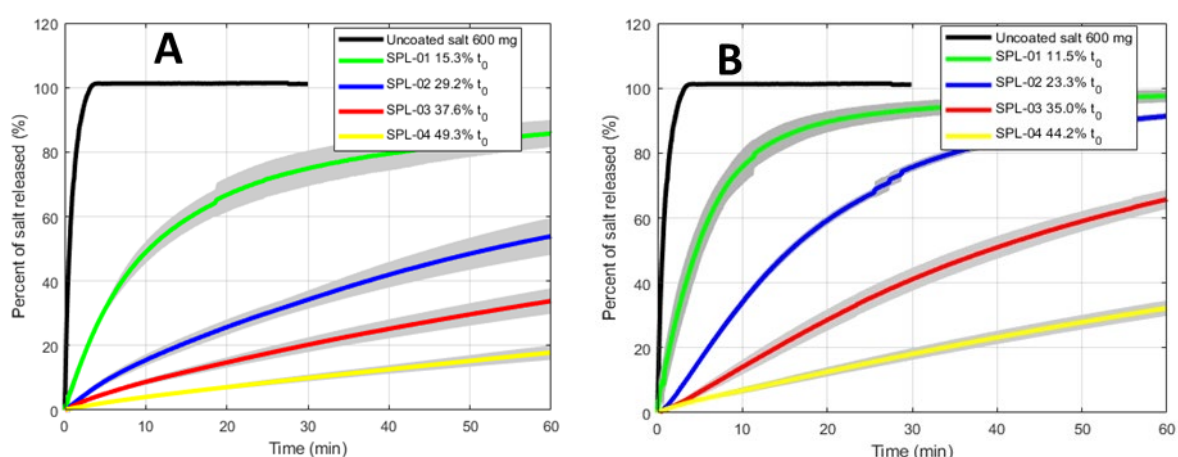


Figure 3-21. Comparative dissolution profile of uncoated salt and salt particles coated with different coating contents using **F1** (A) and **F2** (B).

Table 7. Release constants and exponents obtained after data fitting to selected models for salt coated with **F1** at four coating content (%w/w)

Coating content (%w/w)	Zero order		First order		Korsmeyer-Peppas			Peppas-Sahlin			Higuchi			Hopfenberg	
	$k_0$ (h <sup>-1</sup> )	R <sup>2</sup>	$k_1$ (h <sup>-1</sup> )	R <sup>2</sup>	$k_{KP}$ (h <sup>-n</sup> )	n	R <sup>2</sup>	$k_D$ (h <sup>-m</sup> )	m	$k_{R-E}$ (h <sup>-m</sup> )	R <sup>2</sup>	$k_H$ (h <sup>-1</sup> )	R <sup>2</sup>	$k_B$ (h <sup>-1</sup> )	R <sup>2</sup>
15.3%	3.70	0.9752	4.50	0.9975	2.31	0.81	0.9980	2.31	0.81	0.00	0.9980	1.04	0.9098	1.3972	0.9924
29.2%	0.71	0.9460	0.87	0.9851	0.57	0.73	0.9991	0.57	0.73	0.00	0.9991	0.46	0.9385	0.2678	0.9760
37.6%	0.41	0.9644	0.46	0.9839	0.35	0.77	0.9999	0.35	0.77	0.00	0.9999	0.27	0.9248	0.1366	0.9800
49.3%	0.19	0.9831	0.20	0.9917	0.18	0.83	0.9999	0.17	0.80	0.01	1.0000	0.15	0.9019	0.0658	0.9896

Table 8. Release constants and exponents obtained after data fitting to selected models for salt coated with **F2** at four coating content (%w/w)

Coating content (%w/w)	Zeroth order		First order		Korsmeyer-Peppas			Peppas-Sahlin			Higuchi			Hopfenberg	
	$k_0$ (h <sup>-1</sup> )	R <sup>2</sup>	$k_1$ (h <sup>-1</sup> )	R <sup>2</sup>	$k_{KP}$ (h <sup>-n</sup> )	n	R <sup>2</sup>	$k_D$ (h <sup>-m</sup> )	m	$k_{R-E}$ (h <sup>-m</sup> )	R <sup>2</sup>	$k_H$ (h <sup>-1</sup> )	R <sup>2</sup>	$k_B$ (h <sup>-1</sup> )	R <sup>2</sup>
11.5%	7.63	0.9757	9.28	0.9942	4.21	0.81	0.9965	4.12	0.81	0.41	0.9965	1.49	0.9102	2.90	0.9908
23.3%	2.01	0.9944	2.37	0.9797	2.41	1.09	0.9977	2.41	1.09	0.00	0.9977	0.71	0.8063	0.75	0.9860
35.0%	0.85	0.9988	1.00	0.9918	0.85	1.00	0.9988	0.85	1.00	0.00	0.9988	0.47	0.8374	0.32	0.9958
44.2%	0.34	0.9876	0.40	0.9985	0.33	0.85	0.9997	0.33	0.85	0.00	0.9997	0.28	0.8929	0.13	0.9964

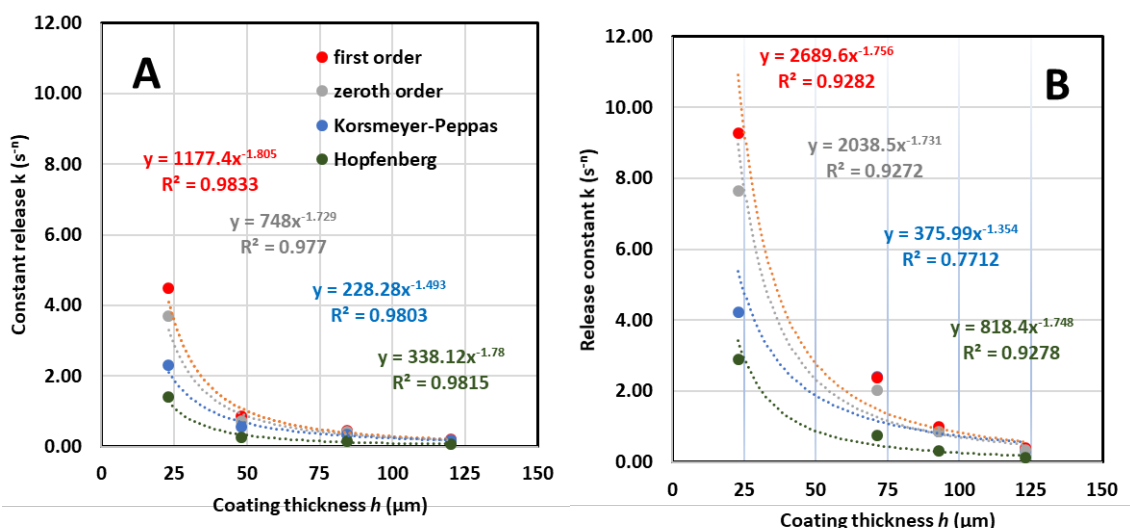


Figure 3-22. Relationship between release constants of different models and estimated mean coating thickness. Closed and open markers represent the values obtained with the formulations **F1** (A) and **F2** (B), respectively. Red, grey, blue and green closed circles denote the release constants associated with first order, zeroth order, Korsmeyer-Peppas and Hopfenberg, accordingly. Dotted line indicates the inverse power relationship.

Therefore, for this approach the inverse exponential relationship (based on the results in Figure 21) can be written as  $k \times h^a = \text{constant}$ , where  $a$  represents the dimensionality of dissolution. Intuitively,  $a$  is hardly to be found as an integer as it depends on multiple factors of coating quality (e.g. intraparticle and interparticle distribution of coating thickness, porosity).

Thirdly, the exponent of Korsmeyer-Peppas model is  $n$  (indicative of release mechanism). This is to show that this approach is limited to first order, zeroth order and Hopfenberg models which were shown to be relevant to chemical composition of **F1** and **F2**.

Based on this and the results of assay uniformity, it is reasonable to conclude that coating with **F1** and **F2** from 15.3% and 23.3% w/w yields homogeneous coating for salt particles whose size is between 400 and 630  $\mu\text{m}$ .

In conclusion, for a good conclusion of the minimal coating content, the use of empirical release models needs considerations of biological formulation properties and measurements of release kinetics from substrate particles coated with at least four different coating contents in the same batch, which are well integrated in this multiple-sampling experimental approach.

### 3. Conclusions

The study was focused on the processability of HMC formulations with **challenging properties i.e. solidification, melt viscosity and adhesiveness**. Two experimental approaches were performed in parallel:

- A **multiple-point-sampling** approach comprised of mass balance, assay uniformity, optical observations, and release testing. This approach was tested and proved useful for early development of HMC formulations, although other complementary characterisations may also be useful;

▪ A **single-point-sampling** approach comprised of mass balance, assay uniformity, PSD measurement, SEM imagery and release testing. This approach is conventional and normally adopted for quality control in the case of coating with developed HMC formulations.

It was demonstrated that formulation properties – solidification, melt viscosity and adhesiveness of coating materials – all have a determinative impact on processing performance and coating quality. The most important is adhesion and cohesion of BW and SMS. Adjustment of process parameters was less effective than improvement of formulation properties. In fact, combination of BW and SMS was shown to contribute to improvement of its processing performance.

Addition of a small fraction of hydrophilic surfactant PS80 had a neglectable effect on adhesiveness of the formulation and cohesiveness of coated particles, but release mechanism via the impact on water uptake of the lipid coating. Together with assay uniformity and optical observations, measurements of salt release kinetics from particles coated with different coating amounts can help conclude a minimal coating content that could guarantee a good coating homogeneity, i.e. over 15% and 23% w/w for **F1** and **F2**, respectively. As a precaution, this conclusion depends on granulometry of initial substrate particles, in this case 400-630  $\mu\text{m}$ .

The multiple-point sampling approach is worth transferring to HMC studies with other types of lipid-based formulations (e.g., triglycerides). The utilities of this approach lie on the fact that it enables exploring the effect of formulation properties on specification of process parameters and thereafter processing performance and coating quality. The model drug, NaCl crystals (Clarkson et al., 1971), has proved to be very useful as it facilitates rapid characterisation of HMC process and product performance. Despite the high solubility of salt in the dissolution medium and the sink conditions maintained, the lipid coating was able to limit the dissolution rate compared to uncoated salt. As expected, the type of coating clearly influences the rate and extent of salt release without any burst effect. The lipid coating controls release of the drug.

As for product stability and release properties, this study warrants further research studies on the evolution of solid-state in the presence of additives. Future research studies would be planned to understand the impact of additives addition and link with long-term stability of formulations ranging from microscopic scale (e.g., solid-state) to macroscopic scale (e.g., release rate) and also to study salt release mechanism changes in simple buffer and in biologically simulated medium.

## Part 2

# Coating Lipid Composition: Physical Coating Stability

After studying the impact of lipid-based coating properties on coating performance in **Part 1**, **Part 2** focuses on their physical coating stability and, analyses, as a consequence, the impact of their physical stability on the release control in simple and complex dissolution media.

### 1. Materials and Methods

#### 1.1. Materials

Beeswax (BW) and additives, Montane™ 60 PHA PREMIUM (sorbitan stearate, SMS) and Montanox™ 80 PHA PREMIUM (polysorbate 80, PS80), were provided by SEPPIC (Castres, France).

Sodium chloride (NaCl) salt crystals were used as model substrate. From a commercial food source, the crystals were sieved between 400 and 630 µm.

The studied formulations were **F0**, **F1**, **F2** and **F3** already described in Part 1 (See *Materials*).

#### 1.2. Methods

##### 1.2.1. Hot-melt coating processing

As already described, HMC trials were performed using lab-scale Ventilus® fluidised bed technology (Romaco© Group, Germany). The sample preparation process for **F0**, **F1**, **F2** and **F3** has already been detailed in Part 1 (See *Methods*).

##### 1.2.2. Solid-state Monitoring

As seen in the literature review, crystallized metastable lipid forms can be converted to stable forms. For freshly melt-coated products, it is important to evaluate a possible evolution of the solid-state of the coating during storage under controlled temperature and humidity conditions. All coated products were then stored for three months in a climatic chamber (Mettler, Germany) under tempering conditions of 25°C/60%RH, based on ICH guidelines (ICH Topic Q 1 A (R2), 2003), and analysed (DSC, XRPD, SEM, release profiles) at pre-determined points during this period.

##### 1.2.3. Coated-product characterisation

###### 1.2.3.1. *Assay of coating contents*

According to the methodology already described in Part 1 (See *Methods*).

###### 1.2.3.2. *Differential scanning calorimetry (DSC)*

According to the methodology already described in Part 1 (See *Methods*).



### 1.2.3.3. X-Ray powder diffraction

Polymorphic identification with X-ray powder diffraction was conducted using Malvern PANalytical Empyrean with reflection applied. The device is equipped with an anticathode tube (radiation Cu K $\alpha$  ( $\lambda = 1.5418 \text{ \AA}$ )) and a detector 1Der.

Diffractograms were collected using X-ray source at 45 keV and 40 mA over a  $2\theta$  range from  $2^\circ$  to  $45^\circ$  recorded at every step of  $0.033^\circ$  (2) with an acquisition time of 160.02 s per step. The powder was filled in a sample holder and rotated at 2 s/revolution. Short d-spacing is calculated using **Equation 46** (Schertel, Salar-Behzadi, Karrer, et al., 2021):

Equation 46 :

$$\text{Short } d - \text{spacing} = \frac{\text{order of reflection } (n) \times \text{wavelength } (\lambda)}{2 \times \sin\theta}$$

Furthermore, quantity of polymorph could be estimated using a suggested expression for complex lipids (Kushwah et al., 2020) using **Equation 47**:

Equation 47 :

$$\beta \text{ contents } (\%) = \frac{\text{peak intensity of about } 19^\circ 2\theta}{(\text{peak intensity of about } 19^\circ 2\theta + \text{peak intensity of about } 21^\circ 2\theta)}$$

### 1.2.3.4. Polarized Light Microscopy

Polarized images were acquired using Zeiss IMAGER.M2m powered by Power Supply 232, equipped with a tube lens 1.25x and external long-distance objectives 5x and 20x for use with a heating plate. In addition, automatic image acquisition was conducted by the camera Aixocam 305 Color and 10x magnification should also be considered.

A polarized angle of  $75^\circ$  was chosen for all observations. Light intensity was manually set at about 80% on the date of observation. Four formulations were prepared on lamellas using thermal conditions mimicking coating operations: holding at  $100^\circ\text{C}$  for 5 min and cooling at  $10^\circ\text{C}/\text{min}$  till  $20^\circ\text{C}$ . These lamellas were then used for the whole stability study. Four to six polarized light micrographs are taken for each time of observation, i.e. freshly after preparation  $t_0$ , 6 weeks and 12 weeks after  $t_0$ .

Furthermore, those images were ultimately utilised in a quantitative interpretation using particle-counting method with Fractal analysis package (version 1.0.3) (Frydendahl, 2023), in order to evaluate density of microstructure with monitoring time.

*Particle-counting fractal dimension,  $D_f$*  (Tang & Marangoni, 2006). The concept of particle-counting fractal dimension  $D_f$  is derived from the mass fractal dimension  $D_m$ , where  $D_m$  relates the number of particles  $N$  to the linear size of the fractal object  $R$  (e.g. crystal clusters, flocs, crystal network), and the linear size of one particle (microstructure element – crystallites for lipids)  $a$  with **Equation 48**.

Equation 48 :

$$N = \left(\frac{R}{a}\right)^{D_m}$$

Assumed the average size of the microstructural element is constant, the previous equation becomes **Equation 49**.

*Equation 49 :*

$$N \propto R^{D_f}$$

where  $D_f$  is the particle-counting fractal dimension. To calculate the value of  $D_f$ , the two-dimensional polarised light micrographs of lipid crystal networks are used. The logarithm of the number of microstructure elements  $\log N$  is plotted against  $\log R$  for varying values of  $R$ . The slope of the linear regression curve is the particle-counting fractal dimension  $D_f$ . Take an example of a square of one unit (1) divided into 16 equal parts so that each of them side have a quarter of the side length of this square  $R = 1/4$ . This means:

$$\frac{1}{16} = \left(\frac{1}{4}\right)^2$$

where the particle-counting fractal dimension  $D_f$  is obviously 2 (Frydendahl, 2023). A fractal analysis is to measure the filled space of lipid crystal networks which is fractal or formed by one building unit aggregated with another throughout multiple length scales. Therefore,  $D_{f,max} = 2$  where all the space of a micrograph is filled with crystals.

The particle counting fractal dimension algorithm should be carried out within the range between 100% and 35% of the original image size (Tang & Marangoni, 2006).

#### 1.2.3.5. *Scanning Electron Microscopy*

According to the methodology already described in Part 1 (See *Methods*).

#### 1.2.3.6. *Measurements of Release Kinetics*

Release in water medium

Release kinetics of coated salt was experimentally performed in water as a simple release medium for evaluation of coating quality subject to aging. The experimental procedure used has already been described in Part 1 (See *Methods*).

Release in lipolysis conditions

For solid lipid-based formulations, release kinetics of active substance is not only as a function of its physicochemical properties and product characteristics (e.g., size, morphology) but also depends on lipid composition. The use of biorelevant media and lipolytic enzyme is necessary for testing polar and digestible formulations. Otherwise, evaluation of release kinetics might not be appropriate.

The experiment was performed, with a pH STAT Titrand 901 (Metrohm, Switzerland) equipped with a dosing unit Dosino 800 (Metrohm, Switzerland) and a thermostat (LUDA, Germany) (See **Figure 2-4**). For each experiment, a sample equivalent to 120 mg NaCl was placed inside a 100-mesh stainless steel sinker basket, which was added into a thermostatic reaction vessel containing 36 mL of fasted-state

simulated intestinal fluid (FaSSIF) (*Ref-* FaSSIF/FeSSIF/FaSSGF (Biorelevant, UK)). In the interests of clarity, detailed composition is given in the **Appendix 01**.

The digestion experiments were initiated by the addition of substrate. The content was kept at 37°C with continuously stirring. The pH-Stat automatic titration unit was used to maintain the pH around  $6.50 \pm 0.05$  by titrating with 0.20 M NaOH. Salt release kinetics was monitored directly and continuously using the conductometer pHenomenal® CO 3100 H (VWR). For each sample, release testing was performed in triplicate ( $n = 3$ ).

Pancreatin extract was prepared by dispersing 1.28 g of porcine pancreatin powder (containing pancreatic lipase and co-lipase) to 5.2 mL tris-maleate buffer pH 6.5. The mixture was vortexed for 15 min at 5°C and underwent centrifugation at 1,600 g (4,000 rpm) at 5°C for 15 min according to the reported method (Arnold et al., 2012). The supernatant was collected into a vial of 10 mL.

Activity of lipases in pancreatin was priorly assayed following a standardised method (Brodkorb et al., 2019). After dilution with FaSSIF, the final medium should have an activity of about 286 TBU/mL state, i.e. a half of the reported fasted state activity (Christophersen, Vaghela, et al., 2014b).

Pancreatin extracts were prepared at the start of a week and stored in freezer for a series of experiments. Before each experiment, a vial of 4 ml frozen pancreatin extract was thawed at room conditions for about 15 min. After adding the extract into the reactor, the whole digestion medium was titrated immediately to the setpoint pH 6.5.

#### 1.2.3.7. Analysis of Release Kinetics

Statistical method and model-independent method are used simultaneously to compare their applicability to a small number of samples. In practice, model-independent method is largely applied to a number of 3 release testing repetitions. Besides, Peppas-Sahlin model is used again to investigate hypothetically any change in salt release mechanisms from coated products with storage time.

##### Statistical method

Release profiles between two time points –  $t_0$  and  $t_{3M}$  – were compared by deploying ANOVA-based methods (Yuksel, 2000) at specific time points 5, 10, 15, 20, 25, 30 minutes of release testing.

##### Model-independent method

Release profiles between two time points –  $t_0$  and  $t_{3M}$  – were compared by applying calculations of similarity ( $f_2$ ) factors:

Equation 50 :

$$f_2 = 50 \times \log \left\{ \left[ 1 + (1/n) \sum_{i=1}^n (R_t - T_t)^2 \right]^{-0.5} \times 100 \right\}$$

Model-dependent method

Peppas-Sahlin model is used to data fit salt release kinetics during lipolysis with the objective to relate change in release kinetics (if any) to destabilisation mechanisms of solid lipid-based formulations (See Part 1 – *Methods*).

## 2. Results and Discussion

### 2.1. Solid-State Monitoring of the Four Lipid-Based Coating Compositions

Samples of products coated with the proposed lipid formulations were evaluated at several time points:

- **F0 and F3** (3 timepoints): after production ( $t_0$ ), after 6 weeks ( $t_1$ ) and after 12 weeks ( $t_2$ ) (stored in freezer before analyses);
- **F1 and F2** (5 timepoints): after production ( $t_0$ ), after 1 week ( $t_1$ ), after 4 weeks ( $t_2$ ), after 8 weeks ( $t_3$ ) and after 12 weeks ( $t_4$ ).

The thermal analyses acquired over the period of stability study are presented in **Figure 3-23**. Due to the difficulty to generate beeswax-based coated products, as an exception, for preparation of DSC samples for the physical stability study, F0 was produced under the form of a cast film as follows: F0 was melt at 80°C, then poured in a small vial, let solidify at ambient conditions and then kept hermetically together with coated samples in the climatic chamber. For preparation of XRPD samples, F0 was solidified in one sample carrier support and this sample was kept together with coated samples in the climatic chamber for all testing time points.

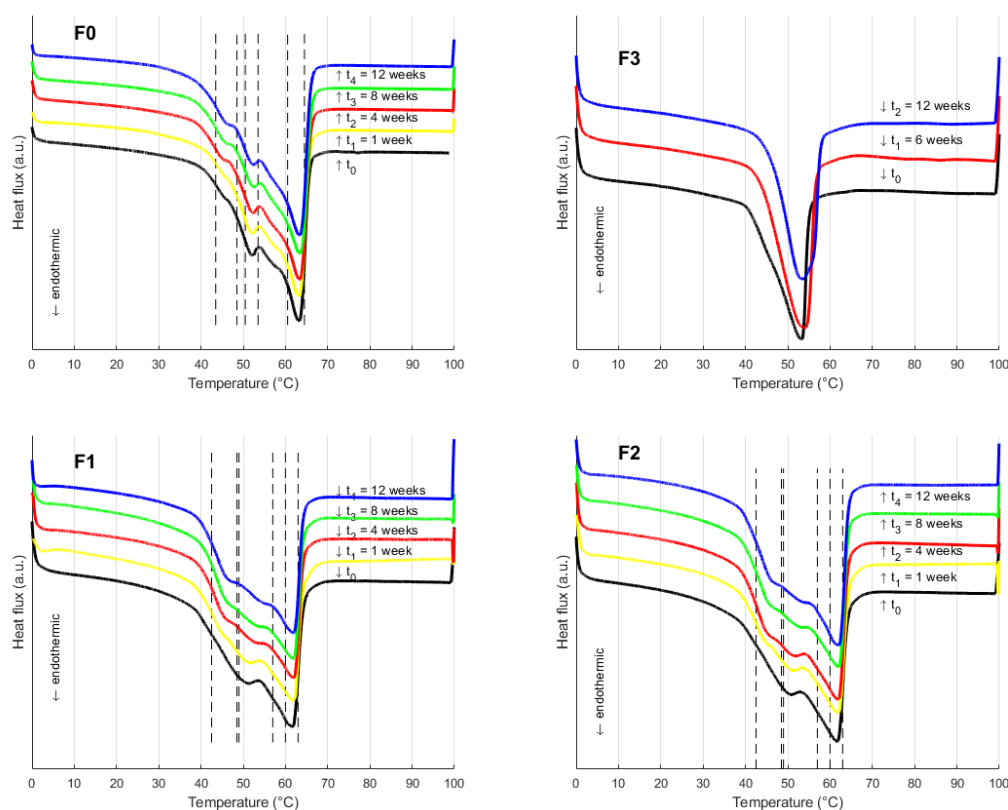


Figure 3-23. Thermal behaviours of 04 formulations **F0**, **F3**, **F1** and **F2** monitored over 12 weeks.

**Figure 3-23** shows that three formulations (**F0**, **F1** and **F2**) exhibit three distinct regions delimited by dashed lines which evolved with observation time. In the case of beeswax (**F0**), onset of melting was detected around 37.35-38.27°C from  $t_0$  till after 12 weeks. The characteristic peaks of low- and high-melting fractions were identified at about 52.39-52.81°C and 63.48-63.73°C, respectively. There was only a shoulder shift starting from  $t_2$  (4 weeks), i.e. 45.43-46.46°C to 46.45-47.59°C. By visual inspection, the form of thermal curves obtained at  $t_2$ ,  $t_3$  and  $t_4$  are comparable to each other and to that of the initially received beeswax.

In the case of SMS (**F3**), melting onset changed from 41.66°C to 45.57°C at the end of stability study, which could hint at growth of crystallites in crystal network (Schertel, Salar-Behzadi, Karrer, et al., 2021; Takeguchi et al., 2020). The melting peak increases slightly from 53.42°C to 53.95°C.

For both **F0** and **F3**, the observations indicate that **F0** should start to transform from  $t_2$ . There is no polymorphic change for **F3** as SMS was reported to be non-polymorphic (Nilsson et al., 2020). This is confirmed with the diffractogram patterns shown in **Figure 3-24**.

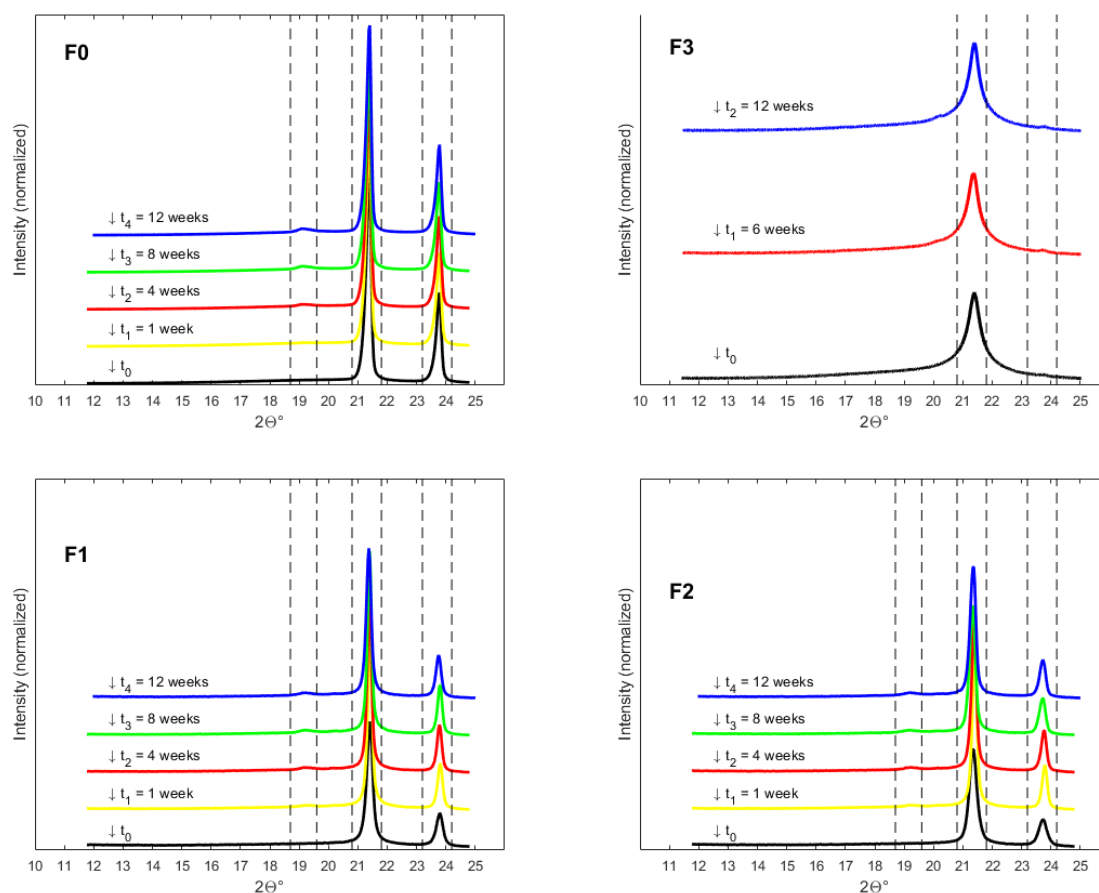


Figure 3-24. Diffractograms obtained for 4 formulations under stability study over 12 weeks.

In fact, as for **F0**, initially, the diffractogram displays two peaks at about  $21.40^\circ$  ( $4.2 \text{ \AA}$ ) and  $23.78^\circ$  ( $3.7 \text{ \AA}$ ), which show probably the occurrence of the orthorhombic structures of hydrocarbons (alkanes) (Bucio et al., 2021; Gaillard et al., 2011). The peak at  $19.12^\circ$  ( $4.6 \text{ \AA}$ ) only appeared from  $t_2$  and this implies development of the stable  $\beta$  polymorph of fatty acids (Attama et al., 2006; Bucio et al., 2021).

The diffractograms of **F3** at 3 time points show a principal peak  $21.38^\circ$  ( $4.2 \text{ \AA}$ ) that indicates the occurrence of hexagonal packing - form  $\alpha$  (Nilsson et al., 2020). **These two types of analyses complement each other with respect to the polymorphic transformation of F0 and in addition DSC pinpoints the growth of crystallite size within the SMS crystal network.**

As for combinations, unlike **F0**, DSC patterns of **F1** and **F2** (as shown in **Figure 3-23**) illustrate 2 shoulders and 1 characteristic peak. The first shoulder developed only after  $t_1$  to  $t_4$  was situated over  $44.69\text{-}45.52^\circ\text{C}$  and  $44.28\text{-}45.52^\circ\text{C}$ , respectively. The second shoulder underwent a larger shift from  $51.45^\circ\text{C}$  to  $55.52^\circ\text{C}$  and from  $50.98^\circ\text{C}$  to  $54.42^\circ\text{C}$ , respectively. The peak of the high-melting fraction appears to be depressed and have a stable value about  $61.86\text{-}62.06^\circ\text{C}$  and  $61.84\text{-}62.23^\circ\text{C}$ , respectively. In addition, the onset of melting was raised to  $37.38\text{-}40.75^\circ\text{C}$  and  $38.41\text{-}39.70^\circ\text{C}$ , respectively. The last two findings indicate the effect of SMS-addition (**F1**), while the presence of a low content of PS80 (**F2**) does not affect many positions of peaks and shoulders.

In addition, considering X-ray diffraction patterns of **F1** and **F2** (shown in **Figure 3-24**), the form  $\beta'$  could be also determined as indicated by two peaks each,  $21.40^\circ$  ( $4.2 \text{ \AA}$ ) and  $23.78^\circ$  ( $3.7 \text{ \AA}$ ),  $21.37^\circ$  ( $4.2 \text{ \AA}$ ) and  $23.74^\circ$  ( $3.7 \text{ \AA}$ ), respectively. The development of the  $\beta$  polymorph was noticed as early as at  $t_1$  with the appearance of the peak  $19.21^\circ$  ( $4.6 \text{ \AA}$ ). It could be hypothesized that initially fraction of fatty acids occurred in  $\alpha$  or liquid and gradually recrystallised into  $\beta$ . In summary, **both DSC and XRPD show the effect of mixing surfactants to BW with respect to melting point depression and induction of polymorphic transformation.**

From a quantitative perspective, polymorphic transformation kinetics could be evaluated considering changes in total melting enthalpies ( $H_m$ ) (Reitz & Kleinebudde, 2007) and estimated  $\beta$  contents ( $\beta\%$ ) (Kushwah et al., 2020) with time as demonstrated in **Figure 3-25**.

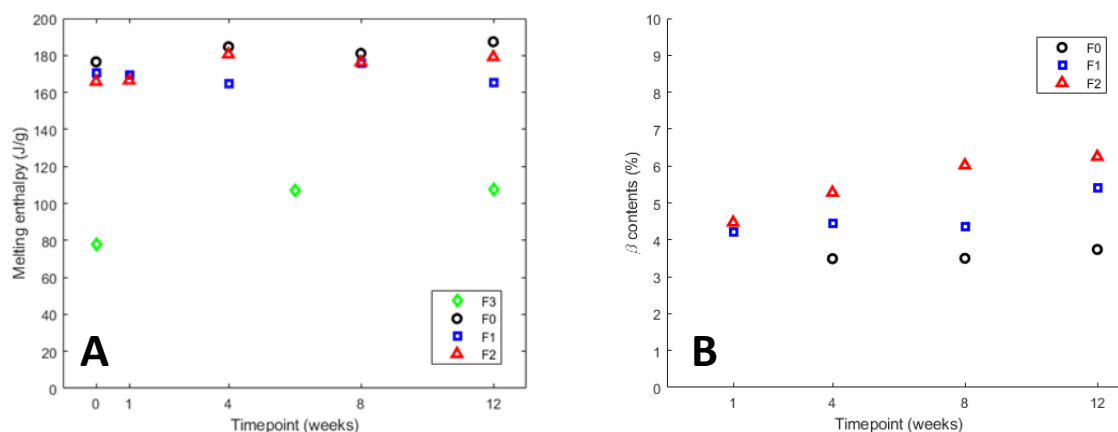


Figure 3-25. Evolution of melting enthalpy of 4 formulations (A) and estimated  $\beta$  contents (%) in samples coated with 3 beeswax-containing formulations (B) during stability study over 12 weeks.

Concerning thermal analyses (**Figure 3-25-A**), melting enthalpies of products coated with **F1**, **F2** and **F3** were adjusted with their coating contents 27.1%, 28.9% and 32.6%, respectively. The values of  $H_m$  of **F0** and **F1** do not vary with time. In fact, by considering the form of thermal curves, note that DSC curves of **F0** show separation of peaks with time while for **F1** the second peak lost from  $t_1$  and two

shoulders were formed after. On the other hand, the values of  $H_m$  of **F2** and **F3** increased and levelled off from 4 weeks. The values of  $H_m$  of **F2** are slightly higher than those of **F1**. However, the shape of DSC curves of **F2** resembles to that of DSC curves of **F1**, correspondingly.

Concerning crystallographic measurements (**Figure 3-25-B**),  $\beta$  contents of **F0**, **F1** and **F2** increased continually during study period with the final  $\beta\%$  at  $t_4$  equal to 0.25%, 1.21% and 1.78%, respectively. This again demonstrates the inductor effect of addition of surfactants in BW (**F0**) and this effect is more remarkable using the ternary combination (**F2**).

To summarise, except **F3**, all the beeswax-containing formulations underwent polymorphic transformation under storage conditions of 25°C/60% RH during three months. An endpoint of this process cannot be concluded from both qualitative and quantitative perspectives. In fact, beeswax is a complex-mixture lipid, its polymorphic transformation can be long. In this case, a prolonged stability study up to 12 months may be necessary to determine this endpoint. For **F3**, despite its being not polymorphic, the fact its melting peak increases with time indicates an increase in its crystal size due to the process of Ostwald ripening (Boistelle, 1988).

## 2.2. Changes in Surface Properties

Lipid blooming is a known physical phenomenon encountered with fat-based products. By nature, it could be ascribed to the physical process of Ostwald ripening which takes place on lipid-based product surface (Delbaere et al., 2016). This was observed on solid lipid-based products after polymorphic transformation and/or after storage in a certain time (Bertoni et al., 2021; D. G. Lopes et al., 2015; D. G. Lopes, Koutsamanis, et al., 2017; Witzleb et al., 2012).

**Figure 3-26** shows SEM images taken on products coated with beeswax alone (**F0**) observed from  $t_0$  till 12 weeks. At  $t_0$ , primary structures (e.g., solidified droplets, fin-like surface) prevailed on the scale of observation at 50  $\mu\text{m}$ . The image on a magnitude of 200  $\mu\text{m}$  shows a highly rough surface not due to fat blooming. After 6 weeks (not shown), secondary structures developed with the appearance of flat needle-like scattered features and agglomerations. It could be observed that certain parts of the surface remain unaffected by blooms. After 12 weeks ( $t_2$ ), those secondary structures (at 50  $\mu\text{m}$ ) include flowers with needle-like petals which can be seen to invade all the observed surfaces.

**Figure 3-27** shows SEM images taken on products coated with sorbitan monostearate (**F3**) alone observed from  $t_0$  till 12 weeks. At  $t_0$ , filaments as main primary structures prevailed on the scale of observation at 200  $\mu\text{m}$ . These primary structures were probably formed due to the occurrence of high viscosity of SMS in the process of deposition on substrate surface and film formation, as presented in the first part.

In comparison with beeswax, both scales show a rather smooth surface. After 6 weeks (not shown), bloom as secondary structures developed rather on the rough part of the surface. After 12 weeks ( $t_2$ ), small and petal-like features (secondary structures) can be observed more clearly but scattered.



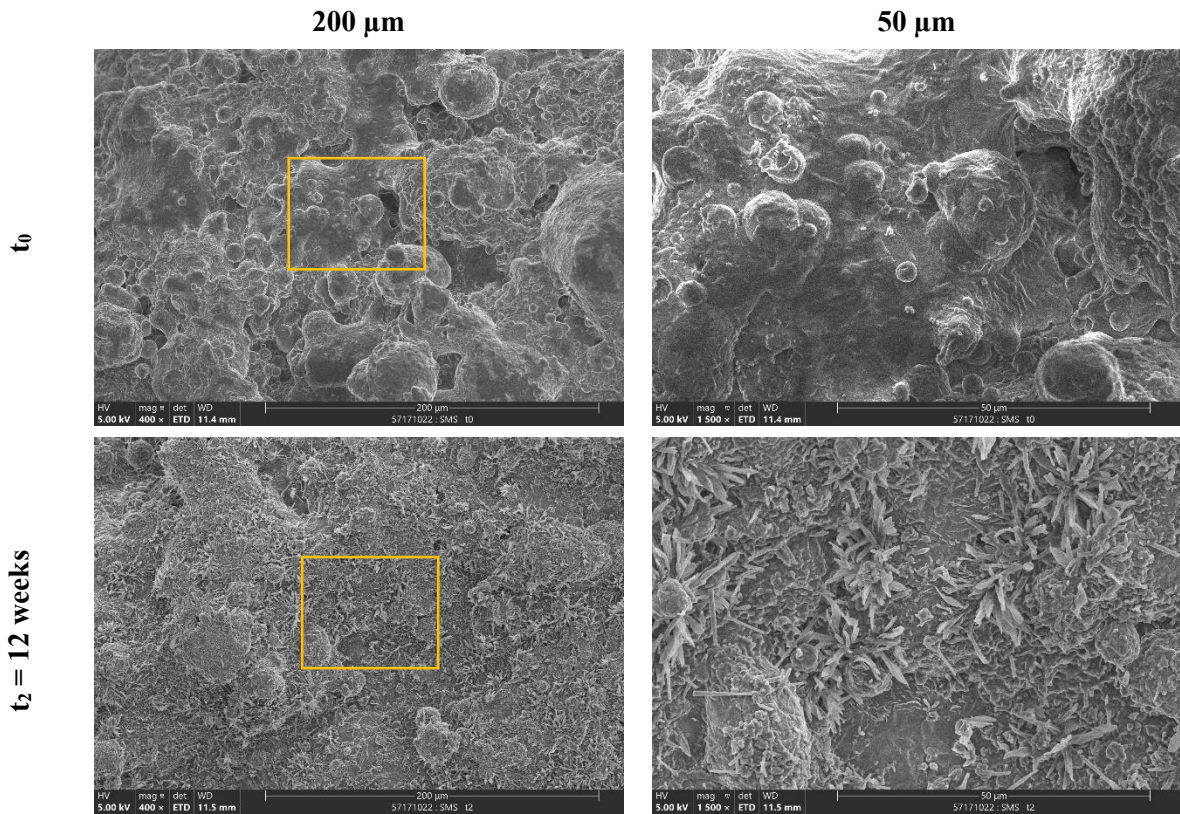


Figure 3-26. SEM micrographs of salt coated with formulation **F0** obtained at 2 timepoints ( $t_0$ ,  $t_2$ ) in stability study (the orange rectangle shows the enlarged image at 50  $\mu\text{m}$  on the left side.)

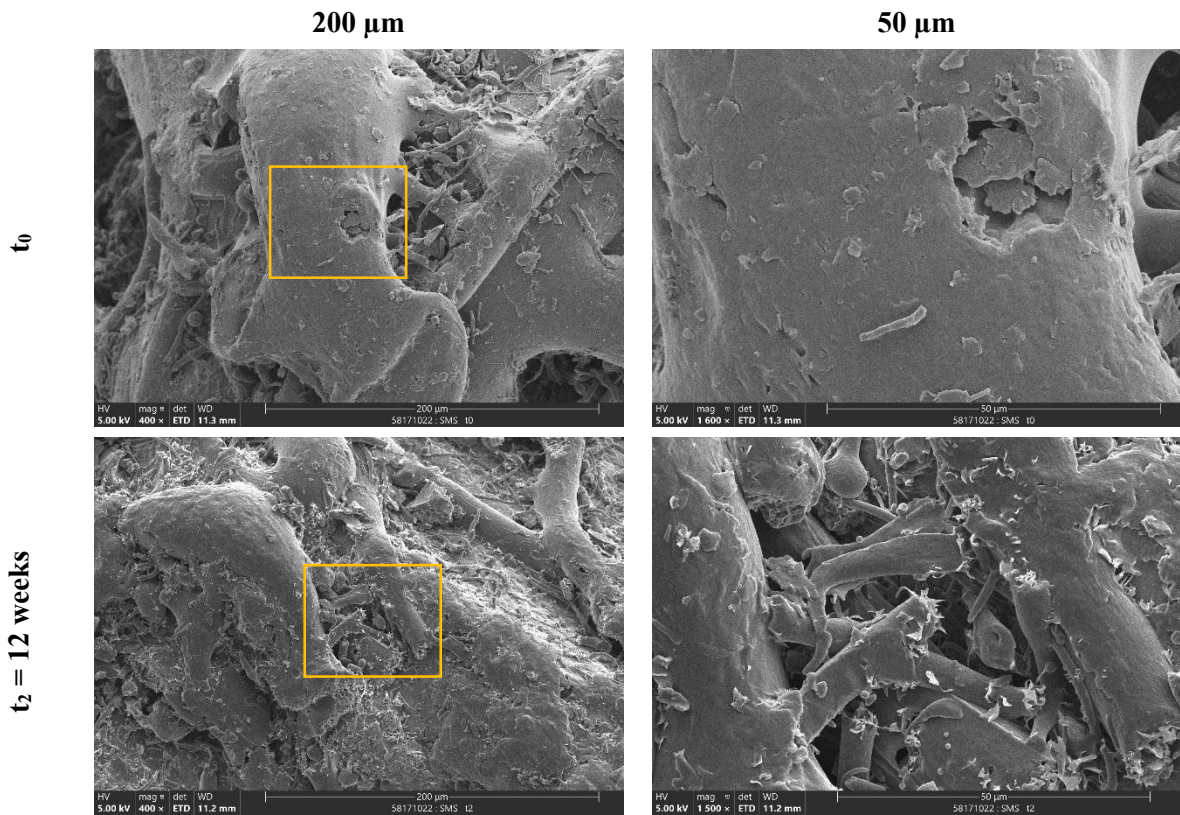


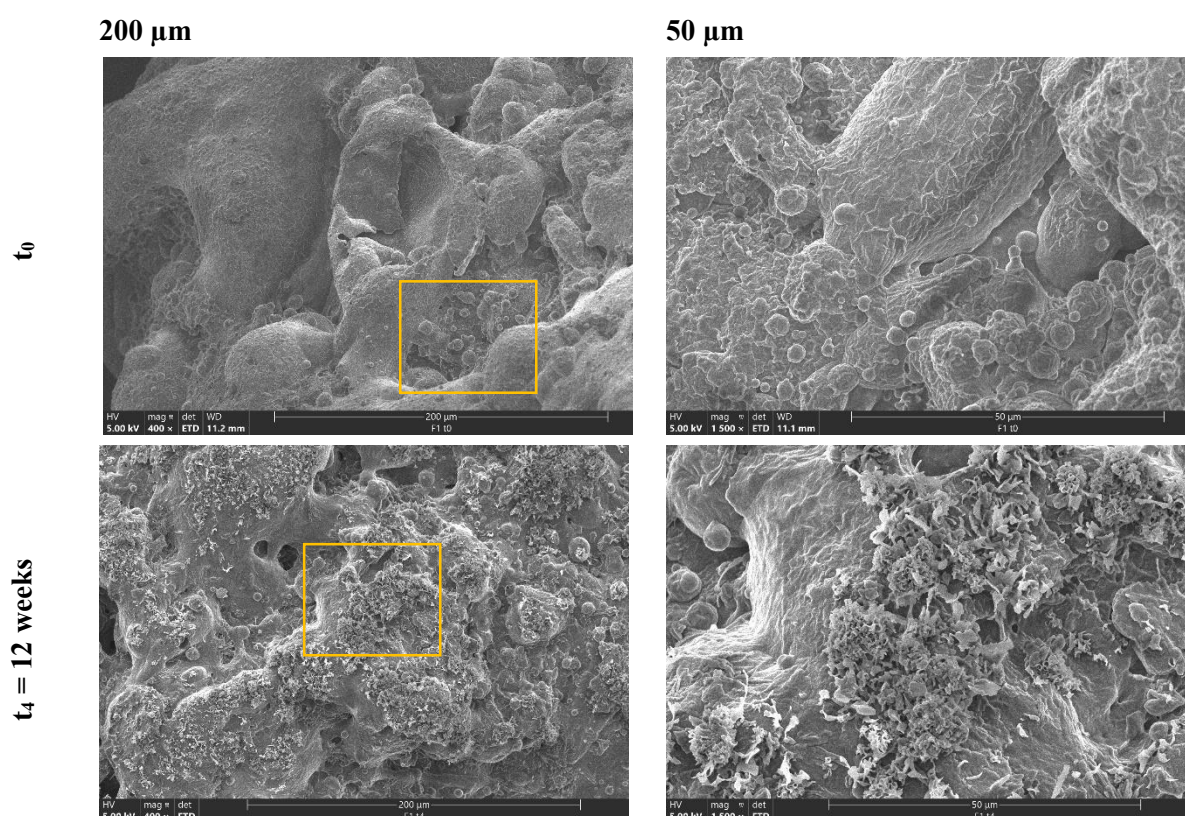
Figure 3-27. SEM micrographs of salt coated with formulation **F3** obtained at 2 timepoints ( $t_0$ ,  $t_2$ ) in a stability study (the orange rectangle shows the enlarged image at 50  $\mu\text{m}$  on the left side.)



**Figure 3-28** shows SEM images taken on products coated with the binary combination (**F1**) observed from  $t_0$  till 12 weeks. At  $t_0$ , the image on a magnitude of 200  $\mu\text{m}$  shows a rough surface and almost no blooming is detected, while primary structures (e.g., solidified droplets, folds) prevailed on the scale of observation at 50  $\mu\text{m}$ . After 1 week (not shown), petal-like features as secondary structures developed scattered all over the surface. After 4 weeks (not shown), those secondary structures concentrated into small agglomerations on the surface. After 8 weeks (not shown), star-like structures appeared and almost the surface was covered with secondary structures. After 12 weeks ( $t_4$ ), larger agglomerations of rose-like features were observed but the surface was still not covered completely.

**Figure 3-29** shows SEM images taken on products coated with the ternary combination (**F2**) observed from  $t_0$  till 12 weeks. At  $t_0$ , as can be detected at the scale of 50  $\mu\text{m}$ , not only primary structures (e.g., solidified droplets) prevailed but also secondary structures (e.g., petal-like flakes) appeared. The image of both scales shows a smooth surface. After 1 week (not shown), petal-like features continued to develop but did not cover all the surface. From 4 weeks (not shown) to 12 weeks ( $t_4$ ), those secondary structures concentrated into small groups and their surface coverage increased but did not attain the maximum.

All the observations above show the development of lipid blooming to different extent and rate. See **Appendix 01** for more observations in this stability monitoring study.



*Figure 3-28. SEM micrographs of salt coated with formulation **F1** obtained at 2 time points ( $t_0$ ,  $t_4$ ), in stability study (the orange rectangle shows the enlarged image at 50  $\mu\text{m}$  on the left side.)*

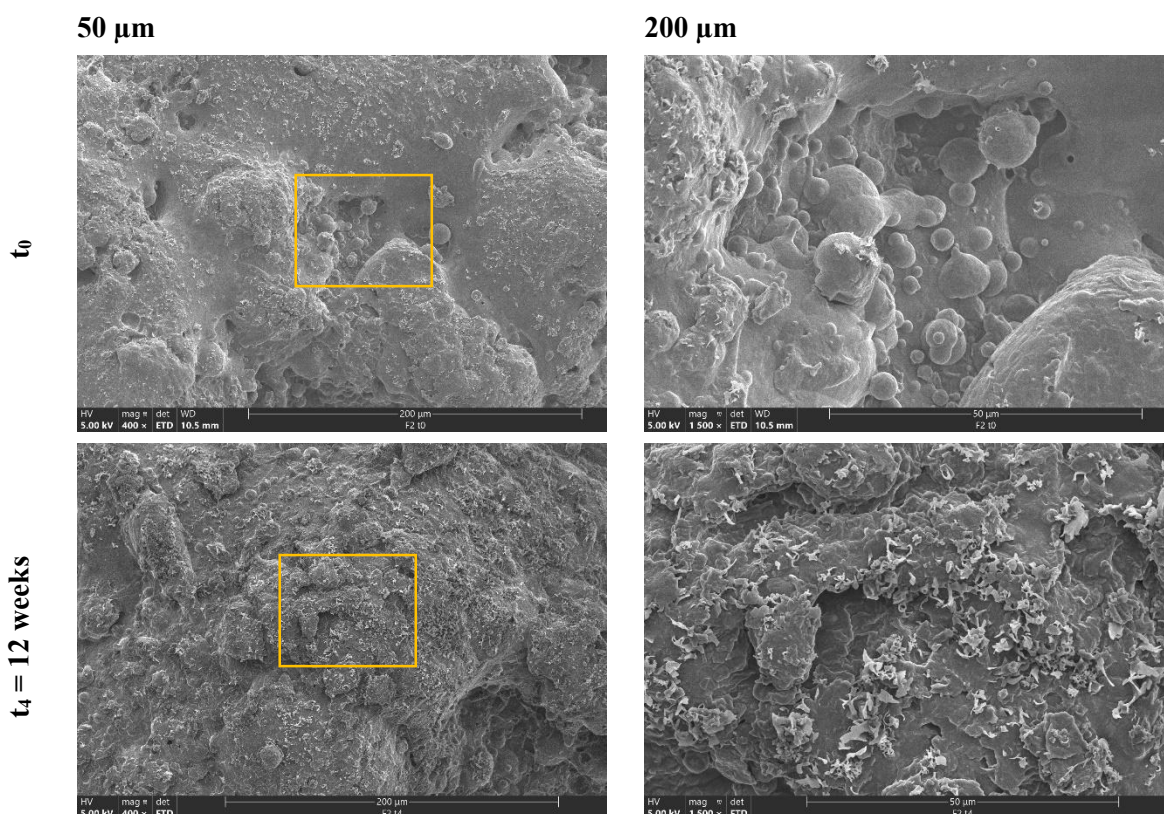


Figure 3-29. SEM micrographs of salt coated with formulation **F2** obtained at 2 timepoints ( $t_0$ ,  $t_4$ ), in stability study (the orange rectangle shows the enlarged image at 50  $\mu\text{m}$  on the left side.)

**To conclude this part**, although **F0** and **F1** coated surfaces remained smooth (without bloom) after production, they underwent rapid bloom formation from 6 and 8 weeks, respectively. After 12 weeks, the surface of products coated with these two formulations displayed bloom agglomerations large in size with specific structures, i.e. needle-like flowers and rose-like agglomerations, respectively.

The surface coated with **F3** was subject to blooming to a small degree. As a reminder, its anti-bloom effect often exploited in the food industry (Cottrell & Peij, 2014; Delbaere et al., 2016).

By considering the binary combination **F1** again, note that this effect of SMS could maintain till 4 weeks after production. The addition of a small content of polysorbate 80 led to remarkable anti-blooming impact. This hydrophilic surfactant is also known for this use (Cottrell & Peij, 2014) and the surface of salt particles coated with **F2** underwent lipid bloom formation to a lesser extent from 1 to 3 months and looks like the surface of **F1** observed at 4 weeks. The combined effect of both added surfactants should be additive.

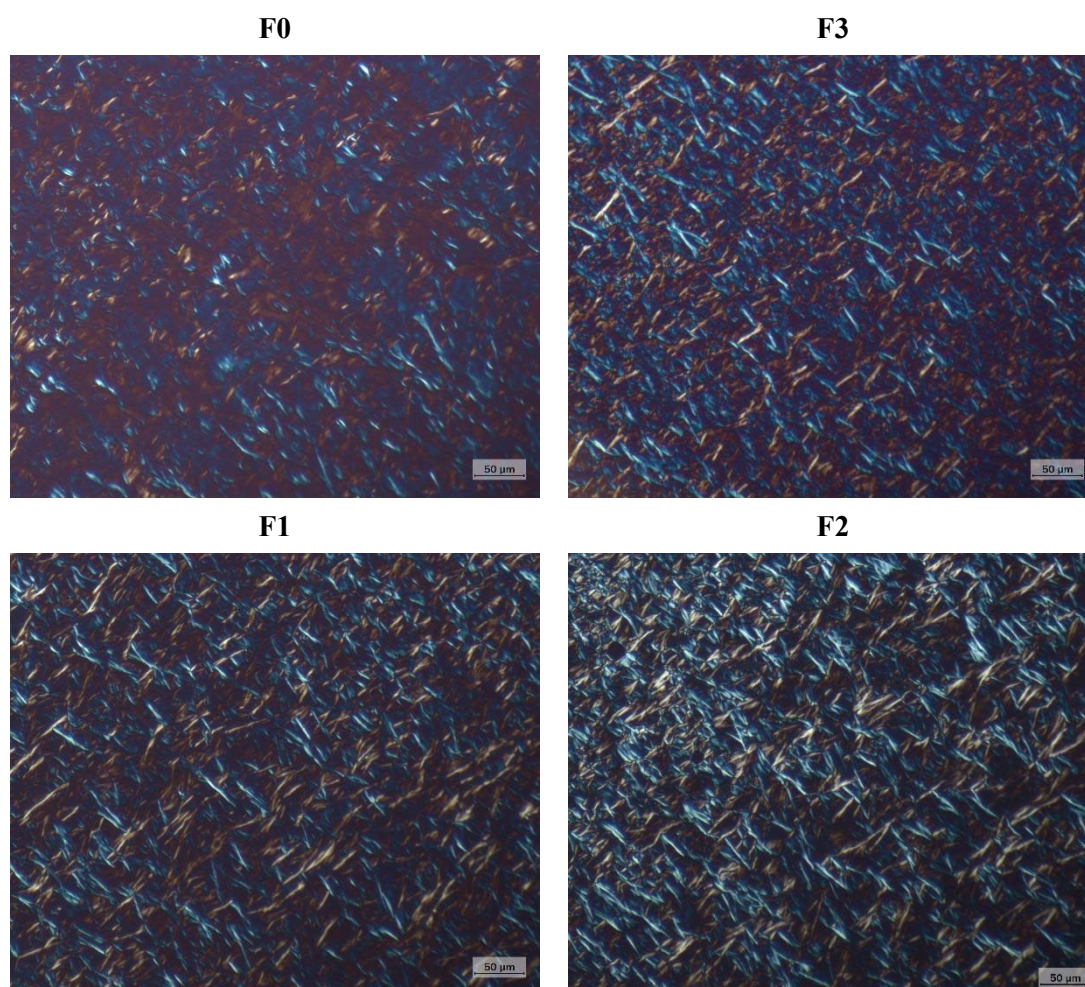
### 2.3. Microstructure Characterisation

Polarised light microscopy was deployed to observe density of lipid crystal network, crystal morphology and redistribution of crystal sizes and phases within. After transformation or direct crystallisation in the stable polymorph, lipid crystal network is still continuously subject to Ostwald ripening in such a way that the total interfacial area between crystals become minimized or one single crystal of the largest initial size exist (Boistelle, 1988).



For pharmaceutical products, this time scale is hardly achieved and therefore Ostwald ripening is always occurring. In fact, the evolution of lipid crystal network with time (e.g. growth of crystallite size, liquid-solid phase separation) was reported to alter release kinetics as reported in the literature (D. G. Lopes, Koutsamanis, et al., 2017; Schertel, Salar-Behzadi, Karrer, et al., 2021; Schertel, Salar-Behzadi, & Zimmer, 2021).

**Figure 3-30** illustrates the crystal network of **F0**, **F1**, **F2** and **F3** observed at  $t_0$ . Visually, one can observe small needle-like crystals in all the four formulations. Besides, crystal density of **F3** is obviously denser than that of **F0**. Crystal density of **F2** is obviously denser than that of **F1**. Note again that **F0** (beeswax) and **F3** (sorbitan monostearate) are natural and semi-synthetic complex-mixture lipids, respectively. Both **F1** and **F2** are combinations of **F0** and **F3**.



*Figure 3-30. Micrographs of formulations F0, F1, F2 and F3 captured at  $t_0$*

In the case of **F0**, at  $t_0$ , at 63.75°C a mixture of small needle-shape crystals with contrasting colours appears in the pure phase (rose background) upon cooling at 5°C/min (See **Appendix 01** for record of dynamic crystallization of **F0**, **F1** and **F2** upon cooling till 40°C at 5°C/min). Down to 40°C, beeswax crystal network became denser with narrowed rose space, which might hint at some domains blind to polarised light. In fact, beeswax was reported to naturally occur in both crystalline and amorphous forms (Gaillard et al., 2011). Crystallisation of **F1** and **F2** start at about 62.5°C and 60°C also with the

appearance of needle-like crystals. This suggests a depression effect on beeswax crystallisation when adding surfactants. Furthermore, the crystal size of **F1** was found to be larger in comparison to those of **F0** and **F2**. In the literature, the crystallisation of beeswax was reported to be random with formation of small needle-like crystals (Y. Chen et al., 2021; L. Wang & Wang, 2007). In the case of **F3**, at  $t_0$ , it crystallises at a lower temperature and the shape of crystals is also needle-like.

The evolution of crystal size distribution of beeswax crystal network was reported to be difficult to notice with time (Attama et al., 2006). Therefore, in this study, **fractal analyses** were applied in an attempt to detect any changes in its crystal network preserved under 25°C/60% RH within 3 months.

All the micrographs were converted into black and white photos and then subjected to fractal analyses using a code MatLab (Frydendahl, 2023). These analyses give the quantitative aspect about the crystal network of **F0**, **F1**, **F2** and **F3**.

**Figure 3-31** shows the mean fractal dimension  $D_{f,mean}$ ,  $D_f$  of 10%, 50% and 90% of counted particles. At  $t_0$ , the order of  $D_{f,mean}$  of 4 formulations is **F0** (1.41) < **F3** (1.47) < **F1** (1.52) < **F2** (1.53). This might reflect increase in the crystal density of crystallised lipids or faster nucleation and more homogeneous crystal growth in the observed area (Y. Chen et al., 2021; Liu et al., 2019; Zhang et al., 2014). In other words, addition of surfactants induced nucleation in comparison with **F0** or **F3** alone and the effect of combination is probably higher than that of SMS alone.

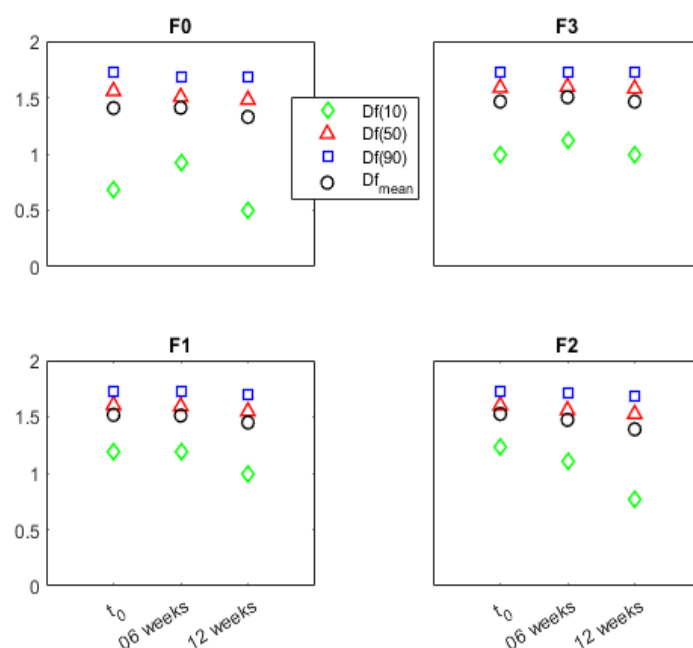


Figure 3-31. Change in fractal dimension of all studied lipidic coating formulations monitored over 12 weeks.

Concerning the stability reflected in the evolution of crystal network density, in the case of **F0**,  $D_{f,mean}$  decreases with time. As a hypothesis, this might imply slow crystallisation of a certain lipid fraction in beeswax, which corroborate the increase of crystallinity with time and the appearance of the peak 19.21° (4.6 Å).

This tendency was also observed with the case of **F1** and **F2** as beeswax is the main constituent, but the mentioned peak appeared earlier. By considering the decrease in  $D_{f,(10)}$ , this suggests that addition of the second hydrophilic additive leads to faster crystallisation in comparison with adding SMS alone. The mechanism could be attributed to the formation of a solidified emulsion. In fact, while the mixture of beeswax and sorbitan monostearate (HLB 4.7) likely occurs in solution, addition of a small fraction of polysorbate 80 should lead to formation of a melt emulsion. This justifies the increase in melt viscosity of **F2** in comparison with **F1**. Droplets can also be observed in the melt of **F2** (See **Appendix 01**). The interface of dispersed phase and dispersing phase could have a templating effect.

Another complementary hypothesis is that initial crystal clusters would be subject to Ostwald ripening. In this case, the initial mixing phases of beeswax, sorbitan monostearate with/without polysorbate tend to separate and those components recrystallised with time. As a consequence, the network tends to become less compact with the decrease of  $D_{f,mean}$  (Omar et al., 2015).

In the case of **F3**, the density of the crystal network seems to stabilise in terms of  $D_{f,(10)}$ ,  $D_{f,(50)}$  and  $D_{f,(90)}$  parameters. This might more or less correlate with an increase in the melting peak of this formulation. With the aim of complementing these findings with optical observations and fractal analyses, measurements of specific surface BET were done (data not shown) and they showed no significant change for all formulations between  $t_0$  and 12 weeks.

## 2.4. Release Kinetics

### 2.4.1. Salt release in water medium

Measurements of salt release kinetics were performed only within 30 minutes as the focus was to interpret evolving quality of coating of the 4 formulations. **Figure 3-32** and **Figure 3-33** shows comparative dissolution profiles of the studied formulations at time 0 (freshly produced), 6 and 12 weeks, respectively for **F0** and **F3** and **F1** and **F2**.

Regarding **F0**-coated products (**Figure 3-32**), at  $t_0$ , the percentage of salt released could reach almost 20% at the end of 30 min. After 12 weeks, the release extent and rate were reduced by about a half. There is no significant difference between salt release profile between 6 and 12 weeks. The deceleration of salt release between  $t_0$  and  $t_1$  could be attributed to solid-state transitions, i.e. polymorphic transformation, lipid blooming and re-distribution of crystal size in the crystal network, as reported elsewhere (D. G. Lopes et al., 2015; D. G. Lopes, Koutsamanis, et al., 2017; Schertel, Salar-Behzadi, Karrer, et al., 2021; Schertel, Salar-Behzadi, & Zimmer, 2021; Witzleb et al., 2012).

With the additive SMS as coating material alone (**Figure 3-32**), at  $t_0$ , 100% salt was released within 15 min. Over observation time, salt release rate decreased and after 12 weeks the release was complete within 30 min. As discussed in the above sections, SMS did not undergo significantly polymorphic transitions, lipid blooming as well as change in crystal network density. However, suspected growth of crystallite size as suggested via DSC could be likely the cause (D. G. Lopes, Koutsamanis, et al., 2017; Schertel, Salar-Behzadi, Karrer, et al., 2021; Schertel, Salar-Behzadi, & Zimmer, 2021).

In the case of F1 formulation (**Figure 3-33**), at  $t_0$ , the final release extent was about 60% whereas this extent was found around 70% after 12 weeks. The similarity factor ( $f_2$ ) calculated between the 12 weeks stability compare to the  $t_0$  as reference is lower than the limit of 50% indicating a difference between the two profiles.

For the reader's information, the fact that  $f_2$  factors were calculated for each timepoints shows that a release testing duration of 30 min is appropriate for evaluation of coating quality subject to aging. Although the conditions for applying calculations of  $f_2$  factors is for at least 12 repetitions, this model-independent method (**Table 3-7**) appears more sensitive than two-sample t-test (**Table 3-8**) for detecting changes in release kinetics. A possible improvement is conduct of a sufficient number of tests in the future as measurements of salt release kinetics are simple. In addition, this could be an alternative to testing lipid erosion in water which has been adopted for testing if solid lipid-based formulations are subject to phase separation (Kreye et al., 2011; D. G. Lopes, Koutsamanis, et al., 2017).

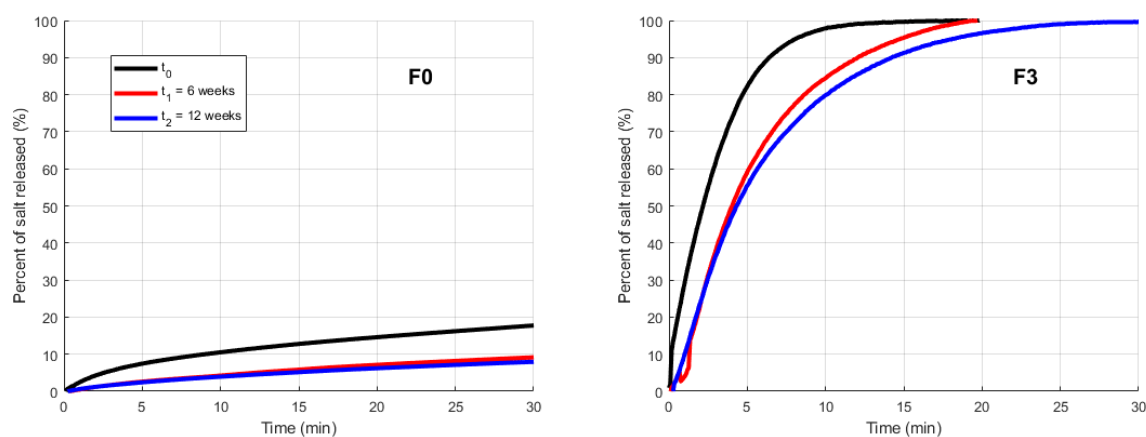


Figure 3-32. Comparative dissolution profile of salt particles coated with 33.8% w/w F0 and 32.6% w/w F3 monitored over 12 weeks.

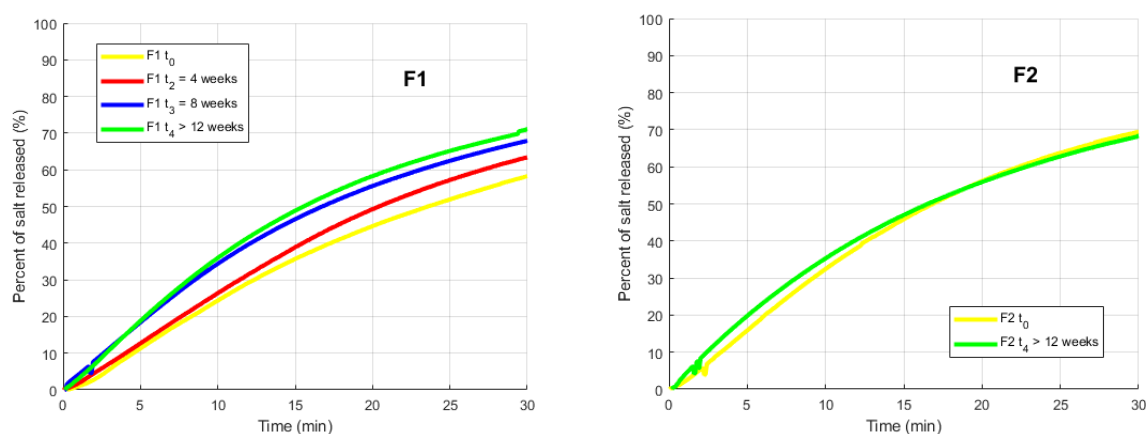


Figure 3-33. Comparative dissolution profile of salt particles coated with 27.1% w/w F1 and 28.9% w/w F2 monitored over 12 weeks.



Table 3-7.  $f_2$  factors calculated for dissolution profile obtained with salt coated with **F1** (left) and **F2** (right)

Timepoints (min)	$t_1$ vs $t_0$	$t_2$ vs $t_0$	$t_3$ vs $t_0$	$t_4$ vs $t_0$	Timepoints (min)	$t_1$ vs $t_0$	$t_2$ vs $t_0$	$t_3$ vs $t_0$	$t_4$ vs $t_0$
5	87,6	90,5	56,8	55,5	5	78,6	65,5	70,1	68,8
10	84,4	87,1	52,5	49,9	10	75,9	69,3	75,0	71,4
15	83,5	81,3	50,8	47,5	15	77,1	73,2	78,7	74,9
20	84,5	75,4	49,9	46,2	20	79,3	75,6	79,5	77,6
25	86,1	71,9	49,7	45,7	25	81,2	76,4	78,9	79,5
30	87,3	70,2	49,8	45,5	30	82,8	76,3	78,3	80,8

$f_2 > 50$  indicates similarity in the salt release profiles between two time points.

Table 3-8. Two-sample t-test  $p$  values calculated for dissolution profile obtained with salt coated with **F1** (left) and **F2** (right)

Timepoints (min)	$t_1$ vs $t_0$	$t_2$ vs $t_0$	$t_3$ vs $t_0$	$t_4$ vs $t_0$	Timepoints (min)	$t_1$ vs $t_0$	$t_2$ vs $t_0$	$t_3$ vs $t_0$	$t_4$ vs $t_0$
5	0.63	0.63	0.06	0.09	5	0.14	0.03	0.04	0.04
10	0.69	0.68	0.11	0.09	10	0.16	0.11	0.27	0.11
15	0.74	0.56	0.13	0.08	15	0.42	0.66	0.86	0.54
20	0.84	0.45	0.15	0.09	20	0.68	0.72	0.39	0.95
25	0.93	0.40	0.17	0.10	25	0.90	0.51	0.27	0.75
30	0.94	0.45	0.21	0.12	30	0.95	0.41	0.25	0.69

$p < 0.05$  indicate difference in the salt release profiles between two time points.

Polymorphic transitions started from 1 week ( $t_1$ ) and lipid blooming developed largely from 4 weeks ( $t_2$ ), which should in theory decelerate salt release kinetics according to established proofs for hot-melt coating formulations (Salar-Behzadi et al., 2019; Witzleb et al., 2012). Against expectations, salt release kinetics was accelerated from  $t_2$  to  $t_3$  but maintained at  $t_4$ . According to the second hypothesis proposed in the discussion on optical microscopic observations, loosening of the crystal network indicated by decrease in  $D_{f,mean}$  could be the cause. This implies that phase separation should take place to a greater extent in this system in comparison with other physical processes. This was observed with other systems polysorbate 65/tripalmitin (D. G. Lopes, Koutsamanis, et al., 2017) and poloxamer/glyceryl behenate (Kushwah et al., 2020). However, these solid-state behaviours could likely have stopped or diminished in extent and rate from  $t_3$  (8 weeks).

For **F2**-coated products, at 30 min the release is about 65% at  $t_0$  and all the release profiles appear to be relatively stable from  $t_0$  till 12 weeks. This is confirmed with the calculations of similarity factor  $f_2$  between  $t_0$  and T 12 weeks is 80.8%. Despite the same physical processes undergone by **F1** and **F2**, the mechanism of release stability might rely on the fact that the presence of 1% w/w polysorbate 80 already facilitated water penetration (as discussed in Part 1) and salt release throughout the membrane. The possible solid-state changes, i.e. polymorphic transformation and Ostwald ripening related physical processes, might compensate each other in addition to increased water permeation imparted to the ternary formulation right at the beginning. In fact, there was a similar case of hot-melt coating formulations. The fact that high concentration of polysorbate 65 (30% w/w) was combined with

tripalmitin rendered the influence of phase separation neglectable in comparison with the combination of tripalmitin/polysorbate 65 90:10 (D. G. Lopes, Koutsamanis, et al., 2017).

**To conclude this part**, stability of formulations made of complex-mixture lipids was expected to be challenging as polymorphic transitions and other solid-state behaviours were shown to be more or less chronological. With the study of four formulations, it showed by serendipity an approach to overcoming potential stability issues of this type of formulations. In effect, all the possible solid-state behaviours (e.g., polymorphism, Ostwald ripening) of the tested systems should be considered with respect to their effects to accelerate or decelerate release kinetics. The solubility of substrate should not be overlooked either. From these elements, one can choose one surfactant or one combination of surfactants to deal with stability challenges associated with complex polymorphism and variable chemical composition of natural lipids such as beeswax.

#### 2.4.2. Release of NaCl during lipolysis

Salt release kinetics was also measured during lipolysis, aiming to investigate the impact of digestion of salt release from lipid-coated particles.

As shown in **Figure 3-34**, from a qualitative perspective, all dissolution of salt release from products coated almost accelerated slightly between  $t_0$  and after 12 weeks, except **F3**. More than 85% salt was released from **F3**-coated products within 15 min while at the end of release testing, the release extent of **F0**-coated products reached about 30-40%. For **F1** and **F2** formulations, the release rate is slow and the final extent is between 70% and 90% respectively.

Interestingly, in comparison with the results in **Figure 3-32** and **Figure 3-33**, there is also no significant difference between release in pure water or in digestion media. This might be due to the choice of NaCl as a highly dissolved substrate. On the other hand, beeswax is composed of non-digestible lipids such as fatty acids, esters of fatty acids and fatty alcohols and hydrocarbons (Buchwald et al., 2008; Gaillard et al., 2011). Inclusion of surfactants aims at imparting an immediate release to coated salt by the mechanism by which lipid coating is subject to digestion in the presence of lipases. However, in this case, coating contents might be the limiting factor for this purpose. Therefore, lower coating contents are required.

From these experiments, salt release data of products coated with all coating formulations were fitted using the Peppas-Sahlin to investigate release mechanisms. Estimated model parameters are given in **Table 3-9**. Overall, there is not much difference in terms of release rate constants, except **F3**, estimated at  $t_0$  and after 12 weeks. However, as indicated by the release exponents “ $m$ ” of each formulations **F0**, **F1**, **F2** and **F3**, release mechanisms appeared to change. For all the formulations, the value of “ $m$ ” tended to increase within three months.

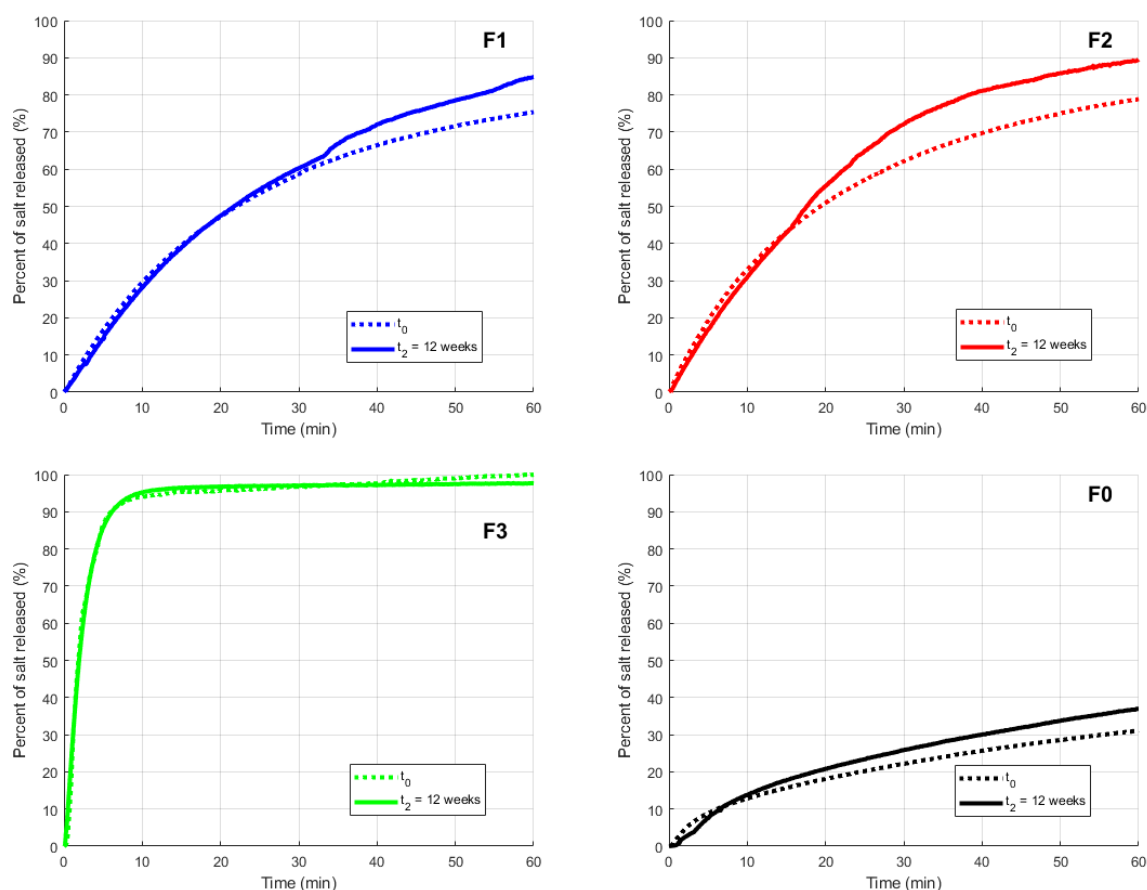


Figure 3-34. Comparative dissolution-digestion profile of salt particles coated with **F0**, **F1**, **F2** and **F3**

Table 3-9. Estimated release parameters for dissolution of salt coated with 04 formulations at  $t_0$  and 12 weeks

Coating content (%w/w) and (Formulation)		Peppas-Sahlin			
		$k_D$ (h <sup>-m</sup> )	$m$	$k_{R-E}$ (h <sup>-m</sup> )	$R^2$
33.8% F0	$t_0$	0.314	0.508	4.992e-10	0.998
	12 weeks	0.378	0.572	3.893e-09	0.991
27.1% F1	$t_0$	1.250	0.815	6.229e-12	0.980
	12 weeks	1.389	0.902	2.167e-12	0.980
28.9% F2	$t_0$	1.347	0.788	5.081e-11	0.997
	12 weeks	1.512	0.888	8.058e-09	0.999
32.6% F3	$t_0$	1.261e-12	0.611	36.397	0.996
	12 weeks	8.288e-08	0.950	479.096	0.991

The shift, i.e. from Fickian to non-Fickian transport (**F0**), and towards Case II (**F1**, **F2** and **F3**) – indicates an increase in swelling of lipid-based coatings which allows for more water penetration (See again the description of these release mechanisms in **Part 1**). This agrees with the hypothesis that a phase separation should likely happen. In fact, other solid-state behaviours like polymorphic transitions and lipid blooming should result in denser packing and water-repellent surface, respectively, which should decelerate release kinetics. In the case of **F3**, the fact that erosion of the coating membrane become important might correlate with the suspected growth of crystallite.

**To conclude this part**, the application of release testing in biorelevant and lipolytic media was not able to accelerate salt release as expected. However, note that salt is a very soluble drug in water and release testing was performed in sink conditions. Non-sink conditions can make a difference but these should be tested with poorly water-soluble drugs.

### 3. Conclusions

The research work was focused on the effect of surfactants added to beeswax-based formulations on hot-melt coating process manufacturability (**Part 1**) and product stability (**Part 2**).

The results presented in both parts intended to demonstrate firstly a new experimental approach which integrates considerations of formulation properties and process parameters and to reveal secondly a new strategy to formulate stable solid lipid-based formulations with a complex-mixture lipid such as beeswax.

In this part, the effect of surfactant addition was demonstrated to accelerate crystallisation, polymorphic transformation and to inhibit lipid blooming on the surface. While solid-state behaviours (e.g., polymorphism, Ostwald ripening) evolved, the system constituted by beeswax combined with both lipophilic and hydrophilic surfactants (**F2**) yielded a relatively stable release kinetics in both simple and biologically simulated dissolution media over the whole period of stability study.

This finding suggests that for the case of complex-mixture lipids, drug release instability from solid lipid-based formulations should be treated with considerations of all the potential solid-state behaviours of the tested systems and combination of surfactants can help overcome stability challenges. In fact, possible physical changes observed in the stability study might compensate for each other and don't significantly affect release kinetics of NaCl. This is remarkably noticed with the ternary combination.

Last but not least, the use of NaCl, as model drug, proved its usefulness once more as measurements of its release kinetics in water can serve as a stability-indicating test for any phase separation in the lipid coatings. This is complementary to the other four characterisation techniques. As perspectives, the mechanism(s) to stabilise combinations of beeswax and additives with diverse lipophilicity / hydrophilicity warrants further studies.

## Chapter 4.

# MELT CRYSTALLISATION AND HOT-MELT COATING OF TRISTEARIN-BASED FORMULATIONS: FROM LIPID FUNDAMENTALS TO APPLICATIONS

---

### General Introduction

Lipid crystallization and transformation behaviours are in general the fundamental principles of melt processing. In effect, lipid crystallisation kinetics determines the formation of lipid crystal network and eventually functionalities (e.g., release kinetics) and stability of solid lipid-based formulated products (Bayés-García et al., 2015).

This fundamental knowledge of crystallization, including nucleation and crystal growth, has not been fully acquired, although successful treatments subject to set crystallization temperature, cooling rate and presence of additive(s) have been introduced.

To investigate crystallisation behaviours and polymorphism of lipids, thermal analyses often represent key characterisation to probe thermal properties (e.g. occurrence of polymorphs, melting points, solidification profile) but provide limited screening throughput.

On the other hand, knowledge of nucleation and crystal is not so interesting as its applications. In fact, some successful case studies of melt processing underlaid by this knowledge have reveal its importance. There have been scarcely established proofs of multifunctionality of lipids with respect to their processing possibilities.

For several melt technologies (for instance, extrusion, high-shear granulation, spray-chilling), the same target temperature could be defined with the objective of generating the targeted polymorph but the strategy to specify process parameters (normally mechanical) is distinct due to characteristics of each transformation mode (e.g. heat and mass transfer, use of shear or pressure, residence time). **In this context, the treatment of material- and process-specific aspects constitute the two studies of this chapter.**

**Tristearin (SSS)** was used as a model material for these studies. Tristearin has been a triglyceride base widely used in formulation of conventional solid dosage forms using established melt-based processing technologies (e.g., spray-congealing, extrusion, hot-melt coating) (Bertoni, Dolci, et al., 2018; Bertoni et al., 2020, 2021; D. G. Lopes et al., 2015; Pluntze et al., 2023; Traub-Hoffmann et al., 2020; Windbergs et al., 2009e).

Parallely, tristearin has been a popular lipid model in food research (J. S. Aronhime et al., 1987, 1988; Garti et al., 1982; MacNaughtan et al., 2006; Oh et al., 2002) as it would be more straightforward to investigate its polymorphism and crystallisation behaviours than a complex-mixture lipid (e.g.

beeswax). Therefore, it will be reasonable to evaluate results of method development against documented evidences.

On the other hand, a single component is hardly an interesting formulation, and multi-component blends could give rise to new functionalities. That is the reason why tristearin has been oftentimes mixed with another lipid or formulated with an additive. However, despite the interest, choice of one additive can still be limiting to stabilising or customising release properties (Bertoni et al., 2021; Windbergs et al., 2009d).

In our study, to widen the scope of applications of those additives, tristearin was mixed to one, two or three additives. Besides the impact of the composition of the tristearin-based formulations on stability and release profile, another aspect often neglected in the research work was studied here, which is the **impact of additives on the formulation processability (e.g. solidification)**.

As additives, hydrophilic and lipophilic surfactants (**polysorbate 20 –PS20, sorbitan monolaurate – SML and sorbitan monostearate – SMS**, respectively) and a mineral (**talc - T**) were tested using different mass ratios with tristearin.

In development of lipid-based formulations, use of surfactants retains much attraction as these components can play a role of polymorphic controllers and modifiers of release profile – functional impact. However, their impact on processing performance – operational impact – has not been well studied even for combination-based lipid systems.

**The first part of this chapter** concerns the development of a fast method to screen combination-based lipid systems considering their crystallisation behaviours. **Crystal16®** was the device fitted for this purpose. For this screening, two types of research were performed:

- (1) **Non-isothermal crystallisation**: The first objective was to measure crystallisation point of the most stable polymorph of tristearin using different additives and diverse combinations;
- (2) **Isothermal crystallisation**. The second objective was to evaluate the effect of additives and diverse combinations on nucleation behaviours (e.g. induction time, nucleation randomness).

Other techniques (differential scanning calorimetry, Raman spectroscopy and polarised light microscopy) were deployed as complementary characterisation to identify crystallised polymorphs and crystallisation mechanisms (including crystal growth) in similar conditions.

**In the second part of this chapter**, two formulations were chosen from the screening study for an exploratory case study with hot-melt coating. They contain tristearin and binary additive combination at mass ratios 97:3 and 91:9. Talc was not used in this study.

The principal objective was to test their multifunctionality and adaptability to different thermal operational conditions. In fact, in hot-melt coating operations, **traditionally**, the thermal setpoint in fluidized bed is regulated at a value inferior to the melting point of metastable forms ( $T_{m,metastable\ form(s)}$ ) to avoid agglomeration. As for **non-traditional** HMC approach, operating thermal conditions were set above that  $T_{m,metastable\ form(s)}$ , aiming direct crystallization of the most stable polymorph.



NaCl crystals are still used as a model substrate and the multiple-sampling approach (developed in Chapter 3) was applied to evaluate the operational and functional impact using known formulation properties and process parameters.

Raman spectroscopy, atomic force microscopy, observations of film formation and solidification time were employed for monitoring polymorphic conversion, defining process variables, and predicting coating quality, respectively. Also, long-term stability of products generated via two HMC approaches was investigated using X-ray powder diffraction, polarised light microscopy, and release testing.

The chapter ends with a general summary of the main conclusions drawn from these studies with **tristearin, surfactants and talc**.

# Part 1

## A New Fast Lipid-Additive Formulation Screening Approach used in Formulating Solid Lipids for Melt-Processing

---

### 1. Materials and Methods

#### 1.1. Materials

##### 1.1.1. Strategy for choice of lipids for this study

The additives used can be divided into three categories:

- derivatives of fatty acids and polymers (e.g. polysorbates);
- derivatives of only fatty acids (sorbitan esters of fatty acids);
- inorganic substances (e.g. talc).

In this study tristearin was formulated with a binary additive combination between a polysorbate (i) and a sorbitan (ii) at different ratios. Technically, the choice of liquid surfactants is based on their effect to accelerate the polymorphic transformation process of tristearin in the solid lipidic formulations (Garti & Yano, 2001). Furthermore, this combination permits tuning release profile of an active substance from the coated products by varying the combination ratios between the two surfactants.

Normally, an additive might have four possible effects: (i) both nucleation and crystal growth promoted, (ii) nucleation promoted and crystal growth retarded, (iii) nucleation retarded and crystal growth promoted and (iv) both nucleation and crystal growth retarded (K. W. Smith & Sato, 2018). Talc as third additive was parallelly evaluated by considering its known effect to enhance crystallisation rate (both nucleation and crystal growth) (Yoshikawa, 2016; Yoshikawa et al., 2014, 2015).

Ultimately, the objective of this study was to investigate the effect of binary additive combination  $\pm$  talc on crystallisation properties (nucleation and crystal growth) which is linked to processability of lipid-based formulations.

##### 1.1.2. Description of used materials

Dynasan<sup>®</sup> 118 (tristearin, SSS) and Luzenac PHARMA M (talc, T) were kindly donated by IOI Oleo GmbH (Witten, Germany) and Azelis (Courbevoie, France).

Montanox<sup>™</sup> 20 Premium Pharma (polysorbate 20, PS20), Montane<sup>™</sup> 20 Premium Pharma (sorbitan monolaurate, SML) and Montane<sup>™</sup> 60 Premium Pharma (sorbitan monostearate, SMS) were provided by SEPPIC (Castres, France).

Those materials were composed into coded formulations subject to screening as shown in **Table 4-1**.

Table 4-1. Lipid-based coating formulations composition

Formulation	Excipients (% w/w)				Formulation	Excipients (% w/w)			
	SSS	PS20	SML	T		SSS	PS20	SML	T
<b>Control</b>					<b>HBAC4-3</b>	97	2.25	0.75	-
<b>SSS</b>	100	-	-	-	<b>HBAC4-3-T 0.1%*</b>	97	2.25	0.75	0.1
<b>SSS-T 0.1%</b>	99.9	-	-	0.1	<b>HBAC4-3-T 0.5%*</b>	97	2.25	0.75	0.5
<b>SSS-T 0.5%</b>	99.5	-	-	0.5	<b>HBAC4-3-T*</b>	97	2.25	0.75	1.0
<b>SSS-T</b>	99.0	-	-	1.0	<b>HBAC4-9</b>	91	6.75	2.25	-
<b>PS20-3</b>	97	3	-	-	<b>HBAC4-9-T 0.1%*</b>	91	6.75	2.25	0.1
<b>PS20-3-T 0.1%*</b>	97	3	-	0.1	<b>HBAC4-9-T 0.5%*</b>	91	6.75	2.25	0.5
<b>PS20-3-T 0.5%*</b>	97	3	-	0.5	<b>HBAC4-9-T*</b>	91	6.75	2.25	1.0
<b>PS20-3-T*</b>	97	3	-	1.0	<b>NBAC4-3</b>	97	1.50	1.50	-
<b>PS20-9</b>	91	9	-	-	<b>NBAC4-3-T 0.1%*</b>	97	1.50	1.50	0.1
<b>PS20-9-T 0.1%*</b>	91	9	-	0.1	<b>NBAC4-3-T 0.5%*</b>	97	1.50	1.50	0.5
<b>PS20-9-T 0.5%*</b>	91	9	-	0.5	<b>NBAC4-3-T*</b>	97	1.50	1.50	1.0
<b>PS20-9-T*</b>	91	9	-	1.0	<b>NBAC4-9</b>	91	4.50	4.50	-
<b>SML-3</b>	97	-	3	-	<b>NBAC4-9-T 0.1%*</b>	91	4.50	4.50	0.1
<b>SML-3-T 0.1%*</b>	97	-	3	0.1	<b>NBAC4-9-T 0.5%*</b>	91	4.50	4.50	0.5
<b>SML-3-T 0.5%*</b>	97	-	3	0.5	<b>NBAC4-9-T*</b>	91	4.50	4.50	1.0
<b>SML-3-T*</b>	97	-	3	1.0	<b>LBAC4-3</b>	97	0.75	2.25	-
<b>SML-9</b>	91	-	9	-	<b>LBAC4-3-T 0.1%*</b>	97	0.75	2.25	0.1
<b>SML-9-T 0.1%*</b>	91	-	9	0.1	<b>LBAC4-3-T 0.5%*</b>	97	0.75	2.25	0.5
<b>SML-9-T 0.5%*</b>	91	-	9	0.5	<b>LBAC4-3-T*</b>	97	0.75	2.25	1.0
<b>SML-9-T*</b>	91	-	9	1.0	<b>LBAC4-9</b>	91	2.25	6.75	-
<i>* indicates 1%w/w talc to the total 99%w/w of other components</i>					<b>LBAC4-9-T 0.1%*</b>	91	2.25	6.75	0.1
					<b>LBAC4-9-T 0.5%*</b>	91	2.25	6.75	0.5
					<b>LBAC4-9-T*</b>	91	2.25	6.75	1.0
					<b>SSS</b>			<b>SMS</b>	
					<b>SSS-SMS-3</b>	97	-	3	-
					<b>SSS-SMS-9</b>	91	-	9	-
<i>* indicates 1%w/w talc to the total 99%w/w of other components</i>									

## 1.2. Methods

### 1.2.1. Measurements of Melting and Crystallisation Points

Measurements of melting and crystallisation points were performed using a Crystall16® parallel crystallizer (Technobis Crystallization Systems) which combines automation with integrated turbidity measurements. According to the principles of turbidimetry, the characterisation consists of measuring disappearance or appearance of melting or crystallising solids in molten media, respectively.

Crystal 16® is a device used to monitor crystallisation at the scale of mL. This device is capable of (1) controlling the temperature of vials of 1.5 mL, (2) probing dissolution/precipitation during crystallisation via turbidity measurements by laser (detection of crystal appearance), and (3) having a small well-stirred system in each vial.

Crystal 16® has four blocks (and 4 vials/block) which are equipped with a temperature controller. When using the same lipid in the four blocks, we wanted to test the effect of additive in 16 samples at the same

time as follows: by adding in each block (4 vials) a different amount of the same additive or combination and specifying one identical temperature programme for four blocks.

About 700 mg of each formulation listed above was weighed and introduced in a 1.5 mL vial of specific design. This quantity was found sufficient to cover the light transmission pathway.

After preliminary trials, bottom stirring mode was chosen and a stirring rate was set at 200 rpm, which assures homogeneous mixing of molten media. A typical run programme is illustrated in **Figure 4-1**.

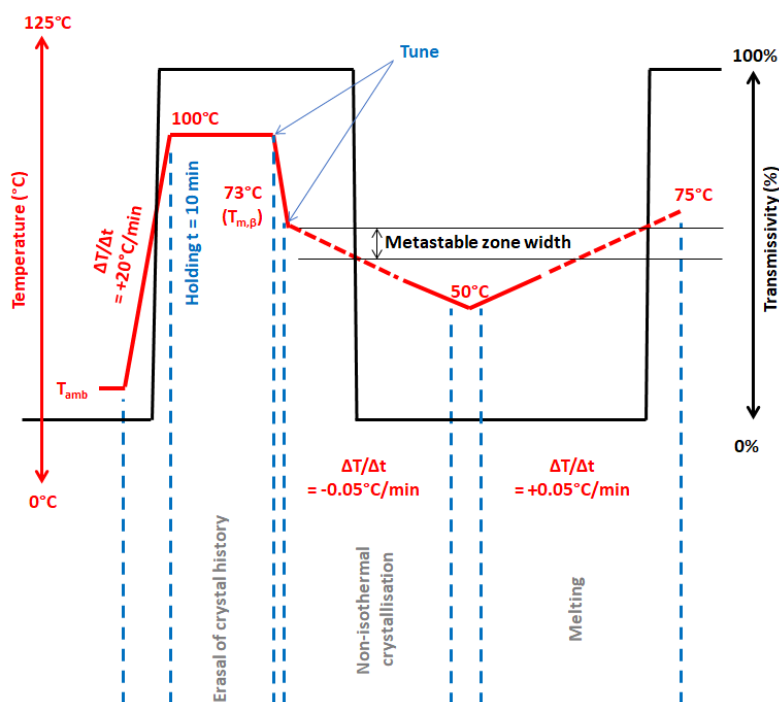


Figure 4-1. Thermal programme set for non-isothermal experiments in Crystal16®

Firstly, it starts when heating is launched till  $100^\circ\text{C}$  and held for 10 min at this point to erase all the crystal history. Then the first step of “tuning” will be performed in order to reset the transmissibility through one block (4 vials) to 100% as there might be a difference due to mixing heterogeneity. Cooling is performed at  $20^\circ\text{C}/\text{min}$  from  $100^\circ\text{C}$  till  $73^\circ\text{C} - T_{m,\beta}$  of tristearin. At this point, the second step of “tuning” is performed to reset all the transmissibility values to zero as they might diminish with temperature decrease. From  $73^\circ\text{C}$  to  $50^\circ\text{C}$  a cooling rate of  $0.05^\circ\text{C}/\text{min}$  is defined as the condition for non-isothermal crystallisation. When the programme temperature reaches  $55^\circ\text{C}$ , the system will then be heated again up to  $75^\circ\text{C}$  at the same velocity. **The objective of this last step is to measure melting point** of the system in the vial.

For information, at  $55^\circ\text{C}$ , all the tristearin-based systems should be solidified. Onset melting point or crystallisation point are identified as the temperature at which the transmissivity start to increase or decrease significantly, accordingly. As shown in **Figure 4-1**, by definition, the difference of melting point and crystallisation point is the width of metastable zone (MSZW) (Kulkarni et al., 2013), which will be considered as proof of thermal feasibility of tristearin under the effect of different additive-combinations. In addition, non-isothermal experiments were also conducted with a cooling rate at -

5°C/min and -10°C/min, which might represent the cooling capacity of certain melt-processing technologies. The measurements for each formulation were performed in triplicate (n = 3).

### 1.2.2. Measurements of Induction Time

Measurements of **induction time** were also performed with Crystal16®. The same settings (sample quantity, stirring rate) were applied except that the isothermal period was defined at 1h. The similarity in sample quantity was assured in order to eliminate the effect of volume on nucleation (Adachi et al., 2014). A typical run programme is illustrated in **Figure 4-2**.

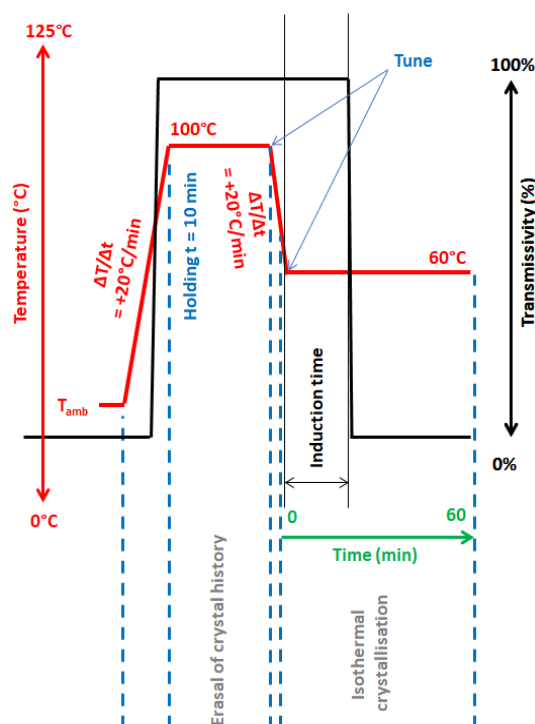


Figure 4-2. Thermal programme set for isothermal experiments in Crystal16®

Firstly, it starts when heating is launched till 100°C and held for 10 min at this point to erase all the crystal history. Then the first step of “tuning” is performed in order to reset the transmissibility through one block (4 vials) to 100% as there might be a difference due to mixing heterogeneity.

Cooling is performed at 20°C/min (maximum rate of the apparatus) from 100°C till 60°C. At this point, the second step is performed to reset all the transmissibility values to zero as they might diminish with temperature decrease. This point (60°C) is defined as the condition for isothermal crystallisation. All the lipid systems are held at this temperature for 1h. This period is reasonable to assure that all the tristearin-based formulations should crystallise.

By definition, induction time is the time difference between the moment where the temperature reaches target isothermal condition (60°C) and the moment where the transmissivity changes even by 1% (Kulkarni et al., 2013). This physical quantity will be used to evaluate **the effect of different additive-combinations on tristearin crystallisation** behaviours. The temperature 60°C was chosen as isothermal condition to crystallise directly  $\beta$  polymorph as this temperature has been used in different

researches with melt-processing technologies (Bertoni et al., 2021; Lopes et al., 2015; Windbergs et al., 2009d). The measurements for each formulation were performed 40 times ( $n = 40$ ).

Each set of induction times obtained for each formulation was fitted to the cumulative Gaussian-Laplace (normal) distribution,  $F(x)$ , in order to estimate parameters of the probability density function,  $P(x)$ , (Nooraiepour et al., 2021) using **Equation 51** and **Equation 52**:

*Equation 51 :*

$$P(x) = \frac{1}{\sigma\sqrt{2\pi}} e^{-\frac{(x-\mu)^2}{2\sigma^2}}$$
$$0 \leq x \leq 2\mu$$

*Equation 52 :*

$$F'(x) = P(x)$$

where  $x$  is the measured induction time (s),  $\mu$  the mean induction time (s) and  $\sigma$  the standard deviation (s) to be found.

### 1.2.3. Polymorph Identification by Raman Spectroscopy

Samples in vials used in the measurements of melting and crystallisation point were observed using RAMAN-AFM Alpha 300 AR (WITec, Ulm, Germany) based on a microscope with a magnification of x50 and a laser of 785 nm wavelength.

Other parameters include a resolution of  $3 \text{ cm}^{-1}$  and an integration time of 1.0 s defined for combinations of tristearin and additives. Measurements were carried out at the middle and bottom of each vial. Raw data was treated using an in-house code MatLab for visualising Raman spectra. Analyses with Raman spectroscopy was **performed with the objective of identifying polymorphs crystallised at the end of non-isothermal experiments.**

### 1.2.4. Polymorph Identification by Differential Scanning Material (DSC)

Isothermal and non-isothermal crystallisation experiments were also performed using DSC Q200 (TA Instrument, USA). The objective was to identify polymorphs occurring under thermal conditions like those used with Crystal16® and to confirm the effect of additives on induction time and crystallisation points, respectively.

All the analyses are performed in non-hermetic aluminium pans under nitrogen purge at  $50 \text{ mL}\cdot\text{min}^{-1}$ . The thermal programme is described in **Figure 4-3**.



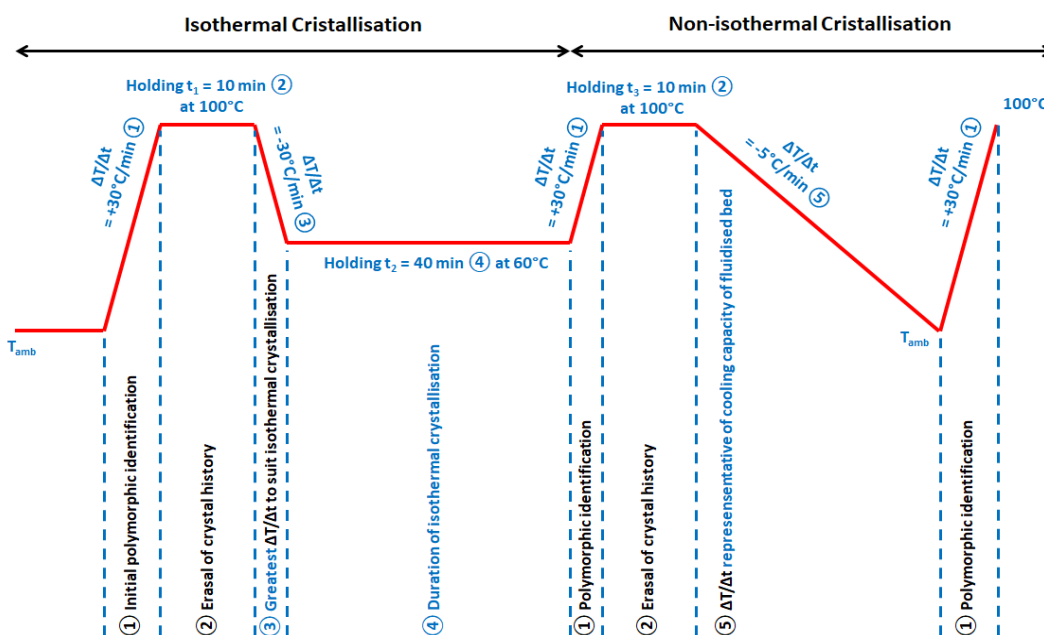


Figure 4-3. Thermal programme used in DSC analyses for isothermal and non-isothermal crystallisation

Heating rate of 30°C/min was used to identify different occurring polymorphs (if it is the case) by preventing solid-solid transformation (Takeguchi et al., 2020). A cooling rate of 30°C/min and an isothermal period of 40 min were set according to the results reported by a research group (Bertoni et al., 2021). A cooling rate of 5°C/min was used in non-isothermal experiments with the aim of simulating the cooling capacity of fluidised bed (Becker et al., 2016).

Thermal data in the crystallisation step was also exploited to construct solidification profile and the same conversion method as described in **Chapter 3 – Part 1** was applied.

### 1.2.5. Crystallisation Mechanisms Investigations by Polarised light microscopy

Isothermal crystallisation with some typical formulations was performed using Zeiss IMAGER.M2m powered by Power Supply 232, equipped with a tube lens 1.25x and external long-distance objectives 5x and 20x for use with a heating plate controlled via Linkam. The aim was **to investigate the effect of additives on tristearin crystallisation behaviours**.

These formulations were studied under the conditions mimicking processing operations (e.g. hot-melt coating): holding at 100°C for 5 min, cooling at 10°C/min till 40°C (non-isothermal crystallisation) or 60°C (isothermal crystallisation) and holding at this temperature for 2h.

Experiments might terminate earlier depending on nucleation and growth rate of the formulation. For sample preparation, the lower lamella was cleaned and preheated in hot plate, a small quantity of sample was put on it, then the upper lamella was carefully covered to spread the samples. After the holding at 100°C, automatic image acquisition was initiated by the software controlling the camera Aixocam 305 Color. 10x magnification should also be considered. Capturing velocities of 1 image/15s and 1 image/30s were chosen for isothermal crystallisation. A polarized angle of 75° was chosen for all observations. Light intensity was manually set at about 80% on the date of observation.

## 2. Results and Discussion

### 2.1. Measurements of Melting and Crystallisation Points

A slow cooling rate (0.05°C/min) has been used for three reasons. Firstly, this is for comparison with the results already obtained with DSC in the same conditions. In fact, it was reported that measurements of crystallisation points of tristearin and its combinations with a variety of additives at such a cooling rate could reveal which additive is an inductor of  $\beta$  nucleation (J. S. Aronhime et al., 1988). At the end of cooling cycle,  $\beta$  should be the crystallised form, except the combinations between tristearin and sorbitan monostearate. Secondly, a slow heating cycle should be performed right after slow-cooling crystallization to measure melting points of the target crystallised polymorph supposed to be  $\beta$  in this case. Thirdly, slow rate of heating and cooling helps overcome limitations in heat transfer of the device. Note that the choice of heating and cooling rate depends on the nature of lipid systems.

As discussed in the literature review (**Chapter 1**), knowing the concepts of metastable zone width (MSZW) could be useful for determining thermal conditions for melt-processing. With the example of tristearin, from measured melting and crystallisation points of different solid forms  $\alpha$ ,  $\beta'$  and  $\beta$ , several regions could be distinguished. In this section, there are two parts: (i) correlation of MSZW with processing evidence and (ii) effect of additive addition.

#### 2.1.1. Correlation of MSZW with processing evidence – the case of tristearin

Melting (red) and solidification (blue) points determined at 3 different cooling rates for tristearin-based formulations without surfactant added are displayed in **Figure 4-4**. The crystallisation points of tristearin (SSS) measured at 10°C/min, 5°C/min and 0.05°C/min are 47.6°C, 49.2°C and 60.0°C, respectively.

The melting points of the three polymorphs  $\alpha$ ,  $\beta'$  and  $\beta$  of tristearin are used as reference (Moorthy, 2018) : 72.5 °C ( $T_{m,\beta}$ ), 64.3°C ( $T_{m,\beta'}$ ) and 54.7°C ( $T_{m,\alpha}$ ).

Above  $T_{m,\beta}$ , tristearin is in molten state. In the regions of  $\beta$  supercooling,  $\beta$  could crystallise sporadically following homogeneous or heterogeneous nucleation mechanisms. For a cooling rate of 0.05°C/min, pure tristearin crystallised spontaneously at 60.0°C (blue square). However, its crystallisation also depends on set temperature during an isothermal period. This justifies the successful hot-melt coating with tristearin at 60°C reported recently (D. G. Lopes et al., 2015).

In practice, a processing temperature could be chosen around the inferior limit of the observed MSZW for  $\beta$  tristearin. Indeed, a set temperature from 59°C could be set to generate  $\beta$  (Bertoni et al., 2021), 2021). As a precaution, unexpected  $\beta'$  could occur between 56.5°C and 58.5°C (Bertoni et al., 2021; MacNaughtan et al., 2006; Oh et al., 2002).

It is noticed that  $\beta'$  crystallisation kinetics is slower than that of  $\beta$ . Furthermore, it was reported that  $\beta$  tristearin was extruded successfully at 65°C (Windbergs et al., 2009e). Cooling capacity of extruder is not equal to that of fluidised bed. This suggest a possible involvement of both primary and secondary nucleation for this case.

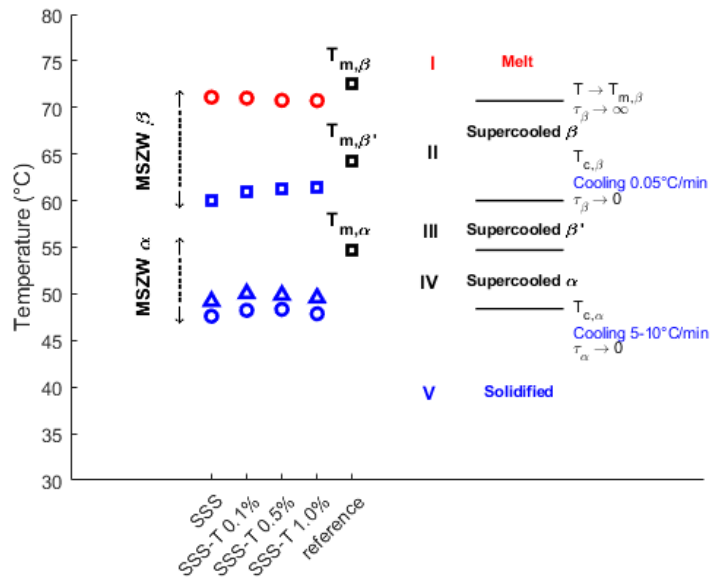


Figure 4-4. Metastable zone widths (MSZW) map constituted by measurements of melting and crystallisation points of tristearin. Melting points at 0.05°C/min (red open circles), crystallisation points at 0.05°C/min (blue open squares), 5°C/min (blue open triangles) and 10°C/min (blue circles), reference melting points of polymorphs  $\alpha$ ,  $\beta'$  and  $\beta$  (black open squares). Standard deviation (See **Appendix 02**)

The region of  $\alpha$  supercooling is delineated by its melting point and the two lower values obtained at 5-10°C/min (blue triangles and circle, correspondingly). These two latter values should reflect the crystallisation point of  $\alpha$ . In accord with the MSZW map, supercooling of this polymorph was found low compared to that of  $\beta$  (Kellens & Reynaers, 1992). Generation of  $\alpha$  tristearin at ambient conditions is often the case of processing by spray-chilling (Bertoni et al., 2020, 2021). In a study, low temperature (13-15°C) was set to assure cooling of tristearin-based droplets (Traub-Hoffmann et al., 2020). This thermal condition might be dictated by the thermolability of the substrate itself.

To conclude this part,  $\alpha$  and  $\beta$  MSZW maps were shown to correlate with the thermal conditions for crystallisation of  $\alpha$  or  $\beta$  in melt processing technologies. In the case of hot-melt coating, by considering the MSZW map, cooling rate and crystallisation temperature of each tristearin polymorph could be interdependent for one processing technology. For instance, cooling rate of fluidised bed could vary between 2-10°C/min (Becker et al., 2016; Chansanroj et al., 2007b) and it should hinge on the set temperature of the fluidisation air. With the constant cooling capacity provided by the fluidisation air, cooling rates from the melt temperature (thermal conditions to maintain formulations for feeding and pulverisation) down to the temperature at a supercooling level of  $\beta$  (for instance, 60.0°C) and  $\alpha$  (< 55°C) should differentiate from each other.

### 2.1.2. Effect of adding talc

In the case of talc addition, the crystallisation points of  $\beta$  increases with talc concentration whereas those of  $\alpha$  increase then decrease at 0.1% or 0.5%. It is probable that effects of talc and cooling rate neutralise each other. The increase in crystallisation point of  $\beta$  is the target effect with additive addition as this implies an increase in nucleation rate.

Talc was reported to act as templating agent by creating nucleation sites. As expected, the more the talc concentration, the higher the templating effect of talc. Note that the talc used in this study has a  $d_{50,laser} = 10.5 \mu\text{m}$  (technical information). It was reported that talc particles whose mean size is  $2.5 \mu\text{m}$  had the highest effect (indicated by an increase in crystallisation point obtained at  $1^\circ\text{C}/\text{min}$ ) (Yoshikawa et al., 2015). Talc of larger or smaller size is not so effective due to limited total surface area or aggregation. This is to justify that based on the current results of four levels of talc concentration 1.0% w/w yielded the highest effect on nucleation rate and there should also be minimal or no segregation of talc in the melt at this level.

Considering melting points of tristearin and its combinations with talc obtained at a slow heating rate of  $0.05^\circ\text{C}/\text{min}$ , they decrease when the talc concentration increases from 0 to 1.0% w/w. These values appear to be close to that of reference ( $72.5^\circ\text{C}$ ). Note that the value of measured (onset) melting points depends on crystallite size of lipids and heating rate or their processing history (Ravotti et al., 2020; Takeguchi et al., 2020). From the current observations, as nucleation rate increases with the increase of talc concentration, crystal size in lipid crystal network should decrease and as a consequence melting point decreases accordingly.

Tristearin MSZW was demonstrated with crystallisation data of both  $\alpha$  and  $\beta$  polymorphs with the aim of linking its relevance to the crystallisation of this triglyceride documented throughout abundant processing experiences. In the following part on formulations composed of tristearin and surfactants, the focus will be on crystallisation behaviours of  $\beta$ . In fact, intuitively, if a tristearin system can crystallise in  $\beta$  form, obviously it can also crystallise in  $\alpha$  form, but the inverse is not completely certain as reported with some surfactants such as sorbitan monostearate and glyceryl monostearate (J. S. Aronhime et al., 1988).

**To conclude this part**, melting and crystallisation point of tristearin is regarded as a milestone for evaluating the effect on tristearin crystallisation rate of an additive or combination. The case where tristearin is combined with four levels of talc concentration provides some key hypotheses for discussion in the next. On the one hand, in comparison with pure tristearin ( $T_{c,pure \beta} = 60.0^\circ\text{C}$ ) an increase in crystallisation point indicates a positive effect on nucleation rate.

On the other hand, measurements of melting points can be indirectly indicative of the effect of additive addition on crystal growth. As discussed above, the lower the melting point of a system the higher the effect of additive addition on nucleation rate and as a matter of fact the lower of crystal size in the tested system. Furthermore, one can apply a hypothesis that an increase in melting point can inform a decrease in crystal growth rate of the tested system. This is the first hypothesis to be investigated further in this research.

### 2.1.3. Effect of adding a surfactant in combinations of tristearin and talc

The principle of this study is inspired from an example in food research. It was possible to detect additives which are inductors of  $\beta$  nucleation by applying a cooling rate ( $0.05^{\circ}\text{C}/\text{min}$ ) (J. S. Aronhime et al., 1988). At this very low cooling rate, when adding an inductor of  $\beta$  nucleation to tristearin, the system will crystallise more or less the crystallisation point of (pure)  $\beta$  tristearin. On the other hand, when adding an inhibitor of  $\beta$  nucleation, the system will crystallise more or less the crystallisation point of (pure)  $\alpha$  tristearin. This means if a  $\beta$  MSZW is detected for one formulation, additive or additive combination can be regarded as inductor of  $\beta$  tristearin nucleation. This is the second hypothesis to be investigated in this research.

**Figure 4-5** and **Figure 4-6** show the MSZW maps constituted by crystallisation points (blue) and melting points (red) of the polymorph  $\beta$  in formulations composed of tristearin plus solely one hydrophilic surfactant (PS20) or one lipophilic surfactant (SML) with or without talc, respectively.

In general, in the presence of talc, crystallisation points augmented. Crystallisation points also increase with the increase in talc concentration whereas melting points follow the inverse tendency, except 1.0% w/w. There are some findings from these observations. In the first place, nucleation of the systems of SSS plus PS20 or SSS plus SML behaves like the case of pure SSS when adding talc.

In the second place, solubility of the surfactant relates partially to its effect on nucleation rate. Based on the solubility, it is presumably that the systems of SSS plus PS20 (HLB 16.7 – water-soluble) or SSS plus SML (HLB 8.6 – oil soluble) are melt dispersions and melt solutions, respectively. Of all these additives/additive combinations tested on tristearin, templating effect of SML appears to be weaker by considering that crystallisation points of the  $\beta$  polymorph in these melt solutions were smaller in comparison with those of pure SSS and other systems (including SSS plus PS20). In fact, one highly soluble surfactant in the melt can retard the formation of nuclei, therefore the nucleation rate or reduce the crystallisation point in this case (K. W. Smith & Sato, 2018).

In the third place, the fact that an increase in melting point was commonly observed for all the systems with 1% w/w talc might hint at larger crystal size in these systems. Hypothetically, this could result from a slow growth rate.

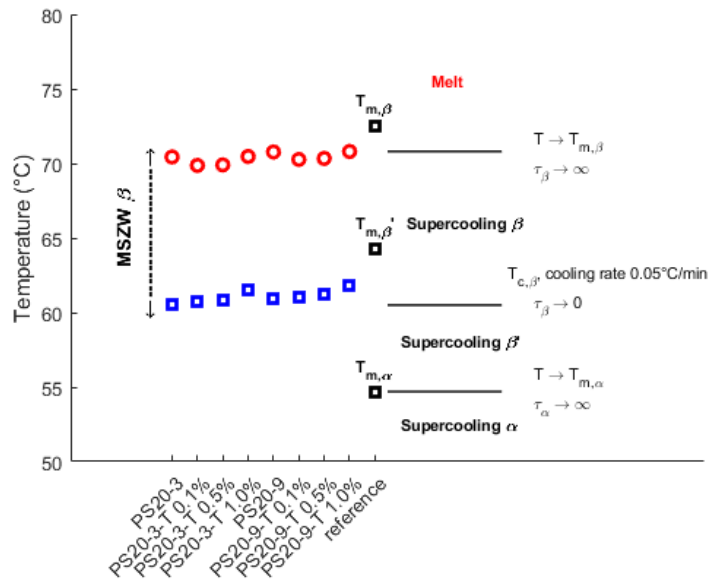


Figure 4-5. MSZW map constituted by melting points (red) and crystallisation points (blue) of formulations composed of tristearin, polysorbate 20 (hydrophilic surfactant) and talc at different ratios. Standard deviation (See **Appendix 02**)

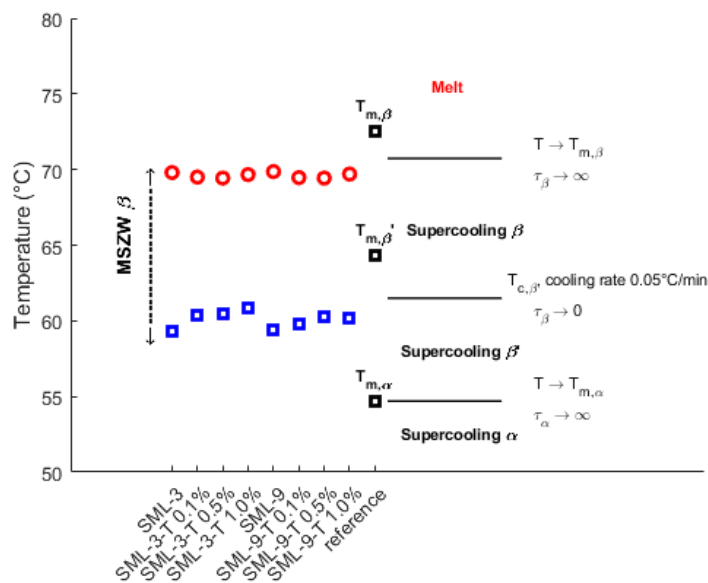


Figure 4-6. MSZW map constituted by melting points (red) and crystallisation points (blue) of formulations composed of tristearin, sorbitan monolaurate (lipophilic surfactant) and talc at different ratios. Standard deviation (See **Appendix 02**)

#### 2.1.4. Effect of adding a combination of surfactants in combinations of tristearin and talc

**Figure 4-7, Figure 4-8 and Figure 4-9** show the MSZW maps constituted by crystallisation points (blue) and melting points (red) of the polymorph  $\beta$  in formulations composed of tristearin plus binary additive combinations with or without talc, where H, L, and N stand for hydrophilic, lipophilic and “neutral” balance depending on the blend ratios of PS20 and SML 3:1, 1:3 and 1:1, respectively. From the chemical composition, the systems of tristearin and two surfactants can be regarded as melt emulsions.



For these melt emulsions, the effect of talc addition did not follow a specific trend like the three groups presented above. This implies that there should be an effect of interactions between talc and BACs on tristearin nucleation behaviours.

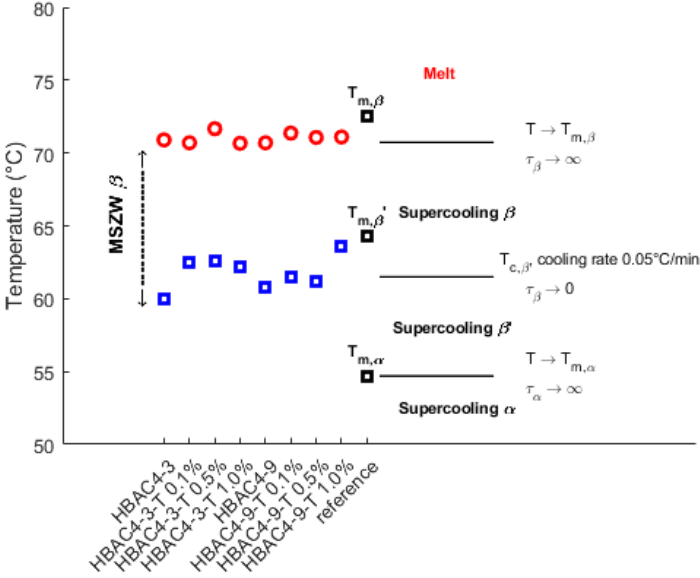


Figure 4-7. MSZW map constituted by melting points (red) and crystallisation points (blue) of formulations composed of tristearin, hydrophilic binary additive combinations (HBAC) and talc at different ratios. Standard deviation (See Appendix 02)

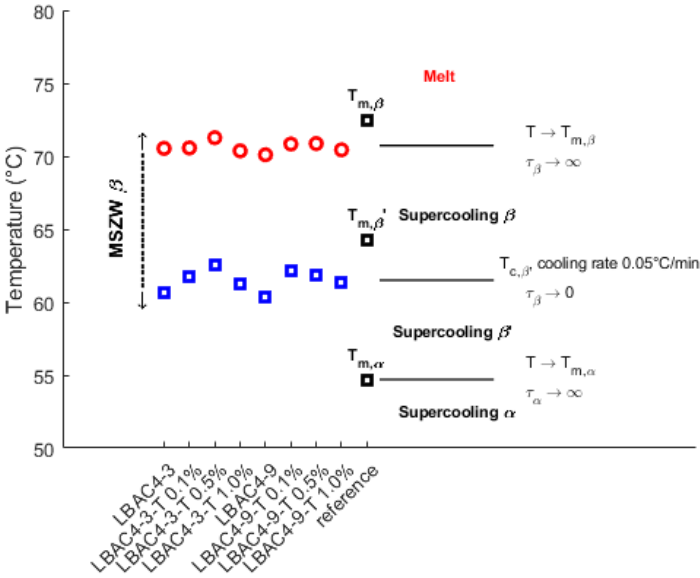


Figure 4-8. MSZW map constituted by melting points (red) and crystallisation points (blue) of formulations composed of tristearin, lipophilic binary additive combinations (LBAC) and talc at different ratios. Standard deviation (See Appendix 02)

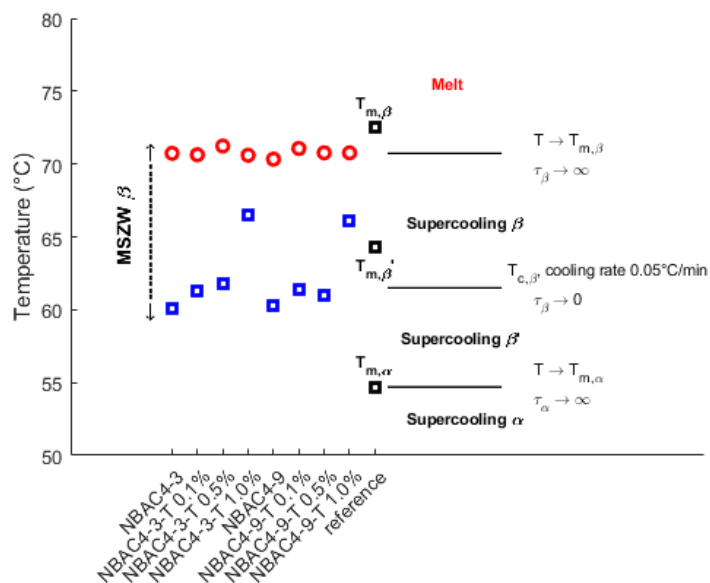


Figure 4-9. MSZW map constituted by melting points (red) and crystallisation points (blue) of formulations composed of tristearin, “neutral” binary additive combinations (NBAC) and talc at different ratios. Standard deviation (See **Appendix 02**)

In general, in the presence of talc, crystallisation points of all these formulations augmented in comparison with pure SSS. Crystallisation points of tristearin were raised more remarkably in the presence of both talc and BACs: HBAC4-3-T 0.1% ( $62.5 \pm 1.6^\circ\text{C}$ ), HBAC4-3-T 0.5% ( $62.6 \pm 0.5^\circ\text{C}$ ), HBAC4-3-T 1.0% ( $62.2 \pm 1.4^\circ\text{C}$ ), HBAC4-9-T 1.0% ( $63.6 \pm 1.8^\circ\text{C}$ ), LBAC4-3-T 0.5% ( $62.5 \pm 0.4^\circ\text{C}$ ), LBAC4-9-T 0.1% ( $62.1 \pm 0.6^\circ\text{C}$ ), NBAC4-3-T 1.0% ( $66.5 \pm 0.6^\circ\text{C}$ ) and NBAC4-9-T 1.0% ( $66.1 \pm 0.4^\circ\text{C}$ ) (See Appendix 02 for full tabulated data for comparison). The BACs in these systems all can potentially promote nucleation of  $\beta$  tristearin in comparison with pure SSS.

To simplify the discussion, one can disregard the formulations with 0.5% or 0.1% w/w. Concerning HBAC-3 and HBAC-9, NBAC-3 and NBAC-9, LBAC-3 and LBAC-9 with and without 1% w/w T (12 formulations in total), a same tendency was observed. At low concentration of surfactant combinations, adding talc reduces melting point while at high concentration of surfactant combinations, adding talc raises melting point. These could be related to their effect on crystal growth rate based on the initial hypothesis.

To conclude this part, the concept of MSZW map (as shown in **Figure 4-4**, **Figure 4-5**, **Figure 4-6**, **Figure 4-7**, **Figure 4-8** and **Figure 4-9**) could be useful for defining at which cooling rate (vertically) and at which temperature (horizontally) a certain solid form of tristearin could be crystallised intentionally. The former factor is mainly associated with one specific melt-processing technology and setup of thermal operational conditions whereas the latter factor is associated with effect of additive addition.

Except SMS (data not shown), two liquid surfactants, talc and their combinations at different ratios were shown to be inductors of  $\beta$  tristearin nucleation. This is the first hypothesis. To confirm again, representative formulations will be analysed with RAMAN spectroscopy and DSC to identify the polymorph crystallised in similar thermal conditions and investigate nucleation kinetics.

The current results show that combinations of both liquid surfactants can induce nucleation and the crystallisation point of these systems all increases in comparison with pure SSS. Melt solutions appear to nucleate at a temperature lower than melt dispersion or melt emulsions. These findings support the advantage of targeting  $\beta$  crystallisation for control of product stability. In fact, as presented in Chapter 1, while lipid-based  $\beta$  solid solutions (i.e. tristearin/oil or liquid surfactant) for spray-congealing tend to yield a relatively stable product profile in long-term storage (Bertoni et al., 2021), products hot-melt coated with lipid-based  $\beta$  solid dispersions (i.e. tripalmitin/polysorbate 65) was reported with several stability issues whose cause could be resumed in one physical process – Ostwald ripening (D. G. Lopes, Koutsamanis, et al., 2017; Schertel, Salar-Behzadi, Karrer, et al., 2021; Schertel, Salar-Behzadi, & Zimmer, 2021). Among the strategies to overcome stability challenges due to Ostwald ripening proposed in food researches (Boistelle, 1988),  $\beta$  crystallisation and use of additives represent two solutions which are the main subjects of this study. With the proof of  $\beta$  crystallisation feasibility, the interesting additive or combination of additives can be selected for testing with hot-melt coating. Now arises the question: *How can this fundamental finding be translated into successful applications?*

## 2.2. Measurements of Induction Time

**Figure 4-10-A** shows accumulative distribution curves of induction time measurements and its model obtained for SSS  $\pm$  T at four talc concentrations. Mean induction time appears to decrease with the increase in talc concentration. At the moment, increase in crystallisation point and decrease in induction time are shown to reflect an effect of additive or combination to enhance nucleation rate.

Furthermore, the distribution of measured induction time values reveals clearly that nucleation of  $\beta$  tristearin is a stochastic phenomenon and its randomness decreases when talc concentration increases. This effect is important for applications in melt processing because randomness of nucleation might compromise repeatability of processing operations.

Extrusion of pure tripalmitin ( $T_{m,\alpha} \cong 45^\circ\text{C}$ ) at  $55^\circ\text{C}$  could be an example. It was reported that extrusion with 1.0- and 0.3-mm dies made such a difference between two processing operations that tripalmitin was cooled slowly or rapidly at ambient conditions under the effect of extrudate surface and friction imposed by presson. In fact, slow cooling maintained the thermal condition favourable for  $\beta$  crystallisation ( $T_c > T_{m,\alpha}$ ) whereas rapid cooling (fast heat removal) led to  $\alpha$  crystallisation ( $T_c < T_{m,\alpha}$ ). In this case, if the nucleation time were more controlled, i.e. less subject to randomness,  $\beta$  crystallisation could occur in a repeatable manner within a short time at the defined temperature.

**Figure 4-10-B** and **-C** shows accumulative distribution curves of induction time measurements for combinations of tristearin plus one surfactant (PS20 or SML) with or without talc. Qualitatively, these curves show that adding talc reduces to a smaller extent the nucleation randomness of PS20-containing systems (**Figure 4-10-B**) while SML-containing systems (**Figure 4-10-C**) tend to nucleate slower than any groups of other systems. However, a common tendency is that increase in talc concentration resulted in decrease in nucleation time but the effect of talc to reduce nucleation randomness appears to be reduced or cancelled.

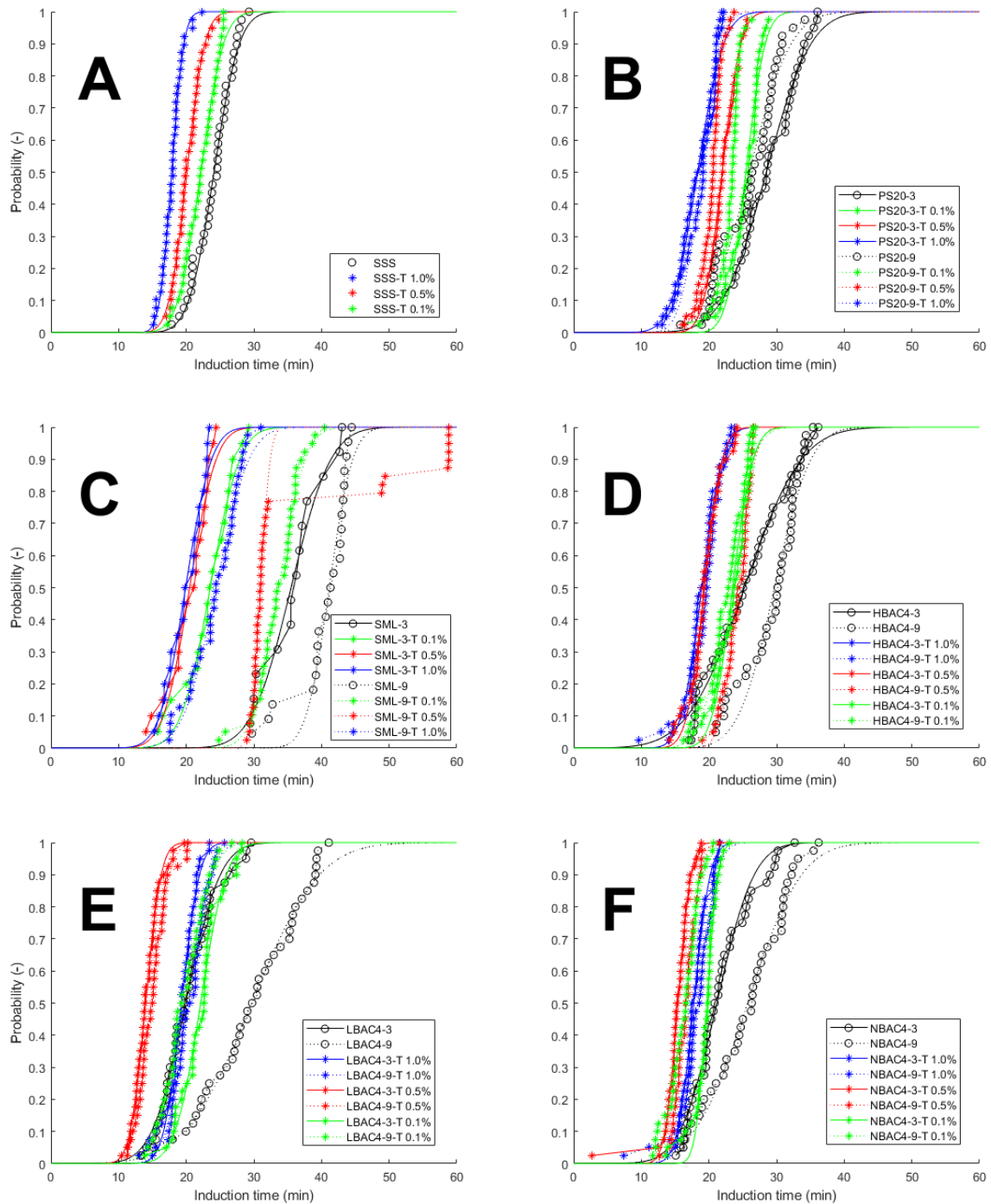


Figure 4-10. Accumulative distribution of induction time measurements and its model obtained for forty-four formulations

Outliers are observed for formulations composed of tristearin, sorbitan monolaurate and talc at different ratios (see **Figure 4-10-C**). Particularly, the distribution curve obtained for SML-9-T 0.5% displays 9 points outside the estimated model. However, these points conform to the condition  $0 \leq x \leq 2\mu$  and therefore are still included. This group of formulations SML behaves in such a different manner that not all samples did crystallise within 60 minutes, which is the isothermal period set for all the formulations under research for a good comparison. In fact, the number of induction time measurements for almost

the formulations in **Figure 4-10-C** acquired were smaller: SML-3 (13), SML-3-T 0.1% (20), SML-3-T 0.5% (20), SML-3-T 1.0% (20) and SML-9 (22). These observations complement the fact that SML was previously shown to depress  $T_c$  or retard its nucleation in comparison with of pure SSS. Besides, intuitively, formulating with PS20 (hydrophilic surfactant) alone risks causing de-mixing in the SSS systems in both liquid and solid state. This justifies the need to blend two surfactants with different HLB values.

**Figure 4-10-D, -E and -F** shows accumulative distribution curves of induction time measurements for formulations composed of SSS and combinations of surfactants – HBAC4, LBAC4 and NBAC4, respectively. For formulations without talc, induction time and nucleation randomness are higher than talc-loaded formulations. Furthermore, the effect of adding talc also did not follow a specific trend like the three groups presented above.

In comparison with the systems of SSS plus one surfactant (**Figure 4-10-B and -C**), the effect of adding talc might not be significantly different between talc-loaded formulations by considering closeness or overlapping of the distribution curves. A shift towards reduction in induction time can be observed from HBAC4, LBAC4 to NBA4. This might hint at a good combination of surfactants at the equal ratio 1:1.

For all the three groups, 0.5% w/w talc was noticed to reduce the most both induction time and nucleation randomness. This could be ascribed to some interactions between binary additive combinations and talc. This effect could be meaningful as it suggests a possible reduction in talc quantity used for hot-melt coating formulations.

In addition, a set of outliers was also noticed at the head of some distribution curves (e.g., PS20-3, HBAC3, HBAC4-9). It is possible that certain metastable form(s) of tristearin nucleated earlier than its stable form. In reality, it was recently reported that triglycerides can occur in multiple  $\beta$  forms (Takeguchi et al., 2020).

Above, all the results were presented qualitatively considering **Figure 4-10**. Quantitatively, **Figure 4-11** shows estimated induction time of 28 formulations with standard deviation values (excluding 16 systems of SSS plus one surfactant). In general, almost induction time was observed less than 30 minutes and almost formulations have an induction time less than that of pure SSS (except NBAC4-9, HBAC4-3, HBAC4-9, HBAC4-9-T 0.5 and LBAC4-9. In the presence of talc, formulations constituted by SSS and BACs have an accelerated nucleation kinetics by considering induction time and nucleation randomness.

In this study, combinations of SSS and SMS at 97:3 and 91:9 w/w did not crystallise using the same thermal programme. They should crystallise at a temperature below 55°C. In fact, the  $T_c$  of SSS:SMS 90:10 was reported to be 51.5°C (just below  $T_{m,\alpha}$ ) at 0.05°C/min via DSC and SMS was noticed to inhibit  $\beta$  formation (J. S. Aronhime et al., 1988). For information, SMS has been known as a crystal modifier which stabilises polymorph  $\alpha$  and delays  $\beta$  formation/conversion (J. S. Aronhime et al., 1987; Elisabettini et al., 1996; Garti et al., 1982).

To conclude this part, on the one hand, both increase in crystallisation point (related to MSZW) and decrease in nucleation time were shown to indicate an effect of additive or combination to enhance nucleation rate. While metastable zone widths (MSZW) could be interpreted as proof of processing

feasibility of the  $\beta$  polymorph of tristearin, induction time ( $\tau_{ind}$ ) could indicate impact level of additive addition on its nucleation. The latter physical quantity should have a link to processing fluidity. In reality, take the case of hot-melt coating for example. The unique case of non-traditional hot-melt coating (setting  $T_c > T_{m,pure \alpha}$ ) was also reported with tristearin but no additives were used (D. G. Lopes et al., 2015). In the cited study, another particular feature is switching feeding rate in the course of coating. In fact, the initial lower feeding rate (0.5 g/min) should be related to nucleation induction time whereas the sequential higher feeding rate (10 g/min) should be related to high crystallisation kinetics of  $\beta$  tristearin once nucleation occurred (Bertoni et al., 2021). It justifies the reason to combine non-isothermal and isothermal crystallisation studies.

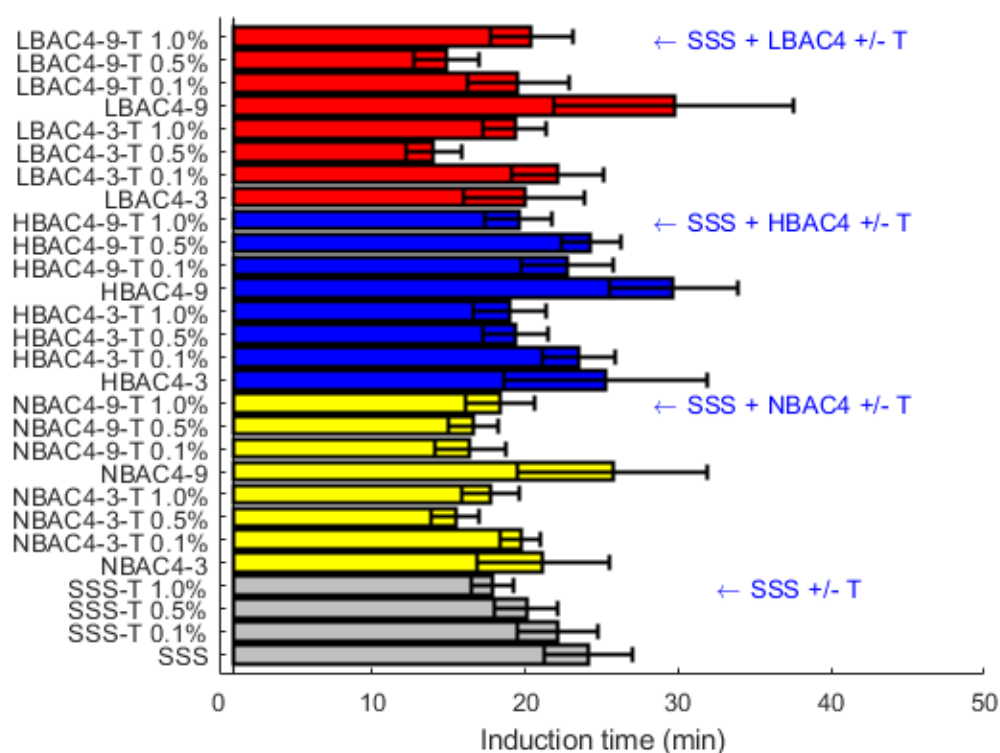


Figure 4-11. Comparison of induction time obtained for 28 formulations

Besides, for the case of inhibitors of  $\beta$  nucleation such as sorbitan monostearate tested in this study, it would be not reasonable to launch an isothermal crystallisation study comprising 40 cycles in order to construct distribution curves of induction time shown in **Figure 4-10** without having a prior proof of processing feasibility. It justifies the order to conduct non-isothermal and isothermal crystallisation studies. For information, the number of 40 cycles was proved practical to distinguish the effect of additive addition on nucleation behaviours of tristearin instead of launching up to 80 cycles to search for a statistical significance (obtained with 80 cycles) (Xiao et al., 2017).

Talc was confirmed in this study as a  $\beta$  tristearin crystallisation promoter in addition to the work performed in food research on other triglycerides (i.e., trilaurin, trimyristin and tripalmitin) (Yoshikawa, 2016; Yoshikawa et al., 2014, 2015).



On the other hand, these results highlight the applicability of the use of Crystal® for fast screening additives in search of an effect of nucleation induction or inhibition as well as an effect of nucleation promotion or retardation. Preliminary hot-melt coating trials were successfully performed at 60°C to validate the proof of feasibility of SSS plus different BACs. It is to show the quick link of fundamental research to applications detectable by this fast-track screening method.

However, the hypotheses whether the crystallised form in two sets of designed experiments with Crystal16® is  $\beta$  and whether increase or decrease in melting pointing correlate indirectly with crystal growth will be tested with other characterisation techniques in the next parts.

## 2.3. Polymorph Identification

### 2.3.1. By Raman Spectroscopy

As one of limitations of Crystal16® is related to the principle of measurements – turbidimetry, it is not possible to identify the polymorph of solids. Therefore, Raman spectroscopy was performed on samples which have been subject to non-isothermal crystallisation for detecting metastable zone widths.

It would rather perform with Raman spectroscopy as a complementary test with Crystal16® than repeat analyses via DSC (time-consuming to run a cycle with each sample using 0.05°C/min as cooling rate). Furthermore, as crystallisation point of tristearin in the presence of additives was available in the literature (J. S. Aronhime et al., 1988), it is possible to make a comparison.

For a better comparison between spectra of different samples, all the spectral data were normalised with the intensity of the peak at 1370 cm<sup>-1</sup> which was said to not to change much in polymorphic transitions (Motoyama, 2012).

Polymorph identification between  $\alpha$  and  $\beta$  forms of tristearin could be indicated by certain characteristic peaks in Raman spectra:

- intensities at 1180 (CH<sub>2</sub> rocking mode),
- 1438 and 1460 cm<sup>-1</sup> (CH<sub>2</sub> scissoring mode),
- presence/absence of 1728 cm<sup>-1</sup> (ester C=O stretching C<sub>3</sub>-C<sub>2</sub> gauche),
- 1743 cm<sup>-1</sup> (ester C=O stretching C<sub>3</sub>-C<sub>2</sub> trans) (Motoyama, 2012).

Forms  $\alpha$  and  $\beta$  of tristearin were made in-house for spectral comparison. For the reader's information,  $\alpha$  form was generated by melting commercial powder tristearin ( $\beta$ ) and letting it solidify in a rectangular mould at ambient conditions. For preparation of  $\beta$  form,  $\alpha$  form was then cured at 50°C during 12h following a reported procedure (D. G. Lopes et al., 2015).

A qualitative approach for determining polymorphs could be applied based on considerations of the appearance of single or double peaks in the range of 1650-1750 cm<sup>-1</sup> in high frequency region and an intensity shift at 113 to 140 cm<sup>-1</sup> in low frequency region. In effect, as shown in **Figure 4-12** and **Figure 4-13**, the spectrum of in-house  $\alpha$  displays a peak positioned at 113 cm<sup>-1</sup> in low frequency region and a single peak 1736 cm<sup>-1</sup> in high frequency region.

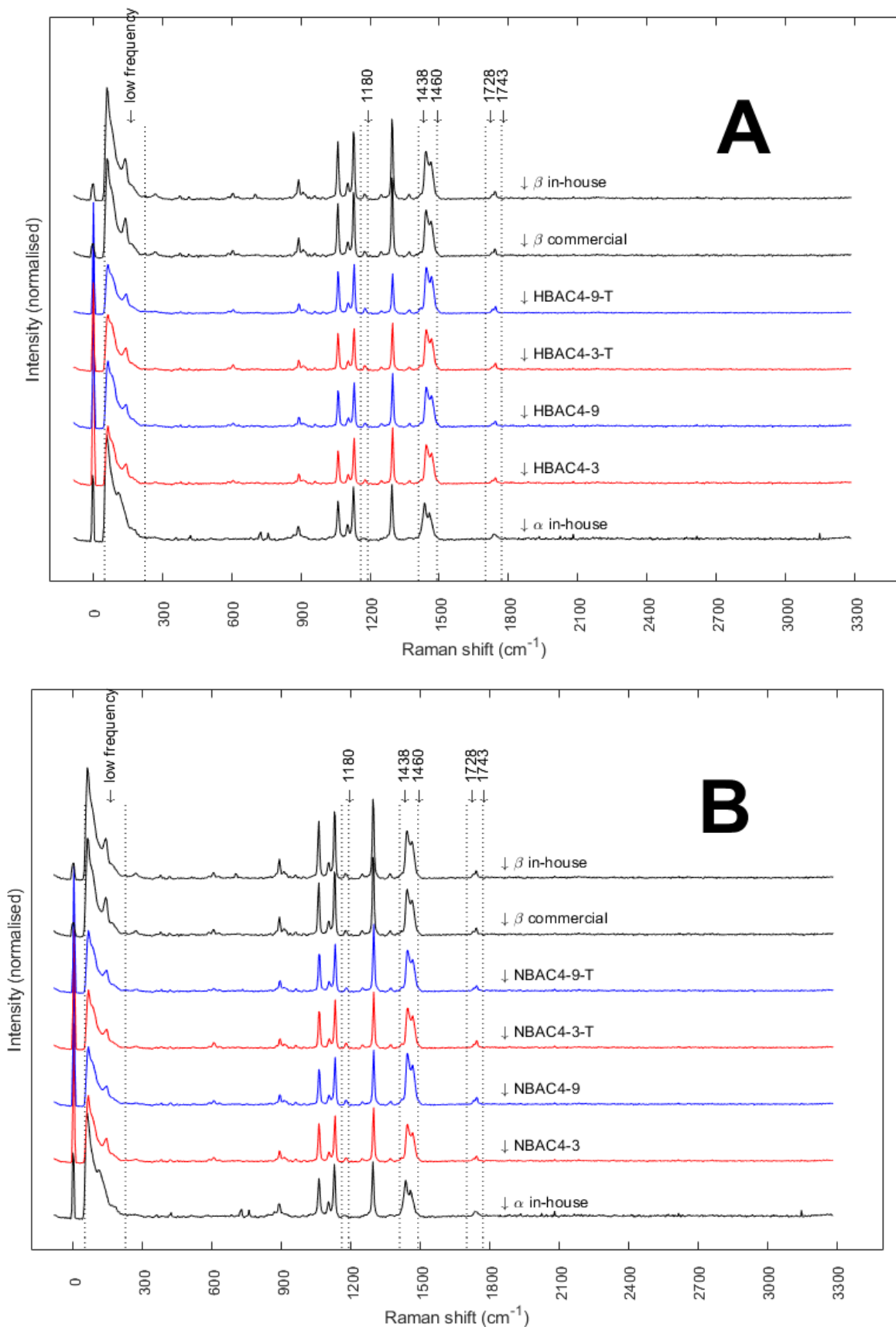


Figure 4-12. Raman spectra of 16 formulations subject to non-isothermal crystallisation in Crystal16®. A, SSS plus HBAC4 with/without T; B, SSS plus NBAC4 with/without T

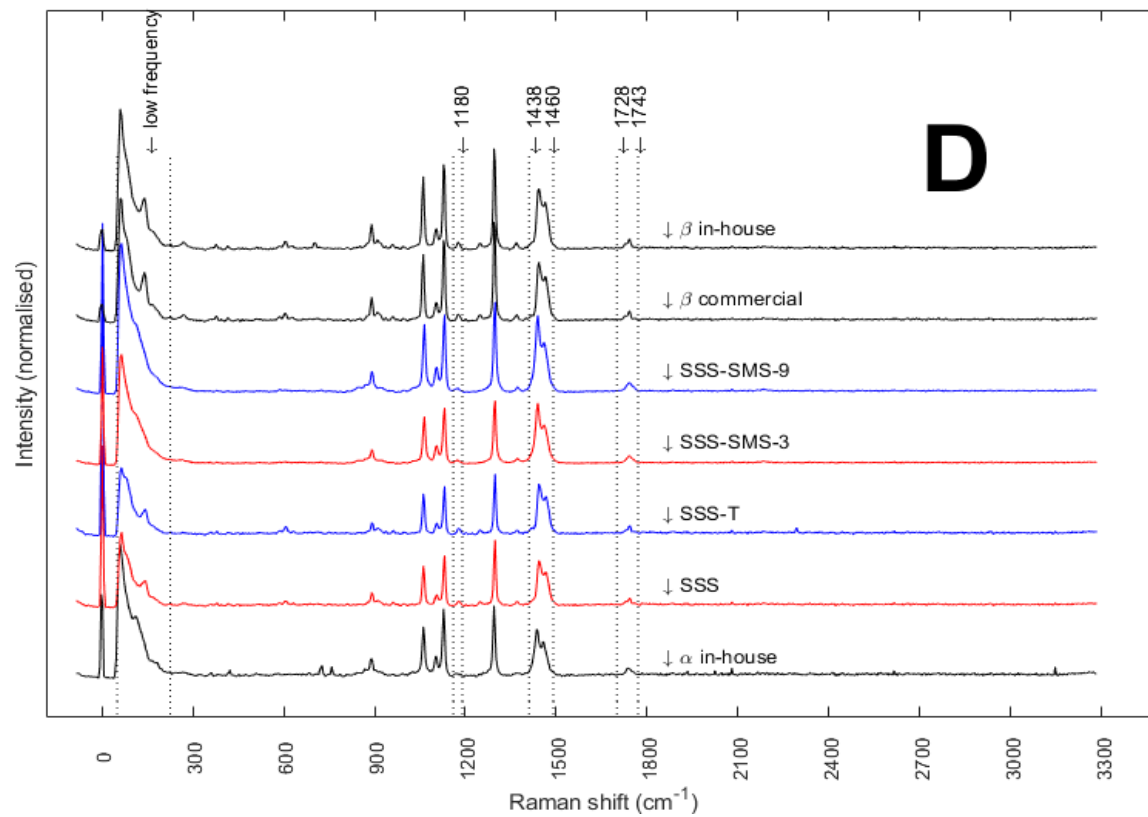
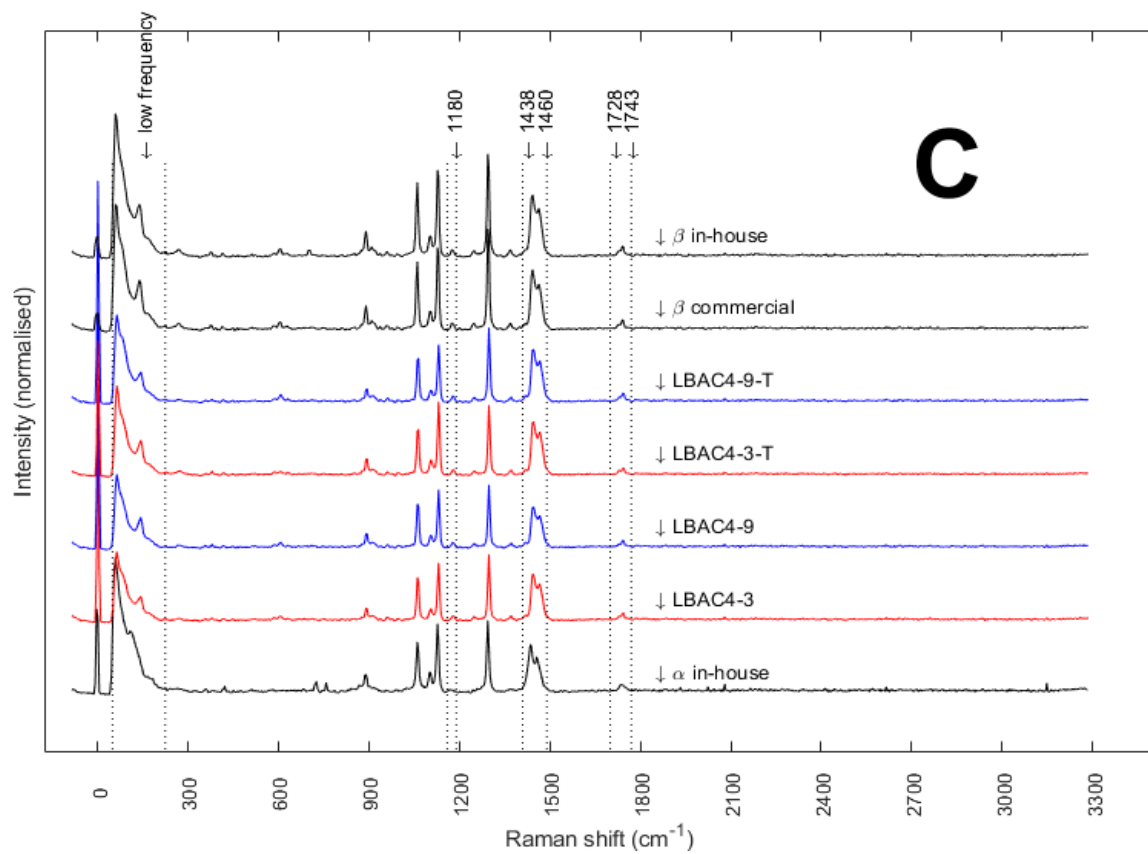


Figure 4-13. Raman spectra of 16 formulations subject to non-isothermal crystallisation in Crystall16® : C, SSS plus LBAC4 with/without T; D, SSS plus SMS and SSS with/without T

On the other hand, the spectrum of in-house  $\beta$  displays a peak positioned at  $140\text{ cm}^{-1}$  in low frequency region and a presence of two peaks  $1728\text{ cm}^{-1}$  and  $1743\text{ cm}^{-1}$ . In addition, the peak at  $1180\text{ cm}^{-1}$  of  $\beta$  is higher than that of  $\alpha$ . It can be seen that all the formulations composed of SSS and H-, N- and L-BAC4 at ratios of 97:3 and 91:9 with or without talc exhibit a polymorph  $\beta$ , as shown in **Figure 4-12-A, -B** and **Figure 4-13-C**, respectively. Besides, it is reasonable to conclude that hybrid spectra of  $\alpha$  and  $\beta$  forms (as indicated by the absence of  $113$  or  $140\text{ cm}^{-1}$  in low frequency region) were obtained for both combinations of SSS and SMS, as shown in **Figure 4-13-D**. The system of SSS plus one surfactant (PS20 or SML) were not analysed but the crystallised form could be deduced as the  $\beta$  polymorph.

### 2.3.2. By DSC

**As presented in the previous part, to complement the limitation of Crystal16®** in terms of polymorphic identification, RAMAN spectroscopy was applied for testing samples freshly crystallised in non-isothermal crystallisation study with Crystal® at  $0.05^\circ\text{C}/\text{min}$ . Parallely, DSC was applied for simulating isothermal crystallisation conditions of those samples in Crystal® and identifying the polymorph generated in these conditions.

Fourteen representative formulations were selected: SSS, SSS-T, HBAC4-3, HBAC4-3-T, HBAC4-9, HBAC4-9-T, LBAC4-3, LBAC4-3-T, LBAC4-9, LBAC4-9-T, NBAC4-3, NBAC4-3-T, NBAC4-9, and NBAC4-9-T. SSS and SSS-T serve as control for comparison. Only formulations with combinations of two surfactants were selected by considering that the effect of combinations is more important than adding solely a surfactant. Talc concentration (if present) was fixed at  $1.0\%$  w/w. T was always an accompanying additive by considering its effect to enhance both nucleation and crystal growth.

**Figure 4-14-A and -B** shows solidification kinetics of crystallised formulations in isothermal crystallisation study and melting curve of a polymorph, respectively. As the isothermal period at  $60^\circ\text{C}$  was limited to 40 minutes, only nine formulations crystallised. Of these, only two formulations with binary surfactant combinations without talc crystallised in comparison with all the talc-loaded formulations. Induction time obtained with Crystal16® and DSC might differ as experimental conditions were different and a large number of experiments were conducted for Crystal16®. Importance is put on the fact that **Crystal16® setup** with chosen experimental conditions **was sensible to distinguish the effect of different additives and additive combinations**. Experiments with Crystal16® **were also able to show the stochastic nature of nucleation with obviously higher throughput than an analytical plan with DSC**.

Except LBAC4-9-T, they nucleate to a greater or equal rate of SSS-T. Almost the formulations display the same S-shaped curve which could hint at a similar solidification kinetics. This might imply that crystal growth following sporadic nucleation is rapid. The form  $\beta$  was the crystallised polymorph for all of these cases considering its solidification kinetics and melting temperature (Bertoni et al., 2021; Moorthy, 2018; Oh et al., 2002; Ravotti et al., 2020). For the other six formulations which did not crystallise within the isothermal period of 40 minutes as well as the others in 44 formulations in total subject to experiments with Crystal16®, it is reasonable to say that the polymorph crystallised should also be  $\beta$ .

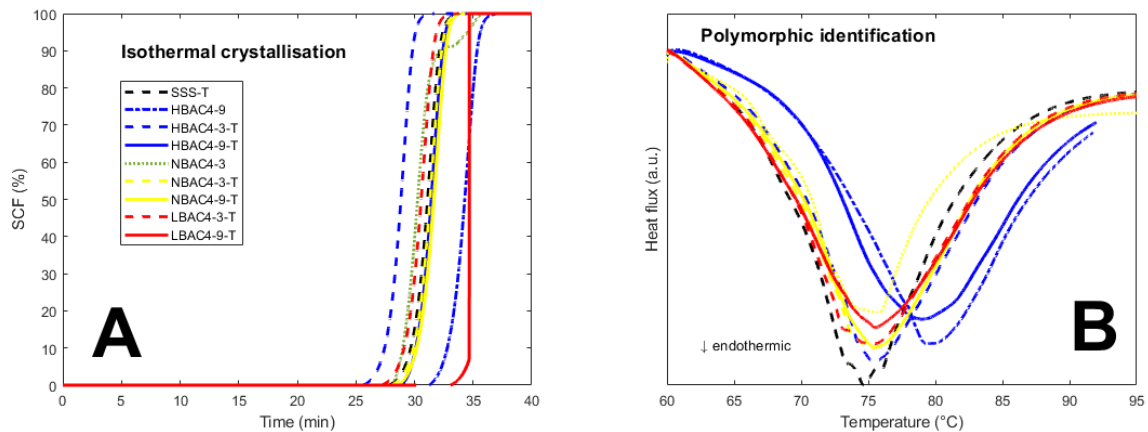


Figure 4-14. Isothermal crystallisation at 60°C (A) and melting at 30°C/min (B)

**Figure 4-15-A** and **-B** shows solidification kinetics of crystallised formulations in non-isothermal crystallisation study and melting curve of a polymorph, respectively.

The form  $\alpha$  was the crystallised polymorph for all of these cases considering its melting temperature (Moorthy, 2018; Oh et al., 2002; Ravotti et al., 2020).

All the formulations exhibit a rapid solidification kinetics which might imply that crystal growth following spontaneous nucleation is rapid. There should presumably be no effect of additives on this property of tristearin. However, as can be noticed from the results of DSC, a small depression in crystallisation point of  $\alpha$  could be observed for all the formulations without talc in comparison with SSS (51.1°C): HBAC4-3 (50.8°C), HBAC4-9 (50.5°C), NBAC4-3 (50.7°C), NBAC4-9 (50.5°C), LBAC4-3 (50.7°C) and LBAC4-9 (50.3°C).

For all these cases, as an effect of additive, depression in  $T_{c,\alpha}$  or increase in  $\alpha$  supercooling could indeed be considered insignificant. However, for other lipid systems, this could be adverse from a processing point of view. For instance, inclusion of certain active substances could inhibit solidification of a lipid system at its original crystallisation point (Qi et al., 2010). This justifies an application of turbidimetry integrated Crystal16® for detecting such a problem with a large number of formulations in early stage.

As can be noticed from the results of DSC and Crystal®, there is a difference between the value of  $T_{c,\alpha}$  measured via DSC and that by turbidimetry (49.2°C) at the same cooling rate (5°C/min). The value is still comparable for tristearin by accounting for the heat transfer mode of each apparatus.

Another remark for DSC results is that at least two  $\beta$  forms could be detected, which is indicated by an offsetting of melting points at the same heating rate. In fact, there has been reported that  $\beta$  tristearin occurs in four forms (Takeguchi et al., 2020). In the cited research, melting peaks of  $\beta$  forms were detected around 75°C (at 40°C/min), which support these DSC results of polymorph identification. As an exception, the offsetting (both  $\alpha$  and  $\beta$ ) towards higher melting peaks was only observed for HBAC4-9 (with/without talc). This implies that this particular additive combination at 9% w/w might induce nucleation of a new  $\beta$  form.

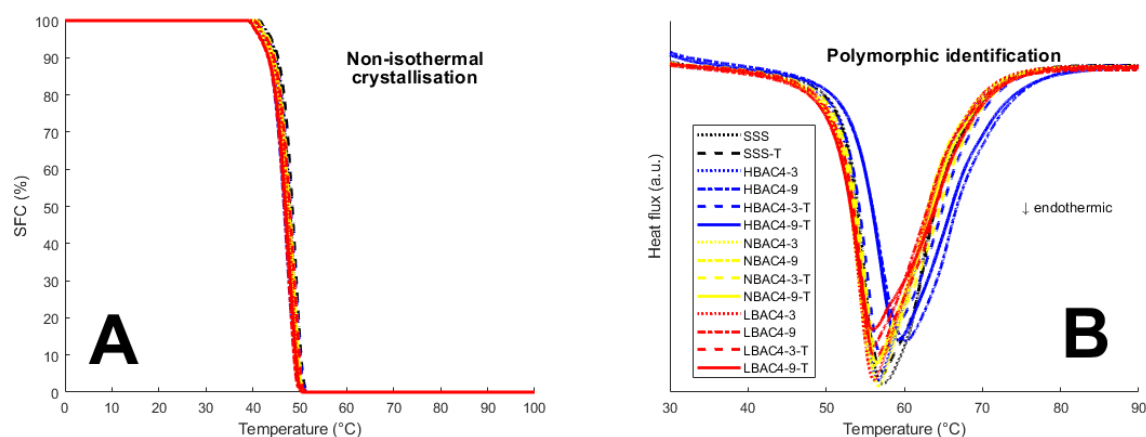


Figure 4-15. Non-isothermal crystallisation at a cooling rate of 5°C/min (A) and melting at 30°C/min (B)

## 2.4. Crystallisation Mechanisms Investigations

In this final part, the second hypothesis related to crystal growth will be investigated with polarised light microscopy. Six representative formulations in terms of talc inclusion and additive concentration were chosen: SSS, SSS-T, NBAC4-3, NBAC4-3-T, NBAC4-9, and NBAC4-9-T. SSS and SSS-T again serve as control. NBAC4-3 and NBAC4-9 with/without talc are selected by considering their plausibly superior effects on nucleation (indicated by crystallisation point, induction time, nucleation randomness).

Talc has been emerged as an interesting additive in food research field. It plays a role of nucleation inductor for monoacid triglycerides (Bayés-García et al., 2022; Yoshikawa et al., 2014). Action mechanism of talc as inductor of heterogeneous nucleation was attributed to hydrophobic cleavage surfaces of its particles (Yoshikawa et al., 2015).

**Figure 4-16** shows images of isothermal crystallisation study performed for six selected formulations (the whole process of crystal growth captured for the four formulations NBAC4-3, NBAC4-9, NBAC4-3-T and NBAC4-9-T can be visualized in the Appendix 02).

The arrows indicate droplets of additives or solid particles. For SSS and SSS-T, induction time was detected after about 16 and 21 minutes. Solidification time, as the time from first sign of crystal till full crystallisation in lamella, was about 8 and 10 minutes, respectively. The difference lies in the underlying crystallisation mechanisms, homogeneous nucleation for SSS and heterogeneous nucleation for SSS-T, as concluded in a study for triglycerides (Yoshikawa et al., 2014). In fact, talc particles serve as template and first nuclei of  $\beta$  tristearin were observed on the surface of talc particles.

In the case of NBAC4-3 and NBAC4-9, droplets of binary additive combinations were observed and their size increases with additive concentration. At the appearance of crystals, these droplets turn blurred. Induction time of about 15.5 and 39 minutes was measured for formulations with low and high additive concentrations, respectively. It is possible that an interface-mediated crystallisation mechanism would apply in this case where two phases exist at the same time (A. R. Patel & Dewettinck, 2015; Stewart et al., 2017).



For NBAC4-3, from the moment of first nuclei, the population of nuclei increases rapidly until solidification ended in about 24 minutes.

For NBAC4-9, nuclei took more time to appear, and it seems that they grew around a net interface (See **Appendix 02** for more details). When they grew, a few smaller nuclei started to appear nearby and grew a net interface. This could be attributed to secondary nucleation. Gradually, they formed an agglomeration of growing crystals aligned linearly or perpendicularly. Since their birth crystallites continued till the bulk was completely consumed. The number of nuclei was less but their size was larger. Solidification of NBAC4-9 took more than 51 minutes.

Concerning NBAC4-3-T and NBAC4-9-T, with the addition of talc, measured values of induction time were reduced close to that of SSS-T. A shorter solidification time was also achieved for NBAC4-3-T and NBAC4-9-T (about 15 min and more than 42 min, respectively). Crystallisation of these formulations might involve a complexity of factors: templating effect of talc, interface created in the presence of binary additive combinations. As discussed above, interactions between talc and binary additive combinations should not be excluded.

At low concentration of additives, both mechanisms contribute to crystallisation of tristearin. On the one hand, first sign of nuclei could be detected on talc particles in the image. On the other hand, shortly after that, nuclei also appear abundantly in the observation field and even away from talc surface. The solidification terminates promptly.

At high concentration of additives, the presence of talc seems to promote nucleation earlier than the case of NBAC4-9. Nuclei started to appear abundantly and seem to grow rapidly. Until a certain size was achieved, growth slowed down. Then small nuclei came to birth nearby and they continue to grow till the complete consumption of the bulk. At the end, an even distribution of crystal size could be noticed. In comparison with NBAC4-9, no interface was observed in the centre of crystals. In this case, it is possible that additives and talc interact with others to catalyse nucleation of tristearin but also control crystal growth.

**To conclude this part, on the one hand, a difference in induction time values can be observed for three characterisation techniques** and this might be due to involvement of shear (Xiao et al., 2017) and surface/volume effect (Adachi et al., 2014). Furthermore, if polarized light microscopy (PLM) is not deployed to observe crystallization progress in real time, solidification kinetics could be overestimated. In fact, despite having the same S-shaped curve solidification profile obtained via DSC, solidification time of NBAC4-3, NBAC4-3-T, and NBAC4-9-T observed via PLM differs distinctly.

On the other hand, the effect of talc to enhance both nucleation and crystal growth can be concluded from PLM experiments with the six selected formulations. In fact, adding talc not only reduced nucleation time but also accelerated crystal growth. Therefore, solidification time of the concerned formulations diminished.

Adding surfactant combination appeared to induce nucleation by another mechanism – heterogenous nucleation at the interface. However, surfactants were shown to decrease crystal growth. They are called “poisoning” agents which interact with growth sites during the process of crystallisation.

After about 15 min at 60°C

SSS

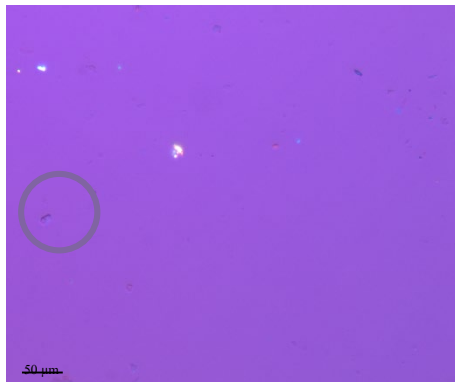


After about 21 min at 60°C  
(solidification time ≈ 8 min)

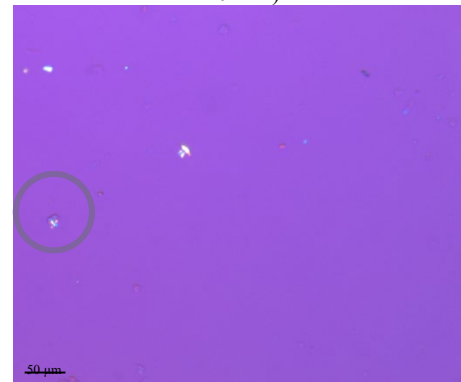


After about 15 min at 60°C

SSS-T



After about 16 min at 60°C  
(solidification time ≈ 10 min)



After about 10 min at 60°C

NBAC4-3



After about 15.5 min at 60°C  
(solidification time ≈ 24 min)

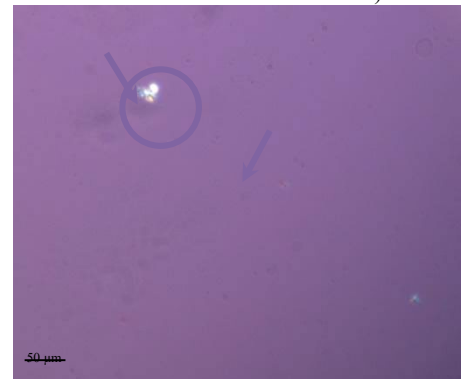


After about 10 min at 60°C

NBAC4-9



After about 39 min at 60°C  
(solidification time ≈ more than 51 min)



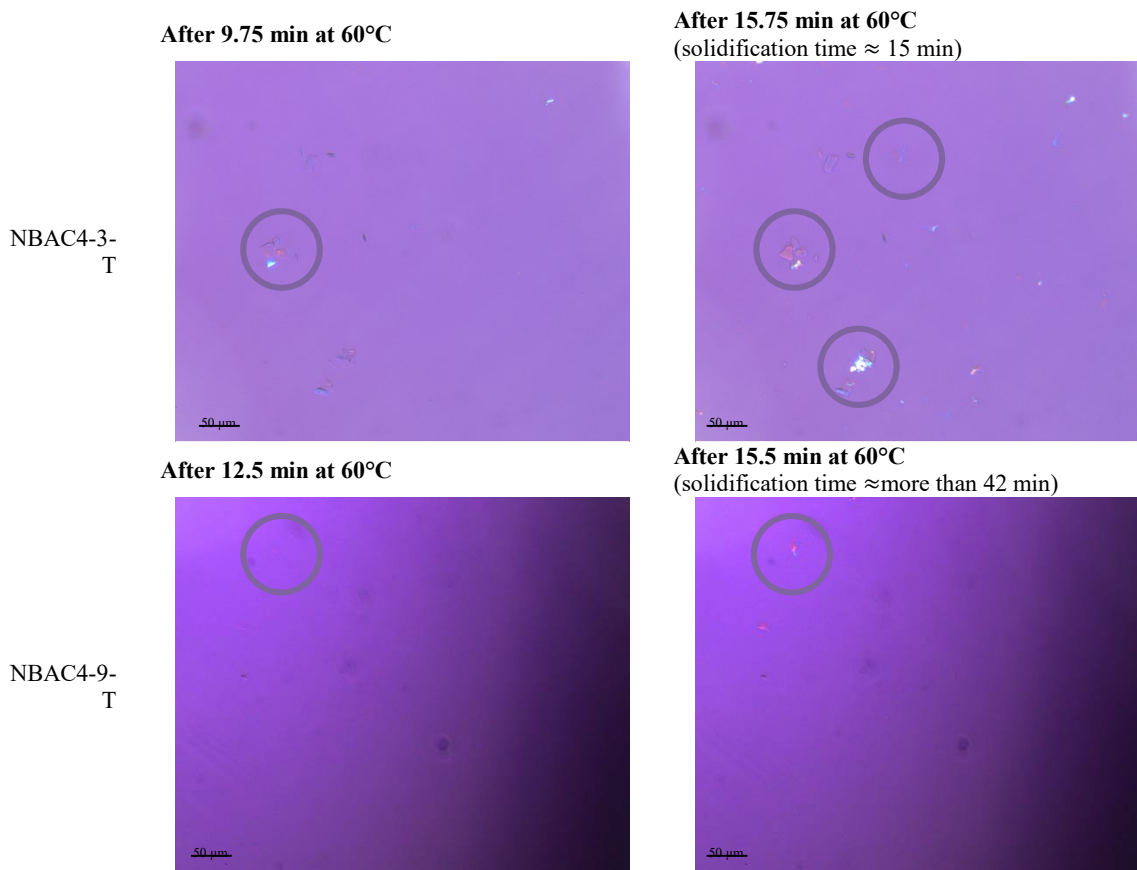


Figure 4-16. Optical observations of isothermal crystallisation for 6 representative formulations SSS, SSS-T, NBAC4-3, NBAC4-3-T, NBAC4-9, and NBAC4-9-T: images before (left) and after (right) nucleation.

In the case where both talc and surfactant combination are present, there might be an interaction. In fact, the interface for growing crystals did not appear when the nucleation started. Talc particles were also not observed at high concentration of surfactant combination. This could be due to affinity between talc and surfactant combination. Dispersed droplets of surfactant combination in the melt were supposed to adsorb onto hydrophilic surface while hydrophobic of talc particles should still be exposed for a templating effect. This hypothesis is possible by considering the closeness in induction time observed for SSS-T, NBAC4-3-T and NBAC4-9-T and discovered action mechanism of talc particles. As a consequence, the “poisoning” effect of surfactant combination was partially cancelled, which led to an increase of crystal growth and solidification kinetics in the presence of talc.

The second hypothesis that increase in melting point hints at a decrease in crystal growth rate can only be observed between one group of formulations, i.e. between SSS and SSS-T, between NBAC4-3 and NBAC3-T, NBAC4-3-T and NBAC4-9-T. Investigation of crystal growth is indispensable to compensate the studies with Crystal16®.

### 3. Conclusions

To summarise, the results of this study (**Part 1 of Chapter 4**) supported the development of a fast-screening method of lipid-additive systems using Crystal16® which allow for two types of crystallisation studies: non-isothermal and isothermal crystallisation.

The advantages of this method have been based on its higher throughput in comparison with DSC. Polymorph identification investigated with Raman spectroscopy and DSC confirmed the temperature associated with the crystallisation of a specific polymorph.

For a conclusion on solidification kinetics and crystallisation mechanisms, it is recommended to perform polarised light microscopy as a technique to investigate crystal growth, which is complementary to turbidimetry.

In particular, tristearin was chosen as a model by considering its popular use in drug formulation. The temperature of 60°C is confirmed again as the crystallisation temperature for the most stable polymorph. Except sorbitan monostearate, all the tested surfactants, binary combinations, talc, and ternary combinations were found to be nucleation inductors of  $\beta$  polymorph.

Addition of binary surfactant combination decelerated crystal growth and this effect increased with its concentration.

Talc was confirmed as  $\beta$  stabiliser for tristearin, inductor of nucleation and crystal growth. In the presence of binary surfactant combination regardless of its concentration, talc acts against their poisoning effect. Therefore, the solidification kinetics of these formulations could be improved but also crystallite size seems to be controlled.

## Part 2.

# Development of Multifunctional Tristearin-based Formulations for Hot-Melt Coating in Fluidised Bed

---

In HMC operations, traditionally, product temperature in fluidized bed is regulated at a value inferior to melting point of metastable forms ( $T_{m, \text{metastable form(s)}}$ ) to avoid agglomeration.

As for non-traditional HMC approach, operating thermal conditions are set above that  $T_{m, \text{metastable form(s)}}$ , aiming direct crystallization of the most stable polymorph.

The **second part of Chapter 4** evaluated the feasibility of non-conventional HMC approach with formulations composed of tristearin and binary additive combinations (polysorbate 20 plus sorbitan monolaurate) for the model substrate (NaCl crystals), as well as the long-term stability of coated products produced via these two coating approaches.

Within this study, new characterisation techniques were developed for each coating approach:

- On the one hand, Raman spectroscopy and atomic force microscopy were deployed to investigate the effect of binary additive combination on the transformation kinetics of tristearin and the resultant evolution of surface properties.

- On the other hand, measurements of contact angle during liquid-solid transitions were applied to explain/predict a two-step feeding rate, key to success of non-traditional HMC.

For all coated products, solid-state behaviours and release stability were monitored using X-ray powder diffraction, polarised microscopy, and release testing in simple media.

## 1. Materials and Methods

### 1.1. Materials

#### 1.1.1. Raw materials

Dynasan© 118 (tristearin, SSS) was kindly donated by IOI Oleo GmbH (Witten, Germany). Melting points of its three polymorphs  $\alpha$ ,  $\beta'$ , and  $\beta$  are given as follows:  $T_{m, \alpha} = 54.7^{\circ}\text{C}$ ,  $T_{m, \beta'} = 64.3^{\circ}\text{C}$  and  $T_{m, \beta} = 72.5^{\circ}\text{C}$ .

Montanox™ 20 Premium Pharma (polysorbate 20, PS20) and Montane™ 20 Premium Pharma (sorbitan monolaurate, SML) were provided by SEPPIC (Castres, France).

Sodium chloride (NaCl) salt crystals used as model substrate in this study, were commercially sourced (Baleine SA, Salins, France).

NaCl crystals were sieved between 400 and 630  $\mu\text{m}$ .

### 1.1.2. Tristearin-based coating compositions

The composition of the studied formulations is provided in **Table 4-2**.

NBAC4 means neutral binary additive combinations in which the ratio of PS20 and SML is 1:1.

NBAC4-3-40, NBAC4-3-60, NBAC4-9-40 and NBAC4-9-60 stand for formulations composed of tristearin and NBAC4 in ratios of 97:3% and 91:9% w/w, respectively.

The numbers 40 and 60 indicate the temperature of inlet air set in coating operations.

*Table 4-2. Lipid-based coating formulations composition*

Formulation	Excipients (% w/w)		
	SSS	PS20	SML
NBAC4-3-40	97	1.5	1.5
NBAC4-9-40	91	4.5	4.5
NBAC4-3-60	97	1.5	1.5
NBAC4-9-60	91	4.5	4.5
Controls in preformulation study			
SSS-PS20-3	97	3	-
SSS-PS20-9	91	9	-
SSS-SML-3	97	-	3
SSS-SML-9	91	-	9

## 1.2. Methods

### 1.2.1. Measurements of Melt Viscosity

The same experimental procedure already described in **Chapter 3 – Part 1** (See **Methods**) is applied.

### 1.2.2. Measurements of Contact Angle

The characterisation is adapted to tristearin-based formulations, using the same device in the previous work (**Chapter 3 – Part 1**). For each formulation, measurements ( $n = 3$ ) were performed at a temperature close to that of fluidisation temperature (i.e. 40°C and 60°C) at 5 cm as this allows for good observations of film formation in the course of liquid-solid transitions. During a measurement, the evolution of droplet was captured each in a 1- or 10-minute video at a rate of 1 frame per second. Solidification time was directly estimated from taken images.



### 1.2.3. Preparation of Coated Products

#### 1.2.3.1. Hot-Melt Coating (HMC)

HMC trials are performed using lab-scale Ventilus® fluidised bed technology (Romaco© Group, Germany). Process parameters were selected based on preliminary trials (data not presented) and are presented in **Table 4-3**. The difference lies on the specification of the inlet air ( $T_{air,f}$ ):

- $T_{air,f} = 40^{\circ}\text{C} < T_{m,\alpha}$
- $T_{air,f} = 60^{\circ}\text{C} > T_{m,\alpha}$

These two approaches were performed with pure tristearin in a study of another research group (Lopes et al., 2015). The present study was focused on the effect of additives on feasibility of those two coating approaches and stability of products generated in this way.

Except setting thermal conditions (as above) and process variables adapted to tristearin-based formulations (See **Table 4-3**), the same experimental procedure already described in **Chapter 3 – Part 1** (See **Methods**) is applied.

Table 4-3. Process parameters and their values specified for each formulation

Parameters	Values specified for each formulation	
Formulation	NBAC4-3-40, NBAC4-9-40	NBAC4-3-60, NBAC4-9-60
Reactor volume (L)	1	1
Batch size (g)	250	250
Final coating content (% w/w)	30	30
Temperature of fluidisation air (°C)	40 (setpoint)	60 (setpoint)
Quantity of process air (m <sup>3</sup> /h)	37	37
Feeding rate (g/min)	≈7	≈2 (first 7-8 min) ≈7 after that
Temperature of melt media (°C)	100	100
Temperature of feeding system (°C)	100	100
Temperature of spraying air (°C)	100	100
Pressure of spraying air (°C)	0.5	0.5

#### 1.2.3.2. Curing – a study of polymorphic transformation

This study only applies to products coated with NBAC4-3-40 and NBAC4-9-40. They are coated products generated at 40°C at which conditions the metastable form  $\alpha$  is formed. Hence, curing is an extra unit operation to convert  $\alpha$  into  $\beta$  form.

#### 1.2.3.3. In situ measurements of polymorphic transformation by Raman spectroscopy

The same experimental procedure already described in **Chapter 4 – Part 1** (See *Methods*) is applied.

Analytical plan with Raman spectroscopy was displayed in **Table 4-4**.

Table 4-4. Analytical plan for curing study with Raman spectroscopy

Coated products	Analysis timepoints during curing					
	Freshly produced	30 min after	2h after	4h after	8h after	24h after
NBAC4-3-40 NBAC4-9-40	t <sub>0</sub>	t <sub>1</sub>	t <sub>2</sub>	t <sub>3</sub>	t <sub>4</sub>	t <sub>6</sub>

#### 1.2.3.4. *In situ* evaluation of surface of the coat subject to curing by AFM

Surface of coated particles was observed using RAMAN-AFM Alpha 300 AR (WITec, Ulm, Germany) based on a microscope with a magnification of x20 and a laser of 532 nm wavelength. Topography maps were obtained using contact mode at ambient temperature and a relative humidity of 40–60%. The pyramidal cantilevers were used, with a spring constant of 0.28 N/m. Other parameters include a setpoint of 0.8-1.2, P-gain and I-gain of 6-12, driving amplitude of 2 V, times/line for 1-2 s (trace) and 1-2 s (retrace), respectively.

Measurements were carried out on three separate areas of 15 x 15 µm on the similar surface of the same sample (n = 3). The measured positions were marked with a marker to assure measurements to be conducted on the similar positions. Analytical plan with AFM was displayed in **Table 4-5**.

Table 4-5. Analytical plan for curing study with AFM

Coated products	Analysis timepoints during curing			
	Freshly produced	30 min after	2h after	22h after
NBAC4-3-40 NBAC4-9-40	t <sub>0</sub>	t <sub>2</sub>	t <sub>3</sub>	t <sub>6</sub>

#### 1.2.3.5. Stability Monitoring

Lipid-based products are often subject to curing during a certain time after production so that metastable forms freshly crystallised could be converted into stable forms and this is to assure a thermodynamic polymorphic profile over the product shelf-life thereafter.

Coated products with two formulations NBAC4-3-40, NBAC4-3-60, NBAC4-9-40 and NBAC4-9-60 generated at two temperatures are stored in a climatic chamber (Mettler, Germany) under tempering conditions of 25°C/60%RH. Analytical plan was displayed in **Table 4-6**.

Table 4-6. Analytical plan for stability study with XRPD, SEM, PLM and release testing

Coated products	Analysis timepoints		
	Freshly produced	06 weeks after	12 weeks after
All	t <sub>0</sub>	t <sub>1</sub>	t <sub>2</sub>

### 1.2.4. Product Characterisation

#### 1.2.4.1. Assay of Coating Contents

The same experimental procedure already described in **Chapter 3 – Part 1** (See **Methods**) is applied.

#### 1.2.4.2. Particle Size Distribution

The same experimental procedure already described in **Chapter 3 – Part 1** (See **Methods**) is applied.

#### 1.2.4.3. Scanning Electron Microscopy

The same experimental procedure already described in **Chapter 3 – Part 1** (See **Methods**) is applied.

#### 1.2.4.4. X-ray powder diffraction

Polymorphic identification with X-ray powder diffraction was conducted using Malvern PANalytical Empyrean with reflection applied. The device is equipped with an anticathode tube (radiation Cu K $\alpha$  ( $\lambda = 1.5418 \text{ \AA}$ )) and a detector 1Der. Diffractograms were collected using X-ray source at 45 keV and 40 mA over a  $2\theta$  range from  $2^\circ$  to  $45^\circ$  recorded at every step of  $0.033^\circ$  ( $2$ ) with an acquisition time of 160.02 s per step. The powder was filled in a sample holder and rotated at 2 s/revolution. Short d-spacing is calculated using the following expression (Schertel, Salar-Behzadi, Karrer, et al., 2021):

Equation 7 :

$$\text{Short } d - \text{spacing} = \frac{\text{order of reflection } (n) \times \text{wavelength } (\lambda)}{2 \times \sin\theta}$$

Crystallite size of tristearin  $\beta$  was estimated from the peak (003) in X-ray diffraction patterns, after being fitted with the function Pearson VII, using Scherrer's equation (D. G. Lopes et al., 2015):

Equation 8 :

$$D(003) = \frac{K \times \lambda}{FWHM \times \cos \theta}$$

where FWHM is the width in radians of the diffraction maximum measured at half-way height between background and peak, typically known as full width at half maximum (FWHM),  $\theta$  is the diffraction angle,  $\lambda$  is the X-ray wavelength (1.5418  $\text{\AA}$ ). K (Scherrer constant) is a dimensionless number that provides information about the shape of the crystal and in case of the absence of detailed shape information,  $K = 0.9$  is a good approximation for spherical geometry.

#### 1.2.4.5. Measurements of Release Kinetics

The same experimental procedure already described in **Chapter 3 – Part 1** (See **Methods**) is applied.

### 1.2.5. Analysis of Release Kinetics

Statistical method

Release profiles between two time points –  $t_0$ ,  $t_{6w}$  and  $t_{12w}$  – were compared by deploying ANOVA-based method (Yuksel, 2000) at specific time points 5, 10, 15, 30, 45 and 60 minutes of release testing. This method was chosen to assure statistical meaning due to the limited of sample number.

Model-dependent method:

Peppas-Sahlin model is used to data fit salt release kinetics during lipolysis with the objective to relate change in release kinetics (if any) to destabilisation mechanisms of solid lipid-based formulations (**Chapter 3 – Part 1 (See Methods)**).

## 2. Results and Discussion

### 2.1. Shear Viscosity

**Figure 4-17-A** shows flow curves of two formulations NBAC4-3 and NBAC4-9 in molten state measured at two temperatures – 80°C and 100°C. A shear rate range of 50-500 1/s was chosen as it might reflect the shear rate of pumping in practice (Carnicer et al., 2021). Despite stark shear, these molten formulations behave like Newtonian fluids.

Mean viscosities of NBAC4-3 and NBAC4-9 vary from 9.28 to 19.56 mPa.s and from 12.79 to 23.67 mPa.s, respectively. **Figure 4-17-B** shows the viscosity-temperature relationship at a shear rate of 50 1/s. A temperature interval of 80°C and 120°C was chosen to mimic the temperature defined for maintaining NBAC4-3 and NBAC4-9 in molten state. The temperature at the tip of pulverisation nozzle in operation which is kept heated with a spray air temperature of 100°C.

As a hypothesis, the temperature of freshly atomised melt droplets should fall within this interval. The viscosity of all formulations decreases from about 18 to 6 mPa.s with temperature increase. These graphs show that the effect of additives is neglectable, i.e. not above one order of multitude, on viscosity profile of tristearin. The measured viscosity of these mixed formulations is noticed to agree with that of tristearin reported in the literature (Valeri & Meirelles, 1997) and should respond to technical requirements for hot-melt coating.

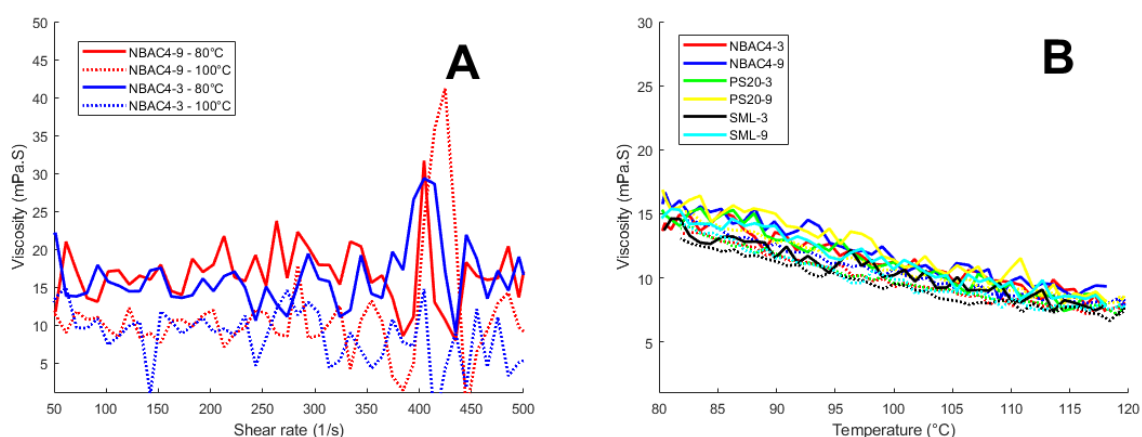


Figure 4-17. Viscosity of lipid-based formulations as a function of shear rate (A) and of temperature (B)

### 2.2. Solidification Time and Film Formation

Measurements of contact angle were performed for two ternary formulations at two thermal conditions. The principal application was to observe film formation and solidification process as adopted from a study of the same type (Kim & Ulrich, 2003). SSS was further included and served as control in terms of

solidification time lag, which could be considered from the moment where curvature of the molten droplet started to deform (See **Appendix 02**).

**Figure A.4.1** shows film formation and solidification process of NBAC4-3, NBAC4-9 and SSS on NaCl surface and the surface of the same formulation at 40°C. Both types of surfaces were investigated to observe solidification time lag under both primary and secondary nucleation, respectively.

Generally, at this temperature, three formulations all wet well both types of surface. They start to solidify few seconds later upon contact, which is indicated by the loss in transparency (change of background from white to black). As a consequence, the contact angle remains almost constant during observation time. This is the spontaneous nucleation process. The film formation was complete only 60-150 s after impingement, which is denoted by a deformation in curvature of the deposited solidified droplet. Visually, there is no significant difference observed on both types of surface in terms of solidification time lag.

**Figure A.4.2** demonstrates film formation and solidification process of NBAC4-3, NBAC4-9 and SSS on NaCl surface and the surface of the same formulation at 60°C. At this temperature, solidification did not start right after the contact. It requires a solidification time lag considered from the moment where curvature of the molten droplet starts to deform. Solidification time was estimated from this point till the moment when the film did not change anymore. The two types of surface were studied and showed significant differences in terms of solidification time lag and duration.

In the case of NaCl used as substrate surface, solidification time lag of NBAC4-3, NBAC4-9 and SSS amounts to 150 s, 300 s and 300 s, respectively. Their solidification duration was around 150 s. This is the sporadic nucleation process. Particularly, for NBAC4-3, at the end of solidification process, pieces of solidified lipid tended to detach. In the case of the formulation itself used as substrate surface, solidification time lag was all reduced to about 60 s and solidification terminated during approximately 90 s. Note that solidification time lag was only approximate. The importance is to compare apparent solidification time lag and duration between formulations in two instances – primary nucleation (spontaneous and sporadic) and secondary nucleation.

Based on the results of the first part, solidification time lag observed for NBAC4-3, NBAC4-9 and SSS agrees with their induction time obtained with polarised light microscopy. But solidification duration of NBAC4-9 observed with goniometry appeared much less than solidification time measured with polarised light microscopy but comparable to that of NBAC4-3 and SSS. This suggests that there is a remarkable effect of NaCl surface – i.e. induction of heterogeneous nucleation.

These observations on contact angle and solidification time of two formulations at two thermal conditions led us to the following statements:

- When dealing with non-traditional hot-melt coating, it is necessary to consider applying two feeding rates if primary nucleation rate is less than secondary nucleation rate. In fact, in the proof of concept of non-traditional hot-melt coating approach where the condition  $T_{air,f} > T_{m,\alpha}$  was defined, 0.5 g/min during the first 5 min and then 10 g/min were applied (D. G. Lopes et al., 2015). The first feeding rate should relate to a step to wait for nucleation to occur. Interestingly, only 5 min was set in

comparison with 20 min of induction time measured for pure SSS (Bertoni et al., 2021). This implies heterogeneous nucleation between coating and substrate surface.

- In this study, based on the current observations with hot goniometry, a two-step feeding rate was still necessary. In fact, for the hot-melt coating with NBAC4-3 and NBAC4-9 at 60°C, the feeding rate was initially set at about 2 g/min and then changed to about 7 g/min.

- Theoretically, one feeding rate is only possible if primary nucleation rate approaches secondary nucleation rate. For instance, it is the case of spontaneous nucleation where a droplet of the formulation (NBAC4-3 and NBAC4-9) was deposited on two types of surface at 40°C. This justifies the relevance of the objective to apply this hot goniometry.

- The second application of this technique is for observing the film formation process. Two mechanisms can be suggested. For spontaneous nucleation, a smooth film is supposedly constituted by deposition of droplets which well wet the surface of substrate and coated substrate and solidify momentarily. For sporadic nucleation, a rough film is supposedly formed as droplets have to spread and the solidification is time-dependent. In fact, the lipid-based formulation normally tends to contract its volume in this process (Rishoi & Sharp, 1938). Furthermore, if the formulation is not sufficiently cohesive and/or viscous, the droplet of the formulation can break into small particles before contact or splash upon contact with the surface (Wongprasert et al., 2022). This likely causes fine overproduction.

- The third application of this technique is for evaluating qualitatively adhesion of the formulation onto two types of surface. On the one hand, adhesion can be evaluated at the time of contact between the droplet and the surface of substrate or coated substrate. The more adhesive the formulation the more wetted the surface (Von Fraunhofer, 2012). On the other hand, adhesion can be evaluated after solidification. Even if the droplet well wet the surface under another influence (e.g., impact velocity) as demonstrated in Chapter 3 – Measurements of Contact Angle in Molten State, poorly adhesive material could tend to detach. This likely causes delamination.

- In this study, delamination of NBAC4-3 and NBAC4-9 was observed on the substrate surface after isothermal crystallisation. This was not observed on the surface of the formulation itself at 60°C. This was also not observed in droplet deposition on two types of surface at 40°C (the case of spontaneous nucleation). These observations imply that  $\alpha$  form is more adhesive  $\beta$  form, as suggested by another study of hot-melt coating (Woerthmann et al., 2022).

- From all the aforementioned elements, it can be said that goniometry serves several purposes. It permits evaluation of solidification, film formation and adhesion which are related to the processing-specific formulation properties (as presented in Chapter 1 – Processing-Specific Properties). The most important factor which determines these properties upon contact with the surface is the crystallisation temperature (fluidisation air temperature). Besides, one can vary the impact velocity, which reflects the definition of principal process variables (i.e. atomisation air pressure, fluidisation air flowrate and feeding rate), to verify if adjustment of these parameters can improve in the case of inadequate formulation properties.



**To conclude this part**, hot goniometry although qualitative can potentially help link formulation properties and definition of process variables to hot-melt coating performance and product quality. In fact, its relevance was shown with the traditional approach in **Chapter 3 – Measurements of Contact Angle in Molten State**. All the above observations will be considered with the results of other characterisation in the next parts.

## 2.3. Processing Performance

### 2.3.1. Yield and Process efficiency

For coating by fluidised bed, it is possible to generate products with different drug or coating contents in the same batch. This strategy was adopted as a multiple-sampling approach for HMC process and product characterisation.

Process yield for HMC with NBAC4-3-40, NBAC4-9-40, NBAC4-3-60 and NBAC4-9-60 was recorded as 97%, 96%, 94% and 92%, accordingly.

**Figure 4-18** shows coating contents of samples taken during each trial. Coating process efficiency observed for all formulations (red continuous line), approaches to 100% at the end of operation. This could also be indicated by the small difference between the theoretically calculated values (black filled squares) and the practical assay results (blue columns).

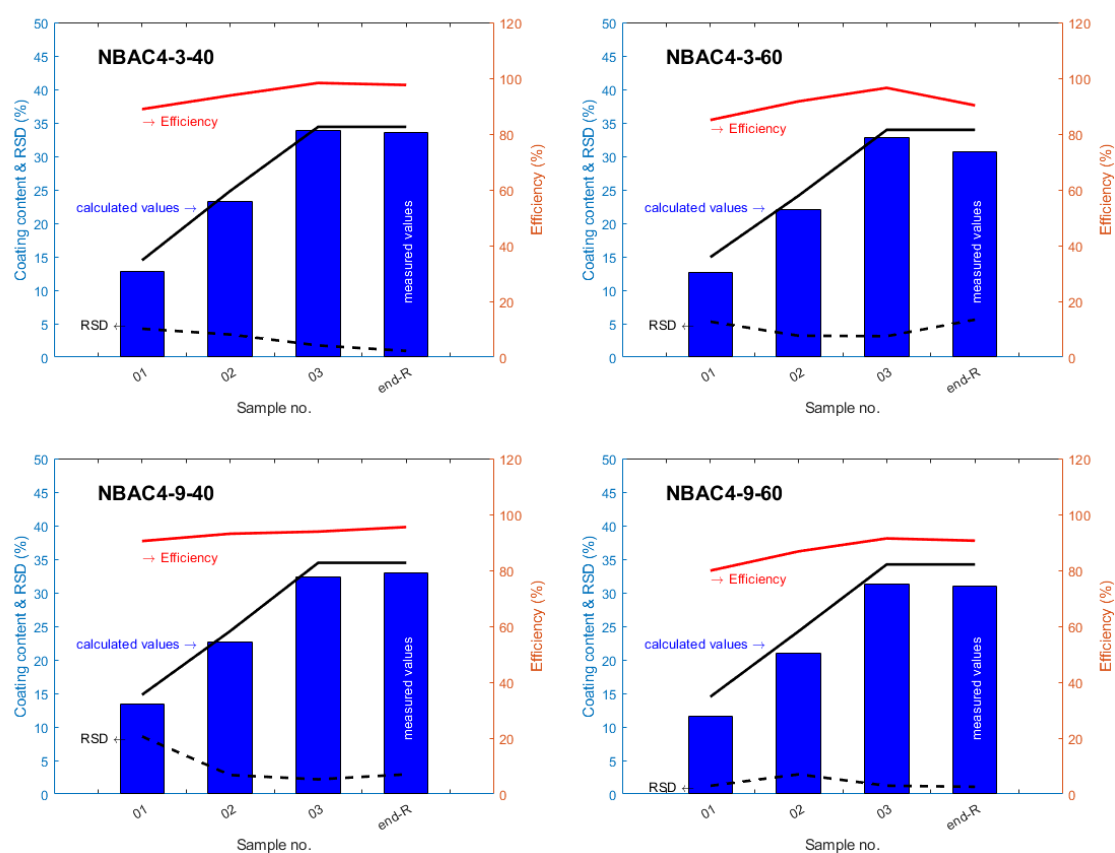


Figure 4-18. Assay of samples taken during coating trials with formulations NBAC4-3-40, NBAC4-3-60, NBAC4-9-40 and NBAC4-9-60. Sample no. 03, sample taken at the stop of feeding; end-R, sample taken while particles were still in fluidisation

The samples 03 (sample taken at the discontinuation of feeding) and end-R (sample taken while particles were still in fluidisation), shown just to verify the uniformity of sample recovery, were found similar. In general, good yield and process efficiency were obtained with two formulations regardless of thermal processing conditions.

In addition, a coefficient of variation based on assay results ( $n = 3$ ) equal to or less than 5% is considered indicating dosage uniformity with a coating content at 20% w/w (Bánfai et al., 2007). However, our previous results with beeswax-based formulations (as shown in **Chapter 3 – Measurements of Contact Angle in Molten State**) have demonstrated that  $CoV \leq 5\%$  was not a good indicator of coating completeness and homogeneity. In the continuity of this study, coating quality was then investigated directly via SEM observations and indirectly via release testing.

### 2.3.2. Identification of process regime

The process regime was analysed by interpreting PSD and its parameters  $SPAN$  and  $D_{v(90)}/D_{v(10)}$ .

**Figure 4-19** shows superimposed PSD curves expressed in volume measured for initial NaCl particles, first, second and third particles sampled during coating trials corresponding with the three assayed coating contents in the previous section. All coating operations follow the same tendency: all first PSD curves (blue lines) display a higher median peak and a narrower distribution width in comparison with those observed for initial NaCl particles.

From then on, the second and third PSD curves exhibit the inverse characteristics. This behaviour is interpreted as follows: At first a coating regime was established, and then a mixed regime (coating and agglomeration) occurred till the end of each coating operation.

In addition, fine generation was observed for two formulations processed at two thermal operational conditions. It could be due to fast solidification kinetics of tristearin. As can be seen with measurements of solidification time and film formation, low adhesiveness of  $\beta$  form of NBAC4-3 and NBAC4-9 could also be the cause.

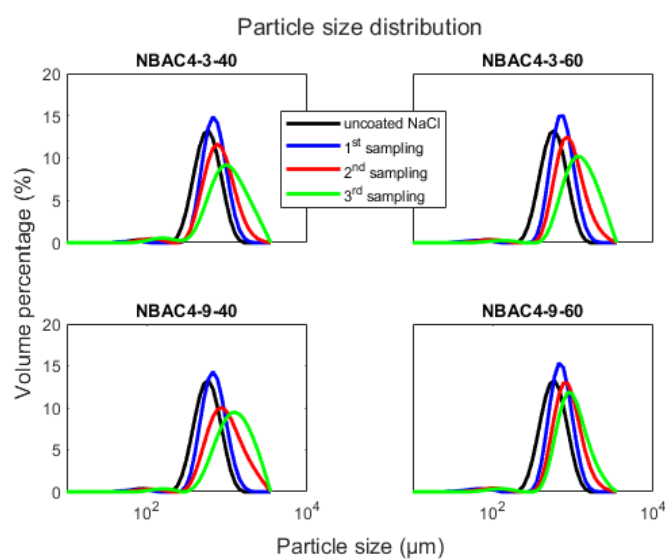


Figure 4-19. PSD in volume measured for salt particles coated with four products NBAC4-3-40, NBAC4-3-60, NBAC4-9-40 and NBAC4-9-60

The evolution of PSD parameters SPAN and  $D_{v(90)}/D_{v(10)}$ , as shown in **Figure 4-20**, corroborates with the discussion on PSD curves. In fact, an initial decrease in both SPAN and  $D_{v(90)}/D_{v(10)}$  indicates a coating regime whereas the following increasing tendency denotes a mixed regime of coating and agglomeration. These arguments agree with a hypothesis that, when a coating regime dominates, fine particles tend to gain more coating materials with time in comparison with larger particles, the width of PSD should reduce and the median peak  $D_{v(50)}$  should sharpen. In the other case, agglomeration leads to an enlargement of particle size and a rapid shift of PSD to greater class size bins.

The fact that the initial coating process was established might suggest that crystallisation of NBAC4-3 and NBAC4-9 on NaCl surface was good with the defined process variables (e.g. feeding rate). Later, agglomeration results likely from two hypotheses:

- On the one hand, the highest bed temperature of 56-57°C was documented for NBAC4-3-40 and NBAC4-9-40 and 74-76°C for NBAC4-3-60 and NBAC4-9-60, respectively. These levels of temperature approach to  $T_{m,\alpha}$  and  $T_{m,\beta}$ . The increase in product temperature is due to heat release from crystallisation of NBAC4-3 and NBAC4-9. It is possible that the coating re-melt and the coated particles tend to collide in this case.

On the other hand, an elevated thermal condition could slow down solidification kinetics of the formulation. In the case of spontaneous nucleation, nucleation and crystal growth can be Arrhenius temperature-dependent (Vyazovkin, 2020). In this case, the formulation remained in liquid state on the surface for a longer time and colliding wetted particles could agglomerate when a solid bridge was formed. Definition of a higher fluidisation air flowrate, a lower feeding rate or augmentation of the batch size are possible solutions to maintain a balance between cooling (heat removal) and wetting of the substrate particles as well as to increase particle bed density for collection of melt droplets.

For hot-melt coating at 60°C, the solidification rate of the formulation NBAC4-3 and NBAC4-9 is the limiting factor, as determined in experiments with the polarised light microscopy in Part 1 of this chapter (**Crystallisation Mechanisms Investigations**). The mechanism of agglomeration as presented above also holds true for this case. Reduction of a feeding rate is a possible solution as at the beginning with a small feeding rate a coating regime was established. However, improvement of formulation properties by adding additives could be more effective.

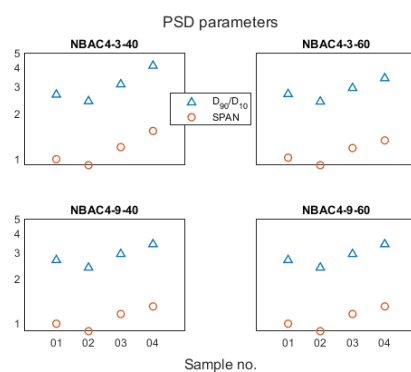


Figure 4-20. PSD parameters –  $D_{v(90)}/D_{v(10)}$  (blue triangles) and SPAN (red circles) – used to identify process regime with four products NBAC4-3-40, NBAC4-3-60, NBAC4-9-40 and NBAC4-9-60. Log scale applied for better visualisation between  $D_{v(90)}/D_{v(10)}$  and SPAN

Besides, according to preliminary trials where the bed temperature of 60°C was set as thermal setpoint, the fluctuations of inlet air temperature, below  $T_{m,\alpha}$  at times, led to simultaneous formation of  $\alpha$  and  $\beta'$  and accumulative sticking of coated particles in the reactor. The incidence could be due to slow solidification kinetics of  $\beta'$ . The level of the inlet air temperature was therefore fixed at 60°C which is the crystallisation of the polymorph  $\beta$ . This justifies for lipids whose polymorphic profile is sensible to short-term temperature exposure that the fluidisation air temperature should be the thermal setpoint.

In addition, **Figure 4-19** demonstrates the presence of fine fraction in all the samples taken in the course of coating operation for both formulations processed at two temperatures. In this case, abundant overspray also results likely from two hypotheses:

- At 40°C, fine overproduction could be due to a low viscosity of NBAC4-3 and NBAC4-9 as well as their probably poor cohesiveness (as observed with sorbitan monostearate in Chapter 3). As a consequence, finer droplets might be generated and then subject to faster cooling when travelling in the fluidisation air.

- At 60°C, slow solidification kinetics could be likely the cause of such incidence. In this case, the formulation remained in liquid state on the surface for a longer time and due to its supposedly low cohesiveness it could suffer from splashing to generate more fine particles. Furthermore, weak adhesiveness of  $\beta$  tristearin is also another contributing factor. As presented above, improvement by modification of formulation composition could be more effective.

**To conclude this part**, together with slow solidification kinetics, low viscosity, cohesiveness and adhesiveness can be said to cause a complex process regime – abundant fine generation, coating and agglomeration.

## 2.4. Coating quality

### 2.4.1. SEM images (chemical contrast mode)

**Figure 4-21** shows SEM images of particles coated with NBAC4-3 and NBAC4-9 processed at two thermal conditions. These images were taken at **chemical contrast mode**. This mode enables evaluation of coating completeness based on the interactions of chemical elements with X-ray. Higher-atomic-weight elements display a brighter aspect compared to lower-atomic-weight elements. Therefore, NaCl crystals brighten, and coated parts of these crystals darken.

As shown in **Figure 4-21**, single particles and clusters of agglomerated particles could be observed in all images, corroborating the previous observations and hypotheses that a mixed regime of coating and agglomeration was established for all the operations. There is no observed difference on the surface of coated particles before and after tempering using this mode of observation.

Defects in coating membrane observed for particles coated at 40°C could be due to incomplete coverage as well as breakage of agglomerates, considering the form of border of those particles. In the contrary, coating defects of particles coated at 60°C might be principally due to delamination resulting from low adhesiveness of  $\beta$  form and volume contraction confirmed in measurements with hot goniometry.

Besides, cracks observed on the surface (for instance, NBAC4-3-40) could be due to sudden cooling in the current practices sampling and final product recovery. Furthermore, coating with  $\alpha$  rather yields a continuously smooth surface whereas surface made of  $\beta$  form appears irregular, porous and rough. These observations are in accord with the recorded process of film formation.

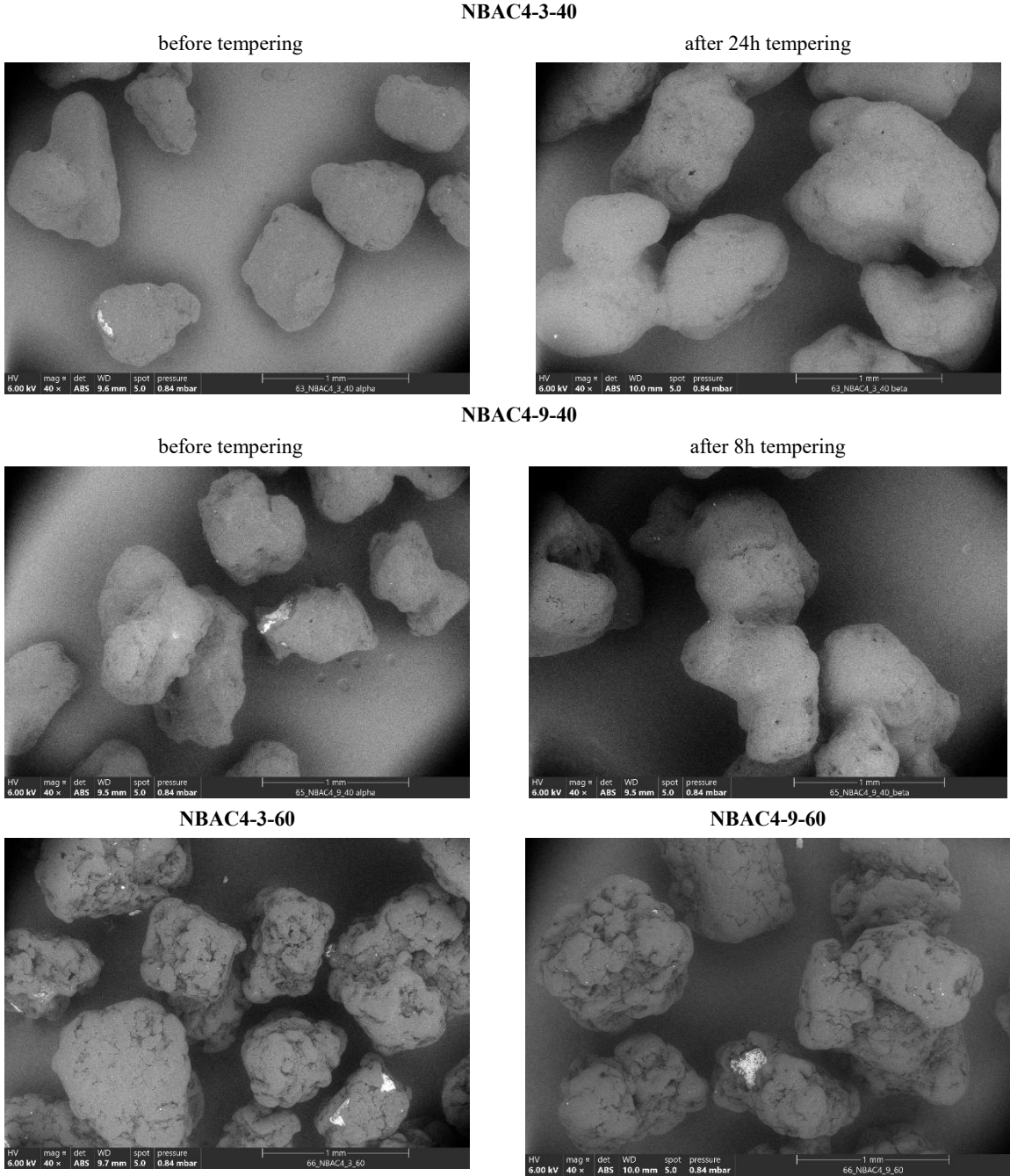


Figure 4-21. Images taken on chemical contrast mode (at length-scale of 1 mm) for particles coated with NBAC4-3-40, NBAC4-9-40 (before and after tempering), NBAC4-3-60, and NBAC4-9-60

2.4.2. SEM images (topographical contrast mode)

2.4.2.1. Case of particles coated with NBAC4-3 and NBAC4-9 at 40°C



Figure 4-22 displays SEM images, taken at **topographical contrast mode**, of particles coated with NBAC4-3 and NBAC4-9 processed at two thermal conditions.

For coated particles generated at 40°C, the crystallised polymorph of tristearin is  $\alpha$ . Coated products were then subject to tempering at 40°C in a hot even for an appropriate time depending on the concentration of binary additive combination.

The surface of both particles freshly produced looks smooth.

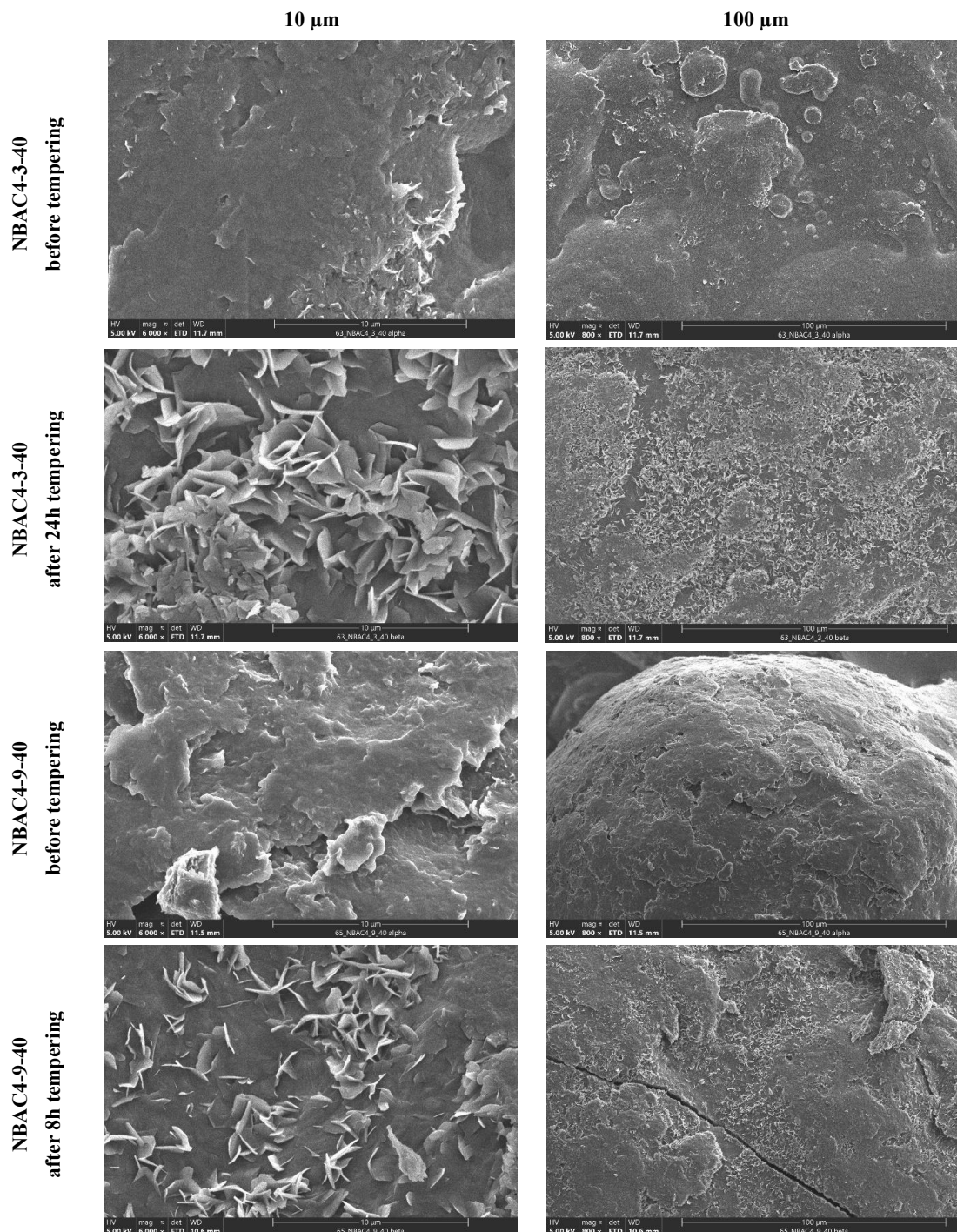


Figure 4-22. Images taken on topographical contrast mode (at length-scales of 10  $\mu\text{m}$  and 100  $\mu\text{m}$ ) for particles coated with NBAC4-3-40, NBAC4-9-40 (before and after tempering)



The surface of NBAC4-3 coated particles (after being tempered at 40°C) has developed flake-like structures which are invasive all over the surface at both scales 10 and 100 μm. This phenomenon is called lipid blooming, which has been reported in pharmaceutical research (D. G. Lopes et al., 2015; D. G. Lopes, Koutsamanis, et al., 2017; Witzleb et al., 2012). The mechanism has been reported to be tilting of triglyceride molecules during  $\alpha$ - $\beta$  transitions at the molecular level and superficial crystal growth at the macroscopic level (Delbaere et al., 2016; Khan & Craig, 2004; Mayama, 2009).

In turn, the surface of NBAC4-9 coated particles displays smaller flake-like structures which are sparsely observed at 100 μm scale. The comparison between the surface of NBAC4-3 and NBAC4-9 coated particles (both after being tempered at 40°C) suggests that higher binary additive concentration might inhibit blooming induced by polymorphic transformation to some extent. The mechanism of action could be ascribed to reduction of more surface energy when a higher additive concentration is used which acts against the Ostwald ripening process (Boistelle, 1988).

#### 2.4.2.2. Case of particles coated with NBAC4-3 and NBAC4-9 at 60°C

The surface of both freshly produced particles looks rough at the scale of 10 μm (See **Figure 4-23**). Flake-like reliefs are observed. The difference is that these are primary structures, and their thickness is obviously greater. However, at the scale of 100 μm, regions of smooth surface could be detected. The surface of coated particles generated at 60°C shows characteristics (roughness and crystallite size) like that of particles coated with pure tristearin previously reported (D. G. Lopes et al., 2015).

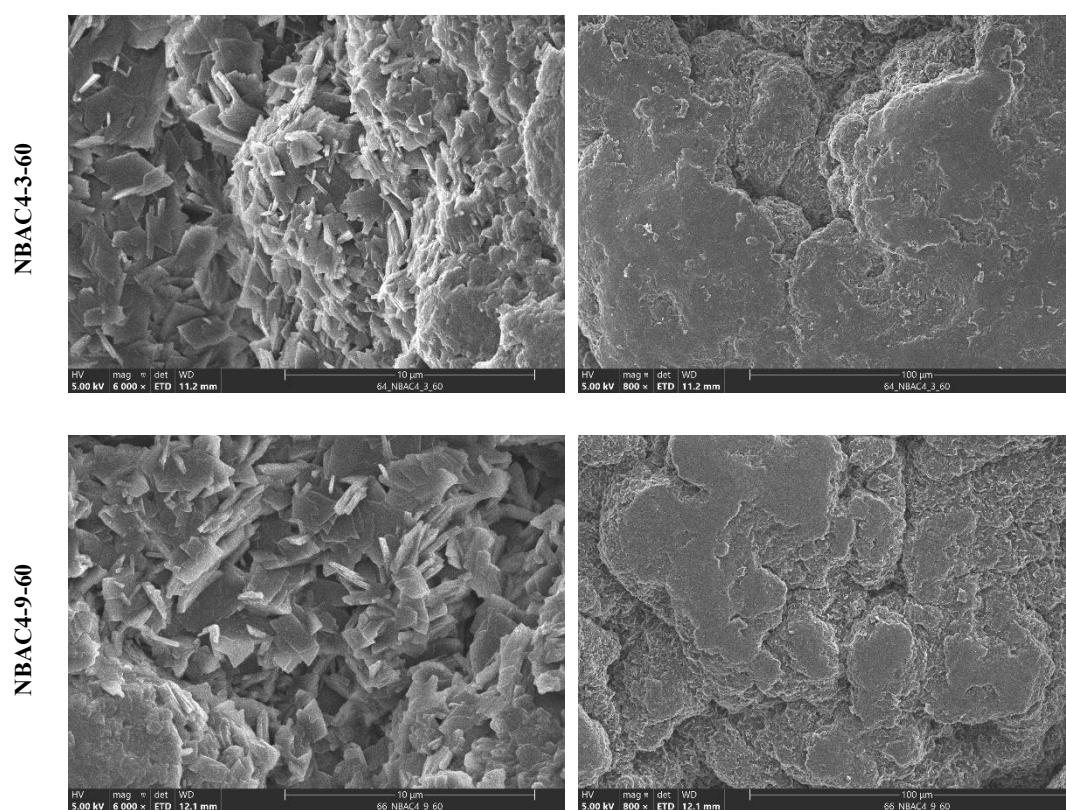


Figure 4-23. Images taken on topographical contrast mode (at length-scales of 10 μm and 100 μm) for particles coated with NBAC4-3-60, and NBAC4-9-60

### 2.4.3. Transformation Kinetics

#### 2.4.3.1. Measurements of Conversion Rate of $\alpha$ into $\beta$

RAMAN spectroscopy is a rapid, non-destructive and *in situ* available characterisation technique. It is therefore applied here to **monitor polymorphic transformation** of freshly coated samples produced at 40°C.

The course of polymorphic conversion from  $\alpha$  into  $\beta$  form of tristearin is indicated by certain characteristic peaks in RAMAN spectra: intensities at 1438 and 1460  $\text{cm}^{-1}$  ( $\text{CH}_2$  scissoring mode), presence/absence of 1728  $\text{cm}^{-1}$  (ester C=O stretching  $\text{C}_3\text{-C}_2$  gauche) and 1743  $\text{cm}^{-1}$  (ester C=O stretching  $\text{C}_3\text{-C}_2$  trans) (Motoyama, 2012; Pasquarella et al., 2023).

For spectral comparison, forms  $\alpha$  and  $\beta$  of tristearin were made in-house as follows:

- $\alpha$  form was generated by melting commercial powder tristearin ( $\beta$ ) at 100°C and letting it solidify in a silicone mould 9.5 x 2.9 cm at ambient conditions;
- For preparation of  $\beta$  form,  $\alpha$  form was then cured at 50°C during 12h following a reported procedure (Lopes et al., 2015). The smooth surface of the cured film was used for analyses.

For a better comparison between spectra of different samples, all the spectral data were normalised with the intensity of the peak at 1370  $\text{cm}^{-1}$  which was said to not to change much in polymorphic transitions (Motoyama, 2012).

Spectral data are interpreted into quantitative and qualitative approaches based on considerations of the ratio  $I_{1460}/I_{1438}$  and appearance of single or double peaks in the range of 1650-1750  $\text{cm}^{-1}$ , respectively. Considering the quantitative approach, as shown in Figure 7,  $\alpha$ - $\beta$  conversion is indicated by an evolution of  $I_{1460}/I_{1438}$  with time. According to a publication (Simpson, 1983), the values of  $I_{1460}/I_{1438}$  are 0.67, 0.58 (or 0.65) and 0.84 calculated for  $\alpha$ ,  $\beta'$  and  $\beta$ . In practice, the measured  $I_{1460}/I_{1438}$  of  $\alpha$  form is close to the published value while for  $\beta$  form there are several values of  $I_{1460}/I_{1438}$ , which are far equal to the published value.

Difference in  $I_{1460}/I_{1438}$  observed for  $\beta$  form could be ascribed to surface quality of samples (e.g., cast film, powder, coated particles) when the preparation of samples was not available in the reference article. Therefore, in this study, the endpoint of curing was considered to be the value closest to the lowest  $I_{1460}/I_{1438}$  of  $\beta$  form.

As shown in **Figure 4-24**, the ratio  $I_{1460}/I_{1438}$  initially decreases till 15-30 min after curing, then increases gradually. By considering that  $I_{1460}/I_{1438}$  of  $\alpha$  form is greater than  $I_{1460}/I_{1438}$  of  $\beta'$  form (Simpson, 1983), the transformation kinetics is presumably initiated by slow  $\alpha$ - $\beta'$  conversion and then followed by fast  $\alpha$ - $\beta$  conversion.

By considering the values of  $I_{1460}/I_{1438}$  obtained at 24h, 28h and 96h and that of commercial powder, it is reasonable to conclude that at 24h  $\alpha$ - $\beta$  transformation should be complete.

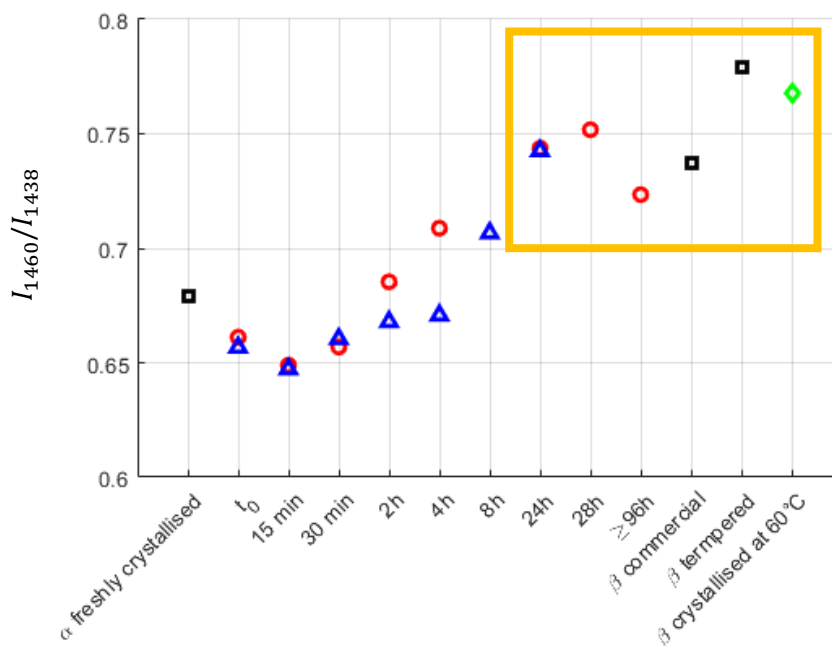


Figure 4-24. Transformation kinetics of NBAC4-3-40 indicated by evolution of  $I_{1460}/I_{1438}$  in RAMAN spectra (performed twice): NBAC4-3-40 1<sup>st</sup> time (red circles), 2<sup>nd</sup> time (blue triangles), reference values of  $\alpha$  and  $\beta$  (black squares), and NBAC4-3-60 (green diamond)

Taking a qualitative approach, RAMAN spectra obtained with NBAC4-3 and NBAC4-9 coated samples after being thermally treated at 40°C for 24h are shown in **Figure 4-25** and **Figure 4-26**, respectively. The main observations summarized from these figures are as follows:

- At lower additive concentration (NBAC4-3) a change in spectra was noticed only starting from 8h, which is indicated by a separation of two peaks in 1650-1750  $\text{cm}^{-1}$ ;
- The higher additive concentration (NBAC4-9) formulation displays earlier transitions starting from 2h.

In comparison with RAMAN spectra obtained with  $\beta$  form generated at 60°C and  $\beta$  form occurring in commercial powder, an end point of 8h where transformation should terminate could be attributed to high-additive-concentration formulation. In addition, spectral information in the low frequency region also corroborates these features in the high frequency region through an intensity shift at 113 to 140  $\text{cm}^{-1}$  at the same timepoints (Pasquarella et al., 2023).

Time to convert  $\alpha$  into  $\beta$  tristearin in the presence of additives (3% and 9% w/w) used in this study is considerable compared to 12h at 50°C (Khan & Craig, 2004) or more than 2 months at 25°C (Windbergs et al., 2009c) for pure tristearin. For tristearin combined with oil/liquid surfactants (e.g., polysorbate 80 10% w/w), tempering duration is about from 6h to 7 days at 25°C (Bertoni et al., 2021).

In this study, tempering was performed at 40°C, as a compromise for thermally sensitive substrates (e.g. amorphous solid dispersions) and for a shorter temperature-exposure time in the curing step.

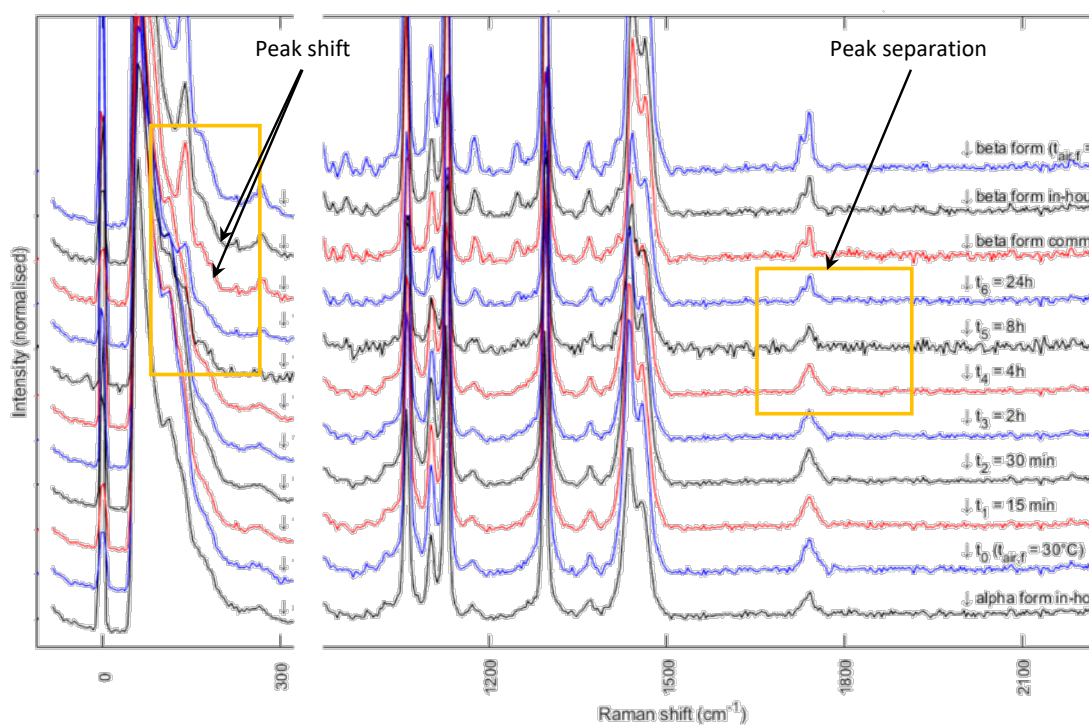


Figure 4-25. RAMAN spectra obtained for samples coated with NBAC4-3 in the course of curing at 40°C

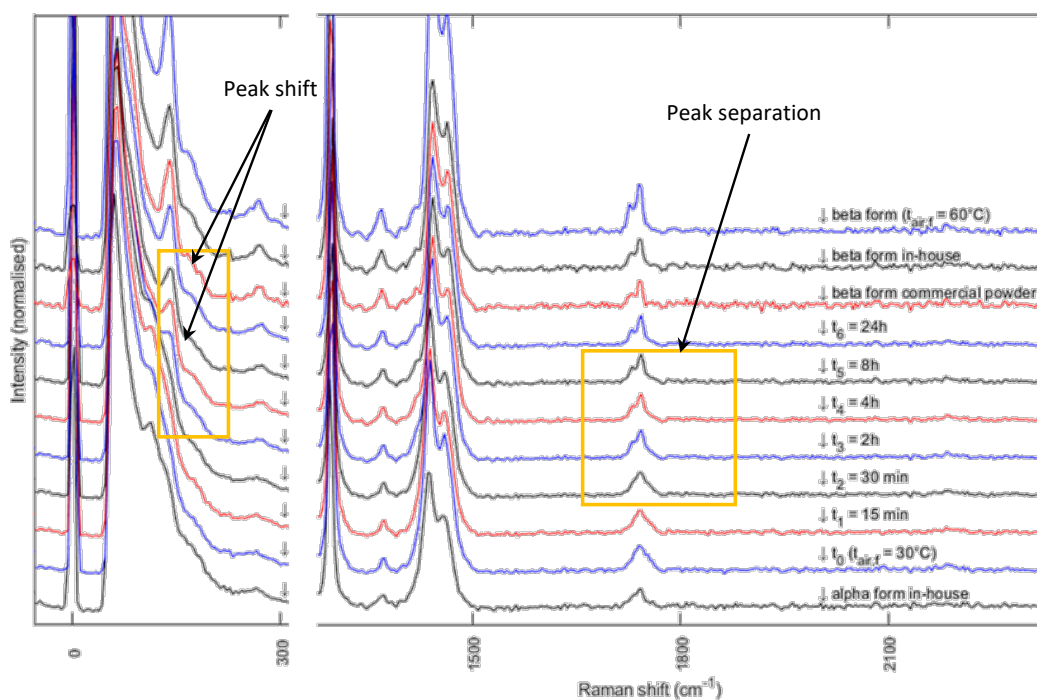


Figure 4-26. RAMAN spectra obtained for samples coated with NBAC4-9 in the course of curing at 40°C

#### 2.4.3.2. Evaluation of Coated Particles Surface

The phenomenon of lipid blooming has been scarcely monitored in pharmaceutical research but more in food research (Sonwai & Rousseau, 2008). Following the example of the cited research, AFM was



deployed in this study with the aim of monitoring **lipid blooming development** at nanometric scale. In parallel, impact of additive concentration on surface properties of coated samples subjected to tempering was evaluated via AFM.

**Figure 4-27** and **Figure 4-28** show topographical maps taken at the same area on coated samples at representative timepoints during the course of polymorphic transformation. By considering a quantitative approach, arithmetic mean height (SA) and root-mean-square (SQ) values were used as indices of rugosity (Seitavuopio et al., 2005).

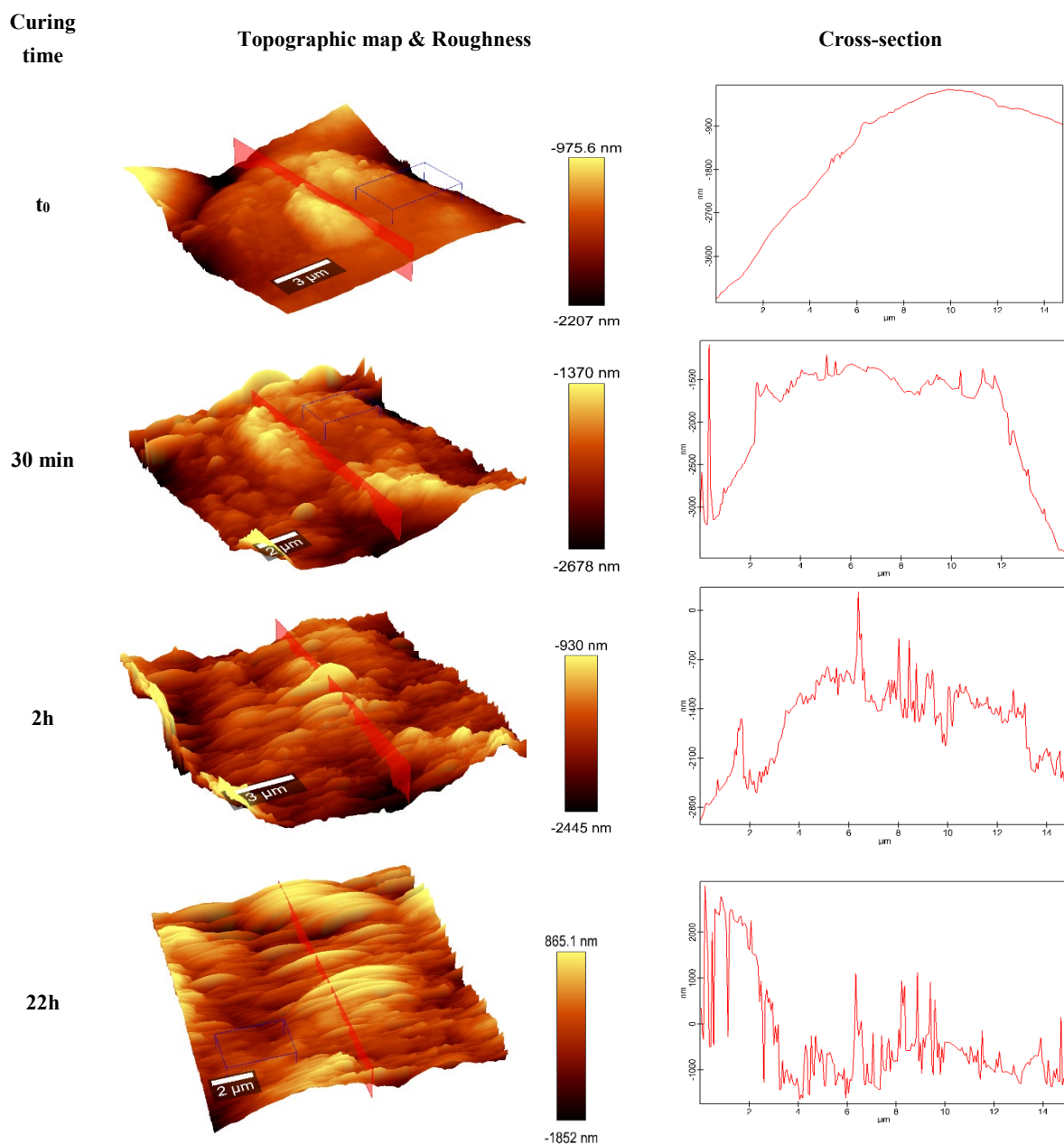


Figure 4-27. Evolution of surface properties in the course of polymorphic transformation of NBAC4-3

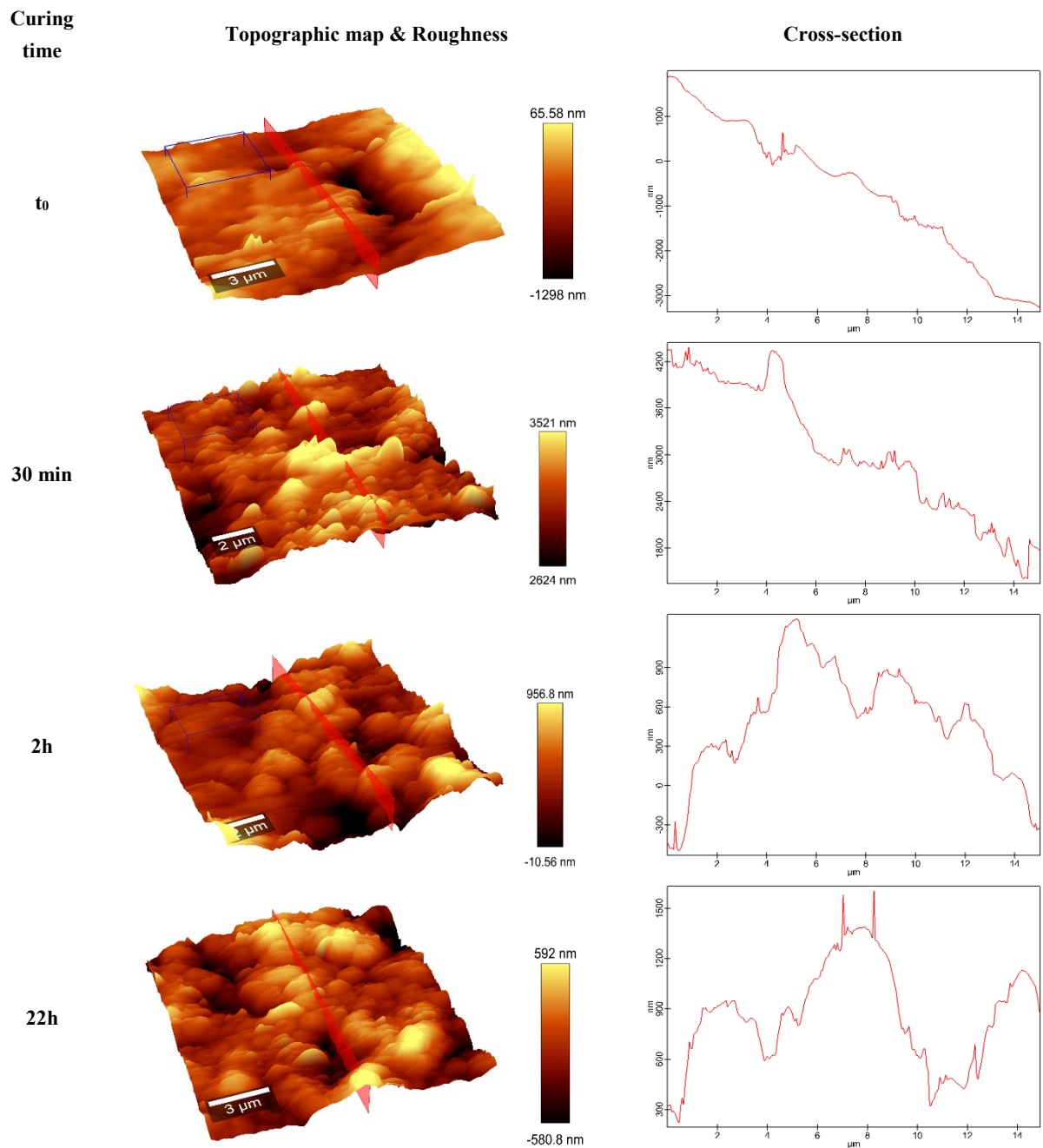


Figure 4-28. Evolution of surface properties in the course of polymorphic transformation of NBAC4-9

From a quantitative approach, **an evolution of (SA, SQ) values** was reported as follows:

- (SA, SQ) for NBAC4-3-40 increases remarkably at 22h, as this timepoint was close to the end curing time concluded in the previous section: (188.5 nm, 249.7 nm) at  $t_0$ , (215.6 nm, 283.3 nm) at 30 min, (228.8 nm, 295.9 nm) at 2h and (416.0 nm, 534.8 nm) at 22h.
- (SA, SQ) for NBAC4-9-40 appears smaller, decreases during the following 2h and then increases at 22h and this timepoint surpassed its defined curing time of 8h: (191.0 nm, 255.4 nm) at  $t_0$ , (127.6 nm, 172.5 nm) at 30 min, (143.1 nm, 188.0 nm) at 2h and (361.0 nm, 458.1 nm) at 22h.



The increase in (SA, SQ) indicates an increase in roughness of the coated surface and these values appear comparable. However, by considering a qualitative, cross-sections of analysed surface area (Figure 4-27 and Figure 4-28) demonstrate better the impact of additives on surface of coated samples, as discussed below:

- At the lower additive concentration (for NBAC4-3-40), from 30 min to 22h, the surface appears to develop a discontinuity with alternating crests and valleys. This agrees with observations of flake-like structures via scanning electron microscopy (SEM) at the same scale of 2  $\mu\text{m}$  for pure tristearin as reported in the literature (D. G. Lopes et al., 2015; D. G. Lopes, Koutsamanis, et al., 2017).
- At the higher additive concentration (for NBAC4-9-40), the surface seems to remain rather smooth throughout analysis time. This is also in agreement with one SEM observation obtained with a tristearin-based formulation containing polysorbate 80 10% w/w after curing and storage over one year at 25°C also reported in the literature (Bertoni et al., 2021).

AFM topographical maps measured at 22h agree with SEM observations performed on tempered coated particles during 24h and 8h for NBAC4-3-40 and NBAC4-9-40. It would be reasonable to say that the higher additive concentration could stabilise surface properties of coated samples undergoing tempering at 40°C up to 22h. In fact, polysorbates, sorbitans and their combinations were reported to be used as anti-blooming agents in food research (Delbaere et al., 2016).

These observations of ADM agree with those of SEM in the fact that less lipid blooming was developed for NBAC4-9 than NBAC4-3 after curing.

## 2.5. Stability monitoring of coated products

### 2.5.1. Polymorphic Identification and Crystal Microstructure Characterisation

#### 2.5.1.1. *X-ray powder diffraction*

X-ray powder diffraction was performed to acquire both types of information - **polymorphic identification and crystallite size** – using long and short d-spacings in the wide and small angle regions, respectively.

Figure 4-29 and Figure 4-30 show wide- and small-angle X-ray diffraction patterns obtained from four samples in the stability study over 3 months at 25°C/60% relative humidity. In general, wide-angle X-ray diffraction patterns are similar for all products in terms of characteristic peaks at about 19.4°, 23.0° and 24.0°  $2\theta$ . After a conversion, short d-spacings of 0.46 nm, 0.39 nm and 0.37 nm indicate the occurrence of the polymorph  $\beta$ . These findings agree with data reported in the literature (J. S. Aronhime et al., 1987).

From small-angle X-ray diffraction, patterns peak (003) was identified around 5.80-5.90°  $2\theta$  which also **corresponds with d-spacing of  $\beta$  tristearin** (Bertoni et al., 2021).

Using  $d = 46 \text{ \AA}$  as a lamellar thickness (D. G. Lopes et al., 2015), the number of stacked lamellas for a crystallite was estimated and given in Table 4-7. Note that the obtained value represents the mean size

of the whole crystallites of crystal network (Den Adel et al., 2018) and the estimated values are approximate to demonstrate product stability. For more precise estimation, measurements should be performed with a transmission mode using a capillary configuration. Crystallite size obtained for coated products generated at 40°C in this study is similar to that of cured samples coated with pure tristearin at 25°C given in the literature (D. G. Lopes et al., 2015).

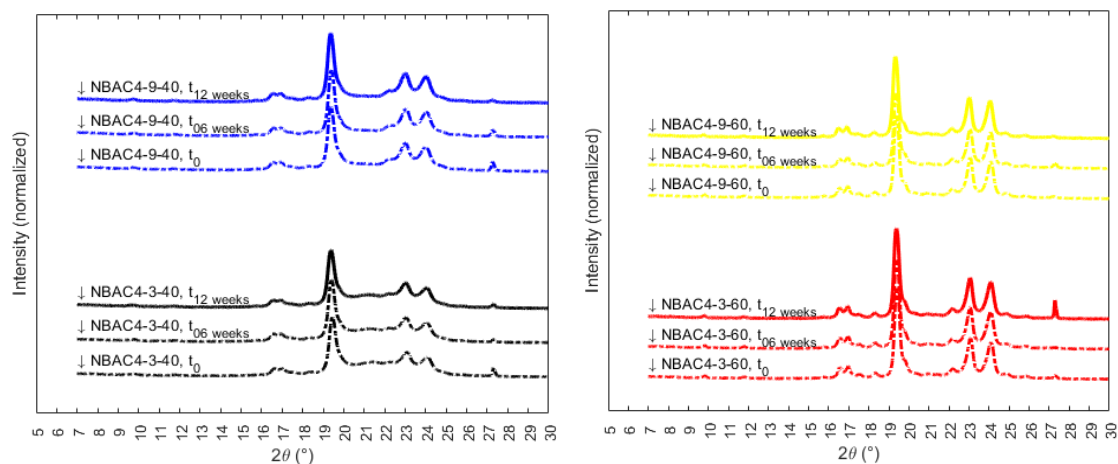


Figure 4-29. Wide-angle X-ray diffraction patterns obtained for 2 formulations processed at 2 thermal conditions over stability study period

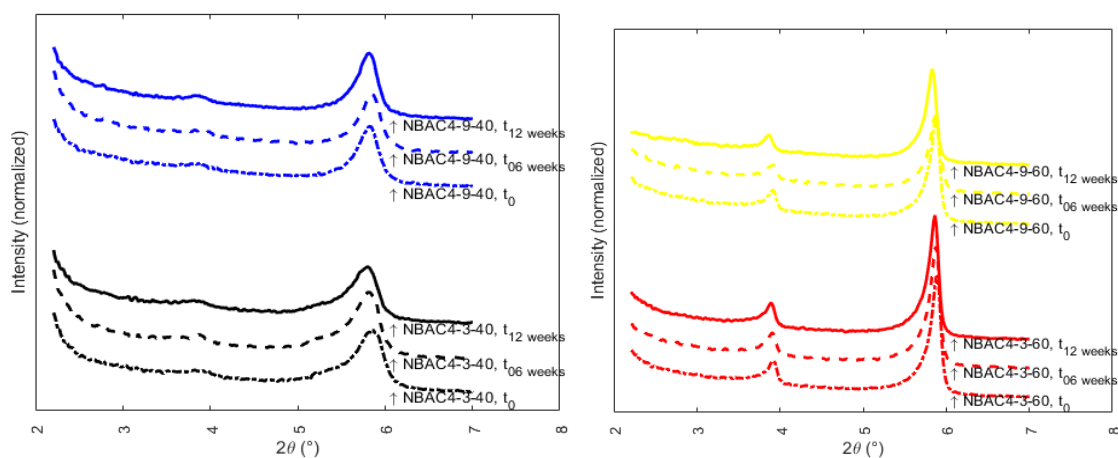


Figure 4-30. Small-angle X-ray diffraction patterns obtained for 2 formulations processed at 2 thermal conditions over stability study period

From **Table 4-7** it can also be observed that crystallite size estimated for coated products generated at 60°C was found two- or three-fold larger and even than the value obtained for samples coated with pure tristearin at the same temperature (D. G. Lopes et al., 2015). Firstly, this might explain the difference in thickness of flake-like structures observed via SEM for each formulation processed at two levels of temperature. Secondly, adding surfactants were shown to slow down growth rate of tristearin (See **Crystallisation Mechanisms Investigations** in the first part). As a consequence, higher crystallite size developed during isothermal crystallisation should be expected for formulations composed of SSS and

surfactants in comparison with pure SSS. In definitive, crystallite size and number of stacked lamellas did not vary significantly during 3 months.

Table 4-7. Estimated crystallite size and number of stacked lamellas in each crystallite

Formulation		Crystallite size (Å)	Stacking no. of lamellas <sup>#</sup>
NBAC4-3-40	t <sub>0</sub>	223	5
	t <sub>1</sub>	237	5
	t <sub>2</sub>	234	5
NBAC4-3-60	t <sub>0</sub>	840	18
	t <sub>1</sub>	844	18
	t <sub>2</sub>	882	19
NBAC4-9-40	t <sub>0</sub>	342	7
	t <sub>1</sub>	353	8
	t <sub>2</sub>	355	8
NBAC4-9-60	t <sub>0</sub>	842	18
	t <sub>1</sub>	748	16
	t <sub>2</sub>	864	19

<sup>#</sup>Rounded values were shown.

#### 2.5.1.2. Polarised light microscopy

As a complement test for stability study, polarised optical images were generated and observed in the interval of 6 weeks.

**Figure 4-31**, **Figure 4-32** and **Figure 4-33** show polarised optical images obtained for **SSS**, **NBAC4-3** and **NBAC4-9** prepared at 40°C (left) and 60°C (right) observed over three months. In all the images, there are disordered spherulites with strong birefringent patterns (Oh et al., 2002).  $\beta$  form should be the main polymorph observed as the samples were prepared under thermal conditions like those set in coating operations.

In the case of **SSS** (**Figure 4-31**), crystal size and number differ for those generated at 40°C and 60°C. These observations agree with those obtained in studies with tristearin (Oh et al., 2002; R. C. D. Silva et al., 2016). With time, converted  $\beta$  form appears to expand horizontally and its contrast becomes more and more important. This might suggest an increase in crystallite size.

In the contrary, directly crystallised  $\beta$  form exhibits no significant change over observation time and all images show a high contrast of crystals. These observations with pure tristearin serve as control for explaining results obtained for NBAC4-3 and NBAC4-9.

In the case of **NBAC4-3** (**Figure 4-32**), crystals formed at 40°C exhibit various sizes and their contrast appears more important than those observed for pure converted SSS. Qualitatively, their size distribution and their contrast did not change significantly. This corroborates the crystallite size via XRPD in small angle region. These observations hint at a possible effect of binary additive combination on density of crystal network.

Considering  $\beta$  crystals directly formed at 60°C (**Figure 4-32 – NBAC4-3-60**), it was difficult to observe as they should be arranged in such a direction where they become almost extinct under polarised light. The principles of the application of polarised light microscopy work for anisotropic materials such as



lipids (Nyqvist, 1993). However, the second image (6 weeks) shows almost some birefringent crystals whose size is similar.

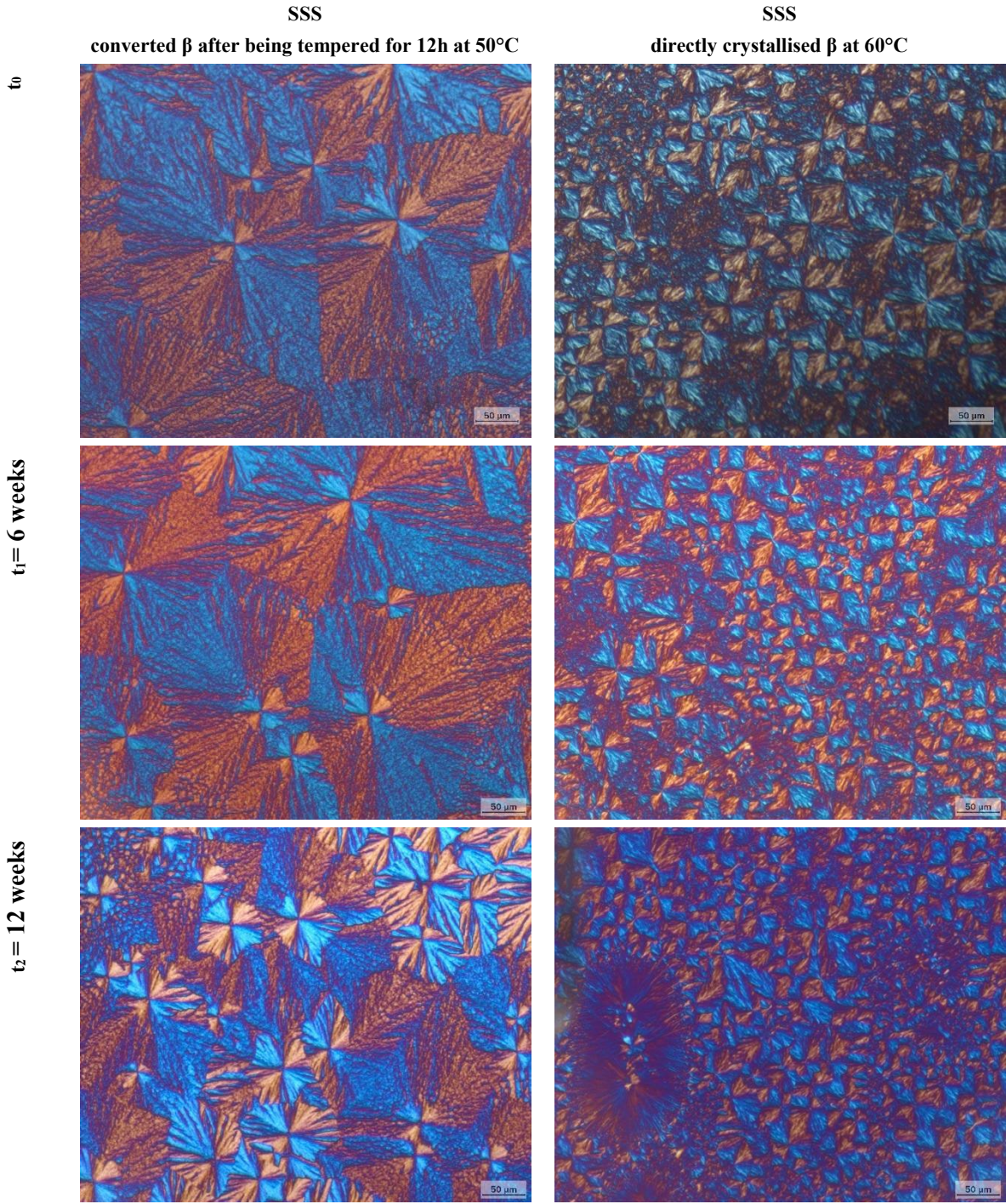


Figure 4-31. Polarised optical images of *tristearin* (converted  $\beta$ ) after being tempered at 50°C for 12h (left column) and *tristearin* (directly crystallised  $\beta$ ) directly crystallised at 60°C (right column)



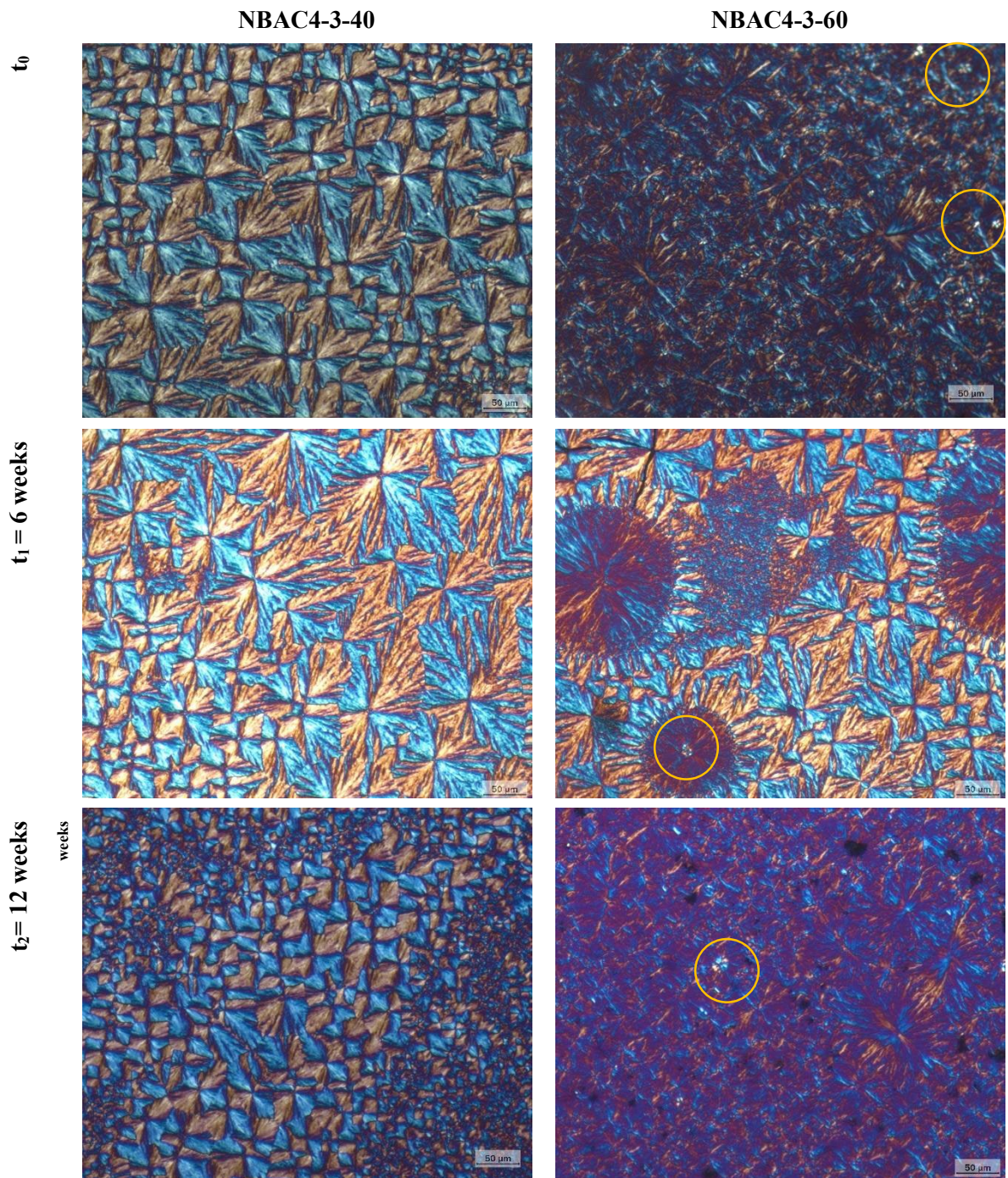


Figure 4-32. Polarised optical images of NBAC4-3-40 (converted  $\beta$ ) after being tempered at 40°C for 24h (left column) and NBAC4-3-60 (directly crystallised  $\beta$ ) directly crystallised at 60°C (right column)

In comparison with the image of NBAC3-40 obtained on the same date (Figure 4-32 – NBAC4-3-40), the only difference in brightness of crystals might explain the observed difference in crystallite size estimated. Small flower-like features (indicated in orange circles) can be observed in the middle of polarised light-extinct crystals. In fact, these features were supposed to be interface which acts a nucleation site in isothermal crystallisation (See **Crystallisation Mechanisms Investigations** in the first part).



In the case of NBAC4-9 (Figure 4-33), crystals formed at 40°C (NBAC4-9-40) exhibit an apparently even size distribution and their size appears larger than those observed for NBAC4-3-40 (Figure 4-32). This might be the consequence of decelerated crystal growth rate under the effect of higher additive concentration. Their size appeared not to change significantly with time and this hint at the expected effect of this combination of two surfactants to stabilise the density of crystal network against the Ostwald ripening process (Boistelle, 1988).

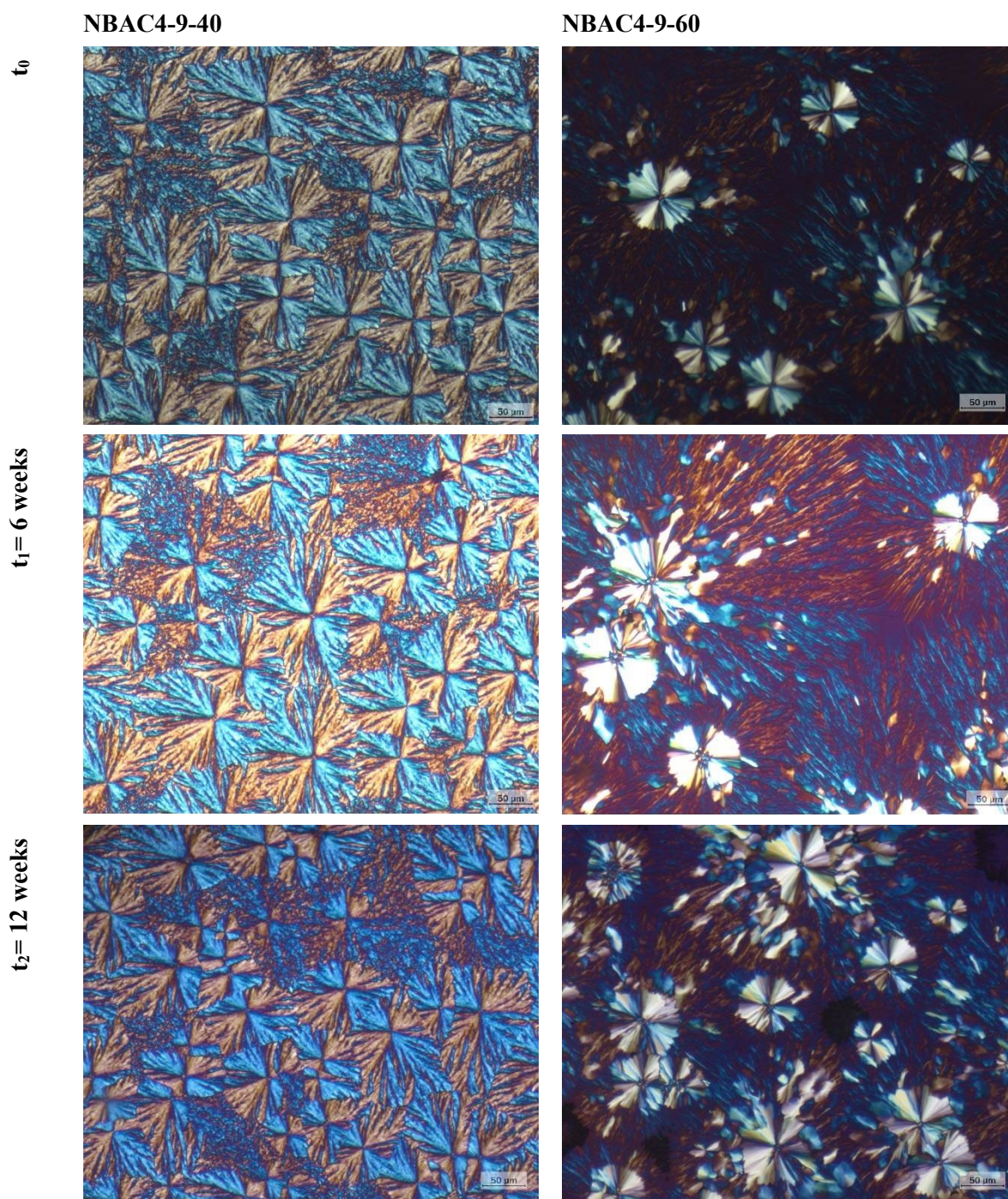


Figure 4-33. Polarised optical images of NBAC4-9-40 ( $\alpha$ - $\beta$ ) after being tempered at 40°C for 24h (left column) and NBAC4-9-60 ( $\beta$ ) directly crystallised at 60°C (right column)



Considering  $\beta$  crystals directly formed at 60°C (**Figure 4-33-NBAC4-9-60**), most crystals were not extinct in all the images acquired. As a first remark, their crystal size appears clearer and larger but uneven in comparison with NBAC4-3-60 (**Figure 4-32**). As a second remark, larger flower-like features can also be observed in the middle of each crystal unit which is birefringent under polarised light. Again, as already discussed (See **Crystallisation Mechanisms Investigations** in the first part), this might be attributed to the interface formed in the presence of surfactant combination serving as template for nucleation. These features indicate probably the trapping site of additives in crystal network of tristearin. In general, the size of both structures also did not change significantly with time and this agrees with the estimated values of crystallite size via XRPD in small angle region. This confirms the effect of surfactant combination at higher concentration against the Ostwald ripening process (Boistelle, 1988).

### 2.5.2. Salt Release Kinetics

Measurements of salt release kinetics were performed **not only to relate to physical changes in coating membrane in stability study but also, they represent themselves a technique to investigate phase separation in the formulation** (as stated in **Chapter 3 – Release kinetics**). The other objective was to attribute a pharmacokinetic property (e.g. immediate release, prolonged release) to each product based on its release profile.

**Figure 4-34** shows comparative dissolution profile of products coated obtained for two formulations (NBAC4-3 and NBAC4-9) processed at two thermal conditions over 12 weeks. Their coating contents are close: 33.8% NBAC4-3-40, 32.8% NBAC4-3-60, 32.3% NBAC4-9-40, and 31.3% NBAC4-9-60.

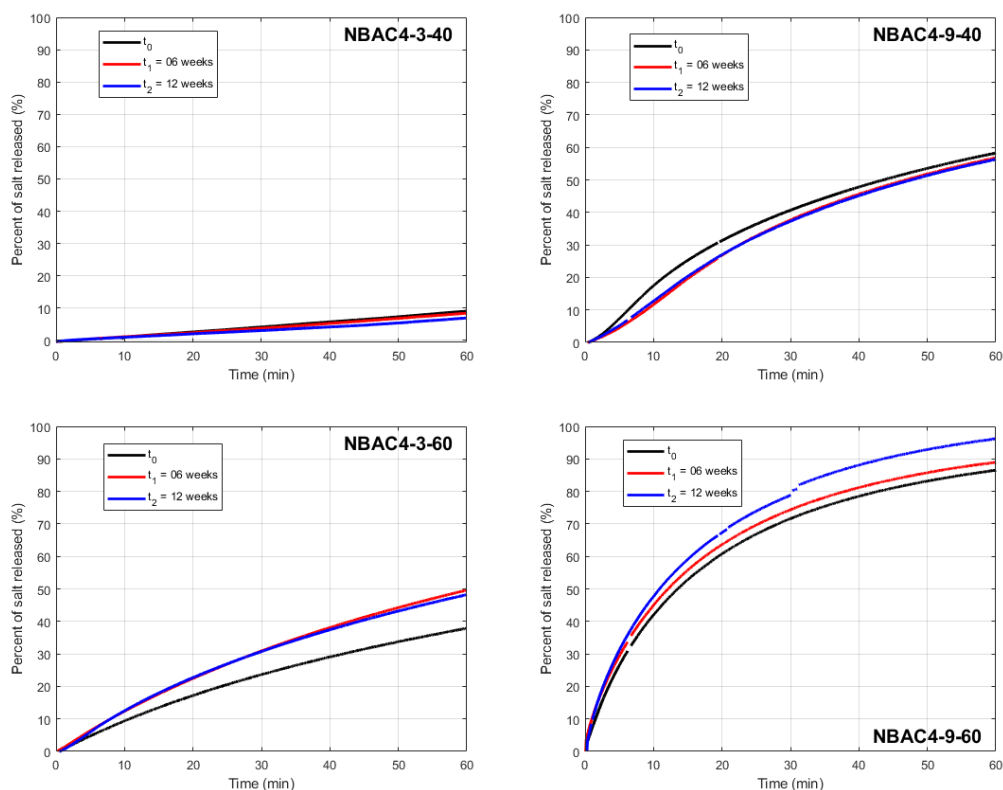


Figure 4-34. Comparative dissolution profile of products coated obtained for two formulations (NBAC4-3 and NBAC4-9) processed at 2 thermal conditions over stability study period.

At the same processing conditions, formulation comprising the higher additive concentration yields faster release profile in terms of percentage of salt dissolved:

- NBAC4-3-40 (about 10%) vs. NBAC4-9-40 (about 60%) at 1h;
- NBAC4-3-60 (about 40%) vs. NBAC4-9-60 (about 85%) at  $t_0$ .

Considering the same formulation processed at two temperatures, products generated at high temperature, i.e. with directly crystallised  $\beta$  form, exhibit faster salt release. This is controversial as due to denser crystal network products coated with directly crystallised  $\beta$  form should release active substance slower than those coated with converted  $\beta$  form (Lopes et al., 2015). Higher occurrence of coating defects observed with SEM for coated products generated at 60°C might justify these findings. In addition, particularly rough morphology of directly crystallised  $\beta$  form coating membrane might be a contributing factor. As a result, unexpected **immediate release profile** was noticed for NBAC4-9-60 whereas all three other cases yield **prolonged salt release**.

From a **stability point of view**, **Figure 4-34** also shows that:

- Salt release from coated products generated at 40°C slightly reduces with time and this might be due to continuous crystal growth of  $\beta$  triglyceride under Ostwald ripening effect in bulk (Schertel, Salar-Behzadi, Karrer, et al., 2021) and/or on surface (Mayama, 2009).
- On the contrary, the inverse tendency is noticed for salt release from those produced at 60°C. Although density of crystal network seems to be stabilised from the time of production, microphase separation could be the cause in this case (D. G. Lopes, Koutsamanis, et al., 2017).

However, all products exhibit relatively stable release profile monitored during three months at 25°C/60% relative humidity, which is indicated by two-sample t-test at 5% significance level. In the future, it is advisable to increase the number of tests to check with  $f_2$  factor calculation.

By comparing the current release testing results with a recent study, caffeine-loaded microspheres whose matrix was constituted by tristearin and one lipophilic lipid at 90:10 show that all their release profile displayed minor changes (all  $f_2 > 50$ ) (Bertoni et al., 2021). Despite the difference in product structure, i.e. microspheres vs. microcapsules, it is reasonable to conclude that NBAC4-3 and NBAC4-9 yield a relatively stable release profile to products produced at 40°C.

To further assess theoretically release mechanisms, the empiric model – Peppas-Sahlin was applied to fit dissolution data and estimated release parameters were given in **Table 4-8**.

For NBAC4-3-40 and NBAC4-3-60 coated products generated at 40°C, salt release mechanisms appear to change, as indicated by the variations of the release exponent “m”. Considering the faster release of salt from NBAC4-3-60 over 3 months, the possible explanation could be that lipid-based coating would relax more in the water. For the slight change (reduction) on salt release from NBAC4-3-40, the hypothesis more plausible could be a reduction of water penetration over 3 months (even if not too impacting), as in this case continuous development of lipid blooming could be expected.

Table 4-8. Estimated release parameters for dissolution of coated salt obtained for two formulations (NBAC4-3 and NBAC4-9) processed at 2 thermal conditions over stability study period

Formulation	Observation	Peppas-Sahlin			
	time	$k_D$ (h <sup>-m</sup> )	m	$k_{R-E}$ (h <sup>-m</sup> )	R <sup>2</sup>
NBAC4-3-40	t <sub>0</sub>	0.091	1.142	9.36e-13	0.999
	12 weeks	0.047	0.924	0.021	0.999
NBAC4-9-40	t <sub>0</sub>	0.389	0.758	3.14e-14	0.997
	12 weeks	0.497	0.735	6.86e-09	0.995
NBAC4-3-60	t <sub>0</sub>	0.684	0.759	4.76e-10	0.986
	12 weeks	0.743	0.963	3.26e-13	0.993
NBAC4-9-60	t <sub>0</sub>	1.648	0.744	2.95e-09	0.998
	12 weeks	1.820	0.715	8.96e-09	0.995

For NBAC4-9-40 and NBAC4-9-60 coated products generated at 60°C, salt release mechanism seems to remain unchanged, considering the very slight variation of release exponent “m”. On the one hand, release of salt from NBAC4-9-40 coated products tended to decrease during the first 6 weeks and then did not change significantly up to 12 weeks. The initial change might be due to a continuous development of lipid blooming on the surface of coated particles. Note that despite an effect of anti-blooming it is possible that bloom was just retarded or slowed down as observed with beeswax-based formulations in **Chapter 3 – Part 2**. As blooming can be said to related to Ostwald ripening, this process seems more important on the surface than in the bulk in this case.

Concerning both NBAC4-9-60 and NBAC4-3-60 coated products, salt release tended to accelerate over 3 months. In this case, normal solid-state behaviours (e.g., polymorphism, lipid blooming and increase in crystal size distribution induced by Ostwald ripening, phase separation) should have limited influence with the application of non-traditional hot-melt coating approach. One possible reason relates to coating defects and poor adhesiveness of  $\beta$  tristearin. As certain salt particles were observed not to be completely coated, the open coating membrane might continue to delaminate, which facilitate salt dissolution. **Generally, release rate of all coated products did not change beyond an order of magnitude after three months of storage.**

### 3. Conclusions

**In summary**, this study (**part 2**) showed successful application of both traditional and non-traditional hot-melt coating approaches using formulations composed of **tristearin and binary additive combination (polysorbate 20 plus sorbitan monolaurate 1:1) at ratios of 97:3 and 91:9.**

For traditional HMC approach, Raman spectroscopy and AFM were developed for monitoring  $\alpha$ - $\beta$  conversion kinetics and crystal growth on the surface induced by polymorphic transitions. Addition of surfactant combination was found to facilitate the  $\alpha$ - $\beta$  conversion at both concentrations and higher additive concentration yielded an anti-blooming effect. A curing time could be concluded for each formulation.

For non-traditional HMC approach, hot goniometry appears to be a perfect technique to evaluate hot-melt coating formulations. It is useful not only for aiding in definition of process variables (e.g.,

fluidisation air temperature, feeding rate) but also for predicting coating quality (e.g., film formation). In fact, in this study, any issues with process performance and coating quality, especially concerning coating at high temperature, can be linked to challenging formulation properties (e.g., slow solidification, low viscosity, poor adhesiveness) of  $\beta$  tristearin combined with two surfactants. Improvement by modification of coating composition should be more effective than adjustment of process variables as the lowest crystallisation temperature for  $\beta$  crystallisation should be fixed at 60°C.

Regarding the impact of both coating approaches on release properties, release profile of all products is relatively stable over three months. With a strategy to formulate tristearin with blend of hydrophilic and lipophilic surfactants, it was possible to control initial polymorphism and to stabilise long-term crystal size distribution in crystal network regardless of thermal processing conditions. This study shows the combination of two surfactants whose lipophilicity and hydrophilicity are complementary and the direct  $\beta$  crystallisation represents two strategies to stabilise solid lipid-based coated formulations. However, coating defects led to faster salt release kinetics from coated particles generated at 60°C than expected and are suspected to cause a slight increase in release kinetics.

## Chapter 5.

# EFFECT OF TALC AND VITAMIN E TPGS ON MANUFACTURABILITY, STABILITY AND RELEASE PROPERTIES OF TRILAURIN-BASED FORMULATIONS FOR HOT-MELT COATING

---

### General Introduction

This chapter is focused on one particular case of hot-melt coating with **trilaurin – a medium-chain monoacid glyceride**.

The challenge resides in the fact that its melting profile is relatively low: 15.6°C ( $T_{m,\alpha}$ ), 35.1°C ( $T_{m,\beta'}$ ) and 45.7°C ( $T_{m,\beta}$ ). It concerns not only its processability but also stability and release properties imparted on NaCl crystals as substrate model.

From a material perspective, processability of trilaurin relates principally to its solidification properties which were evaluated via turbidimetry, calorimetry, goniometry during liquid-solid phase transition and polarised light microscopy in preformulation.

From a process perspective, the only possibility to generate products coated with formulations composed of trilaurin was to set thermal operational conditions above  $T_{m,\alpha}$ . Samples were then analysed to investigate processing performance, coating quality, stability and release properties of products encapsulated with three selected formulations: **(i) trilaurin, (ii) trilaurin plus talc, (iii) trilaurin plus vitamin E TPGS and talc**.

For product characterisation, analytical techniques consist of conductometry, laser diffraction, optical microscopy, differential scanning calorimetry, X-ray powder diffraction, dynamic vapour sorption, and release testing in simple and complex dissolution media.

**This chapter has been submitted as scientific paper to the *International Journal of Pharmaceutics* and published on 28/01/2024.**

V.-T.-T. Huynh, S. de Paiva Lacerda, F. Espitalier, E. Beyssac, M.-I. Ré, Effect of Talc and Vitamin E TPGS on Manufacturability, Stability and Release Properties of Trilaurin-Based Formulations for Hot-Melt Coating, *International Journal of Pharmaceutics* (2024), doi: <https://doi.org/10.1016/j.ijpharm.2024.123866>

## GENERAL INTRODUCTION

From a process perspective, there has been rarely publications where **trilaurin** was used for melt-processing. Actually, two studies reported the use of trilaurin with/without polyethylene glycol 10000 (PEG) successfully extruded at 40°C to encapsulate theophylline (Windbergs et al., 2009e, 2009a). It was concluded that the most stable form was achieved at this temperature (Windbergs et al., 2009e). It is noted that even for a mixture of trilaurin-additive-drug 45:5:50 direct crystallisation of  $\beta$  solid form still occurred (Windbergs et al., 2009a). The role of drug and PEG in trilaurin crystallisation represents a question for this application. Otherwise, it was necessary to quench LLL melt to 5°C to recover its  $\alpha$  solid form with an extreme cooling rate (Takeguchi et al., 2020). Until now, there is lack of fundamental studies to expose the link between crystallisation/solidification properties of lipids (e.g., **trilaurin** in particular) and their processability with melt technologies.

From a material perspective, trilaurin is a monoacid triglyceride the polymorphs of which exhibit low melting points compared to the ambient temperature. After a cycle of melting and solidifying, kinetics of  $\beta'$ - $\beta$  trilaurin conversion is also rapid and could be complete within a day at room conditions whereas  $\alpha$ - $\beta$  tripalmitin or tristearin transformation takes place at 40°C for one day and more than two months, respectively (Windbergs et al., 2009c). Furthermore, additive addition was reported to depress to various degrees crystallisation points of trilaurin using emulsifiers such as spans and tween 60 (J. S. Aronhime et al., 1988). Additives which are lauric-acid-derivatives were concluded to exert the most effect on trilaurin crystallisation in comparison with other fatty-acid-derivatives (P. R. Smith et al., 1994; P. R. Smith & Povey, 1997). Lauric/stearic-acid derived emulsifiers were found to disturb more or less the crystal lattice of trilaurin (Schlichter et al., 1988). Recently, **talc**, regarded as a new type of additives due to its inorganic nature, was reported to exert an templating effect on crystallisation of triglycerides (Yoshikawa et al., 2014). In fact, talc addition was found to induce heterogeneous crystallisation of trilaurin and  $\beta'$ - $\beta$  transformation was instantaneous. Moreover usually, scientists significantly owe fundamentals on trilaurin crystallisation and polymorphism to food research.

From a products perspective, biopharmaceutical properties of trilaurin appear much overlooked as a matrix excipient. In fact, trilaurin belongs to triglycerides constituted of medium-chain fatty acids (Jadhav & Annapure, 2023) which are normally used to formulate (liquid) lipid-based bio-enabling formulations (Feeney et al., 2016). These formulations are in favour of pharmacokinetic properties oftentimes owing to their digestibility. Trilaurin is unique with its solid state at room conditions and its susceptibility to digestion in comparison with other monoacid triglycerides made of saturated long-chain fatty acids (e.g., trimyristin, tripalmitin, tristearin) (Christophersen, Vaghela, et al., 2014b; Christophersen, Zhang, et al., 2014b).

On the one hand, fast digestion of trilaurin in alignment with rapid release of a peptide was found to protect it from proteolytic degradation (Christophersen, Zhang, et al., 2014b). On the other hand, digestion of trilaurin was reported to be a contributing factor to enhanced bioavailability of drugs (Nishihata et al., 2011; Watanabe et al., 1993; Yoshitomi et al., 2011). In addition, this property has been exploited to design gastro-resistant or enteric coated tablets even with very low concentrations of trilaurin (Yoshitomi et al., 1992, 1993). It should be noted that those dosage forms were prepared with



recourse to aqueous vehicles/organic solvents. However, there is no proof of concept of trilaurin-based formulated microparticulate products prepared via melt-processing and no correlation on release of active substance and digestion of lipid coating membrane (Jannin & Cuppok, 2013).

Based on the aforementioned material-, process- and product-specific aspects on the use of trilaurin in food and pharmaceutical research, this study was designed to investigate **the effect of talc and vitamin E TPGS, as new types of additives**, on technical feasibility, product stability and release properties.

Firstly, a fundamental study for formulations screening was performed with turbidimetry-integrated Crystal16 for measurements of crystallisation points and induction time.

Secondly, hot-melt coating of our model substrate (crystals of NaCl) with representative trilaurin-based formulations was studied. The coated products were analysed via calorimetry, goniometry, and polarised light microscopy in order to investigate deeply polymorphism and underlying mechanisms of crystallisation possibly involved in processing.

Finally, coated products were used for evaluation of processing performance, coating quality, release properties as well as long-term stability.

## 1. Materials and Methods

### 1.1. Materials

Trilaurin (LLL,  $T_{m,\alpha} = 15.6^{\circ}\text{C}$ ,  $T_{m,\beta'} = 35.1^{\circ}\text{C}$ ,  $T_{m,\beta} = 45.7^{\circ}\text{C}$ ) and vitamin E TPGS (VitE\_TPGS) were purchased from TCI Europe N.V. and PMC Isochem (France). Luzenac PHARMA M (talc, T) ( $d_{50,laser} = 10.5 \mu\text{m}$ ) was kindly donated by Azelis (Courbevoie, France).

LLL was chosen as the lipid for the crystallization experiments, as it has been scarcely researched for pharmaceutical applications. Talc was used as an additive who acts a templating agent while vitamin E D- $\alpha$ -tocopherol polyethylene glycol 1000 succinate (HLB  $\approx 13$ ) should provide a possibility to accelerate release kinetics. Those materials were composed into formulations detailed in **Table 5-1** and **Table 5-2**.

Table 5-1. Lipid-based formulations composition for screening with Crystal16 crystallization systems

Formulation	Excipients (% w/w)		
	LLL	VitE_TPGS	T
LLL	100	-	-
LLL+T 0.1%*	99.9	-	0.1
LLL+T 0.5%*	99.5	-	0.5
LLL+T 1.0%*	99.0	-	1.0
LLL+VitE_TPGS	90	10	-
LLL+VitE_TPGS+T 0.1%*	90	10	0.1
LLL+VitE_TPGS+T 0.5%*	90	10	0.5
LLL+VitE_TPGS+T 1.0%*	90	10	1.0

\* indicates 1.0%, 0.5%, 0.1% w/w talc to the total 99%w/w of other components  
# denotes that it is only used in preformulation study

Table 5-2. Lipid-based formulations composition for hot-melt coating

Formulation		Excipients (% w/w)		
		LLL	VitE-TPGS	T
LLL-1F	LLL	100	-	-
LLL-2F*	LLL+T 1.0%	99	-	1
LLL-3F*	LLL+VitE_TPGS+T 1.0%	90	10	1
LLL-3F-1#	LLL+VitE_TPGS	90	10	-

\* indicates 1% w/w talc to the total 99%w/w of other components  
# denotes that it is only used in preformulation study

## 1.2. Methods

### 1.2.1. Trilaurin-based lipid formulation characterisation

#### 1.2.1.1. Turbidimetry with Crystal16 Crystallization Systems

The same experimental procedure already described in **Chapter 4 – Part 1** (See **Methods**) is applied, except that the thermal programme was adapted for performing isothermal crystallisation of trilaurin-based formulations. A typical run programme is illustrated in **Table 5-1**.

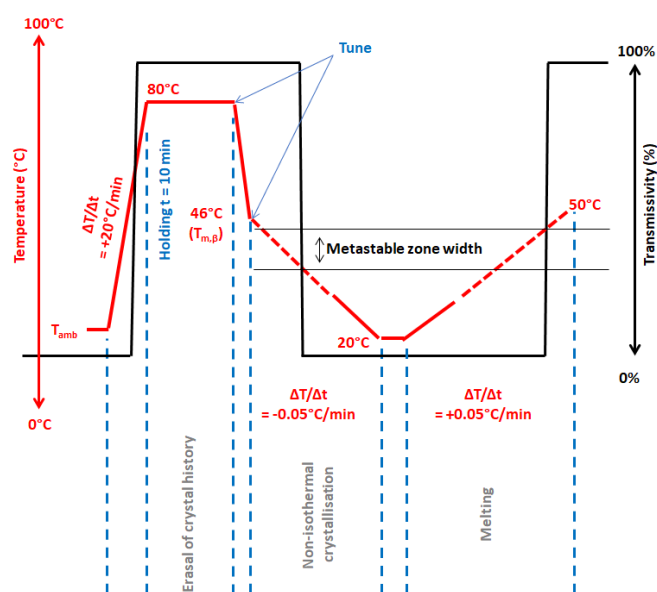


Figure 5-1. Thermal programme set for non-isothermal experiments with trilaurin in Crystal16®

Firstly, it starts when heating is launched till 80°C and held for 10 min at this point to completely melt all the crystals. Then the first step of “tuning” is performed in order to reset the transmissibility through one block (4 vials) to 100% as there might be a difference due to mixing heterogeneity, for example. Cooling is performed at 20°C/min from 80°C till 46°C –  $T_{m,\beta}$  of trilaurin.

At this point, the second step of “tuning” is performed so as to reset all the transmissibility values to zero as they might diminish with temperature decrease. From 46°C to 20°C a cooling rate of 0.05°C/min is defined as the condition for non-isothermal crystallisation. When the programme temperature reaches 20°C, the system will then be heated again up to 50°C at the same velocity. The objective of this last

step is to measure melting point of the system in the vial. Onset melting point or crystallisation point are identified as the temperature at which the transmissivity starts to increase or decrease significantly, accordingly.

As shown in **Figure 5-1**, by definition, the difference of melting point and crystallisation point is the width of metastable zone (Kulkarni et al., 2013), which will be considered as proof of thermal feasibility of tristearin under the effect of different additive-combinations.

In addition, non-isothermal experiments were also conducted with a cooling rate of 5°C/min and 10°C/min, which might represent the cooling capacity of certain melt-processing technologies. The measurements for each formulation were performed in triplicate (n = 3).

#### 1.2.1.2. *Differential Scanning Calorimetry (DSC)*

The same experimental procedure already described in **Chapter 3 – Part 1** (See **Methods**) is applied.

For isothermal crystallisation, the thermal programme, spanning over a temperature range of 0°C and 100°C, consists of a first heating to 80°C, holding for a period to melt all the crystals, cooling at 30°C min<sup>-1</sup> till 30°C, holding time for 2h at 30°C and a second heating, for which a heating rate of 30°Cmin<sup>-1</sup> for polymorph identification.

Thermal data in the crystallisation step was also exploited to construct solidification profile and the same conversion method as described in **Chapter 3 – Part 1** was applied.

#### 1.2.1.3. *Measurements of Contact Angle*

The same experimental procedure already described in **Chapter 3 – Part 1** (See **Methods**) is applied, except that the thermal testing conditions were adapted for performing isothermal crystallisation of trilaurin-based formulations.

Each formulation was melted beforehand in an oven at 80°C, agitated and poured into a single-use 1 mL syringe. The latter is then placed in the heat-control box of the goniometer. For each formulation, measurements (n = 3) were performed at a temperature close to that of fluidisation temperature – 30°C – at a distance of 5 cm as this allows for good observations of film formation in the course of liquid-solid transitions. During a measurement, the evolution of droplet was captured each in a 1- or 10-minute video at a rate of 1 frame per second. Solidification time was directly estimated from taken images.

The substrate was also salt pastilles produced using the procedure already described in **Chapter 3 – Part 1** (See **Methods**)

#### 1.2.1.4. *Polarised Light Microscopy*

The same experimental procedure already described in **Chapter 4 – Part 1** (See **Methods**) is applied, except the fact that thermal testing conditions were adapted for performing isothermal crystallisation of trilaurin-based formulations.

Four formulations were prepared on lamellas using thermal conditions mimicking coating operations: holding at 80°C for 5 min and cooling at 10°C/min till 30°C and holding at this temperature till complete

crystallisation. These lamellas were then used for the whole stability study. Four to six images were taken for each time of observation, i.e. freshly after preparation  $t_0$ , 06 weeks and 12 weeks after.

## 1.2.2. Hot-Melt Coated Products: Preparation and Characterisation

### 1.2.2.1. *HMC processing*

HMC trials are performed using lab-scale Ventilus® fluidised bed technology (Romaco© Group, Germany). Process parameters were selected based on preliminary trials. The same experimental procedure already described in **Chapter 3 – Part 1** (See **Methods**) is applied, except the fact that thermal conditions and process variables were adapted to trilaurin-based formulations in **Table 5-3**.

Table 5-3. Process parameters and their values specified for hot melt coating of LLL-1F, LLL-2F and LLL-3F

Parameters	Set-up values
Reactor volume (L)	1
Batch size (g)	250
Final coating content (% w/w)	30
Temperature of fluidisation air (°C)	30 (setpoint)
Quantity of process air (m <sup>3</sup> /h)	37
Temperature of melt media (°C)	80
Temperature of feeding system (°C)	80
Temperature of spraying air (°C)	80
Pressure of spraying air (bar)	0.5
Formulation feeding rate (g/min):	≈ 18-19 (LLL-1F, LLL-3F) ; ≈ 24-25 (LLL-2F):

### 1.2.2.2. *Stability Monitoring*

Curing was bypassed as trilaurin occurs in  $\beta$  form right after production. Coated products with three formulations were stored in a climatic chamber (Memmert, Germany) under tempering conditions of 25°C/60%RH, based on the official guidelines (ICH Topic Q 1 A (R2), 2003). Characterisation techniques involved in stability study consist of XRPD, DSC, DVS, PLM and release testing. All products were analysed at three time points:  $t_0$  (freshly produced),  $t_1$  (6 weeks after),  $t_2$  (12 weeks after).

## 1.2.3. Coated Product Characterisation

### 1.2.3.1. *Assay of Coating Contents*

The same experimental procedure already described in **Chapter 3 – Part 1** (See **Methods**) is applied.

### 1.2.3.2. *Particle Size Distribution*

The same experimental procedure already described in **Chapter 3 – Part 1** (See **Methods**) is applied.

### 1.2.3.3. *X-ray powder diffraction*

The same experimental procedure already described in **Chapter 3 – Part 1** (See **Methods**) is applied, except the fact that diffractograms were collected using X-ray source at 45 keV and 40 mA over a  $2\theta$

range from 1° to 30° recorded at every step of 0.033° (2) with an acquisition time of 135.255 (or 280.035) s per step. Long d-spacings and crystallite size were estimated using the same conversion method as described in **Chapter 4 – Part 2** was applied.

#### 1.2.3.4. *Dynamic Vapour Sorption*

Dynamic vapour sorption profiles were recorded using a DVS Resolution instrument (Surface Measurement Systems, London, UK). Samples were loaded onto the quartz balance and dried at 25°C and 0% RH (setpoints) until a constant weight was reached. Next, the relative humidity was increased from 10% up to 95% with a step size of 5-10% with the condition that a minimum equilibration time of 5 minutes was achieved when change in mass remained less than 0.01%. Otherwise, the relative humidity continued to increase/decrease when the holding time at that step attained 360 minutes. The temperature was maintained 25°C (setpoint) during the measurements.

#### 1.2.3.5. *Release Kinetics*

Release in water medium

The same experimental procedure already described in **Chapter 3 – Part 1** (See **Methods**) is applied.

Digestibility in complex medium

The same experimental procedure (including preparation of FaSSIF and pancreatin extract) already described in **Chapter 3 – Part 2** (See **Methods**) is applied, except the need for addition of lipase inhibitor and back-titration up to pH 9.0. At the end of 3-hour digestion, a volume of 200 µL 4-bromophenyl-boronic acid 1 M in methanol was added to stop lipolysis. Then, back titration was performed till pH 9.0 would be reached using the same titrant. For each sample, release testing is performed in triplicate (n = 3). Extent of digestion (%) was estimated using the following formula:

Equation 53 :

$$\text{Extent of digestion (\%)} = \frac{n_{FA,ionised} + n_{FA,non-ionised}}{n_{max,FA in LbF}} \times 100$$

where  $n_{FA,ionised}$  number of moles ionised, fatty acid neutralised by NaOH 0.2 M at pH 6.5 (mol),  $n_{FA,non-ionised}$  number of moles non-ionised fatty acid back-titrated at pH 9.0 (mol),  $n_{max,FA in LbF}$  number of moles fatty acid occurring in the lipid-based formulation (mol).

Release studies from coated salt under digestion.

The same experimental procedure already described in **Chapter 3 – Part 2** (See *Methods*) is applied.

#### 1.2.3.6. *Statistical data analysis.*

Statistics-based method (Yuksel, 2000) at specific time points 5, 10, 15, 30, 45 and 60 minutes of release testing. This method was chosen to assure statistical meaning due to a limited sample number.

## 2. Results and Discussion

### 2.1. Solidification Properties

#### 2.1.1. Non-Isothermal Crystallisation

The objective here was to measure melting and crystallisation points of trilaurin (LLL). Four levels of talc concentration, 0, 0.1%, 0.5% and 1.0% w/w, were investigated to test impact of talc and its concentration on thermal behaviours of this triglyceride and then to select a good level for use in hot-melt coating formulations. Talc concentration was limited to the maximal value of 1.0% w/w in order to avoid segregation in molten state (Beaupere et al., 2018).

**Figure 5-2** shows metastable zone width (MSZW) map constituted by melting and crystallisation points of LLL combined with 4 levels of talc concentration. In melt crystallisation, MSZW could be construed as the difference between the melting point of a solid form and its corresponding crystallisation point measured at a certain cooling rate. In other words, one MSZW applies to each polymorph of a triglyceride but one MSZW map could serve as a guide for melt-processing of that triglyceride.

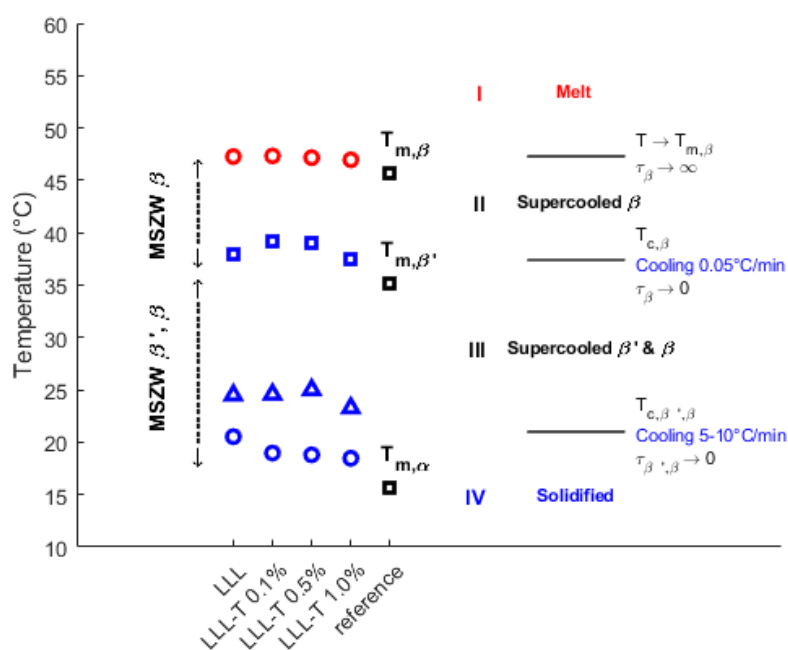


Figure 5-2. MSZW map measured for LLL with 4 levels of talc concentration. Melting points at 0.05°C/min (red circles), crystallisation points at 0.05°C/min (blue squares), 5°C/min (blue triangles) and 10°C/min (blue circles), reference melting points of polymorphs  $\alpha$ ,  $\beta'$  and  $\beta$  (black squares). (See **Appendix 03**)

As indicated by the column to the right of measured melting and crystallisation points, MSZW map of LLL based formulations could be divided into 4 regions: I, II, III, and IV. In effect, above the liquidus line of  $\beta$  (I) indicated by the experimental melting temperature of pure  $\beta$  LLL ( $T_{m,\beta} = 47.3 \pm 0.1^\circ\text{C}$ ), LLL remains in molten state. At  $T_{m,\beta}$ , its induction time of  $\beta$  approaches the infinity. In this case study, MSZW (II) where the triglyceride in general and  $\beta$  LLL in particular is supercooled was identified by melting and crystallisation points ( $T_{c,\beta} = 38.0 \pm 1.9^\circ\text{C}$ ) measured at 0.05°C/min heating and cooling,



respectively. The values of measured  $T_{m,\beta}$  of LLL based formulations are close to the reference value (Moorthy, 2018) as this discrepancy could be explained by the fact that  $T_{m,\beta}$  varies as function of crystallite size in the sample (Takeguchi et al., 2020). Down from  $T_{c,\beta}$  to  $T_{c,\beta'-\beta}$  lies the region where both  $\beta'$  and  $\beta$  LLL (III) are supercooled and they can nucleate at any time. For LLL, the length of constituent fatty acid chains is shorter, therefore  $\beta'$  LLL is more stable and can occur upon cooling (Yoshikawa, 2016). For other long-chain triglycerides (data not shown), there are five regions of MSZW map (I, II, III, IV and V) as their  $\beta'$  solid form can crystallise separately from  $\beta$  depending on thermal treatment. Below  $T_{c,\beta'-\beta}$  measured at 5°C/min and 10°C/min (IV), LLL solidifies spontaneously. For the reader's information,  $T_{c,\beta'-\beta}$  measured by turbidimetry was found close to the values obtained via DSC (data not shown).

As a possible application, MSZW map could serve as a guide to choose a thermal condition corresponding to formation of a specific polymorph. Except the region (I) where LLL occurs in molten state, all the 3 remaining regions could be considered for crystallisation of an LLL polymorph in final products. For instance, in a study, successful extrusion of a binary mixture of drug and  $\beta$  SSS LLL conditioned by setting a processing temperature of 40°C which falls within the  $\beta$  MSZW (II) (Windbergs et al., 2009e). In another study, it was reported that even when adding 10% w/w polyethylene glycol (PEG) to the binary system,  $\beta$  LLL could be also obtained at 40°C (Windbergs et al., 2009a). In these cases, drug and PEG can either have no effect on LLL crystallization or be a nucleation inductor.

Definition of thermal conditions in the region (III) where  $\beta'$  and  $\beta$  are likely in the state of undercooling, respectively, was possible in preliminary trials with hot-melt coating when the temperature of fluidisation air (inlet air) was kept at 20-25°C. Several fundamental studies reported a multiplicity of cases where  $\beta'$  LLL was generated (Kellens et al., 1991; Takeguchi et al., 2020; Windbergs et al., 2009c).  $\beta'$  LLL is more stable than  $\alpha$  LLL but the former is converted overnight into  $\beta$  LLL at room conditions (Windbergs et al., 2009c). Direct crystallisation of  $\beta$  LLL was possible at the same thermal conditions with the addition of an additive (Yoshikawa, 2016; Yoshikawa et al., 2014, 2015). In the last region (IV) of LLL MSZW map, in order to obtain  $\alpha$  LLL it is necessary to quench the melt at an extreme cooling rate (Takeguchi et al., 2020). It implies that this approach is not technically viable for industrial large-scale production. In addition,  $\alpha$  LLL is not stable at room conditions by considering its melting point.

Talc addition led to a general reduction in crystallisation points of  $\beta$ ,  $\beta'$  measured at cooling rates of 5-10°C/min whereas those of long-chain triglycerides (tripalmitin, tristearin) were not significantly affected. This could be ascribed to the occurrence of a more stable  $\beta'$  LLL. Talc appears to influence the solidification point of trilaurin, because adding 0.1% or 0.5% w/w, an increase in solidification point was observed. This implies lowered supercooling level, which might be in favour of nucleation. Addition of 1% w/w talc resulted in a decrease in melting point. This is controversial in comparison with documented data (Yoshikawa et al., 2015) but the cause could be the difference in granulometry of talc particles used. In fact, in the cited study, when mean size of talc particles increases to a critical value (2.5  $\mu\text{m}$ ), its effect on crystallisation point of trilaurin (cooled at 1°C/min) turned in reverse. It should

be noticed that there might be also shear effect for homogeneous mixing brought about by a specification of 200 rpm in experiments.

Talc was used as an additive for it is a common excipient (glidant, lubricant) used in formulating solid dosage forms. Its effect on crystallisation of triglycerides and fat-based systems has been discovered recently (Bayés-García et al., 2022; Yoshikawa et al., 2014, 2015). By considering  $T_{m,\beta}$  of pure LLL, the fact that talc-loaded formulations were shown to possess a relative  $\beta$  MSZW indicates evidently that talc can induce nucleation of  $\beta$  LLL. It is because this nucleation occurs above  $T_{m,\beta'}$  of pure LLL. This highlights an advantage of the fact that construction of MSZW map by turbidimetry should be performed prior to another characterisation (e.g., DSC, optical microscopy).

Figure 5-3 shows MSZW map constituted by melting and crystallisation points measured for all the trilaurin-based formulations where vitamin E TPGS was also included. Though measurements of crystallisation points (5-10°C/min) were not performed, four regions could also be deduced. The importance was that addition of 10% w/w vitamin E TPGS did not also affect crystallisation of  $\beta$  LLL as indicated by the presence of a similar  $\beta$  MSZW.

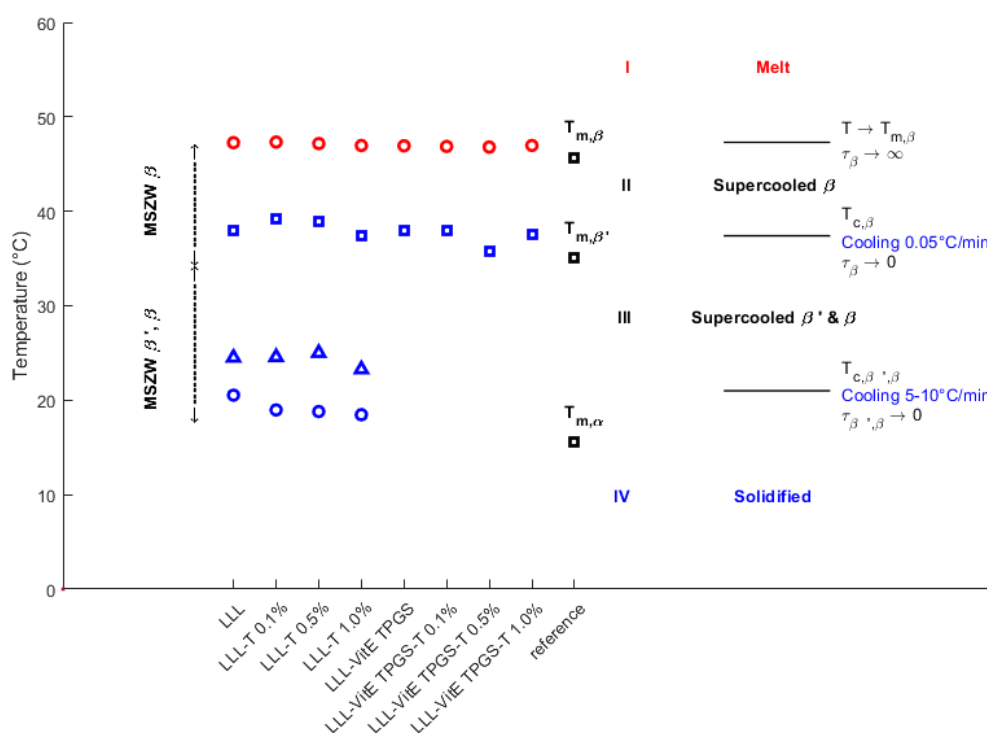


Figure 5-3. MSZW map measured for all formulations containing trilaurin. Melting points at 0.05°C/min (red circles), crystallisation points at 0.05°C/min (blue squares), 5°C/min (blue triangles) and 10°C/min (blue circles), reference melting points of polymorphs  $\alpha$ ,  $\beta'$  and  $\beta$  (black squares)

**To conclude this part**, sporadic crystallisation in  $\beta$  MSZW (region II) can yield a stable crystal form while formation of metastable form(s) likely results from spontaneous crystallisation below their melting points (region V). By showcasing the example of LLL, this signifies that each triglyceride in general can be adapted to at least two processing approaches depending on the level of thermal

conditions in relation to the melting point of metastable form(s). From the overview of documented researches with monoacid triglycerides, one melt-based processing technology could be more adapted to direct crystallisation of  $\beta$  polymorph than the other depending on their characteristics (e.g., mass and heat transfer mode, use of pressure, residence time). With the help of MSZW map as processability map, it can help select a transformation method with good thermal conditions, especially when additive addition or complex-mixture combinations are necessary, and even shun the use of high-capacity cooling unit. However, the dependence of other properties (e.g. solidification kinetics, adhesiveness, degradability of substrate) as function of temperature, additive quality and quantity should be also considered as they could influence processing performance.

### 2.1.2. Isothermal Crystallisation

#### 2.1.2.1. *Measurements of induction time and polymorph identification by DSC*

**Figure 5-4** shows solidification profile of the four selected formulations at 30°C during 2h (**A**) and polymorph identification after crystallisation (**B**). According to DSC results converted into solid fraction contents (%) as function of time (see **Figure 5-4-A**), four formulations **LLL-1F**, **LLL-2F**, **LLL-3F** and **LLL-3F-1** exhibit an induction time of 751.2 s, 79.2 s, 14.4 s and 948.6 s, respectively. Solidification profile of four formulations can also be ranked as follows: **LLL-3F** > **LLL-2F** > **LLL-1F** > **LLL-3F-1**.

According to DSC thermograms of four formulations as shown in **Figure 5-4-B**, all the formulations exhibit  $\beta$  form the melting point of which peaks at 48.2°C (**LLL-1F**), 50.9°C (**LLL-2F**), 49.0°C (**LLL-3F**) and 47.4°C (**LLL-3F-1**). Without talc, there is occurrence of  $\beta'$  and  $\beta'_1$  forms indicated by peaks at 37.7°C and 43.6°C (**LLL-1F**), at 37.3°C and 42.8°C (**LLL-3F-1**), respectively (Hagemann, 1988). In the case of **LLL-3F-1**, the peak at 35.8°C is attributed to melting of vitamin E TPGS.

Particularly, thermogram of **LLL-3F** also displays a peak of 41.5°C (black arrow) which could be attributed to either vitamin E TPGS or  $\beta'_1$  form of trilaurin. For information, isothermal crystallisation of vitamin E TPGS at 30°C (data not shown) was also performed but there was no sign of thermal events during 2h. This characteristics should be noted for multi-sourced vitamin E TPGS as this semi-synthetic substance was reported to crystallise at this temperature upon continuous cooling (J. Li et al., 2011). The value of these melting peaks is higher than the reference value of trilaurin polymorphs because of a high heating rate of 30°C/min applied (Takeguchi et al., 2020; Yoshikawa et al., 2015).

Measurements of induction time via calorimetry yield a completely different landscape from those via turbidimetry. In fact, talc addition results in the fact that induction time was reduced about 9.5 and 65.9 times for trilaurin and its combination with vitamin E TPGS. In reality, **LLL-3F** contains about 2.5%w/w talc and therefore the effect of talc addition on nucleation of **LLL-3F** might be magnified one order of magnitude in comparison with **LLL-2F**.

It should be noted that neither Crystal16 nor DSC could provide a faster cooling rate to suit the principle of isothermal crystallisation. Therefore, cooling time was significant to be taken into account. In fact, in the absence of vitamin E TPGS, nucleation of all the formulations containing only trilaurin and talc was

recorded in Crystall16 earlier than those with vitamin E TPGS added. However, both techniques can discriminate the effect of additive addition on nucleation of trilaurin. Furthermore, the difference in measurements of induction time via two techniques might be due to setting a shear rate of 200 rpm in turbidimetry. In experiments with turbidimetry, shear was indispensable for homogeneously mixing the content in each vial. A possible effect of involvement of shear and interfacial interactions between solids and liquid phases of hydrophilic vitamin E TPGS in melt LLL warrants for further investigations in the future.

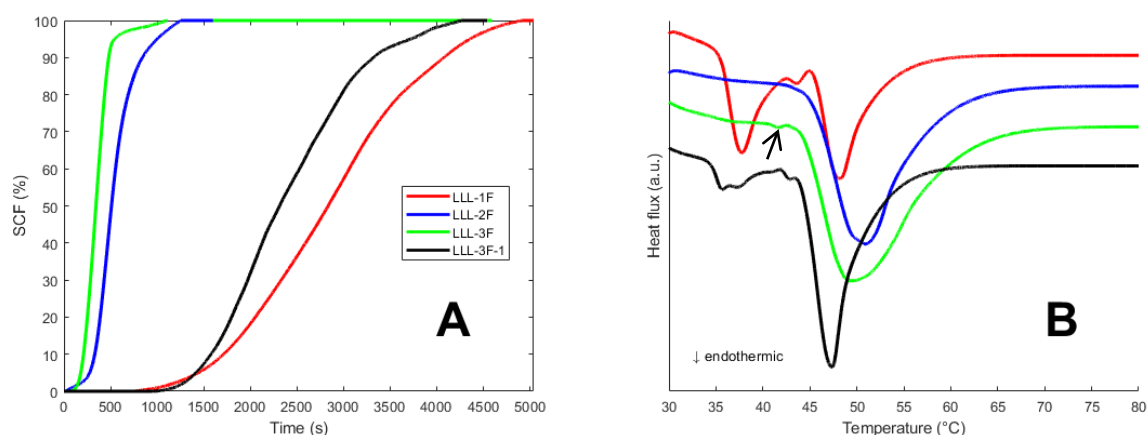


Figure 5-4. Isothermal crystallisation of 4 selected trilaurin-based formulations (A) and polymorphic identification of crystallised form(s) (B)

Another important aspect for melt processing is that the inclusion of talc accelerated solidification of trilaurin and its combination with vitamin E TPGS. In fact, slow solidification appears to be characteristics of  $\beta'$  form of triglycerides (e.g., trilaurin, tristearin) (Bertoni et al., 2021; Yoshikawa et al., 2015). In the presence of talc,  $\beta'$ - $\beta$  conversion was catalysed and finished rapidly in the course of cooling (Yoshikawa et al., 2015). This justifies no observation of  $\beta'$  in polymorphic identification of **LLL-2F** and **LLL-3F** (see **Figure 5-4-B**).

In summary, in the presence of vitamin E TPGS, crystallisation behaviours of **LLL-1F** and **LLL-3F-1** are similar in terms of polymorphic profile. In addition, when it comes to the case of **LLL-3F-1**, trilaurin seems to induce nucleation of vitamin E TPGS because the latter alone did not crystallise during an isothermal period of 2h at 30°C. With all the elements discussed, only **LLL-1F**, **LLL-2F** and **LLL-3F** were used as coating materials in this study where processing performance, quality, stability and release properties of coated products would be evaluated. **LLL-3F-1** was characterised for comparison in terms of solidification properties as well as solid-state evolution with time.

#### 2.1.2.2. Measurements of solidification time lag and film formation

Finally, solidification behaviours of four formulations **LLL-1F**, **LLL-2F** and **LLL-3F** (used for hot-melt coating) were investigated by means of goniometry. The pictures taken over time (from deposition of a drop on the substrate's hot surface to solidification) can be seen in **Appendix**. They demonstrate contact angle upon impingement, solidification and film formation of **LLL-1F**, **LLL-2F** and **LLL-3F**

on the surface of compressed NaCl and that of the formulation itself. The main objective is to observe solidification and film formation in the case that primary or secondary nucleation takes place.

For all the cases, **LLL-1F**, **LLL-2F** and **LLL-3F** in molten state exhibit good wetting behaviours with a contact angle less than 90°. On this macroscopic scale, solidification time lag is considered as the time between the first contact (0 s) and the moment where the curve of the molten droplet started to deform. Solidification time lags of around 60 s, 60 s and 150 s were noticed for **LLL-1F**, **LLL-2F** and **LLL-3F** on NaCl surface and the solidification times were estimated to be about 240 s, 240 s and 300 s, respectively. On the other hand, the solidification process started about 30 s, 60 s and 30 s after its impact with the film of the same nature and finished within approximately 120 s, 240 s and 120 s, accordingly. At the end, all the solidified droplets display a rough surface but no sign of detachment on NaCl surface. This implies that trilaurin-based formulations have a good affinity to substrate.

**To conclude this part**, solidification of molten formulation on NaCl and on the surface of the same nature was homologous to primary nucleation and secondary nucleation, respectively. It is presumed that when solidification time lag of both nucleation phenomena approaches it is possible to set only one feeding rate instead of two as was applied to the case of tristearin (D. G. Lopes et al., 2015). Therefore, in this study, for all the coating trials, only one feeding rate was specified for the whole operation by considering also the solidification profile obtained for each formulation via DSC.

## 2.2. Process Performance and Coating Quality

### 2.2.1. Process Efficiency

For coating by fluidised bed, it is possible to generate products with different drug or coating contents in the same batch. This strategy was adopted as a multiple-sampling approach for HMC process and product characterisation.

Process yield for HMC with **LLL-1F**, **LLL-2F** and **LLL-3F** was recorded as 84%, 91% and 88%, accordingly. **Figure 5-5** shows coating contents of samples taken during each trial. Coating process efficiency observed for **LLL-1F** and **LLL-3F**, depicted by the red continuous line, approaches 100% at the end of operation but that of **LLL-2F** falls close to 80%. It could be also indicated by the gap between the theoretically calculated values (black filled squares) and the practical assay results (blue columns). In the case of **LLL-1F** and **LLL-3F**, assay of the samples 03 and end-R was found similar whereas results of **LLL-2F** display a difference. An explanation could be that at the moment of third sampling a large amount of fine trilaurin was collected and at the end of coating this fine fraction was segregated while coated particles were still in fluidisation.

In general, good yield and process efficiency were obtained with three formulations. This might be due to the propensity of trilaurin to generate fine. Actually, process data (not shown) indicates a continuous increase in filter pressure. All the coating operations lasted less than 6 minutes. For information, preliminary trials were performed with **LLL-2F** by augmenting feeding rate from 6-7, 11-12 to 18-19 g/min. At the final rate, fine powder was not observed evidently on the process wall. As trilaurin-

containing formulations (**LLL-1F** and **LLL-3F**) exhibit a fast solidification kinetics, it is not advisable to specify a lower feeding rate. Otherwise, fine generation would be important.

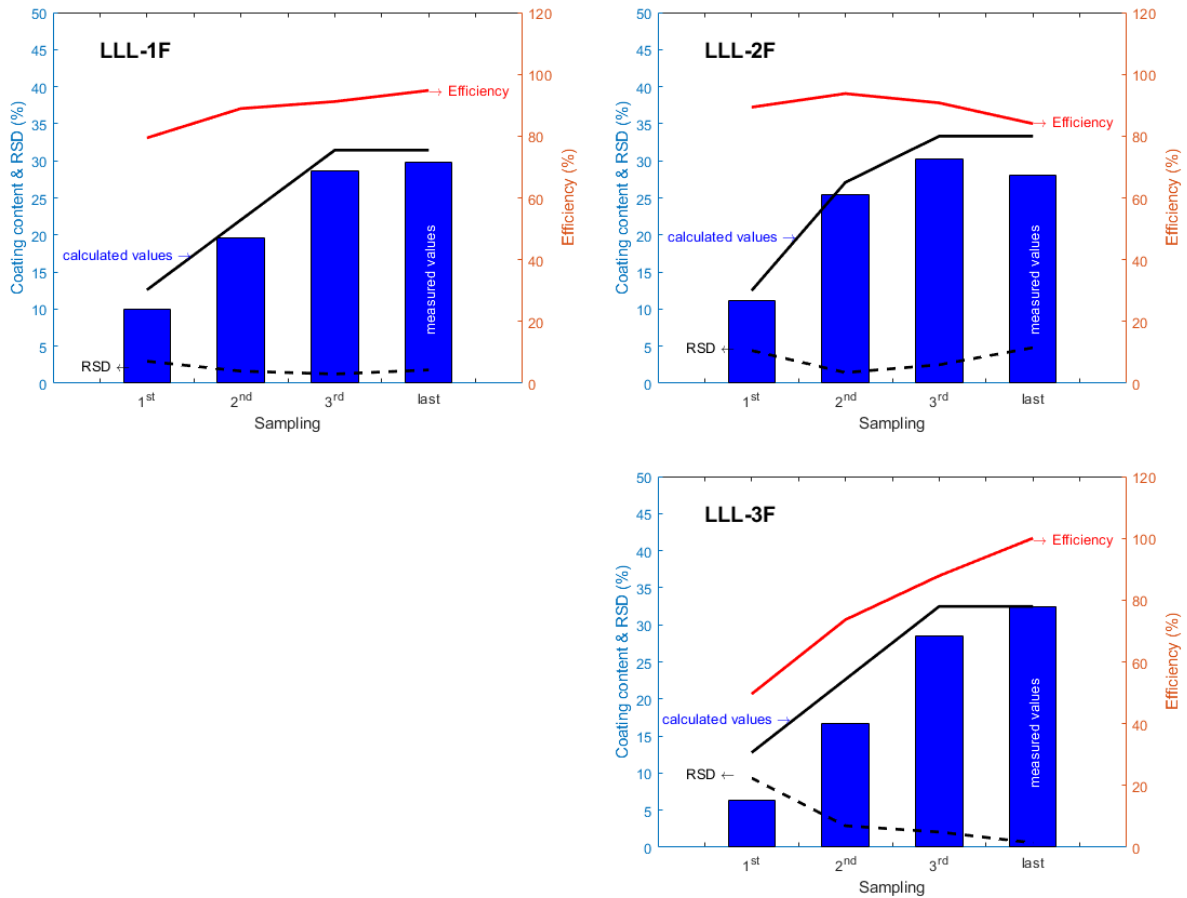


Figure 5-5. Assay results of coating trials performed with LLL-1F, LLL-2F and LLL-3F

### 2.2.2. Identification of Process Regime

The process regime could be determined by interpreting PSD and its parameters SPAN and  $D_{90}/D_{10}$ .

**Figure 5-6** shows superimposed PSD curves expressed in volume (left) measured for initial NaCl particles, 1<sup>st</sup>, 2<sup>nd</sup> and 3<sup>rd</sup> sampling during coating trials corresponding with the three assayed coating contents in the previous section. Evolution of all the PSD curves indicates a progressive coating regime.



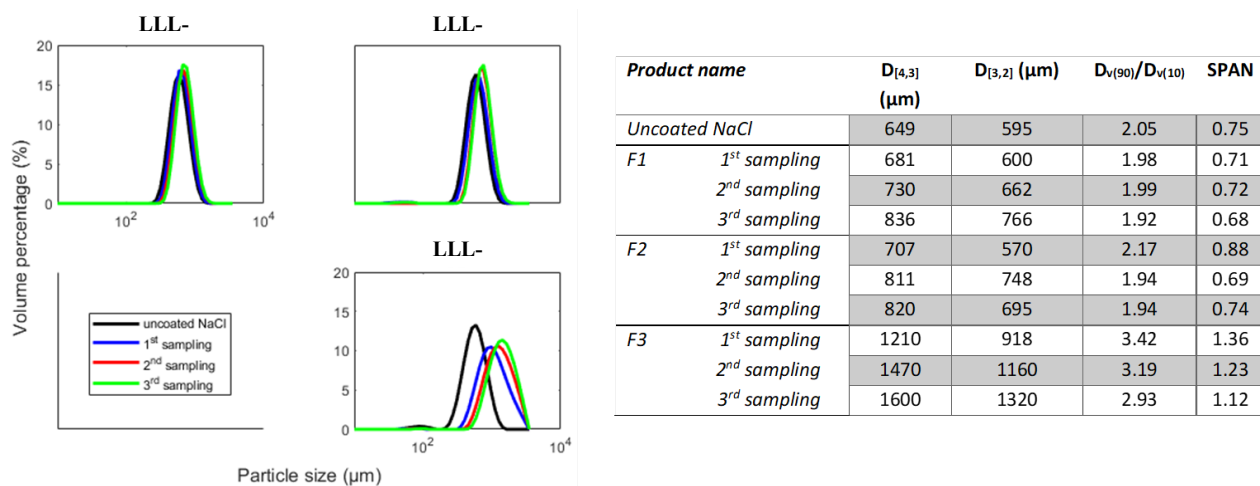


Figure 5-6. Evolution of particle size distribution in volume(left) and PSD parameters (right) obtained for products coated with **LLL-1F**, **LLL-2F** and **LLL-3F**

As an exception, in the case of **LLL-3F**, the first PSD curve of first sampled particles display a reduced median peak but the trends reverse after that. This implies particles were agglomerated but then a strict coating regime was maintained. Initial agglomeration is probably the resultant of specifying one feeding rate for the whole agglomeration. This corroborates the hypothesis where it is possible to apply merely one feeding rate in the case of non-traditional coating (where temperature of fluidisation air  $> T_{m,\alpha}$ ) when induction time of primary nucleation approaches that of secondary nucleation. It is not the case of **LLL-3F**. Measurements of solidification time with goniometry are rather appropriate for justifying a strategy to define process variables than DSC. In fact, **LLL-3F** and **LLL-2F** display both a similarly rapid solidification profile but this information appears irrelevant for setting a good feeding rate.

Besides, fine generation was observed for **LLL-2F** processed at the same thermal operational conditions as **LLL-1F** and **LLL-3F**. Fast solidification kinetics is likely the only cause. Measurements of solidification time and film formation demonstrated that all trilaurin-containing formulations adhere well to NaCl substrate and itself.

The evolution of PSD parameters SPAN and  $D_{v(90)}/D_{v(10)}$ , as given in **Figure 5-6** (right), is in accordance with the discussion on PSD curves. For **LLL-1F** and **LLL-2F**, constant decrease in both SPAN and  $D_{v(90)}/D_{v(10)}$  indicates a progressive coating regime. However, in the case of **LLL-3F**, the initial jump from 2.05 ( $D_{v(90)}/D_{v(10)}$  of uncoated particles) to 3.42 ( $D_{v(90)}/D_{v(10)}$  of 1<sup>st</sup> sampling) denotes a mixed regime of coating and agglomeration. These arguments agree with a hypothesis that when a coating regime dominates fine particles tend to gain more coating materials with time in comparison with larger particles, the width of PSD should reduce and the median peak  $D_{v(50)}$  should sharpen. Otherwise, agglomeration leads to an enlargement of particle size and a rapid shift of PSD to greater class size bins.

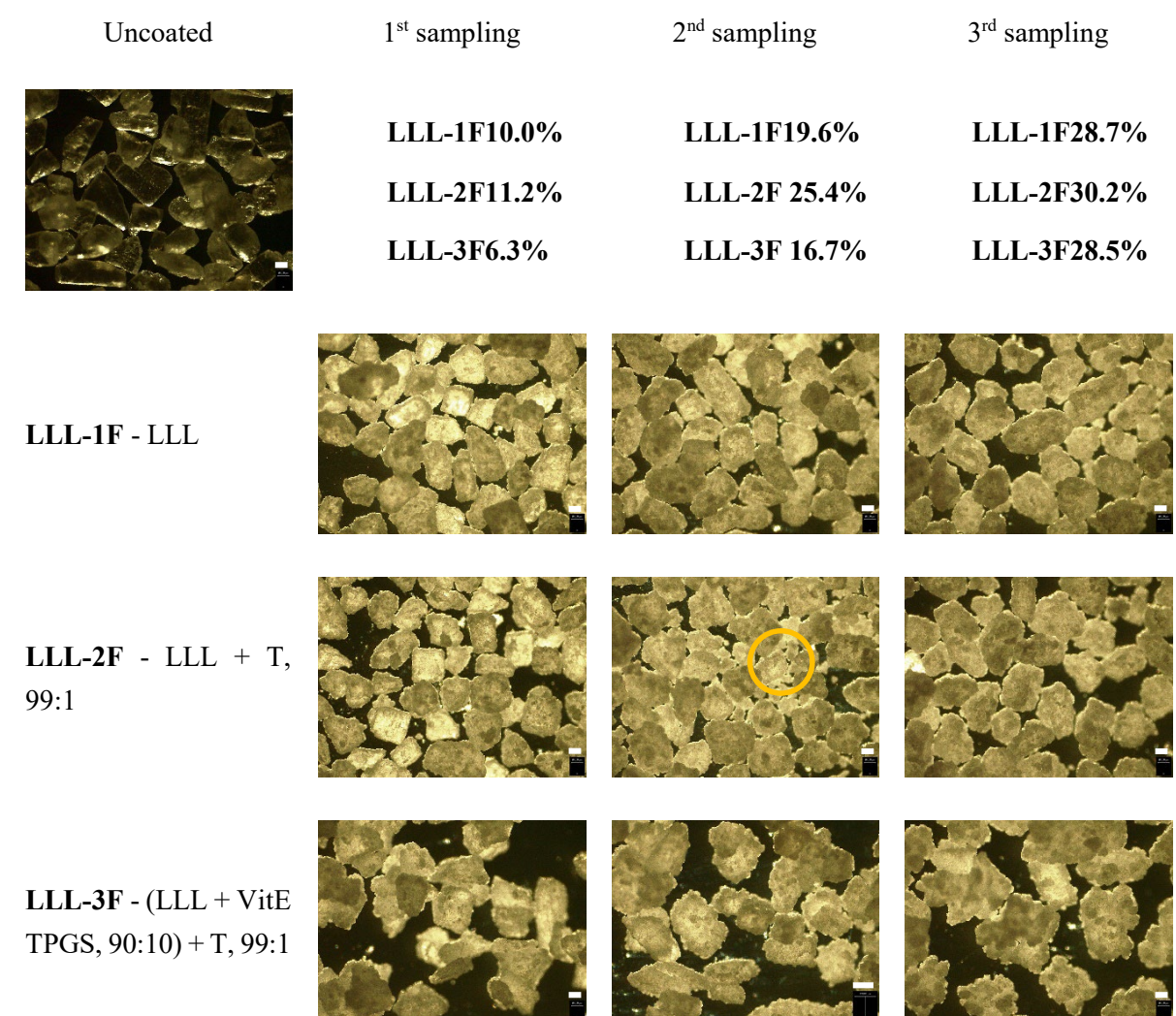
Highest product temperature – 44.1°C, 46.4°C and 43.9°C – was noted for coating with **LLL-1F**, **LLL-2F** and **LLL-3F**, respectively. Despite its closeness to  $T_{m,\beta}$ , a strict coating regime with trilaurin-containing formulations was identified. This suggests that fast solidification of these three formulations

may be the contributing factor of the expected coating regime whereas slow solidification could cause agglomeration.

For information, in **Chapter 4 – Part 2**, slow solidification of NBAC4-3 and NBAC4-9 at 60°C could be now confirmed to be the cause of agglomeration. Furthermore, higher feeding rate seems to decrease fine overproduction as not demonstrated in **Figure 5-6**. Adding talc or other inductor of both nucleation and growth could be a key formulation variable for successful non-traditional hot-melt coating with triglycerides.

### 2.3. Coating Quality

Coating quality of salt particles coated with **LLL-1F**, **LLL-2F** and **LLL-3F** was assessed visually using an optical microscope. Talking pictures are displayed in **Figure 5-7**.



*Figure 5-7. Optical images of salt particles uncoated and coated with **LLL-1F**, **LLL-2F**, and **LLL-3F** with increasing contents.*

*The white bar (right bottom of each image) indicates 200 μm.*

**Figure 5-7** shows images salt particles uncoated and coated with increasing contents of **LLL-1F**, **LLL-2F**, and **LLL-3F**, correspondingly. The thick white bar indicates an observation scale of 200  $\mu\text{m}$ . Uncoated salt particles had bright and almost translucent aspect, polygonal shape and rather sharp edges which were gradually rounded with coating. It should be noted that these observations were performed under the same lighting conditions. Reduction in brightness of salt crystals reflects increase in coating coverage. Fine particles less than 200  $\mu\text{m}$  (orange circle) were detected among **LLL-2F**-coated particles, which was also observed in PSD. In the case of **LLL-3F**-coated particles, as discussed before (see *Identification of Process Regime*), both coated and agglomerated particles could be observed, and the image of first sampling shows mostly agglomerates formed by two collided particles. These particles were still observed with a larger size in second and third sampled populations, which implies a strictly coating established after initial agglomeration. This agrees with considerations of process regime using particle size distribution parameters – **Figure 5-6** (right).

## 2.4. Release Properties and Product Stability

### 2.4.1. Polymorphism

Samples of products coated with the proposed lipid formulations were stored in freezer before analyses and then evaluated at several timepoints: **LLL-1F**, **LLL-2F** and **LLL-3F** (3 timepoints): after production ( $t_0$ ), after 6 weeks ( $t_1$ ) and after 12 weeks ( $t_2$ ).

**Figure 5-8** shows thermograms obtained for products coated with three formulations. Those of **LLL-1F** and **LLL-2F** both display close melting points 48.6 and 48.3°C, respectively. This indicates that the crystallised form  $\beta$  was obtained after production (Kaneko et al., 2020; Y. L. Lee et al., 2010). It should be noted that for trilaurin without talc, the crystallised form  $\beta'$  could be formed at the moment of production but at the time of analysis (more than 1 day of delay)  $\beta'$  was not stable enough in freezer and transformed completely into  $\beta$  (Windbergs et al., 2009c). In the case of **LLL-3F**, the thermogram has two melting peaks at 34.5°C (black arrow) and 47.5°C, which indicates solid-solid phase separation and depression in melting points of trilaurin.

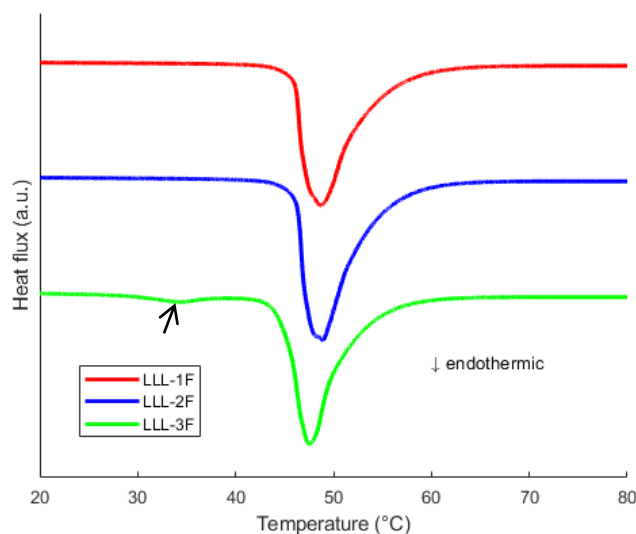


Figure 5-8. Polymorphic identification performed on products coated with LLL-1F, LLL-2F and LLL-3F at  $t_0$

Figure 5-9-A1, A2, B1, B2, C1 and C2 shows small-angle and wide-angle XRPD patterns obtained for products coated with LLL-1F, LLL-2F and LLL-3F over three months, respectively. According to these XRPD patterns, long d-spacings of LLL-1F (A1), LLL-2F (B1) and LLL-3F (C1) were found between 31.2 and 31.8 Å ( $2.830$ - $2.776^\circ 2\theta$ ) and short d-spacings of LLL-1F (A2), LLL-2F (B2) and LLL-3F (C2) have the values of 4.6 Å ( $19.286$ - $19.249^\circ 2\theta$ ), 3.9 Å ( $23.196$ - $23.023^\circ 2\theta$ ) and 3.7 Å ( $23.978$ - $23.720^\circ 2\theta$ ). These long and short d-spacings correspond to  $\beta$  polymorph of trilaurin (Kaneko et al., 2020; Y. L. Lee et al., 2010). With a chain of polyethylene in its structure, vitamin E TPGS alone seems to exhibit sub- $\alpha$  or  $\beta'$  packing (J. Li et al., 2011) and incorporate well with trilaurin crystal network. Hence, XRPD appears not capable to detect phase separation of vitamin E TPGS at 10% w/w.

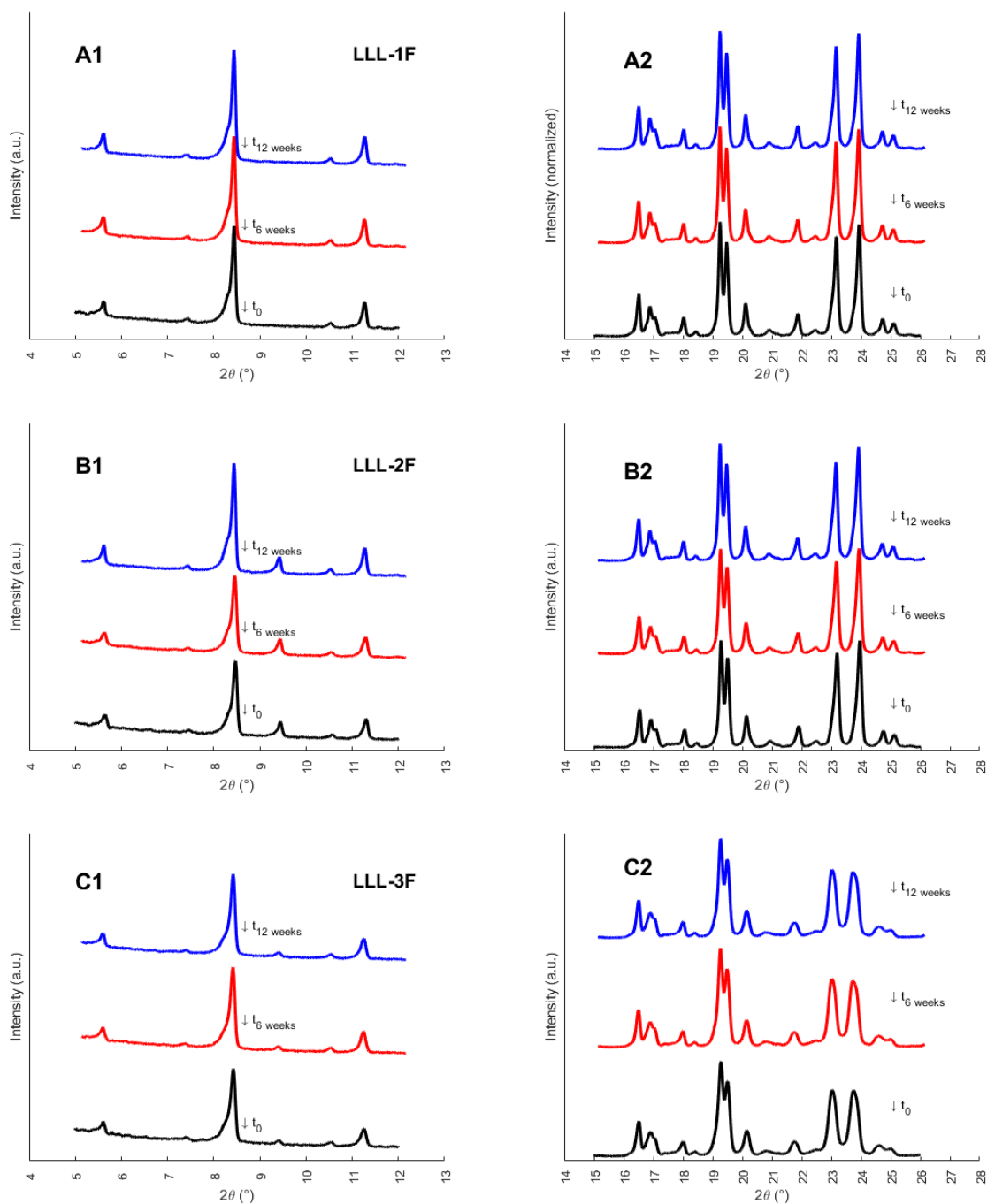


Figure 5-9. Small-angle (left) and wide-angle X-ray powder diffraction patterns obtained for products coated with **LLL-1F**, **LLL-2F** and **LLL-3F** at  $t_0$  (black line), 6 weeks (red line) and 12 weeks (blue line) after that

#### 2.4.2. Crystal Network and Phase Behaviours

Crystal network was evaluated based on monitoring crystallite size via XRPD analyses and polarised-light optical observations. **Table 5-4** shows estimated crystallite size and number of stacked lamellas measured for coated products with the ranking order of **LLL-1F** > **LLL-2F** > **LLL-3F**. Melting point of **LLL-1F**, **LLL-2F** and **LLL-3F** measured at  $t_0$  appears to correlate with estimated crystallite size. In fact, melting point increases when estimated crystallite size increases as expected (Takeguchi et al.,

2020). Without additive, crystal network of **LLL-1F** displays larger crystallite size than that of **LLL-2F** and **LLL-3F** formed under the effect of talc. This is in agreement with polarised light optical observations published in a research on talc (Yoshikawa et al., 2014). Polarised light optical images performed in-house with **LLL-1F**, **LLL-2F**, **LLL-3F** and **LLL-3F-1** will be discussed in the following.

Table 5-4. Estimated crystallite size and number of stacked lamellas

Formulation		Crystallite size (Å)	Stacking no. of lamellas#
<b>LLL-1F</b>	t <sub>0</sub>	1597	50.7
	t <sub>1</sub>	1613	51.2
	t <sub>2</sub>	1726	54.8
<b>LLL-2F</b>	t <sub>0</sub>	1205	38.3
	t <sub>1</sub>	1205	38.3
	t <sub>2</sub>	1435	45.6
<b>LLL-3F</b>	t <sub>0</sub>	979	31.1
	t <sub>1</sub>	1166	37.0
	t <sub>2</sub>	1190	37.8

#Rounded values were shown.

**Figure 5-10** shows in parallel representative polarised light optical images of **LLL-1F** and **LLL-2F** taken in intervals of 6 weeks. For the reader's information, the samples were kept in lamellas and preserved hermetically at 25°C/60% relative humidity. **LLL-1F** at the time of formation (t<sub>0</sub>) was constituted of large spherulite crystals (Yoshikawa et al., 2014). Both images taken at 6 weeks and 12 weeks (**LLL-1F**) show that such spherulite crystals were transformed into β in the form of small loosely packed crystals. In the case of **LLL-2F**, images taken at t<sub>0</sub>, 6 weeks and 12 weeks display crystal morphology characterised for β and not changed significantly with time : spherulites with strong birefringent patterns (Oh et al., 2002; Yoshikawa et al., 2014).

**Figure 5-11** shows polarised light optical images of vitamin E TPGS crystallised at room conditions (not at 30°C). It can be seen that large crystallites stack one on top of another. Crystallite size also seems not to evolve with time. These observations of vitamin E TPGS were performed to complement those of **LLL-3F** and **LLL-3F-1** in the following.

**Figure 5-12** shows in parallel representative polarised light optical images of **LLL-3F** and **LLL-3F-1** taken in intervals of 6 weeks. Image of **LLL-3F-1** (t<sub>0</sub>) appears to display hybrid features of large spherulites β' and β and large crystallites of vitamin E TPGS without net borders. After 6 weeks, demixing of vitamin E TPGS was detected easily like its morphology observed in **Figure 5-11**. After 12 weeks, appearance of spherulites of vitamin E TPGS could be indicative of net phase separation between two components of the system. The crystal network of β **LLL-3F** (t<sub>0</sub>) also comprised of spherulites with birefringent patterns. There seems not to be significant changes in crystal morphology at 6 weeks and 12 weeks. At the last timepoints, a small piece of vitamin E TPGS like crystals could be also observed.



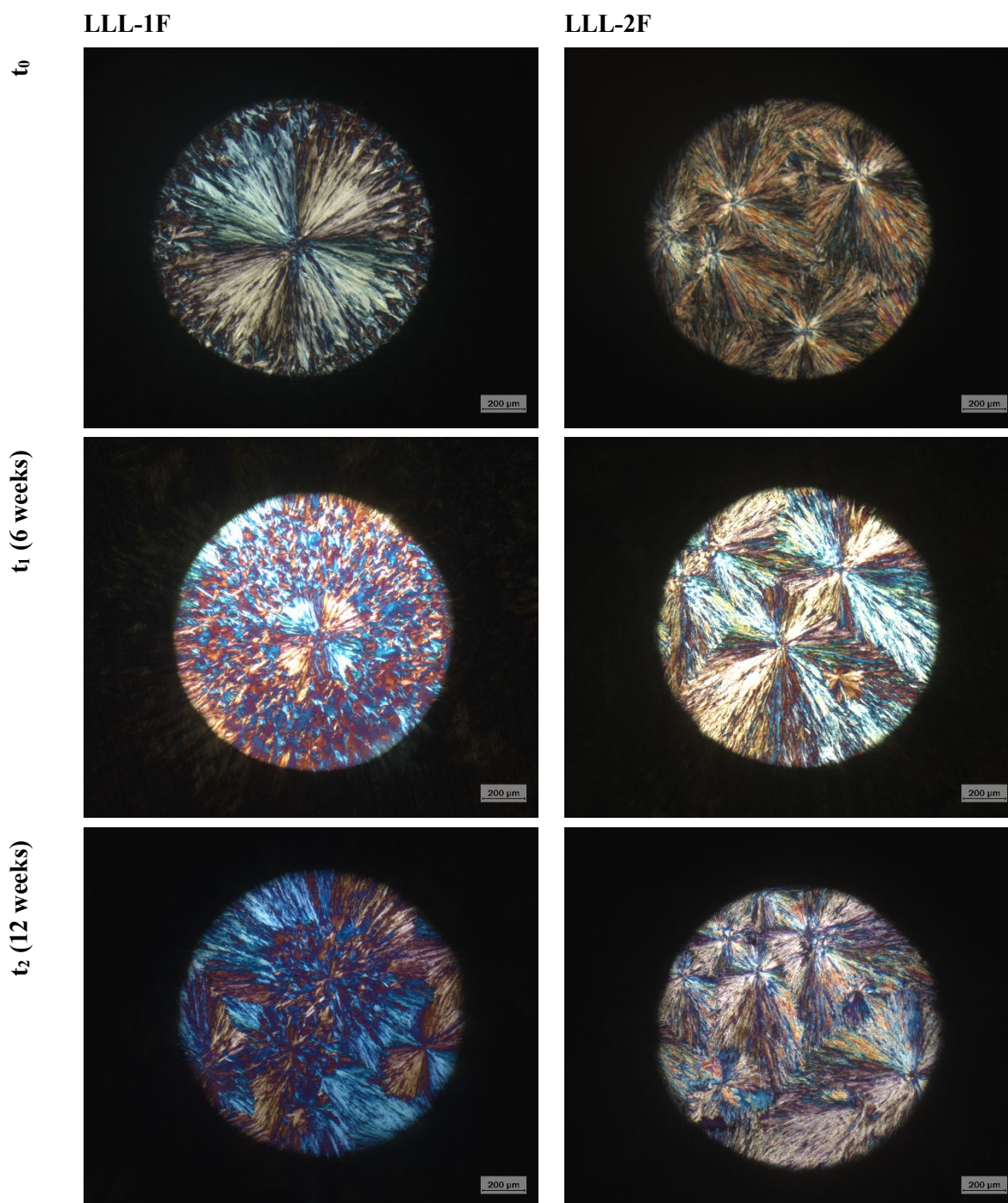


Figure 5-10. Polarised light optical images performed for LLL-1F and LLL-2F at  $t_0$ , 6 and 12 weeks after that

These observations show at least two advantages of formulating trilaurin and vitamin E TPGS with talc. On the one side, talc promoted an even crystal network populated with  $\beta$  polymorph spherulites the size of which seems not to change significantly over three months. On the other side, fast solidification kinetics of  $\beta$  form appears to trap vitamin E TPGS which crystallised under the effect of trilaurin. Therefore, despite the immiscibility of two components at the ratio 90:10, phase separation could be overcome via fast crystallisation induced by talc. The whole crystallisation of the ternary formulation, composed of trilaurin, vitamin E TPGS and talc, (90:10),99:1 was recorded as an evidence (data not shown).

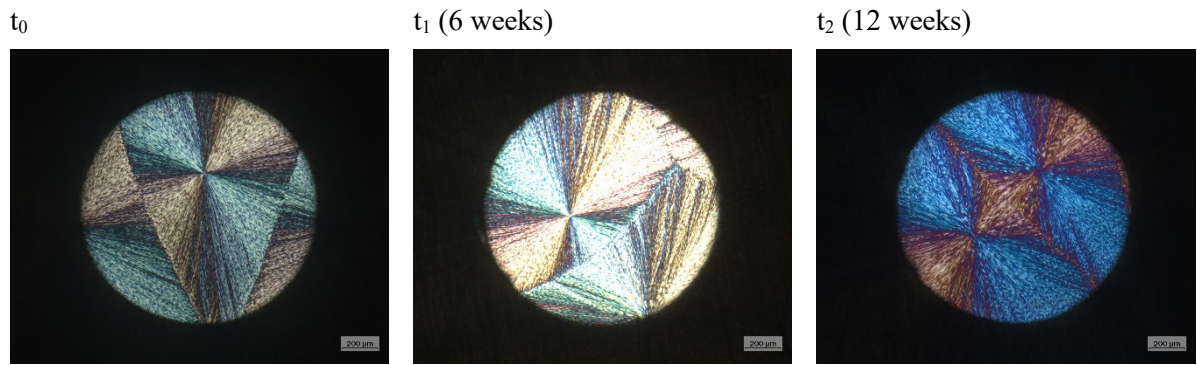


Figure 5-11. Polarised light optical images performed for vitamin E TPGS at  $t_0$ , 6 and 12 weeks after that

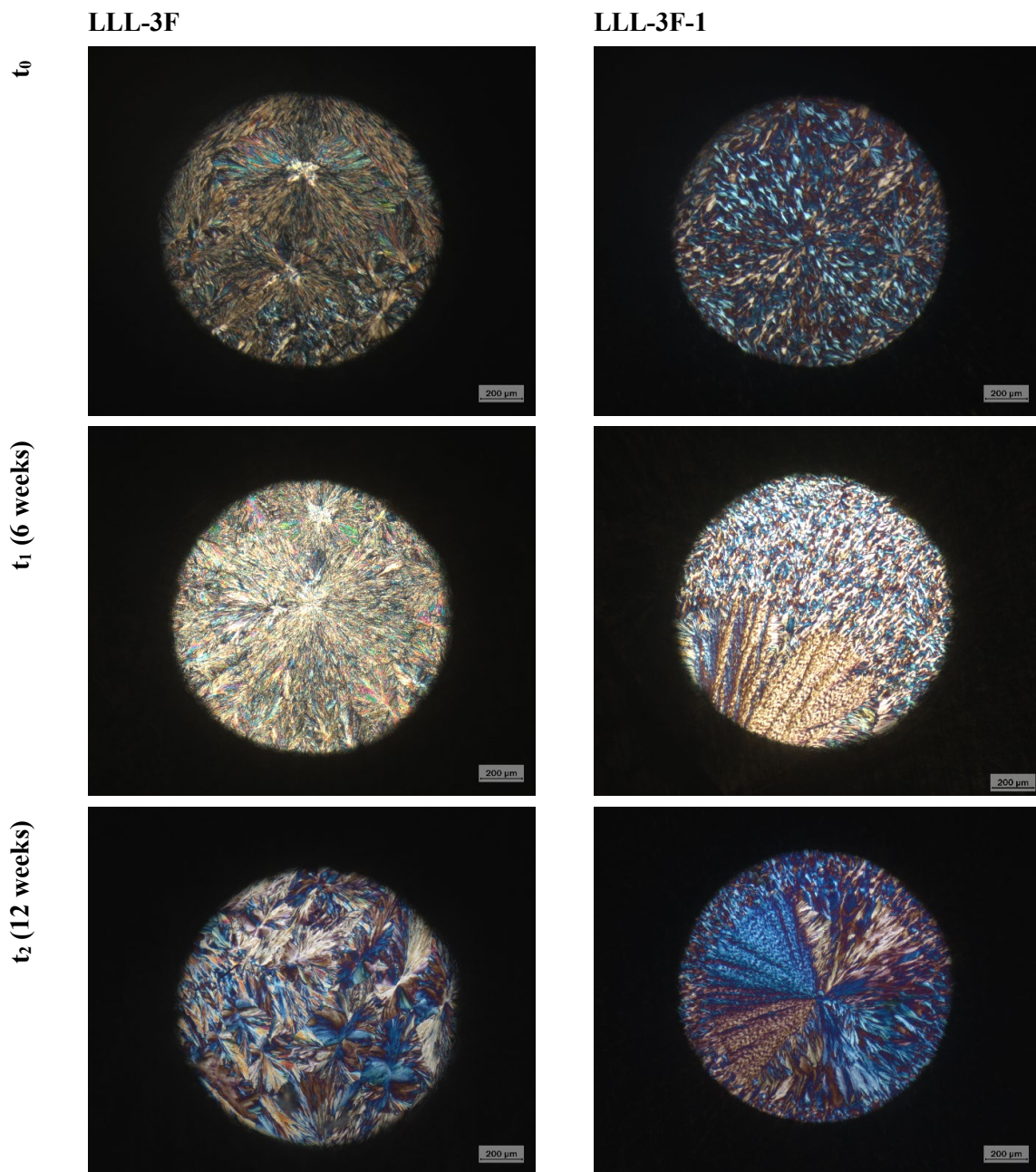
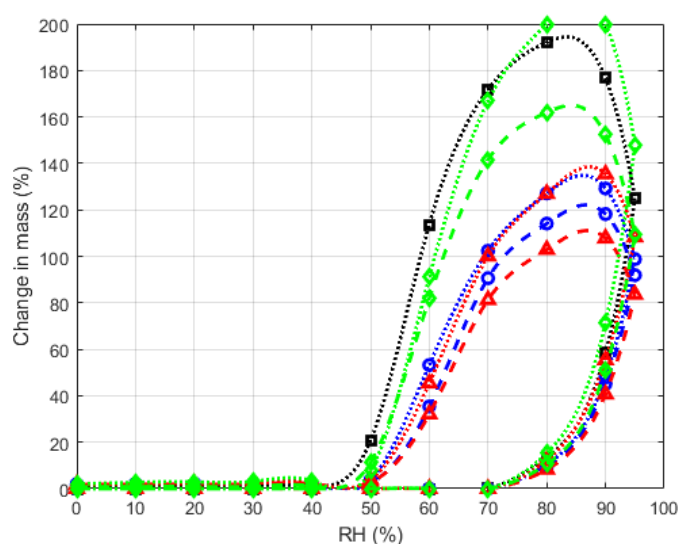


Figure 5-12. Polarised light optical images performed for LLL-3F and LLL-3F-1 at  $t_0$ , 6 and 12 weeks after that

### 2.4.3. Hygroscopicity profile

As NaCl crystals are very soluble in water (360 mg/mL (25°C)), trilaurin is water-resistant and formulating with additives could modify its property, salt particles coated with trilaurin-based formulations were tested with dynamic vapour sorption with the objective of (i) monitoring any physical changes when these products were subject to aging at 25°C/60% relative humidity and (ii) testing a technological functionality, i.e. moisture-proofing property of each formulation.

**Figure 5-13** shows the results of dynamic vapour sorption obtained for NaCl and its products coated **LLL-1F**, **LLL-2F** and **LLL-3F**. The sorption curves show evidently that at some moisture increments of 10% to 95% change in mass (%) had not attain its most because of insufficient equilibrium time set for each step. In fact, as a humidity regulating agent, NaCl can absorb 10-100 times higher its mass and experimentation could be long-lasting (Sängerlaub et al., 2018). Therefore, provided that the same protocol was applied, the results should be comparable.



*Figure 5-13. Dynamic vapour sorption profile obtained for uncoated NaCl and products coated with **LLL-1F**, **LLL-2F** and **LLL-3F** at  $t_0$  and 12 weeks after that; uncoated NaCl (black open square), **LLL-1F** (blue open circle), **LLL-2F** (red open triangle), **LLL-3F** (green open diamond), measurements at  $t_0$  (dotted lines) and at 12 weeks after that (dashed lines)*

All the samples start to absorb vapour above 70% relative humidity which is near the deliquescence point of NaCl (Sängerlaub et al., 2018). Both uncoated NaCl and **LLL-3F**-coated products ( $t_0$ ) exhibit the highest vapour sorption kinetics with a peak up to 2 times change in mass. This implies that vapour absorbed would dissolve both NaCl and vitamin E TPGS occurring in the products. Without inclusion of the hydrophilic surfactant **LLL-1F**- and **LLL-2F**-coated products have a similar and milder vapour sorption kinetics which attain its peak at about 1.4 times change in mass. For all the cases, desorption process was faster for coated products than uncoated NaCl.

After 3 months of storage, all the coated products exhibit lower vapour sorption kinetics with the ranking order of **LLL-2F** < **LLL-1F** < **LLL-3F**. Reduced in sorption kinetics after three months suggests that the coating quality in terms of surface and microstructure could evolve. This observation is in agreements with the increase in estimated crystallite size during storage. In fact, fat blooms (or



continuous crystal growth on surface) often happen to lipid-based products and trilaurin-based formulations could not be exempt from this physical process. There have been reports of triglycerides affected by fat blooming (Bertoni et al., 2021; Mayama, 2009; Witzleb et al., 2012). When blooms are developed, normally the surface will become more water-repellent (W. Fang et al., 2007) and release kinetics of active substance could therefore decelerate.

In practice, sorption isotherms have been interpreted to evaluate moisture-proofing of the hot-melt coat (A. S. Achanta et al., 2001; H. Chen et al., 2010). In this case, moisture-proofing property of bloomed lipid-coated salt could be deemed improved in comparison with  $t_0$ . However, it is advisable to coat with trilaurin without hydrophilic additive if the applications of its formulations were for moisture protection.

#### 2.4.4. Release properties

Measurements of salt release kinetics not only reflect the impact of solid-state evolution on performance stability. As NaCl crystals represent a simple active model, it can also help verify susceptibility of formulations in development to phase separation. This has been reported to cause release instability of lipid-based formulated products (D. G. Lopes, Koutsamanis, et al., 2017).

**Figure 5-14** demonstrates comparative release profile of salt particles coated with **LLL-1F**, **LLL-2F**, and **LLL-3F** during a stability period of three months. For **LLL-1F** and **LLL-2F**, a prolonged release was obtained. Qualitatively, salt was released from **LLL-1F**- or **LLL-2F**-formulated products to similar rate and extent at  $t_0$  and 12 weeks. Salt release was observed to decelerate between these two timepoints. This could be probably due to growth of crystallite size and fat blooming (Schertel, Salar-Behzadi, Karrer, et al., 2021; Witzleb et al., 2012). In the case of **LLL-3F**, it imparts an immediate release (i.e. more than 85% dissolved within 30 min) to salt coated with a similar content. The incorporation of vitamin E TPGS might create hydrophilic channels that facilitates in turn water transfer throughout lipid coat.

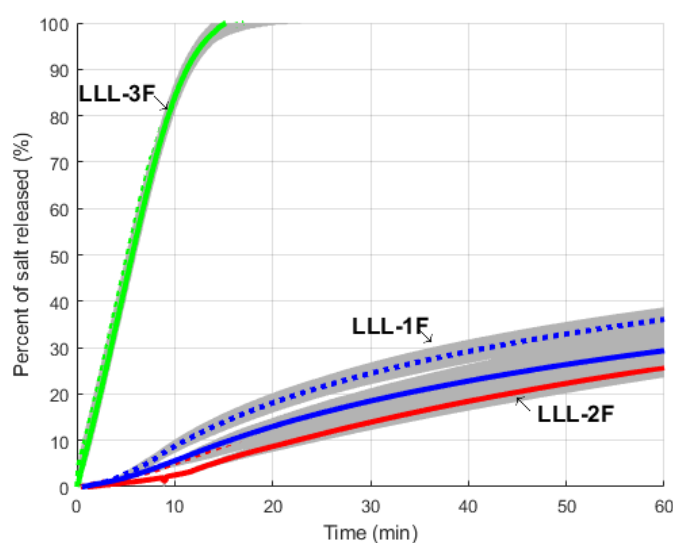


Figure 5-14. Salt release profile obtained for products coated with **LLL-1F** (red), **LLL-2F** (blue) and **LLL-3F** (green) at  $t_0$  (dotted lines) and 12 weeks (solid lines) after that. Error bar (grey region)

Notably, release profile of salt coated with **LLL-3F** appears not to change over three months despite initial phase separation and continuous evolution of its solid-state behaviours. On the one hand, in spite of phase immiscibility of vitamin E TPGS at 10% w/w, this component could also crystallise at the time the crystal network of trilaurin formed and was found to be evenly dispersed therein. In other words, it is reasonable to state that there formed a non-solid solution system where mobility of solid vitamin E TPGS was minimised. As discussed before, trilaurin acts as a crystallisation inductor for vitamin E TPGS (see **Section 2.1.2.1**) while talc acts as a promoter of both nucleation and crystal growth for trilaurin (see **Crystal Network and Phase Behaviours**).

From a quantitative perspective, two-sample t-test confirms that there is no significant difference ( $\alpha = 5\%$ ) in salt release kinetics between  $t_0$  and 6 weeks, between 6 weeks and 12 weeks for all the three formulations. LLL-2F factor test could be more discriminative but it necessitates a larger number of tests.

#### 2.4.5. Digestibility

Trilaurin is a medium chain triglyceride (Jadhav & Annapure, 2023) but its digestibility sometimes goes unnoticed when formulating solid lipid formulations (Windbergs et al., 2009e, 2009d, 2009a). In this section, products coated with **LLL-1F**, **LLL-2F** and **LLL-3F** were tested with a focus on the digestibility of these formulations.

**Figure 5-15-A** shows digestion kinetics of the three trilaurin-based formulations. In this graph, digestion kinetics is indicated by the rate of NaOH consumption. As can be seen, **LLL-1F** and **LLL-2F** appear to be digested to the similar rate during the whole experiments. It implies that talc 1% w/w has no significant effect on digestion of trilaurin. In the case of **LLL-3F**, digestion was slow at beginning in comparison with **LLL-1F** and **LLL-2F** but after 150 min its digestion rate reached that of those two formulations. As shown in **Figure 5-15-B**, both digestion extents (%) determined via direct titration and back titration were close, showing that at 3h all the three formulations were digested to the similar extent. Addition of vitamin E TPGS changed the digestion mechanism of the formulation at the beginning but its digestion extent is equivalent to trilaurin after 3h.

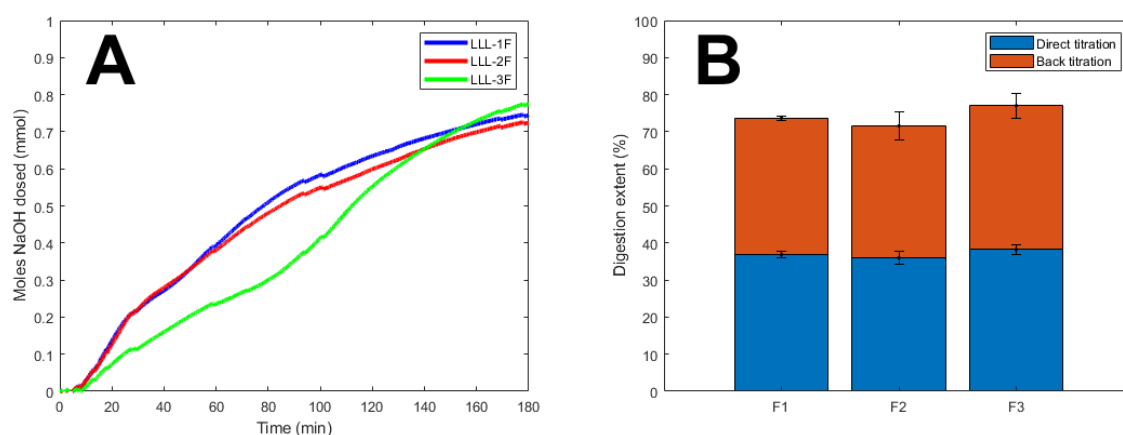


Figure 5-15. Digestion profile of 500 mg each formulation **LLL-1F**, **LLL-2F** and **LLL-3F** ( $t_0$ )

Following a normal mechanism of triglyceride digestion, a triglyceride is firstly attacked by lipase, at positions sn-1 and sn-3, to produce one fatty acid and one 1,2-diacylglyceride. The latter is then cleaved by lipase to yield one fatty acid and 2-monoglyceride. The latter should be then converted to 1-monoglyceride so that lipase could hydrolyse it into one fatty acid and one glycerol (Benito-Gallo et al., 2015; Jensen et al., 1963). The difference in digestion kinetics is indubitably due to the presence of vitamin E TPGS which is not digestible but known to inhibit lipolysis to some extent (Christiansen et al., 2010).

It was reported to mimic binding of co-lipase and thereby blocking the association of co-lipase with pancreatic lipase but different mechanisms were also suggested (Christiansen et al., 2010). As a hypothesis, vitamin E TPGS could compete with pancreatic lipase at the beginning and this resulted in retarded digestion kinetics. In the course of lipolysis, more digestion products were generated and they might have a more or less affinity with vitamin E TPGS to form solubilising structures (Jensen et al., 1963). This should free gradually active sites of enzymes. Furthermore, at this point, almost trilaurin should have been digested into digestion products. The more they are solubilised, the faster they could be digested (Christophersen et al., 2013b; Witzleb et al., 2012).

The quantity of each sample was normalised to 500 mg of each formulation. To compare digestibility of different liquid lipid types, the tests could be performed on the same quantity of lipids with all the same parameters (Arnold et al., 2012). To compare digestibility of different solid lipid types or formulations, total surface area of solid systems should be considered as an important factor (Vithani et al., 2019a). As is demonstrated in this case study, use of coated microparticulate systems could be a viable suggestion for this type of comparative study. In fact, digestion of monolithic systems was also tested but a digestion extent obtained at the end of 3h was neglectable in comparison with that of multiparticulate systems (data not shown). Previous studies performed on lipid digestibility (Bertoni et al., 2018, Christophersen, Vaghela, et al., 2014; Christophersen, Zhang, et al., 2014) also agrees that the size of the system is important to design a comparative lipid digestibility study.

#### 2.4.6. Effect of Digestion

When it comes to solid lipid-based formulations, release testing in biologically simulated media in the presence of lipolytic enzymes has been sparsely conducted.

**Figure 5-16** shows the results of release testing coupled with *in vitro* lipolysis which was performed on three types of coated products. The graph shows that for all the coated products an immediate release profile, i.e. at least 85% active substance released within 45 min (Siewert et al., 2003) could be obtained instead of an extended release profile for **LLL-1F** and **LLL-2F** when performing release testing without lipolysis. Therefore, it is important for testing solid lipid-based formulated products that release testing coupled with *in vitro* lipolysis should be performed. As discussed before (see **Section 2.4.4**), release testing in simple media is always, though, practical, and vital for evaluation of quality in batch release and long-term stability.



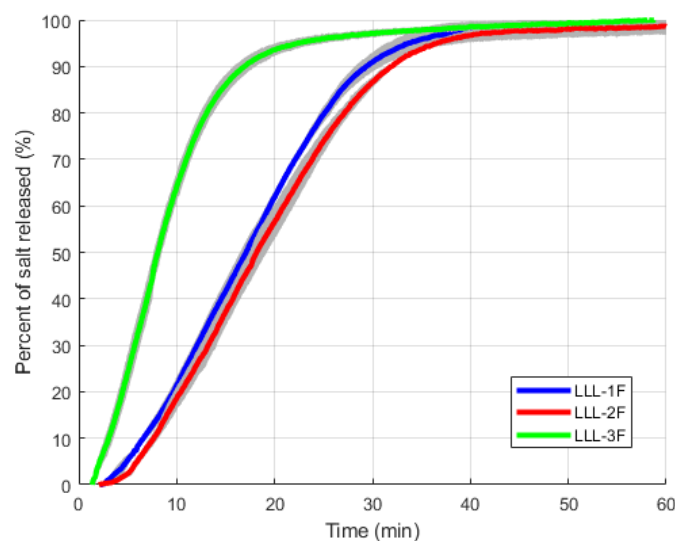


Figure 5-16. Salt release profile of products coated with **LLL-1F**, **LLL-2F** and **LLL-3F** ( $t_0$ ) in the course of lipolysis

Again, as fat in general, triglycerides in particular and notably trilaurin are likely to be substrate of *in vivo* lipolysis, combination of dissolution and digestion should become a normal testing for solid lipid-based formulated products in order to explore a full landscape of their functionalities.

To exploit lipids for their functionalities (e.g., taste-masking, enteric coating, prolonged release), it is of utmost importance to overcome processability and stability issues.

All the development work performed in the previous sections is till this point to highlight trilaurin – a medium-chain triglyceride – which could be used in hot-melt coating for several projective applications (e.g. moisture-proofing, taste-masking).

### 3. Conclusions

This research work demonstrates the effect of talc and vitamin E TPGS on manufacturability, release properties and stability of products hot-melt coated with trilaurin-containing formulations.

Firstly, as showcased by the study of trilaurin, for saturated monoacid triglycerides whose polymorphic profile comprises different polymorphs, two melt-based processing approaches are possible according the choice of either  $\beta$  MSZW (II) or thermal conditions less than  $T_{m,\alpha}$  (IV or V). This highlights the impact of additives on processability of solid lipid-based formulations as well as adds more values to already developed triglyceride-based formulas.

Secondly, with technical feasibility proof for the addition of vitamin E TPGS, its combination with trilaurin and talc was chosen for hot-melt coating compared to trilaurin without/with talc. There is a link between solidification properties of these formulations, specification of process variables and processing performance.

Thirdly, the advantages of non-conventional hot-melt coating are guaranteed as a stable polymorphic profile obtained after production with no need for curing. Despite the evolution of solid-state behaviours, a new strategy to improve release stability of lipid-based formulated products was revealed: fast

crystallisation of trilaurin-based formulations induced by talc. In fact, though phase separation for the ternary combination was observed from the beginning, salt release kinetics was found relatively stable with time.

Last but not least, coating with these formulations imparted a lower humidity sorption in comparison with uncoated NaCl. Addition of talc 1% w/w or vitamin E TPGS 10% w/w did not influence significantly the digestibility of trilaurin at the end of 3h lipolysis. As expected, digestion of trilaurin with a coating content around 30% w/w results in an immediate release profile for trilaurin and its binary combination. In conclusion, the results of this case study highlight the fact that a thorough understanding of material properties (e.g. crystallisation, polymorphism, digestibility) is of utmost importance for melt-processing, stabilising and customising release profile of solid lipid-formulated products.

## Chapter 6.

# HOT-MELT COATED SUBSTRATES: SALT AND AMORPHOUS SOLID DISPERSIONS OF PRAZIQUANTEL, TWO DIFFERENT CASES

---

### General Introduction

#### Sodium chloride

As said before, the first motivation to use NaCl crystals as a model substrate was the simplicity of checking membrane integrity during release tests on coated products (salt dissolves instantaneously in the dissolution media used in this thesis if it is not coated).

However, NaCl crystals have been coated aiming a slow release for the treatment and prevention of sodium chloride deficiency (Clarkson et al., 1971; Claviez et al., 1999) or sodium reduction in the food industry (Cai & Lee, 2020; Christina & Lee, 2016)

In the **first part of this chapter**, some selected coated NaCl crystals (with formulations from chapters 3,4 and 5) will be briefly compared with the coated commercial salt form (Slow Sodium Tablets®) in terms of release profile.

#### Amorphous solid dispersions of praziquantel

Solid amorphous dispersions are challenging drug systems in terms of physical stability. The **second part of this chapter** is dedicated to a more detailed study on an amorphous solid dispersion of praziquantel coated with some selected lipid-based formulations also selected from the previous chapters.

# Part 1.

## Hot-Melt Coated Sodium Chloride Crystals: Comparison with a Slow Release Reference Product

---

### 1. Materials and Methods

#### 1.1. Materials

Coated salt in **Chapter 3** – Part 1, **Chapter 4** – Part 2 and **Chapter 5** is used for this comparative study.

Salt hot-melt coated with three types of formulations:

- Beeswax-based formulations (**Chapter 3**): F1 and F2.
- Tristearin-based formulations (**Chapter 4**): NBAC4-3-40, NBAC4-9-40, NBAC4-3-60 and NBAC4-9-60.
- Trilaurin-based formulations (**Chapter 5**): LLL-1F, LLL-2F and LLL-3F.

The reference product: Slow Sodium Tablets® 600 mg NaCl (purchased in a pharmacy in England).

#### 1.2. Methods

##### 1.2.1. Measurements of release kinetics

The same experimental procedure already described in **Chapter 3 – Part 1** (See **Methods**) is applied. The tests were performed in water medium without enzymes.

### 2. Results and Discussion

#### 2.1. Beeswax-based formulations (from Chapter 3)

Release profiles of salt coated with varying coating contents of **F1** and **F2** (**Chapter 3**) were compared with that of a commercial product, used for the treatment and prevention of sodium chloride deficiency (Slow Sodium Tablets® 600 mg NaCl). According to the summary of product characteristics, excipients other than NaCl are low or not chargeable in aqueous media. It is safe to perform real-time measurements of salt release kinetics from this product applying the conductometry.

As demonstrated in **Figure 6-1**, with coating contents 49.3% **F1** and 44.2% **F2**, salt was released from coated products to the similar rate and extent up to 2h30 min in comparison with Slow Sodium Tablets®. Then, the release rate was slowed down for **F1**-coated products. However, if the general profile is considered, they are still comparable in terms of quantity released over time.

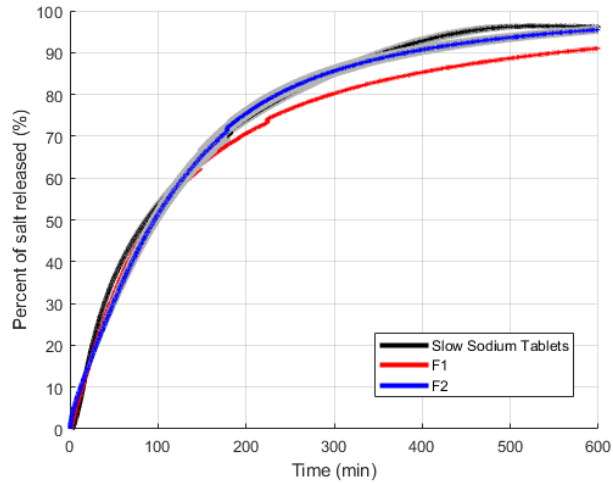


Figure 6-1. Comparative dissolution profile in water (37°C) with the reference product Slow Sodium Tablets® : Coating content in F1 and F2: 49.3% F1 and 44.2% F2

## 2.2. Tristearin-based formulations (from Chapter 4)

Figure 6-2 shows a comparative release profile between salt coated with two tristearin-based formulations processed at two different temperatures obtained in Chapter 4– Part 2. It shows that all products coated with tristearin-based formulations show an effect of coating (different release extents) in comparison with uncoated NaCl (100% dissolved within 5 min) (data not shown).

To conclude their release profiles, it is possible to use a single point value at 1h (FDA, CDER, 1997). A possibly immediate release profile was noticed for NBAC4-9-60 whereas all three other cases yield prolonged salt release, with that of the product NBAC4-3-60 close to the release profile of the commercial product Slow Sodium Tablets®.

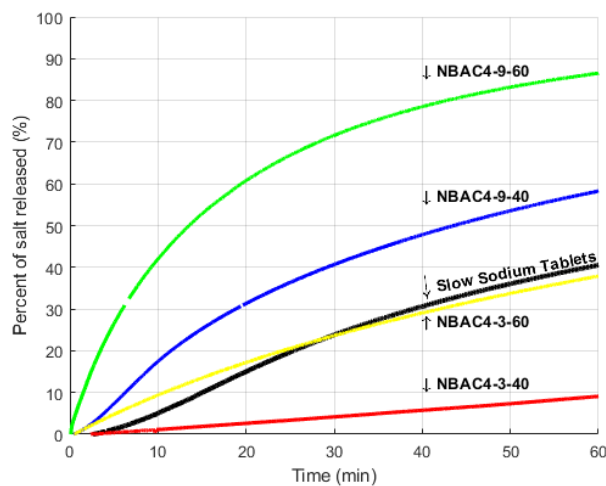


Figure 6-2. Comparative dissolution profile in water (37°C) of salt coated with two tristearin-based formulations processed at 2 thermal conditions: 33.8% NBAC4-3-40 (red line), 32.8% NBAC4-3-60 (yellow line), 32.3% NBAC4-9-40 (blue line), and 31.3% NBAC4-9-60 (green line).

### 2.3. Trilaurin-based formulations (from Chapter 5)

Figure 6-3 shows a comparative release profile of salt coated with three trilaurin-based formulations from Chapter 5. As shown in Figure 6-3, with release testing in water media, an immediate release profile can be obtained with LLL-3F while LLL-1F and LLL-2F yielded a prolonged release profile. However, in this case, as trilaurin is a highly digestible lipid in microparticulate systems (Christophersen, Zhang, et al., 2014b), release testing in biorelevant and lipolytic media can make all the difference. In fact, the three trilaurin-based formulations studied in this thesis yield an immediate release profile when considering their digestibility (Chapter 5). They could not be suitable for controlled-release dosage forms.

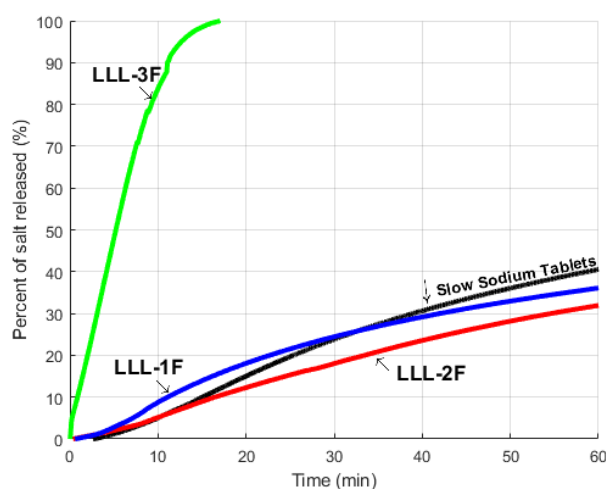


Figure 6-3. Salt release profile in water (37°C) obtained for salt coated with LLL-1F (blue line), LLL-2F (red line) and LLL-3F (green line).

### 3. Conclusions

By considering the dissolution results of the beeswax-based formulations (F1, F2) and the reference product, about 40% salt released at 1h could be set as a criterion for a comparable controlled release profile.

In the case of tristearin-based formulations, coating with about 30% w/w NBAC4-3-40 and NBAC4-3-60 (low concentration of surfactants) responds to this criterion. For the tristearin-based formulation with higher concentration of surfactants, a higher coating content is required to attain a controlled release profile comparable to that of the reference product. On the other hand, despite the results shown in Figure 6-3, trilaurin-based formulations are not suitable for extended release (by considering their digestibility, as presented in Chapter 5).

By comparing the current salt release profiles of all lipid-based formulations proposed and studied in this doctoral thesis, it could be shown that some of these formulations could correspond to the profile targeted for the application for which the commercial product (Slow Sodium Tablets®) is intended. This analysis is made only for comparative purposes, to have a benchmark in terms of target profile for a slow salt release, but it is not the intention of the current work to make a proposal in this sense.



## Part 2.

# Stability and *in vitro* Performance of Amorphous Solid Dispersions Hot-Melt Coated with Lipid-based Formulations of Diverse Digestibility

---

### Motivation

#### Reasons for coating amorphous drug solid dispersions

To improve solubility of poorly water-soluble drugs, amorphous solid dispersions (ASDs) have been considered as a formulation technology solution that can provide solids with high dissolution rate and supersaturation conditions (B. J. Boyd et al., 2019; Van Den Mooter, 2012). These systems consist of an amorphous active pharmaceutical ingredient stabilized in a matrix (generally a polymer). They can be produced by different processes, from a homogeneous mixture of the drug and the ‘matrix’ in a liquid state, which is then solidified by solvent evaporation (from a solvent solution) or cooling (from a molten state) (Alzahrani et al., 2022; Dedroog et al., 2019).

Formulating ASD is associated with several challenges, among them, the physical instability of the drug amorphous form which depends on their susceptibility to recrystallise post-production, during use (Descamps, 2020). Recrystallisation could occur in the course of amorphization processing (i), storage (ii) or dissolution when solids are placed in a biologically simulated fluid (iii) (Descamps, 2020). To deal with the case (i), it depends strongly on the glass forming ability of the molecule and the choice of an appropriate bio-enabling technology (Baird et al., 2010; Ditzinger et al., 2019).

Coating ASDs could help overcome the stability challenge (ii) during storage. In this case, recrystallisation takes place at the temperature less than the glass transition temperature of ASDs ( $T_g$ ). While utilisation of polymer as anti-plasticizer (for increasing  $T_g$ ) could act well against local and global molecular mobility (corresponding to  $\beta$  and  $\alpha$  relaxations, respectively) in the bulk, it is less effective against rapid recrystallisation occurring in the vicinity of free surface or plastification under the effect of humidity (Descamps, 2020).

Coating of the surface even with a thin thickness (a few nm) has been successful to prevent recrystallisation of amorphous drugs in many instances (Bansal et al., 2011; Bosselmann et al., 2011; Duong et al., 2022; Novakovic et al., 2020; Puri et al., 2012; Wu et al., 2007).

Hot-melt coating an amorphous drug was also reported but recrystallisation was found be induced by the coat itself (Bannow et al., 2020). In this case, coating ASDs caused an adverse effect. These incidences could be due to the fact that coatings acted as heterogeneous nucleation inductor (Descamps, 2020). Technically, solvent-based coating risks to dissolve highly soluble drug or component(s) from ASDs (Kleinbach & Riede, 1995) and furthermore solvent contact has been reported to induce recrystallisation and heterogeneity in ASDs in a recent study (Boel & Van Den Mooter, 2023).

Solventless coating represents implicitly a preferable method from a processing point of view. Therefore, it always justifies the motivation of this study to evaluate **solid-state behaviours of ASDs hot-melt coated with lipid-based formulations of a diverse nature.**

Recrystallisation of ASDs in the course of dissolution (iii) pertains to biopharmaceutics study. In the case of solid lipid-based formulations, release testing with *in vitro* lipolysis in biologically simulated media is necessary (Bannow et al., 2020) as wetting of lipids should not be ignored and digestion of the lipidic coat could also contribute to drug release kinetics depending on their digestibility (Bertoni, Albertini, et al., 2018; Christophersen et al., 2013b; Witzleb et al., 2012).

ASDs coated with digestible solid lipids represent a special case for *in vitro* testing for two reasons:

- not only presence of bile salts but also surfactants, digestion products could change apparent solubility of drug via partition in micellar structures occurring in the media and in the course of lipolysis, which should influence its release kinetics in a dynamic manner (Gautschi et al., 2016).
- fast dissolution, supersaturation and precipitation are relevant to amorphous drug in ASDs, which makes complex to predict the biopharmaceutical behaviours of an orally administered drug involving multiple kinetic processes (Gray et al., 2020; Z. Wang et al., 2023).

Hence, by considering solubilising capacity of lipid species and supersaturating capacity of ASDs, the use of a static release testing model alone could fail to rank bioperformance (B. J. Boyd et al., 2019; Nora et al., 2022). A good *in vitro* testing approach should reflect the dynamics of *in vivo* formulation processing of ASDs coated with digestible lipid-based formulation and therefore it warrants for **application of an multicompartmental gastrointestinal digestion model** (Blanquet et al., 2004; López Mármol et al., 2022).

### **Raisons for coating amorphous solid dispersions of praziquantel**

According to the World Health Organization, schistosomiasis is a global parasitic disease affecting over 250 million people, for which Praziquantel (PZQ) is the most widely used drug (World Health Organization, 2022).

PZQ is a safe racemic compound with a good safety window, but its low efficacy against juvenile stages of the parasites, poor compliance in children (10-13 years, the most exposed population) due to the bitter taste and size of the oral forms given the dose to be administered (600mg), and highly irregular pharmacokinetic profiles limit its effectiveness.

Consequently, in order to eliminate infection, repeated doses are required, which limits its use in paediatrics and increases the risk of developing tolerance to the disease (Doenhoff et al., 2009; W. Wang et al., 2012). In this context, our research group has been studying new supersaturated forms of praziquantel capable of offering advantages over standard praziquantel, such as improved pharmacokinetic parameters and efficacy on adult *S. Mansoni* stages.

The main search for new solid forms of PZQ focuses on supersaturated forms such as amorphous solid dispersions (Ferreira Marques et al., 2018). Dissolution of these forms in aqueous biological media leads to PZQ concentrations well above the equilibrium concentration (compared to the crystalline form). To

reap the benefits of the supersaturated state, it must be maintained for a sufficiently long time to promote absorption. Although various formulations have already been studied, supersaturated forms need to be mastered in terms of stability. For example, in the solid state, amorphous solid dispersions may be susceptible to phase conversion in high humidity. *How can we avoid these undesirable changes in supersaturated forms in the solid state, and then in solution?* Maintaining the supersaturation of the PZQ molecule at physiological pH, good absorption in order to reach the biological target efficiently (as the parasitic worm lives in blood vessels, in the mesenteric veins close to the human intestine) and the impact on biological activity are the scientific hurdles to be overcome.

Coating with lipid/additive mixtures such as those developed in the present thesis, is a strategy not explored for these PZQ forms. The aim of taking a supersaturated form of PZQ developed as part of another PhD thesis (Boniatti, 2021) in the group is to propose coating it with the formulations developed in **Chapter 3**, **Chapter 4**, and **Chapter 5** in order to modulate the release profile of this supersaturated form and verify the impact of coating on its physical stability.

By considering all the elements discussed above, **this part of Chapter 6** reports the following properties of **hot-melt coated amorphous solid dispersions of PZQ**:

- Monitored stability of samples stored during 6 months at 25°C/60% relative humidity.
- Release patterns from coated ASDs and drug bioaccessibility.

## 1. Materials and Methods

### 1.1. Materials

#### 1.1.1. Composition of amorphous solid dispersions:

Praziquantel (C<sub>19</sub>H<sub>24</sub>N<sub>2</sub>O<sub>2</sub>, PZQ), was kindly provided by Farmanguinhos (Fiocruz, Brazil). Kollidon VA64 (copolymer of vinylpyrrolidone with vinyl acetate, PVP/VA) and Montane™ 20 Premium Pharma (sorbitan monolaurate, SML) were provided by BASF (Germany) and SEPPIC (Castres, France), respectively.

Amorphous solid dispersions (ASD-PZQ) were composed of PZQ, PVP/VA and SML in a mass proportion of 35:60:5.

#### 1.1.2. Coating materials

The lipid-based coating formulations chosen for this study have been extensively studied in **Chapters 3, 4 - Part 2**, and **Chapter 5** thoroughly with respect to their manufacturability, release properties and three-month stability under long-term storage conditions in the former researches. Their composition is presented in **Table 6-1**.

Hot-melt coating of ASD-PZQ was executed on the first attempt right after generation of this product via hot melt extrusion.

*Table 6-1. Composition of lipid-based coating formulations*

Formulation	Excipients (% w/w)		
	BW	SMS	PS80
BWbF	Qs 100	1 to 20	1 to 10
	SSS	PS20	SML
SSSbF	91	4.5	4.5
	LLL	VitE TPGS	T
LLLbF*	90	10	1

\* indicates 1%w/w talc to the total 99%w/w of other components

## 1.2. Methods

### 1.2.1. Preparation of Praziquantel-containing Amorphous Solid Dispersions by Hot-Melt Extrusion

A twin-screw extruder Pharma 16 (ThermoFischer Scientific, Karlsruhe, Germany) was used to prepare ASDs. Following the previous work (Boniatti, 2021), the HME process parameters set were given in **Table 6-2** and shown in **Figure 6-4** to replicate production of high loading ASD-PZQ (35% w/w PZQ). PZQ and PVP/VA were initially mixed (72 rpm, 8 min) at the defined ratio using the mixer Turbula® T2F (WAB) and fed into the extruder using a single screw feeder (FW 18, Brablander Technologies, Germany). The extrudate was immediately spun, cooled and pelletized using a Varicut Pelletizer (ThermoFischer Scientific, Karlsruhe, Germany) to produce pellets 1 mm in size. The pellets were then milled (Scalable Lab System™ QUADRO® COMIL®) with 5000 rpm for speed and a sieve of 1143 µm of size. Only milled fraction 200-630 µm was used for hot-melt coating.

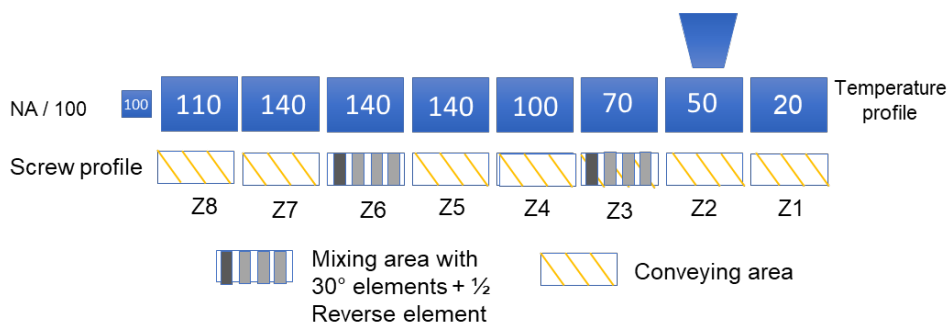


Figure 6-4. Simplified diagram of the screw profile and operating conditions of the hot extrusion process used to produce the amorphous solid dispersion of interest (ASD\_PZQ uc)

Table 6-2. HME process parameters for production of praziquantel-containing ASD (ASD\_PZQ uc)

conveying and extrusion			mixing		conveying and adding of additive		mixing		conveying		conveying and adding of mixture of powders
13.0 L/D			1.5 L/D		6.5 L/D		1.5 L/D		17.0 L/D		
100°C	110°C	140°C	140°C		140°C	100°C	100°C		100°C	70°C	50°C
			½ Rev	F30			½ Rev	F30			
			1	5			1	5			

## 1.2.2. Hot-Melt Coating of Praziquantel-containing Amorphous Solid Dispersions

### 1.2.2.1. Hot-Melt Coating (HMC)

HMC trials are performed using lab-scale Ventilus® airflow bed technology (Romaco© Group, Germany). The HMC process parameters are presented in **Table 6-3**. At the start of each coating trial, the process chamber was pre-heated with the entry of fluidisation and atomisation air flows. The substrate particles were then introduced to equilibrate with the temperature briefly and the coating operation was initiated. Coating operations were terminated until an estimated **30% w/w** could be reached.

Table 6-3. Process parameters and their values specified for each formulation

Parameters	Values specified for each formulation		
	BWbF	SSSbF	LLLbF
Formulation			
Reactor volume (L)	1		
Batch size (g)	250		
Final coating content (% w/w)	30		
Temperature of fluidisation air (°C)	20 (setpoint)	30 (setpoint)	30 (setpoint)
Quantity of process air (m <sup>3</sup> /h)	37		
Feeding rate (g/min)	≈ 7	≈ 12	≈ 12
Temperature of melt media (°C)	100	100	80
Temperature of feeding system (°C)	80	100	80
Temperature of spraying air (°C)	80	100	80
Pressure of spraying air (°C)	0.5		

Amorphous solid dispersions uncoated and coated with beeswax-, tristearin- and trilaurin-containing formulations are named as ASD-PZQ-uc (or uncoated ASD-PZQ), ASD-PZQ-cBWbF, ASD-PZQ-cSSSbF and ASD-PZQ-cLLLbF, respectively.

### 1.2.2.2. Curing

The product ASD-PZQ-cSSSbF was hermetically contained and subject to heating at 40°C during 8h in order to convert  $\alpha$  into  $\beta$  tristearin, using a climatic chamber (Memmert, Germany). The curing time is defined based on the results obtained in **Chapter 4 Curing – a study of polymorphic transformation**.

### 1.2.2.3. Stability study

Coated and uncoated ASDs are stored in open glass vials (see **Table 6-4**) in a climatic chamber temperature and humidity controlled at 25°C and 60 % UR, respectively. For any transport or any delay in analytical planning, samples were conserved in the freezer.



Table 6-4. Open glass vials containing PZQ-ASDs stored in climatic chamber (25°C/6%RH) for 3 months.

### 1.2.3. Product characterisation

The PZQ-ASD samples were analysed at zero (fresh production), 3 and 6 months after production.

#### 1.2.3.1. Assay Uniformity

For each sample, an amount equivalent to 9 mg PZQ was weighed and introduced into a 50 mL volumetric flask. Acetonitrile was used as solvent. Firstly, a small quantity of solvent was added. Then, all the contents should be kept hermetically and heated mildly on a plaque at a temperature of about 80°C in order to remove coating membrane and release active substance. After that, all the flasks were made up to 50 mL with acetonitrile and weighed again. For each analysis, the samples were pre-filtered via acetate cellulose membrane 0.45  $\mu\text{m}$ . Quantification was carried out using an integrated UPLC system (Agilent 1260 Infinity II) for data acquisition and processing. Assay uniformity was conducted in triplicate ( $n = 3$ ) on gravimetric basis and then converted onto volumetric basis. Calibration curve was performed using concentration series from about 2 to 230  $\mu\text{g/mL}$  ( $R^2 = 1$ ).

The UPLC assay was performed with the injection of 10  $\mu\text{L}$  samples through a Protosil C18 column at room temperature (25 °C) (250  $\times$  4.60 mm–5  $\mu\text{m}$ ) (Phenomenex, Bologna, Italy) in an isocratic mode with mobile phase consisting of acetonitrile and water (60:40 v/v) at a flow rate of 1 mL/min. A wavelength of 210 nm was used for detection. The retention time was found to be approximately 5.4 min and the run time was set at 10 min.

#### 1.2.3.2. Measurement of Particle Size Distribution (PSD) by Laser Diffraction

Measurements of PSD were performed (under dry dispersion mode (Mastersizer 3000, Aero Module - Malvern Instruments, Malvern, United Kingdom). Particle size measurements (Dv10, Dv50, and Dv90,



corresponding to the particle size below which 10%, 50% and 90% of the particles by volume are smaller than, and the volume mean diameter, VMD, the volume weighted mean particle size of the sample) calculated using Fraunhofer theory.

#### 1.2.3.3. Optical Microscopy

Images were obtained using a Leica EZ4 HD® microscope (Leica, Wetzlar, Germany) with an integrated high-definition digital camera, set to 10× magnification. The images were then edited with the Leica LAS EZ software program. For calibration purposes, an image (obtained under the same conditions) of a standard slide containing a straight 1 cm segment, with 100 divisions, was employed.

#### 1.2.3.4. Scanning Electron Microscopy

SEM images were obtained using a scanning electron microscope HITACHI TM3030 Plus (Hitachi, Tokyo, Japan) with an acceleration voltage of 15 kV. Samples were fixed on a support using a double-sided adhesive and covered with platinum using a high-resolution SEM coated spray Polaron SC7640 (Quorum Technologies, Lewes, UK).

#### 1.2.3.5. Modulated Differential Scanning Calorimetry

Thermal properties of formulations such as melting point ( $T_m$ ), phase transitions are studied using DSC Q200 (TA Instrument, USA). All the analyses are performed in non-hermetic aluminium pans under nitrogen purge at 50 mL.min<sup>-1</sup>. The DSC was calibrated with indium and an empty aluminium pan was used as a reference. The thermal programme was given in **Table 6-5**:

Table 6-5. Parameters of heating-cooling cycles applied in mDSC

Run	T <sub>start</sub> (°C)	T <sub>end</sub> (°C)	Rate (°C/min)	Amplitude (°C)	Duration (s)
1 <sup>st</sup> heating	180	-20	2	0.2	40
1 <sup>st</sup> cooling	-20	180	10	0	0
2 <sup>nd</sup> heating	180	-20	2	0.2	40

Crystallinity is estimated using the following formula:

Equation 54 :

$$\%Crystallinity = \Delta H_{i,meas} \times \frac{m_{DSC}}{\Delta H_{i,ref}} \times \frac{\Delta H_{A,ref}}{\Delta H_{i,ref}} \times \frac{100}{m_{DSC} \times \%PZQ_{sample}}$$

where  $\Delta H_{i,meas}$  is melting of polymorph B or C of PZQ measured in thermograph (J/g),  $m_{DSC}$  sample weight used for DSC measurement (g),  $\Delta H_{i,ref}$  reference melting enthalpy value of polymorph B or C of PZQ (J/g),  $\Delta H_{A,ref}$  reference melting enthalpy value of polymorph A (J/g),  $\%PZQ_{sample}$  contents of praziquantel in the sample (%). Reference melting enthalpy values were based on the study (De Moraes et al., 2023). Calculations are performed assumed no interference between thermal events recorded in DSC measurements.

#### 1.2.3.6. X-ray Powder Diffraction

A Philips X'Pert Panalytical X-ray diffractometer (Malvern Panalytical, Malvern, UK) using CuK $\alpha$  radiation ( $\lambda = 1.5418 \text{ \AA}$ ), 40 mA of current, and 45 kV of voltage was used. The recording spectral range was set at 3–45° with a measuring step (angular deviation between 2 consecutive points) of 0.0167° and an acquisition time of 240 s per point. The powder was filled in a sample holder and rotated at 2 s/revolution.

#### 1.2.3.7. Dynamic Vapour Sorption

Samples were loaded onto the quartz balance and dried at 25°C and 0% RH (setpoints) until a constant weight was reached (Surface Measurement Systems, London, UK). Relative humidity was increased from 10% up to 95% with a step size of 5-10% and maintained at each step until a change in mass per unit of time less than 0.01%/s. The temperature was maintained 25°C (setpoint) during the measurements.

#### 1.2.3.8. Release testing

Release from lipolysis study

Release kinetics of PZQ from uncoated and coated amorphous solid dispersions in biologically simulated media was performed using an *in vitro* static lipid digestion model pH STAT Titrand 901 (Metrohm, Switzerland) equipped with a dosing unit Dosino 800 (Metrohm, Switzerland) and a thermostat (LUDA, Germany). For each experiment, a quantity of samples equivalent to 25 mg PZQ was put inside a hard capsule 00 (Cooper). At the start of experiment, this dosage form would be added into a thermostated reaction vessel containing 36 mL of fasted-state simulated intestinal fluid (FaSSIF) whose detailed composition is given in **Table 6-6**.

The digestion experiments were initiated by the addition of substrate. At 5, 10, 15, 30, 45, 60, 90, 120 and 180 min, analytical samples (about 0.8 mL each, not compensated) were manually and simultaneously withdrawn and prefiltered via acetate cellulose membrane 0.45  $\mu\text{m}$ . They were then diluted twice with FaSSIF medium and assayed by means of HPLC. The content was kept at 37°C with continuously stirring. The pH-Stat automatic titration unit was used to maintain the pH around  $6.50 \pm 0.05$  by titrating with 0.20 M NaOH. For each sample, release testing is performed in triplicate ( $n = 3$ ).

Pancreatin extract was prepared by dispersing 1.28 g of porcine pancreatin powder (containing pancreatic lipase and co-lipase) to 5.2 mL tris-maleate buffer pH 6.5. The mixture was vortexed for 15 min at 5°C and underwent centrifugation at 1,600 g (4,000 rpm) at 5°C for 15 min according to the reported method (Arnold et al., 2012). The supernatant was collected into a vial of 10 mL. Activity of lipases in pancreatin was priorly assayed following a standardised method (Brodkorb et al., 2019). After dilution with FaSSIF, the final medium should have an activity of about 286 TBU/mL state, i.e. about a half of the reported fasted state activity (Christophersen, Vaghela, et al., 2014b). Pancreatin extracts were prepared at the start of a week and stored in freezer for a series of experiments. Before each experiment, a vial of 4 ml frozen pancreatin extract was thawed at room conditions for about 15 min. After adding the extract into the reactor, the whole digestion medium was titrated immediately to the setpoint pH 6.5.

Table 6-6. FaSSIF and FeSSIF composition and properties

	FaSSIF	FeSSIF
<b>Component</b>	Concentration	
Sodium taurocholate	3mM	15 mM
Lecithin	0.75 mM	3.75
<b>Buffer</b>		
NaH <sub>2</sub> PO <sub>4</sub> ·2H <sub>2</sub> O	5.14 g	
Glacial Acetic Acid		8.65 g
NaCl	6.19 g	11.87 g
NaOH	<i>qs ad</i> pH 6.5	<i>qs ad</i> pH 5.0
Water	<i>qs ad</i> 1000 mL	<i>qs ad</i> 1000 mL
pH	<i>pH 6.5 ± 0.05</i>	<i>pH 5.0 ± 0.05</i>
Buffer capacity	10	75
Osmolarity (Osm/L)	270	670

#### Release in biorelevant media

Release of PZQ from uncoated and coated amorphous solid dispersions was performed in a flow-through dissolution apparatus (USP4 apparatus, CE7 smart, SOTAX, Switzerland) equipped with the cell for powder and granulates (**Figure 6-5**) as described in European Pharmacopeia [Ref European Pharmacopoeia 11.4, 2.9.43 Apparent dissolution].

A 5 mm diameter ruby bead was placed at the bottom of the cone of the lower part of each cell, followed by glass beads of 1 mm diameter, a sieve of 0.2 mm aperture, a 0.7 µm Whatman® glass microfiber filter (GF/F, Millipore-Sigma, Burlington, MA, USA), and a 2nd sieve of 0.2 mm aperture on top of the lower part. Once the middle part was fit onto the lower part, an amount of uncoated and coated amorphous solid dispersions corresponding to 50 mg of PZQ was introduced into the cell and precisely weighted. The insert, used to prevent agglomerates of particles, was placed cone upwards on the clip midway down the middle part. A sieve of 0.112 mm aperture and a 0.7 µm Whatman® glass microfiber filter, were placed on top of the middle part and the upper part was fit onto the other parts. The dissolution medium consisted of 250 mL of buffer pH5 (blank FeSSIF) and in the following biorelevant media: Fasted State Simulated Intestinal Fluid (FaSSIF), Fed State Simulated Intestinal Fluid (FeSSIF) and Simulated intestinal fluid with pancreatin (SIF), each at a flow rate of 20 mL/min and 37°C. Detailed composition of FaSSIF and FeSSIF media are given in **Table 6-6**. Buffer pH 5 correspond to a blank FeSSIF without lecithin and taurocholate and SIF was prepared according to European Pharmacopeia (77.0 mL of 0.2 M sodium hydroxide, 250.0 mL of a solution containing 6.8 g of potassium dihydrogen phosphate R, and 500 mL of water R. Add 10.0 g of pancreas powder R, mix and adjust the pH to 6.8 if necessary. Dilute to 1000.0 mL with water R. Dissolution apparatus was used in a closed-loop configuration considering 3 independent samples of each uncoated and coated amorphous solid dispersions equivalent

to 50 mg of PZQ. Experiment with Sif was performed only on coated formulations. The samples were collected manually (1mL) at the following times: 5, 10, 15, 20, 30, 45, 60, 90, 120, 180 and 240 samples. The samples were analysed by HPLC.

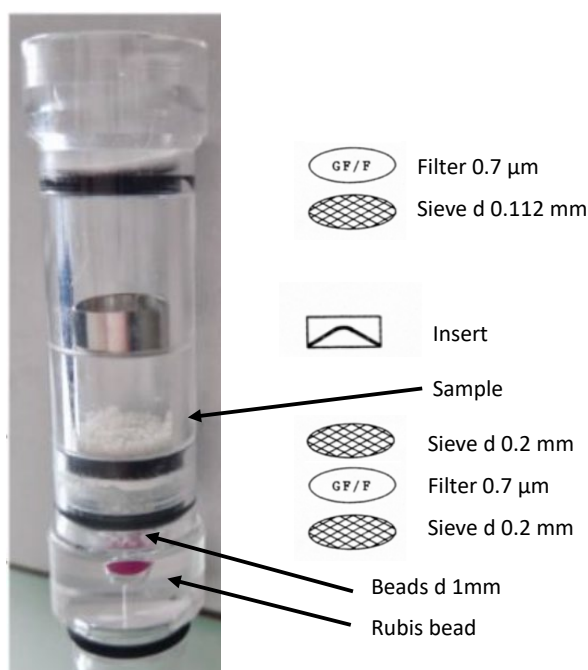


Figure 6-5. The flow cell for powder

#### Usage of artificial gastrointestinal model TIM-1

Bioaccessibility of PZQ released from uncoated and coated amorphous solid dispersions was assessed using the TNO gastro-Intestinal Model (TIM1). The TIM1 Model is a multi-compartment, dynamic and computer-controlled system developed at TNO Nutrition and Food Research (Zeist, the Netherlands) to reproduce the digestive process occurring in the luminal part of the human upper digestive tract (Dupont et al., 2019; Lvova et al., 2012; Minekus et al., 1995).

It consists of four serial compartments simulating the stomach and the three segments of the small intestine: duodenum, jejunum, and ileum. It enables control of the main mechanical, physical and biochemical parameters of digestion such as pH, temperature, peristaltic movements, volumes, transit times of the chyme, digestive secretions and passive absorption of water, salts and soluble small compounds through hollow fibers that continuously dialyse the jejunal and ileal contents. Each compartment is composed of glass jacket with flexible wall between which heated water flows to control both the temperature inside compartment (37°C) and the pressure on flexible walls inducing the mixing of the chyme by alternate compression and relaxation (**Figure 6-6**). Chyme transit is then regulated by opening or closing the peristaltic valves that connect the compartments. With respect to the computerised control of chyme transit, gastric and ileal deliveries are conducted following the exponential equation as below:

Equation 55 :

$$F = 100 \times 2^{-(t/t_{1/2})^\beta}$$

where  $F$  represents the fraction of meal delivered,  $t$  the time of delivery (min),  $t_{1/2}$  the half-time of delivery (min) and  $\beta$  is a coefficient describing the shape of the curve (Minekus, 2015).

The volume in each compartment is monitored by a pressure sensor connected to the computer. The pH is computer-monitored and continuously controlled by secreting either water or 0.3 M HCl ( $0.25 \text{ mL}\cdot\text{min}^{-1}$ ) into the stomach compartment and either electrolytes or 0.5M NaHCO<sub>3</sub> ( $0.25 \text{ mL}\cdot\text{min}^{-1}$ ) into the three small intestine compartments. Simulated gastric ( $0.5 \text{ mL}\cdot\text{min}^{-1}$ ), biliary ( $0.5 \text{ mL}\cdot\text{min}^{-1}$ ), and pancreatic ( $0.25 \text{ mL}\cdot\text{min}^{-1}$ ) secretions (pepsin, lipase, bile salts, and pancreatin) are delivered into the corresponding compartment by computer-controlled pumps. The model is equipped with hollow fiber membranes Sureflux-L (SF-09L,  $0.90 \text{ m}^2$ , cut-off 10 kDa, Nipro Medical France) connected to the jejunal and ileal compartments. Water and small molecules including the drug studied are removed from the lumen of the compartments by pumping dialysis fluid ( $10 \text{ mL}\cdot\text{min}^{-1}$ ) through the hollow fibers.

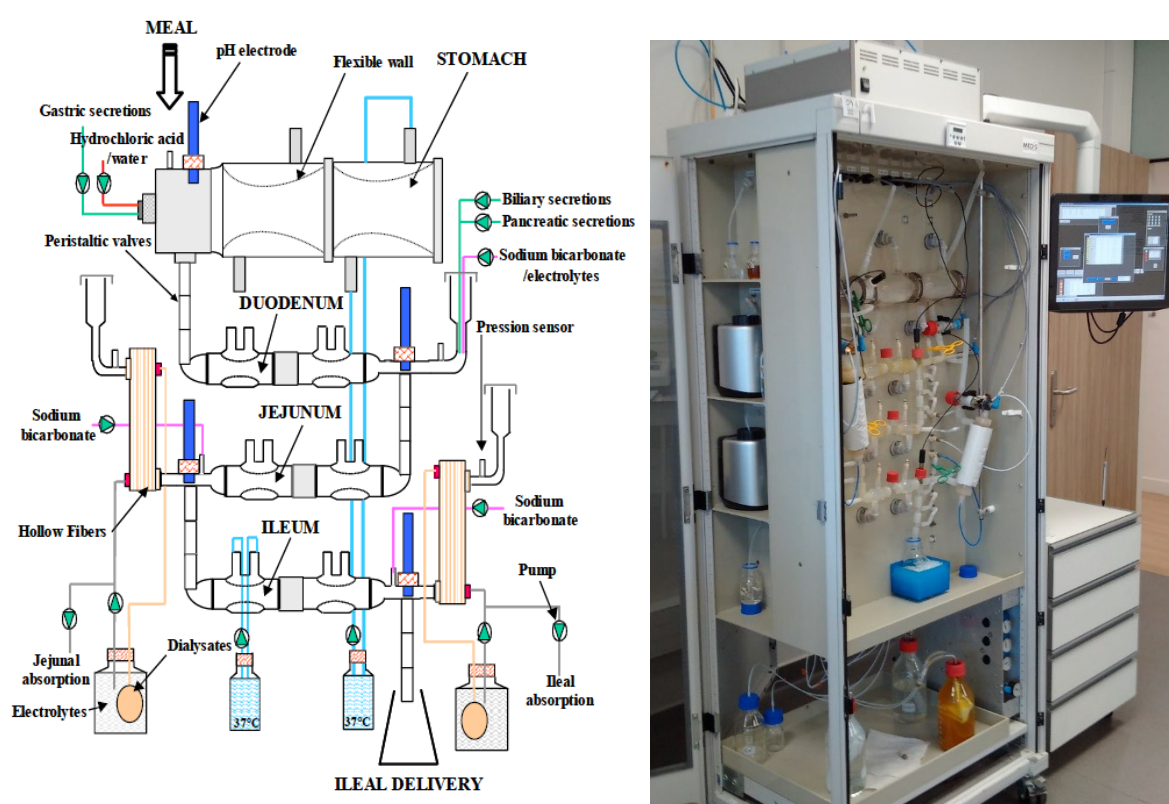


Figure 6-6. Schematic representation of the artificial digestive system comprising a stomach compartment and three segments of small intestine (duodenum, jejunum, and ileum) reproducing the *in vivo* digestive conditions of humans (adapted from Minekus et al., 1995) and picture of the system.

The TIM-1 system was set to simulate the fasted state, a digestion of a glass of water, in a healthy human adult for a total duration of 4 h according to *in vivo* data (Minekus, 2015) (See **Table 6-7**). For each formulated product, two hard gelatine capsules 00 (Cooper) containing an amount equivalent to 150 mg of PZQ were administered with 200 mL of mineral water (Volvic®, Volvic, France) in the TIM-1 system, in triplicate. During digestion, cumulated dialysis fluids (jejunal and ileal dialysates) and cumulated ileal effluents were regularly collected. Volumes were measured and PZQ determination in samples was performed using HPLC protocol previously described.

Table 6-7. Digestive conditions applied for in vitro digestion in the TIM-1 system. The TIM-1 was programmed to reproduce the digestion of a glass of water in a healthy adult

Compartment	Volume (mL) at initial time	pH/time (min)	Secretions	T(min); $\beta$ coefficient
<b>Stomach</b>	10 gastric residue	1.8/0;6.0/1;3.2/10; 2.4/20; 1.8/40 1.6/60; 1.5/240	Pepsine Lipase HCl	20; 1
	200 mL water			
<b>Duodenum</b>	50	Maintained at 6.4	Bile extract Pancreatin NaHCO <sub>3</sub>	
<b>Jejunum</b>	130	Maintained at 6.9	NaHCO <sub>3</sub>	
<b>Jejunal dialysis</b>	10mL.min <sup>-1</sup>		phosphate buffer pH 6.9	
<b>Ileum</b>	130	Maintained at 7.2	NaHCO <sub>3</sub>	150, 2.4
<b>Ileal dialysis</b>	10mL.min <sup>-1</sup>		phosphate buffer pH 7.2	

#### 1.2.3.9. Analysis of Release Kinetics

To analyze the release mechanism, several release models were tested such as Higuchi, Korsmeyer-Peppas and Harland.

*Higuchi Model.* This model is widely used to describe drug release from several types of modified release pharmaceutical dosage forms such as matrix tablets. The drug release mechanism is a diffusion process based on Fick's law, dependent on the square root of time:

Equation 56 :

$$Q_t = K_H \sqrt{t} \quad (5)$$

where  $Q_t$  is the fraction of drug released at time  $t$  and  $K_H$  is the Higuchi dissolution constant.

*Korsmeyer-Peppas Model.* This model is generally used to analyze the release of pharmaceutical polymeric dosage forms when the release mechanism is not well known or when more than one type of release phenomena could be involved:

Equation 57 :

$$\frac{M_t}{M_\infty} = K_{KP} t^n \quad (6)$$

where  $M_t/M_\infty$  is the fraction of drug released at time  $t$ ,  $K_{KP}$  is the Korsmeyer-Peppas kinetic constant characteristic of the drug/polymer,  $n$  is the diffusional exponent for drug release.

For a cylindrical-shaped matrix, if the exponent  $n = 0.45$  indicates Fickian release (case I),  $0.45 < n < 0.89$  indicates non Fickian (anomalous) release,  $n = 0.89$  indicates case II (zero order) release, and  $n > 0.89$  indicates super case II type of release



*Harland Model.* This model is used to the case of dissolution-controlled, diffusional release of drugs from mono- and polydisperse, non-swellable porous polymeric microparticles. It allows to define the predominant release mechanism erosion or diffusion according to the equation:

Equation 58 :

$$\frac{Mt}{M_{\infty}} = A\sqrt{t} + Bt$$

$Mt/M_{\infty}$  is the fraction of drug released at time  $t$ ,  $A$  and  $B$  are diffusion and erosion terms. When  $A > B$ , the diffusion factor prevails in the release system, whereas when  $A < B$ , erosion predominates. If  $A = B$ , the release mechanism includes both diffusion and erosion equally.

## 2. Results and Discussion

### 2.1. Processing Performance

Evaluation of a coating operation is based on three criteria: yield, efficiency and process regime. **Table 6-8** shows yield and efficiency of extrusion and hot-melt coating process. The ‘yield’ of the ASD-PZQ production by HME process covers the various involved operations with filament production by extrusion, followed by filament milling).

Encapsulation efficiencies of both HME and HMC processes were high (> 90%). During these coating operations, initially milled uncoated ASD-PZQ particles were found difficult to be fluidised, indicating poor flowability. After the coating was initiated movement of particles became more and more fluid.

Table 6-8. Yield, efficiency and content of praziquantel in uncoated and coated ASDs monitored every 3 months

Product name	Yield (%)	Efficiency (%)	PZQ content (%)	CoV (%)	PZQ content (%)	CoV (%)	PZQ content (%)	CoV (%)
ASD-PZQ	77.3	94.0	32.9	4.1	31.1	0.1	30.7	0.3
<b>Timepoints</b>	After production $t_0$				$t_1 = 3$ months		$t_2 = 6$ months	
ASD-PZQ cBWbF	86.0	98.6	23.8	0.7	21.6	2.3	22.5	0.2
ASD-PZQ cSSSbF	86.9	96.6	23.3	0.7	20.5	0.2	21.0	0.2
ASD-PZQ cLLLbF	88.7	99.1	23.0	0.3	22.2	0.5	22.1	0.1

Assay values of PZQ was interpreted as mass content of PZQ (mg) in relation to 100 mg total product mass. Assay ( $n = 3$ ) could be deemed as homogeneous as all CoV (%) were found less than 5% (Bánfai et al., 2007).

For verifying if a target process regime, i.e. strictly coating, was assured in HMC operations, size distribution and its parameters could be informative. **Figure 6-7** shows particle size distribution curve of non-fluidised, fluidised (but not coated), (fluidised) and coated ASD-PZQ in black dashed line, black and blue continuous lines, respectively. As can be seen, partial loss of fine fraction was demonstrated by both the absence of the shoulder observed in black dashed curve and an increase in the median peak of the black curve. The fact that the median peak of all the blue curves augmented indicated a coating regime obtained for all the three formulations. In fact, a raise in the median peak height suits a hypothesis

that fine fraction tends to consume more coating material than coarse fraction and if this continues to infinity solely one size class would be obtained. As a precaution, a slight displacement of PSD measured for ASD-PZQ cLLLbF towards the right might indicate partial agglomeration that occurred during coating.

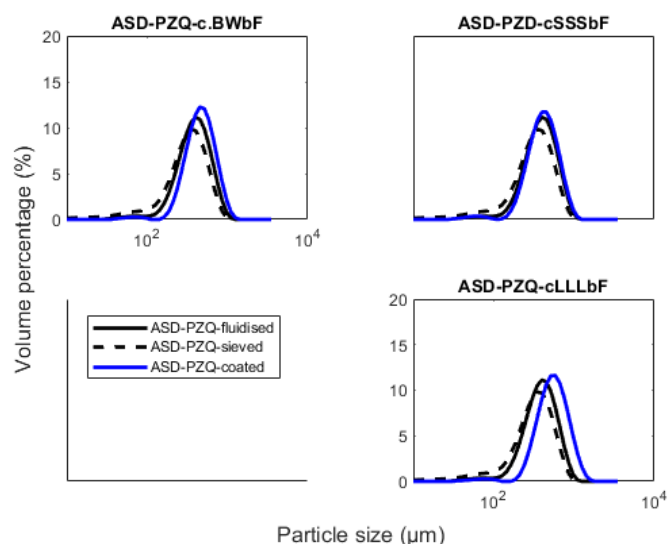


Figure 6-7. Particle size distribution (PSD) of uncoated and coated PZQ amorphous solid dispersions. Size distribution curve of initial ASD-PZQ, i.e. sieved but not fluidised, (dashed line), that of fluidised ASD-PZQ, i.e. not coated, (black line) and that of coated ASD-PZQ (blue line)

By considering PSD parameters shown in **Table 6-9**, coating regime can also be confirmed by the decrease in  $D_{v(90)}/D_{v(10)}$  and SPAN observed between coated ASD-PZQ and fluidised (but not coated) ASD-PZQ.

The same observation was found for PSD parameters between non-fluidised and fluidised ASD-PZQ but in this case this is due to the loss of fine fraction. Except PSD parameters of ASD-PZQ fluidised (but not coated), all these values would be considered in the discussion on dissolution results.

Table 6-9. PSD parameters measured for all the products containing PZQ

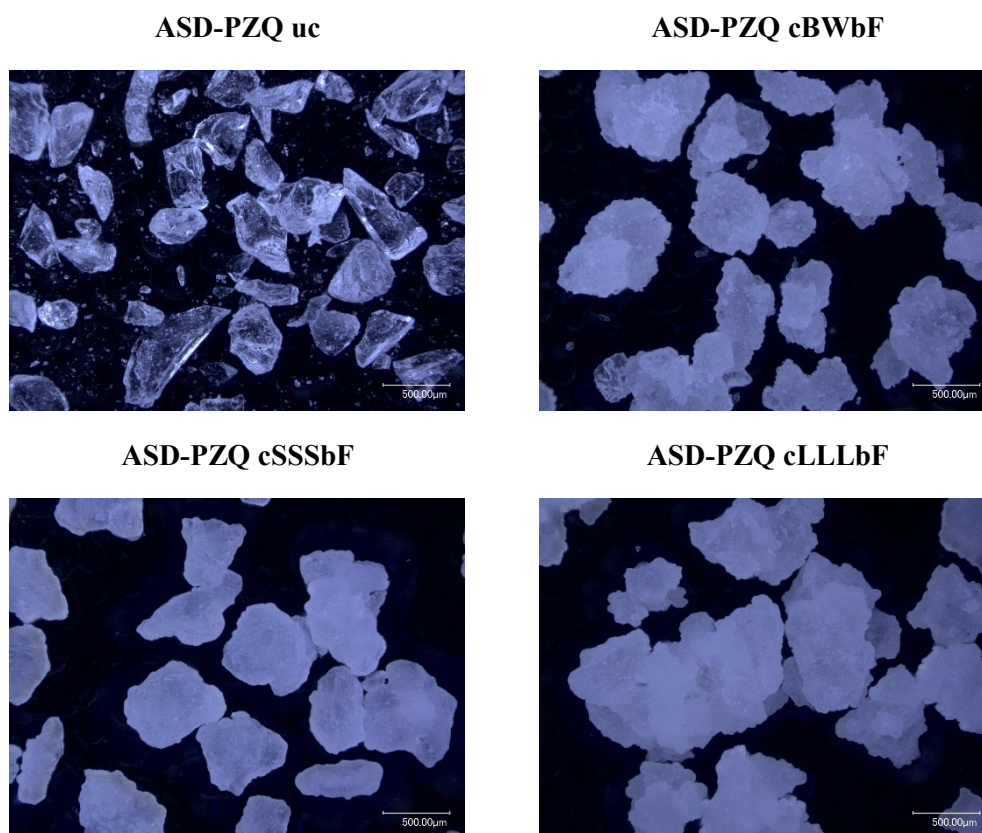
Product name	$D_{[4,3]}$ ( $\mu\text{m}$ )	$D_{[3,2]}$ ( $\mu\text{m}$ )	$D_{v(90)}/D_{v(10)}$	SPAN
PZQ	9.85	1.92	-	-
ASD-PZQ sieved	362	172	5.27	1.46
ASD-PZQ fluidised	439	334	3.28	1.19
ASD-PZQ cBWbF	523	423	2.84	1.07
ASD-PZQ cSSSbF	467	361	2.98	1.11
ASD-PZQ cLLLbF	622	483	2.99	1.13

## 2.2. Coating Quality

### 2.2.1. Optical microscopic observations

For evaluating coating quality in terms of surface coverage, microscopy was applied.

**Figure 6-8** shows optical images with a scale bar of 500  $\mu\text{m}$ . As can be seen, uncoated ASD-PZQ contained also fine fraction while this fraction was not evident for coated ASD-PZQ. The sharp edge of milled ASD-PZQ was rounded off as well as its translucence was lost after coating.



*Figure 6-8. Optical observations of uncoated and coated PZQ amorphous solid dispersions*

For ASD-PZQ cLLLbF, agglomerated particles were observed, which corroborate the finding its PSD curve.

As coating with LLLbF is a non-conventional approach where  $T_{\text{air},f}$  was set above  $T_{m,\alpha}$ , the setup of feeding rate is so laborious that nucleation of  $\beta$  LLLbF should occur on time in maintaining the fluidity of the operation as non-solidified particles could agglomerate while colliding with each other. This case study also shows initial agglomeration while a smaller feeding rate was defined in comparison with a previous work, i.e., about 12 g/min vs. 18-19 g/min. For future work, the feeding rate of LLLbF could be reduced for coating ASD-PZQ or alike as this should not significantly affect the rapidity of HMC.

However, the occurrence of initial agglomeration could be due the nature of substrate surface as it could induce or inhibit nucleation of LLLbF to a certain rate. This justifies the application of hot-melt goniometry to check solidification time lag of molten formulation on substrate surface in previous work.

### 2.2.2. Chemical contrast mode SEM images

The surface coverage post-coating could be verified via SEM using chemical contrast mode. Based on the principles of this SEM mode, substrate and coating formulation could be distinguished depending on their colour reflected by their different interactions with back-scatter electrons. A molecule whose

atomic mass is greater renders itself brighter under X-ray radiation. As shown in Figure 6-9. Images taken on chemical contrast mode for ASD\_PZQ cBWbF, ASD\_PZQ cSSSbF and ASD\_PZQ cLLLbF: Intact particles (500  $\mu\text{m}$  – left) and cross-sectioned particles (200  $\mu\text{m}$  – right) **Figure 6-9**, in this case, fortunately, there was a contrast between substrate (the core) and coating formulation (the coat).

The particles of the batch **ASD-PZQ cBWbF** observed by SEM product (at both scales) displays a not perfectly coated surface with many hemi-spherical shapes attached thereon. Cross-section of one particle shows no delamination between the coat and the core, which hints at a good affinity between BWbF and ASD-PZQ.

The particles of the batch **ASD-PZQ cSSSbF** was found also not to be perfectly coated. There are less hemi-spherical shapes observed but a rather smooth surface. With the image of a cross-section at 200  $\mu\text{m}$ , the coat was also found attached well to the core. The particles of the batch **ASD-PZQ cLLLbF** has a rough surface which suggests a more integral coating in comparison with those observed for the two latter formulation. White spots disseminated in the image at 500  $\mu\text{m}$  are talc particles whose atomic mass is the heaviest. Cross-section at 200  $\mu\text{m}$  also shows a good affinity between the coat and the core and in addition an irregular border of the coated particle.

The coating imperfections observed in the analysed particles could be due to the fact that the presence of fine fraction should have demanded a higher coating quantity to cover completely ASD-PZD than the minimal coating content concluded in **Chapter 3 – Part 1**. Furthermore, a higher surface coverage could be visually observed with the analysed particle of ASD-PZQ cLLLbF. This could be attributed to the advantage of non-conventional HMC approach where  $T_{\text{air},f}$  was set above  $T_{m,\alpha}$ . In this case, LLLbF once impacting the core had more time to spread before solidification whereas BWbF and SSSbF should solidify immediately (within seconds) at the defined temperature. The difference in film formation by either of two mechanisms of solidification in the case of sporadic nucleation (LLLbF) and spontaneous nucleation (BWbF and SSSbF) can be observed. In fact, hot-melt coating by direct  $\beta$  crystallisation was said to require less coating content to achieve a homogenous coating (D. G. Lopes et al., 2015).

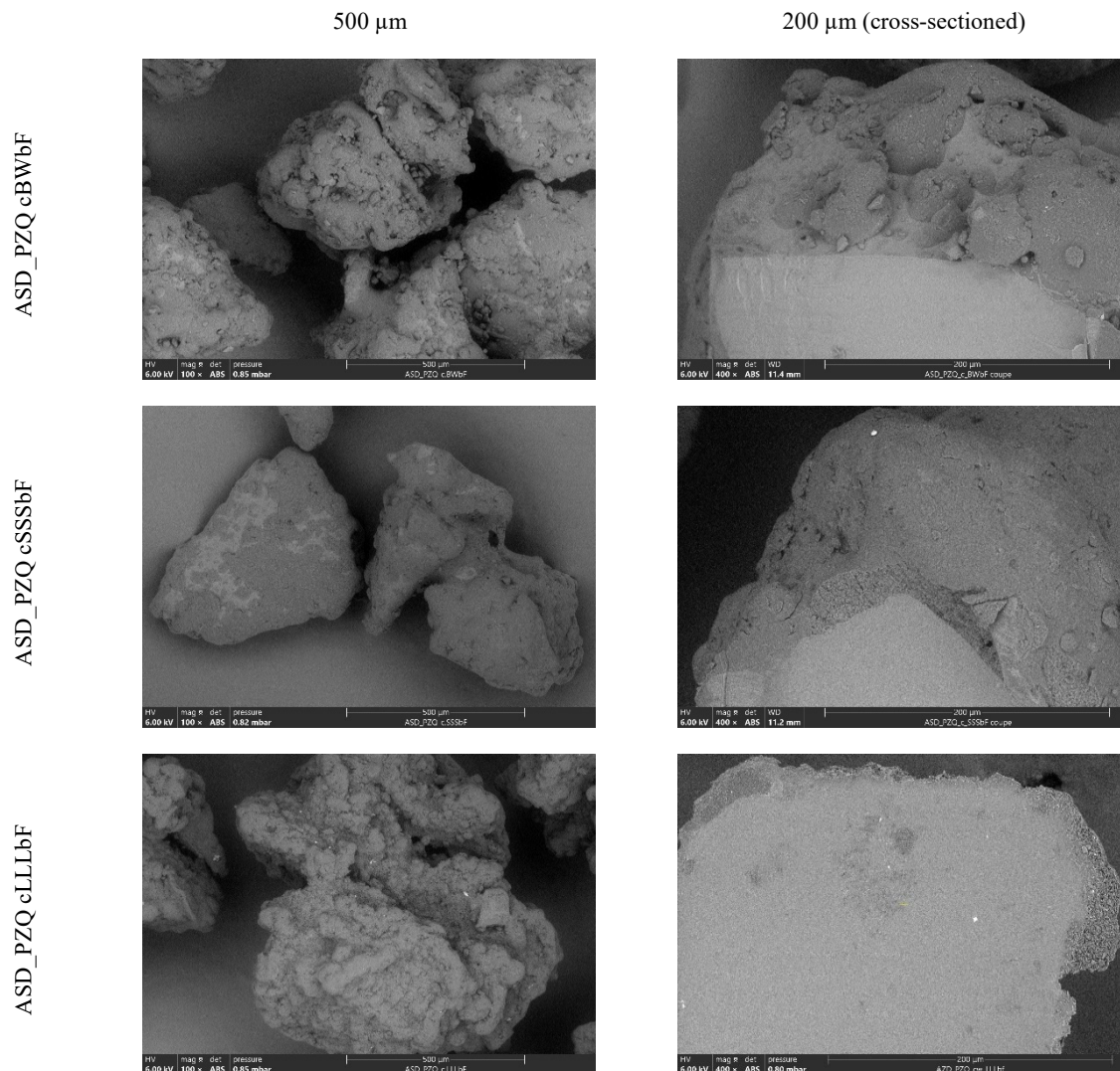


Figure 6-9. Images taken on chemical contrast mode for ASD\_PZQ cBWbF, ASD\_PZQ cSSSbF and ASD\_PZQ cLLLbF: Intact particles (500  $\mu\text{m}$  – left) and cross-sectioned particles (200  $\mu\text{m}$  – right)

### 2.2.3. Topographical contrast mode SEM images

At a smaller scale of observation, once the samples were coated a thin layer of metal, the resultant higher conduction allows for observing the topography of uncoated and coated surfaces of ASD-PZQ, as demonstrated in **Figure 6-10**.

- Surface of uncoated particles of ASD-PZQ was smooth, attached with loads of finer particles and marked with scratches which should be created in the course of milling.
- The analysed particles of ASD-PZQ cBWbF displays a smooth surface on which solidified droplets attaches in the form of hemi-spheres. There was not much blooming as expected but occurring needle-like features spread on the coat. This structure should be related to uncoated fine fraction of ASD-PZQ. On an exposed uncoated surface which was marked by the presence of scratches, those needle-like features were detected abundantly together with solidified hemi-spherical droplets of BWbF. This indicates again a high affinity of BWbF and ASD-PZQ which sustained despite the drag force in the fluidised bed.



- The analysed particles of ASD-PZQ cSSSbF exhibits, in the contrary, dense blooming which seems to mingle with needle-like features.
- The analysed particles of ASD-PZQ cLLLbF displays, as expected, a rough surface with irregular crests and troughs. The surface of troughs was formed by layered thick and fin-like flakes. These are not secondary structures (like bloom) but should be characteristic of a surface formed by directly crystallised  $\beta$  polymorph, as observed for tristearin.

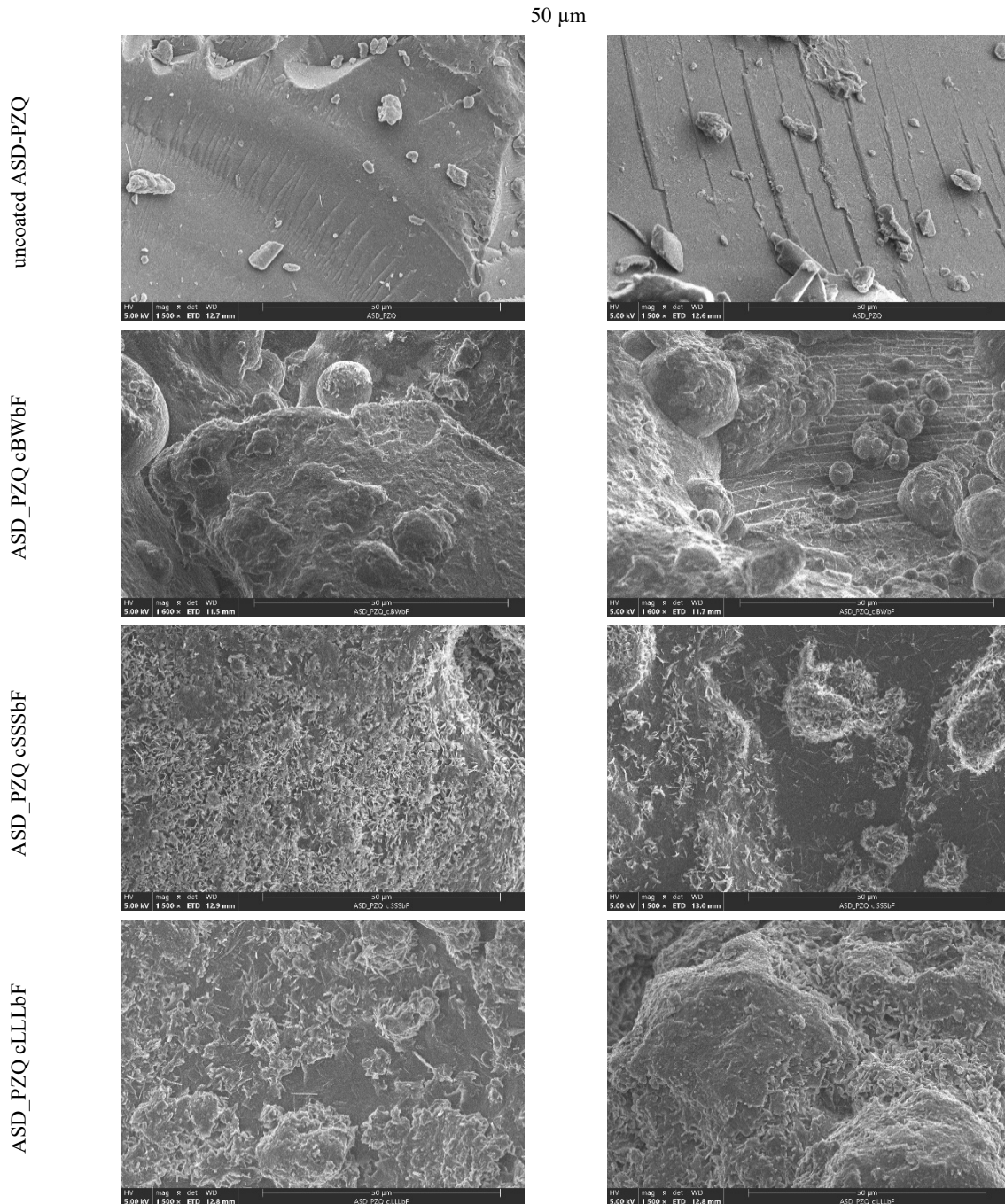


Figure 6-10. Images taken on topographical contrast mode (at length-scales of 50  $\mu$ m) for uncoated ASD\_PZQ, ASD\_PZQ cBwBF, ASD\_PZQ cSSSbF and ASD\_PZQ cLLLbF



## 2.3. Solid state behaviour

Coated and uncoated ASDs are stored in **open vials** in a climatic chamber, temperature and humidity controlled at 25°C and 60 % RH, respectively. The samples were analysed at time zero (fresh production), 3 and 6 months after production of the coated ASDs.

### 2.3.1. Hygroscopicity profile

As amorphous solid dispersions could be more hygroscopic than crystalline materials, dynamic vapour sorption was applied to monitor water sorption capacity of uncoated and coated ASD-PZQ with time. **Figure 6-11** demonstrates vapour sorption profile of uncoated ASD-PZQ (A), ASD-PZQ cBWbF (B), ASD-PZQ cSSSbF (C) and ASD-PZQ cLLLbF (D). According to the protocol, each sample was left in equilibrium with the dry condition (few degrees of relative humidity) till its mass did not change significantly between two recordings. Therefore, water vapour already attached on at the sample surface should be removed at the start of a new measurement.

Generally, **coating was found to reduce the maximal moisture absorption content** by considering uncoated ASD-PZQ (31.2%) in comparison with ASD-PZQ cBWbF (22.9%), ASD-PZQ cSSSbF (22.8%) and ASD-PZQ cLLLbF (22.6%). The fact of visualising change in mass plot allows for reading the rate and content of water sorption which all evolved within during storage.

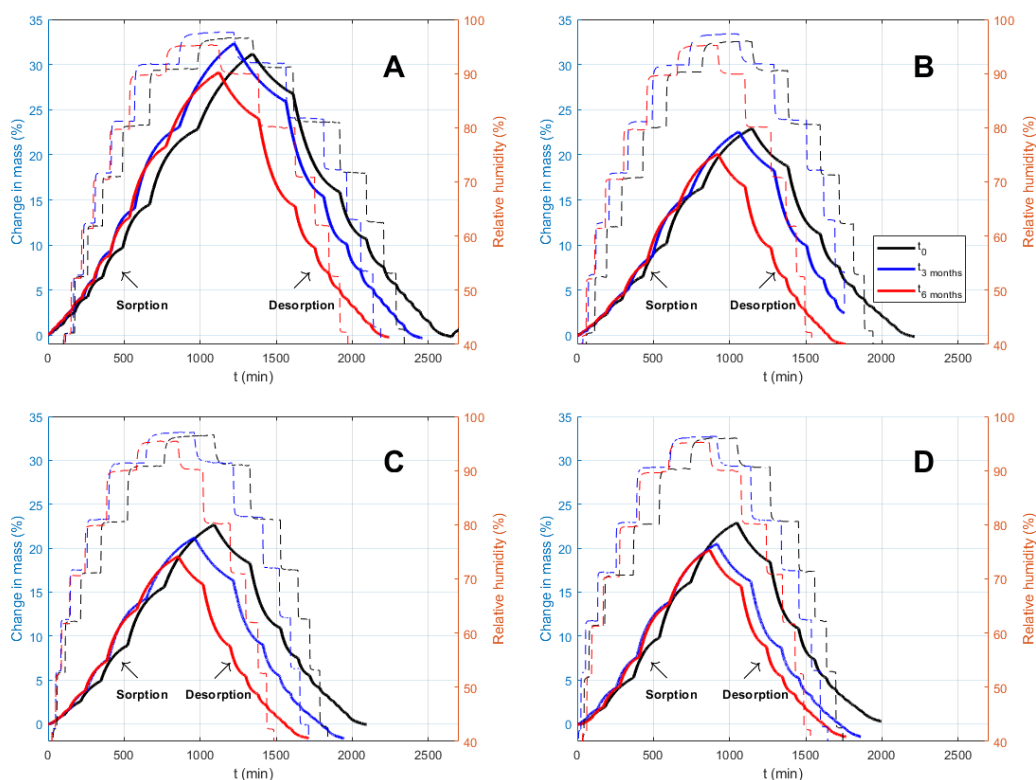


Figure 6-11. Vapour sorption and desorption kinetics of ASD\_PZQ (A), ASD\_PZQ cBWbF (B), ASD\_PZQ cSSSbF (C) and ASD\_PZQ cLLLbF (D): black line ( $t_0$ ), blue line (3 months\*) and red line (6 months\*). Dashed line in corresponding colour represents the programmed relative humidity. \* after months in open vial exposed to 25°C/60%RH

As observed, all the coated ASD-PZQ products had a common tendency to absorb less water with time at both  $t_1$  (3 months) and  $t_2$  (6 months). Water sorption extent of all the products was given in **Table 6-10**.

Table 6-10. Water sorption extent (%) at the maximal exposure to humidity in DVS measurements during storage

Product name	Water sorption extent (%)		
	$t_0$ (after production)	$t_1$ (3 months)	$t_2$ (6 months)
Uncoated ASD-PZQ	31.2	32.3	29.1
ASD-PZQ cBWbF	22.9	22.5	20.0
ASD-PZQ cSSSbF	22.6	21.2	18.9
ASD-PZQ cLLLbF	22.9	20.5	19.8

However, there were also particular sorption behaviours specific to each ASD-PZQ coated with SSSbF, LLLbF and BWbF, that will be better understood with information from the analysis of the evolution of the solid state of the samples, which will be done in the following with other analysis techniques.

### 2.3.2. Solid state evolution

#### 2.3.2.1. X-ray powder diffraction (XRPD)

For monitoring stability of amorphous form, XRPD and DSC are common techniques of first choice. **Figure 6-12** shows X-ray powder diffraction patterns obtained for uncoated and coated ASD-PZQ during six months of stability study: uncoated ASD-PZQ (A), ASD-PZQ cBWbF (B), ASD-PZQ cSSSbF (C) and ASD-PZQ cLLLbF (D). Grey continuous line denotes XRPD patterns of PZQ polymorph A (initial solid form, PZQ A), black, blue and red lines denote XRPD patterns of uncoated and coated ASD-PZQ at  $t_0$  (after production),  $t_1$  (3 months after) and  $t_2$  (6 months after). There was no sample of uncoated ASD-PZQ analysed at  $t_2$  because the uncoated granules were consolidated.

For a good interpretation, certain characteristic peaks in XRPD pattern of each occurring polymorph are to be identified. For PZQ A, peaks at 6.3, 8.0 and 20.0° ( $2\theta$ ) (marked by red dashed line) are present in its XRPD patterns but absent in those of PZQ C and PZQ B. Both the latter polymorphs are characterised by several common peaks, i.e. 6.9, 8.5, 16.4, 18.0, 19.7 and 21.5° ( $2\theta$ ) (marked by purple dashed line). XRPD pattern of PZQ C displays some of its characteristic peaks at 13.9, 15.3, 22.5 and 26.0° ( $2\theta$ ) whereas that of PZQ B possesses the peaks at 13.6 and 25.6° ( $2\theta$ ) to distinguish itself from the others (De Moraes et al., 2023). On the other hand, characteristic peaks indicating the polymorphic profile of lipid-based coating formulations are marked by a black dashed dotted line.

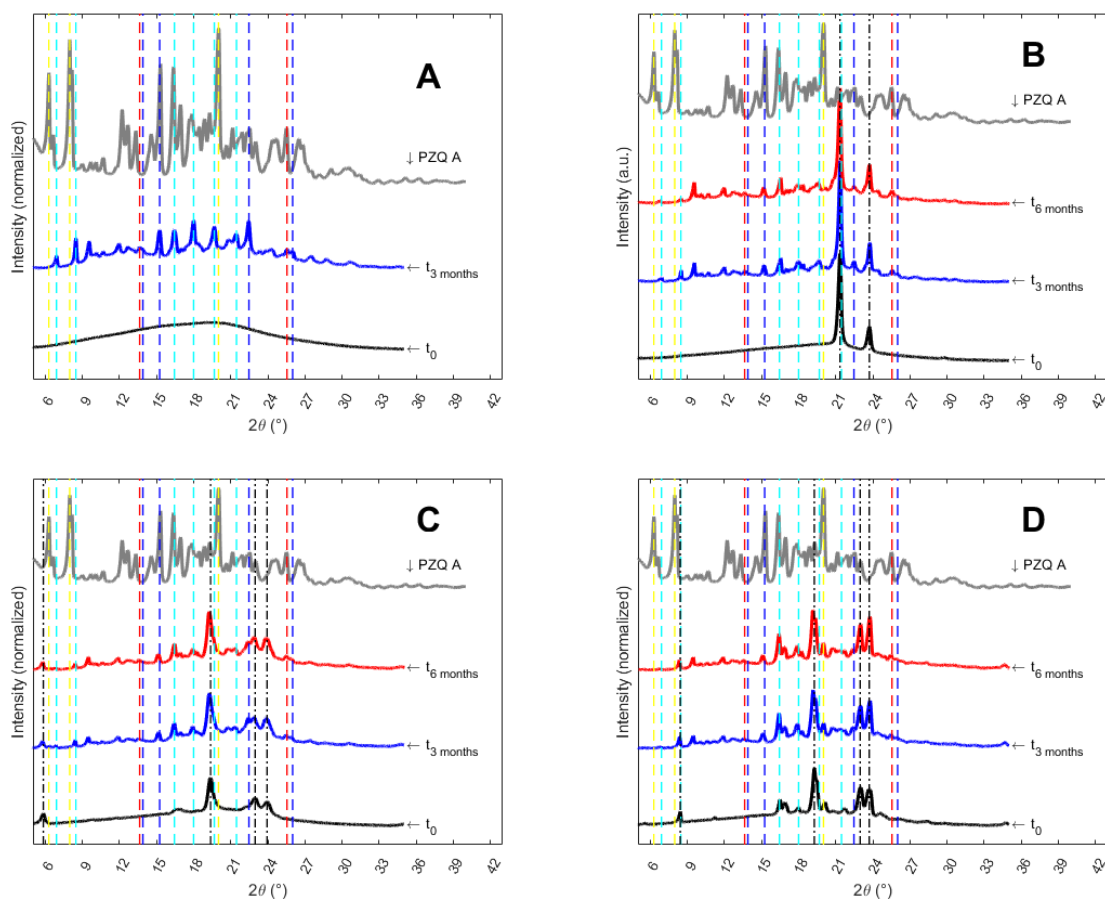


Figure 6-12. Normalised X-ray powder diffraction patterns obtained for ASD\_PZQ uc (A), ASD\_PZQ cBwBF (B), ASD\_PZQ cSSSbF (C) and ASD\_PZQ cLLLbF (D) over 3 months of stability study: black line ( $t_0$ ), blue line (3 months), red line (6 months) and grey line (PZQ initial form A). Yellow, red, blue and cyan dashed lines represent XRPD characteristic peaks of PZQ polymorph A, B, C or both B and C, respectively; dash-dotted line, XRPD characteristic peaks of lipid polymorph.

At the start of the stability study ( $t_0$ ), all the XRPD patterns (**Figure 6-12**) demonstrate the occurrence of PZQ amorphous form by the presence of a characteristic halo. In particular, the patterns of coated ASD-PZQ also show the polymorphic profile of sub- $\alpha$  or  $\beta'$  BWbF (**B**),  $\beta$  SSSbF (**C**) and  $\beta$  LLLbF (**D**).

Three months after  $t_0$ , peaks appeared in all the XRPD patterns. PZQ A was not identified as its characteristic peaks were absent. PZQ C and PZQ B could be identified by considering their XRPD fingerprints (De Moraes et al., 2023). Six months after  $t_0$ , PZQ A was still not identified while PZQ C and PZQ B were always present.

In the particular case of ASD-PZQ cLLLbF (**Figure 6-12-D**), XRPD patterns of  $\beta$  LLL share some close peaks with those of PZQ C and PZQ B at 8.4, 9.5, 16.5 and 18.0° ( $2\theta$ ). This could cast doubt on possible initial recrystallisation of ASD-PZQ coated with this formulation. However, this hypothesis could be excluded as the characteristic peaks of PZQ C and PZQ B (**D**) whose intensities are remarkable were absent in the XRPD patterns of ASD-PZQ cLLLbF obtained at  $t_0$ .

The position of characteristic peaks indicating polymorphic profile of the three lipid-based formulations was unchanged after 3 and 6 months of preservation. In fact, the stable polymorph  $\beta$  could be obtained

for trilaurin (LLLbF) and tristearin (SSSbF) right after production or after curing, respectively. Polymorph occurring in beeswax (BWbF) could evolve with time, but its release kinetics was deemed as “relatively stable” throughout a three-month period of stability study under the same conditions.

### 2.3.2.2. Differential scanning calorimetry (DSC)

As complementary characterisation, mDSC allows for identifying kinetic thermal events (e.g., melting, recrystallisation) and jump in the specific heat, where  $T_g$  could be detected.

**Figure 6-13** shows thermograms obtained for uncoated ASD-PZQ (**A**), ASD-PZQ cBWbF (**B**), ASD-PZQ cSSSbF (**C**) and ASD-PZQ cLLLbF (**D**) over six months. The dashed lines show the position of all the possible thermal events encountered by uncoated and coated ASD-PZQ. No melting peak of PZQ A was observed for all the thermograms.

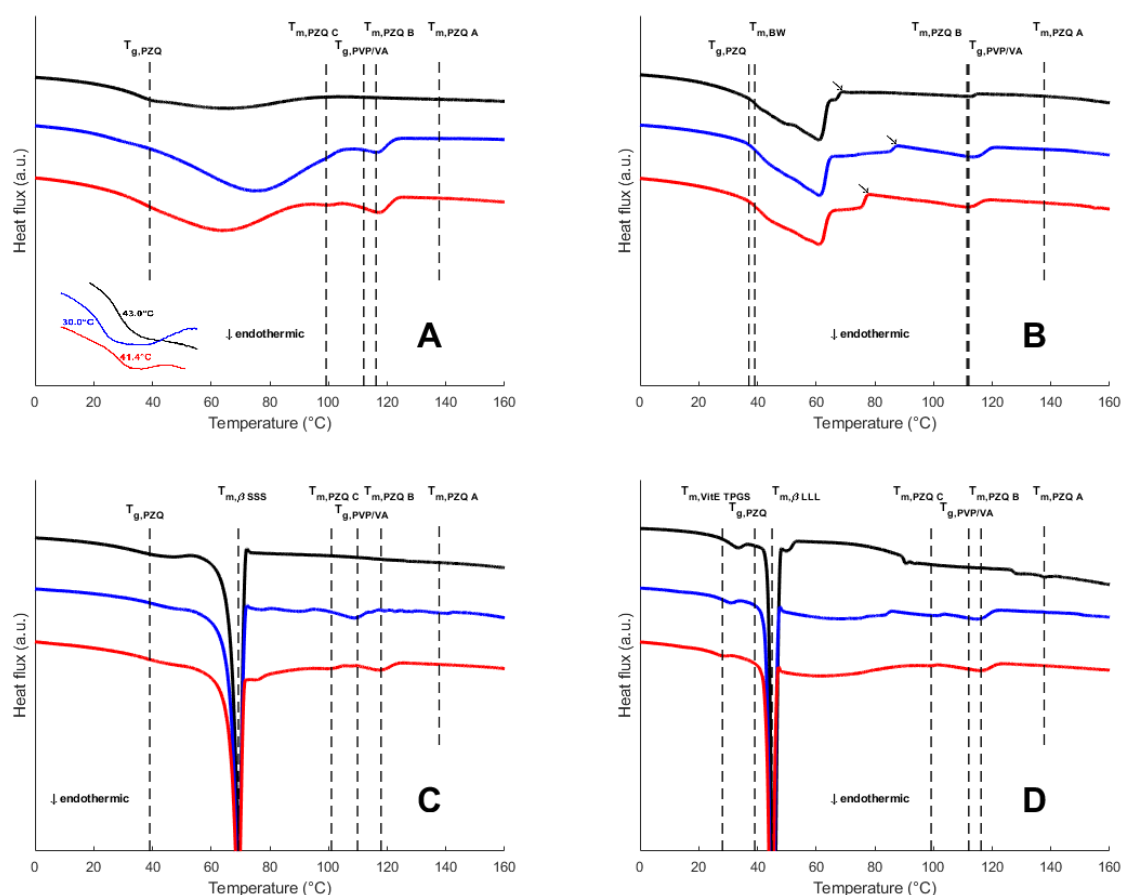


Figure 6-13. Normalised DSC thermograms obtained for ASD\_PZQ uc (A), ASD\_PZQ cBWbF (B), ASD\_PZQ cSSSbF (C) and ASD\_PZQ cLLLbF (D) over 3 months of stability study: black line ( $t_0$ ), blue line (3 months) and red line (6 months)

Thermograms of uncoated ASD-PZQ (**Figure 6-13-A**) at first sight show an evolution in  $T_g$  and specific heat jump from 43.0°C (0.334 J/(g.°C)) at  $t_0$ , 30.0°C (0.241 J/(g.°C)) at  $t_1$  (3 months after) to 41.4°C (0.146 J/(g.°C)) at  $t_2$  (6 months). In this case, water plasticised clearly ASD-PZQ at  $t_1$  but not this effect was less intense at  $t_2$ . It is presumed that after 3 months improved dispersibility of uncoated ASDs granules resulting from a small extent of crystallisation facilitated water penetration and reduction in  $T_g$

in the earlier period of stability study. As a consequence, the amount of amorphous form was reduced and the crystallinity increased with time. From  $t_1$  (3 months after), only melting peak of PZQ B appeared against the observation with XRPD patterns. In this case, melting peak of PZQ C could be hidden by relaxation enthalpy of the polymer PVP/VA spanning a range between 40°C and 120°C. From  $t_2$  (6 months after), both melting peaks of PZQ C and PZQ B were evident but it is doubtful that area under curve of those two melting peaks were masked by relaxation enthalpy of the polymer PVP/VA.

$T_g$  could not be detected for the three coated ASD-PZQ due to overlapping of onset melting peak of BW, crushing by large signal of SSS melting enthalpy and intertwining with melting peaks of vitamin E TPGS and  $\beta$  LLL in the vicinity.

In the case of ASD-PZQ cBWbF (**Figure 6-13-B**), it was unexpected that melting peak of PZQ B was observed at  $t_0$  against the observation in XRPD patterns. When carefully verifying the thermogram, it can be seen that this melting peak was preceded by an exothermic event which could be attributed to recrystallisation. This observation could be explained by the fact that melting of BWbF probably induces recrystallisation of PZQ B (indicated by a black arrow) at the time of analysis. At the timepoints  $t_1$  (3 months) and  $t_2$  (6 months), recrystallisation and melting peak of PZQ B was developed to a greater extent with time. However, despite its presence in XRPD patterns, PZQ C was not detected in these two analyses, which suggests its melting peak might be masked either by recrystallisation exothermic peak or by polymer relaxation endothermic enthalpy or by both. It is logical that PZQ C should occur before PZQ B according to the Ostwald rule of stages (Nývlt, 1995).

In both the cases of ASD-PZQ cSSSbF and ASD-PZQ cLLLbF (**Figure 6-13-C and D**), no melting peak was observed initially ( $t_0$ ). At the timepoints  $t_1$  (3 months) and  $t_2$  (6 months), melting peaks of PZQ C and PZQ B were noticed to an increasing extent with time. Relaxation enthalpy was still visible in the thermograms of ASD-PZQ cLLLbF whereas in those of ASD-PZQ cSSSbF it appeared to be masked by melting point of  $\beta$  SSS.

From the melting enthalpies of PZQ A (initial form) and PZQ C and PZQ B (re-crystallised during storage), crystallinity of PZQ A was approximately estimated and the results were given in **Figure 6-14**. At the beginning of stability study ( $t_0$ ), except ASD-PZQ cBWbF, no crystallinity could be detected via the current mDSC. Therefore, an immediate adverse effect of coatings on recrystallisation of ASD-PZQ could be excluded by considering a HMC case study (Bannow et al., 2020).

In the case of uncoated ASD-PZQ, crystallinity appeared to increase quasi-linearly from 0 ( $t_0$ ), through 18.3% ( $t_1$ ) up to 40.3% ( $t_2$ ). This shows an effect of moisture on the evolution of PZQ recrystallisation from the amorphous form.

In the case of ASD-PZQ cBWbF, as explained above, the initial presence of crystallinity for ASD-PZQ cBWbF was likely due to the recrystallisation of PZQ B and/or PZQ C induced by melting of BWbF while the sample was being analysed. This observation for coated ASD-based medicines has not been reported elsewhere in the literature. Nevertheless, this thermal behaviour is possible. For example, mixture of two monoacid triglyceride bearing different chain-lengths could induce melt-mediated recrystallisation of  $\beta'$  form, which is normally not the case when mixing a triglyceride and a surfactant

(J. S. Aronhime et al., 1988). By collating XRPD and DSC data, the initial crystallinity of ASD-PZQ cBWbF cannot be attributed to immediate instability of coated ASD like the reported case (Bannow et al., 2020). To estimate its crystallinity, a difference between melting and recrystallisation enthalpies was considered. Interestingly, the crystallinity of this product did not evolve significantly within 6 months. Despite a non-complete surface coverage, BWbF provides a good protection against the long-term exposition to high moisture (60% relative humidity). The fact that the crystallinity between the three timepoints was estimated to a similar quantity might due to the lack of resolution in thermal events. Melting of PZQ C should be expected whereas it was not noticed in all its three thermograms. As a precaution, it can only be concluded that recrystallisation of PZQ in ASD-PZQ cBWbF was either stopped or slowed down significantly in comparison with the other three products.

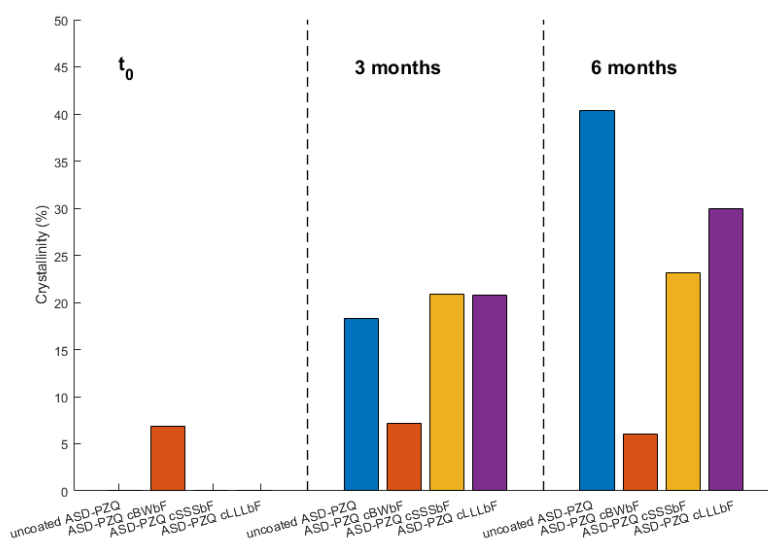


Figure 6-14. Evolution in crystallinity of praziquantel for ASD-PZQ uc (blue column), ASD-PZQ cBWbF (red column), ASD-PZQ cSSSbF (green column) and ASD-PZQ cLLLbF (purple column) during 6 months

By considering both products ASD-PZQ cSSSbF and ASD-PZQ cLLLbF, crystallinity seems to develop to a similar rate and extent, i.e. 20.9% and 20.8% (3 months), 23.1% and 30.0% (6 months), respectively. The fact that crystallinity of uncoated ASD-PZQ and these two products is comparable might be counterintuitive. In this case study, ASD-PZQ were probably not completely coated but a moisture-proofing effect by coating should not be excluded. A possible cause for this observation is that recrystallisation of ASD-PZQ was initiated at a certain moment during the stability study. In this case, recrystallisation was caused by both moisture and a latent induction activity of these two coatings. After 6 months, the extent of recrystallisation of these two coated products was much less than that of uncoated ASD-PZQ. With this further observation, it can be presumed that coating prevented recrystallisation of ASD-PZQ to some degree similar to the case of BWbF and this effect should be possibly constant with time. In the meanwhile, once the recrystallisation was activated by the long-term contact between the coat and the core, it evolved steadily but not so speedily when ASD-PZQ was exposed totally to moisture.



We can conclude that the use of both XRPD and DSC was judicious here to monitor stability of ASD-PZQ. In fact, XRPD is a sensitive technique in terms of its limit of detection whereas DSC enabled quantification of different polymorphs in the sample. The estimation of crystallinity should be considered as approximative as interpretation of DSC thermograms was complex. The fact that relaxation enthalpy of the polymer PVP/VA covers a wide range of temperature could interfere with thermal events of concern and disrupt the construction of a good baseline (Parker, 2000).

Specifically, stability of ASD-PZQ was mainly affected by moisture and coating did provide some protection effect.

Hot-melt coating with BWbF, SSSbF and LLLbF did not induce an immediate recrystallisation of ASD-PZQ but the two latter formulations could activate latently this unexpected physical process during storage. BWbF could be concluded to be more effective to stabilise ASD-PZQ with the double mechanisms: (i) protection against plasticisation by moisture and (ii) free surface modification to reduce molecular mobility. However, these findings should not negate the benefit of hot-melt coating in general and of a particular solid lipid-based formulation SSSbF, LLLbF or alike (Bannow et al., 2020). As the statement “no-size-fits-all” can apply, one hot-melt coating formulation can stabilise one product of ASDs but destabilise another. Furthermore, depending on the nature of ASDs, it could be probably stabilised by hot-melt coating in general regardless of the type of lipid-based formulations. Further mechanistic investigations could associate the choice of a specific group of lipids or additives to coating ASDs. However, it would be best to have a method which enables fast screening good combinations of one ASD in development and a variety of solid lipid-based formulations depending on stability and usage properties.

### 2.3.3. Effect of storage conditions

The products monitored during this storage period under controlled temperature and humidity conditions (25°C, 60%RH) were stored in open vials. However, we also stored the same products in parallel, at ambient temperature (~25°C), less exposed to the effect of humidity (in closed vials). **Figure 6-15** (presents some pictures of the vials, showing differences in color between them, depending on storage conditions (open x closed vial).

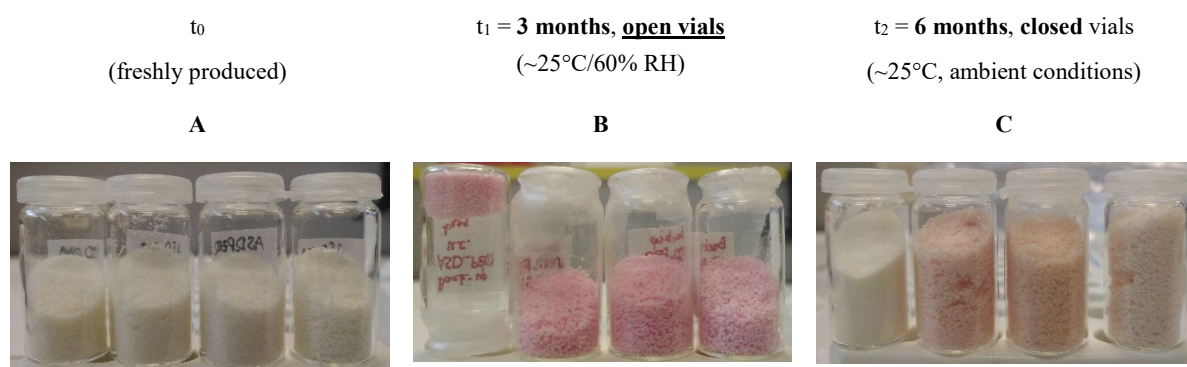


Figure 6-15. Appearance of uncoated and coated ASD-PZQ in the stability study. For each set of 4 vials, **from left to right**: uncoated ASD-PZQ, ASD-PZQ cBWbF, ASD-PZQ cSSSbF and ASD-PZQ cLLLbF.

Initially ( $t_0$ ), uncoated and coated ASD-PZQ were presented as fluid powder or granules very slightly orange (almost unnoticeable in Figure 10.A). In open vials, from 3 months of storage, all these products changed their colour into pink (Figure 6-15-B). Particularly, uncoated ASD-PZQ was densified into a monolithic compact. In fact, its compact was shown no longer flow when the vial was kept upside down. It was necessary to scratch its surface to generate some powder for further analyses.

In turn, after 3 months of storage in closed vials (Figure 10-C), the appearance of uncoated ASD-PZQ hasn't changed visually. The coated ASD-PZQ stored in closed vials visually changed colour to a more visible orange, but differently from the pink colour of the same samples stored in open vials, and less perceptible. This implies that humidity is a destabilising factor for uncoated and coated ASD-PZQ, and storage in closed vials could be the ideal conditions for these products to minimize any changes brought about by humidity.

## 2.4. Release properties

### 2.4.1. Release from lipolysis study

Measurements of **release kinetics coupled with lipolysis in biorelevant media** were performed in non-sink conditions in order to investigate potential of ASD-PZQ (e.g. fast dissolution, supersaturation, precipitation) subject to aging. Uncoated ASD-PZQ was also subjected to the same test, although lipolysis should only influence PZQ release from lipid-coated products.

Figure 6-16 demonstrates the corresponding dissolution profile of uncoated ASD-PZQ (A), ASD-PZQ cBWbF (B), ASD-PZQ cSSSbF (C) and ASD-PZQ cLLLbF (D) obtained over 3 months.

For uncoated ASD-PZQ (Figure 6-16-A), at  $t_0$ , a large variation was noticed during the first 60 minutes. This is ascribed to its poor dispersion behaviour, as observed experimentally. Besides, dissolution kinetics of PZQ from uncoated ASD-PZQ measured at  $t_1$  and  $t_2$  given the variability of the measurements, were not really very different.

Call  $C_{maximum}$  as kinetic solubility in this case. The  $C_{maximum}$  levels of all the products at 3 timepoints were given in Table 6-11.

Table 6-11.  $C_{maximum}$  levels recorded when testing uncoated and coated ASD-PZQ

Product name	Maximal concentration that PZQ could attain in the experiment ( $\mu\text{g/mL}$ )		
	$t_0$ (after production)	$t_1$ (3 months)	$t_2$ (6 months)
PZQ A <sup>#</sup>	302.0	-	-
Uncoated ASD-PZQ	466.5 $\pm$ 13.5	461.5 $\pm$ 0.4	445.0 $\pm$ 1.6
ASD-PZQ cBWbF	552.0 $\pm$ 9.7	445.0 $\pm$ 8.5	430.9 $\pm$ 9.6
ASD-PZQ cSSSbF	454.6 $\pm$ 5.9	424.3 $\pm$ 17.6	418.3 $\pm$ 21.1
ASD-PZQ cLLLbF	518.7 $\pm$ 3.6	460.0 $\pm$ 8.4	447.8 $\pm$ 14.8

<sup>#</sup> This experiment was performed once ( $n = 1$ ).

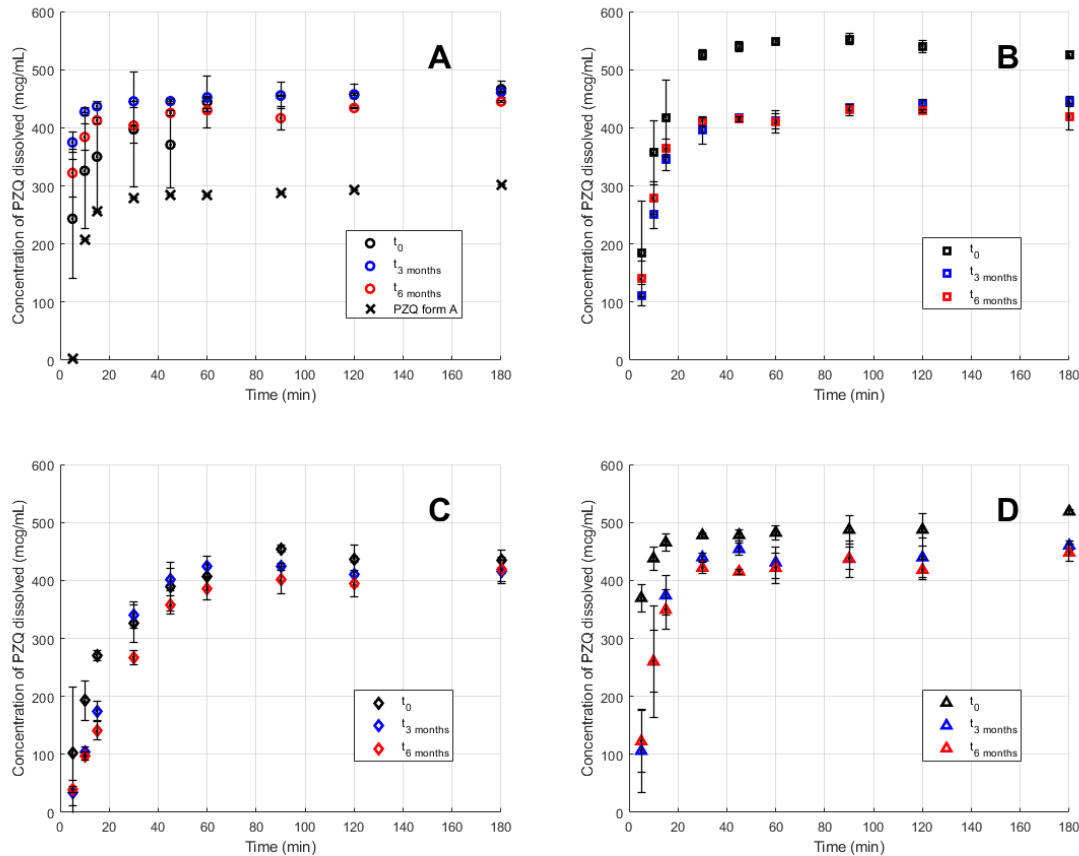


Figure 6-16. Dissolution profile of uncoated and coated amorphous solid dispersions in the presence of lipases: ASD\_PZQ uc (A), ASD\_PZQ cBWBf (B), ASD\_PZQ cSSSbF (C) and ASD\_PZQ cLLLbF (D)

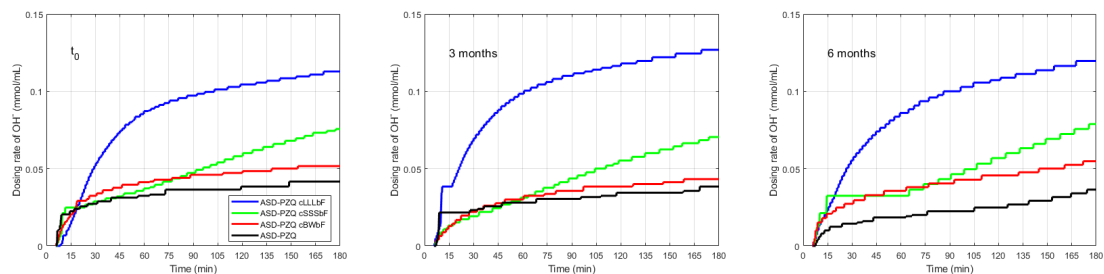


Figure 6-17. Digestion profile recorded for uncoated and coated products in stability study. ASD-PZQ (black line), ASD-PZQ cBWBf (red line) ASD-PZQ cSSSbF (green line), ASD-PZQ cLLLbF (blue line).

For the PZQ A fine powder, the  $C_{maximum,PZQ A}$  value obtained is  $302 \mu\text{g/mL}$ . For information, this result is comparable to the PZQ solubility in FaSSIF of  $289 \pm 77 \mu\text{g/mL}$  reported in a study (Eason et al., 2022). In comparison the kinetic solubility of PZQ A measured at about  $200 \mu\text{g/mL}$  (Boniatti, 2021), a solubilisation effect of FaSSIF was confirmed for crystalline PZQ A.

This effect was also observed for amorphous PZQ. In effect, the  $C_{maximum,PZQ amorph}$  of praziquantel corresponding to the ASD-PZQ 35:60:5 was around  $325 \mu\text{g/mL}$  at 30 min and 1h, as reported in the previous thesis (Boniatti, 2021).

In the course of dissolution of praziquantel, digestion of the lipid coatings took place simultaneously. **Figure 6-17** shows the digestion profile recorded for uncoated and coated ASD-PZQ. In this case, tests with uncoated ASD-PZQ could be regarded as “blank digestion tests” where there were no digestible coatings. As expected, digestibility (reflected by dosing rate of NaOH) decreases from LLLbF, SSSbF to BWbF. Digestion profile of each lipid coating seems not to change with time by considering the form of digestion curve and the final digestion extent.

For ASD-PZQ cBWbF (containing digestible surfactants) and ASD-PZQ cLLLbF, the  $C_{maximum}$  levels at  $t_0$  were raised over 500  $\mu\text{g/mL}$ . This might show the additive effect of supersaturation of amorphous PZQ and/or solubilisation by digestion products. This effect was notable in comparison with the solubility of crystalline PZQ in fed-state simulated intestinal fluid (FeSSIF) ( $581 \pm 20 \mu\text{g/mL}$ ) and far less than the solubility of crystalline PZQ in digestion medium (about threefold that of FeSSIF) (Eason et al., 2022).

According to **Table 6-11**, the  $C_{maximum}$  levels of PZQ in all the tests diminished remarkably from  $t_0$  to 3 months, except uncoated ASD-PZQ which tended to agglomerate at. From 3 to 6 months, a slight decrease was observed for all of them. This should reflect a reduction in their amorphous content, which is complemented by DSC analyses. The decrease in  $C_{maximum}$  from  $t_0$  to 3 months could be due to recrystallisation of the amorphous fine fraction content (much less than 50  $\mu\text{m}$ ) on the surface (indicated by a change in product colour) while coated amorphous solid dispersions (coarse fraction between 200 and 630  $\mu\text{m}$ ) should remain mostly amorphous at the timepoint of 3 months.

This also justifies the high  $C_{maximum}$  levels of PZQ obtained at  $t_0$  but not at 3 and 6 months after that. In this case,  $C_{maximum}$  could be said to be dependent on the size of ASD particles as observed with one similar case of drug-loaded PVP/VA polymer-based matrix (K. Zheng et al., 2019). Furthermore, by considering a comparable level of  $C_{maximum}$  between ASD-PZQ and ASD-PZQ cLLLbF, the solubilisation effect could be excluded in this case and it was the fine fraction of amorphous PZQ that impacted on the supersaturation level at  $t_0$ .

Furthermore, by considering high levels of  $C_{maximum}$  at  $t_0$ , solubilisation effect might be less important than the effect of coatings on dispersibility of ASD-PZQ and the effect of fine fraction of ASD-PZQ. In fact, despite the fact that PZQ had not been completely dissolved in the course of digestion, its concentration did not increase with the liberation of digestion products (indicated by the increase in the amount of consumed OH<sup>-</sup>). This signifies that amorphous PZQ did not dissolve anymore in the presence of digestion products. Furthermore, a higher  $C_{maximum}$  obtained for ASD-PZQ cBWbF than for ASD-PZQ cLLLbF might be due to coating imperfections, as discussed with SEM images. The increase in PZQ concentration in the lipolytic testing with ASD-PZQ cLLLbF could attributed to its higher coating uniformity. In fact, fine fraction of ASD-PZQ probably entrapped in the coatings could be released in the course of digestion and dissolve to increase its concentration.

Furthermore, although these dissolution experiments were performed under non-sink conditions, the percentage of PZQ dissolved reached 50-90%. (See **Appendix 04**) within 1h depending on the type of

product. Under non-sink conditions, it is plausible that 100% PZQ could be obtained within 1h for all the products. Therefore, an immediate release profile could be expected (Siewert et al., 2003).

#### 2.4.2. Release in biorelevant media

The dissolution of PZQ and PZQ from uncoated and coated amorphous solid dispersions in blank FeSSIF (pH 5), FaSSIF, FeSSIF and SIF are presented in **Figure 6-18**, **Figure 6-19** and **Figure 6-20** respectively.

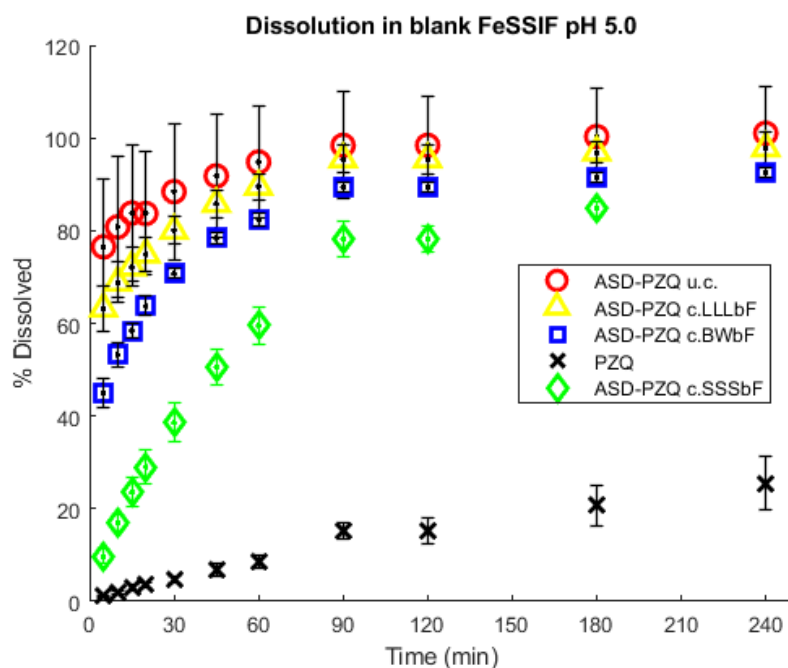


Figure 6-18. Dissolution in blank FeSSIF pH 5

As expected, in blank FeSSIF (pH 5) the dissolution rate of active substance PZQ is very low, less than 30% is dissolved in 240 min. PZQ is sparingly soluble in aqueous buffer, it is a class 2 drug with a poor solubility and a low dissolution rate that could be related to a lack of wettability and drug-solvent interaction, particles tended to agglomerate into a mass in the cell.

Considering the solubility of PZQ in phosphate buffer reported as  $282 \pm 149 \mu\text{g/mL}$  (Eason et al., 2022), the total amount of drug (50mg) should be able to dissolve in the volume of dissolution medium (250 mL). The hydrophobicity of drug, its lack of wettability and dispersibility limit its dissolution rate.

The solid dispersion (PZQ-ASD) exhibits a greater solubility and dissolution rate compared to pure drug. The amorphization overcomes the high cohesion energy in the packing of the PZQ crystal lattice. More than 90% of the drug is dissolved in less than 30 min and total solubilisation of the drug is maintained throughout the dissolution kinetic (240 min) without any decrease or parachute effect.

The release of the coated amorphous solid dispersion is dependent of the formulation. Whatever the coating formulation, the release is slower compared to ASD-PZQ. The coating acts as a barrier that limits the solvent penetration and PZQ diffusion. Furthermore, the coating reduces the variability (SD <5%) compared to ASD-PZQ (SD >10%).

The Trilaurin-based formulation (ASD-PZQ cLLLbf) and Beeswax-based formulation (ASD-PZQ cBWbF) had low impact on drug release compared to Tristearin-based formulation (ASD-PZQ cSSSbF). Note that inclusion of vitamin E TPGS in trilaurin was to accelerate release of PZQ, like the case of adding pore formers reported (Windbergs et al., 2009d). In the case of ASD-PZQ cBWbF, inclusion of lipophilic sorbitan monostearate and hydrophilic polysorbate was to modulate release of this active substance based on the reported digestibility of these two surfactants (Koehl et al., 2020; Vithani et al., 2017).

ASD-PZQ cSSSbF coating controls the release of the drug during the first 90 min of the kinetic. Despite the deemed “imperfect” coated based on SEM observations, it acts as a barrier that limits the diffusion of the drug. The obtained release profile was as expected for long-chain triglycerides (Rosiaux et al., 2015, 2022).

Because of their more physiologically relevant composition, compared to compendial media classically used in dissolution testing for quality control purposes, biorelevant media have been used to simulate the human gastrointestinal tract (Dressman et al., 1998). They not only simulate the pH, the buffer capacity and the osmolality of the gastrointestinal tract, but they also contain micelles, composed of sodium taurocholate and lecithin that mimic the human bile salts in fasted and fed state and allow the biorelevant media to better estimate the solubility and/or dissolution rate of poorly soluble drugs (Xie et al., 2014). The small intestine plays a particularly important role since bioavailability of drug depends on how much drug is dissolved in intestinal media. The determination of dissolution in FaSSIF and FeSSIF is an important tool to predict the behaviour of the dosage form in intestinal environment.

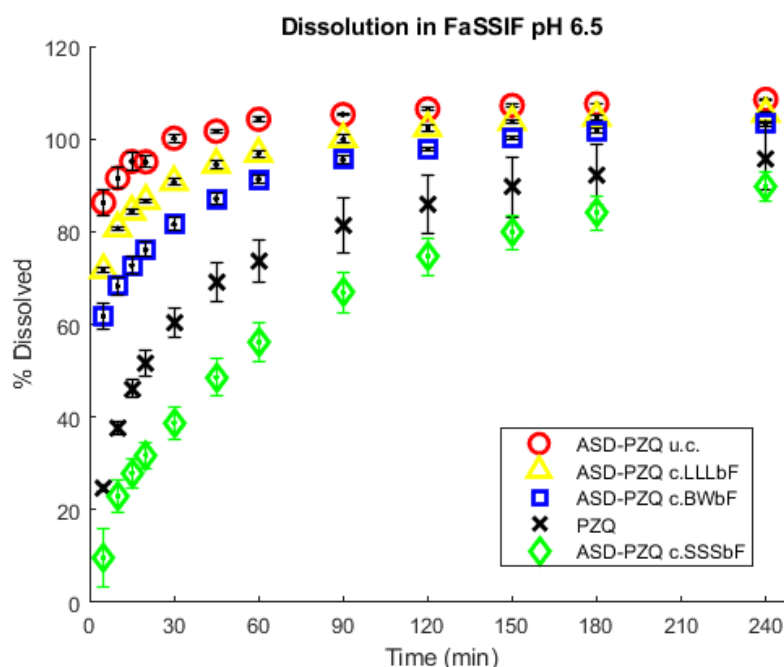


Figure 6-19. Dissolution in FaSSIF



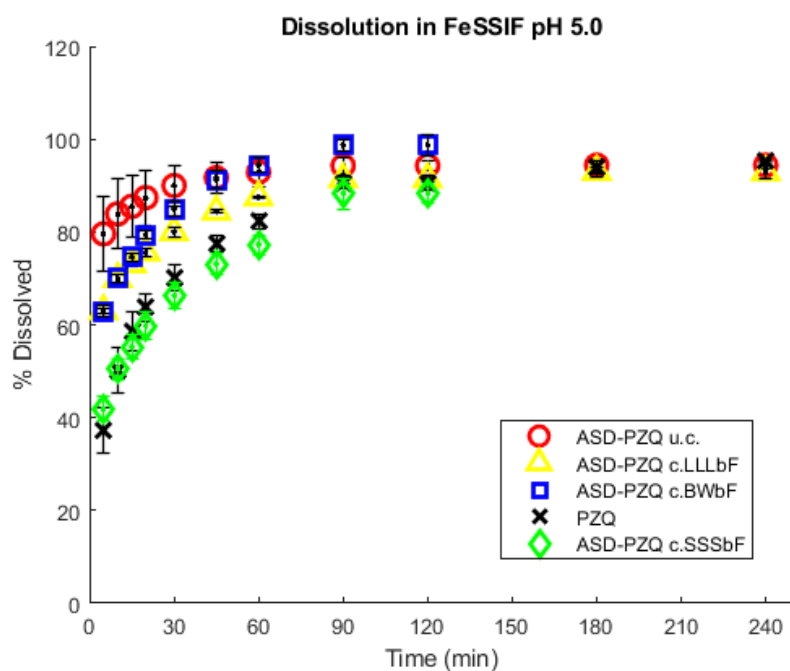


Figure 6-20. Dissolution profile in FeSSIF

In FaSSIF and FeSSIF, the release of PZQ is faster than in blank FeSSIF due to the presence of surfactants that increase the wettability and dispersibility of particles and the micelles that enhance its solubility. In FeSSIF, the amount of tensio active substance allows the sink conditions to be maintained, as the total % released is 100% in 4 hours, and in such conditions, the dissolution of PZQ is no more limited by its solubility but by its dissolution rate.

The main factors that will influence the dissolution rate are particle size, surface area and wettability of pure drug. These results are in accordance with the published solubility value of PZQ in FaSSIF and FeSSIF from  $289 \pm 77 \mu\text{g/mL}$  to  $581 \pm 20 \mu\text{g/mL}$  respectively. The results obtained in FaSSIF and FeSSIF for PZQ suggest a large food effect of the drug when given with meal. They are in accordance with published data showing that area under plasmatic curve of PZQ increased 180 and 271 % after administration with a high-lipid diet and a high-carbohydrate diet respectively (Castro et al., 2000).

In the literature reported that mixed micelles of sodium taurocholate and lecithin were formed when small amounts of lecithin were solubilized in bile salt and the structure was transformed into mixed vesicles only when the intramicellar concentration of lecithin exceeded the micellar critical concentration (Chakrabarty et al., 2005). The molecular structure of sodium taurocholate and lecithin mixed micelles explains the dissolution performance of biorelevant media. Sodium taurocholates interact either by their hydrophilic or hydrophobic phase to give a bilayer stable model in which the lecithin molecule can insert its long carbon chain. The micelle structure is stable and can enhance dissolution of hydrophobic molecules by hydrophobic interaction with the numerous hydrophobic spaces available in the multilayer hydrophilic/hydrophobic layer (Xie et al., 2014). Depending to the amount of lecithin and sodium taurocholate present in the dissolution medium, 3 times more in FeSSIF compared to FaSSIF, nearly sink conditions could be obtained and lead to a complete dissolution of the poorly soluble drug PZQ.

FaSSIF and FeSSIF had no influence on ASD-PZQ as the drug is soluble without the help of micelles and the dissolution rate is fast.

The influence of FaSSIF and FeSSIF is of less importance on coated PZS-ASD compared to blank FeSSIF for Besswax -based and trilaurin- based formulations as the release rate was already fast and almost complete.

For tristearin based formulation, the presence of large amount of surfactants substance increases the rate of release with close to 80% of drug released in FeSSIF at 60 min. These results in biorelevant media simulating the gastrointestinal environment in fasted and fed state suggest that, depending of the lipid material selected, the coating could act as a simple barrier that limit the contact of the drug with saliva after oral administration or is a barrier that could limit and control the release of the drug.

**Table 6-12.** gathered the main model parameters estimated for all dissolution profiles obtained at buffer pH 5, in FaSSIF and FeSSIF media for ASD-PZQ and all ASD-PZQ coated particles.

Table 6-12. Model parameters estimated for all dissolution profiles

Formulation	Korsmeyer-Peppas			Higuchi	Harland	Conclusion
	n	K <sub>KP</sub> (h <sup>-1</sup> )	R <sup>2</sup>	R <sup>2</sup>		
<b>Buffer pH 5</b>						
ASD-PZQ	0.081	2.67	0.9822	--	A>B	Fickian Diffusion
ASD-PZQ cLLLbF	0.131	1.33	0.9805	--	A>B	Fickian Diffusion
ASD-PZQ BWbF	0.211	1.61	0.9684	--	A>B	Fickian Diffusion
ASD-PZQ SSSbF	0.626	2.64	0.9709	0,962	A>B	Fickian Diffusion
<b>FaSSIF</b>						
ASD-PZQ	0.046	1.09	0.9188	--	A>B	Fickian Diffusion
ASD-PZQ cLLLbF	0.086	1.20	0.959	--	A>B	Fickian Diffusion
ASD-PZQ BWbF	0.128	1.34	0.9872	--	A>B	Fickian Diffusion
ASD-PZQ SSSbF	0,540	3.38	0.9461	0,9801	A>B	Fickian Diffusion
<b>FeSSIF</b>						
ASD-PZQ	0.050	1.13	0.9414	--	A>B	Fickian Diffusion
ASD-PZQ cLLLbF	0.113	1.31	0.9753	--	A>B	Fickian Diffusion
ASD-PZQ BWbF	0.137	1.33	0.9553	--	A>B	Fickian Diffusion
ASD-PZQ SSSbF	0.233	2.69	0.9912	0,8504	A>B	Fickian Diffusion

Whatever the dissolution medium studied, the release of PZQ from pure ASD or coated ASD with lipids excipients can be well integrated in a Fickian diffusion.

The Korsmeyer-Peppas model fits well all the data with a n value indicating a fickian diffusion.

With Harland model, for all the dissolution, A>B indicating a diffusion of drug from the AS-PZQ and all the coated formulations.

For tristearin based formulation, the release is controlled by the coating either in Blank FeSSIF, FaSSIF and FeSSIF and it can be well integrated in a Higuchi model corresponding to a diffusion process. The ASD-PZQ and the coating particles were well dispersed in the cell during the dissolution with a constant

flow of dissolution medium crossing the cell. The only phenomenon of release was diffusion of ASD-PZQ across the coating depending of the type of lipid in the formulation and the driven force generated by the surfactants in the dissolution medium.

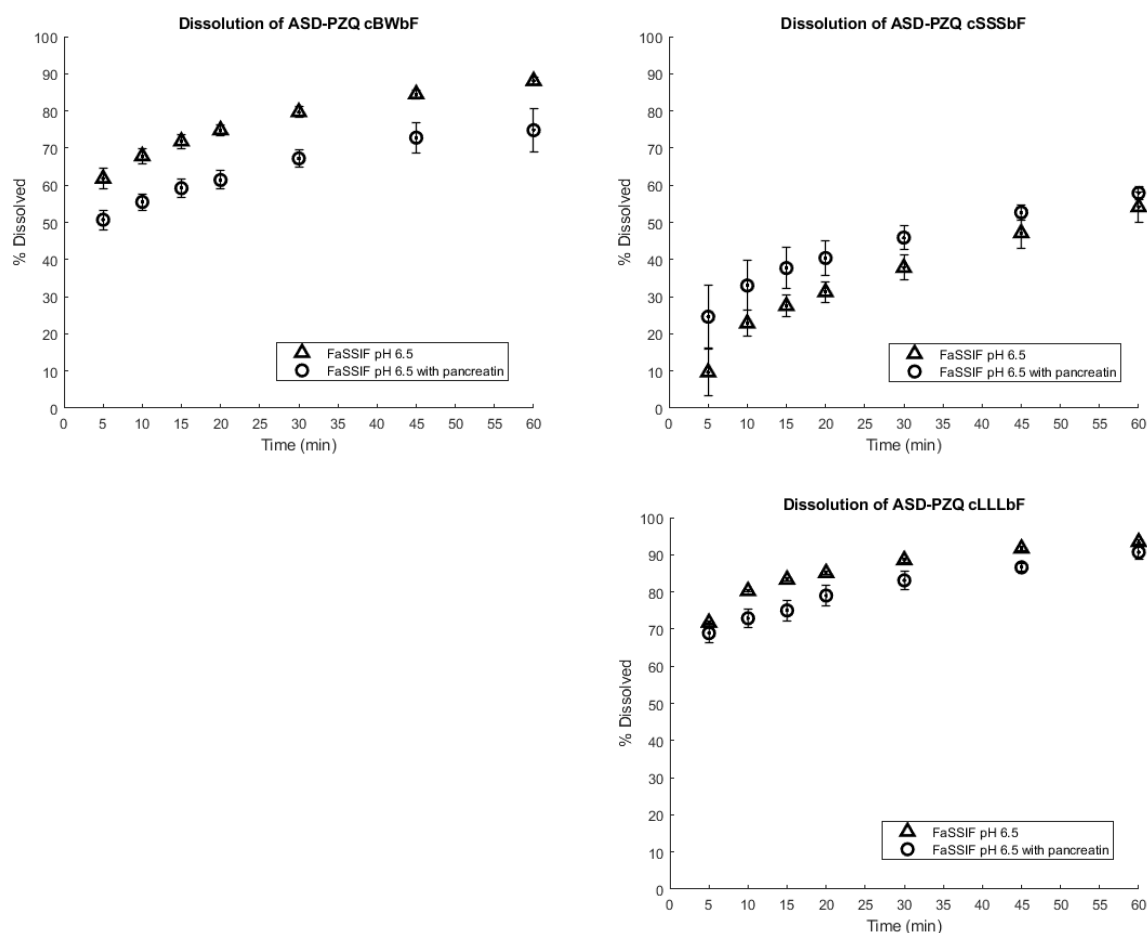


Figure 6-21. Dissolution of ASD coated with BWbF, SSSbF and LLLbF in SIF with pancreatin compared to FaSSiF

As shown in **Figure 6-21**, there is no difference between the release in FaSSiF, corresponding to a pH 6.5 with taurocholate and lecithin and SIF, corresponding to pH 6.8 with 10 g/L of pancreatin. There is no impact of pancreatin enzyme over the period of time studied (120 min) and there is no change in dissolution profile.

The diffusion of PZQ from the coated formulations is not affected by pancreatin. Pancreatin is a mixture of digestive enzymes containing amylase (breaks down starch), lipase (breaks down fats), and protease (breaks down proteins). The lack of influence of pancreatin could be related to either the amount of enzyme in the dissolution medium as well as the digestibility of lipids in the formulation.

As discussed with the results of *in vitro* lipolysis, the influence of pancreatin could be limited to its digestion impact on the release. In the case of ASD-PZQ cSSSbF, an increase in praziquantel release kinetics might be thanks to lipolysis of the coating simultaneous to dissolution (see **Figure 6-16** and **Figure 6-17**). In the case of ASD-PZQ cLLLbF and ASD-PZQ cBWbF, the lack of influence of pancreatin might be due to high coating contents up to about 30% w/w as well as no effect of solubilisation expected from digestion products.

## 2.5. Pharmacokinetic properties

### 2.5.1. Dissolution with artificial gastrointestinal model TIM-1

For the final assessment of the behaviour of the different formulations under complex physiological conditions, all formulations were evaluated in triplicate in the TIM model.

The TIM-1 system is a relevant *in vitro* model previously used to study the release of chemical compounds from food matrices and drugs (Blanquet-Diot et al., 2009; Souliman et al., 2007), it was used for the **first time to investigate lipid based formulations in this study**.

**Figure 6-22** depicts the temporal course of PZQ concentrations in the gastric and the intestinal compartment (jejunum + ileal) for all the formulations. As the TIM model is a dynamic system with continuous movements, secretions and removal of liquids, these concentrations can give a picture at time of sampling of the solubilisation of drug between the different formulations.

In the gastric compartment there is a large release of drug for ASD-PZQ uncoated and coated compared to pure PZQ. The gastric compartment concentrations emphasized the increase in wettability and dispersibility of the formulations towards pure drug. In the stomach the hard gelatin capsule released quickly the content, but it can take between 15 min to 30 min for the lipid-based formulation to reach the duodenum compartment.

The highest concentrations are obtained for tristearine-based formulation indicating either a lack of controlled release or a burst effect in the gastric environment. Whatever the location of the formulation, there is a large release of drug in the stomach and in the intestine. In the intestinal compartment, the concentration in jejunal compartment is greater than ileal compartment and after 30 min the concentration decreased in the intestinal part. The peak value is dependant of the sampling protocol but in all cases, it is lower than 60 min. The dissolution profiles for the intestinal compartment showed similar kinetics of the formulations with a difference in amount dissolved.

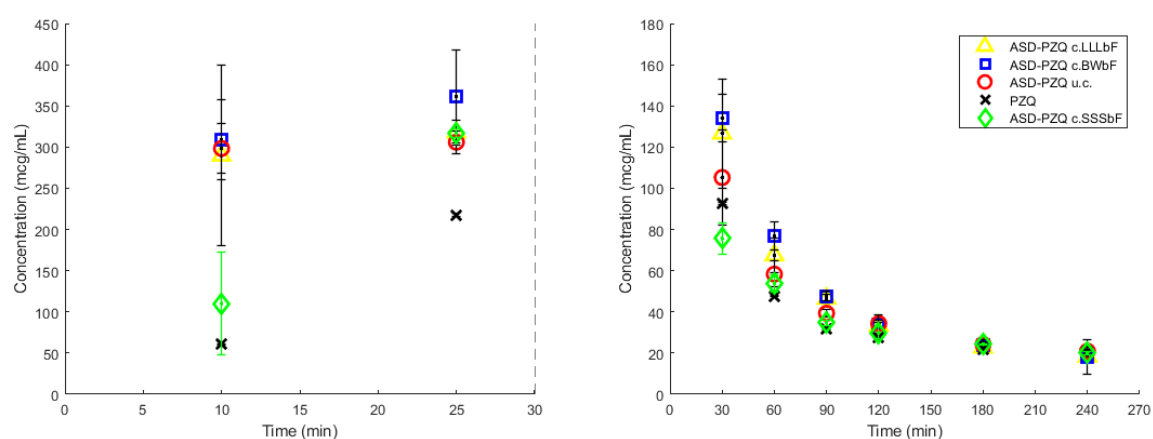


Figure 6-22. Concentration ( $\mu\text{g/mL}$ ) in gastric compartment (**left**) and in intestinal compartment (jejunum + ileon) (**right**)

The bioaccessibility of PZQ and PZQ from uncoated and coated amorphous solid dispersions are presented in **Figure 6-23**.

The results are expressed in % of the dose administered (corresponding to 150mg of PZQ), they correspond to the amount of drug that is recovered in the jejunal et duodenal dialysis during the experiment. It can be considered as the amount of drug available for absorption.

PZQ was mainly released in the proximal part of the artificial digestive system since less than 5 % PZQ were recovered in the jejunal dialysis whatever the formulation studied. After 4 h of digestion in the TIM-1 model 26% to 37% were available for absorption.

The PZQ and ASD-PZQ gave lower bioaccessibility compared to Beewax and Trilaurin based formulations. Coating with lipids could limit a possible precipitation of drug in the gastrointestinal tract and increase the dispersibility of the ASD-PZQ and the surface properties towards intestinal content.

In case of Tristearin-based formulation, the lower bioaccessibility could be related to a prolonged release kinetic. After a burst effect in the gastric compartment, the release is controlled by diffusion through the coating, associated with a lower digestibility of the formulation. Small amounts of drug were released over a longer period of time and available for dialysis, compared to other coated formulations.

The TIM-1 experiment allowed to highlight the influence of the different parameters during digestion. Beside the influence of pH and enzyme, the presence of bile salts and the dynamic movements of the formulation throughout the gastrointestinal tract lead to different behaviours of uncoated and coated formulations. The solubilisation of PZQ and ASD-PZQ are increased, but the bioaccessibility is still limited, related to possible precipitation of drug in the different compartments of the gastrointestinal tract. Coated lipid-based formulation exhibits fast release, burst effect and prolonged release according to the lipid excipient employed.

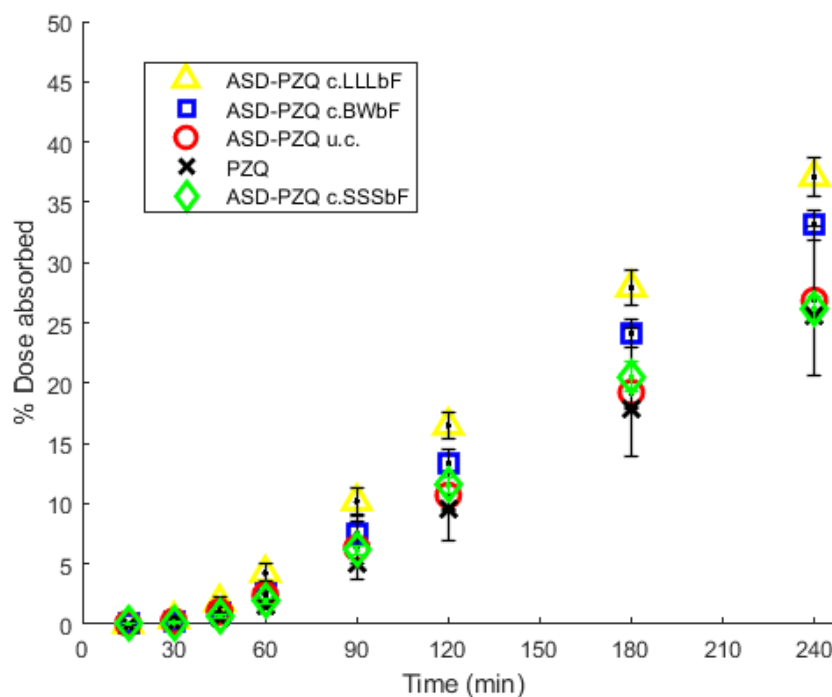


Figure 6-23. Bioaccessibility of praziquantel from uncoated and coated amorphous solid dispersions

### 3. Conclusions and Perspectives

This case study highlights the functional impact of hot-melt coating on amorphous solid dispersions of a poorly water-soluble drug model – praziquantel (PZQ). To explore this impact, amorphous solid dispersions comprising praziquantel, copolymer of vinylpyrrolidone with vinyl acetate and sorbitan monolaurate 35:60:5 (ASD-PZQ) were hot-melt coated with three formulations mainly constituted by either beeswax (BWbF), tristearin (SSSbF) and trilaurin (LLLbF). These formulations differ in chemical composition, physical and biological properties.

From a biopharmaceutics point of view, hot-melt coating combination of ASD-PZQ with lipids of diverse digestibility constitute a new concept of drug development. In effect, in addition to supersaturation potential of ASD formulation, digestion of lipids provided solubilisation capacity as well as permeation enhancing effect.

As a matter of fact, the usage of a dynamic gastro-intestinal dissolution-permeation model (TIM-1) was found indispensable to investigate dissolution and bioaccessibility of different hot-melt coated ASD-PZQ products.

Bioperformance of hot-melt coated ASD-PZQ products corresponded to the intended use of each solid lipid-based formulation. In the first place, formulation composed of trilaurin and vitamin E TPGS was able to increase bioaccessibility of praziquantel.

In the second place, formulation constituted by beeswax, sorbitan monostearate and polysorbate 80 was able to impart an immediate release profile with the coating content around 30% w/w.

In the third place, formulation comprising tristearin, polysorbate 20 and sorbitan monolaurate was able to prolong release kinetics as it is by nature poorly digestible.

Last but not least, hot-melt coating helps overcome flowability and aqueous dispersibility issues eventually encountered with ASDs. In conclusion, hot-melt coating can give rise to new functionalities to ASDs which represent high-tech products and hot topics for research.

Hot-melt coating did provide a protection effect against plasticisation induced by water sorption under long-term storage conditions. However, coating with BWbF was found to be the most suitable formula to coat ASD-PZQ as it should also inhibit PZQ recrystallisation by reducing molecular mobility in the vicinity of free surface.

SSSbF and LLLbF were also able to provide some protection effect against humidity but induced latently a slow recrystallisation of PZQ in ASDs. However, these observations should not be generalised to the fact that coating ASDs of other molecules with SSSbF and LLLbF might always cause such issues as well as the fact that BWbF could suit all ASDs products. Considerations on an *ad hoc* basis are important. It justifies again the purpose to investigate stability of ASD-PZQs coated with lipid-based formulations of a diverse nature in this case study.



## General Conclusions and Suggestions for Future Work

This doctoral thesis addressed the challenges of hot-melt coating and formulation of solid lipids by providing a methodological approach to characterising process, materials, and products. The initial objectives laid out were concretised progressively throughout the experimentation.

**Concerning the first objective**, despite the complexity of hot-melt coating by fluidised bed, the starting point of one research could be placed on investigating the processing-specific properties of lipids and combinations. The three case studies showed how to define process variables as a function of formulations properties.

- In the development of beeswax-based formulations (BWbFs), a thorough physics-based experimental approach was established for early development of hot-melt coating formulations. Concerning materials, adhesion of BWbFs was found to be such a limiting factor that they should be processed as at the lowest thermal setpoint as possible. Besides, one cannot treat solely one of processing-specific properties as these properties (e.g., melt viscosity, inherent solidification rate) of one (monocomponent) formulation could be more challenging than those of another. However, it was possible to predict the interlink between the formulation properties, the definition of process variables and their impact on process performance and coating quality. The application of hot-melt goniometry was found to respond to the objective. These conclusions are drawn from **Chapter 3 – Part 1**.

- Concerning hot-melt coating process, the established experimental approach was based on one of the advantages of air suspension coating to generate different drug loadings in the same batch. Analyses of this series of samples with incremental target coating contents provided, for decision-making, useful information on tendency of coating efficiency, evolution of process regime and determination of a minimal coating content which assures a homogenous coating. Effective adjustment of process parameters was based on the four principal variables: (i) fluidisation air flowrate, (ii) feeding rate, (iii) atomisation air pressure and (iv) batch size. Further, poor processing-specific properties led to poor processing performance and ultimately poor coating quality (case of F0 and F3). This physics-based experimental approach could be adaptable to other class of solid lipid-based formulations and other substrate(s). These conclusions are drawn also from **Chapter 3 – Part 1**.

- In the development of tristearin-based formulations (SSSbFs), advancement of non-traditional hot-melt coating should go together with understanding fundamentals of melt crystallisation (nucleation and crystal growth). Note that  $\alpha$  crystallisation is associated to traditional hot-melt coating while  $\beta$  crystallisation is associated with non-traditional hot-melt coating. When  $\beta$  crystallisation is possible for one solid lipid-based formulation,  $\alpha$  crystallisation is also possible but the inverse conclusion is not certain. This is the rationale to develop multifunctional hot-melt coating formulations.

Concerning materials, in the case of SSSbFs, crystallisation of  $\beta$  polymorph imposes a specific thermal setpoint (neither too high nor too low). Due to longer residence time of the liquid state, melt cohesion and solid adhesion of this polymorph was also challenging, which caused fine overproduction and delamination. Conclusions drawn from **Chapter 4 – Part 2**.

- Concerning hot-melt coating by a non-traditional approach, applications of hot-melt goniometry are still relevant as it also helps predict the necessity for a switch of two feeding rates due to the occurrence of sequential processes of  $\beta$  crystallisation, i.e. primary nucleation, secondary nucleation and growth. Agglomeration was found to be due to slow solidification kinetics (case of NBAC4-3 and NBAC4-9). In summary, understanding fundamentals of melt crystallisation could open new opportunities (e.g., streamlining a tempering unit operation, overcoming Ostwald ripening stability issues). In fact, for the sake of product stability,  $\alpha$  crystallisation necessitates  $\alpha$ - $\beta$  conversion (tempering) which was shown to be time- and energy-consuming (case of NBAC4-3). Conclusions drawn from **Chapter 4 – Part 2**.

- In the development of trilaurin-based formulations (LLLbFs), application of the non-traditional hot-melt coating is the only possibility for trilaurin, a typical lipid whose melting point of the most stable form is close to the ambient temperature. In effect, the cooling capacity of the melt technology is the limiting factor. In the case of LLLbFs, solidification rate is more important than other processing-specific properties. Hot-melt goniometry again successfully predicted this instance. In effect, it was possible to define only one feeding rate for coating operations thanks to faster solidification kinetics of LLLbFs than SSSbFs. The operation of hot-melt coating with LLLbFs was shown to be the shortest in comparison with BWbFs and SSSbFs. Conclusions drawn from **Chapter 5**.

**To add further**, while for BWbF or LLLbFs only traditional or non-traditional hot-melt coating approach can be applied, SSSbF can respond to both processing methods. Therefore, there are many processing possibilities depending on the needs of formulators: bypassing post-processing thermal treatment (e.g., tempering) (case of NBAC4-3/9-60), consuming less coatings for the same homogeneous coating (case of LLLbF), coating thermosensitive substrates (case of NBAC4-9-30). Furthermore, concerning additive addition, it is interesting to notice that adding of glass or liquid materials might require a reduction in feeding rate (case of SSSbFs and LLLbFs) whereas adding a crystalline matter the inverse trend applies (case of F1 and F2).

**Concerning the second objective**, a methodological approach to selection and combination of lipids and additives based on a mechanistic understanding of their structure-property-function relationship was proved for each category of solid lipid-based formulations:

- In the development of beeswax-based formulations, beeswax and sorbitan monostearate have contrasting adhesiveness and cohesiveness. Whether adhesiveness and cohesiveness are too low

or too high, these properties are not good for hot-melt coating. Their consequences were processing issues such as loss in productivity due to stickiness of coated particles, delamination and fine powder overproduction. Combination of both substances (F1) resulted in **improved processability of the compounded formulation**, which permitted good yield, good coating efficiency, target process regime achieved and good coating quality. Conclusions drawn from **Chapter 3 – Part 1**.

- Adding a small content of polysorbate 80 did not change significantly its processability and therefore did not affect processing performance. On the other hand, it increased water penetrability of the compounded formulation (F2) in release testing. This **change of release mechanism** was found by chance to contribute to **stabilisation** of the total lipid system. In fact, for complex-mixture lipids like beeswax, concurrence of multiple solid-state behaviours was anticipated. The difference in release profile between F1 and F2 in the stability study gave showed how different solid-state behaviours evolved and compensated each other. This led to early or late stabilisation of F2 and F1, respectively. Conclusions drawn from **Chapter 3 – Part 2**.

- In the development of tristearin-based formulations, the focus was put on **development of a fast screening of additives and combinations of additives** based on nucleation “performance” of  $\beta$  tristearin (i.e. occurrence of nucleation, induction time, randomness). With combinations of tristearin and talc at four levels of concentration as control, it showed that melt emulsions (H-, L-, N-BAC4) were more performant than melt solutions (SSS-SML with only lipophilic surfactant added) or melt dispersions (SSS-PS20 with only hydrophilic surfactant added). Among these melt emulsions, combinations of lipophilic and hydrophilic surfactants at equal ratios (NBAC4-3/9) were even more performant than others. Although all the surfactants and their combinations can induce nucleation of  $\beta$  tristearin but they could tend to decrease crystal growth (case of NBAC4-3/9 demonstrated). Without changing its mechanism of action, talc addition was found to resolve this adverse effect regardless of the surfactant concentration. These findings could be transferable to other triglyceride-based formulations. Conclusions drawn from **Chapter 4 – Part 1**.

- Furthermore, two representative formulations, NBAC4-3 and NBAC4-9 without talc, were tested with both hot-melt coating approaches for exploring their impact on processing performance and long-term stability. Concerning their manufacturability, a mixed process regime of coating and agglomeration occurred. This shows two consequences of their crystallisation behaviours: (i) feasibility of the two formulations for the non-traditional coating approach (induced nucleation) and (ii) not good coating quality (decreased crystal growth). These results show a **link between fundamentals and hot-melt coating applications**. However, adding other additives (e.g., talc) should be considered for improving their solidification rate, cohesion and adhesion. Conclusions drawn from, **Chapter 4–Part 2**.

- Concerning their stability, combination of two surfactants appeared to have an effect of stabilisation especially when traditional hot-melt coating ( $\alpha$  crystallisation) was performed. On the one

hand, with a higher concentration of surfactants, NBAC4-9 was shown to be less subject to lipid blooming during polymorphic transformation. On the other hand, crystal size appeared to remain constant being exposed to 25°C/60%RH over 3 months of stability study. The same results were obtained with non-traditional coating approach ( $\beta$  crystallisation). This shows in general an **effect of stabilisation on Ostwald ripening** and liquid-solid phase separation should be not expected (NBAC4-3-60 and NBAC4-9-60). However, coating defects were suspected to cause increase in release kinetics with time. Conclusions drawn from **Chapter 4 – Part 2**.

- In the development of trilaurin-based formulations, adding talc particles was shown to affect coating operations. In fact, setting a higher feeding rate was for LLL-1F than LLL-2F. Notably, adding talc not only rendered the combination of trilaurin and vitamin E TPGS feasible but also stable. In fact, adding talc induced fast solidification of the binary combination of trilaurin vitamin E TPGS, whose inherent solidification rate is slow. Fast solidification was found to lead to homogeneous  $\beta$  crystal network and this trapped droplets of vitamin TPGS E which slowly crystallised over time. Little phase separation observed for the ternary formulation. Conclusions drawn from **Chapter 5**.

**To add more elements**, for each class of BWbF, SSSbF and LLLbFs one mechanism of action for long-term stabilisation could be revealed. In these instances of formulation development, almost solid-state behaviours related to stability of solid lipid-based formulations were considered. This was reflected in the selection of solid-state characterisation techniques adopted in each study together with the physics-based experimental approach. As lipid crystallisation is the core principle of hot-melt coating, rapid feasibility screening could be based on nucleation but crystal growth must not be overlooked. DSC might have limited application due to its low throughput and yield less information on crystal growth. Combination of Crystal16® and polarised-light microscopy were found to be useful for this purpose (case of NBAC4-3/9 and LLLbFs).

**Concerning the third objective**, throughout these three case studies, the use of sodium chloride as model drug was shown to accelerate the process of developing hot-melt coating formulations in the early stage. Furthermore, it was shown to simplify evaluation of coating quality by measurement of release kinetics by conductometry. Last but not least, throughout these three case studies, release mechanisms of salt from different lipid systems: they were shown to involve water penetration, drug diffusion and interactions of lipids with aqueous systems. Conclusions drawn from **Chapter 3, Chapter 4 and Chapter 5**.

**Concerning the fourth objective**, for this doctoral thesis, pharmaceutical applications were targeted with a challenging model drug (amorphous solid dispersions of praziquantel) for hot-melt coating with candidate beeswax/tristearin/trilaurin-based formulations (BWbF/SSSbF/LLLbF). For biopharmaceutical applications (controlled release, bioavailability enhancement), this justifies the

choice of three representative formulations from three classes of lipids whose biological properties (i.e. digestibility) are different.

Coated praziquantel amorphous solid dispersions were tested using biorelevant media and lipolytic enzymes for determining the most suitable release profile for each lipid-based formulation. Based on the conclusions of **Chapter 6**, LLLbF and SSSbF were found to respond to intended use for bioavailability enhancement and controlled release despite coating imperfections, respectively. In fact, LLLbF could be ranked the first with its highest bioaccessibility determined by means of the artificial gastro-intestinal digestion/dissolution/permeation model in comparison with uncoated amorphous solid dispersions. With different biorelevant models, SSSbF and BWbF were found to be sensitive to food effect while fed state did not influence the performance of LLLbF.

On top of these results, BWbF, with second ranked bioaccessibility, was found to be the most performant to suit technological applications. In effect, BWbF could protect amorphous solid dispersions against exposure to high humidity the most effectively with less evolution of crystallinity. All the three formulations could provide some protective effect but LLLbF and SSSbF induced lately recrystallisation of amorphous praziquantel. The reason for such a result would be a question for future work. This again justifies the choice of lipid-based formulations of a different nature to anticipate this attrition rate in development. Furthermore, by the work on three classes of lipids, hot-melt coating was shown to prevent amorphous solid dispersions from sintering/being consolidated with time, to improve their flow properties and aqueous dispersibility, which represent technical challenges of these high-tech products.

For future work, the following question should be addressed. *Which are the underlying principles to coat any amorphous solid dispersions with a certain lipid-based formulation which will not induce recrystallisation?* Or is it more viable to develop a fast-track approach to selecting appropriate formulations from a multiplicity of choices. This supports the work done within this doctoral thesis for fast-track development of solid lipid-based formulations.

Within the limited time framework, this doctoral thesis represents only exploratory studies by proposing a systematic approach to (i) characterising hot-melt coating by the new technology Ventilus®, (ii) selecting lipids and additives and (iii) designing solid lipid-based formulated products with sufficient stability and quality. Again, the driver of hot-melt coating is the build-up of knowledge on lipid crystallisation, polymorphism and additive addition. To add further, there will be more possibilities for developing solid lipid-based formulations given the versatility of hot-melt coating by fluidised bed and lipid-based excipients.

## Bibliography

- Abramczyk, H., Imiela, A., Brozek-Pluska, B., & Kopec, M. (2019). Advances in Raman imaging combined with AFM and fluorescence microscopy are beneficial for oncology and cancer research. *Nanomedicine*, *14*(14), 1873-1888. <https://doi.org/10.2217/nmm-2018-0335>
- Aburahma, M. H., & Badr-Eldin, S. M. (2014). Compritol 888 ATO: a multifunctional lipid excipient in drug delivery systems and nanopharmaceuticals. *Expert opinion on drug delivery*, *11*(12), 1865-1883.
- Acevedo, N. C., & Marangoni, A. G. (2015). Nanostructured Fat Crystal Systems. *Annual Review of Food Science and Technology*, *6*(1), 71-96. <https://doi.org/10.1146/annurev-food-030713-092400>
- Achanta, A. (1999). *Elucidation of Hot Melt Wax Coating Systems* [University of Rhode Island]. <https://doi.org/10.23860/thesis-achanta-anand-1999>
- Achanta, A. S., Adusumilli, P. S., James, K. W., & Rhodes, C. T. (1997). Development of hot melt coating methods. *Drug development and industrial pharmacy*, *23*(5), 441-449.
- Achanta, A. S., Adusumilli, P. S., James, K. W., & Rhodes, C. T. (2001). Hot-Melt Coating : Water Sorption Behavior of Excipient Films. *Drug Development and Industrial Pharmacy*, *27*(3), 241-250. <https://doi.org/10.1081/DDC-100000242>
- Adachi, T., Daudah, D., & Tanaka, G. (2014). Effects of supercooling degree and specimen size on supercooling duration of erythritol. *Isij International*, *54*(12), 2790-2795.
- Adachi, T., Nakashima, T., & Tanaka, G. (2013). *Study on Supercooling of Erythritol –Influence of Sample Volume, Contact Area and Insoluble Particle*. <https://doi.org/10.11322/tjsrae.30.203>
- Adhikari, B., Howes, T., Bhandari, B. R., & Truong, V. (2001). Stickiness in foods : A review of mechanisms and test methods. *International Journal of Food Properties*, *4*(1), 1-33. <https://doi.org/10.1081/JFP-100002186>
- Alany, R. (2017). Lipid and surfactant-based formulations, drug delivery systems, and dosage forms. *Pharmaceutical Development and Technology*, *22*(3), 301-301. <https://doi.org/10.1080/10837450.2017.1297220>
- Albertini, B., Bertoni, S., Perissutti, B., & Passerini, N. (2019). An investigation into the release behavior of solid lipid microparticles in different simulated gastrointestinal fluids. *Colloids and Surfaces B: Biointerfaces*, *173*, 276-285. <https://doi.org/10.1016/j.colsurfb.2018.09.056>
- Albertini, B., Di Sabatino, M., Melegari, C., & Passerini, N. (2014). Formulating SLMs as oral pulsatile system for potential delivery of melatonin to pediatric population. *International journal of pharmaceutics*, *469*(1), 67-79.
- Al-Shehri, B. M., Haddadi, T., M. Alasmari, E., Ghramh, H. A., Khan, K. A., Mohammed, M. E. A., Sager Alotaibi, M., El-Niweiri, M. A. A., Hamdi Assiri, A., & Khayyat, M. M. (2022). Effect of Storage Time and Floral Origin on the Physicochemical Properties of Beeswax and the Possibility of Using It as a Phase Changing Material in the Thermal Storage Energy Technology. *Foods*, *11*(23), 3920. <https://doi.org/10.3390/foods11233920>
- Alzahrani, A., Nyavanandi, D., Mandati, P., Youssef, A. A. A., Narala, S., Bandari, S., & Repka, M. (2022). A systematic and robust assessment of hot-melt extrusion-based amorphous solid dispersions : Theoretical prediction to practical implementation. *International Journal of Pharmaceutics*, *624*, 121951. <https://doi.org/10.1016/j.ijpharm.2022.121951>
- Amidon, G. L., Lennernäs, H., Shah, V. P., & Crison, J. R. (1995). A theoretical basis for a biopharmaceutic drug classification : The correlation of in vitro drug product dissolution and in vivo bioavailability. *Pharmaceutical research*, *12*(3), 413-420.
- Ammar, H. O., Ghorab, M. M., Felton, L. A., Gad, S., & Fouly, A. A. (2016). Effect of Antiadherents on the Physical and Drug Release Properties of Acrylic Polymeric Films. *AAPS PharmSciTech*, *17*(3), 682-692. <https://doi.org/10.1208/s12249-015-0397-7>
- Appelgren, C., & Eskilson, C. (1993). Size enlargement and coating by the use of melts. In *Industrial Aspects of Pharmaceutics*. Swedish Pharmaceutical Press.
- Aquilano, D., & Sgualdino, G. (2001). Fundamental aspects of equilibrium and crystallization kinetics. *Crystallization processes in fats and lipid systems*, 1-51.
- Arnold, Y. E., Imanidis, G., & Kuentz, M. (2012). In vitro digestion kinetics of excipients for lipid-based drug delivery and introduction of a relative lipolysis half life. *Drug development and industrial pharmacy*, *38*(10), 1262-1269.



- Aronhime, J. S., Sarig, S., & Garti, N. (1987). Mechanistic considerations of polymorphic transformations of tristearin in the presence of emulsifiers. *Journal of the American Oil Chemists' Society*, 64(4), 529-533. <https://doi.org/10.1007/BF02636388>
- Aronhime, J. S., Sarig, S., & Garti, N. (1988). Dynamic control of polymorphic transformation in triglycerides by surfactants : The button syndrome. *Journal of the American Oil Chemists' Society*, 65(7), 1144-1150.
- Aronhime, J., Sarig, S., & Garti, N. (1990). Emulsifiers as additives in fats : Effect on polymorphic transformations and crystal properties of fatty acids and triglycerides. *Food structure*, 9(4), 1.
- Arwidsson, H. G., & Rudén, M. (1993). Film coating by the spray process. In *Industrial Aspects of Pharmaceutics* (p. 212-226). Swedish Pharmaceutical Press.
- Atomic Force Microscopy (AFM)—WITec Raman Imaging*. (s. d.). Oxford Instruments. Consulté 9 décembre 2023, à l'adresse <https://raman.oxinst.com/techniques/scanning-probe-microscopy>
- Attama, A., Schicke, B., & Mullergoymann, C. (2006). Further characterization of theobroma oil-beeswax admixtures as lipid matrices for improved drug delivery systems. *European Journal of Pharmaceutics and Biopharmaceutics*, 64(3), 294-306. <https://doi.org/10.1016/j.ejpb.2006.06.010>
- Baird, J. A., Van Eerdenbrugh, B., & Taylor, L. S. (2010). A Classification System to Assess the Crystallization Tendency of Organic Molecules from Undercooled Melts. *Journal of Pharmaceutical Sciences*, 99(9), 3787-3806. <https://doi.org/10.1002/jps.22197>
- Banerjee, S., Joshi, U., Singh, A., & Saharan, V. A. (2021). Lipids for Taste masking and Taste assessment in pharmaceutical formulations. *Chemistry and Physics of Lipids*, 235, 105031.
- Bánfai, B., Ganzler, K., & Kemény, S. (2007). Content uniformity and assay requirements in current regulations. *Journal of Chromatography A*, 1156(1-2), 206-212. <https://doi.org/10.1016/j.chroma.2006.10.067>
- Bannow, J., Koren, L., Salar-Behzadi, S., Löbmann, K., Zimmer, A., & Rades, T. (2020). Hot melt coating of amorphous carvedilol. *Pharmaceutics*, 12(6), 519.
- Bansal, A., Dantuluri, A., & Puri, V. (2011). Barrier Coated Drug Layered Particles for Formulation Design of an Amorphous Solid Dispersion. *Proceedings of The 1st Electronic Conference on Pharmaceutical Sciences*, 518. <https://doi.org/10.3390/ecps2011-00518>
- Barthelemy, P., Laforet, J. P., Farah, N., & Joachim, J. (1999). Compritol® 888 ATO: an innovative hot-melt coating agent for prolonged-release drug formulations. *European journal of pharmaceutics and biopharmaceutics*, 47(1), 87-90.
- Bauer, K. H. (2015). Sind Wirbelschichten in pharmazeutischen Granulations- und Umhüllungs-Verfahren gleich Fließbetten und was sind Luftgleitschichten? *Pharm. Ind.*, 77(7), 1088-1095.
- Bayés-García, L., Patel, A. R., Dewettinck, K., Rousseau, D., Sato, K., & Ueno, S. (2015). Lipid crystallization kinetics—Roles of external factors influencing functionality of end products. *Current Opinion in Food Science*, 4, 32-38. <https://doi.org/10.1016/j.cofs.2015.04.005>
- Bayés-García, L., Sato, K., & Ueno, S. (2005). Polymorphism of triacylglycerols and natural fats. *Bailey's Industrial Oil and Fat Products*, 1-49.
- Bayés-García, L., Yoshikawa, S., Aguilar-Jiménez, M., Ishibashi, C., Ueno, S., & Calvet, T. (2022). Heterogeneous Nucleation Effects of Talc Particles on Polymorphic Crystallization of Cocoa Butter. *Crystal Growth & Design*, 22(1), 213-227. <https://doi.org/10.1021/acs.cgd.1c00859>
- Beaupere, N., Soupremanien, U., & Zalewski, L. (2018). Nucleation triggering methods in supercooled phase change materials (PCM), a review. *Thermochimica Acta*, 670, 184-201. <https://doi.org/10.1016/j.tca.2018.10.009>
- Becker, K. (2016). *Hot melt coating with lipid-based excipients : Development of a solvent-free technology for the coating of multiparticulate drug delivery systems/Karin Dagmar Frieda Becker (B. Sc./M. Sc.)*. Karl-Franzens-Universität Graz.
- Becker, K., Salar-Behzadi, S., & Zimmer, A. (2015). Solvent-free melting techniques for the preparation of lipid-based solid oral formulations. *Pharmaceutical research*, 32(5), 1519-1545.
- Becker, K., Saurugger, E.-M., Kienberger, D., Lopes, D., Haack, D., Köberle, M., Stehr, M., Lochmann, D., Zimmer, A., & Salar-Behzadi, S. (2016). Advanced stable lipid-based formulations for a patient-centric product design. *International journal of pharmaceutics*, 497(1-2), 136-149.
- Bendjaballah, M., Canselier, J. P., & Oumeddour, R. (2010). Optimization of Oil-in-Water Emulsion Stability : Experimental Design, Multiple Light Scattering, and Acoustic Attenuation Spectroscopy. *Journal of Dispersion Science and Technology*, 31(9), 1260-1272. <https://doi.org/10.1080/01932690903224888>
- Benito-Gallo, P., Franceschetto, A., Wong, J. C. M., Marlow, M., Zann, V., Scholes, P., & Gershkovich, P. (2015). Chain length affects pancreatic lipase activity and the extent and pH-time profile of triglyceride lipolysis.

*European Journal of Pharmaceutics and Biopharmaceutics*, 93, 353-362.  
<https://doi.org/10.1016/j.ejpb.2015.04.027>

Bennett-Lenane, H., O'Shea, J. P., O'Driscoll, C. M., & Griffin, B. T. (2020). A retrospective biopharmaceutical analysis of > 800 approved oral drug products: Are drug properties of solid dispersions and lipid-based formulations distinctive? *Journal of Pharmaceutical Sciences*.

Benoît, J.-P., Richard, J., & Venier-Julienne, M.-C. (2013). Microencapsulation. In *Techniques de l'ingénieur Cosmétiques : Procédés de formulation: Vol. base documentaire : TIB634DUO*. (Numéro ref. article : j2210). Editions T.I. <https://www.techniques-ingenieur.fr/base-documentaire/procedes-chimie-bio-agro-th2/cosmetiques-procedes-de-formulation-42634210/microencapsulation-j2210/>

Berthelsen, R., Klitgaard, M., Rades, T., & Müllertz, A. (2019). In vitro digestion models to evaluate lipid based drug delivery systems; present status and current trends. *Advanced Drug Delivery Reviews*, 142, 35-49. <https://doi.org/10.1016/j.addr.2019.06.010>

Bertoni, S., Albertini, B., Dolci, L. S., & Passerini, N. (2018). Spray congealed lipid microparticles for the local delivery of  $\beta$ -galactosidase to the small intestine. *European Journal of Pharmaceutics and Biopharmaceutics*, 132, 1-10. <https://doi.org/10.1016/j.ejpb.2018.08.014>

Bertoni, S., Albertini, B., & Passerini, N. (2019). Spray Congealing : An Emerging Technology to Prepare Solid Dispersions with Enhanced Oral Bioavailability of Poorly Water Soluble Drugs. *Molecules*, 24(19), 3471. <https://doi.org/10.3390/molecules24193471>

Bertoni, S., Dolci, L. S., Albertini, B., & Passerini, N. (2018). Spray congealing : A versatile technology for advanced drug-delivery systems. *Therapeutic delivery*, 9(11), 833-845.

Bertoni, S., Passerini, N., & Albertini, B. (2021). Liquid Lipids Act as Polymorphic Modifiers of Tristearin-Based Formulations Produced by Melting Technologies. *Pharmaceutics*, 13(7), 1089.

Bertoni, S., Tedesco, D., Bartolini, M., Prata, C., Passerini, N., & Albertini, B. (2020). Solid Lipid Microparticles for Oral Delivery of Catalase : Focus on the Protein Structural Integrity and Gastric Protection. *Molecular Pharmaceutics*, 17(9), 3609-3621. <https://doi.org/10.1021/acs.molpharmaceut.0c00666>

Blanquet, S., Garrait, G., Beyssac, E., Perrier, C., Denis, S., Hébrard, G., & Alric, M. (2005). Effects of cryoprotectants on the viability and activity of freeze dried recombinant yeasts as novel oral drug delivery systems assessed by an artificial digestive system. *European Journal of Pharmaceutics and Biopharmaceutics*, 61(1-2), 32-39. <https://doi.org/10.1016/j.ejpb.2005.03.009>

Blanquet, S., Zeijdner, E., Beyssac, E., Meunier, J.-P., Denis, S., Havenaar, R., & Alric, M. (2004). A Dynamic Artificial Gastrointestinal System for Studying the Behavior of Orally Administered Drug Dosage Forms Under Various Physiological Conditions. *Pharmaceutical Research*, 21(4), 585-591. <https://doi.org/10.1023/B:PHAM.0000022404.70478.4b>

Blanquet-Diot, S., Soufi, M., Rambeau, M., Rock, E., & Alric, M. (2009). Digestive Stability of Xanthophylls Exceeds That of Carotenes As Studied in a Dynamic in Vitro Gastrointestinal System. *The Journal of Nutrition*, 139(5), 876-883. <https://doi.org/10.3945/jn.108.103655>

Boel, E., & Van Den Mooter, G. (2023). The impact of applying an additional polymer coating on high drug-loaded amorphous solid dispersions layered onto pellets. *International Journal of Pharmaceutics*, 630, 122455. <https://doi.org/10.1016/j.ijpharm.2022.122455>

Boerefijn, R., & Hounslow, M. J. (2005). Studies of fluid bed granulation in an industrial R&D context. *Chemical Engineering Science*, 60(14), 3879-3890. <https://doi.org/10.1016/j.ces.2005.02.021>

Boistelle, R. (1988). Fundamentals of nucleation and crystal growth. *Crystallization and polymorphism of fats and fatty acids*, 31, 189-226.

Boniatti, J. (2021). *Development and characterization of Praziquantel amorphous solid dispersions for paediatric use by hot melt extrusion and 3D printing* [PhD Thesis, Ecole des Mines d'Albi-Carmaux]. <https://theses.hal.science/tel-03683835>. <https://www.arca.fiocruz.br/handle/icict/55434>

Bosselmann, S., Owens, D. E., Kennedy, R. L., Herpin, M. J., & Williams, R. O. (2011). Plasma deposited stability enhancement coating for amorphous ketoprofen. *European Journal of Pharmaceutics and Biopharmaceutics*, 78(1), 67-74. <https://doi.org/10.1016/j.ejpb.2010.12.011>

Boyd, B. J., Bergström, C. A., Vinarov, Z., Kuentz, M., Brouwers, J., Augustijns, P., Brandl, M., Bernkop-Schnürch, A., Shrestha, N., & Préat, V. (2019). Successful oral delivery of poorly water-soluble drugs both depends on the intraluminal behavior of drugs and of appropriate advanced drug delivery systems. *European Journal of Pharmaceutical Sciences*, 137, 104967.

- Boyd, J., Parkinson, C., & Sherman, P. (1972). Factors affecting emulsion stability, and the HLB concept. *Journal of Colloid and Interface Science*, 41(2), 359-370. [https://doi.org/10.1016/0021-9797\(72\)90122-1](https://doi.org/10.1016/0021-9797(72)90122-1)
- Bradley, D. (2007). Finding new formulas for pharma success. *Nature Reviews Drug Discovery*, 6(6).
- Bransford, P., Cook, J., Gupta, M., Haertter, S., He, H., Ju, R., Kanodia, J., Lennernäs, H., Lindley, D., & Polli, J. E. (2019). ICH M9 guideline in development on biopharmaceutics classification system-based biowaivers : An industrial perspective from the IQ consortium. *Molecular pharmaceutics*, 17(2), 361-372.
- Brodkorb, A., Egger, L., Alming, M., Alvito, P., Assunção, R., Ballance, S., Bohn, T., Bourliou-Lacanal, C., Boutrou, R., Carrière, F., Clemente, A., Corredig, M., Dupont, D., Dufour, C., Edwards, C., Golding, M., Karakaya, S., Kirkhus, B., Le Feunteun, S., ... Recio, I. (2019). INFOGEST static in vitro simulation of gastrointestinal food digestion. *Nature Protocols*, 14(4), 991-1014. <https://doi.org/10.1038/s41596-018-0119-1>
- Brubach, J. B., Jannin, V., Mahler, B., Bourgaux, C., Lessieur, P., Roy, P., & Ollivon, M. (2007). Structural and thermal characterization of glyceryl behenate by X-ray diffraction coupled to differential calorimetry and infrared spectroscopy. *International Journal of Pharmaceutics*, 336(2), 248-256. <https://doi.org/10.1016/j.ijpharm.2006.11.057>
- Buchwald, R., Breed, M. D., & Greenberg, A. R. (2008). The thermal properties of beeswaxes : Unexpected findings. *Journal of Experimental Biology*, 211(1), 121-127.
- Bucio, A., Moreno-Tovar, R., Bucio, L., Espinosa-Dávila, J., & Anguebes-Franceschi, F. (2021). Characterization of Beeswax, Candelilla Wax and Paraffin Wax for Coating Cheeses. *Coatings*, 11(3), 261. <https://doi.org/10.3390/coatings11030261>
- Butler, J. M., & Dressman, J. B. (2010). The developability classification system : Application of biopharmaceutics concepts to formulation development. *Journal of pharmaceutical sciences*, 99(12), 4940-4954.
- Cai, J., & Lee, Y. (2020). Controlling sodium release using maltodextrin and octenyl-succinic-anhydride-modified starch with two types of spray-dryer nozzles. *Journal of Food Process Engineering*, 43(5), e13238. <https://doi.org/10.1111/jfpe.13238>
- Capece, M., & Davé, R. N. (2014). Solventless polymer coating of microparticles. *Powder Technology*, 261, 118-132. <https://doi.org/10.1016/j.powtec.2014.04.012>
- Carnicer, V., Alcázar, C., Orts, M. J., Sánchez, E., & Moreno, R. (2021). Microfluidic rheology : A new approach to measure viscosity of ceramic suspensions at extremely high shear rates. *Open Ceramics*, 5, 100052. <https://doi.org/10.1016/j.oceram.2020.100052>
- Castro, N., Medina, R., Sotelo, J., & Jung, H. (2000). Bioavailability of Praziquantel Increases with Concomitant Administration of Food. *Antimicrobial Agents and Chemotherapy*, 44(10), 2903-2904. <https://doi.org/10.1128/AAC.44.10.2903-2904.2000>
- Castro-Alayo, E. M., Balcázar-Zumaeta, C. R., Torrejón-Valqui, L., Medina-Mendoza, M., Cayo-Colca, I. S., & Cárdenas-Toro, F. P. (2023). Effect of tempering and cocoa butter equivalents on crystallization kinetics, polymorphism, melting, and physical properties of dark chocolates. *LWT*, 173, 114402. <https://doi.org/10.1016/j.lwt.2022.114402>
- Chakrabarty, D., Chakraborty, A., Seth, D., Hazra, P., & Sarkar, N. (2005). Binding and relaxation behavior of Coumarin-153 in lecithin-taurocholate mixed micelles : A time resolved fluorescence spectroscopic study. *Chemical Physics Letters*, 412(4-6), 255-262. <https://doi.org/10.1016/j.cplett.2005.06.098>
- Chambin, O., & Jannin, V. (2005). Interest of multifunctional lipid excipients : Case of Gelucire® 44/14. *Drug development and industrial pharmacy*, 31(6), 527-534.
- Chansanroj, K., Betz, G., Leuenberger, H., Mitrevej, A., & Sinchaipanid, N. (2007a). Development of a multi-unit floating drug delivery system by hot melt coating technique with drug-lipid dispersion. *Journal of drug delivery science and technology*, 17(5), 333-338.
- Chansanroj, K., Betz, G., Leuenberger, H., Mitrevej, A., & Sinchaipanid, N. (2007b). Polymorphic change of a triglyceride base in hot melt coating process and stability acceleration by tempering process. *Journal of drug delivery science and technology*, 17(5), 347-352.
- Chauhan, G., Shaik, A. A., Kulkarni, N. S., & Gupta, V. (2020). The preparation of lipid-based drug delivery system using melt extrusion. *Drug Discovery Today*, 25(11), 1930-1943. <https://doi.org/10.1016/j.drudis.2020.07.025>
- Chauhan, R. R., Dullens, R. P. A., Velikov, K. P., & Aarts, D. G. A. L. (2017). The effect of colloidal aggregates on fat crystal networks. *Food & Function*, 8(1), 352-359. <https://doi.org/10.1039/C6FO01622G>

- Chen, H., Shi, S., Liu, A., & Tang, X. (2010). Combined application of extrusion-spheronization and hot-melt coating technologies for improving moisture-proofing of herbal extracts. *Journal of pharmaceutical sciences*, 99(5), 2444-2454.
- Chen, J., Ghazani, S. M., Stobbs, J. A., & Marangoni, A. G. (2021). Tempering of cocoa butter and chocolate using minor lipidic components. *Nature communications*, 12(1), 1-9.
- Chen, Y., Gavaliatsis, T., Kuster, S., Städeli, C., Fischer, P., & Windhab, E. J. (2021). Crust treatments to reduce bread staling. *Current Research in Food Science*, 4, 182-190. <https://doi.org/10.1016/j.crfs.2021.03.004>
- Christiansen, A., Backensfeld, T., & Weitschies, W. (2010). Effects of non-ionic surfactants on in vitro triglyceride digestion and their susceptibility to digestion by pancreatic enzymes. *European Journal of Pharmaceutical Sciences*, 41(2), 376-382. <https://doi.org/10.1016/j.ejps.2010.07.005>
- Christina, J., & Lee, Y. (2016). Modification of Sodium Release Using Porous Corn Starch and Lipoproteic Matrix. *Journal of Food Science*, 81(4). <https://doi.org/10.1111/1750-3841.13251>
- Christophersen, P. C., Vaghela, D., Müllertz, A., Yang, M., Nielsen, H. M., & Mu, H. (2014a). Solid lipid particles for oral delivery of peptide and protein drugs III—the effect of fed state conditions on the in vitro release and degradation of desmopressin. *The AAPS journal*, 16(4), 875-883.
- Christophersen, P. C., Vaghela, D., Müllertz, A., Yang, M., Nielsen, H. M., & Mu, H. (2014b). Solid lipid particles for oral delivery of peptide and protein drugs III—the effect of fed state conditions on the in vitro release and degradation of desmopressin. *The AAPS journal*, 16(4), 875-883.
- Christophersen, P. C., Zhang, L., Müllertz, A., Nielsen, H. M., Yang, M., & Mu, H. (2014a). Solid lipid particles for oral delivery of peptide and protein drugs II—the digestion of trilaurin protects desmopressin from proteolytic degradation. *Pharmaceutical research*, 31(9), 2420-2428.
- Christophersen, P. C., Zhang, L., Müllertz, A., Nielsen, H. M., Yang, M., & Mu, H. (2014b). Solid lipid particles for oral delivery of peptide and protein drugs II—the digestion of trilaurin protects desmopressin from proteolytic degradation. *Pharmaceutical research*, 31(9), 2420-2428.
- Christophersen, P. C., Zhang, L., Yang, M., Nielsen, H. M., Müllertz, A., & Mu, H. (2013a). Solid lipid particles for oral delivery of peptide and protein drugs I—Elucidating the release mechanism of lysozyme during lipolysis. *European Journal of Pharmaceutics and Biopharmaceutics*, 85(3), 473-480.
- Christophersen, P. C., Zhang, L., Yang, M., Nielsen, H. M., Müllertz, A., & Mu, H. (2013b). Solid lipid particles for oral delivery of peptide and protein drugs I—Elucidating the release mechanism of lysozyme during lipolysis. *European Journal of Pharmaceutics and Biopharmaceutics*, 85(3), 473-480.
- Clarkson, E. M., Curtis, J. R., Jewkes, R. J., Jones, B. E., Luck, V. A., De Wardener, H. E., & Phillips, N. (1971). Slow sodium : An oral slowly released sodium chloride preparation. *Br Med J*, 3(5775), 604-607.
- Claviez, A., Thies, R., Kleinebudde, P., & Suttrop, M. (1999). Microencapsulated NaCl for Oral Salt-Replacement Therapy in Infants. *JNCI Journal of the National Cancer Institute*, 91(17), 1513-1514. <https://doi.org/10.1093/jnci/91.17.1513>
- Cole, A. S., & Eastoe, J. E. (1988). Lipids. In *Biochemistry and Oral Biology* (p. 100-108). Elsevier. <https://doi.org/10.1016/B978-0-7236-1751-8.50015-6>
- Corzo, C., Lopes, D. G., Lochmann, D., Reyer, S., Stehr, M., & Salar-Behzadi, S. (2020). Novel approach for overcoming the stability challenges of lipid-based excipients. Part 1 : Screening of solid-state and physical properties of polyglycerol esters of fatty acids as advanced pharmaceutical excipients. *European Journal of Pharmaceutics and Biopharmaceutics*, 148, 134-147.
- Corzo Dardón, C. C. (s. d.). *Lipid-microparticles for advanced and safe inhalable formulations*. Consulté 9 novembre 2023, à l'adresse <http://unipub.uni-graz.at/obvugrhs/content/titleinfo/6722954>
- Costa, M. C., Rolemberg, M. P., Boros, L. A., Krähenbühl, M. A., de Oliveira, M. G., & Meirelles, A. J. (2007). Solid–liquid equilibrium of binary fatty acid mixtures. *Journal of Chemical & Engineering Data*, 52(1), 30-36.
- Costa, M. C., Sardo, M., Rolemberg, M. P., Coutinho, J. A., Meirelles, A. J., Ribeiro-Claro, P., & Krähenbühl, M. A. (2009). The solid–liquid phase diagrams of binary mixtures of consecutive, even saturated fatty acids. *Chemistry and Physics of Lipids*, 160(2), 85-97.
- Costa, P., & Sousa Lobo, J. M. (2001). Modeling and comparison of dissolution profiles. *European Journal of Pharmaceutical Sciences*, 13(2), 123-133. [https://doi.org/10.1016/S0928-0987\(01\)00095-1](https://doi.org/10.1016/S0928-0987(01)00095-1)
- Costard, E. M. (2017). *Control of fat crystallisation by adding additives and changing the process* [PhD Thesis, University of Birmingham]. <https://etheses.bham.ac.uk/id/eprint/7589/>
- Cottrell, T., & Peij, J. V. (2014). Sorbitan Esters and Polysorbates. In V. Norn (Éd.), *Emulsifiers in Food Technology* (p. 271-296). John Wiley & Sons, Ltd. <https://doi.org/10.1002/9781118921265.ch12>



- Couffin, A.-C., & Delmas, T. (2013). Vecteurs lipidiques en tant que nanomédicaments. In *Techniques de l'ingénieur Mise en forme des médicaments et autres produits de santé: Vol. base documentaire : TIB611DUO*. (Numéro ref. article : j2310). Editions T.I. <https://www.techniques-ingenieur.fr/base-documentaire/biomedical-pharma-th15/mise-en-forme-des-medicaments-et-autres-produits-de-sante-42611210/vecteurs-lipidiques-en-tant-que-nanomedicaments-j2310/>
- Da Silva, E., Bresson, S., & Rousseau, D. (2009). Characterization of the three major polymorphic forms and liquid state of tristearin by Raman spectroscopy. *Chemistry and physics of lipids*, 157(2), 113-119.
- da Fonseca Antunes, A. B., De Geest, B. G., Vervaet, C., & Remon, J. P. (2013). Gelucire 44/14 based immediate release formulations for poorly water-soluble drugs. *Drug development and industrial pharmacy*, 39(5), 791-798.
- Dasgupta, S. (2017). *Metastable zone determination and nucleation kinetics during melt crystallization of polyunsaturated fatty acids* [PhD Thesis]. BTU Cottbus-Senftenberg.
- De Moraes, M. G. F., Barreto, A. G., Secchi, A. R., De Souza, M. B., Lage, P. L. D. C., & Myerson, A. S. (2023). Polymorphism of Praziquantel : Role of Cooling Crystallization in Access to Solid Forms and Discovery of New Polymorphs. *Crystal Growth & Design*, 23(2), 1247-1258. <https://doi.org/10.1021/acs.cgd.2c01381>
- Déat, E., Blanquet-Diot, S., Jarrige, J.-F., Denis, S., Beyssac, E., & Alric, M. (2009). Combining the Dynamic TNO-Gastrointestinal Tract System with a Caco-2 Cell Culture Model : Application to the Assessment of Lycopene and  $\alpha$ -Tocopherol Bioavailability from a Whole Food. *Journal of Agricultural and Food Chemistry*, 57(23), 11314-11320. <https://doi.org/10.1021/jf902392a>
- Dechsiri, C. (2004). *Particle transport in fluidized beds : Experiments and stochastic models*. Groningen.
- Dedroog, S., Huygens, C., & Van Den Mooter, G. (2019). Chemically identical but physically different : A comparison of spray drying, hot melt extrusion and cryo-milling for the formulation of high drug loaded amorphous solid dispersions of naproxen. *European Journal of Pharmaceutics and Biopharmaceutics*, 135, 1-12. <https://doi.org/10.1016/j.ejpb.2018.12.002>
- Delbaere, C., Van de Walle, D., Depypere, F., Gellynck, X., & Dewettinck, K. (2016). Relationship between chocolate microstructure, oil migration, and fat bloom in filled chocolates. *European Journal of Lipid Science and Technology*, 118(12), 1800-1826.
- Den Adel, R., Van Malssen, K., Van Duynhoven, J., Mykhaylyk, O. O., & Voda, A. (2018). Fat Crystallite Thickness Distribution Based on SAXD Peak Shape Analysis. *European Journal of Lipid Science and Technology*, 120(9), 1800222. <https://doi.org/10.1002/ejlt.201800222>
- Descamps, M. (2020). États amorphe et vitreux des composés moléculaires et pharmaceutiques—Applications et utilisations. *Médicaments et produits pharmaceutiques*. <https://doi.org/10.51257/a-v1-pha2032>
- Descamps, M., & Dudognon, E. (2014). Crystallization from the Amorphous State : Nucleation–Growth Decoupling, Polymorphism Interplay, and the Role of Interfaces. *Journal of Pharmaceutical Sciences*, 103(9), 2615-2628. <https://doi.org/10.1002/jps.24016>
- Dewettinck, K., & Huyghebaert, A. (1999). Fluidized bed coating in food technology. *Trends in Food Science & Technology*, 10(4-5), 163-168. [https://doi.org/10.1016/S0924-2244\(99\)00041-2](https://doi.org/10.1016/S0924-2244(99)00041-2)
- Ditzinger, F., Price, D. J., Nair, A., Becker-Baldus, J., Glaubitz, C., Dressman, J. B., Saal, C., & Kuentz, M. (2019). Opportunities for Successful Stabilization of Poor Glass-Forming Drugs : A Stability-Based Comparison of Mesoporous Silica Versus Hot Melt Extrusion Technologies. *Pharmaceutics*, 11(11), 577. <https://doi.org/10.3390/pharmaceutics11110577>
- Dobrosielska, M., Dobrucka, R., Kozera, P., Brząkalski, D., Gabriel, E., Głowacka, J., Jałbrzykowski, M., Kurzydłowski, K. J., & Przekop, R. E. (2023). Beeswax as a natural alternative to synthetic waxes for fabrication of PLA/diatomaceous earth composites. *Scientific Reports*, 13(1), 1161. <https://doi.org/10.1038/s41598-023-28435-0>
- Doenhoff, M. J., Hagan, P., Cioli, D., Southgate, V., Pica-Mattoccia, L., Botros, S., Coles, G., Tchuem Tchuenté, L. A., Mbaye, A., & Engels, D. (2009). Praziquantel : Its use in control of schistosomiasis in sub-Saharan Africa and current research needs. *Parasitology*, 136(13), 1825-1835. <https://doi.org/10.1017/S0031182009000493>
- Dong, Y., Hengst, L., Hunt, R., Patel, D., Vo, A., Choi, S., Ashraf, M., Cruz, C. N., & Xu, X. (2019). Understanding drug distribution and release in ophthalmic emulsions through quantitative evaluation of formulation-associated variables. *Journal of Controlled Release*, 313, 96-105. <https://doi.org/10.1016/j.jconrel.2019.09.010>
- Dressman, J. B., Amidon, G. L., Reppas, C., & Shah, V. P. (1998). Dissolution testing as a prognostic tool for oral drug absorption : Immediate release dosage forms. *Pharmaceutical Research*, 15(1), 11-22. <https://doi.org/10.1023/A:1011984216775>

- Dudzińska, N. M. (2017). *Development of lipid-based enteric coatings*. 1 Online-Ressource (125 Seiten). <https://doi.org/10.25673/1986>
- Duong, V. T., Nguyen, H. T., Wang, F., Wang, M., Narwankar, P. K., & Taylor, L. S. (2022). Surface nanocoating of high drug-loading spray-dried amorphous solid dispersions by atomic layer coating : Excellent physical stability under accelerated storage conditions for two years. *International Journal of Pharmaceutics*, 620, 121747. <https://doi.org/10.1016/j.ijpharm.2022.121747>
- Dupont, D., Alric, M., Blanquet-Diot, S., Bornhorst, G., Cueva, C., Deglaire, A., Denis, S., Ferrua, M., Havenaar, R., Lelieveld, J., Mackie, A. R., Marzorati, M., Menard, O., Minekus, M., Miralles, B., Recio, I., & Van Den Abbeele, P. (2019). Can dynamic *in vitro* digestion systems mimic the physiological reality? *Critical Reviews in Food Science and Nutrition*, 59(10), 1546-1562. <https://doi.org/10.1080/10408398.2017.1421900>
- Eason, T., Ramirez, G., Clulow, A. J., Salim, M., & Boyd, B. J. (2022). Revisiting the Dissolution of Praziquantel in Biorelevant Media and the Impact of Digestion of Milk on Drug Dissolution. *Pharmaceutics*, 14(10), 2228. <https://doi.org/10.3390/pharmaceutics14102228>
- Ebnesaajjad, S. (2014). Surface and Material Characterization Techniques. In *Surface Treatment of Materials for Adhesive Bonding* (p. 39-75). Elsevier. <https://doi.org/10.1016/B978-0-323-26435-8.00004-6>
- El Mafadi, S., & Poncelet, D. (2007). L'enrobage en lit fluidisé pour la production de microcapsules. In *Microencapsulation des sciences aux technologies*. TEC & DOC.
- Elder, D. P., Holm, R., & Kuentz, M. (2017). Medicines for pediatric patients—Biopharmaceutical, developmental, and regulatory considerations. *Journal of pharmaceutical sciences*, 106(4), 950-960.
- Elisabettoni, P., Desmedt, A., & Durant, F. (1996). Polymorphism of stabilized and nonstabilized tristearin, pure and in the presence of food emulsifiers. *Journal of the American Oil Chemists' Society*, 73(2), 187-192. <https://doi.org/10.1007/BF02523893>
- Faham, A., Prinderre, P., Farah, N., Eichler, K. D., Kalantzis, G., & Joachim, J. (2000). Hot-melt coating technology. I. Influence of Compritol® 888 Ato and granule size on theophylline release. *Drug development and industrial pharmacy*, 26(2), 167-176.
- Faham, A., Prinderre, P., Piccerelle, P., Farah, N., & Joachim, J. (2000). Hot melt coating technology : Influence of Compritol 888 Ato and granule size on chloroquine release. *Die Pharmazie*, 55(6), 444-448.
- Fahy, E., Cotter, D., Sud, M., & Subramaniam, S. (2011). Lipid classification, structures and tools. *Biochimica et Biophysica Acta (BBA)-Molecular and Cell Biology of Lipids*, 1811(11), 637-647.
- Fan, Y., & Zhang, Q. (2013). Development of liposomal formulations : From concept to clinical investigations. *Asian Journal of Pharmaceutical Sciences*, 8(2), 81-87. <https://doi.org/10.1016/j.ajps.2013.07.010>
- Fang, S., Wei, Y., Fu, L., Tian, G., & Qu, H. (2020). Modeling of the Minimum Fluidization Velocity and the Incipient Fluidization Pressure Drop in a Conical Fluidized Bed with Negative Pressure. *Applied Sciences*, 10(24), 8764. <https://doi.org/10.3390/app10248764>
- Fang, W., Mayama, H., & Tsujii, K. (2007). Spontaneous formation of fractal structures on triglyceride surfaces with reference to their super water-repellent properties. *The Journal of Physical Chemistry B*, 111(3), 564-571.
- FDA, CDER. (1997). *Guidance for Industry—Dissolution Testing of Immediate Release Solid Oral Dosage Forms*. <https://www.fda.gov/regulatory-information/search-fda-guidance-documents/dissolution-testing-immediate-release-solid-oral-dosage-forms>
- Feeney, O. M., Crum, M. F., McEvoy, C. L., Trevaskis, N. L., Williams, H. D., Pouton, C. W., Charman, W. N., Bergström, C. A., & Porter, C. J. (2016). 50 years of oral lipid-based formulations : Provenance, progress and future perspectives. *Advanced drug delivery reviews*, 101, 167-194.
- Feeney, O. M., Williams, H. D., Pouton, C. W., & Porter, C. J. H. (2014). 'Stealth' lipid-based formulations : Poly(ethylene glycol)-mediated digestion inhibition improves oral bioavailability of a model poorly water soluble drug. *Journal of Controlled Release*, 192, 219-227. <https://doi.org/10.1016/j.jconrel.2014.07.037>
- Felton, L. A. (2013). Mechanisms of polymeric film formation. *International Journal of Pharmaceutics*, 457(2), 423-427. <https://doi.org/10.1016/j.ijpharm.2012.12.027>
- Fernanda, P. (2018). Methods Used in the Study of the Physical Properties of Fats. In *Structure-Function Analysis of Edible Fats* (p. 313-385). Elsevier. <https://doi.org/10.1016/B978-0-12-814041-3.00011-3>
- Fernandes, C. P., Mascarenhas, M. P., Zibetti, F. M., Lima, B. G., Oliveira, R. P. R. F., Rocha, L., & Falcão, D. Q. (2013). HLB value, an important parameter for the development of essential oil phytopharmaceuticals. *Revista Brasileira de Farmacognosia*, 23(1), 108-114. <https://doi.org/10.1590/S0102-695X2012005000127>
- Ferreira Marques, C. S., Rezende, P., Andrade, L. N., Mendes, T. M. F., Allegretti, S. M., Bani, C., Chaud, M. V., Batista De Almeida, M., Souto, E. B., Pereira Da Costa, L., & Severino, P. (2018). Solid dispersion of praziquantel



- enhanced solubility and improve the efficacy of the schistosomiasis treatment. *Journal of Drug Delivery Science and Technology*, 45, 124-134. <https://doi.org/10.1016/j.jddst.2018.03.009>
- Floeter, E., Haeupler, M., & Sato, K. (2018). Molecular Interactions and Mixing Phase Behavior of Lipid Crystals. In K. Sato (Éd.), *Crystallization of Lipids* (1<sup>re</sup> éd., p. 61-104). Wiley. <https://doi.org/10.1002/9781118593882.ch3>
- Foroughi-Dahr, M., Mostoufi, N., Sotudeh-Gharebagh, R., & Chaouki, J. (2017). Particle Coating in Fluidized Beds. In *Reference Module in Chemistry, Molecular Sciences and Chemical Engineering* (p. B9780124095472122061). Elsevier. <https://doi.org/10.1016/B978-0-12-409547-2.12206-1>
- Foubert, I., Dewettinck, K., & Vanrolleghem, P. A. (2003). Modelling of the crystallization kinetics of fats. *Trends in Food Science & Technology*, 14(3), 79-92. [https://doi.org/10.1016/S0924-2244\(02\)00256-X](https://doi.org/10.1016/S0924-2244(02)00256-X)
- Frankiewicz, M., & Sznitowska, M. (2022). Design of Experiments as a Tool to Optimize the Process of Coating Minitablets with Commercial Gastro-Resistant Coating Mixtures. *Pharmaceutics*, 14(9), 1816. <https://doi.org/10.3390/pharmaceutics14091816>
- Fratini, F., Cilia, G., Turchi, B., & Felicioli, A. (2016). Beeswax : A minireview of its antimicrobial activity and its application in medicine. *Asian Pacific Journal of Tropical Medicine*, 9(9), 839-843. <https://doi.org/10.1016/j.apjtm.2016.07.003>
- Frenning, G., Tunón, Å., & Alderborn, G. (2003). Modelling of drug release from coated granular pellets. *Journal of Controlled Release*, 92(1-2), 113-123. [https://doi.org/10.1016/S0168-3659\(03\)00300-6](https://doi.org/10.1016/S0168-3659(03)00300-6)
- Frydendahl, C. (2023). *Fractal analysis package* (1.0.3) [Logiciel]. <https://www.mathworks.com/matlabcentral/fileexchange/71770-fractal-analysis-package>
- Gaillard, Y., Mija, A., Burr, A., Darque-Ceretti, E., Felder, E., & Sbirrazzuoli, N. (2011). Green material composites from renewable resources : Polymorphic transitions and phase diagram of beeswax/rosin resin. *Thermochimica Acta*, 521(1-2), 90-97. <https://doi.org/10.1016/j.tca.2011.04.010>
- Garti, N. (1988). Effects of surfactants on crystallization and polymorphic transformation of fats and fatty acids. *Crystallization and polymorphism of fats and fatty acids*, 267-303.
- Garti, N., & Aserin, A. (2012). Effect of Emulsifiers on Cocoa Butter and Chocolate Rheology, Polymorphism, and Bloom. In *Cocoa Butter and Related Compounds* (p. 275-305). Elsevier. <https://doi.org/10.1016/B978-0-9830791-2-5.50015-3>
- Garti, N., Schlichter, J., & Sarig, S. (1986). Effect of food emulsifiers on polymorphic transitions of cocoa butter. *Journal of the American Oil Chemists' Society*, 63(2), 230-236.
- Garti, N., Wellner, E., & Sarig, S. (1982). Crystal structure modifications of tristearin by food emulsifiers. *Journal of the American Oil Chemists' Society*, 59(4), 181-185. <https://doi.org/10.1007/BF02680272>
- Garti, N., & Yano, J. (2001). The roles of emulsifiers in fat crystallization. *Crystallization processes in fats and lipid systems*, 211-250.
- Gautschi, N., Bergström, C. A. S., & Kuentz, M. (2016). Rapid determination of drug solubilization versus supersaturation in natural and digested lipids. *International Journal of Pharmaceutics*, 513(1-2), 164-174. <https://doi.org/10.1016/j.ijpharm.2016.09.015>
- Geldart, D. (1973). Types of gas fluidization. *Powder Technology*, 7(5), 285-292. [https://doi.org/10.1016/0032-5910\(73\)80037-3](https://doi.org/10.1016/0032-5910(73)80037-3)
- Gibson, L. (2007). Lipid-based excipients for oral drug delivery. In *Oral Lipid-Based Formulations* (p. 55-84). CRC Press.
- Girod Fullana, S., & Aubert-Pouessel, A. (2019). Excipients verts en émergence pour l'industrie pharmaceutique. *Chimie verte*. <https://doi.org/10.51257/a-v1-chv4024>
- Girod Fullana, S., & Aubert-Pouessel, A. (2019). *Excipients verts en émergence pour l'industrie pharmaceutique* (Numéro ref. article : chv4024). Editions T.I. <https://www.techniques-ingenieur.fr/base-documentaire/procedes-chimie-bio-agro-th2/elaboration-des-formulations-42335210/excipients-verts-en-emergence-pour-l-industrie-pharmaceutique-chv4024/>
- Gore, A. J., Bhagwat, S. S., Mhaskar, S., & Saxena, S. (2023). Determination of required HLB value and emulsifiers for the preparation of water in coconut oil emulsions for application in food process industries. *Journal of Dispersion Science and Technology*, 44(8), 1363-1370. <https://doi.org/10.1080/01932691.2021.2016438>
- Grant, D. J. W., & Liversidge, G. G. (1983). Influence of Physicochemical Interactions on the Properties of Suppositories. III. Reecological Behaviour of Fatty Suppository Bases and its Effect on Spreading in Rats. *Drug Development and Industrial Pharmacy*, 9(1-2), 247-266. <https://doi.org/10.3109/03639048309048556>
- Grant, D. J. W., Liversidge, G. G., & Bell, J. (1983). Influence of physicochemical interactions on the properties of suppositories V. The in vitro release of ketoprofen and metronidazole from various fatty suppository bases and

correlations with in vivo plasma levels. *International Journal of Pharmaceutics*, 14(2-3), 251-262. [https://doi.org/10.1016/0378-5173\(83\)90098-4](https://doi.org/10.1016/0378-5173(83)90098-4)

Gray, V. A., Mann, J. C., Barker, R., & Pepin, X. J. H. (2020). The Case for Physiologically Based Biopharmaceutics Modelling (PBBM) : What do Dissolution Scientists Need to Know? *Dissolution Technologies*, 27(3), 6-19. <https://doi.org/10.14227/DT270320P6>

Green, N. L., & Rousseau, D. (2018). Lipid Crystallization in Water-in-Oil Emulsions. In K. Sato (Éd.), *Crystallization of Lipids* (1<sup>re</sup> éd., p. 405-429). Wiley. <https://doi.org/10.1002/9781118593882.ch14>

Greth, G. G., & Wilson, J. E. (1961). Use of the HLB system in selecting emulsifiers for emulsion polymerization. *Journal of Applied Polymer Science*, 5(14), 135-148. <https://doi.org/10.1002/app.1961.070051402>

Grundy, M. M. L., Abrahamse, E., Almgren, A., Alming, M., Andres, A., Ariëns, R. M. C., Bastiaan-Net, S., Bourliou-Lacanal, C., Brodkorb, A., Bronze, M. R., Comi, I., Couëdelo, L., Dupont, D., Durand, A., El, S. N., Grauwet, T., Heerup, C., Heredia, A., Infantes Garcia, M. R., ... Carrière, F. (2021). INFOGEST inter-laboratory recommendations for assaying gastric and pancreatic lipases activities prior to in vitro digestion studies. *Journal of Functional Foods*, 82, 104497. <https://doi.org/10.1016/j.jff.2021.104497>

Guan, T., Wang, J., Li, G., & Tang, X. (2011). Comparative study of the stability of venlafaxine hydrochloride sustained-release pellets prepared by double-polymer coatings and hot-melt subcoating combined with Eudragit® NE30D outercoating. *Pharmaceutical Development and Technology*, 16(3), 269-277. <https://doi.org/10.3109/10837451003664081>

Hagemann, J. W. (1988). Thermal behavior and polymorphism of acylglycerides. In *Crystallization and polymorphism of fats and fatty acids* (Vol. 31, p. 9-95). Marcel Dekker New York.

Hampel, N., Roydeva, E., Bück, A., & Tsotsas, E. (2018). Coating of finely dispersed particles by two-fluid nozzle. *Particuology*, 38, 80-93. <https://doi.org/10.1016/j.partic.2017.05.015>

Hate, S. S. (2015). *Investigation of physico-chemical properties of lipid-based excipients in a hot-melt fluid bed coating process* [PhD Thesis, Rutgers University-Graduate School-New Brunswick]. <https://rucore.libraries.rutgers.edu/rutgers-lib/47410/>

Hautala, J., Kääriäinen, T., Hoppu, P., Kemell, M., Heinämäki, J., Cameron, D., George, S., & Juppo, A. M. (2017). Atomic layer deposition—A novel method for the ultrathin coating of minitables. *International Journal of Pharmaceutics*, 531(1), 47-58. <https://doi.org/10.1016/j.ijpharm.2017.08.010>

Hede, P. D., Bach, P., & Jensen, A. D. (2008). Validation of the flux number as scaling parameter for top-spray fluidised bed systems. *Chemical Engineering Science*, 63(3), 815-828. <https://doi.org/10.1016/j.ces.2007.10.017>

Hippalgaonkar, K., Majumdar, S., & Kansara, V. (2010). Injectable Lipid Emulsions—Advancements, Opportunities and Challenges. *AAPS PharmSciTech*, 11(4), 1526-1540. <https://doi.org/10.1208/s12249-010-9526-5>

Hohl, R., Scheibelhofer, O., Stocker, E., Behzadi, S. S., Haack, D., Koch, K., Kerschhaggl, P., Lochmann, D., Sacher, S., & Zimmer, A. (2017). Monitoring of a hot melt coating process via a novel multipoint near-infrared spectrometer. *AAPS PharmSciTech*, 18(1), 182-193.

Holm, R., Kuentz, M., Ilie-Spiridon, A.-R., & Griffin, B. T. (2023). Lipid based formulations as supersaturating oral delivery systems: From current to future industrial applications. *European Journal of Pharmaceutical Sciences*, 189, 106556. <https://doi.org/10.1016/j.ejps.2023.106556>

Hondoh, H., Ueno, S., & Sato, K. (2018). Fundamental aspects of crystallization of lipids. *Crystallization of Lipids: Fundamentals and Applications in Food, Cosmetics and Pharmaceuticals*, 105-136.

Hüttlin, H. (2011). Coatings mittels INNOJET®-Verfahren. In M. Kumpugdee-Vollrath & J.-P. Krause (Éds.), *Easy Coating* (p. 120-132). Vieweg+Teubner. [https://doi.org/10.1007/978-3-8348-9896-8\\_5](https://doi.org/10.1007/978-3-8348-9896-8_5)

Huynh, V.-T.-T., De Paiva Lacerda, S., Espitalier, F., Beyssac, E., & Ré, M.-I. (2024). Effect of talc and vitamin E TPGS on manufacturability, stability and release properties of trilaurin-based formulations for hot-melt coating. *International Journal of Pharmaceutics*, 653, 123866. <https://doi.org/10.1016/j.ijpharm.2024.123866>

ICH Q3C. (2022). *ICH guideline Q3C (R8) on impurities : Guideline for residual solvents* (Version R8).

ICH Q8 (R2). (2009). *Pharmaceutical development, ICH Harmonized Tri- partite Guidelines. International Conference on Harmonization of Technical Requirements for Registration of Pharmaceuticals for Human Use.*

ICH Topic Q 1 A (R2). (2003). *Stability Testing of new Drug Substances and Products.* [https://www.ema.europa.eu/en/documents/scientific-guideline/ich-q-1-r2-stability-testing-new-drug-substances-and-products-step-5\\_en.pdf](https://www.ema.europa.eu/en/documents/scientific-guideline/ich-q-1-r2-stability-testing-new-drug-substances-and-products-step-5_en.pdf)

- Ignjatović, J., \DJuriš, J., \DJuriš, M., Bočarski, T., Vasiljević, V., Aleksić, I., & Cvijić, S. (2021). Assessment of hot-melt coating methods for multiparticulate substrates: Mortar-coating vs. pan-coating. *Arhiv za farmaciju*, 71(1), 35-54.
- Inoue, T., Hisatsugu, Y., Ishikawa, R., & Suzuki, M. (2004). Solid-liquid phase behavior of binary fatty acid mixtures: 2. Mixtures of oleic acid with lauric acid, myristic acid, and palmitic acid. *Chemistry and physics of lipids*, 127(2), 161-173.
- Inoue, T., Hisatsugu, Y., Suzuki, M., Wang, Z., & Zheng, L. (2004). Solid-liquid phase behavior of binary fatty acid mixtures: 3. Mixtures of oleic acid with capric acid (decanoic acid) and caprylic acid (octanoic acid). *Chemistry and physics of lipids*, 132(2), 225-234.
- Inoue, T., Hisatsugu, Y., Yamamoto, R., & Suzuki, M. (2004). Solid-liquid phase behavior of binary fatty acid mixtures: 1. Oleic acid/stearic acid and oleic acid/behenic acid mixtures. *Chemistry and physics of lipids*, 127(2), 143-152.
- Jacobsen, N. M. Y., Nedergaard, H. B., Kock, A., Caglayan, I., Laursen, M. M., Lange, E.-M., Marcial-Coba, M. S., Bar-Shalom, D., Nielsen, D. S., & Müllertz, A. (2021). Development of gastro-resistant coated probiotic granulates and evaluation of viability and release during simulated upper gastrointestinal transit. *LWT*, 144, 111174. <https://doi.org/10.1016/j.lwt.2021.111174>
- Jadhav, H. B., & Annapure, U. S. (2023). Triglycerides of medium-chain fatty acids: A concise review. *Journal of Food Science and Technology*, 60(8), 2143-2152. <https://doi.org/10.1007/s13197-022-05499-w>
- Jannin, V. (2004). *Valorisation de la fonctionnalité des poudres microenrobées par des lipides (Improvement of the functionality of lipid-coated particles)*. PhD thesis, Université de Bourgogne, Dijon, France, 1-145.
- Jannin, V. (2010). *Valorisation des propriétés physico-chimiques et biologiques d'excipients lipidiques destinés à l'administration orale de substances actives*. Université Claude Bernard Lyon I, Lyon.
- Jannin, V., Bérard, V., & Andrès, C. (2005). *Modification of the drug release of ibuprofen by hot-melt coating with mixes of Compritol® 888 ATO and non-ionic surfactants*. <https://doi.org/10.13140/RG.2.2.26168.65282>
- Jannin, V., Bérard, V., N'Diaye, A., Andrès, C., & Pourcelot, Y. (2003). Comparative study of the lubricant performance of Compritol® 888 ATO either used by blending or by hot melt coating. *International Journal of Pharmaceutics*, 262(1-2), 39-45. [https://doi.org/10.1016/S0378-5173\(03\)00316-8](https://doi.org/10.1016/S0378-5173(03)00316-8)
- Jannin, V., & Cuppok, Y. (2013). Hot-melt coating with lipid excipients. *International journal of pharmaceutics*, 457(2), 480-487.
- Jannin, V., Pochard, E., & Chambin, O. (2006). Influence of poloxamers on the dissolution performance and stability of controlled-release formulations containing Precirol® ATO 5. *International journal of pharmaceutics*, 309(1-2), 6-15.
- Jannin, V., Rodier, J.-D., & Musakhanian, J. (2014). Polyoxylglycerides and glycerides: Effects of manufacturing parameters on API stability, excipient functionality and processing. *International Journal of Pharmaceutics*, 466(1-2), 109-121. <https://doi.org/10.1016/j.ijpharm.2014.03.007>
- Jannin, V., Rosiaux, Y., & Doucet, J. (2015). Exploring the possible relationship between the drug release of Compritol®-containing tablets and its polymorph forms using micro X-ray diffraction. *Journal of Controlled Release*, 197, 158-164. <https://doi.org/10.1016/j.jconrel.2014.11.013>
- Jaw, K.-S., Hsu, C.-K., & Lee, J.-S. (2001). The thermal decomposition behaviors of stearic acid, paraffin wax and polyvinyl butyral. *Thermochimica Acta*, 367-368, 165-168. [https://doi.org/10.1016/S0040-6031\(00\)00680-8](https://doi.org/10.1016/S0040-6031(00)00680-8)
- Jensen, R. G., Sampugna, J., Parry Jr, R. M., & Shahani, K. M. (1963). Lipolysis of Laurate Glycerides by Pancreatic and Milk Lipase. *Journal of Dairy Science*, 46(9), 907-910.
- Jeong, K. H., Woo, H. S., Kim, C. J., Lee, K. H., Jeon, J. Y., Lee, S. Y., Kang, J.-H., Lee, S., & Choi, Y. W. (2015). Formulation of a modified-release pregabalin tablet using hot-melt coating with glyceryl behenate. *International Journal of Pharmaceutics*, 495(1), 1-8.
- Jones, D. M. (1985). Factors to consider in fluid-bed processing. *Pharm. Technol*, 9(4), 50.
- Jones, D. M. (1988). Air suspension coating. *Encyclopedia of pharmaceutical technology*, 1, 189-216.
- Jones, D. M., & Percel, P. J. (1994). Coating of multiparticulates using molten materials. Formulation and process considerations. *Drugs and the pharmaceutical sciences*, 65, 113-142.
- Joyce, P., Dening, T. J., Meola, T. R., Schultz, H. B., Holm, R., Thomas, N., & Prestidge, C. A. (2019). Solidification to improve the biopharmaceutical performance of SEDDS: Opportunities and challenges. *Advanced drug delivery reviews*, 142, 102-117.
- Jozwiakowski, M. J., Jones, D. M., & Franz, R. M. (1990). Characterization of a hot-melt fluid bed coating process for fine granules. *Pharmaceutical research*, 7(11), 1119-1126.

- Kalepu, S., Manthina, M., & Padavala, V. (2013). Oral lipid-based drug delivery systems – an overview. *Acta Pharmaceutica Sinica B*, 3(6), 361-372. <https://doi.org/10.1016/j.apsb.2013.10.001>
- Kalish, J. P., Ramalingam, S., Bao, H., Hall, D., Wamuo, O., Hsu, S. L., Paul, C. W., Eodice, A., & Low, Y.-G. (2015). An analysis of the role of wax in hot melt adhesives. *International Journal of Adhesion and Adhesives*, 60, 63-68. <https://doi.org/10.1016/j.ijadhadh.2015.03.008>
- Kaneko, F., Yamamoto, Y., & Yoshikawa, S. (2020). Structural study on fat crystallization process heterogeneously induced by graphite surfaces. *Molecules*, 25(20), 4786.
- Katzhender, I., Hoffman, A., Goldberger, A., & Friedman, M. (1997). Modeling of Drug Release from Erodible Tablets. *Journal of Pharmaceutical Sciences*, 86(1), 110-115. <https://doi.org/10.1021/js9600538>
- Kegel, C., Klein, S., & Mäder, K. (2009). Neue Hilfsstoffe – Mehrwert oder nur Mehrkosten? In *Innovative Arzneiformen—Ein Lehrbuch für Studium und Praxis* (p. 13-35). Wissenschaftliche Verlagsgesellschaft Stuttgart.
- Kellens, M., Meeussen, W., Hammersley, A., & Reynaers, H. (1991). Synchrotron radiation investigations of the polymorphic transitions in saturated monoacid triglycerides. Part 2 : Polymorphism study of a 50:50 mixture of tripalmitin and tristearin during crystallization and melting. *Chemistry and Physics of Lipids*, 58(1-2), 145-158. [https://doi.org/10.1016/0009-3084\(91\)90120-Z](https://doi.org/10.1016/0009-3084(91)90120-Z)
- Kellens, M., & Reynaers, H. (1992). Study of the Polymorphism of Saturated Monoacid Triglycerides I : Melting and Crystallization Behaviour of Tristearin. *Lipid / Fett*, 94(3), 94-100. <https://doi.org/10.1002/lipi.19920940304>
- Kennedy, J. P., & Niebergall, P. J. (1996). Development and Optimization of a Solid Dispersion Hot-Melt Fluid Bed Coating Method. *Pharmaceutical Development and Technology*, 1(1), 51-62. <https://doi.org/10.3109/10837459609031418>
- Kennedy, J. P., & Niebergall, P. J. (1998). Evaluation of Extended-Release Applications for Solid Dispersion Hot-Melt Fluid Bed Coatings Utilizing Hydrophobic Coating Agents. *Pharmaceutical Development and Technology*, 3(1), 95-101. <https://doi.org/10.3109/10837459809028483>
- Khan, N., & Craig, D. Q. (2004). Role of blooming in determining the storage stability of lipid-based dosage forms. *Journal of pharmaceutical sciences*, 93(12), 2962-2971.
- Khobragade, D. S., Wankar, J., Patil, A. T., Potbhare, M. S., Lakhotiya, C. L., & Umathe, S. N. (2014). A novel practical approach for enhancement of bioavailability of a poorly water soluble drug by hot melt coating technique. *Int. J. Pharm. Sci. Rev. Res*, 26(1), 258-263.
- Kim, J.-W. (2003). *Manufacture and characteristics of pastilles and their coating by crystallization process*.
- Kim, J.-W., & Ulrich, J. (2003). Prediction of degree of deformation and crystallization time of molten droplets in pastillation process. *International Journal of Pharmaceutics*, 257(1-2), 205-215. [https://doi.org/10.1016/S0378-5173\(03\)00141-8](https://doi.org/10.1016/S0378-5173(03)00141-8)
- Kleinbach, E., & Riede, Th. (1995). Coating of solids. *Chemical Engineering and Processing: Process Intensification*, 34(3), 329-337. [https://doi.org/10.1016/0255-2701\(94\)04021-4](https://doi.org/10.1016/0255-2701(94)04021-4)
- Knezevic, Z., Gosak, D., Hraste, M., & Jalsenjako, I. (1998). Fluid-bed microencapsulation of ascorbic acid. *Journal of Microencapsulation*, 15(2), 237-252. <https://doi.org/10.3109/02652049809006853>
- Knezevic, Z., Gosak, D., Hraste, M., Rausl, D., & Khan, M. Z. I. (2009). Application of hot-melt coating process for designing a lipid based controlled release drug delivery system for highly aqueous soluble drugs. *Chemical and pharmaceutical bulletin*, 57(5), 464-471.
- Koehl, N. J., Holm, R., Kuentz, M., Jannin, V., & Griffin, B. T. (2020). Exploring the impact of surfactant type and digestion : Highly digestible surfactants improve oral bioavailability of nilotinib. *Molecular Pharmaceutics*, 17(9), 3202-3213.
- Kohli, K., Chopra, S., Dhar, D., Arora, S., & Khar, R. K. (2010). Self-emulsifying drug delivery systems : An approach to enhance oral bioavailability. *Drug Discovery Today*, 15(21-22), 958-965. <https://doi.org/10.1016/j.drudis.2010.08.007>
- Kondo, H., & Toda, A. (2009). Mechanical and Thermal Properties of a Hot-melt Adhesive of Triblock Copolymer Added with a Miscible Homopolymer. *Polymer Journal*, 41(1), 74-82. <https://doi.org/10.1295/polymj.PJ2008162>
- Kreye, F., Siepmann, F., & Siepmann, J. (2008). Lipid implants as drug delivery systems. *Expert Opinion on Drug Delivery*, 5(3), 291-307. <https://doi.org/10.1517/17425247.5.3.291>
- Kreye, F., Siepmann, F., Zimmer, A., Willart, J., Descamps, M., & Siepmann, J. (2011). Cast Lipid Implants for Controlled Drug Delivery : Importance of the Tempering Conditions. *Journal of Pharmaceutical Sciences*, 100(8), 3471-3481. <https://doi.org/10.1002/jps.22574>



- Kucera, S. A., Felton, L. A., & McGinity, J. W. (2013). Physical aging in pharmaceutical polymers and the effect on solid oral dosage form stability. *International Journal of Pharmaceutics*, 457(2), 428-436. <https://doi.org/10.1016/j.ijpharm.2013.01.069>
- Kulah, G., & Kaya, O. (2011). Investigation and scale-up of hot-melt coating of pharmaceuticals in fluidized beds. *Powder Technology*, 208(1), 175-184. <https://doi.org/10.1016/j.powtec.2010.12.016>
- Kulkarni, S. A., Kadam, S. S., Meekes, H., Stankiewicz, A. I., & Ter Horst, J. H. (2013). Crystal Nucleation Kinetics from Induction Times and Metastable Zone Widths. *Crystal Growth & Design*, 13(6), 2435-2440. <https://doi.org/10.1021/cg400139t>
- Kushwah, V., Gomes Lopes, D., Saraf, I., Koutsamanis, I., Werner, B., Zangger, K., Roy, M. C., Bartlett, J. A., Frericks Schmidt, H., Shamblin, S. L., Laggner, P., & Paudel, A. (2022). Phase Behavior of Drug–Lipid–Surfactant Ternary Systems toward Understanding the Annealing-Induced Change. *Molecular Pharmaceutics*, 19(2), 532-546. <https://doi.org/10.1021/acs.molpharmaceut.1c00651>
- Kushwah, V., Lopes, D. G., Koutsamanis, I., Plank, H., Ardelean, I., Sarkar, A., Prpich, A., Am Ende, M. T., Schmidt, H. F., & Doshi, P. (2020). Evolution of the microstructure and the drug release upon annealing the drug loaded lipid-surfactant microspheres. *European Journal of Pharmaceutical Sciences*, 147, 105278.
- Kyobula, M., Adedeji, A., Alexander, M. R., Saleh, E., Wildman, R., Ashcroft, I., Gellert, P. R., & Roberts, C. J. (2017). 3D inkjet printing of tablets exploiting bespoke complex geometries for controlled and tuneable drug release. *Journal of Controlled Release*, 261, 207-215.
- Langguth, P., Fricker, G., & Wunderli-Allenspach, H. (2012). *Biopharmazie*. John Wiley & Sons. <https://books.google.com/books?hl=en&lr=&id=2rb5hcG91LgC&oi=fnd&pg=PT9&dq=Grundlagen+der+Biopharmazie+&ots=4cz7M4t7O&sig=K5nPMfW9yaBa163cMlw6wBrcM>
- Laser Diffraction Particle Size Analysis | Malvern Panalytical*. (s. d.). Consulté 9 décembre 2023, à l'adresse <https://www.malvernpanalytical.com/en/products/technology/light-scattering/laser-diffraction>
- Le, H. T. (2004). *Preparing sustained release dosage forms of nifedipine by hot-melt coating method*. [https://ir.library.oregonstate.edu/concern/graduate\\_thesis\\_or\\_dissertations/4b29b801x](https://ir.library.oregonstate.edu/concern/graduate_thesis_or_dissertations/4b29b801x)
- Leane, M., Pitt, K., Reynolds, G., & Group, M. C. S. (MCS) W. (2015). A proposal for a drug product Manufacturing Classification System (MCS) for oral solid dosage forms. *Pharmaceutical development and technology*, 20(1), 12-21.
- Lee, J. (2004). Intrinsic adhesion force of lubricants to steel surface. *Journal of Pharmaceutical Sciences*, 93(9), 2310-2318. <https://doi.org/10.1002/jps.20124>
- Lee, Y. L., Ristic, R. I., DeMatos, L. L., & Martin, C. M. (2010). Crystallisation Pathways of Polymorphic Triacylglycerols Induced by Mechanical Energy. *Journal of Physics: Conference Series*, 247, 012049. <https://doi.org/10.1088/1742-6596/247/1/012049>
- Leturia, M., & Saleh, K. (2014). Fluidisation gaz-solide—Bases et théorie. *Opérations unitaires. Génie de la réaction chimique*. <https://doi.org/10.51257/a-v2-j4100>
- Li, J., Yang, B., Levons, J., Pinnamaneni, S., & Raghavan, K. (2011). Phase behavior of TPGS–PEG400/1450 systems and their application to liquid formulation : A formulation platform approach. *Journal of Pharmaceutical Sciences*, 100(11), 4907-4921. <https://doi.org/10.1002/jps.22659>
- Li, W., Kong, X. H., Ruan, M., Ma, F. M., Jiang, Y. F., Liu, M. Z., Chen, Y., & Zuo, X. H. (2012). Green waxes, adhesives and lubricants. *Philosophical Transactions of the Royal Society A: Mathematical, Physical and Engineering Sciences*, 370(1970), 3269-3269. <https://doi.org/10.1098/rsta.2012.0141>
- Lin, T. J., Kurihara, H., & Ohta, H. (1977). Prediction of Optimum O/W Emulsification Via Solubilization Measurements. *Journal of Society of Cosmetic Chemists of Japan*, 11(2), 32-42. [https://doi.org/10.5107/sccj1976.11.2\\_32](https://doi.org/10.5107/sccj1976.11.2_32)
- Liu, C., Zheng, Z., Meng, Z., Chai, X., Cao, C., & Liu, Y. (2019). Beeswax and carnauba wax modulate the crystallization behavior of palm kernel stearin. *LWT*, 115, 108446. <https://doi.org/10.1016/j.lwt.2019.108446>
- Liversidge, G. G. (1983). Influence of physicochemical interactions on the properties of suppositories IV. Factors influencing the in vivo release of ketoprofen and metronidazole from fatty suppository bases. *International Journal of Pharmaceutics*, 13(3), 243-251. [https://doi.org/10.1016/0378-5173\(83\)90073-X](https://doi.org/10.1016/0378-5173(83)90073-X)
- Liversidge, G. G., & Grant, D. J. W. (1983). Influence of Physicochemical Interactions on the Properties of Suppositories, II, Interactions Between the Constituents of Fatty Suppository Bases and Ketoprofen or Metronidazole. *Drug Development and Industrial Pharmacy*, 9(1-2), 223-246. <https://doi.org/10.3109/03639048309048555>

- Liversidge, G. G., Grant, D. J. W., & Padfield, J. M. (1981). Influence of physicochemical interactions on the properties of suppositories I. Interactions between the constituents of fatty suppository bases. *International Journal of Pharmaceutics*, 7(3), 211-223. [https://doi.org/10.1016/0378-5173\(81\)90107-1](https://doi.org/10.1016/0378-5173(81)90107-1)
- Lopes, D. G., Becker, K., Stehr, M., Lochmann, D., Haack, D., Zimmer, A., & Salar-Behzadi, S. (2015). Role of Lipid Blooming and Crystallite Size in the Performance of Highly Soluble Drug-Loaded Microcapsules. *Journal of Pharmaceutical Sciences*, 104(12), 4257-4265. <https://doi.org/10.1002/jps.24660>
- Lopes, D. G., Garsuch, V., Becker, K., Paudel, A., Stehr, M., Zimmer, A., & Salar-Behzadi, S. (2016). Improving the granule strength of roller-compacted ibuprofen sodium for hot-melt coating processing. *International journal of pharmaceutics*, 510(1), 285-295.
- Lopes, D. G., Koutsamanis, I., Becker, K., Scheibelhofer, O., Laggner, P., Haack, D., Stehr, M., Zimmer, A., & Salar-Behzadi, S. (2017). Microphase separation in solid lipid dosage forms as the cause of drug release instability. *International journal of pharmaceutics*, 517(1-2), 403-412.
- Lopes, D. G., Salar-Behzadi, S., & Zimmer, A. (2017). Designing optimal formulations for hot-melt coating. *International journal of pharmaceutics*, 533(2), 357-363.
- Lopes, J. D., Grosso, C. R. F., De Andrade Calligaris, G., Cardoso, L. P., Basso, R. C., Ribeiro, A. P. B., & Efraim, P. (2015). Solid lipid microparticles of hardfats produced by spray cooling as promising crystallization modifiers in lipid systems. *European Journal of Lipid Science and Technology*, 117(11), 1733-1744. <https://doi.org/10.1002/ejlt.201400560>
- López Mármol, Á., Fischer, P. L., Wahl, A., Schwöbel, D., Lenz, V., Sauer, K., & Koziol, M. (2022). Application of tiny-TIM as a mechanistic tool to investigate the in vitro performance of different itraconazole formulations under physiologically relevant conditions. *European Journal of Pharmaceutical Sciences*, 173, 106165. <https://doi.org/10.1016/j.ejps.2022.106165>
- Lvova, L., Denis, S., Barra, A., Mielle, P., Salles, C., Vergoignan, C., Di Natale, C., Paolesse, R., Temple-Boyer, P., & Feron, G. (2012). Salt release monitoring with specific sensors in “in vitro” oral and digestive environments from soft cheeses. *Talanta*, 97, 171-180. <https://doi.org/10.1016/j.talanta.2012.04.013>
- MacNaughtan, W., Farhat, I. A., Himawan, C., Starov, V. M., & Stapley, A. G. F. (2006). A differential scanning calorimetry study of the crystallization kinetics of tristearin-tripalmitin mixtures. *Journal of the American Oil Chemists' Society*, 83(1), 1-9. <https://doi.org/10.1007/s11746-006-1167-1>
- Macridachis-González, J., Bayés-García, L., & Calvet, T. (2020). An insight into the solid-state miscibility of triacylglycerol crystals. *Molecules*, 25(19), 4562.
- Majó, M., Sánchez, R., Barcelona, P., García, J., Fernández, A. I., & Barreneche, C. (2021). Degradation of Fatty Acid Phase-Change Materials (PCM): New Approach for Its Characterization. *Molecules*, 26(4), 982. <https://doi.org/10.3390/molecules26040982>
- Marie Le Page, M., & Hervé, M. (2019). *Cristallisation en milieu fondu-Procédés et mises en œuvre*.
- Mathematical models of drug release. (2015). In *Strategies to Modify the Drug Release from Pharmaceutical Systems* (p. 63-86). Elsevier. <https://doi.org/10.1016/B978-0-08-100092-2.00005-9>
- Mayama, H. (2009). Blooming theory of tristearin. *Soft matter*, 5(4), 856-859.
- Metin, S., & Hartel, R. W. (1998). Thermal analysis of isothermal crystallization kinetics in blends of cocoa butter with milk fat or milk fat fractions. *Journal of the American Oil Chemists' Society*, 75(11), 1617-1624. <https://doi.org/10.1007/s11746-998-0102-z>
- Milanovic, A., Aleksic, I., Ibric, S., Parojcic, J., & Cvijic, S. (2018). Hot-melt coating with Precirol ATO 5 in a fluidized-bed apparatus : Application of experimental design in the optimization of process parameters. *Journal of Drug Delivery Science and Technology*, 46, 274-284.
- Milanovic, A., Aleksic, I., Ibric, S., Parojcic, J., & Cvijic, S. (2020). Tableting of hot-melt coated paracetamol granules : Material tableting properties and quality characteristics of the obtained tablets. *European Journal of Pharmaceutical Sciences*, 142, 105121. <https://doi.org/10.1016/j.ejps.2019.105121>
- Minekus, M. (2015). The TNO Gastro-Intestinal Model (TIM). In K. Verhoeckx, P. Cotter, I. López-Expósito, C. Kleiveland, T. Lea, A. Mackie, T. Requena, D. Swiatecka, & H. Wichers (Éds.), *The Impact of Food Bioactives on Health* (p. 37-46). Springer International Publishing. [https://doi.org/10.1007/978-3-319-16104-4\\_5](https://doi.org/10.1007/978-3-319-16104-4_5)
- Minekus, M., Marteau, P., Havenaar, R., & Veld, J. H. J. H. I. (1995). A Multicompartmental Dynamic Computer-controlled Model Simulating the Stomach and Small Intestine. *Alternatives to Laboratory Animals*, 23(2), 197-209. <https://doi.org/10.1177/026119299502300205>



- Mishra, K., Kummer, N., Bergfreund, J., Kämpf, F., Bertsch, P., Pauer, R., Nyström, G., Fischer, P., & Windhab, E. J. (2023). Controlling lipid crystallization across multiple length scales by directed shear flow. *Journal of Colloid and Interface Science*, 630, 731-741. <https://doi.org/10.1016/j.jcis.2022.10.005>
- Montgomery, D. C. (1999). Experimental design for product and process design and development. *Journal of the Royal Statistical Society Series D: The Statistician*, 48(2), 159-177.
- Moorthy, A. S. (2018). Melting and Solidification of Fats. In *Structure-Function Analysis of Edible Fats* (p. 101-118). Elsevier. <https://doi.org/10.1016/B978-0-12-814041-3.00004-6>
- Mörl, L. (2011). Verfahrenstechnische Grundlagen des Coatings. In *Easy Coating* (p. 7-51). Springer.
- Mostefa, M., & Muhr, H. (2019). *Cristallisation en milieu fondu Procédés et mises en œuvre* (Numéro ref. article : j2798). Editions T.I. <https://www.techniques-ingenieur.fr/base-documentaire/procedes-chimie-bio-agro-th2/operations-unitaires-extractions-fluide-fluide-et-fluide-solide-42332210/cristallisation-en-milieu-fondu-j2798/>
- Motoyama, M. (2012). Structure and phase characterization of triacylglycerols by raman spectroscopy. *Bulletin NARO Institute of Livestock and Grassland Science*, 12, 19-68.
- Moyano, M. A., Paris, R., & Martín-Martínez, J. M. (2019). Viscoelastic and adhesion properties of hot-melts made with blends of ethylene-co-n-butyl acrylate (EBA) and ethylene-co-vinyl acetate (EVA) copolymers. *International Journal of Adhesion and Adhesives*, 88, 34-42. <https://doi.org/10.1016/j.ijadhadh.2018.11.001>
- Mu, H. (2004). The digestion of dietary triacylglycerols. *Progress in Lipid Research*, 43(2), 105-133. [https://doi.org/10.1016/S0163-7827\(03\)00050-X](https://doi.org/10.1016/S0163-7827(03)00050-X)
- Mu, H., Holm, R., & Müllertz, A. (2013). Lipid-based formulations for oral administration of poorly water-soluble drugs. *International journal of pharmaceuticals*, 453(1), 215-224.
- Müller, M. G., Lindner, J. A., Briesen, H., Sommer, K., & Foerst, P. (2018). On the properties and application of beeswax, carnauba wax and palm fat mixtures for hot melt coating in fluidized beds. *Advanced Powder Technology*, 29(3), 781-788.
- Murshed, M., Pham, A., Vithani, K., Salim, M., & Boyd, B. J. (2022). Controlling drug release by introducing lipase inhibitor within a lipid formulation. *International Journal of Pharmaceutics*, 623, 121958. <https://doi.org/10.1016/j.ijpharm.2022.121958>
- Nakanishi, K., & Ueno, S. (2020). Mixing Ratio and Cooling Rate Dependence of Molecular Compound Formation in OPO/POP Binary Mixture. *Molecules*, 25(22), 5253. <https://doi.org/10.3390/molecules25225253>
- Narine, S. S., Humphrey, K. L., & Bouzidi, L. (2006). Modification of the Avrami model for application to the kinetics of the melt crystallization of lipids. *Journal of the American Oil Chemists' Society*, 83(11), 913-921. <https://doi.org/10.1007/s11746-006-5046-6>
- Nawar, W. W. (1969). Thermal degradation of lipids. *Journal of agricultural and food chemistry*, 17(1), 18-21.
- N'Goma, J.-C. B., Amara, S., Dridi, K., Jannin, V., & Carrière, F. (2012). Understanding the lipid-digestion processes in the GI tract before designing lipid-based drug-delivery systems. *Therapeutic delivery*, 3(1), 105-124.
- Nguyen, K. T. T., Heijningen, F. F. M., Zillen, D., Van Bommel, K. J. C., Van Ee, R. J., Frijlink, H. W., & Hinrichs, W. L. J. (2022). Formulation of a 3D Printed Biopharmaceutical: The Development of an Alkaline Phosphatase Containing Tablet with Ileo-Colonic Release Profile to Treat Ulcerative Colitis. *Pharmaceutics*, 14(10), 2179. <https://doi.org/10.3390/pharmaceutics14102179>
- Nguyen, T. T.-L. (2017). *Extrusion-spheronization of pharmaceutical products : System for the delivery of active ingredients which are poorly soluble by oral route* [University of Strasbourg]. <https://theses.hal.science/tel-01756974>.
- Nicklasson, M. (1993). In vitro characterization of dissolution rate. In *Industrial Aspects of Pharmaceutics* (p. 64-79).
- Nilsson, E. J., Lind, T. K., Scherer, D., Skansberger, T., Mortensen, K., Engblom, J., & Kocherbitov, V. (2020). Mechanisms of crystallisation in polysorbates and sorbitan esters. *CrystEngComm*, 22(22), 3840-3853. <https://doi.org/10.1039/D0CE00236D>
- Nishihata, T., Yoshitomi, H., & Higuchi, T. (2011). Intestinal absorption of sodium cefoxitin in rats: Effect of formulation. *Journal of Pharmacy and Pharmacology*, 38(1), 69-70. <https://doi.org/10.1111/j.2042-7158.1986.tb04472.x>
- Nora, G.-I., Venkatasubramanian, R., Strindberg, S., Siqueira-Jørgensen, S. D., Pagano, L., Romanski, F. S., Swarnakar, N. K., Rades, T., & Müllertz, A. (2022). Combining lipid based drug delivery and amorphous solid dispersions for improved oral drug absorption of a poorly water-soluble drug. *Journal of Controlled Release*, 349, 206-212. <https://doi.org/10.1016/j.jconrel.2022.06.057>

- Novakovic, D., Peltonen, L., Isomäki, A., Fraser-Miller, S. J., Nielsen, L. H., Laaksonen, T., & Strachan, C. J. (2020). Surface Stabilization and Dissolution Rate Improvement of Amorphous Compacts with Thin Polymer Coatings: Can We Have It All? *Molecular Pharmaceutics*, 17(4), 1248-1260. <https://doi.org/10.1021/acs.molpharmaceut.9b01263>
- Nursakinah, I., Ismail, A. R., Rahimi, M. Y., & Idris, A. B. (2013). Evaluation of HLB values of mixed non-ionic surfactants on the stability of oil-in-water emulsion system. 850-856. <https://doi.org/10.1063/1.4858761>
- Nyqvist, H. (1993). Preformulation. In *Industrial Aspects of Pharmaceutics* (p. 55-63).
- Nývlt, J. (1995). The Ostwald Rule of Stages. *Crystal Research and Technology*, 30(4), 443-449. <https://doi.org/10.1002/crat.2170300402>
- O'Brien, E. P., Germinario, L. T., Robe, G. R., Williams, T., Atkins, D. G., Moroney, D. A., & Peters, M. A. (2007). Fundamentals of hot-melt pressure-sensitive adhesive tapes: The effect of tackifier aromaticity. *Journal of Adhesion Science and Technology*, 21(7), 637-661. <https://doi.org/10.1163/156856107781192328>
- Oh, J.-H., McCurdy, A. R., Clark, S., & Swanson, B. G. (2002). Characterization and thermal stability of polymorphic forms of synthesized tristearin. *Journal of food science*, 67(8), 2911-2917.
- Olbrich, C., Kayser, O., & Müller, R. H. (2002). Lipase degradation of Dynasan 114 and 116 solid lipid nanoparticles (SLN)—Effect of surfactants, storage time and crystallinity. *International journal of pharmaceutics*, 237(1-2), 119-128.
- Omar, Z., Rashid, N. Abd., Fauzi, S. H. M., Shahrim, Z., & Marangoni, A. G. (2015). Fractal dimension in palm oil crystal networks during storage by image analysis and rheological measurements. *LWT - Food Science and Technology*, 64(1), 483-489. <https://doi.org/10.1016/j.lwt.2015.04.059>
- Otun, S. O., Meehan, E., Qi, S., & Craig, D. Q. (2015). The Use of quasi-isothermal modulated temperature differential scanning calorimetry for the characterization of slow crystallization processes in lipid-based solid self-emulsifying systems. *Pharmaceutical research*, 32(4), 1316-1324.
- Padsalgi, A., Bidkar, S., Jadhav, V., & Sheladiya, D. (2008). Sustained release tablet of theophylline by hot melt wax coating technology. *Asian Journal of Pharmaceutics*, 2(1), 26. <https://doi.org/10.4103/0973-8398.41561>
- Palefsky, I. (2022). Creams and Ointments. In Z. D. Draeos (Éd.), *Cosmetic Dermatology* (1<sup>re</sup> éd., p. 101-105). Wiley. <https://doi.org/10.1002/9781119676881.ch10>
- Parker, M. J. (2000). Test Methods for Physical Properties. In *Comprehensive Composite Materials* (p. 183-226). Elsevier. <https://doi.org/10.1016/B0-08-042993-9/00074-7>
- Pashkovskaya, A. A., Vazdar, M., Zimmermann, L., Jovanovic, O., Pohl, P., & Pohl, E. E. (2018). Mechanism of Long-Chain Free Fatty Acid Protonation at the Membrane-Water Interface. *Biophysical Journal*, 114(9), 2142-2151. <https://doi.org/10.1016/j.bpj.2018.04.011>
- Pasquali, R. C., Taurozzi, M. P., & Bregni, C. (2008). Some considerations about the hydrophilic-lipophilic balance system. *International journal of pharmaceutics*, 356(1-2), 44-51.
- Pasquarella, C., Bertoni, S., Passerini, N., Boyd, B. J., & Bērziņš, K. (2023). Comparison of Low-, Mid-, and High-Frequency Raman Spectroscopy for an In Situ Kinetic Analysis of Lipid Polymorphic Transformations. *Crystal Growth & Design*, acs.cgd.3c00737. <https://doi.org/10.1021/acs.cgd.3c00737>
- Patel, A. R., & Dewettinck, K. (2015). Current update on the influence of minor lipid components, shear and presence of interfaces on fat crystallization. *Current Opinion in Food Science*, 3, 65-70. <https://doi.org/10.1016/j.cofs.2015.05.010>
- Patel, N., & Jani, R. (2021a). Development and Optimization of Controlled Release Formulation and Process of Levetiracetam with Hot Melt Coating Technology. *Journal of Pharmaceutical Research International*, 33(26B), 80-102.
- Patel, N., & Jani, R. (2021b). Hot Melt Coating: Development and Optimization of Controlled Release Formulation and Process of Oxcarbazepine. *Journal of Pharmaceutical Research International*, 33(44A), 30-51.
- Patil, A. T., Khobragade, D. S., Chafle, S. A., Ujjainkar, A. P., Umathe, S. N., & Lakhotia, C. L. (2012). Development and evaluation of a hot-melt coating technique for enteric coating. *Brazilian Journal of Pharmaceutical Sciences*, 48, 69-77.
- Pavuluri, S. (2014). *Kinetic approach for modeling salt precipitation in porous-media*. GRIN Verlag.
- Pham, L., & Christensen, J. M. (2014). Preparation of acetaminophen capsules containing beads prepared by hot-melt direct blend coating. *Pharmaceutical Development and Technology*, 19(1), 91-102. <https://doi.org/10.3109/10837450.2012.757783>
- Pichot, R. (2012). *Stability and characterisation of emulsions in the presence of colloidal particles and surfactants*. [PhD Thesis, University of Birmingham]. <https://etheses.bham.ac.uk/id/eprint/3271/>

- Piska, I., Zárubová, M., Loužecký, T., Karami, H., & Filip, V. (2006). Properties and crystallization of fat blends. *Journal of Food Engineering*, 77(3), 433-438. <https://doi.org/10.1016/j.jfoodeng.2005.07.010>
- Pluntze, A. M., Cape, J. L., Klaus, N. D., & Lyon, D. K. (2023). Control of API release with matrix polymorphism in tristearin microspheres. *International Journal of Pharmaceutics*, 636, 122806. <https://doi.org/10.1016/j.ijpharm.2023.122806>
- Porter, C. J., Trevaskis, N. L., & Charman, W. N. (2007). Lipids and lipid-based formulations : Optimizing the oral delivery of lipophilic drugs. *Nature reviews Drug discovery*, 6(3), 231-248.
- Pouton, C. W. (1997). Formulation of self-emulsifying drug delivery systems. *Advanced Drug Delivery Reviews*, 25(1), 47-58. [https://doi.org/10.1016/S0169-409X\(96\)00490-5](https://doi.org/10.1016/S0169-409X(96)00490-5)
- Pouton, C. W. (2000). Lipid formulations for oral administration of drugs : Non-emulsifying, self-emulsifying and 'self-microemulsifying' drug delivery systems. *European journal of pharmaceutical sciences*, 11, S93-S98.
- Pouton, C. W. (2006). Formulation of poorly water-soluble drugs for oral administration : Physicochemical and physiological issues and the lipid formulation classification system. *European Journal of Pharmaceutical Sciences*, 29(3-4), 278-287. <https://doi.org/10.1016/j.ejps.2006.04.016>
- Pouton, C. W., & Porter, C. J. (2008). Formulation of lipid-based delivery systems for oral administration : Materials, methods and strategies. *Advanced drug delivery reviews*, 60(6), 625-637.
- Puri, V., Dantuluri, A. K., & Bansal, A. K. (2012). Barrier Coated Drug Layered Particles for Enhanced Performance of Amorphous Solid Dispersion Dosage Form. *Journal of Pharmaceutical Sciences*, 101(1), 342-353. <https://doi.org/10.1002/jps.22743>
- Pushpakom, S., Iorio, F., Eyers, P. A., Escott, K. J., Hopper, S., Wells, A., Doig, A., Williams, T., Latimer, J., & McNamee, C. (2019). Drug repurposing : Progress, challenges and recommendations. *Nature reviews Drug discovery*, 18(1), 41-58.
- Pustan, M., Birleanu, C., Voicu, R., & Muller, R. (2022). AFM Characterization of Temperature Effect on the SU-8 Mechanical and Tribological Properties. *Polymers*, 14(5), 1009. <https://doi.org/10.3390/polym14051009>
- Qi, S., Deutsch, D., & Craig, D. Q. (2006). An investigation into the interaction between taste masking fatty acid microspheres and alkaline buffer using thermal and spectroscopic analysis. *Journal of pharmaceutical sciences*, 95(5), 1022-1028.
- Qi, S., Deutsch, D., & Craig, D. Q. (2008). An investigation into the mechanisms of drug release from taste-masking fatty acid microspheres. *Journal of pharmaceutical sciences*, 97(9), 3842-3854.
- Qi, S., Marchaud, D., & Craig, D. Q. M. (2010). An investigation into the mechanism of dissolution rate enhancement of poorly water-soluble drugs from spray chilled gelucire 50/13 microspheres. *Journal of Pharmaceutical Sciences*, 99(1), 262-274. <https://doi.org/10.1002/jps.21832>
- Raman Spectroscopy*. (2018, octobre 31). Chemistry LibreTexts. [https://chem.libretexts.org/Bookshelves/Analytical\\_Chemistry/Molecular\\_and\\_Atomic\\_Spectroscopy\\_\(Wenzel\)/5%3A\\_Raman\\_Spectroscopy](https://chem.libretexts.org/Bookshelves/Analytical_Chemistry/Molecular_and_Atomic_Spectroscopy_(Wenzel)/5%3A_Raman_Spectroscopy)
- Ravotti, R., Worlitschek, J., Pulham, C. R., & Stamatiou, A. (2020). Triglycerides as Novel Phase-Change Materials : A Review and Assessment of Their Thermal Properties. *Molecules*, 25(23), 5572. <https://doi.org/10.3390/molecules25235572>
- Reitz, C. (2007). *Extrudierte Fettmatrizes mit retardierter Wirkstofffreigabe*. Cuvillier Verlag.
- Reitz, C., & Kleinebudde, P. (2007). Solid lipid extrusion of sustained release dosage forms. *European Journal of Pharmaceutics and Biopharmaceutics*, 67(2), 440-448.
- Ribeiro, A. P. B., Masuchi, M. H., Miyasaki, E. K., Domingues, M. A. F., Stroppa, V. L. Z., De Oliveira, G. M., & Kieckbusch, T. G. (2015). Crystallization modifiers in lipid systems. *Journal of Food Science and Technology*, 52(7), 3925-3946. <https://doi.org/10.1007/s13197-014-1587-0>
- Rishoi, A. H., & Sharp, P. F. (1938). Volume Changes of Fat in Cooled Cream Held at Constant Temperature. *Journal of Dairy Science*, 21(11), 683-687. [https://doi.org/10.3168/jds.S0022-0302\(38\)93022-X](https://doi.org/10.3168/jds.S0022-0302(38)93022-X)
- Rohan, S., Daniel, E., Enzo, P., & Ian, H. (2014). *Optimisation and stability assessment of solid lipid nanoparticles using particle size and zeta potential*. 25(1), 59-75.
- Ronsse, F., Pieters, J. G., & Dewettinck, K. (2008). Modelling side-effect spray drying in top-spray fluidised bed coating processes. *Journal of Food Engineering*, 86(4), 529-541.
- Rosiaux, Y., Forest, A., Girard, J.-M., Deleglise, C., Sheehan, L., & Marchaud, D. (2018). High shear blending with glyceryl distearate provides individually coated drug particles for effective taste masking. *Journal of Drug Delivery Science and Technology*, 48, 437-449.

- Rosiaux, Y., Jannin, V., Hughes, S., & Marchaud, D. (2015). Solid lipid excipients as matrix agents for sustained drug delivery. *Excipient Applications in Formulation Design and Drug Delivery*, 237-271.
- Rosiaux, Y., Jannin, V., & Morin, C. (2022). Gattefosse : Strategies for MR Formulation Development – Lipids. In E. S. Kostewicz, M. Vertzoni, H. A. E. Benson, & M. S. Roberts (Éds.), *Oral Drug Delivery for Modified Release Formulations* (1<sup>re</sup> éd., p. 205-213). Wiley. <https://doi.org/10.1002/9781119772729.ch11>
- Roy, P., & Shahiwala, A. (2009). Multiparticulate formulation approach to pulsatile drug delivery : Current perspectives. *Journal of Controlled Release*, 134(2), 74-80. <https://doi.org/10.1016/j.jconrel.2008.11.011>
- Saikh, M. A. A. (2022). Coating Processes of Pharmaceutical Applicability : A Glimpse. *Journal of Drug Delivery and Therapeutics*, 12(2), 126-138. <https://doi.org/10.22270/jddt.v12i2.5362>
- Salar-Behzadi, S., Corzo, C., Lopes, D. G., Meindl, C., Lochmann, D., & Reyer, S. (2020). Novel approach for overcoming the stability challenges of lipid-based excipients. Part 2 : Application of polyglycerol esters of fatty acids as hot melt coating excipients. *European Journal of Pharmaceutics and Biopharmaceutics*, 148, 107-117.
- Salar-Behzadi, S., Corzo, C., Schaden, L., Laggner, P., & Zimmer, A. (2019). Correlation between the solid state of lipid coating and release profile of API from hot melt coated microcapsules. *International journal of pharmaceutics*, 565, 569-578.
- Salar-Behzadi, S., Karrer, J., Demiri, V., Barrios, B., Corzo, C., Meindl, C., Lochmann, D., & Reyer, S. (2020). Polyglycerol esters of fatty acids as safe and stable matrix forming tableting excipients : A structure-function analysis. *Journal of Drug Delivery Science and Technology*, 60, 102019. <https://doi.org/10.1016/j.jddst.2020.102019>
- Sängerlaub, S., Seibel, K., Miesbauer, O., Pant, A., Kiese, S., Rodler, N., Schmid, M., & Müller, K. (2018). Functional properties of foamed and/or stretched polypropylene-films containing sodium chloride particles for humidity regulation. *Polymer Testing*, 65, 339-351. <https://doi.org/10.1016/j.polymertesting.2017.12.002>
- Sanopoulou, M., & Papadokostaki, K. G. (2017). Controlled drug release systems : Mechanisms and kinetics. *Biomed. Membr.(Bio) Artif. Organs*, 2, 1-33.
- Sato, K. (2018a). Introduction : Relationships of Structures, Properties, and Functionality. In K. Sato (Éd.), *Crystallization of Lipids* (1<sup>re</sup> éd., p. 1-15). Wiley. <https://doi.org/10.1002/9781118593882.ch1>
- Sato, K. (2018b). Polymorphism of lipid crystals. *Crystallization of Lipids; Sato, K., Ed.; John Wiley & Sons, Ltd.: Chichester, UK*, 17-60.
- Sato, K., & Garti, N. (1988). Crystallization and polymorphic transformation : An introduction. *Crystallization and polymorphism of fats and fatty acids. Marcel Dekker, New York*, 3-7.
- Schertel, S., Corzo, C., Leitner, L., Karrer, J., Engel, D., Teichmann, Y., Zimmer, A., & Salar-Behzadi, S. (2022). Going green : Development of a sustainable lipid-based enteric coating formulation for low-dose aspirin multiparticulate systems. *International Journal of Pharmaceutics*, 614, 121453. <https://doi.org/10.1016/j.ijpharm.2022.121453>
- Schertel, S., Salar-Behzadi, S., Karrer, J., Laggner, P., & Zimmer, A. (2021). Impact of polysorbate 65 on tripalmitin crystal growth and release stability of hot melt coated multiparticulate systems. *International Journal of Pharmaceutics*, 120970.
- Schertel, S., Salar-Behzadi, S., & Zimmer, A. (2021). Impact of Surface Properties of Core Material on the Stability of Hot Melt-Coated Multiparticulate Systems. *Pharmaceutics*, 13(3), 366.
- Schibschid, C. (2017). Evaluation of taste masking of pharmaceutical Products. *Master thesis*.
- Schlichter, J., Mayer, I., Sarig, S., & Garti, N. (1988). The Influence of Emulsifiers on the Crystal Properties of Tristearin and Trilaurin. *Powder Diffraction*, 3(1), 19-22. <https://doi.org/10.1017/S0885715600013051>
- Schmidts, T., Dobler, D., Guldan, A.-C., Paulus, N., & Runkel, F. (2010). Multiple W/O/W emulsions—Using the required HLB for emulsifier evaluation. *Colloids and Surfaces A: Physicochemical and Engineering Aspects*, 372(1-3), 48-54. <https://doi.org/10.1016/j.colsurfa.2010.09.025>
- Schubert, R. (2022). Feste Arzneiformen. In *Pharmazeutische Technologie* (11<sup>e</sup> éd., p. 366-431). Wissenschaftliche Verlagsgesellschaft Stuttgart.
- Scioli Montoto, S., Muraca, G., & Ruiz, M. E. (2020). Solid Lipid Nanoparticles for Drug Delivery : Pharmacological and Biopharmaceutical Aspects. *Frontiers in Molecular Biosciences*, 7, 587997. <https://doi.org/10.3389/fmolb.2020.587997>
- Seitavuopio, P., Rantanen, J., & Yliruusi, J. (2005). Use of roughness maps in visualisation of surfaces. *European Journal of Pharmaceutics and Biopharmaceutics*, 59(2), 351-358. <https://doi.org/10.1016/j.ejpb.2004.08.009>



- Selen, A., Dickinson, P. A., Müllertz, A., Crison, J. R., Mistry, H. B., Cruaños, M. T., Martinez, M. N., Lennernäs, H., Wigal, T. L., & Swinney, D. C. (2014). The biopharmaceutics risk assessment roadmap for optimizing clinical drug product performance. *Journal of pharmaceutical sciences*, *103*(11), 3377-3397.
- Severino, P., Andreani, T., Macedo, A. S., Fangueiro, J. F., Santana, M. H. A., Silva, A. M., & Souto, E. B. (2012). Current State-of-Art and New Trends on Lipid Nanoparticles (SLN and NLC) for Oral Drug Delivery. *Journal of Drug Delivery*, *2012*, 1-10. <https://doi.org/10.1155/2012/750891>
- Sharma, R., Yadav, S., Yadav, V., Akhtar, J., Katari, O., Kuche, K., & Jain, S. (2023). Recent advances in lipid-based long-acting injectable depot formulations. *Advanced Drug Delivery Reviews*, *199*, 114901. <https://doi.org/10.1016/j.addr.2023.114901>
- Shepard, K. B., Adam, M. S., Morgen, M. M., Mudie, D. M., Regan, D. T., Baumann, J. M., & Vodak, D. T. (2020). Impact of process parameters on particle morphology and filament formation in spray dried Eudragit L100 polymer. *Powder Technology*, *362*, 221-230. <https://doi.org/10.1016/j.powtec.2019.12.013>
- Siepmann, J., Faham, A., Clas, S.-D., Boyd, B. J., Jannin, V., Bernkop-Schnürch, A., Zhao, H., Lecommandoux, S., Evans, J. C., & Allen, C. (2019). Lipids and polymers in pharmaceutical technology : Lifelong companions. *International journal of pharmaceuticals*, *558*, 128-142.
- Siepmann, J., & Siepmann, F. (2009). Freisetzungsmechanismen in Retard- und Depotarzneiformen. In *Innovative Arzneiformen* (p. 135-148). Wissenschaftliche Verlagsgesellschaft Stuttgart.
- Siepmann, J., & Siepmann, F. (2013). Stability of aqueous polymeric controlled release film coatings. *International Journal of Pharmaceutics*, *457*(2), 437-445. <https://doi.org/10.1016/j.ijpharm.2013.10.010>
- Siew, A. (2017). Bringing Together the Benefits of Lipid-Based Formulations and Modified-Release Drug Delivery. *Pharmaceutical Technology*, *41*(12), 26.
- Siewert, M., Dressman, J., Brown, C. K., Shah, V. P., Aiache, J.-M., Aoyagi, N., Bashaw, D., Brown, C., Brown, W., & Burgess, D. (2003). FIP/AAPS guidelines to dissolution/in vitro release testing of novel/special dosage forms. *Aaps Pharmscitech*, *4*(1), 43-52.
- Silva, R. C. D., Martini Soares, F. A. S. D., Maruyama, J. M., Dagostinho, N. R., Silva, Y. A., Ract, J. N. R., & Gioielli, L. A. (2016). Microscopic approach of the crystallization of tripalmitin and tristearin by microscopy. *Chemistry and Physics of Lipids*, *198*, 1-9. <https://doi.org/10.1016/j.chemphyslip.2016.04.004>
- Silva, T. L. T. D., Grimaldi, R., & Gonçalves, L. A. G. (2017). Temperature, time and fat composition effect on fat bloom formation in dark chocolate. *Food Structure*, *14*, 68-75. <https://doi.org/10.1016/j.foostr.2017.06.006>
- Simpson, T. D. (1983). Solid phases of trimargarin : A comparison to tristearin. *Journal of the American Oil Chemists' Society*, *60*(1), 95-97. <https://doi.org/10.1007/BF02540901>
- Sinchaipanid, N., Junyaprasert, V., & Mitrevej, A. (2004). Application of hot-melt coating for controlled release of propranolol hydrochloride pellets. *Powder technology*, *141*(3), 203-209.
- Small, D. M. (1968). A classification of biologic lipids based upon their interaction in aqueous systems. *Journal of the American Oil Chemists Society*, *45*(3), 108-119.
- Smith, K. W., Bhaggan, K., Talbot, G., & Van Malssen, K. F. (2011). Crystallization of Fats : Influence of Minor Components and Additives. *Journal of the American Oil Chemists' Society*, *88*(8), 1085-1101. <https://doi.org/10.1007/s11746-011-1819-7>
- Smith, K. W., & Sato, K. (2018). Effects of Foreign and Indigenous Minor Components. In K. Sato (Éd.), *Crystallization of Lipids* (1<sup>re</sup> éd., p. 263-281). Wiley. <https://doi.org/10.1002/9781118593882.ch9>
- Smith, P. R., Cebula, D. J., & Povey, M. J. (1994). The effect of lauric-based molecules on trilaurin crystallization. *Journal of the American Oil Chemists' Society*, *71*(12), 1367-1372.
- Smith, P. R., & Povey, M. J. W. (1997). The effect of partial glycerides on trilaurin crystallization. *Journal of the American Oil Chemists' Society*, *74*(2), 169-171. <https://doi.org/10.1007/s11746-997-0164-3>
- Soares, L. A., & Crema, E. (2020). Study of a delayed-release system for hard and soft capsules coated with eudragit® s100 acrylic polymers. *Acta Scientiarum. Health Sciences*, *42*, e48422. <https://doi.org/10.4025/actascihealthsci.v42i1.48422>
- Sonwai, S., & Rousseau, D. (2006). Structure evolution and bloom formation in tempered cocoa butter during long-term storage. *European Journal of Lipid Science and Technology*, *108*(9), 735-745. <https://doi.org/10.1002/ejlt.200600078>
- Sonwai, S., & Rousseau, D. (2008). Fat Crystal Growth and Microstructural Evolution in Industrial Milk Chocolate. *Crystal Growth & Design*, *8*(9), 3165-3174. <https://doi.org/10.1021/cg070503h>
- Sorgatz, C. (2011). *Physikalische Charakterisierung von Überzugsmaterialien in der Lebensmittelindustrie*. Technische Universität München.

- Souliman, S., Beyssac, E., Cardot, J.-M., Denis, S., & Alric, M. (2007). Investigation of the Biopharmaceutical Behavior of Theophylline Hydrophilic Matrix Tablets Using USP Methods and an Artificial Digestive System. *Drug Development and Industrial Pharmacy*, 33(4), 475-483. <https://doi.org/10.1080/03639040601128654>
- Stegemann, S., Ecker, F., Maio, M., Kraahs, P., Wohlfart, R., Breitzkreutz, J., Zimmer, A., Bar-Shalom, D., Hettrich, P., & Broegmann, B. (2010). Geriatric drug therapy : Neglecting the inevitable majority. *Ageing research reviews*, 9(4), 384-398.
- Stewart, D. I., Chong, P. S., & Stapley, A. G. F. (2017). Investigation of the Crystallization and Melting of the Tripalmitin/Triolein System via Hot Stage Microscopy, Differential Scanning Calorimetry, and Pulsed NMR. *Crystal Growth & Design*, 17(6), 3005-3016. <https://doi.org/10.1021/acs.cgd.6b01621>
- Stiller, B. (2016). *Sprühgranulation in der zirkulierenden Wirbelschicht* (Cuvillier Verlag, Vol. 5).
- Stocker, E., Becker, K., Hate, S., Hohl, R., Schiemenz, W., Sacher, S., Zimmer, A., & Salar-Behzadi, S. (2017). Application of ICH Q9 Quality Risk Management Tools for Advanced Development of Hot Melt Coated Multiparticulate Systems. *Journal of Pharmaceutical Sciences*, 106(1), 278-290. <https://doi.org/10.1016/j.xphs.2016.09.025>
- Sudke, S. G., Sakarakar, D. M., & Sudke, S. G. (2013). Design and characterization of enteric coated pellets of aspirin using hot-melt coating technique. *Int J Pharma Res Rev*, 2(3), 1-10.
- Sugano, K., & Terada, K. (2015). Rate-and extent-limiting factors of oral drug absorption : Theory and applications. *Journal of pharmaceutical sciences*, 104(9), 2777-2788.
- Suresh, G., & Dinesh, M. (2013). Application of hot-melt coating for sustained release pellets of fenoverine. *Der Pharmacia Sinica*. <https://hal.science/hal-03632066/>
- Szűts, A. (2003). Study of the applicability of sucrose esters in hot-melt technology. *PhD Faculty of Pharmacy, Department of Pharmaceutical Technology University of Szeged*.
- Takeguchi, S., Sato, A., Hondoh, H., Aoki, M., Uehara, H., & Ueno, S. (2020). Multiple  $\beta$  Forms of Saturated Monoacid Triacylglycerol Crystals. *Molecules*, 25(21), 5086. <https://doi.org/10.3390/molecules25215086>
- Tan, A., Rao, S., & Prestidge, C. A. (2013). Transforming lipid-based oral drug delivery systems into solid dosage forms: An overview of solid carriers, physicochemical properties, and biopharmaceutical performance. *Pharmaceutical research*, 30(12), 2993-3017.
- Tan, D. K., Davis, D. A., Miller, D. A., Williams, R. O., & Nokhodchi, A. (2020). Innovations in Thermal Processing: Hot-Melt Extrusion and KinetiSol® Dispersing. *AAPS PharmSciTech*, 21(8), 312. <https://doi.org/10.1208/s12249-020-01854-2>
- Tang, D., & Marangoni, A. G. (2006). Microstructure and fractal analysis of fat crystal networks. *Journal of the American Oil Chemists' Society*, 83(5), 377-388. <https://doi.org/10.1007/s11746-006-1216-9>
- Tang, D., & Marangoni, A. G. (2007). Modeling the rheological properties and structure of colloidal fat crystal networks. *Trends in Food Science & Technology*, 18(9), 474-483. <https://doi.org/10.1016/j.tifs.2007.04.015>
- Thakore, S. D., Sood, A., & Bansal, A. K. (2020). Emerging role of primary heterogeneous nucleation in pharmaceutical crystallization. *Drug Development Research*, 81(1), 3-22. <https://doi.org/10.1002/ddr.21622>
- Toro-Vazquez, J., Herrera-Coronado, V., Dibildox-Alvarado, E., Charo-Alonso, M., & Gomez-Aldapa, C. (2002). Induction Time of Crystallization in Vegetable Oils, Comparative Measurements by Differential Scanning Calorimetry and Diffusive Light Scattering. *Journal of Food Science*, 67(3), 1057-1064. <https://doi.org/10.1111/j.1365-2621.2002.tb09453.x>
- Toschkoff, G., & Khinast, J. G. (2013). Mathematical modeling of the coating process. *International journal of pharmaceutics*, 457(2), 407-422.
- Traub-Hoffmann, K., Gegenfurtner, K., Kraft, K.-U., & Friess, W. (2020). Spray congealed solid lipid microparticles as a sustained release delivery system for Gonadorelin [6-D-Phe] : Production, optimization and in vitro release behavior. *European Journal of Pharmaceutics and Biopharmaceutics*, 154, 18-32. <https://doi.org/10.1016/j.ejpb.2020.06.017>
- Tulloch, A. P. (1980). Beeswax—Composition and Analysis. *Bee World*, 61(2), 47-62. <https://doi.org/10.1080/0005772X.1980.11097776>
- Urbina-Villalba, G., Forgiarini, A., Rahn, K., & Lozsán, A. (2009). Influence of flocculation and coalescence on the evolution of the average radius of an O/W emulsion. Is a linear slope of R3vs. T an unmistakable signature of Ostwald ripening? *Physical Chemistry Chemical Physics*, 11(47), 11184. <https://doi.org/10.1039/b915470a>
- Valeri, D., & Meirelles, A. J. A. (1997). Viscosities of fatty acids, triglycerides, and their binary mixtures. *Journal of the American Oil Chemists' Society*, 74(10), 1221-1226. <https://doi.org/10.1007/s11746-997-0048-6>



- Van Den Mooter, G. (2012). The use of amorphous solid dispersions : A formulation strategy to overcome poor solubility and dissolution rate. *Drug Discovery Today: Technologies*, 9(2), e79-e85. <https://doi.org/10.1016/j.ddtec.2011.10.002>
- Van Kampen, A., Hitzmann, B., & Kohlus, R. (2015). Assessment of coating quality by use of dissolution kinetics. *Powder Technology*, 286, 325-331. <https://doi.org/10.1016/j.powtec.2015.08.024>
- van Kampen, A. (2018). *Investigation of fluidised bed coating : Measurement, optimisation and statistical modelling of coating layers* [Kommunikations-, Informations- und Medienzentrums der Universität Hohenheim]. <http://opus.uni-hohenheim.de/volltexte/2018/1508>
- Vargason, A. M., Anselmo, A. C., & Mitragotri, S. (2021). The evolution of commercial drug delivery technologies. *Nature Biomedical Engineering*, 1-17.
- Vergnaud, J.-M. (1993). *Controlled drug release of oral dosage forms*. CRC Press.
- Vithani, K., Goyanes, A., Jannin, V., Basit, A. W., Gaisford, S., & Boyd, B. J. (2019a). A proof of concept for 3D printing of solid lipid-based formulations of poorly water-soluble drugs to control formulation dispersion kinetics. *Pharmaceutical research*, 36(7), 1-13.
- Vithani, K., Goyanes, A., Jannin, V., Basit, A. W., Gaisford, S., & Boyd, B. J. (2019b). An overview of 3D printing technologies for soft materials and potential opportunities for lipid-based drug delivery systems. *Pharmaceutical research*, 36(1), 1-20.
- Vithani, K., Hawley, A., Jannin, V., Pouton, C., & Boyd, B. J. (2017). Inclusion of Digestible Surfactants in Solid SMEDDS Formulation Removes Lag Time and Influences the Formation of Structured Particles During Digestion. *The AAPS Journal*, 19(3), 754-764. <https://doi.org/10.1208/s12248-016-0036-6>
- Von Fraunhofer, J. A. (2012). Adhesion and Cohesion. *International Journal of Dentistry*, 2012, 1-8. <https://doi.org/10.1155/2012/951324>
- Vyazovkin, S. (2020). Activation Energies and Temperature Dependencies of the Rates of Crystallization and Melting of Polymers. *Polymers*, 12(5), 1070. <https://doi.org/10.3390/polym12051070>
- Wang, L., & Wang, T. (2007). Chemical Modification of Partially Hydrogenated Vegetable Oil to Improve its Functional Properties for Candles. *Journal of the American Oil Chemists' Society*, 84(12), 1149-1159. <https://doi.org/10.1007/s11746-007-1147-0>
- Wang, W., Wang, L., & Liang, Y.-S. (2012). Susceptibility or resistance of praziquantel in human schistosomiasis : A review. *Parasitology Research*, 111(5), 1871-1877. <https://doi.org/10.1007/s00436-012-3151-z>
- Wang, X., Wang, P., Huang, C., Lin, X., Gong, H., He, H., & Cai, C. (2017). Hot-melt sub-and outercoating combined with enteric aqueous coating to improve the stability of aspirin tablets. *asian journal of pharmaceutical sciences*, 12(3), 266-278.
- Wang, Z., Lou, H., Dening, T. J., & Hageman, M. J. (2023). Biorelevant Dissolution Method Considerations for the Appropriate Evaluation of Amorphous Solid Dispersions : Are Two Stages Necessary? *Journal of Pharmaceutical Sciences*, 112(4), 1089-1107. <https://doi.org/10.1016/j.xphs.2022.12.008>
- Wangpradit, N., Macha, S., Phootch, N., Yusohyo, N., Waedoloh, A., & Manee, S. (2022). Determination of required hydrophilic-lipophilic balance of *Amesiodendron chinense* (Merr.) Hu oil and development of stable cream formulation. *OCL*, 29, 29. <https://doi.org/10.1051/ocl/2022011>
- Wankhade, R., Sakarkar, D. M., & Singh, R. P. (2018). DESIGN OF SUSTAINED RELEASE PELLETS OF OFLOXACIN USING HOT MELT COATING TECHNIQUE. *European Journal of Biomedical*, 5(1), 882-891.
- Watanabe, Y., Zhao, W., Matsumoto, Y., Suda, M., Takayama, K., Ohgawara, Y., Kobayashi, Y., & Matsumoto, M. (1993). Increasing bioavailability of nifedipine from matrix granules prepared using macrogol and trilaurin. *International journal of pharmaceutics*, 99(2-3), 337-341.
- Watano, S., Nakamura, H., Hamada, K., Wakamatsu, Y., Tanabe, Y., Dave, R. N., & Pfeffer, R. (2004). Fine particle coating by a novel rotating fluidized bed coater. *Powder Technology*, 141(3), 172-176. <https://doi.org/10.1016/j.powtec.2003.03.001>
- Werner, S. R. L., Jones, J. R., Paterson, A. H. J., Archer, R. H., & Pearce, D. L. (2007). Air-suspension coating in the food industry : Part II — micro-level process approach. *Powder Technology*, 171(1), 34-45. <https://doi.org/10.1016/j.powtec.2006.08.015>
- Wik, H. B., & Wik, O. (1993). Rheology of Pharmaceuticals. In *Industrial Aspects of Pharmaceutics* (p. 42-54). Swedish Pharmaceutical Press.
- Williams, H. D., Sassene, P., Kleberg, K., Bakala-N'Goma, J.-C., Calderone, M., Jannin, V., Igonin, A., Partheil, A., Marchaud, D., Jule, E., Vertommen, J., Maio, M., Blundell, R., Benameur, H., Carrière, F., Müllertz, A., Porter, C. J. H., & Pouton, C. W. (2012). Toward the Establishment of Standardized In Vitro Tests for Lipid-Based

Formulations, Part 1 : Method Parameterization and Comparison of In Vitro Digestion Profiles Across a Range of Representative Formulations. *Journal of Pharmaceutical Sciences*, 101(9), 3360-3380. <https://doi.org/10.1002/jps.23205>

Windbergs, M. (2009). *Towards a better understanding of lipid-based matrices–Innovations in the production and analysis of physically stable solid lipid extrudates with tailor-made dissolution profiles*. Cuvillier Verlag.

Windbergs, M., Strachan, C. J., & Kleinebudde, P. (2009a). Influence of structural variations on drug release from lipid/polyethylene glycol matrices. *European Journal of Pharmaceutical Sciences*, 37(5), 555-562. <https://doi.org/10.1016/j.ejps.2009.04.010>

Windbergs, M., Strachan, C. J., & Kleinebudde, P. (2009b). Influence of the composition of glycerides on the solid-state behaviour and the dissolution profiles of solid lipid extrudates. *International Journal of Pharmaceutics*, 381(2), 184-191. <https://doi.org/10.1016/j.ijpharm.2009.03.002>

Windbergs, M., Strachan, C. J., & Kleinebudde, P. (2009c). Investigating the principles of recrystallization from glyceride melts. *Aaps Pharmscitech*, 10(4), 1224-1233.

Windbergs, M., Strachan, C. J., & Kleinebudde, P. (2009d). Tailor-made dissolution profiles by extruded matrices based on lipid polyethylene glycol mixtures. *Journal of Controlled Release*, 137(3), 211-216.

Windbergs, M., Strachan, C. J., & Kleinebudde, P. (2009e). Understanding the solid-state behaviour of triglyceride solid lipid extrudates and its influence on dissolution. *European Journal of Pharmaceutics and Biopharmaceutics*, 71(1), 80-87.

*WITec Raman Imaging*. (s. d.). Oxford Instruments. Consulté 9 décembre 2023, à l'adresse <https://raman.oxinst.com/techniques/raman-imaging>

Witika, B. A., Makoni, P. A., Matafwali, S. K., Chabalenge, B., Mwila, C., Kalungia, A. C., Nkanga, C. I., Bapolisi, A. M., & Walker, R. B. (2020). Biocompatibility of biomaterials for nanoencapsulation : Current approaches. *Nanomaterials*, 10(9), 1649.

Witzleb, R., Müllertz, A., Kanikanti, V.-R., Hamann, H.-J., & Kleinebudde, P. (2012). Dissolution of solid lipid extrudates in biorelevant media. *International journal of pharmaceutics*, 422(1-2), 116-124.

Woerthmann, B. M., Hoffmann, A., Gerber, J., Wittkamp, T., & Briesen, H. (2023). Analyzing the interparticle batch homogeneity of natural hot-melt coatings. *Powder Technology*, 426, 118626. <https://doi.org/10.1016/j.powtec.2023.118626>

Woerthmann, B. M., Lindner, J. A., Kovacevic, T., Pergam, P., Schmid, F., & Briesen, H. (2021). A novel method for assessing the coating uniformity of hot-melt coated particles using micro-computed tomography. *Powder Technology*, 378, 51-59.

Woerthmann, B. M., Totzauer, L., & Briesen, H. (2022). Delamination and wetting behavior of natural hot-melt coating materials. *Powder Technology*, 404, 117443. <https://doi.org/10.1016/j.powtec.2022.117443>

Wolman, M. (1975). Polarized light microscopy as a tool of diagnostic pathology. *Journal of Histochemistry & Cytochemistry*, 23(1), 21-50. <https://doi.org/10.1177/23.1.1090645>

Wong, P. C. H. (2015). *Spray Congealing with Solid Lipid Materials : Rheological, Solid State and Drug Release Investigations* [National University of Singapore]. <https://scholarbank.nus.edu.sg/handle/10635/123724>

Wong, P. C. H., Heng, P. W. S., & Chan, L. W. (2016). Viscosity–temperature relationship of lipid-based excipients amenable for spray congealing : Derivation of a rheological parameter with good correlation to particle size. *European Journal of Lipid Science and Technology*, 118(7), 1062-1073.

Wongprasert, P., Dreiss, C. A., & Murray, G. (2022). Evaluating hyaluronic acid dermal fillers : A critique of current characterization methods. *Dermatologic Therapy*, 35(6). <https://doi.org/10.1111/dth.15453>

World Health Organization. (2022). *WHO guideline on control and elimination of human schistosomiasis*. World Health Organization. <https://books.google.com/books?hl=en&lr=&id=DXVyEAAAQBAJ&oi=fnd&pg=PR5&dq=+WHO+guideline+on+control+and+elimination+of+human+schistosomiasis&ots=h4-IJ9sGZA&sig=bU2Qy5urdLzF34SbEhMk7zYLZGc>

Wu, T., Sun, Y., Li, N., De Villiers, M. M., & Yu, L. (2007). Inhibiting Surface Crystallization of Amorphous Indomethacin by Nanocoating. *Langmuir*, 23(9), 5148-5153. <https://doi.org/10.1021/la070050i>

Xiao, Y., Tang, S. K., Hao, H., Davey, R. J., & Vetter, T. (2017). Quantifying the Inherent Uncertainty Associated with Nucleation Rates Estimated from Induction Time Data Measured in Small Volumes. *Crystal Growth & Design*, 17(5), 2852-2863. <https://doi.org/10.1021/acs.cgd.7b00372>

Xie, X., Cardot, J.-M., Garrait, G., They, V., El-Hajji, M., & Beyssac, E. (2014). Micelle dynamic simulation and physicochemical characterization of biorelevant media to reflect gastrointestinal environment in fasted and fed

- states. *European Journal of Pharmaceutics and Biopharmaceutics*, 88(2), 565-573. <https://doi.org/10.1016/j.ejpb.2014.05.020>
- Xu, Q., Li, M., Zhang, J., & Li, Z. (2017). Hot-Melt Fluidized Bed Encapsulation of Citric Acid with Lipid. *International Journal of Food Engineering*, 13(5), 20160247. <https://doi.org/10.1515/ijfe-2016-0247>
- Yakugaku Zasshi. (2014). *Essential Manual for Pharmaceutical Experimental Methods for Pharmaceutical Scientist*. Nankodo.
- Yang, W., Gadgil, P., Krishnamurthy, V. R., Landis, M., Mallick, P., Patel, D., Patel, P. J., Reid, D. L., & Sanchez-Felix, M. (2020). The evolving druggability and developability space : Chemically modified new modalities and emerging small molecules. *The AAPS Journal*, 22(2), 1-14.
- Yang, Y., Shen, L., Li, J., & Shan, W. (2017). Preparation and evaluation of metoprolol tartrate sustained-release pellets using hot melt extrusion combined with hot melt coating. *Drug Development and Industrial Pharmacy*, 43(6), 939-946. <https://doi.org/10.1080/03639045.2017.1287715>
- Yoshikawa, S. (2016). *Effects of adding foreign particles on crystallization and physical properties of fat-based products*.
- Yoshikawa, S., Kida, H., & Sato, K. (2014). Promotional Effects of New Types of Additives on Fat Crystallization. *Journal of Oleo Science*, 63(4), 333-345. <https://doi.org/10.5650/jos.ess13155>
- Yoshikawa, S., Kida, H., & Sato, K. (2015). Fat crystallization with talc particles is influenced by particle size, concentration, and cooling rate. *European Journal of Lipid Science and Technology*, 117(6), 858-868. <https://doi.org/10.1002/ejlt.201400420>
- Yoshiteru, W., Toru, K., Youichi, A., & Mitsuo, M. (1990). Preparation and evaluation of enteric granules of aspirin prepared by acylglycerols. *International journal of pharmaceutics*, 64(2-3), 147-154.
- Yoshitomi, H., Nishihata, T., Frederick, G., Dillsaver, M., & Higuchi, L. T. (2011). Effect of triglyceride on small intestinal absorption of cefoxitin in rats. *Journal of Pharmacy and Pharmacology*, 39(11), 887-891. <https://doi.org/10.1111/j.2042-7158.1987.tb03123.x>
- Yoshitomi, H., Shizuku, Y., Masuda, Y., Itakura, R., Kanke, M., Okamoto, S., Nishihata, T., & Goto, S. (1992). Evaluation of Enteric Coated Tablet Sensitive to Pancreatic Lipase. I, In Vitro Disintegration Test. *Chemical and Pharmaceutical Bulletin*, 40(7), 1902-1905. <https://doi.org/10.1248/cpb.40.1902>
- Yoshitomi, H., Shizuku, Y., Masuda, Y., Itakura, R., Okamoto, S., Tomida, H., Nishihata, T., & Goto, S. (1993). Evaluation of Enteric Coated Tablet Sensitive to Pancreatic Lipase. II. In vivo Evaluation. *Biological and Pharmaceutical Bulletin*, 16(12), 1260-1263. <https://doi.org/10.1248/bpb.16.1260>
- Yuksel, N. (2000). Comparison of in vitro dissolution profiles by ANOVA-based, model-dependent and -independent methods. *International Journal of Pharmaceutics*, 209(1-2), 57-67. [https://doi.org/10.1016/S0378-5173\(00\)00554-8](https://doi.org/10.1016/S0378-5173(00)00554-8)
- Zaid, A. N. (2020). A Comprehensive Review on Pharmaceutical Film Coating : Past, Present, and Future. *Drug Design, Development and Therapy, Volume 14*, 4613-4623. <https://doi.org/10.2147/DDDT.S277439>
- Zhang, X., Li, L., Xie, H., Liang, Z., Su, J., Liu, G., & Li, B. (2014). Effect of Temperature on the Crystalline Form and Fat Crystal Network of Two Model Palm Oil-Based Shortenings During Storage. *Food and Bioprocess Technology*, 7(3), 887-900. <https://doi.org/10.1007/s11947-013-1078-8>
- Zheng, K., Lin, Z., Capece, M., Kunnath, K., Chen, L., & Davé, R. N. (2019). Effect of Particle Size and Polymer Loading on Dissolution Behavior of Amorphous Griseofulvin Powder. *Journal of Pharmaceutical Sciences*, 108(1), 234-242. <https://doi.org/10.1016/j.xphs.2018.11.025>
- Zheng, N., He, J., Gao, J., Huang, Y., Besenbacher, F., & Dong, M. (2018). Adhesion force measured by atomic force microscopy for direct carbon fiber-epoxy interfacial characterization. *Materials & Design*, 145, 218-225. <https://doi.org/10.1016/j.matdes.2018.02.060>
- Zupančič, O., Spoerk, M., & Paudel, A. (2022). Lipid-based solubilization technology via hot melt extrusion : Promises and challenges. *Expert Opinion on Drug Delivery*, 19(9), 1013-1032. <https://doi.org/10.1080/17425247.2022.2112173>

## List of Figures

Figure 1-1. Thesis outline.....	22
Figure 1-1. Schematic of top spray (left), bottom spray (middle) and tangential spray (right) fluidised beds (adapted from Arwidsson & Rudén, 1993) .....	25
Figure 1-2. Ventilus® Romaco Innojet technology: air flow bed (left) and drawing of the coating technology (right) (Huynh et al., 2024) .....	27
Figure 1-3. Microcapsules and microspheres obtainable with hot-melt coating by fluidised bed .....	29
Figure 1-4. Fluidisation patterns (A to F, left) and pressure drop (right) as a function of superficial gas velocity (adapted from Leturia & Saleh, 2014) .....	31
Figure 1-5. Geldart classification (A) and bubbling fluidisation (B) (adapted from Leturia & Saleh, 2014; Watano et al., 2004).....	32
Figure 1-6. Illustrative schematic of spraying by the device Rotojet®, impacting, wetting, film forming and solidifying in coating process (adapted from Arwidsson & Rudén, 1993).....	34
Figure 1-7. Typical films formed in solvent-based coating (A & B) (adapted from Arwidsson & Rudén, 1993) and hot-melt coating (C & D).....	36
Figure 1-8. Growth regime by layering .....	40
Figure 1-9. Schema of a multiple-sampling experimental approach.....	42
Figure 1-10. Schema of all possible variables for designing a good coating process .....	45
Figure 1-11. Overview of lipids often used for formulating solid dosage forms .....	48
Figure 1-12. Product cycle constituted by formation, maturation, deterioration and (bio-)destruction of lipid crystal network at different times and at different observation scales (adapted from Mishra et al., 2023; Tang & Marangoni, 2007) .....	50
Figure 1-13. Driving force and Gibbs energy in isothermal crystallisation (A, B) and selective crystallisation as a function of cooling rate (C) (adapted from Yoshikawa, 2016).....	52
Figure 1-14. Melt crystallisation: Nucleation of a pure lipid model as a function of additive addition associated with two coating approaches (adapted from Dasgupta, 2017; Marie Le Page & Hervé, 2019).....	53
Figure 1-15. $\beta$ nucleation mechanisms possibly encountered in lipids processing (adapted from Stewart et al., 2017; Yoshikawa et al., 2015) .....	54
Figure 1-16. Crystal growth processes (A) and mechanisms of action of additive impact on these processes (B) (adapted from Thakore et al., 2020).....	55

Figure 1-17. Relevance between crystallisation kinetics, adhesion, cohesion and viscoelasticity to defining $T_c$ (adapted from Kondo & Toda, 2009; Moyano et al., 2019; O'Brien et al., 2007)....	59
Figure 1-18. Monotropic polymorphism and two processing approaches for generation of the stable form $\beta$ (adapted from Yoshikawa, 2016) .....	63
Figure 1-19. Demonstration of Ostwald ripening: growth of crystals (A) and oil droplets (B) .....	67
Figure 1-20. Three typical phase mixing behaviours of solid lipid systems (adapted from Bayés-García et al., 2005) .....	71
Figure 1-21. Incorporation of a surfactant molecule in triglyceride crystal network (J. S. Aronhime et al., 1988).....	78
Figure 1-22. Chemical-composition based comparative classification of solid and liquid lipid-based formulations (adapted from LFCS Consortium 2010 - <a href="http://www.lfcs-consortium.org/background.aspx">http://www.lfcs-consortium.org/background.aspx</a> ) .....	80
Figure 1-23. Possible release patterns of solid lipid-based formulated products: immediate release (A), delayed release (B), sustained release (C) and pulsatile release (D) (adapted from (Selen et al., 2014)).....	84
Figure 1-24. Link between the choice of release testing methods and biopharmaceutical properties of solid lipids.....	88
Figure 1-25. BCS plane (Pn–Do plane) and DCS lines presented via dimensionless numbers; $F_a$ lines, representing the estimated fraction of dose absorbed, distinguish the case of dissolution-limited and solubility-limited following the concept of maximal dose absorbable in DCS (Sugano & Terada, 2015; Tindal & Elder, 2017).....	89
Figure 1-26. Key numbers: number of publications per functionality (left) and per BCS class (right) (not exhaustive). Pro, moisture protection; Lub, lubrication; Others (left), for example, method development; TM, taste masking with immediate release; ER/SR, extended release / sustained release; DR, delayed release; BE, bioavailability enhancement; Others (right), for example, probiotics .....	91
Figure 1-27. A projective process window for hot-melt coating studies with Ventilus® technology (adapted from Ronsse et al., 2008) .....	94
Figure 1-28. Expected process efficiency evolution obtained with multiple-sampling experimental approach.....	96
Figure 1-29. Molecules bearing a stearic-acid moiety on the basis of HLB (Source: Wikipedia).....	98
Figure 1-30. Proposed classification of additives used for solid lipid-based formulated products .....	98
Figure 1-31. Proposal for additive selection by considering manufacturability, stability and functionalities .....	100

Figure 1-32. Proposal for design of solid lipid-coated products as a function of formulation digestibility .....	103
Figure 2-1. Importance of characterisation in formulation development and pharmaceutical applications .....	105
Figure 2-2. Working principles of Crystal16 <sup>®</sup> Crystallization systems (adapted from Yakugaku Zasshi, 2014).....	109
Figure 2-3. Setup of goniometry for contact angle measurements in molten state (Huynh et al., 2024) .....	110
Figure 2-4. Setup of pH STAT for release kinetics measurements in biorelevant media (Huynh et al., 2024).....	115
Figure 2-5. Considerations for selection of release testing conditions.....	119
Figure 2-6. Characterisation plan in the “ <b>formulation development</b> ” phase.....	119
Figure 2-7. Characterisation plan in the “ <b>pharmaceutical application</b> ” phase .....	120
Figure 3-1. Force-distance curve recorded by digital pulsed force mode DPFM .....	125
Figure 3-2. Simplified experimental setup for measurements of contact angle in molten state.....	126
Figure 3-3. Optical microscope setup.....	128
Figure 3-4. Thermograms of formulations <b>F0</b> , <b>F1</b> , <b>F2</b> and <b>F3</b> : red continuous line (first heating), blue line (first cooling), red discontinuous line (second heating).....	131
Figure 3-5. Comparative solidification profile of three formulations <b>F0</b> (black line), <b>F1</b> (blue line), <b>F2</b> (red line) in comparison with that of <b>F3</b> (green line).....	133
Figure 3-6. Melt dynamic viscosity of <b>F0</b> to <b>F3</b> formulations as a function of shear rate at 70°C and 90°C (A) and that as a function of temperature when shear rate is fixed at 50 1/s (B) .....	134
Figure 3-7. Measurements of adhesion of four formulations <b>F0</b> , <b>F1</b> , <b>F2</b> and <b>F3</b> (from top to bottom) .....	135
Figure 3-8. Values of adhesion force measured for each formulation cast in film .....	136
Figure 3-9. Droplets of each formulation (F0 to F3) deposited at a velocity of 1.17 m/s being solidified within 1 minute on <b>NaCl surface</b> .....	138
Figure 3-10. Droplets of each formulation (F0 to F3) deposited at a velocity of 1.17 m/s being solidified within 1 minute on that of the <b>same formulation itself</b> .....	138
Figure 3-11. Images (A) of solidified droplets of each formulation deposited on <b>NaCl surface</b> and contact angles (B) obtained at different velocities.....	139
Figure 3-12. Assay of samples taken during coating trials with formulations <b>F1</b> , <b>F2</b> , <b>F0</b> and <b>F3</b> .....	141



Figure 3-13. PSD curves (left) and parameters (right) obtained for salt particles coated with <b>F0</b> , <b>F1</b> , <b>F2</b> and <b>F3</b> . Left graphs: initial uncoated NaCl (black line), first sampling (blue line), second sampling (red line), third sampling (green line). Right graphs: $D_{v90}/D_{v10}$ ratio (blue triangles), SPAN (red circles) .....	143
Figure 3-14. Yield locus (A) obtained under a representative consolidation stress 9 kPa and flow function (B) of salt particles coated with: <b>F0</b> (black circles), <b>F1</b> (blue squares), <b>F2</b> (red triangles) and <b>F3</b> (green diamonds) .....	145
Figure 3-15. Optical microscopic images of samples taken from coating trial with formulation F0. S, uncoated salt, A, first sampling, D final sampling.....	148
Figure 3-16. Optical microscopic images of samples taken from coating trial with formulation F2. S, uncoated salt, A, first sampling, D final sampling.....	149
Figure 3-17. Optical microscopic images of samples taken from coating trial with formulation F3. S, uncoated salt, A, first sampling, D final sampling.....	150
Figure 3-18. Images taken on chemical contrast mode (length-scale of 500 $\mu\text{m}$ ): uncoated salt (C-1) and salt coated with different formulations at different ratios: 3.2% and 39.3% <b>F1</b> (A-1 & A-2), 3.2% and 38.9% <b>F2</b> (B-1 & B-2), 33.8% <b>F0</b> (C-2), and 32.6% (C-3) <b>F3</b> .....	151
Figure 3-19. Images taken on topographical contrast mode (length-scale of 50 $\mu\text{m}$ ): uncoated salt (C-1) and salt coated with different formulations at different coating contents: 3.2% and 39.3% <b>F1</b> (A-1 & A-2), 3.2% and 38.9% <b>F2</b> (B-1 & B-2), 33.8% <b>F0</b> (C-2) and 32.6% <b>F3</b> (C-3).....	153
Figure 3-20. Comparative dissolution profile of uncoated salt particles and salt coated with four formulations at a similar coating content (% w/w): uncoated salt (yellow line), salt particles coated with 33.8% <b>F0</b> (black line), 29.1% <b>F1</b> (blue line), 35.0% <b>F2</b> (red line) and 32.6% <b>F3</b> (green line). Standard deviation (grey region). .....	155
Figure 3-21. Comparative dissolution profile of uncoated salt and salt particles coated with different coating contents using <b>F1</b> (A) and <b>F2</b> (B). .....	158
Figure 3-22. Relationship between release constants of different models and estimated mean coating thickness. Closed and open markers represent the values obtained with the formulations <b>F1</b> (A) and <b>F2</b> (B), respectively. Red, grey, blue and green closed circles denote the release constants associated with first order, zeroth order, Korsmeyer-Peppas and Hopfenberg, accordingly. Dotted line indicates the inverse power relationship.....	159
Figure 3-23. Thermal behaviours of 04 formulations <b>F0</b> , <b>F3</b> , <b>F1</b> and <b>F2</b> monitored over 12 weeks..	165
Figure 3-24. Diffractograms obtained for 4 formulations under stability study over 12 weeks.....	166
Figure 3-25. Evolution of melting enthalpy of 4 formulations (A) and estimated $\beta$ contents (%) in samples coated with 3 beeswax-containing formulations (B) during stability study over 12 weeks. ....	167

Figure 3-26. SEM micrographs of salt coated with formulation <b>F0</b> obtained at 2 timepoints ( <b>t<sub>0</sub></b> , <b>t<sub>2</sub></b> ) in stability study (the orange rectangle shows the enlarged image at 50 $\mu$ m on the left side.).....	169
Figure 3-27. SEM micrographs of salt coated with formulation <b>F3</b> obtained at 2 timepoints ( <b>t<sub>0</sub></b> , <b>t<sub>2</sub></b> ) in a stability study (the orange rectangle shows the enlarged image at 50 $\mu$ m on the left side.).....	169
Figure 3-28. SEM micrographs of salt coated with formulation <b>F1</b> obtained at 2 time points ( <b>t<sub>0</sub></b> , <b>t<sub>4</sub></b> ), in stability study (the orange rectangle shows the enlarged image at 50 $\mu$ m on the left side.).....	170
Figure 3-29. SEM micrographs of salt coated with formulation <b>F2</b> obtained at 2 timepoints ( <b>t<sub>0</sub></b> , <b>t<sub>4</sub></b> ), in stability study (the orange rectangle shows the enlarged image at 50 $\mu$ m on the left side.).....	171
Figure 3-30. Micrographs of formulations F0, F1, F2 and F3 captured at <b>t<sub>0</sub></b> .....	172
Figure 3-31. Change in fractal dimension of all studied lipidic coating formulations monitored over 12 weeks. ....	173
Figure 3-32. Comparative dissolution profile of salt particles coated with <b>33.8% w/w F0</b> and <b>32.6% w/w F3</b> monitored over 12 weeks. ....	175
Figure 3-33. Comparative dissolution profile of salt particles coated with <b>27.1% w/w F1</b> and <b>28.9% w/w F2</b> monitored over 12 weeks. ....	175
Figure 3-34. Comparative dissolution-digestion profile of salt particles coated with <b>F0, F1, F2</b> and <b>F3</b> .....	178
Figure 4-1. Thermal programme set for non-isothermal experiments in Crystal16® .....	185
Figure 4-2. Thermal programme set for isothermal experiments in Crystal16® .....	186
Figure 4-3. Thermal programme used in DSC analyses for isothermal and non-isothermal crystallisation .....	188
Figure 4-4. Metastable zone widths (MSZW) map constituted by measurements of melting and crystallisation points of tristearin. Melting points at 0.05°C/min (red open circles), crystallisation points at 0.05°C/min (blue open squares), 5°C/min (blue open triangles) and 10°C/min (blue circles), reference melting points of polymorphs $\alpha$ , $\beta'$ and $\beta$ (black open squares). Standard deviation (See <b>Appendix 02</b> ) .....	190
Figure 4-5. MSZW map constituted by melting points (red) and crystallisation points (blue) of formulations composed of tristearin, polysorbate 20 (hydrophilic surfactant) and talc at different ratios. Standard deviation (See <b>Appendix 02</b> ) .....	193
Figure 4-6. MSZW map constituted by melting points (red) and crystallisation points (blue) of formulations composed of tristearin, sorbitan monolaurate (lipophilic surfactant) and talc at different ratios. Standard deviation (See <b>Appendix 02</b> ).....	193
Figure 4-7. MSZW map constituted by melting points (red) and crystallisation points (blue) of formulations composed of tristearin, hydrophilic binary additive combinations (HBAC) and talc at different ratios. Standard deviation (See <b>Appendix 02</b> ).....	194

Figure 4-8. MSZW map constituted by melting points (red) and crystallisation points (blue) of formulations composed of tristearin, lipophilic binary additive combinations (LBAC) and talc at different ratios. Standard deviation (See <b>Appendix 02</b> ).....	194
Figure 4-9. MSZW map constituted by melting points (red) and crystallisation points (blue) of formulations composed of tristearin, “neutral” binary additive combinations (NBAC) and talc at different ratios. Standard deviation (See <b>Appendix 02</b> ).....	195
Figure 4-10. Accumulative distribution of induction time measurements and its model obtained for forty-four formulations .....	197
Figure 4-11. Comparison of induction time obtained for 28 formulations.....	199
Figure 4-12. Raman spectra of 16 formulations subject to non-isothermal crystallisation in Crystal16®. A, SSS plus HBAC4 with/without T; B, SSS plus NBAC4 with/without T .....	201
Figure 4-13. Raman spectra of 16 formulations subject to non-isothermal crystallisation in Crystal16® : C, SSS plus LBAC4 with/without T; D, SSS plus SMS and SSS with/without T .....	202
Figure 4-14. Isothermal crystallisation at 60°C (A) and melting at 30°C/min (B) .....	204
Figure 4-15. Non-isothermal crystallisation at a cooling rate of 5°C/min (A) and melting at 30°C/min (B).....	205
Figure 4-16. Optical observations of isothermal crystallisation for 6 representative formulations SSS, SSS-T, NBAC4-3, NBAC4-3-T, NBAC4-9, and NBAC4-9-T: images before (left) and after (right) nucleation.....	208
Figure 4-17. Viscosity of lipid-based formulations as a function of shear rate (A) and of temperature (B) .....	215
Figure 4-18. Assay of samples taken during coating trials with formulations NBAC4-3-40, NBAC4-3-60, NBAC4-9-40 and NBAC4-9-60. Sample no. 03, sample taken at the stop of feeding; end-R, sample taken while particles were still in fluidisation.....	218
Figure 4-19. PSD in volume measured for salt particles coated with four products NBAC4-3-40, NBAC4-3-60, NBAC4-9-40 and NBAC4-9-60 .....	219
Figure 4-20. PSD parameters – $Dv(90)/Dv(10)$ (blue triangles) and <i>SPAN</i> (red circles) – used to identify process regime with four products NBAC4-3-40, NBAC4-3-60, NBAC4-9-40 and NBAC4-9-60. Log scale applied for better visualisation between $Dv(90)/Dv(10)$ and <i>SPAN</i> .....	220
Figure 4-21. Images taken on chemical contrast mode (at length-scale of 1 mm) for particles coated with NBAC4-3-40, NBAC4-9-40 (before and after tempering), NBAC4-3-60, and NBAC4-9-60... ..	222
<i>Figure 4-22. Images taken on topographical contrast mode (at length-scales of 10 µm and 100 µm) for particles coated with NBAC4-3-40, NBAC4-9-40 (before and after tempering).....</i>	<i>223</i>
Figure 4-23. Images taken on topographical contrast mode (at length-scales of 10 µm and 100 µm) for particles coated with NBAC4-3-60, and NBAC4-9-60 .....	224

Figure 4-24. Transformation kinetics of NBAC4-3-40 indicated by evolution of $I_{1460}/I_{1438}$ in RAMAN spectra (performed twice): NBAC4-3-40 1 <sup>st</sup> time (red circles), 2 <sup>nd</sup> time (blue triangles), reference values of $\alpha$ and $\beta$ (black squares), and NBAC4-3-60 (green diamond).....	226
Figure 4-25. RAMAN spectra obtained for samples coated with <b>NBAC4-3</b> in the course of curing at 40°C.....	227
Figure 4-26. RAMAN spectra obtained for samples coated with <b>NBAC4-9</b> in the course of curing at 40°C.....	227
Figure 4-27. Evolution of surface properties in the course of polymorphic transformation of <b>NBAC4-3</b> .....	228
Figure 4-28. Evolution of surface properties in the course of polymorphic transformation of <b>NBAC4-9</b> .....	229
Figure 4-29. Wide-angle X-ray diffraction patterns obtained for 2 formulations processed at 2 thermal conditions over stability study period.....	231
Figure 4-30. Small-angle X-ray diffraction patterns obtained for 2 formulations processed at 2 thermal conditions over stability study period.....	231
Figure 4-31. Polarised optical images of <b>tristearin (converted <math>\beta</math>)</b> after being tempered at 50°C for 12h (left column) and <b>tristearin (directly crystallised <math>\beta</math>)</b> directly crystallised at 60°C (right column) .....	233
Figure 4-32. Polarised optical images of <b>NBAC4-3-40 (converted <math>\beta</math>)</b> after being tempered at 40°C for 24h (left column) and <b>NBAC4-3-60 (directly crystallised <math>\beta</math>)</b> directly crystallised at 60°C (right column).....	234
Figure 4-33. Polarised optical images of <b>NBAC4-9-40 (<math>\alpha</math>-<math>\beta</math>)</b> after being tempered at 40°C for 24h (left column) and <b>NBAC4-9-60 (<math>\beta</math>)</b> directly crystallised at 60°C (right column) .....	235
Figure 4-34. Comparative dissolution profile of products coated obtained for two formulations (NBAC4-3 and NBAC4-9) processed at 2 thermal conditions over stability study period.....	236
Figure 5-1. Thermal programme set for non-isothermal experiments with trilaurin in Crystall16® ...	243
Figure 5-2. MSZW map measured for LLL with 4 levels of talc concentration. Melting points at 0.05°C/min (red circles), crystallisation points at 0.05°C/min (blue squares), 5°C/min (blue triangles) and 10°C/min (blue circles), reference melting points of polymorphs $\alpha$ , $\beta'$ and $\beta$ (black squares). (See <b>Appendix 03</b> ).....	247
Figure 5-3. MSZW map measured for all formulations containing trilaurin. Melting points at 0.05°C/min (red circles), crystallisation points at 0.05°C/min (blue squares), 5°C/min (blue triangles) and 10°C/min (blue circles), reference melting points of polymorphs $\alpha$ , $\beta'$ and $\beta$ (black squares) ..	249
Figure 5-4. Isothermal crystallisation of 4 selected trilaurin-based formulations (A) and polymorphic identification of crystallised form(s) (B) .....	251

Figure 5-5. Assay results of coating trials performed with LLL-1F, LLL-2F and LLL-3F .....	253
Figure 5-6. Evolution of particle size distribution in volume(left) and PSD parameters (right) obtained for products coated with <b>LLL-1F</b> , <b>LLL-2F</b> and <b>LLL-3F</b> .....	254
Figure 5-7. Optical images of salt particles uncoated and coated with <b>LLL-1F</b> , <b>LLL-2F</b> , and <b>LLL-3F</b> with increasing contents. The white bar (right bottom of each image) indicates 200 $\mu\text{m}$ . .....	255
Figure 5-8. Polymorphic identification performed on products coated with LLL-1F, LLL-2F and LLL-3F at $t_0$ .....	257
Figure 5-9. Small-angle (left) and wide-angle X-ray powder diffraction patterns obtained for products coated with <b>LLL-1F</b> , <b>LLL-2F</b> and <b>LLL-3F</b> at $t_0$ (black line), 6 weeks (red line) and 12 weeks (blue line) after that .....	258
Figure 5-10. Polarised light optical images performed for LLL-1F and LLL-2F at $t_0$ , 6 and 12 weeks after that.....	260
Figure 5-11. Polarised light optical images performed for vitamin E TPGS at $t_0$ , 6 and 12 weeks after that .....	261
Figure 5-12. Polarised light optical images performed for LLL-3F and LLL-3F-1 at $t_0$ , 6 and 12 weeks after that.....	261
Figure 5-13. Dynamic vapour sorption profile obtained for uncoated NaCl and products coated with <b>LLL-1F</b> , <b>LLL-2F</b> and <b>LLL-3F</b> at $t_0$ and 12 weeks after that; uncoated NaCl (black open square), <b>LLL-1F</b> (blue open circle), <b>LLL-2F</b> (red open triangle), <b>LLL-3F</b> (green open diamond), measurements at $t_0$ (dotted lines) and at 12 weeks after that (dashed lines).....	262
Figure 5-14. Salt release profile obtained for products coated with <b>LLL-1F</b> (red), <b>LLL-2F</b> (blue) and <b>LLL-3F</b> (green) at $t_0$ (dotted lines) and 12 weeks (solid lines) after that. Error bar (grey region) .....	263
Figure 5-15. Digestion profile of 500 mg each formulation <b>LLL-1F</b> , <b>LLL-2F</b> and <b>LLL-3F</b> ( $t_0$ ).....	264
Figure 5-16. Salt release profile of products coated with <b>LLL-1F</b> , <b>LLL-2F</b> and <b>LLL-3F</b> ( $t_0$ ) in the course of lipolysis.....	266
Figure 6-1. Comparative dissolution profile in water (37°C) with the reference product Slow Sodium Tablets® : Coating content in F1 and F2: 49.3% F1 and 44.2% F2.....	270
Figure 6-2. Comparative dissolution profile in water (37°C) of salt coated with two tristearin-based formulations processed at 2 thermal conditions: 33.8% <b>NBAC4-3-40</b> (red line), 32.8% <b>NBAC4-3-60</b> (yellow line), 32.3% <b>NBAC4-9-40</b> (blue line), and 31.3% <b>NBAC4-9-60</b> (green line). ....	270
Figure 6-3. Salt release profile in water (37°C) obtained for salt coated .....	271
Figure 6-4.Simplified diagram of the screw profile and operating conditions of the hot extrusion process used to produce the amorphous solid dispersion of interest (ASD_PZQ uc) .....	275
Figure 6-5. The flow cell for powder .....	281

Figure 6-6. Schematic representation of the artificial digestive system comprising a stomach compartment and three segments of small intestine (duodenum, jejunum, and ileum) reproducing the in vivo digestive conditions of humans (adapted from Minekus et al., 1995) and picture of the system. ....	282
Figure 6-7. Particle size distribution (PSD) of uncoated and coated PZQ amorphous solid dispersions. Size distribution curve of initial ASD-PZQ, i.e. sieved but not fluidised, (dashed line), that of fluidised ASD-PZQ, i.e. not coated, (black line) and that of coated ASD-PZQ (blue line) .....	285
Figure 6-8. Optical observations of uncoated and coated PZQ amorphous solid dispersions.....	286
Figure 6-9. Images taken on chemical contrast mode for ASD_PZQ cBWbF, ASD_PZQ cSSSbF and ASD_PZQ cLLLbF: Intact particles (500 $\mu\text{m}$ – left) and cross-sectioned particles (200 $\mu\text{m}$ – right) .....	288
Figure 6-10. Images taken on topographical contrast mode (at length-scales of 50 $\mu\text{m}$ ) for uncoated ASD_PZQ, ASD_PZQ cBWbF, ASD_PZQ cSSSbF and ASD_PZQ cLLLbF .....	289
Figure 6-11. Vapour sorption and desorption kinetics of ASD_PZQ (A), ASD_PZQ cBWbF (B), ASD_PZQ cSSSbF (C) and ASD_PZQ cLLLbF (D): black line ( $t_0$ ), blue line (3 months*) and red line (6 months*). Dashed line in corresponding colour represents the programmed relative humidity. * after months in open vial exposed to 25°C/60%RH.....	290
Figure 6-12. Normalised X-ray powder diffraction patterns obtained for ASD_PZQ uc (A), ASD_PZQ cBWbF (B), ASD_PZQ cSSSbF (C) and ASD_PZQ cLLLbF (D) over 3 months of stability study: black line ( $t_0$ ), blue line (3 months), red line (6 months) and grey line (PZQ initial form A). Yellow, red, blue and cyan dashed lines represent XRPD characteristic peaks of PZQ polymorph A, B, C or both B and C, respectively; dash-dotted line, XRPD characteristic peaks of lipid polymorph. ....	292
Figure 6-13. Normalised DSC thermograms obtained for ASD_PZQ uc (A), ASD_PZQ cBWbF (B), ASD_PZQ cSSSbF (C) and ASD_PZQ cLLLbF (D) over 3 months of stability study: black line ( $t_0$ ), blue line (3 months) and red line (6 months).....	293
Figure 6-14. Evolution in crystallinity of praziquantel for ASD-PZQ uc (blue column), ASD-PZQ cBWbF (red column), ASD-PZQ cSSSbF (green column) and ASD-PZQ cLLLbF (purple column) during 6 months .....	295
Figure 6-15. Appearance of uncoated and coated ASD-PZQ in the stability study. For each set of 4 vials, <b>from left to right</b> : uncoated ASD-PZQ, ASD-PZQ cBWbF, ASD-PZQ cSSSbF and ASD-PZQ cLLLbF.....	296
Figure 6-16. Dissolution profile of uncoated and coated amorphous solid dispersions in the presence of lipases: ASD_PZQ uc (A), ASD_PZQ cBWbF (B), ASD_PZQ cSSSbF (C) and ASD_PZQ cLLLbF (D) .....	298



Figure 6-17. Digestion profile recorded for uncoated and coated products in stability study. ASD-PZQ (black line), ASD-PZQ cBWbF (red line) ASD-PZQ cSSSbF (green line), ASD-PZQ cLLLbF (blue line).....	298
Figure 6-18. Dissolution in blank FeSSIF pH 5 .....	300
Figure 6-19. Dissolution in FaSSIF .....	301
Figure 6-20. Dissolution profile in FeSSIF .....	302
Figure 6-21. Dissolution in SIF with pancreatin compared to FaSSIF .....	304
Figure 6-22. Concentration ( $\mu\text{h/mL}$ ) in gastric compartment and in intestinal compartment (jejunum+ileon) .....	305
Figure 6-23. Bioaccessibility of praziquantel from uncoated and coated amorphous solid dispersions .....	306

## List of Tables

Table 1-1. Physicochemical characteristics of particles generated via some melt-technologies.....	30
Table 1-2. Process variables and their importance in <b>hot-melt coating</b> by fluidised bed .....	46
Table 1-3. Criteria for selection of an ideal lipid used for hot-melt coating .....	48
Table 1-4. Possible consequences when processing-specific properties are in an extreme case.....	61
Table 1-5. Hot-melt coating formulations composed of a lipid and at least a surfactant .....	74
Table 1-6. Comparison of liquid and solid lipid-based formulations with cited references (not exhaustive).....	83
Table 1-7. Publications on hot-melt coating per technological or biopharmaceutical function.....	91
Table 2-1. Beeswax and surfactants .....	106
Table 2-2. Tristearin and additives.....	106
Table 2-3. Trilaurin and additives .....	106
Table 3-1. Lipid-based coating formulations composition.....	124
Table 3-2. Process parameters and their values specified for each formulation .....	127
Table 3-3. Details about pre-shear and shear stresses used in measurements.....	129
Table 3-4. Model-dependent equations for release kinetics .....	130
Table 3-5. Micromeritic properties of salt particles coated with four formulations.....	144
Table 3-6. Release constants and exponents obtained after data fitting to selected models for salt coated with four formulations at a similar coating content (%w/w) .....	155
Table 3-7. $f_2$ factors calculated for dissolution profile obtained with salt coated with <b>F1</b> (left) and <b>F2</b> (right).....	176
Table 3-8. Two-sample t-test p values calculated for dissolution profile obtained with salt coated with <b>F1</b> (left) and <b>F2</b> (right) .....	176
Table 3-9. Estimated release parameters for dissolution of salt coated with 04 formulations at $t_0$ and 12 weeks .....	178
Table 4-1. Lipid-based coating formulations composition.....	184
Table 4-2. Lipid-based coating formulations composition.....	211
Table 4-3. Process parameters and their values specified for each formulation .....	212
Table 4-4. Analytical plan for curing study with Raman spectroscopy .....	213

Table 4-5. Analytical plan for curing study with AFM.....	213
Table 4-6. Analytical plan for stability study with XRPD, SEM, PLM and release testing .....	213
Table 4-7. Estimated crystallite size and number of stacked lamellas in each crystallite.....	232
Table 4-8. Estimated release parameters for dissolution of coated salt obtained for two formulations (NBAC4-3 and NBAC4-9) processed at 2 thermal conditions over stability study period.....	238
Table 5-1. Lipid-based formulations composition for screening with Crystal16 crystallization systems .....	242
Table 5-2. Lipid-based formulations composition for hot-melt coating.....	243
Table 5-3. Process parameters and their values specified for hot melt coating of LLL-1F, LLL-2F and LLL-3F .....	245
Table 5-4. Estimated crystallite size and number of stacked lamellas .....	259
Table 6-1. Composition of lipid-based coating formulations.....	274
Table 6-2. HME process parameters for production of praziquantel-containing ASD (ASD_PZQ uc) .....	276
Table 6-3. Process parameters and their values specified for each formulation .....	276
Table 6-4. Open glass vials containing PZQ-ASDs stored in climatic chamber (25°C/6%RH) for 3 months. ....	277
Table 6-5. Parameters of heating-cooling cycles applied in mDSC.....	278
Table 6-6. FaSSiF and FeSSiF composition and properties .....	280
Table 6-7. Digestive conditions applied for in vitro digestion in the TIM-1 system. The TIM-1 was programmed to reproduce the digestion of a glass of water in a healthy adult.....	283
Table 6-8. Yield, efficiency and content of praziquantel in uncoated and coated ASDs monitored every 3 months .....	284
Table 6-9. PSD parameters measured for all the products containing PZQ.....	285
Table 6-10. Water sorption extent (%) at the maximal exposure to humidity in DVS measurements during storage .....	291
Table 6-11. <i>C<sub>maximum</sub></i> levels recorded when testing uncoated and coated ASD-PZQ .....	297
Table 6-12. Model parameters estimated for all dissolution profiles .....	303

## Poster, Presentations and Publications

Poster: “**Solvent-free Coating Technology for Technological and Biopharmaceutical Applications**” on Research Day (first version on 04/10/2022), Albi, France.

Oral presentation: “**Development of Non-Traditional Hot-Melt Coating of Particles: Manufacturability, Stability and Impact on Biopharmaceutical Properties**” at the Galenus International Particle Engineering Workshop on 29-30/09/2022 at Research Center Pharmaceutical Engineering GmbH, Graz, Austria.

Oral presentation (in French): “**Excipients lipidiques et technologie d’enrobage sans solvant – Impact fonctionnel et biopharmaceutique**” at 18<sup>th</sup> Congress of la Société française de génie des procédés on 07-10/11/2022, Toulouse, France.

Oral presentation: “**Development of Multifunctional Hot-Melt Coating Formulations: Effect of Additives on Polymorphic Transition monitored by RAMAN spectroscopy and AFM**” at 4<sup>th</sup> European Conference on Pharmaceutics on 20-21/03/2023, Marseille, France.

Publication: Van-Trung-Tin Huynh, Suenia de Paiva Lacerda, Fabienne Espitalier, Eric Beyssac, Maria-Inês Ré. **Effect of Talc and Vitamin E TPGS on Manufacturability, Stability and Release Properties of Trilaurin-based Formulations for Hot-Melt Coating.** *International Journal of Pharmaceutics*, 2024, 653, pp.123866.

Possible publications in progress (manuscript in preparation):

Publication: co-author in Huynh et al., 2024, **Hot-Melt Coating with Formulations composed of Beeswax and Surfactants – Part 1: Impact of Coating Composition on Manufacturing Process and Coating Quality.**

Publication: co-author in Huynh et al., 2024, **Hot-Melt Coating with Formulations composed of Beeswax and Surfactants – Part 2: Impact of Coating Composition on Coating Physical Stability.**

Publication: co-author in Huynh et al., 2024, **Development of a New Fast Lipid-Additive Formulation Screening Approach used in Formulating Solid Lipids for Melt-Processing.**

Publication: co-author in Huynh et al., 2024, **Development of Multifunctional Tristearin-based Formulations for Hot-Melt Coating in Fluidised Bed – Proof of Processability and Stability.**

Publication: co-author in Huynh et al., 2024, **Stability and *in vitro* Performance of Amorphous Solid Dispersions Hot-Melt Coated with Lipid-based Formulations of Diverse Digestibility.**

Publication: co-author in Huynh et al., 2024, **Review on Lipid Excipients and Hot-Melt Coating by Fluidised Bed Technology – Operational and Functional Impact of Additive Addition.**

# Appendix 01

## Chapter 3 – Part 2 FaSSIF composition\*

Component	Concentration
Bile micelle containing preparation	
Bile extract porcine	Equivalent to 3.0 mM taurocholate sodium
Cholate sodium (C <sub>24</sub> H <sub>39</sub> NaO <sub>5</sub> .xH <sub>2</sub> O)	
Deoxycholate sodium (C <sub>24</sub> H <sub>39</sub> NaO <sub>4</sub> )	
Soya lecithin	0.75 mM
Tris-maleate buffer pH 6.5	
Tris-maleate (NH <sub>2</sub> C(CH <sub>2</sub> OH) <sub>3</sub> .C <sub>4</sub> H <sub>4</sub> O <sub>4</sub> )	2.0 mM
Calcium chloride (CaCl <sub>2</sub> .2H <sub>2</sub> O)	1.4 mM

\* All NaCl contents were not included in the composition of FaSSIF. This enables measurements of conductivity in the validity range of calibration standards.

**Complementary data (SEM images) during samples monitoring during storage at 25°C/60%RH for 3 months (coating surface solid state monitoring)**

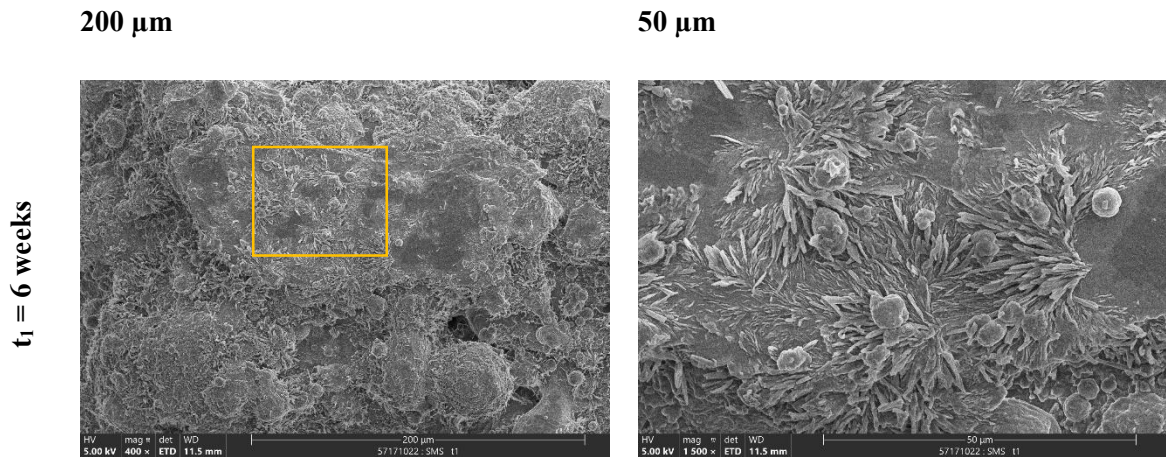


Figure A.2.1. SEM micrographs of salt coated with formulation F0 obtained at 6 weeks intermediary time points ( $t_1$ ), in stability study

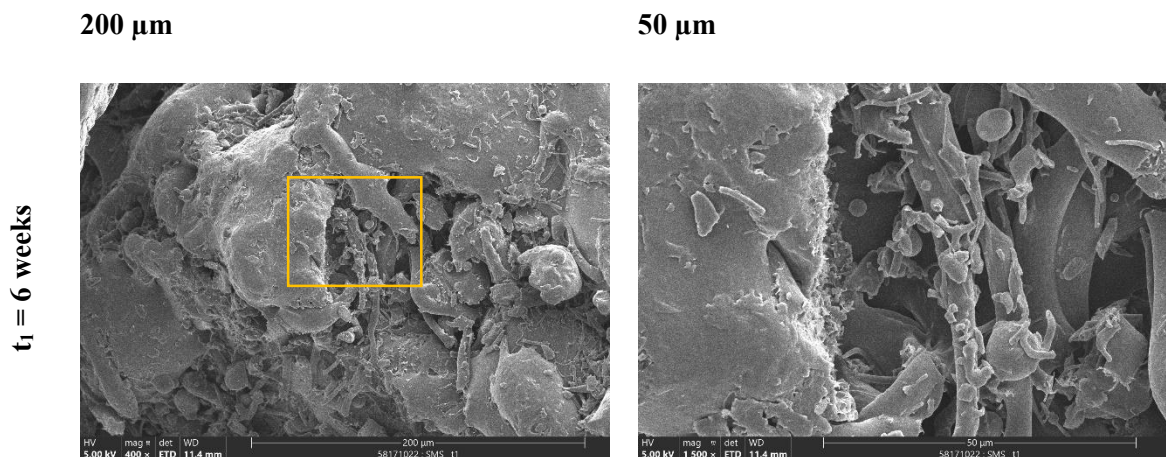


Figure A.2.2. SEM micrographs of salt coated with formulation F3 obtained at 6 weeks intermediary time points ( $t_1$ ), in stability study



**Complementary data (SEM images) during samples monitoring during storage at 25°C/60%RH for 3 months (coating surface solid state monitoring)**

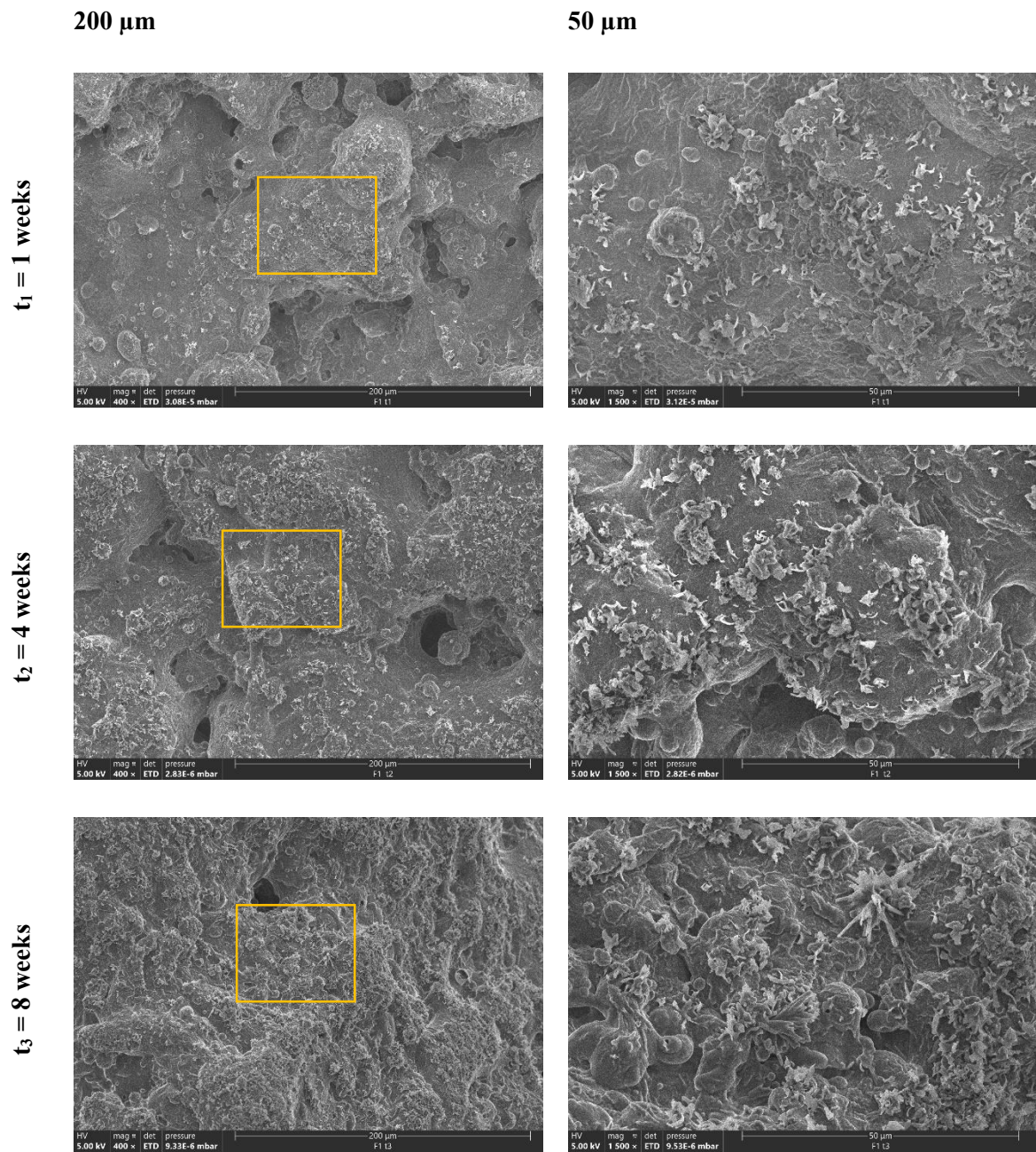


Figure A.2.4. SEM micrographs of salt coated with formulation F1 obtained at 1, 4 and 8 weeks intermediary time points ( $t_1$ ,  $t_2$ ,  $t_3$ ), in stability study



**Complementary data (SEM images) during samples monitoring during storage at 25°C/60%RH for 3 months (coating surface solid state monitoring)**

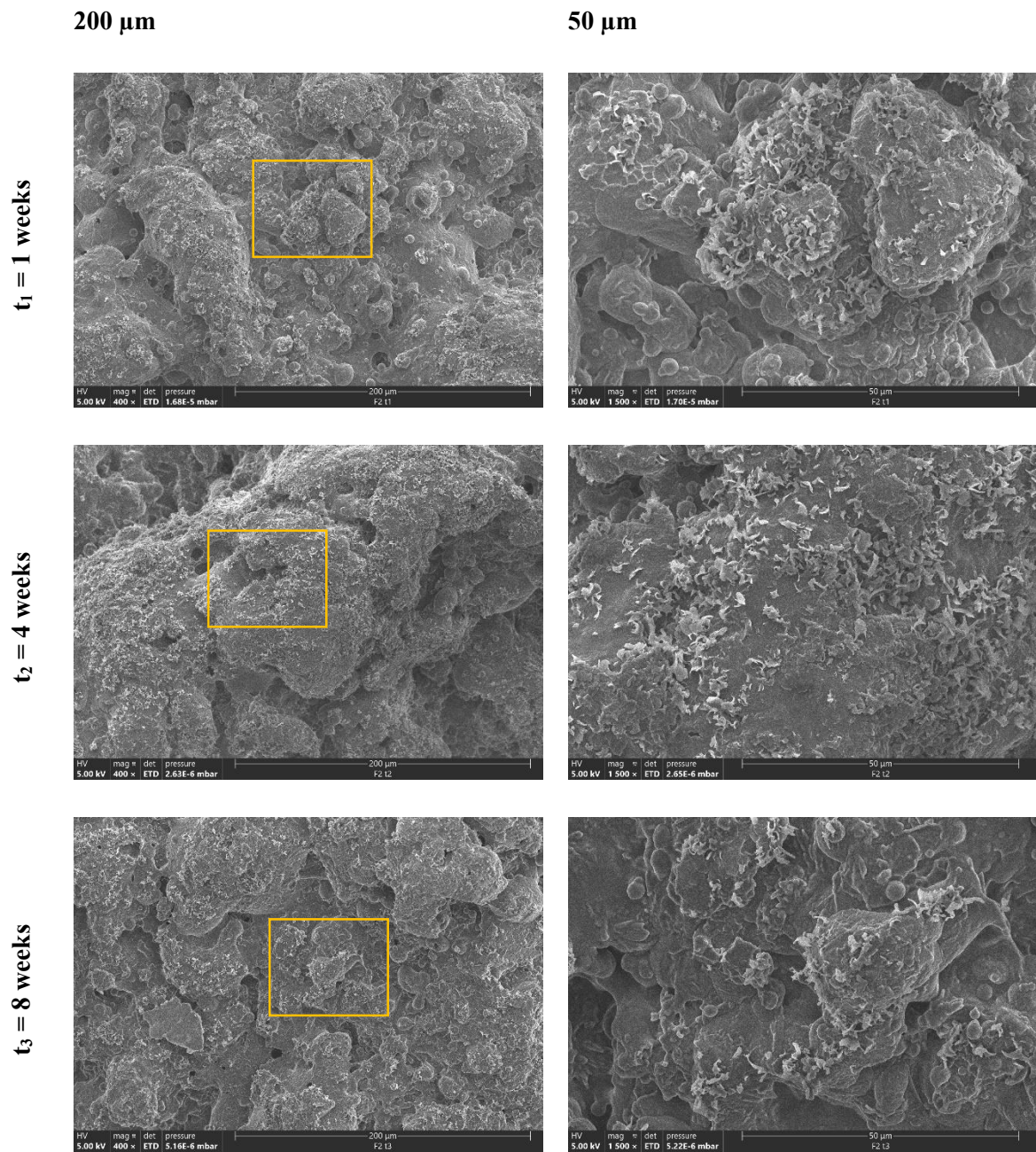
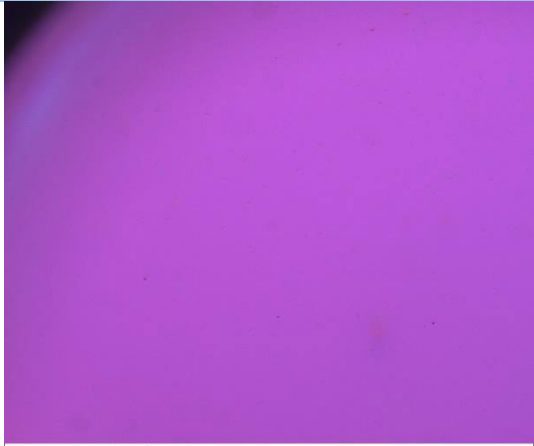

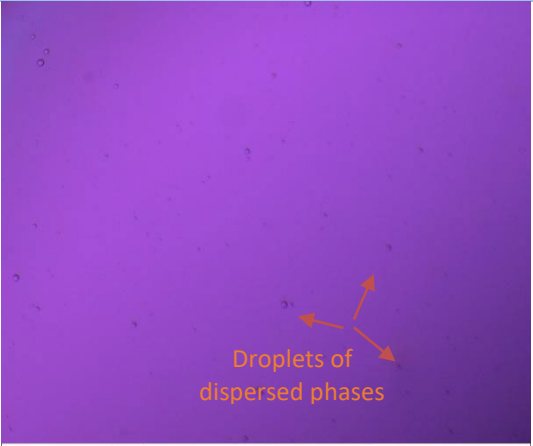
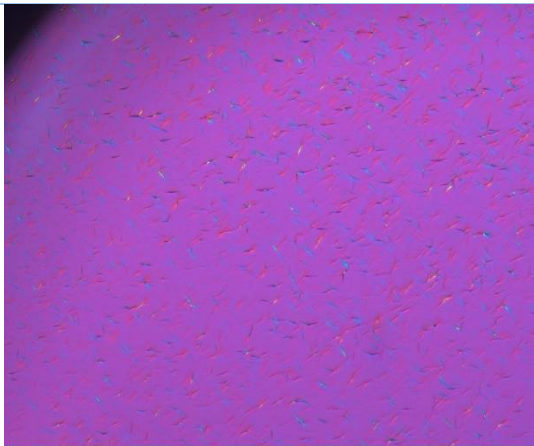




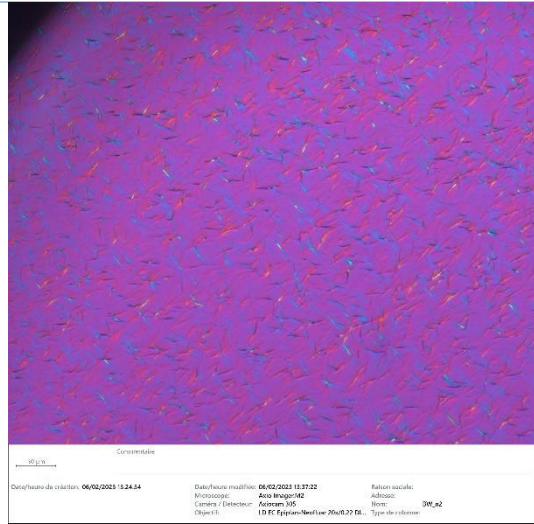
Figure A.2.5. SEM micrographs of salt coated with formulation F2 obtained at 1, 4 and 8 weeks intermediary time points ( $t_1$ ,  $t_2$ ,  $t_3$ ), in stability study

**Complementary data (PLM micrographs):**  
**Spontaneous crystallisation of F0, F1 and F2 upon cooling at 5°C/min**

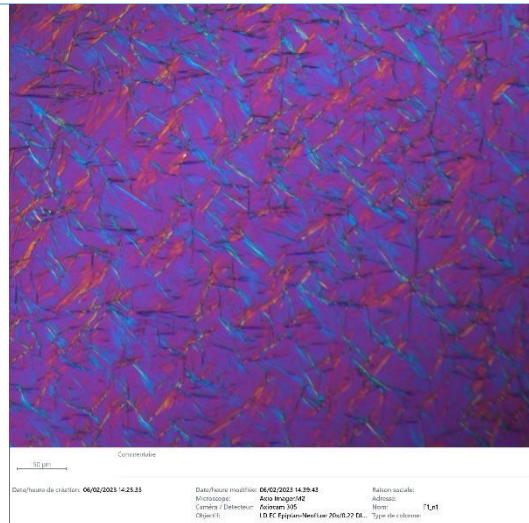
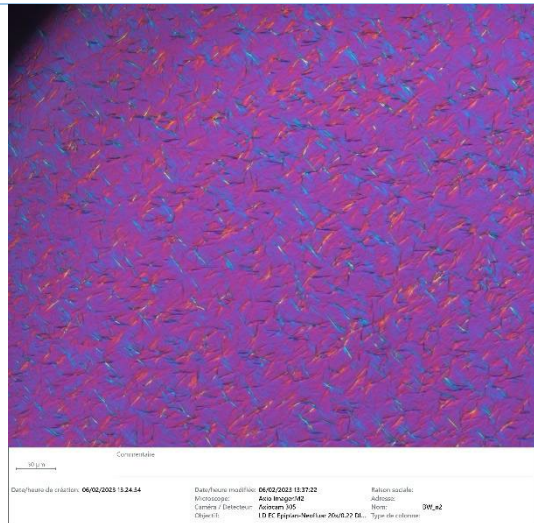
	F0	F1	F2
<b>65°C</b>	 <p>Concentrado</p> <p>100 µm</p> <p>Data/hora de captura: 06/02/2023 13:24:34</p> <p>Data/hora modified: 06/02/2023 13:37:32</p> <p>Microscopio: Axiu Image/162</p> <p>Camera / Detector: AxioCam 305</p> <p>Objetivo: 10.0x Epiplan-Neofluar 20x/0.27 Ed.</p> <p>Rafion social: Adhiso</p> <p>Nombre: DW_#2</p> <p>Tipos de cámara: T1_p1</p>	 <p>Concentrado</p> <p>100 µm</p> <p>Data/hora de captura: 06/02/2023 14:23:13</p> <p>Data/hora modified: 06/02/2023 14:39:43</p> <p>Microscopio: Axiu Image/162</p> <p>Camera / Detector: AxioCam 305</p> <p>Objetivo: 10.0x Epiplan-Neofluar 20x/0.27 Ed.</p> <p>Rafion social: Adhiso</p> <p>Nombre: T1_p1</p> <p>Tipos de cámara: T1_p1</p>	 <p>Concentrado</p> <p>100 µm</p> <p>Data/hora de captura: 06/02/2023 16:44:36</p> <p>Data/hora modified: 06/02/2023 16:55:40</p> <p>Microscopio: Axiu Image/162</p> <p>Camera / Detector: AxioCam 305</p> <p>Objetivo: 10.0x Epiplan-Neofluar 20x/0.27 Ed.</p> <p>Rafion social: Adhiso</p> <p>Nombre: T2_p1</p> <p>Tipos de cámara: T2_p1</p>
<b>63.75°</b>	 <p>Concentrado</p> <p>100 µm</p> <p>Data/hora de captura: 06/02/2023 13:24:34</p> <p>Data/hora modified: 06/02/2023 13:37:32</p> <p>Microscopio: Axiu Image/162</p> <p>Camera / Detector: AxioCam 305</p> <p>Objetivo: 10.0x Epiplan-Neofluar 20x/0.27 Ed.</p> <p>Rafion social: Adhiso</p> <p>Nombre: DW_#2</p> <p>Tipos de cámara: T1_p1</p>	 <p>Concentrado</p> <p>100 µm</p> <p>Data/hora de captura: 06/02/2023 14:23:13</p> <p>Data/hora modified: 06/02/2023 14:39:43</p> <p>Microscopio: Axiu Image/162</p> <p>Camera / Detector: AxioCam 305</p> <p>Objetivo: 10.0x Epiplan-Neofluar 20x/0.27 Ed.</p> <p>Rafion social: Adhiso</p> <p>Nombre: T1_p1</p> <p>Tipos de cámara: T1_p1</p>	 <p>Concentrado</p> <p>100 µm</p> <p>Data/hora de captura: 06/02/2023 16:44:36</p> <p>Data/hora modified: 06/02/2023 16:55:40</p> <p>Microscopio: Axiu Image/162</p> <p>Camera / Detector: AxioCam 305</p> <p>Objetivo: 10.0x Epiplan-Neofluar 20x/0.27 Ed.</p> <p>Rafion social: Adhiso</p> <p>Nombre: T2_p1</p> <p>Tipos de cámara: T2_p1</p>



62.5°C

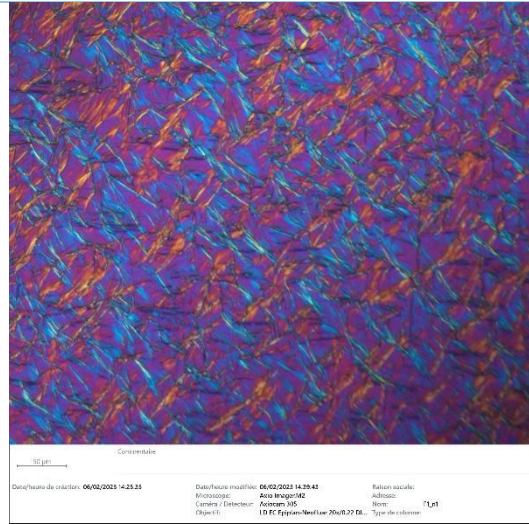


60°C

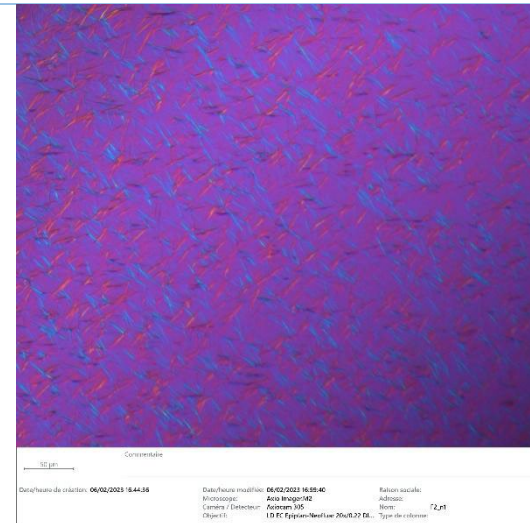
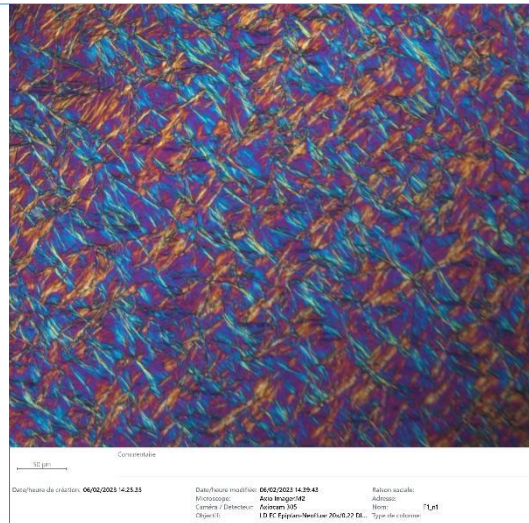




55°C



50°C





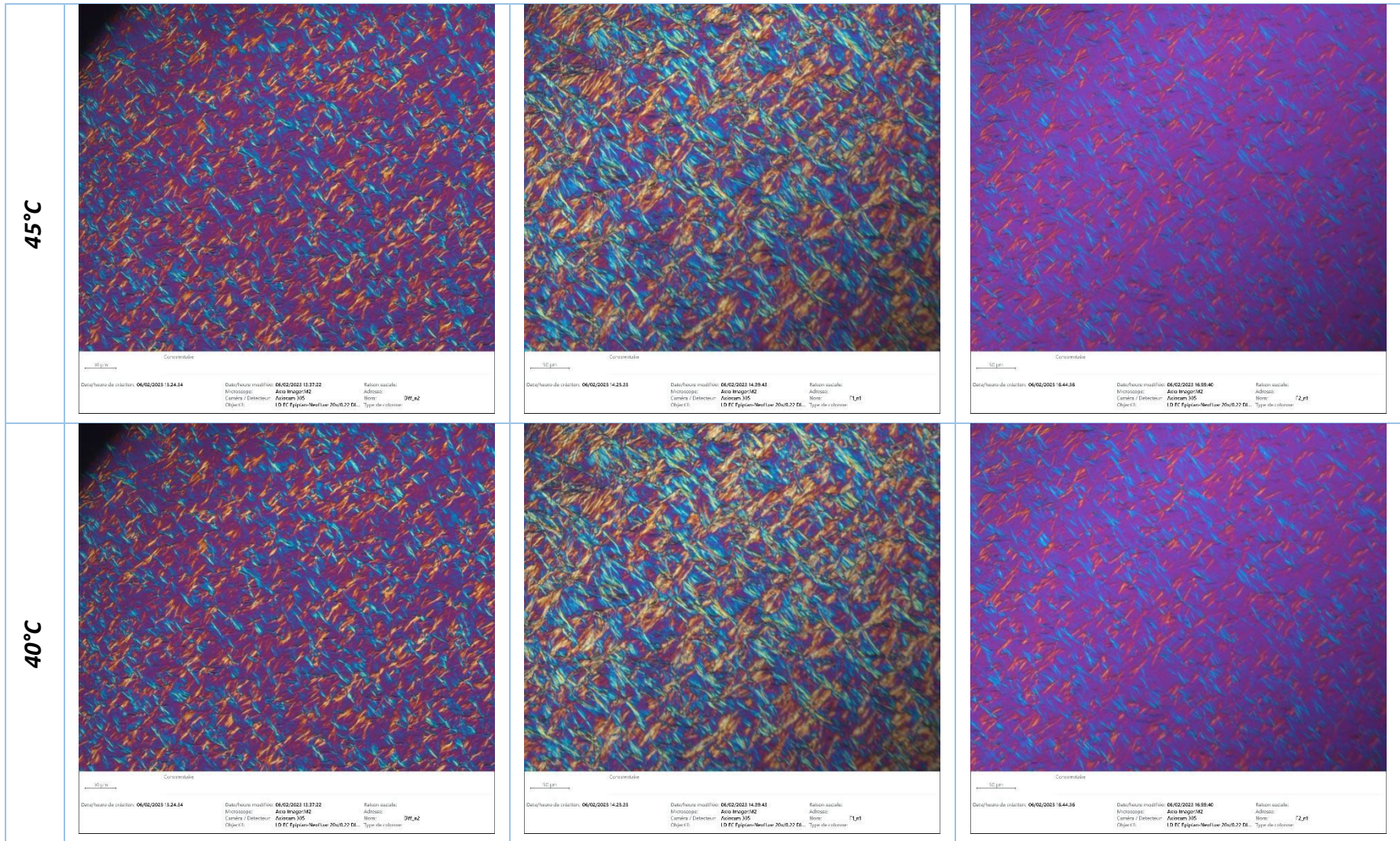


Figure A.2.6. PLM micrographs of spontaneous crystallisation F0, F1 and F2 upon cooling at 5°C/min

# Appendix 02

## Chapter 4 – Part 1

### Tabulated data of melting point and crystallisation points measured using Crystal16 in non-isothermal crystallisation

Formulation	Melting point (°C)	Solidification point (°C)	Formulation	Melting point (°C)	Solidification point (°C)
<b>A. Without surfactant added</b>			<b>D. With two surfactants added</b>		
SSS	71.1 ± 0.0	60.0 ± 0.2	<b>D.1. “Hydrophilic” binary additive combinations</b>		
SSS-T 0.1%	71.0 ± 0.1	61.0 ± 0.0	HBAC4-3*	70.9 ± 0.1	60.0 ± 0.2
SSS-T 0.5%	70.8 ± 0.0	61.3 ± 0.1	HBAC4-3-T 0.1%*	70.7 ± 0.3	62.5 ± 1.6
SSS-T	70.7 ± 0.1	61.5 ± 0.3	HBAC4-3-T 0.5%*	71.7 ± 0.2	62.6 ± 0.5
<b>B. With one hydrophilic surfactant added</b>			HBAC4-3-T*	70.7 ± 0.2	62.2 ± 1.4
PS20-3	70.4 ± 0.2	60.5 ± 0.5	HBAC4-9	70.7 ± 0.1	60.8 ± 0.8
PS20-3-T 0.1%*	69.9 ± 0.2	60.8 ± 0.3	HBAC4-9-T 0.1%*	71.4 ± 0.3	61.5 ± 0.5
PS20-3-T 0.5%*	69.9 ± 0.3	60.9 ± 0.2	HBAC4-9-T 0.5%*	71.1 ± 0.4	61.2 ± 0.4
PS20-3-T*	70.5 ± 0.2	61.5 ± 0.1	HBAC4-9-T*	71.1 ± 0.1	63.6 ± 1.8
PS20-9	70.8 ± 0.2	60.9 ± 0.2	<b>D.2. “Neutral” binary additive combinations</b>		
PS20-9-T 0.1%*	70.3 ± 0.2	61.0 ± 0.2	NBAC4-3	70.7 ± 0.1	60.1 ± 0.1
PS20-9-T 0.5%*	70.3 ± 0.2	61.3 ± 0.2	NBAC4-3-T 0.1%*	70.6 ± 0.1	61.3 ± 0.1
PS20-9-T*	70.8 ± 0.2	61.8 ± 0.1	NBAC4-3-T 0.5%*	71.2 ± 0.1	61.8 ± 0.2
<b>C. With one lipophilic surfactant added</b>			NBAC4-3-T*	70.6 ± 0.1	66.5 ± 0.6
SML-3	69.8 ± 0.4	59.3 ± 0.3	NBAC4-9	70.3 ± 0.2	60.3 ± 0.8
SML-3-T 0.1%*	69.5 ± 0.5	60.4 ± 0.2	NBAC4-9-T 0.1%*	71.1 ± 0.2	61.4 ± 0.1
SML-3-T 0.5%*	69.4 ± 0.4	60.4 ± 0.1	NBAC4-9-T 0.5%*	70.8 ± 0.1	61.0 ± 0.1
SML-3-T*	69.7 ± 0.4	60.9 ± 0.3	NBAC4-9-T*	70.8 ± 0.1	66.1 ± 0.4
SML-9	69.9 ± 0.2	59.4 ± 0.3	<b>D.3. “Lipophilic” binary additive combinations</b>		
SML-9-T 0.1%*	69.5 ± 0.2	59.8 ± 0.3	LBAC4-3	70.5 ± 0.3	60.7 ± 0.2
SML-9-T 0.5%*	69.4 ± 0.2	60.3 ± 0.2	LBAC4-3-T 0.1%*	70.6 ± 0.1	61.8 ± 0.9
SML-9-T*	69.7 ± 0.1	60.2 ± 0.1	LBAC4-3-T 0.5%*	71.3 ± 0.1	62.5 ± 0.4
			LBAC4-3-T*	70.4 ± 0.2	61.2 ± 0.1
			LBAC4-9	70.1 ± 0.2	60.4 ± 0.4
			LBAC4-9-T 0.1%*	70.8 ± 0.1	62.1 ± 0.6
			LBAC4-9-T 0.5%*	70.9 ± 0.1	61.9 ± 0.8
			LBAC4-9-T*	70.4 ± 0.2	61.4 ± 0.1

**Tabulated data of induction measured using Crystall16  
in isothermal crystallisation**

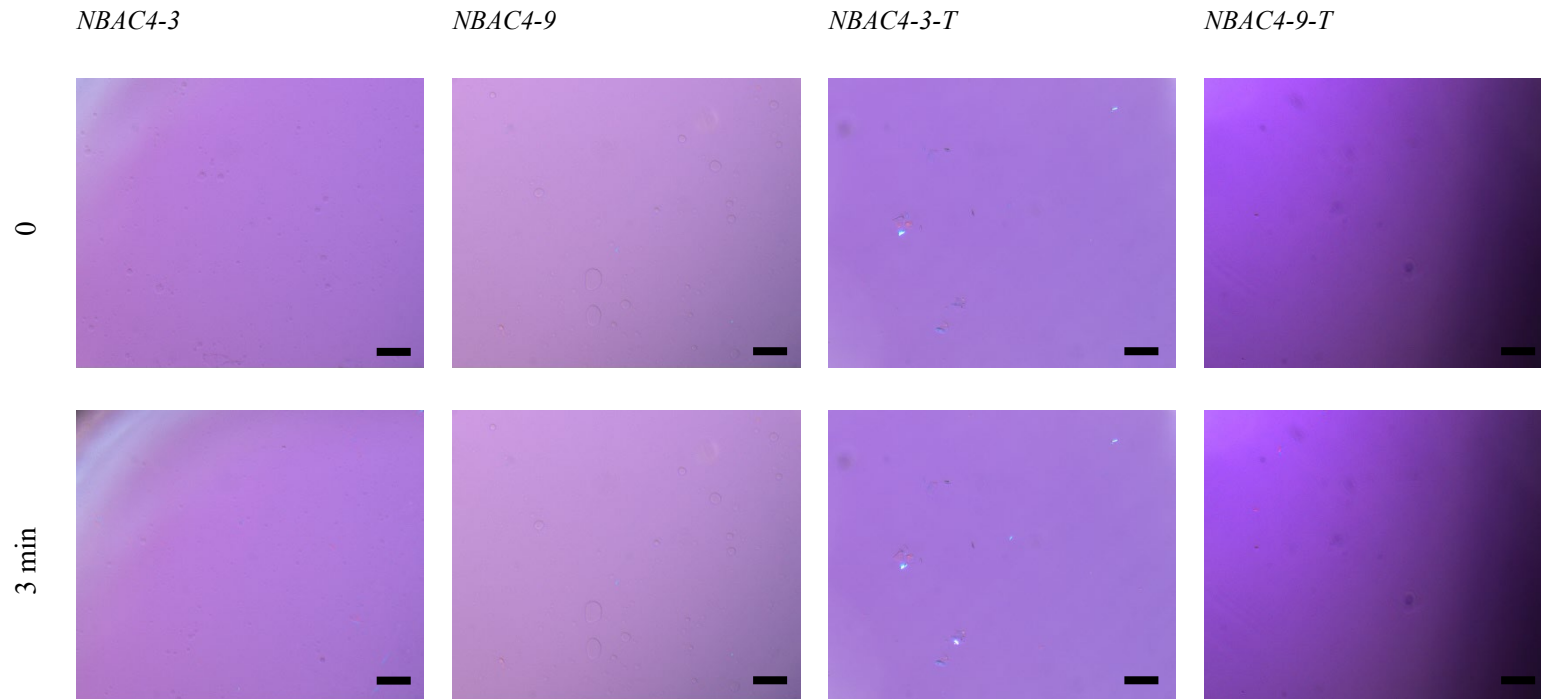
Formulation	$\mu$ (s)	$\sigma$ (s)	$R^2$ (s)
<b>A. Without surfactant added</b>			
SSS	3031.63	322.16	0.992
SSS-T 0.1%	2000.92	211.90	0.979
SSS-T 0.5%	1795.81	266.55	0.986
SSS-T	1906.19	267.53	0.987
<b>B. With one hydrophilic surfactant added</b>			
PS20-3	1709.10	309.44	0.989
PS20-3-T 0.1%*	1528.01	133.97	0.971
PS20-3-T 0.5%*	1317.49	129.59	0.992
PS20-3-T*	1099.21	182.12	0.973
PS20-9	1558.04	289.82	0.963
PS20-9-T 0.1%*	1400.03	70.83	0.969
PS20-9-T 0.5%*	1230.76	82.67	0.984
PS20-9-T*	1129.80	141.63	0.970
<b>C. With one lipophilic surfactant added</b>			
SML-3	2130.28	276.52	0.964
SML-3-T 0.1%*	1412.96	205.25	0.979
SML-3-T 0.5%*	1230.71	184.07	0.969
SML-3-T*	1194.64	180.87	0.970
SML-9	2468.93	163.10	0.946
SML-9-T 0.1%*	2020.93	184.56	0.989
SML-9-T 0.5%*	1859.34	68.04	0.960
SML-9-T*	1465.17	228.53	0.980

Formulation	$\mu$ (s)	$\sigma$ (s)	$R^2$ (s)
<b>D. With two surfactants added</b>			
<b>D.1. "Hydrophilic" binary additive combinations</b>			
HBAC4-3	1514.96	396.80	0.990
HBAC4-3-T 0.1%*	1410.27	143.70	0.962
HBAC4-3-T 0.5%*	1162.00	125.48	0.987
HBAC4-3-T*	1136.25	143.67	0.990
HBAC4-9	1781.02	253.33	0.956
HBAC4-9-T 0.1%*	1365.20	178.83	0.986
HBAC4-9-T 0.5%*	1458.53	119.17	0.971
HBAC4-9-T*	1173.12	130.93	0.989
<b>D.2. "Neutral" binary additive combinations</b>			
NBAC4-3	1270.44	259.31	0.983
NBAC4-3-T 0.1%*	1181.60	79.31	0.981
NBAC4-3-T 0.5%*	925.30	90.87	0.992
NBAC4-3-T*	1065.16	115.22	0.989
NBAC4-9	1543.01	374.09	0.989
NBAC4-9-T 0.1%*	983.83	138.47	0.987
NBAC4-9-T 0.5%*	995.91	100.47	0.993
NBAC4-9-T*	1102.42	133.06	0.987
<b>D.3. "Lipophilic" binary additive combinations</b>			
LBAC4-3	1197.40	238.48	0.991
LBAC4-3-T 0.1%*	1327.87	179.00	0.976
LBAC4-3-T 0.5%*	839.64	108.49	0.993
LBAC4-3-T*	1158.16	124.95	0.989
LBAC4-9	1782.12	468.49	0.991
LBAC4-9-T 0.1%*	1170.73	198.29	0.993
LBAC4-9-T 0.5%*	888.68	127.47	0.993
LBAC4-9-T*	1224.87	160.03	0.988

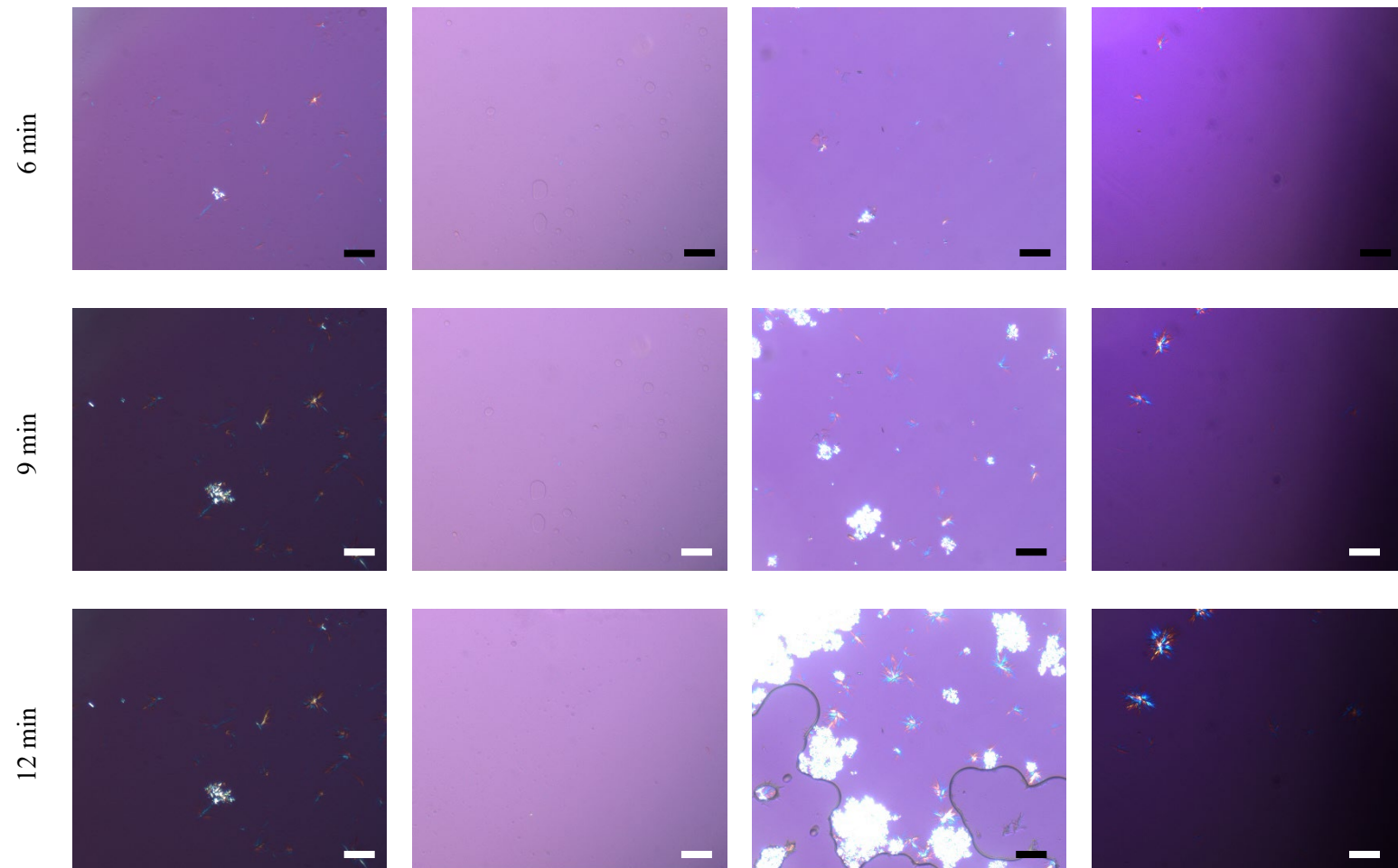
**Supplementary information**

**Crystal growth (solidification) process of NBAC4-3, NBAC4-9, NBAC4-3-T, NBAC4-9-T**

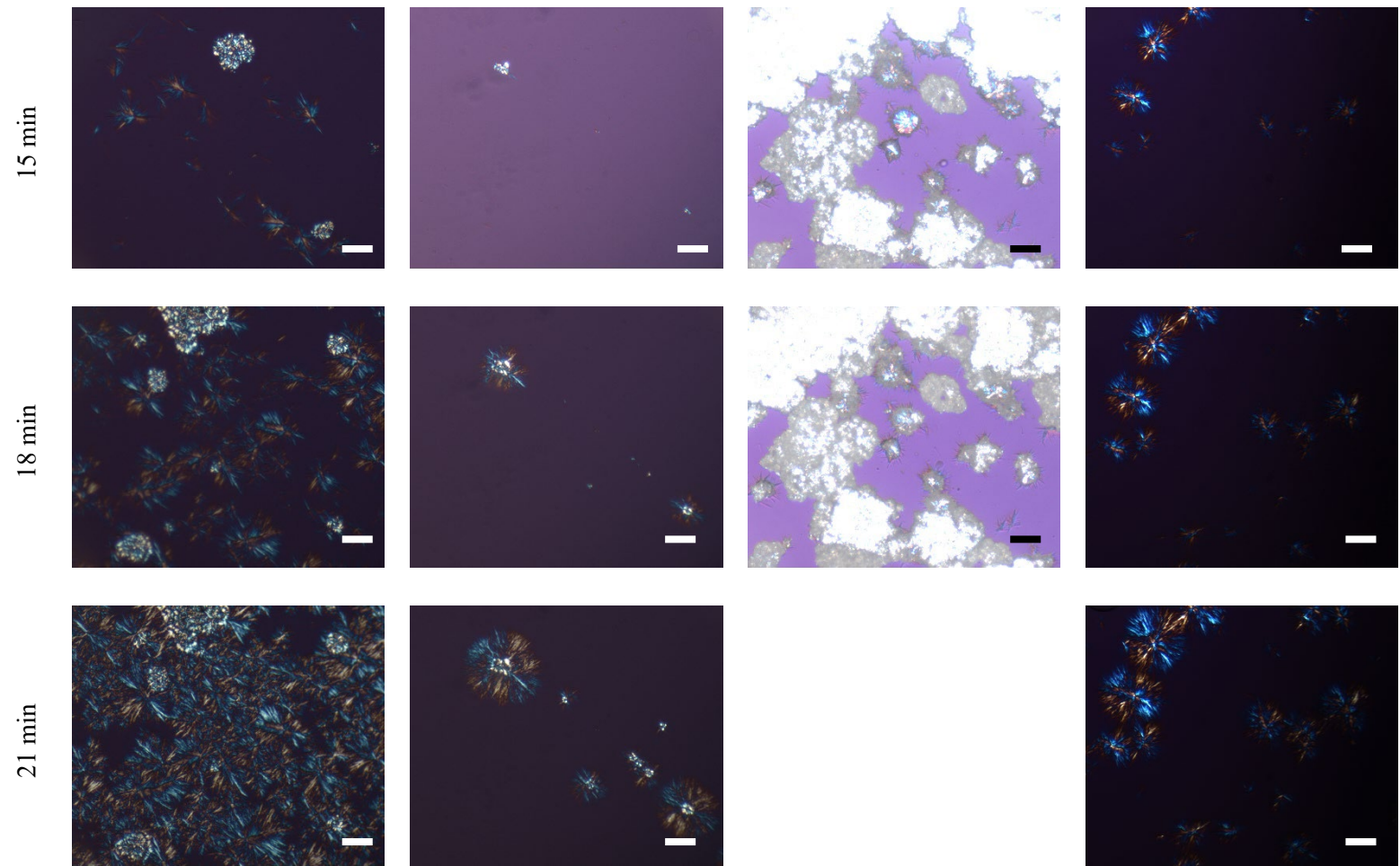
**The black/white bar indicates a length scale of 50  $\mu\text{m}$**



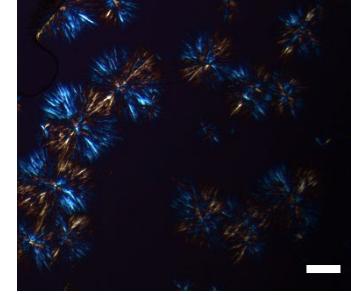
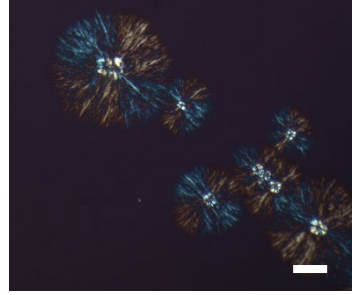
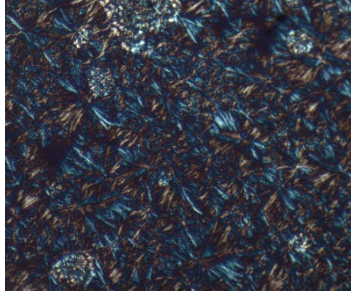




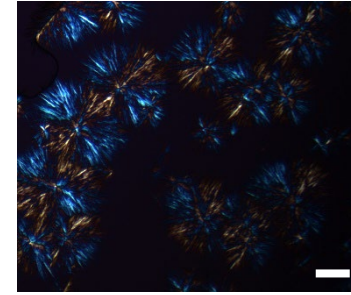
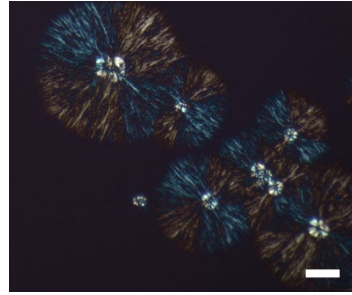




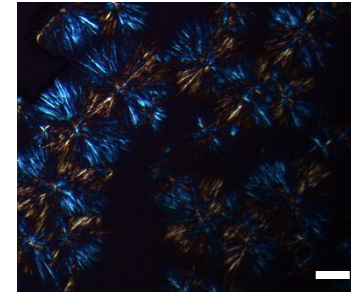
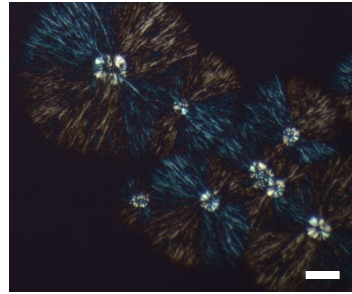
24 min



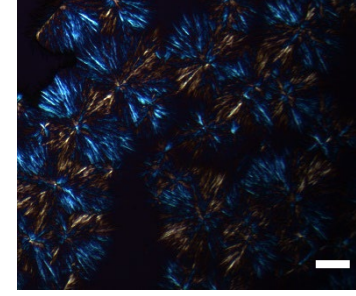
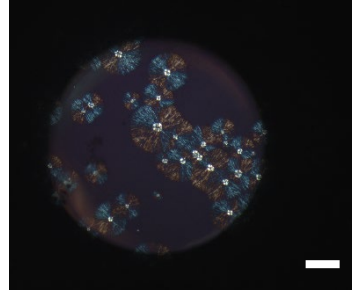
27 min



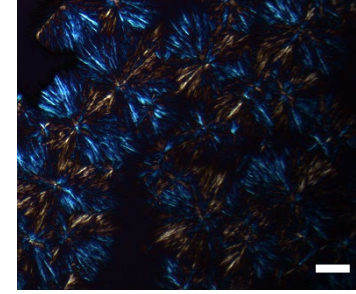
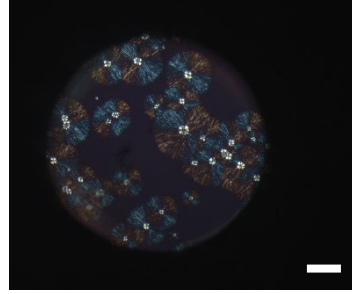
30 min



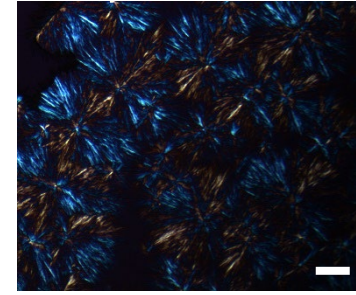
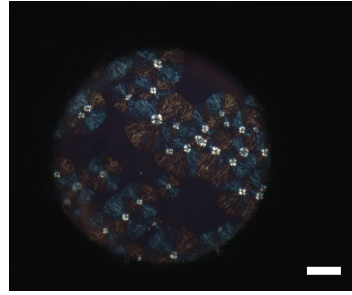
33 min



36 min



39 min



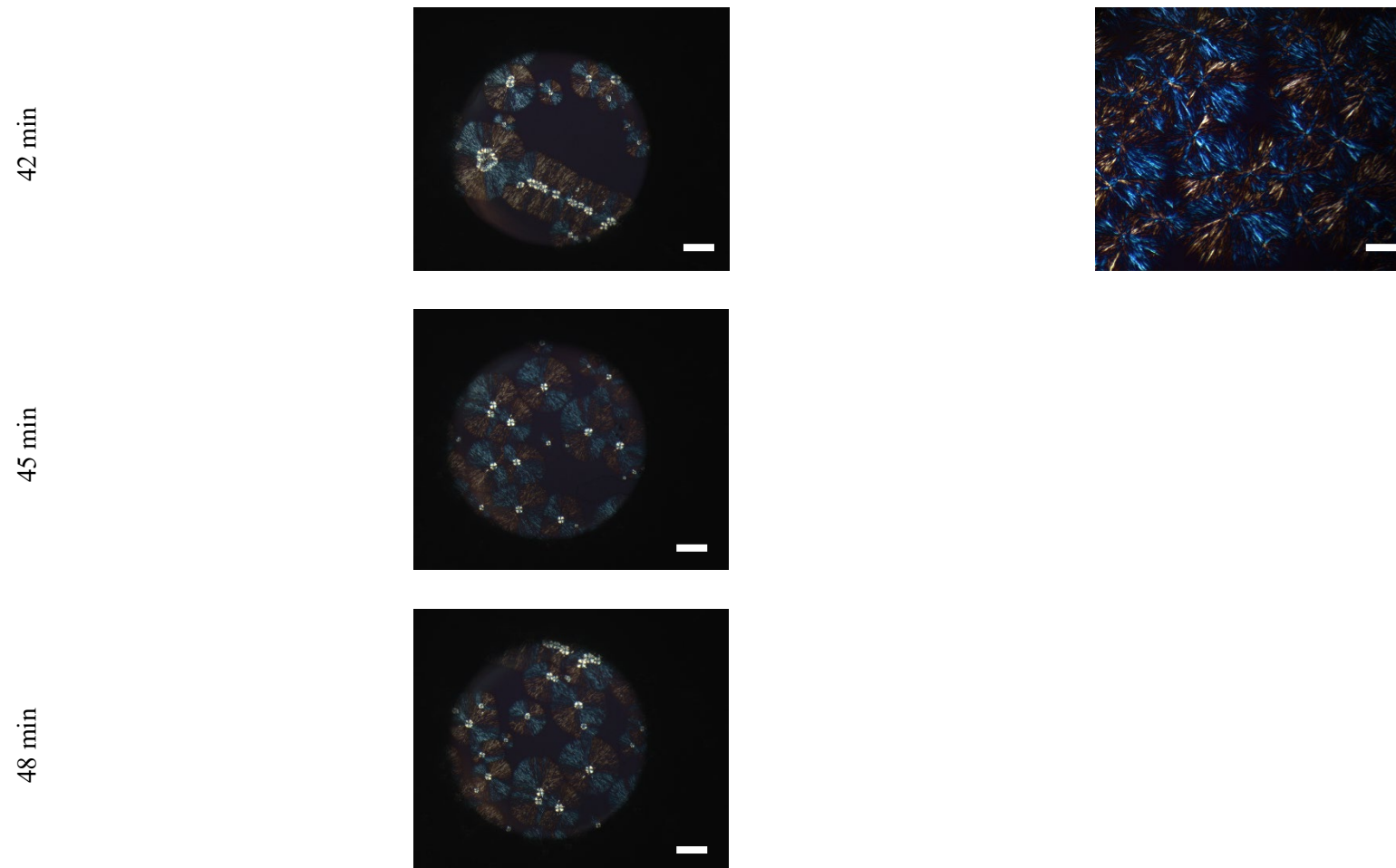
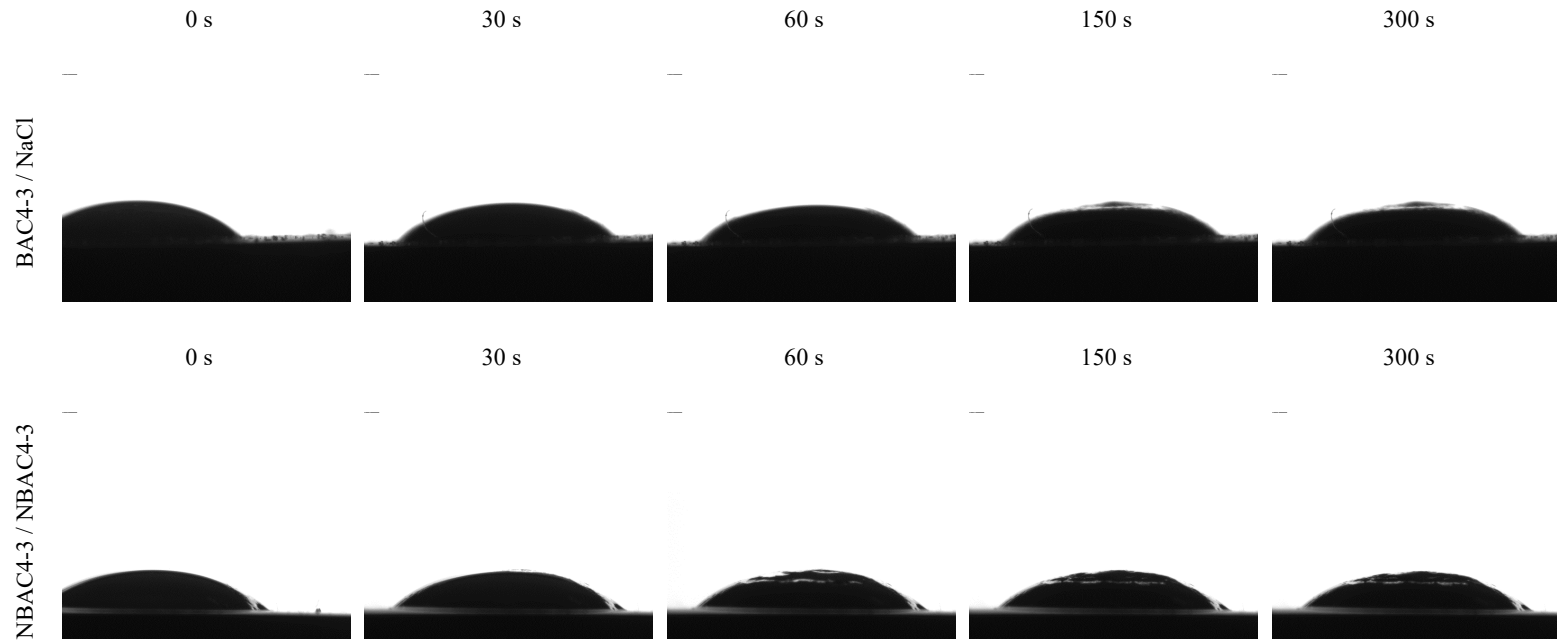


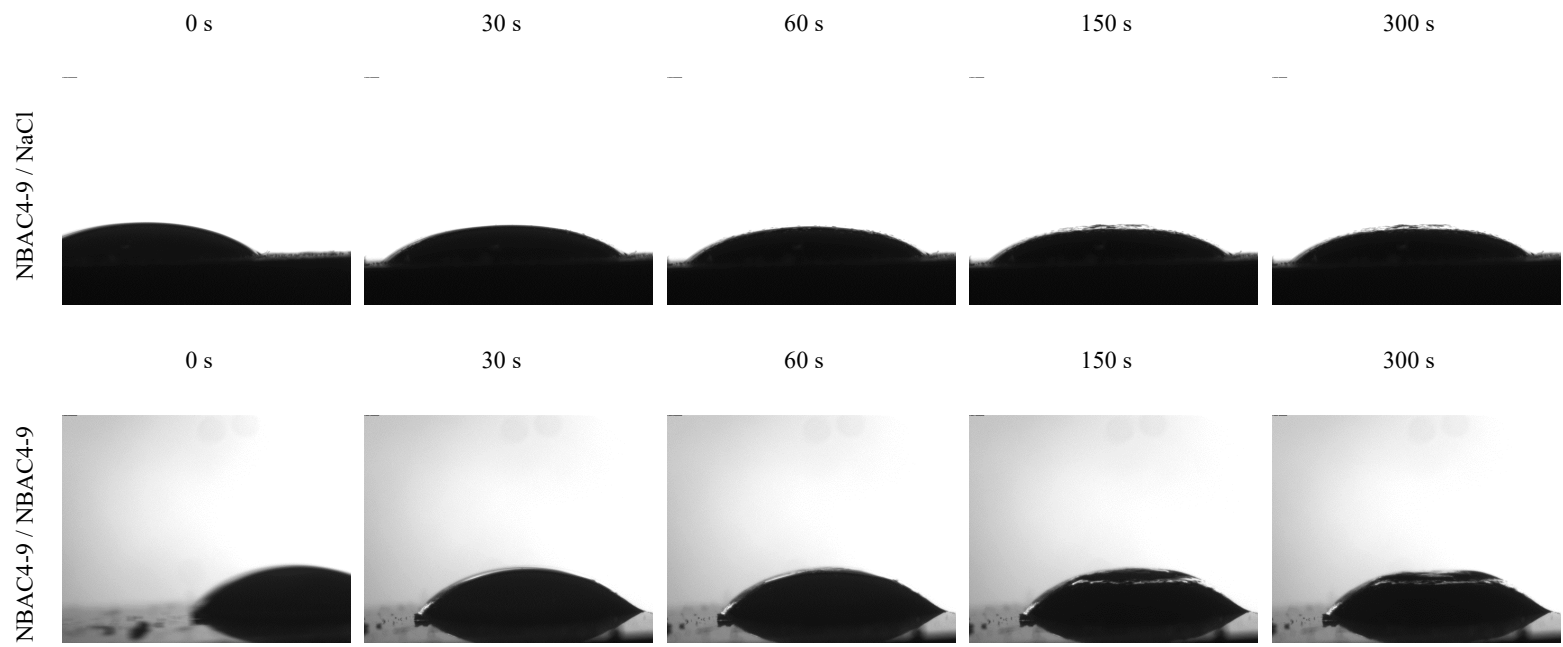
Figure S1. Crystal growth (solidification) process starting from the induction time. White/black bar 50  $\mu\text{m}$ , except for NBAC4-9 from 33 min 200  $\mu\text{m}$ .

Chapter 4 – Part 2

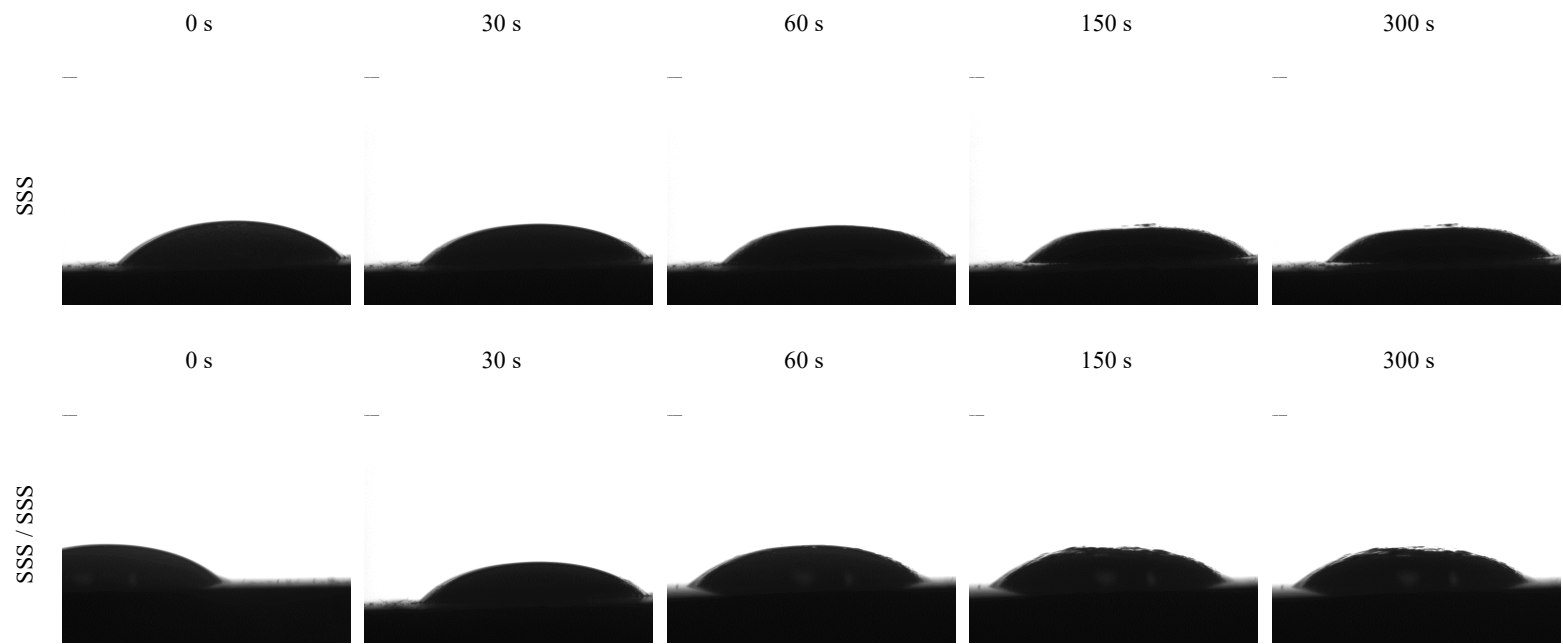
Supplementary information

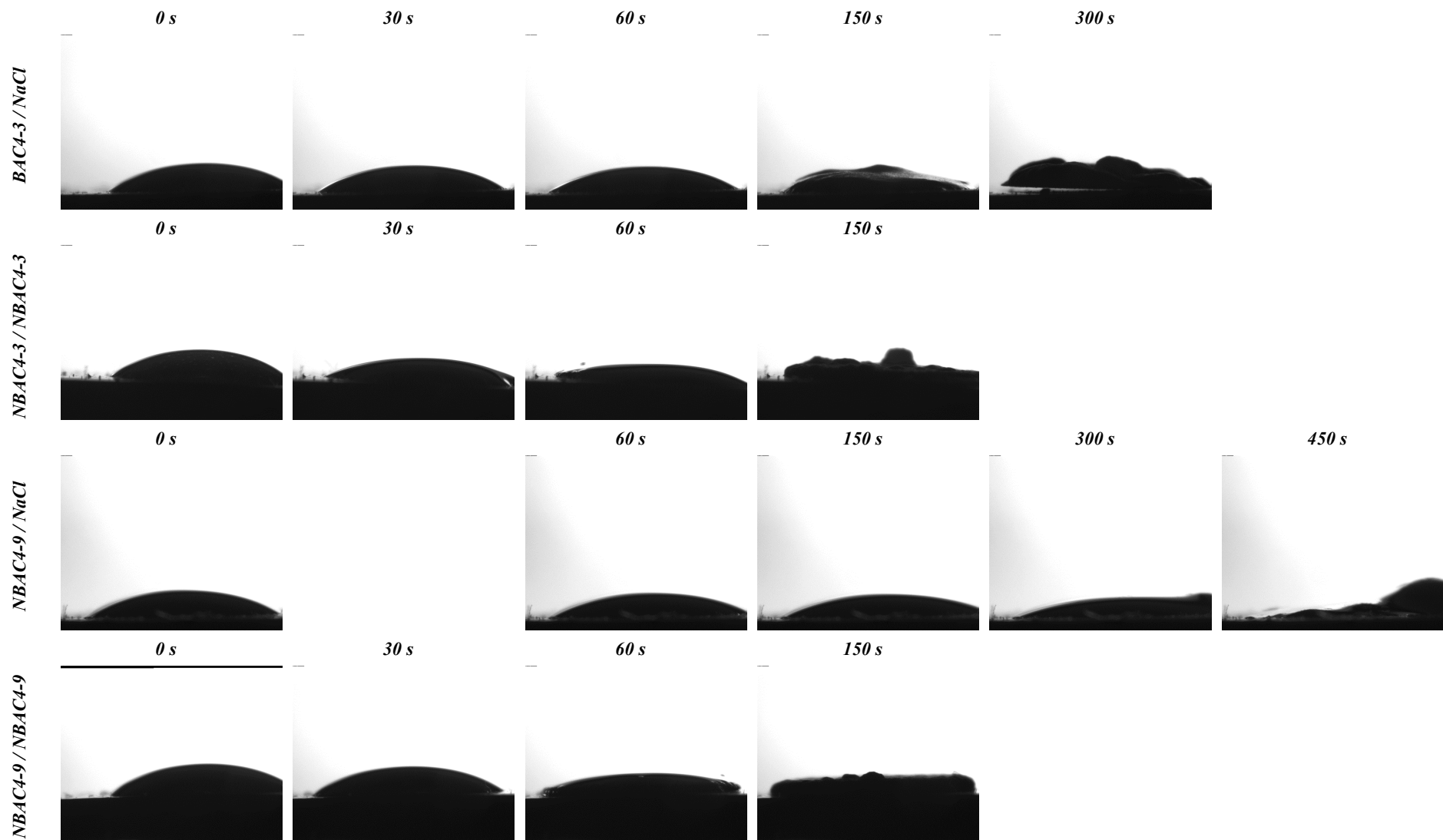
Impact of Additives on Solidification and Deformation Behaviors

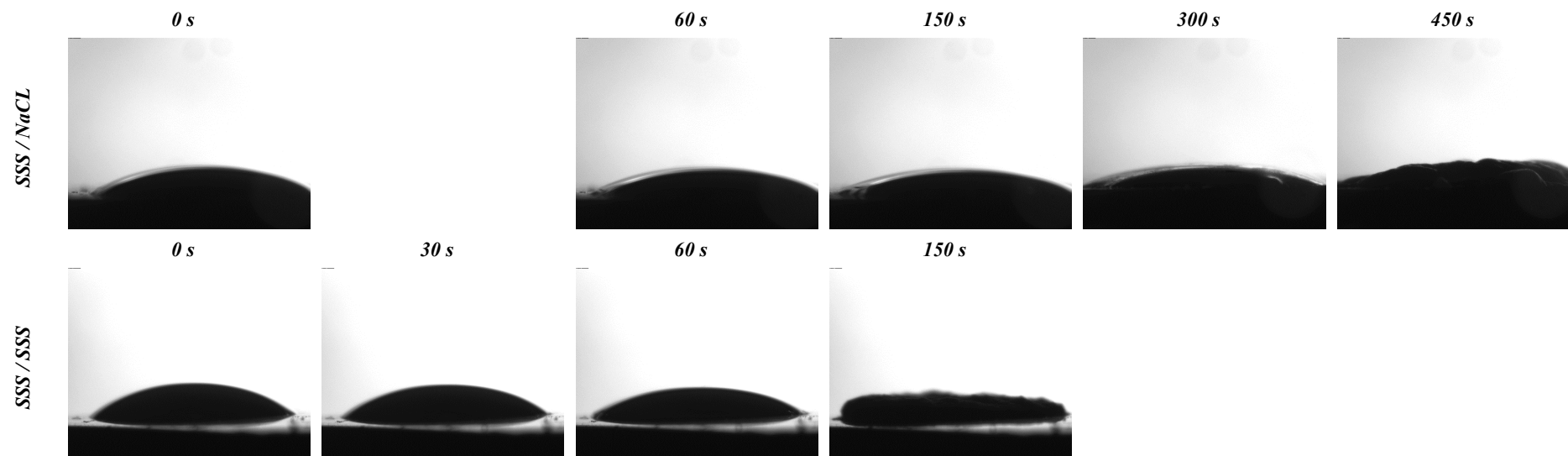












**Figure S1.B.** Solidification and film formation of 3 formulations NBAC4-3, NBAC4-9 and SSS on 2 different types of surface at 60°C

## Appendix 03

### Tabulated data of melting point and crystallisation points measured using Crystall16 in non-isothermal crystallisation

Formulation	Melting point <sup>#</sup> (°C)	Crystallisation point <sup>#</sup> (°C)
<b>1. Trilaurin ± Talc</b>		
LLL	47.3 ± 0.1	38.0 ± 1.9
LLL+T 0.1% w/w*	47.3 ± 0.1	39.2 ± 0.4
LLL+T 0.5% w/w*	47.2 ± 0.1	39.0 ± 0.3
LLL+T 1.0% w/w*	47.0 ± 0.1	37.4 ± 1.0
<b>2. Trilaurin ± Vitamin E TPGS ± Talc</b>		
LLL+VitE_TPGS	46.9 ± 0.1	38.0 ± 0.4
LLL+VitE_TPGS+T 0.1%*	46.9 ± 0.1	37.9 ± 1.1
LLL+VitE_TPGS+T 0.5%*	46.8 ± 0.1	35.7 ± 0.2
LLL+VitE_TPGS+T 1.0%*	47.0 ± 0.2	37.6 ± 1.0

\* indicates 1.0%, 0.5%, 0.1% w/w talc to the total 99%.0, 99.5% and 99.9% w/w of other components, accordingly

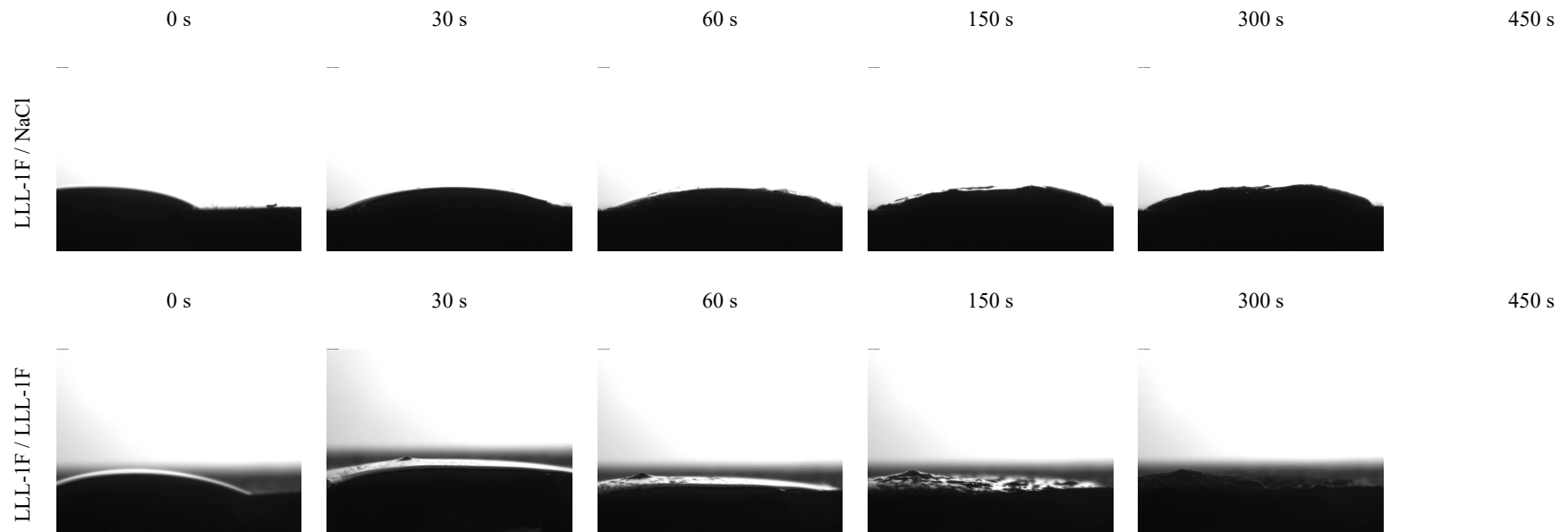
<sup>#</sup> measured at cooling/heating rate of 0.05°C/min

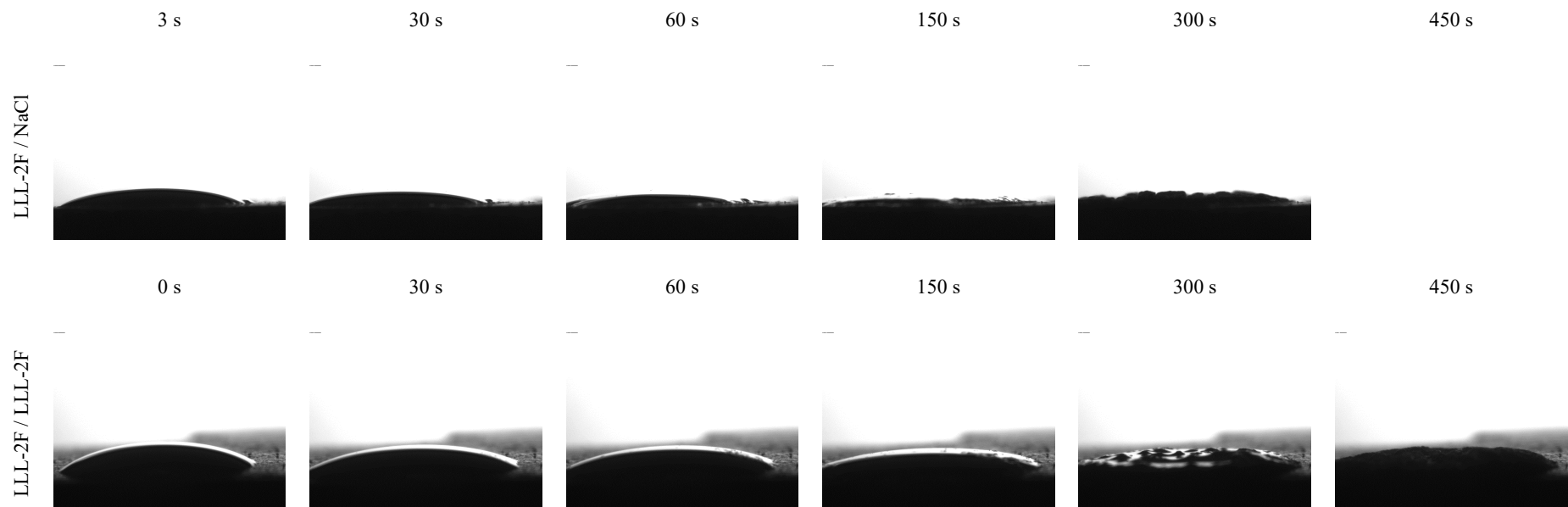
### Tabulated data of induction measured using Crystall16 in isothermal crystallisation

Formulation	$\mu$ (s)	$\sigma$ (s)	$R^2$ (-)
<b>1. Trilaurin ± Talc</b>			
LLL	99.42	13.39	1.00
LLL+T 0.1% w/w*	100.31	19.42	0.99
LLL+T 0.5% w/w*	77.48	7.05	0.99
LLL+T 1.0% w/w*	93.22	8.67	0.99
<b>2. Trilaurin ± Vitamin E TPGS ± Talc</b>			
LLL+VitE_TPGS	151.66	15.12	0.99
LLL+VitE_TPGS+T 0.1%*	152.91	13.90	0.99
LLL+VitE_TPGS+T 0.5%*	168.83	17.78	0.99
LLL+VitE_TPGS+T 1.0%*	158.66	13.92	1.00

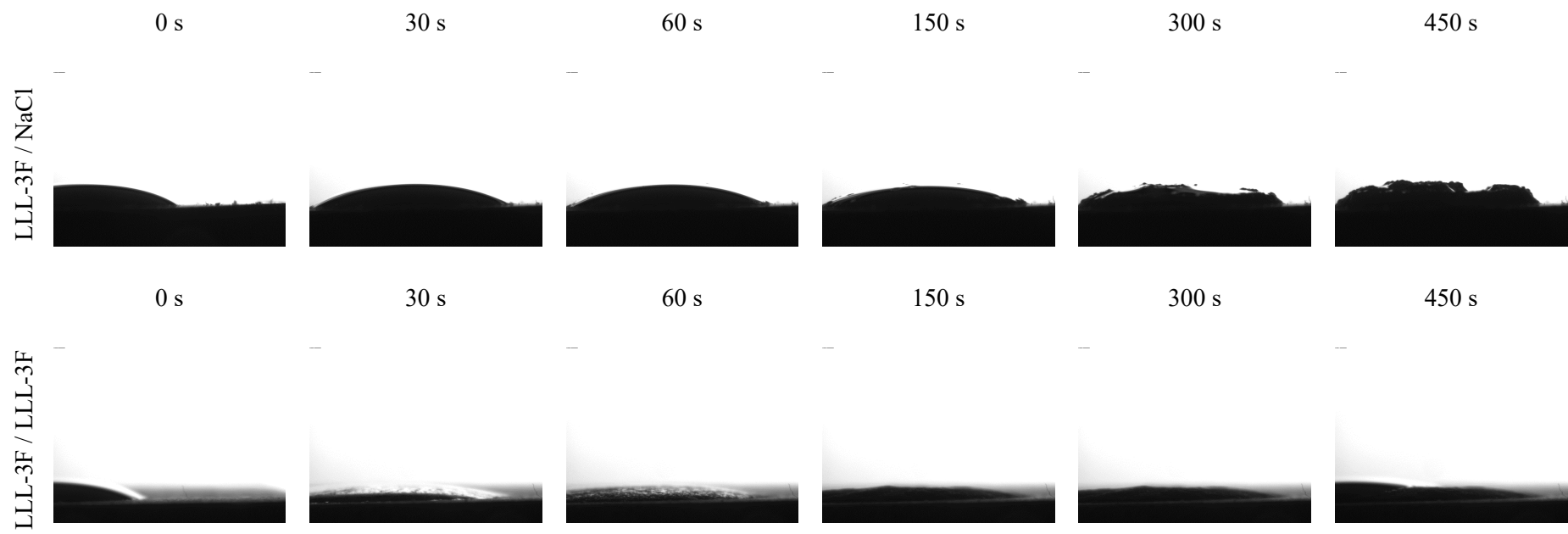
## Supplementary information

### Impact of Additives on Solidification and Deformation Behaviors





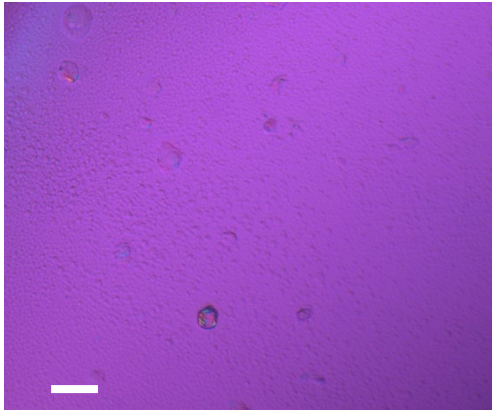




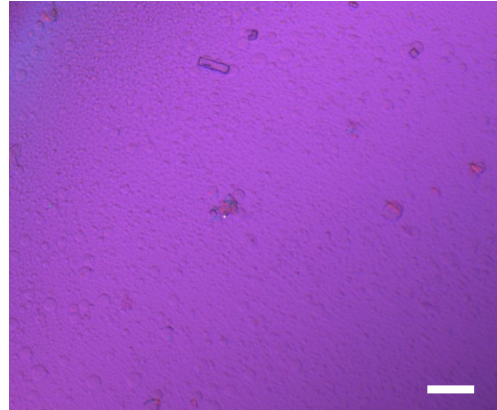
## Supplementary information

### Nucleation & Crystal growth (solidification) process of LLL+VitE\_TPGS+T 1.0% w/w from $t_0$ . White bar 50 $\mu\text{m}$

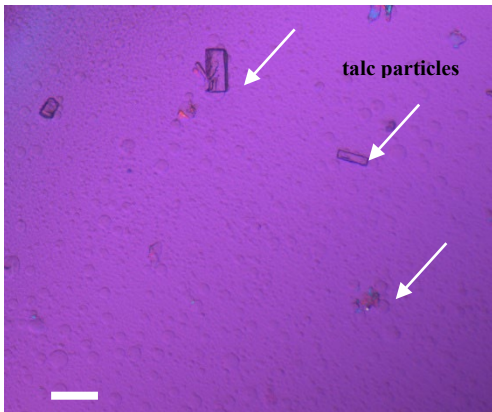
$t_0$  (when the temperature reaches 30°C)



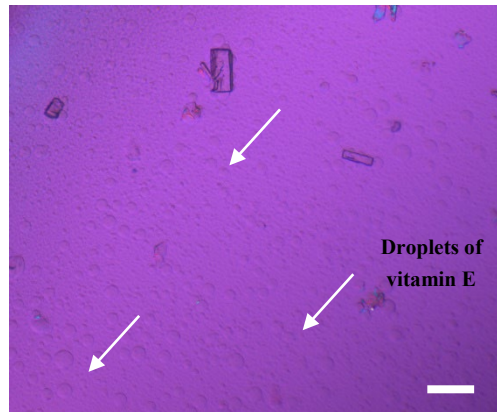
2.5 min



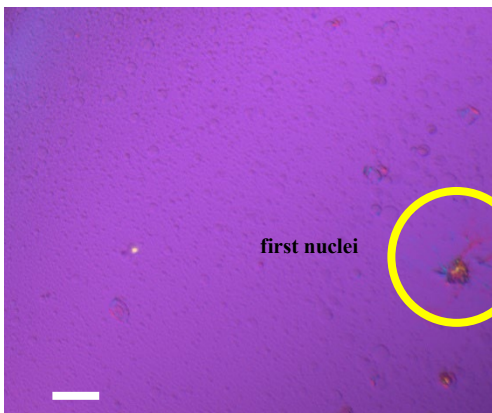
5.0 min



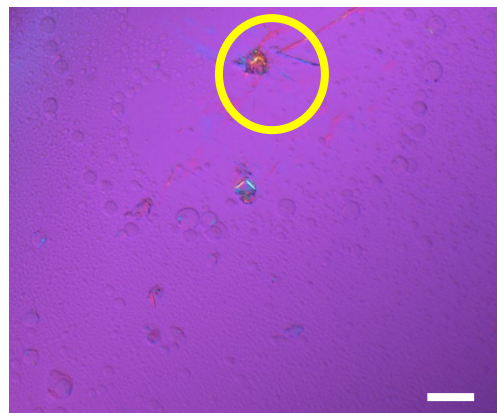
7.5 min



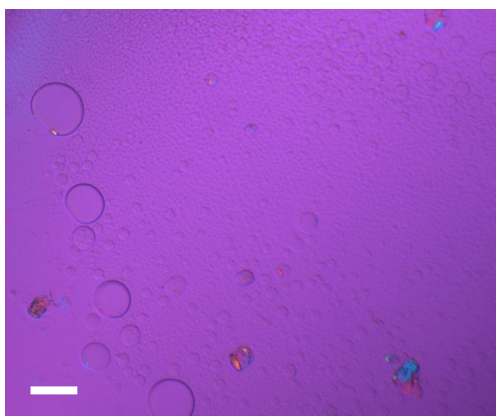
8.75 min (detection of first nuclei)



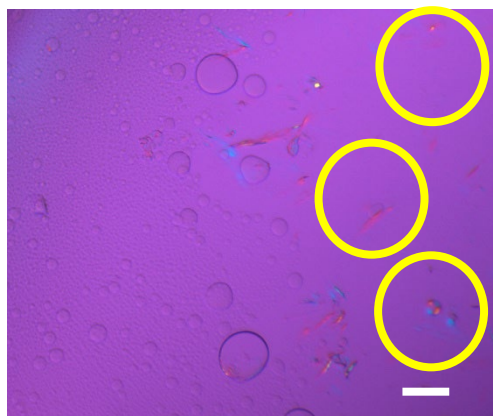
10.0 min



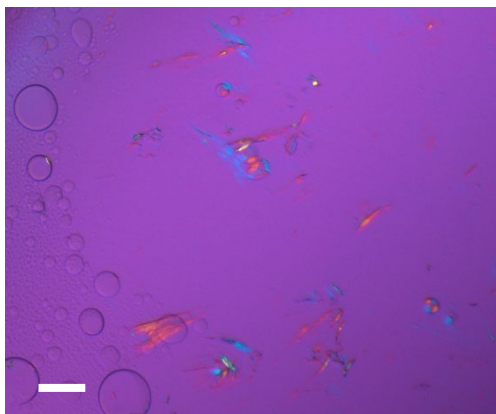
12.5 min



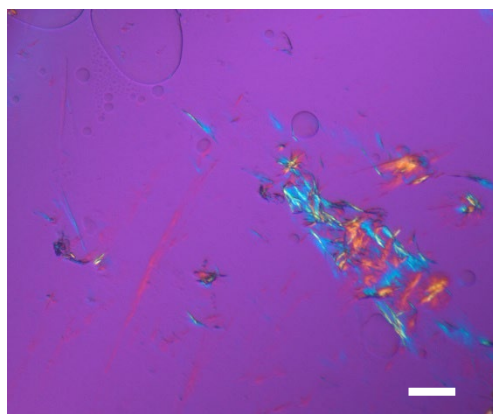
15 min



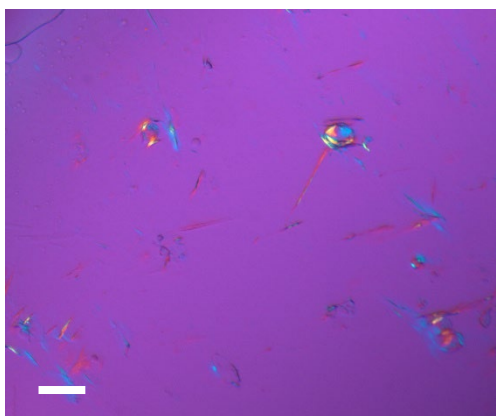
17.5 min



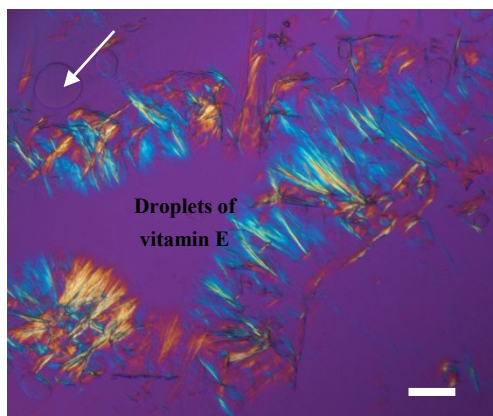
20.0 min



22.5 min

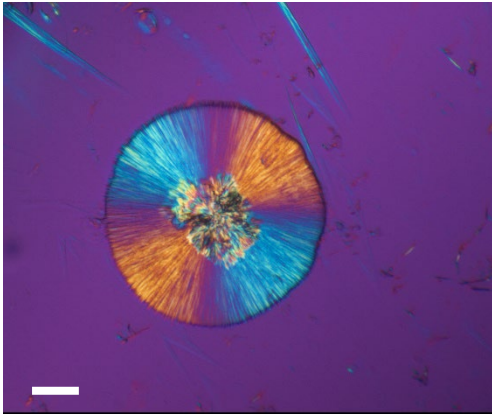


25.0 min (Vitamin E TPGS oily droplet being trapped)

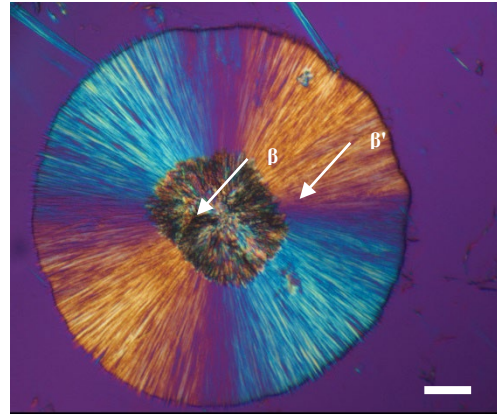




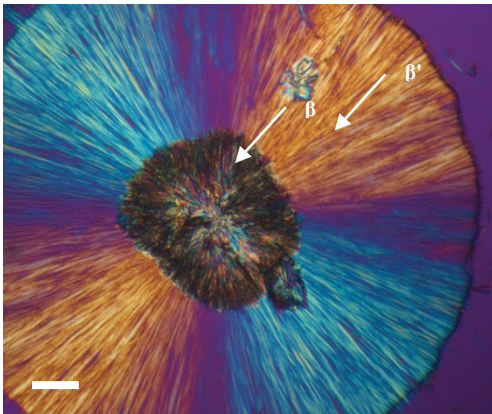
27.5 min



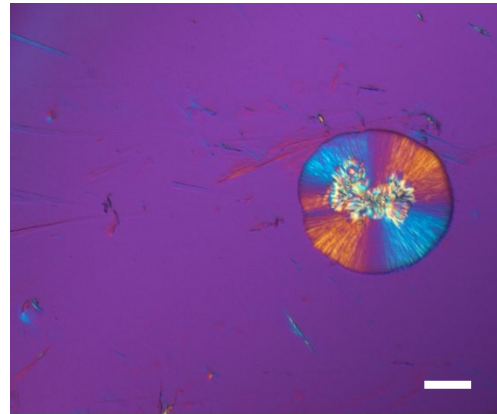
30.0 min (growth of  $\beta'$  nuclei &  $\beta'$ - $\beta$  conversion)



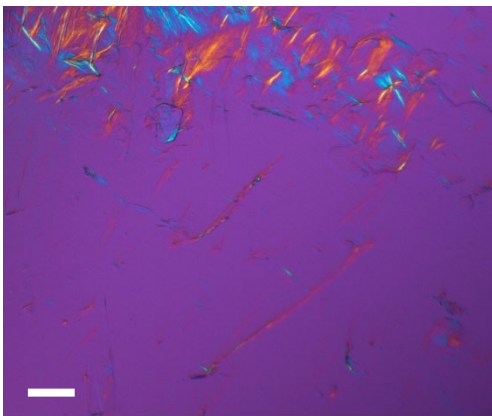
32.5 min



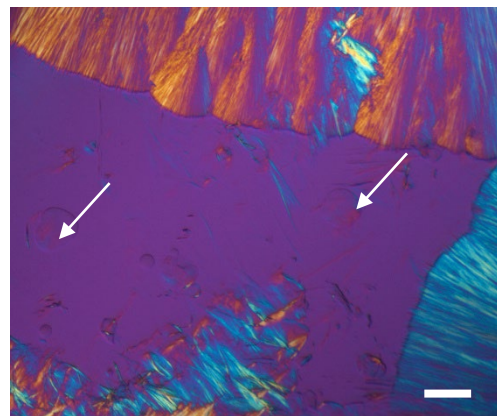
35.0 min



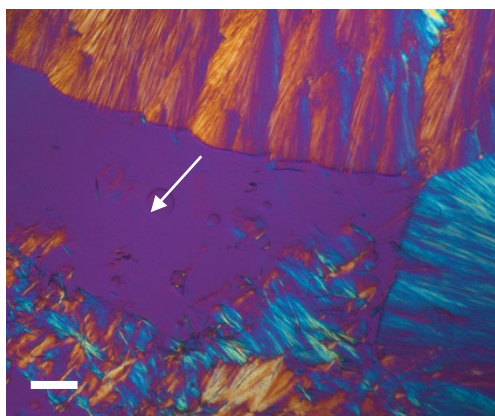
37.5 min



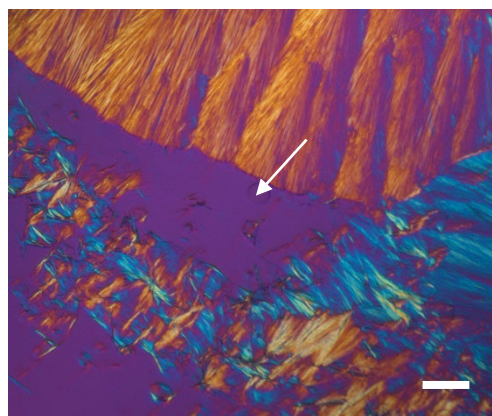
40.0 min (Vitamin E TPGS oily droplet being trapped)



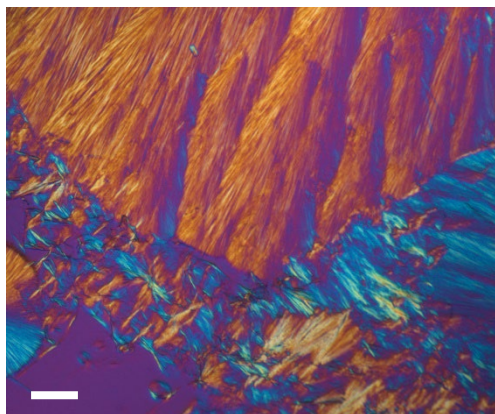
42.5 min (Vitamin E TPGS oily droplet being trapped)



45.0 min (Vitamin E TPGS oily droplet being trapped)



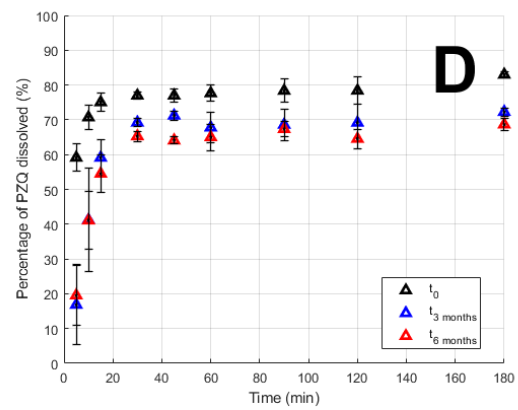
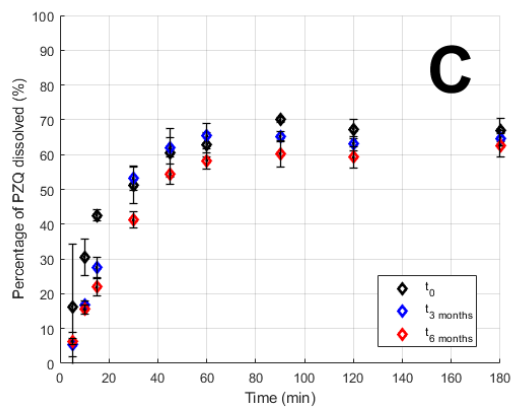
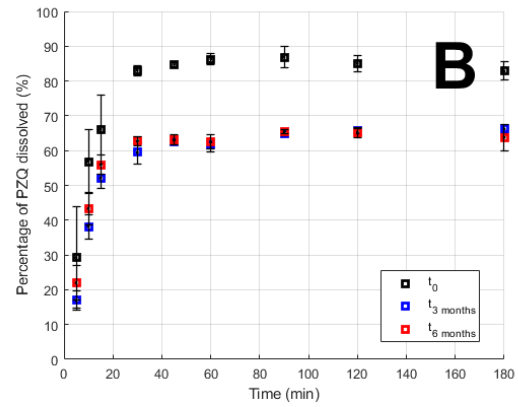
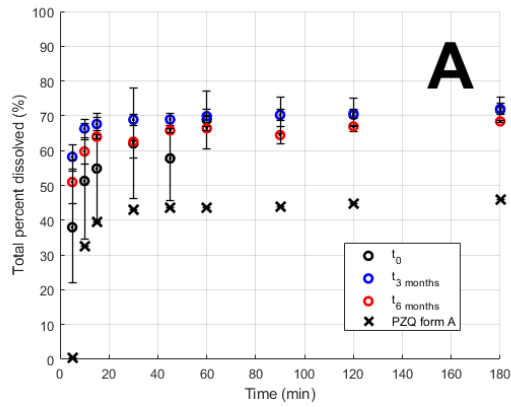
47.5 min (Vitamin E TPGS oily droplet being trapped)



End

## Appendix 04

**Dissolution profile (in percentage) of uncoated and coated amorphous solid dispersions in the presence of lipases: ASD\_PZQ uc (A), ASD\_PZQ cBWbF (B), ASD\_PZQ cSSSbF (C) and ASD\_PZQ cLLLbF (D)**







# Abstract / Résumé

## Lipid Excipients and Hot-Melt Coating Technology: Operational and Functional Impact

Hot-melt coating by fluidised bed consists of delivering molten lipids onto surface of substrate particles in suspension and let them solidify with air-cooling. The process is evidently solventless and therefore time-, cost-efficient and eco-friendly. Lipids constitute a generally-regarded-as-safe class of excipients. Despite those advantages, challenges reside in the fact that their physicochemical and biopharmaceutical properties have not been thoroughly investigated. This thesis dealt with these challenges by considering manufacturability, product stability and release properties. In the first phase “formulation development”, a simple and nimble experimental approach was developed for process and product characterisation in early stage. NaCl, as active substance, allows for fast-track research conduct. With their diverse properties (e.g. complex-mixture vs. pure substance, polymorphism and crystallisation, adaptability to different processing approaches), beeswax, tristearin and trilaurin were chosen as coating materials under research. Additive addition was indispensable and additives of different types were tested with those three lipid systems: (I) polysorbates, (II) sorbitans, (III) vitamin E TPGS and (IV) talc. Besides, several physical and in vitro characterisation techniques have been established, for instance, for rapid screening of solid lipid-additive combinations, in situ monitoring of polymorphic transformation and crystal growth, coupling of digestion and release testing in biologically simulated media. In the second phase “pharmaceutical applications”, three beeswax-, tristearin- and trilaurin-based formulations were selected for coating amorphous solid dispersions of praziquantel. The objectives are (i) to study bioaccessibility of the amorphous active substance coated with lipids of varying digestibility and (ii) to investigate long-term stability of these hot-melt coated products. In conclusion, selection of good additives is important for development of solid lipid-based formulated products. In effect, they can improve productivity of coating operations as well as product performance (stability, release profile).

*Keywords: Hot-melt coating, Solventless processing, Lipids, Bioenabling formulation, Controlled release, Physical stability*

## Excipients lipidiques et technologie d'enrobage à chaud : impact opérationnel et fonctionnel

L'enrobage à l'état fondu en lit fluidisé consiste à déposer du lipide fondu sur la surface des particules de substrat en mouvement et à le laisser refroidir à l'aide de l'air de fluidisation. La mise en forme n'a pas évidemment recours aux solvants. Ainsi, cette technologie fait économiser du temps et des ressources financières et est dite écologique. Les lipides constituent une catégorie d'excipients « généralement reconnus inoffensifs ». Malgré ces avantages, les challenges résident dans le fait que leurs propriétés physico-chimiques et biopharmaceutiques n'ont pas été explorées à fond. Cette thèse traite de ces défis en considérant la manufacturabilité, la stabilité et les propriétés de relargage du produit. Dans la première phase “développement de formulations”, une approche expérimentale facile et agile a été conçue pour la caractérisation de procédé et produits dans un premier temps. L'utilisation de NaCl, comme noyau actif, permet un conduit de recherche très fluide. Dotées des propriétés diverses (e.g. mélange complexe vs. substance pure, polymorphisme et cristallisation, adaptabilité aux approches de mise en forme différentes), la cire d'abeilles, la tristéarine et la trilaurine ont été sélectionnées comme matières enrobantes à l'étude. L'addition d'additif(s) a été indispensable et les additifs de nature différente ont été testés sur ces trois systèmes lipidiques : (I) polysorbates, (II) sorbitanes, (III) vitamine E TPGS et (IV) talc. D'ailleurs, plusieurs techniques de caractérisation physiques et in vitro ont été mises en place, pour l'instant, en vue de cribler rapidement des combinaisons lipide-additif, d'observer in situ la transformation polymorphique et la croissance cristalline, de coupler des tests de digestion et relargage dans le milieu biologiquement simulé. Dans la seconde phase “applications pharmaceutiques”, trois formulations contenant de la cire d'abeilles, de la tristéarine et de la trilaurine ont été choisies afin d'enrober les dispersions solides amorphes du praziquantel. Les objectifs sont (i) d'étudier la bioaccessibilité de ce principe actif amorphe enrobé des lipides dont la digestibilité est différente et (ii) d'investiguer la stabilité à long-terme des produits ainsi enrobés. En conclusion, le choix de bons additifs s'avère important pour le développement des produits formulés à base de lipides solides. En effet, ils peuvent aider à améliorer la productivité d'opérations d'enrobage ainsi que la performance du produit (stabilité, propriétés de relargage).

*Mots clés : Enrobage à chaud, Mise en forme sans solvants, Lipides, Formulation à bioaccessibilité améliorée, Relargage contrôlé, Stabilité*